



Daniel D. Stancil
Anil Prabhakar

Spin Waves

Theory and Applications

 Springer

Spin Waves

Daniel D. Stancil · Anil Prabhakar

Spin Waves

Theory and Applications

 Springer

Daniel D. Stancil
Carnegie Mellon University
Pittsburgh, PA
USA
stancil@cmu.edu

Anil Prabhakar
Indian Institute of Technology
Chennai
India
anilpr@iitm.ac.in

ISBN 978-0-387-77864-8 e-ISBN 978-0-387-77865-5
DOI 10.1007/978-0-387-77865-5

Library of Congress Control Number: 2008936559

© Springer Science+Business Media, LLC 2009

All rights reserved. This work may not be translated or copied in whole or in part without the written permission of the publisher (Springer Science+Business Media, LLC, 233 Spring Street, New York, NY 10013, USA), except for brief excerpts in connection with reviews or scholarly analysis. Use in connection with any form of information storage and retrieval, electronic adaptation, computer software, or by similar or dissimilar methodology now known or hereafter developed is forbidden.

The use in this publication of trade names, trademarks, service marks, and similar terms, even if they are not identified as such, is not to be taken as an expression of opinion as to whether or not they are subject to proprietary rights.

While the advice and information in this book are believed to be true and accurate at the date of going to press, neither the authors nor the editors nor the publisher can accept any legal responsibility for any errors or omissions that may be made. The publisher makes no warranty, express or implied, with respect to the material contained herein.

Printed on acid-free paper

springer.com

To Kathy and Namita

Preface

The properties and physics of spin waves comprise an unusually rich area of research. Under the proper circumstances, these waves can exhibit either dispersive or non-dispersive propagation, isotropic or anisotropic propagation, non-reciprocity, inhomogeneous medium effects, random medium effects, frequency selective nonlinearities, soliton propagation, and chaos. This richness has also led to a number of proposed applications in microwave and optical signal processing, and spin wave phenomena are becoming increasingly important to understand the dynamics of thin-film magnetic recording heads.

The book can be divided into three major parts. The first is comprised of Chapters 1–3 and is concerned with the physics of magnetism in magnetic insulators. The principal goals of these chapters are to provide a basic understanding of the microscopic origins of magnetism and exchange-dominated spin waves, motivate the equation of motion for the macroscopic magnetization, and to construct appropriate susceptibility models to describe the linear responses of magnetic materials to magnetic fields. The second part, Chapters 5–8, focuses on magnetostatic modes and dipolar spin waves, their properties, how to excite them, and how they interact with light. Chapter 4 serves as a bridge between these two parts by discussing how the susceptibility models from Chapter 3 can be used with Maxwell’s equations to describe electromagnetic and magneto-quasi-static waves in dispersive anisotropic media. Finally, Chapters 9 and 10 treat nonlinear phenomena and advanced applications of spin wave excitations.

The problems at the end of each chapter are often used to expand the material presented in the text. To enhance the book’s usefulness as a reference, many of these problems are “show that” problems with the answer given. For example, although the text discussion of dipolar spin waves in Chapter 5 is limited to an isolated film without a ground plane, the dispersion relations in the presence of a ground plane are given in the problems at the end of the chapter.

The book represents a major expansion of the classical, linear treatment of magnetostatic excitations contained in the earlier volume, *Theory of*

Magnetostatic Waves. Major additions include quantum mechanical treatments of angular momentum, exchange, and spin waves; nonlinear phenomena such as solitons and chaos; and applications such as the generation of spin waves using current-induced spin torques.

This book has been fun to write. We hope you find it to be an interesting and useful introduction to spin waves and their applications.

Daniel D. Stancil
Pittsburgh, USA

Anil Prabhakar
Chennai, India

August 2008

Acknowledgments

We are indebted to a number of people for helpful discussions and comments on portions of this book.

The accuracy and readability of the earlier work, *Theory of Magneto-static Waves*, were improved considerably by comments and suggestions from N. Bilaniuk, N. E. Buris, S. H. Charap, D. J. Halchin, J. F. Kauffman, T. D. Poston, A. Renema, S. D. Silliman, M. B. Steer, and F. J. Tischer. In addition, the present volume benefited from our interactions with C. E. Patton, P. E. Wigen, and A. N. Slavin on nonlinear excitations, auto-oscillations, and soliton formation; from discussions with M. Widom on quantum mechanics; and from comments and suggestions relating to spin-transfer torques from J. C. Slonczewski. Of course, the remaining errors and idiosyncrasies are ours.

One of us (DDS) would particularly like to thank his mentor, colleague, and friend, Prof. F. R. Morgenthaler, for teaching him much of the material in this book. He is also grateful to Kathy for her love, support, and patience. AP thanks his wife, Namita, for her encouragement and her indulgence during the many stages of this manuscript. He is also grateful for assistance from IIT-Madras under the Golden Jubilee Book Writing Scheme.

Finally, it has been a pleasure to work with A. Greene, K. Stanne, and their capable team at Springer US.

Contents

1	Introduction to Magnetism	1
1.1	Magnetic Properties of Materials	1
1.1.1	Diamagnetism	3
1.1.2	Paramagnetism	3
1.1.3	Ferromagnetism	3
1.1.4	Ferrimagnetism and Antiferromagnetism	4
1.2	Spinning Top	5
1.3	Magnetism	8
1.3.1	Equation of Motion	8
1.3.2	Gyromagnetic Ratio	10
1.4	Angular Momentum in Quantum Mechanics	12
1.4.1	Basic Postulates of Quantum Mechanics	13
1.4.2	Eigenvalue Equations	14
1.4.3	Angular Momentum	14
1.4.4	Addition of Angular Momenta	20
1.5	Magnetic Moments of Atoms and Ions	23
1.5.1	Construction of Ground States of Atoms and Ions	23
1.6	Elements Important to Magnetism	28
	Problems	28
	References	31
2	Quantum Theory of Spin Waves	33
2.1	Charged Particle in an Electromagnetic Field	33
2.2	Zeeman Energy	36
2.3	Larmor Precession	38
2.4	Origins of Exchange: The Heisenberg Hamiltonian	39
2.5	Spin Wave on a Linear Ferromagnetic Chain	46
2.6	Harmonic Oscillator	50
2.6.1	Harmonic Oscillator Eigenfunctions	50
2.6.2	Raising and Lowering Operators	52

2.7	Magnons in a 3D Ferromagnet: Method of Holstein and Primakoff.....	55
2.7.1	Magnon Dispersion Relation	55
2.7.2	Magnon Interactions	60
	Problems	64
	References	65
3	Magnetic Susceptibilities	67
3.1	Diamagnetism	67
3.2	Paramagnetism	70
3.3	Weiss Theory of Ferromagnetism	73
3.4	Néel Theory of Ferrimagnetism	76
3.5	Exchange Field.....	81
3.5.1	Uniform Magnetization.....	82
3.5.2	Non-uniform Magnetization.....	83
3.6	Magnetocrystalline Anisotropy	84
3.6.1	Uniaxial Anisotropy	84
3.6.2	Cubic Anisotropy	86
3.6.3	Coordinate Transformations	87
3.7	Polder Susceptibility Tensor	91
3.7.1	Equation of Motion for the Magnetization	91
3.7.2	Susceptibility Without Exchange or Anisotropy	91
3.7.3	Susceptibility with Exchange and Anisotropy	93
3.8	Magnetic Damping	94
3.9	Magnetic Switching	102
3.9.1	Stoner–Wohlfarth Particle	102
3.9.2	Damped Precession	104
	Problems	106
	References	108
4	Electromagnetic Waves in Anisotropic-Dispersive Media ...	111
4.1	Maxwell’s Equations	111
4.2	Constitutive Relations	112
4.3	Instantaneous Poynting Theorem	114
4.4	Complex Poynting Theorem	116
4.5	Energy Densities in Lossless Dispersive Media	117
4.6	Wave Equations	119
4.7	Polarization of the Electromagnetic Fields	122
4.8	Group and Energy Velocities	124
4.9	Plane Waves in a Magnetized Ferrite	127
4.9.1	Propagation Parallel to the Applied Field	128
4.9.2	Propagation Perpendicular to the Applied Field	130
4.10	The Magnetostatic Approximation	132
	Problems	134
	References	137

5	Magnetostatic Modes	139
5.1	Walker's Equation	139
5.2	Spin Waves	141
5.3	Uniform Precession Modes	144
5.3.1	Normally Magnetized Ferrite Film	144
5.3.2	Tangentially Magnetized Ferrite Film	145
5.3.3	Ferrite Sphere	146
5.4	Normally Magnetized Film: Forward Volume Waves	151
5.5	Tangentially Magnetized Film: Backward Volume Waves	158
5.6	Tangentially Magnetized Film: Surface Waves	162
	Problems	166
	References	167
6	Propagation Characteristics and Excitation of Dipolar Spin Waves	169
6.1	Energy Velocities for Dipolar Spin Waves	169
6.2	Propagation Loss	171
6.2.1	Relaxation Time for Propagating Modes	171
6.2.2	Surface Waves	173
6.2.3	Volume Waves	174
6.2.4	Summary of the Phenomenological Loss Theory	176
6.3	Mode Orthogonality and Normalization	178
6.3.1	Forward Volume Waves	178
6.3.2	Backward Volume Waves	180
6.3.3	Surface Waves	182
6.4	Excitation of Dipolar Spin Waves	183
6.4.1	Common Excitation Structures	183
6.4.2	Forward Volume Waves	188
6.4.3	Backward Volume Waves	194
6.4.4	Surface Waves	195
6.4.5	Discussion of Excitation Calculations	197
	Problems	199
	References	201
7	Variational Formulation for Magnetostatic Modes	203
7.1	General Problem Statement	203
7.2	Calculus of Variations	204
7.2.1	Formulation for One Independent Variable	204
7.2.2	Extensions to Three Independent Variables	206
7.3	Small-Signal Functional for Ferrites	208
7.4	Interpretation of the Functional	209
7.5	Stationary Formulas	211
7.6	Stationary Formula Examples with Forward Volume Waves	214
7.6.1	Large k -limit	214

7.6.2	Improved Approximation	215
7.6.3	Effect of Medium Inhomogeneity	217
7.7	Finite Element Analysis	218
	Problems	218
	References	221
8	Optical-Spin Wave Interactions	223
8.1	Symmetric Dielectric Waveguides	224
8.1.1	TE Modes	224
8.1.2	TM Modes	227
8.1.3	Optical Mode Orthogonality and Normalization	228
8.2	Magneto-Optical Interactions	231
8.2.1	Can You Tell the Difference Between $\bar{\mu}$ and $\bar{\epsilon}$?	231
8.2.2	Definition of Magnetization at High Frequencies	234
8.2.3	Symmetry Requirements on the Permittivity	235
8.3	Coupled-Mode Theory	236
8.3.1	Coupled-Mode Equations	237
8.3.2	Energy Conservation	238
8.3.3	Solutions to the Coupled-Mode Equations	239
8.4	Scattering of Optical-Guided Modes by Forward Volume Spin Waves	241
8.4.1	Coupled-Mode Equations	241
8.4.2	Coupling Coefficients	245
8.4.3	Tightly Bound Optical Mode Approximation	250
8.4.4	Cotton-Mouton Effect	252
8.5	Anisotropic Bragg Diffraction	253
	Problems	256
	References	260
9	Nonlinear Interactions	263
9.1	Large-Amplitude Spin Waves	263
9.1.1	Foldover and Bistability	267
9.2	Hamiltonian Equations of Motion	271
9.3	Spin Wave Interactions	273
9.3.1	Decay Instability	280
9.3.2	$\mathcal{H}^{(2)}$ Coefficients	282
9.4	Nonlinear Schrödinger Equation	284
9.4.1	Modulational Instability and Solitons	285
9.4.2	Split-Step Fourier Method	287
9.4.3	Anomalous Dispersion	289
9.4.4	Other Aspects	291
9.5	Routes to Chaos	293
9.5.1	Center Manifold Theory	293
9.5.2	Quantizing Low-Dimensional Chaos	296
	Problems	302
	References	305

10 Novel Applications	309
10.1 Nano-Contact Spin-Wave Excitations	309
10.1.1 Current-Induced Spin Torque	310
10.1.2 Magnetic Precession	315
10.2 Magnetic Precession in Patterned Structures	322
10.3 Inverse Doppler Effect in Backward Volume Waves	325
Problems	329
References	330
Appendix A: Properties of YIG	333
References	334
Appendix B: Currents in Quantum Mechanics	335
B.1 Density of States	335
B.2 Electric and Spin Current Densities	337
B.3 Reflection and Transmission at a Boundary	338
B.4 Tunneling Through a Barrier	339
References	341
Appendix C: Characteristics of Spin Wave Modes	343
C.1 Constitutive Tensors	343
C.1.1 Polder Susceptibility Tensor	343
C.1.2 Permeability Tensor	344
C.2 Uniform Precession Mode Frequencies	344
C.3 Spin Wave Resonance Frequencies	344
C.4 General Magnetostatic Field Relations	344
C.5 Forward Volume Spin Waves	345
C.6 Backward Volume Spin Waves	346
C.7 Surface Spin Waves	347
Appendix D: Mathematical Relations	349
D.1 Trigonometric Identities	349
D.2 Vector Identities and Definitions	349
D.3 Fourier Transform Definitions	350
Index	351

Introduction to Magnetism

Spin waves are excitations that exist in magnetic materials and we begin our discussion with an introduction to magnetism. Many aspects of magnetism can be understood in terms of classical analogs, but phenomena such as the quantization of angular momentum and certain interactions between spins are fundamentally quantum mechanical in nature. Consequently, a brief introduction to quantum mechanics is included as well. We will draw from both classical and quantum mechanical models as we gain insight into the basic theory of magnetism.

1.1 Magnetic Properties of Materials

Broadly speaking, all materials can be divided into two classes with regard to their magnetic properties: those that contain atoms or ions possessing permanent magnetic moments and those that do not. Within the group of materials containing permanent magnetic moments, we can further distinguish between those that manifest long-range order among the magnetic moments (below a critical temperature) and those that do not. Finally, we may classify those with magnetic order according to the particular alignment pattern that the moments exhibit. The major classifications of media according to magnetic properties are illustrated in Figure 1.1 and discussed more fully later.¹

The magnetic properties of materials can be conveniently discussed with reference to the magnetic susceptibility $\bar{\chi}$ defined as follows:

$$\mathbf{M} = \mathbf{M}_0 + \bar{\chi} \cdot \mathbf{H}, \quad (1.1)$$

where \mathbf{M} is the net macroscopic magnetic moment per unit volume (also called the magnetization), \mathbf{H} is the applied field (assumed small), and \mathbf{M}_0 is

¹ Although the moment configurations illustrated in Figure 1.1 are the most common, helical and complex-canted configurations are also possible. Further details on magnetic materials are found in [1–4] and in standard texts on solid-state physics such as Ashcroft and Mermin [5] and Kittel [6].

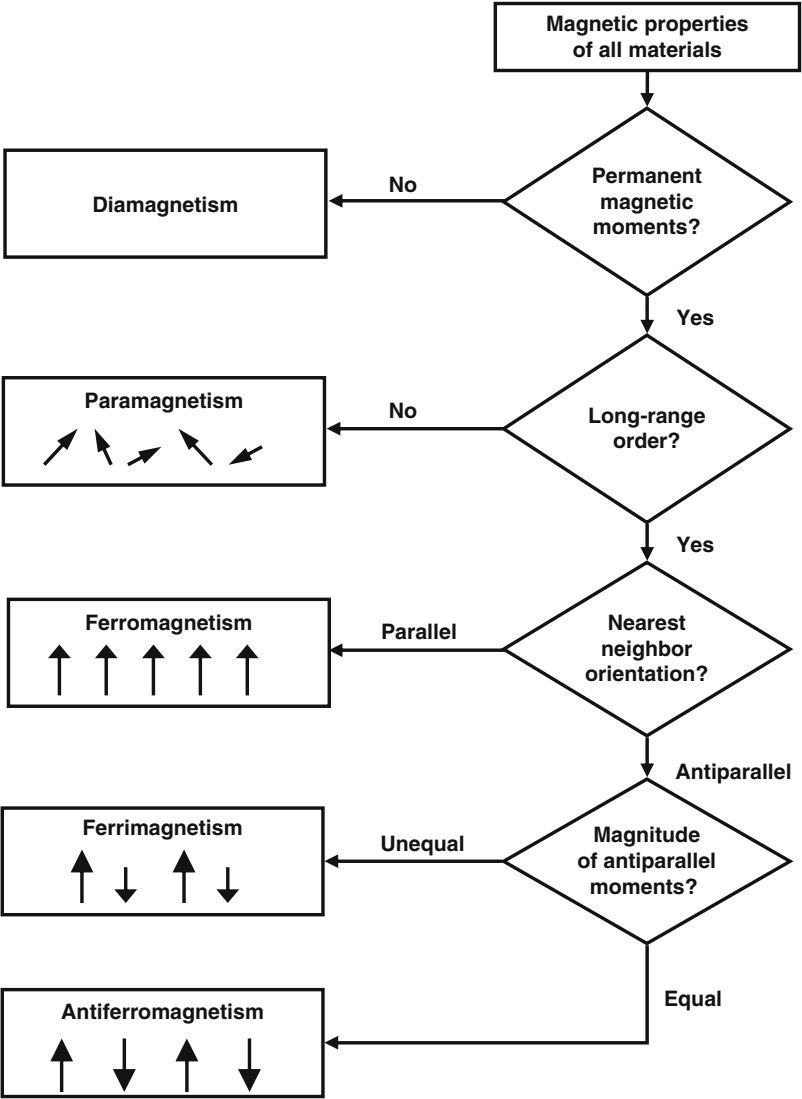


Fig. 1.1. The major classifications of magnetic properties of media. Antiferromagnetism can be viewed as a special case of ferrimagnetism.

the spontaneous magnetization in the absence of an applied field. In general, the susceptibility $\bar{\chi}$ is represented by a 3×3 matrix. For *isotropic* materials, however, the induced magnetization is either parallel or antiparallel to the applied field and the susceptibility is a scalar. In Chapters 1–8, we will restrict our consideration to applied fields that are small enough for the linear relationship between \mathbf{M} and \mathbf{H} described by (1.1) to be valid. Nonlinear effects are discussed in Chapters 9 and 10.

1.1.1 Diamagnetism

Materials that do not contain atoms or ions with permanent magnetic moments respond to an applied field with an induced magnetization that is opposed to the applied field and are called *diamagnetic*. The response of a diamagnetic material to an externally applied magnetic field can be described in terms of a microscopic application of Lenz's law. As a magnetic field is applied to such a material, electronic orbital motions are modified so as to generate an opposing magnetic field. Diamagnetic contributions in electrical insulators come from bound electrons circulating in atomic orbitals. Classically, the diamagnetic contribution from conduction electrons in metals and semiconductors can be shown to vanish in thermal equilibrium.² There is, however, a small non-vanishing diamagnetic effect from conduction electrons that arises from the quantization of angular momentum. Isotropic diamagnets are characterized by a negative scalar susceptibility since the induced moments oppose the applied field. Virtually all materials have a diamagnetic contribution to their total response to a magnetic field. In materials containing permanent magnetic moments, however, the diamagnetic contribution is usually overshadowed by the response of those moments.

1.1.2 Paramagnetism

Materials that contain permanent magnetic moments but not spontaneous long-range order are called *paramagnetic*. In thermal equilibrium without an applied magnetic field, the moments are randomly oriented so that no net magnetic moment is exhibited. Application of an external field then causes a partial alignment of the moments generating a net magnetic moment. Since the moments tend to align parallel to the applied field, isotropic paramagnets exhibit a positive scalar susceptibility.

1.1.3 Ferromagnetism

Ferromagnets are materials in which the elementary permanent moments spontaneously align (below a critical temperature). Although these moments do interact via their dipolar magnetic fields, the interaction giving rise to the spontaneous alignment is orders of magnitude stronger and of quantum mechanical origin. This is called the *exchange* interaction and is discussed in detail in Chapter 2.

In the absence of external fields, the magnetic order of ferromagnets generally breaks up into complex patterns of magnetic *domains*. The moments are all aligned within a given domain but change direction rapidly at the boundaries between domains. Thus, each domain acts like a tiny magnet that

² More generally, no macroscopic property of a material in thermal equilibrium can depend on an applied magnetic field in a purely classical theory. See Section 1.2.

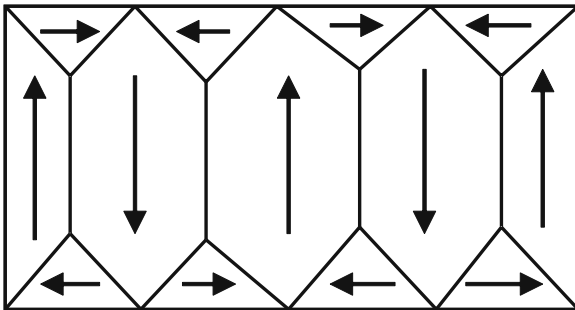


Fig. 1.2. Schematic representation of a magnetic domain pattern in a ferro- or ferrimagnet. Each domain contains a large number of microscopic magnetic moments.

is usually small in volume compared with the size of the material sample, but still contains a large number of elementary magnetic moments. In equilibrium, these domains orient themselves so as to minimize the net magnetic moment of the macroscopic sample (Figure 1.2). This minimizes the magnetic fringing fields external to the sample and thus minimizes the stored magnetostatic energy. When an external field is applied, the domains begin to align with the magnetic field giving rise to a net magnetization. Thus, an isotropic ferromagnet also has a positive scalar susceptibility.³

1.1.4 Ferrimagnetism and Antiferromagnetism

In some materials, the quantum mechanical coupling between moments is such that adjacent moments tend to line up along opposite directions. The long-range order can be described in terms of two opposing ferromagnetic sublattices. If the net magnetizations of the two sublattices are equal, the material is called an *antiferromagnet*. If the net magnetizations are unequal, the material is a *ferrimagnet*. In general, ferrimagnets are not limited to two sublattices; the distinguishing characteristic is that the equilibrium magnetization of at least one of the sublattices must be opposite to the others. For microwave frequencies and below, ferrimagnets can usually be modeled simply as ferromagnets with a total magnetization determined by the net magnetization of the sublattices.

Antiferromagnets, on the other hand, behave like anisotropic paramagnets. In the absence of an external field, the magnetizations of the two sublattices

³ In reality, material defects interfere with domain wall motion with the result that the magnetization at a given time depends not only on the present value of the magnetic field, but also on past values. Under these circumstances, Eq. (1.1) is clearly inadequate for describing the behavior of \mathbf{M} . This phenomenon is called *hysteresis* and is very important when multiple domains are present. For the study of microwave propagation in magnetic materials, we will concentrate on single-domain (saturated) materials.

cancel, yielding no net magnetic moment. The susceptibility along the direction parallel (or antiparallel) to the moments is very small since application of a field parallel (or antiparallel) to a moment yields no net torque. (At finite temperature, however, thermal agitations prevent the moments from being perfectly aligned so that the parallel susceptibility vanishes rigorously only at 0 K.) In contrast, the susceptibility perpendicular to the moments is much larger since the moments on both sublattices will tend to rotate toward the applied field.

At nonzero temperatures, thermal fluctuations prevent perfect alignment in any material exhibiting long-range magnetic order. As the temperature is increased, these fluctuations become larger and larger until the magnetic order is destroyed. The transition temperature above which magnetic order is destroyed is called the *Curie temperature* for ferromagnets and the *Néel temperature* for ferri- and antiferromagnets. Above this transition temperature, ferromagnets, ferrimagnets, and antiferromagnets exhibit a paramagnetic susceptibility.

Materials of particular importance for microwave device applications are magnetic oxides known as ferrites and magnetic garnets. Principal among these for dipolar spin wave applications is single-crystal *yttrium iron garnet* (YIG), $\text{Y}_3\text{Fe}_5\text{O}_{12}$, which is a ferrimagnet with two sublattices. The five iron ions per formula unit are the only magnetic constituents. Three of these ions are on one magnetic sublattice and two are on the other so that the net moment is due to one iron ion per formula unit.

Finally, a word should be said about the small signal susceptibilities of saturated ferro- and ferrimagnets. When a ferromagnet or ferrimagnet is placed in a sufficiently strong static magnetic field, all of the domains become aligned with the applied field, and the material is said to be saturated; strengthening the field will not result in an increased magnetic moment. However, there will still be a susceptibility for small perturbations perpendicular to the static field. Thus, the small signal susceptibility can be seen to be anisotropic in a manner similar to an antiferromagnet. If the perturbations are rapidly varying in time, off-diagonal elements of the susceptibility tensor begin to be important, and the response of the medium becomes considerably more involved. These are precisely the conditions under which dipolar spin waves propagate. Consequently, the small signal susceptibility tensor of a saturated ferromagnet (or ferrimagnet) will be discussed in some detail in Chapter 3.

1.2 Spinning Top

The magnetic properties of materials are due almost entirely to the orbital motion and spin of electrons.⁴ As with all subatomic particles, the dynamics of electrons can only be rigorously described using the language of quantum

⁴ The magnetic moments arising from nuclear particles are smaller by a factor of about 10^3 and may be neglected for our purposes.

mechanics. Indeed, Bohr and van Leeuwen⁵ proved that within the context of classical physics, it is impossible for a macroscopic medium to possess a magnetic moment. A key concept in quantum mechanics needed to overcome this difficulty is the quantization of elementary magnetic moments. However, because macroscopic magnetism involves large numbers of particles, it is still possible to construct classical or semi-classical models that are easy to visualize and accurate enough to be useful. In particular, we shall find that the physics of magnetic resonance phenomena is very similar to that of a spinning top which is a common topic of discussion in classical mechanics [9, 10].

Consider the top shown in Figure 1.3. We assume the gravitational force \mathbf{F}_g is acting on the top's center of gravity located by the vector \mathbf{d} . Let us express \mathbf{F}_g in terms of the gravitational field \mathbf{G} :

$$\mathbf{F}_g = m\mathbf{G}, \quad (1.2)$$

where $\mathbf{G} = -g\hat{\mathbf{z}}$, $g = 9.8 \text{ m/s}^2$ is the gravitational acceleration and m is the mass of the top (kg). The *torque* exerted on the top by gravity is

$$\boldsymbol{\tau} = \mathbf{d} \times \mathbf{F}_g. \quad (1.3)$$

Since the torque is equal to the time rate of change of the *angular momentum* (this follows from the Newtonian law $\mathbf{F} = d\mathbf{p}/dt$), we can also write

$$\frac{d\mathbf{J}}{dt} = \mathbf{d} \times \mathbf{F}_g, \quad (1.4)$$

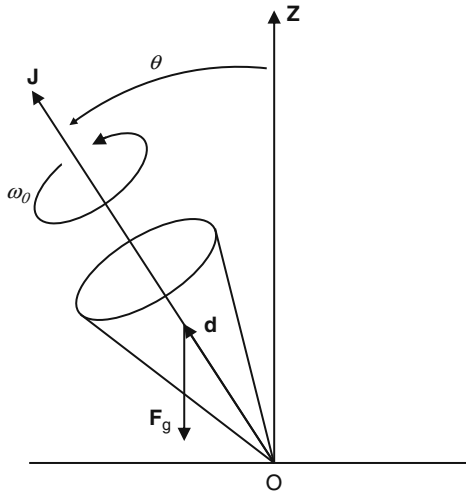


Fig. 1.3. Geometry of a spinning top.

⁵ This was first proved by Niels Bohr in his doctoral thesis [7] and independently by Ms. H.-J. van Leeuwen [8].

where the magnitude of the angular momentum \mathbf{J} is given by

$$|\mathbf{J}| = I\omega_0. \quad (1.5)$$

Here I is the mass moment of inertia and ω_0 is the angular velocity of rotation about the symmetry axis of the top.

In an increment of time Δt , the angular momentum will change by the amount $\Delta\mathbf{J}$ as shown in Figure 1.4. From the geometry, we have

$$\Delta\phi = \frac{\Delta J}{J \sin \theta}, \quad (1.6)$$

where θ is the angle between the \hat{z} -axis and the axis of the top, and we have approximated the arc length by ΔJ for small $\Delta\phi$. Dividing both sides of (1.6) by Δt and taking the limit $\Delta t \rightarrow 0$ we get:

$$\frac{d\phi}{dt} = \omega_P = \frac{dJ}{dt} \frac{1}{J \sin \theta}. \quad (1.7)$$

The angular *precession frequency*, ω_P , is the frequency with which the axis of the top rotates about the vertical. Thus, substituting (1.2) and the magnitude of (1.4) into (1.7) gives

$$\omega_P = \frac{mgd}{J}, \quad (1.8a)$$

or, using (1.5),

$$\omega_P = \frac{mgd}{I\omega_0}. \quad (1.8b)$$

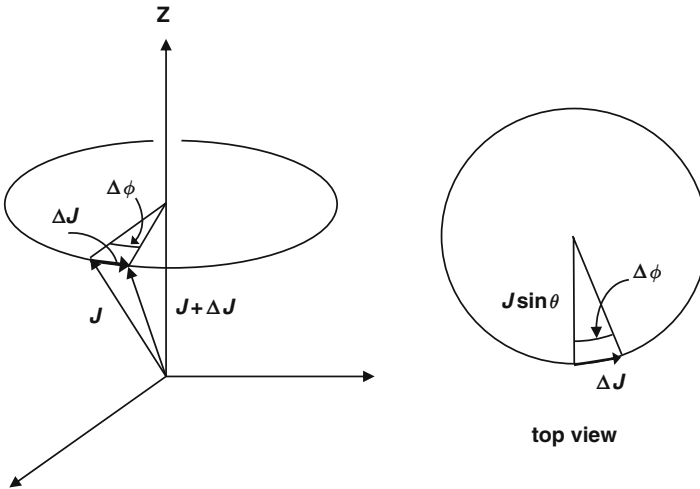


Fig. 1.4. Change in the angular momentum of a spinning top in the time Δt .

Since in our geometry, \mathbf{d} and \mathbf{J} are either parallel or antiparallel, (1.4) can be written as

$$\frac{d\mathbf{J}}{dt} = \frac{md}{J \operatorname{sgn}(\mathbf{d} \cdot \mathbf{J})} \mathbf{J} \times \mathbf{G}$$

or

$$\frac{d\mathbf{J}}{dt} = \boldsymbol{\Omega} \times \mathbf{J}, \quad (1.9)$$

where

$$\boldsymbol{\Omega} = \omega_P \operatorname{sgn}(\mathbf{d} \cdot \mathbf{J}) \hat{\mathbf{z}} \quad (1.10)$$

and $\operatorname{sgn}(x)$ gives the algebraic sign of x .

Note that we have assumed that the total angular momentum of the top is parallel to the top's symmetry axis, thus neglecting the angular momentum associated with rotations about the other principal axes of the top that give rise to the precession. Equation (1.9) is, therefore, the equation of motion for a rapidly spinning top.

1.3 Magnetism

If the spinning top of Section 1.2 is electrically neutral, then the presence of a magnetic field would have no effect. However, if we applied a static electric charge to the top, the spinning motion *would* create a magnetic moment that would interact with an externally applied magnetic field. Consequently, the torques due to both the gravitational and magnetic fields would have to be included in the equation of motion. When dealing with the motions of elementary charged particles, however, the large value of the charge-to-mass ratio permits us to neglect the effects of gravity. Thus, in our discussion of magnetism, an externally applied magnetic flux density \mathbf{B} will take the place of the gravitational field \mathbf{G} .

1.3.1 Equation of Motion

Consider a small current loop in a magnetic field as shown in Figure 1.5 (this could be an electron in an atomic orbital). The magnetic moment is defined as

$$\boldsymbol{\mu} = IA\hat{\mathbf{n}}, \quad (1.11)$$

where $\hat{\mathbf{n}}$ is a unit vector normal to the loop surface according to the right-hand rule. The torque on the loop is

$$\boldsymbol{\tau} = \boldsymbol{\mu} \times \mathbf{B}. \quad (1.12)$$

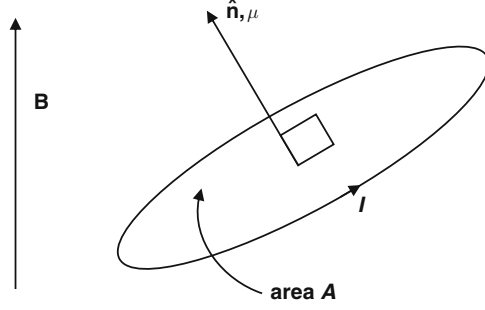


Fig. 1.5. Current loop in a magnetic field.

Since the current is due to the motion of charged particles, the loop will also possess angular momentum along a direction parallel (or antiparallel) to $\hat{\mathbf{n}}$. The constant of proportionality between the magnetic moment and the angular momentum is called the *gyromagnetic ratio* γ :

$$\boldsymbol{\mu} = \gamma \mathbf{J}. \quad (1.13)$$

If the charge is negative, then the directions of the conventional current and the particle velocity will be opposite, $\boldsymbol{\mu}$ and \mathbf{J} will be antiparallel, and γ will be negative. This will be discussed in detail in Section 1.3.2.

The equation of motion can now be written

$$\frac{d\mathbf{J}}{dt} = \gamma \mathbf{J} \times \mathbf{B}. \quad (1.14)$$

In the increment of time Δt , the angular momentum will change by the amount $\Delta \mathbf{J}$. From a construction similar to that of Figure 1.4, we have

$$\Delta \phi = \frac{\Delta J}{J \sin \theta}, \quad (1.15)$$

as before. Dividing both sides of Eq. (1.15) by Δt and taking the limit $\Delta t \rightarrow 0$ gives

$$\frac{d\phi}{dt} = \frac{1}{J \sin \theta} \frac{dJ}{dt}. \quad (1.16)$$

Noting that $d\phi/dt$ is the angular precession frequency ω_P , and using the magnitude of $d\mathbf{J}/dt$ from (1.14) gives

$$\omega_P = |\gamma B|. \quad (1.17)$$

Equation (1.14) can now be written as

$$\frac{d\mathbf{J}}{dt} = \boldsymbol{\Omega} \times \mathbf{J}, \quad (1.18)$$

where

$$\boldsymbol{\Omega} = -\gamma \mathbf{B}. \quad (1.19)$$

Comparing (1.18) with (1.9) shows that the equations of motion for the top and the magnetic moment are of identical form. Because of this, the top is a useful classical analog to aid in visualizing magnetic resonance phenomena. Note, however, that unlike the top, the precession frequency for the magnetization (1.17) is independent of the magnitude of the angular momentum!

1.3.2 Gyromagnetic Ratio

Now let us look more closely at the constant of proportionality between the magnetic moment and angular momentum that we called the gyromagnetic ratio, γ . As stated previously, the dominant angular momentum giving rise to macroscopic magnetism belongs to electrons. Electrons in atoms can have two kinds of angular momenta: orbital \mathbf{L} and spin \mathbf{S} . The total angular momentum is just the vector sum

$$\mathbf{J} = \mathbf{L} + \mathbf{S}. \quad (1.20)$$

Orbital angular momentum is due to the motion of the electron about the atom. Spin, on the other hand, can only be adequately described with quantum mechanics; it has no classical analog. Because orbital angular momentum is easier to visualize, let us first consider it in more detail.

Consider an electron in a classical circular orbit about an atomic nucleus, as shown in Figure 1.6. If the linear momentum of the electron is $\mathbf{p} = m_q \mathbf{v}$ and the position vector is \mathbf{R} , the angular momentum is

$$\mathbf{L} = \mathbf{R} \times \mathbf{p}. \quad (1.21)$$

Thus, according to the right-hand rule, \mathbf{L} is directed out of the page in Figure 1.6 and has the magnitude $Rm_q v$.

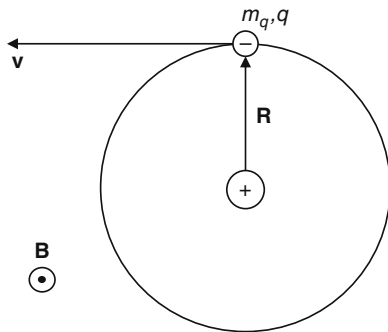


Fig. 1.6. An electron in a classical orbit about an atomic nucleus.

Next, we need the magnetic moment associated with the motion of the electron. We can obtain this by modeling the electron in its orbit as a current loop. The magnetic moment of the loop is

$$\mu = IA, \quad (1.22)$$

where I is the current in the loop and A is the loop area. The current is the charge per unit time passing a particular point along the orbit:

$$I = \frac{v}{2\pi R} (\text{rev/s}) \times q (\text{coul/rev}) = \frac{qv}{2\pi R}. \quad (1.23)$$

Multiplying by the loop area πR^2 gives the magnetic moment

$$\mu = qvR/2. \quad (1.24)$$

The gyromagnetic ratio for orbital angular momentum is therefore

$$\begin{aligned} \gamma_L &= \mu/L \\ &= \frac{q}{2m_q}. \end{aligned} \quad (1.25)$$

The direction of the magnetic moment of the current loop is normal to the loop plane and in a direction determined by the right-hand rule just as with angular momentum. For the case of the electron shown in Figure 1.6, the conventional current is circulating in the opposite direction from the electron so that the magnetic moment is directed into the paper. Thus, for an electron, $\boldsymbol{\mu}$ and \mathbf{L} are oppositely directed. This can be expressed

$$\boldsymbol{\mu} = \gamma_L \mathbf{L} \quad (1.26)$$

where $\gamma_L < 0$ due to the negative electronic charge. Substituting the electronic mass and charge in Eq. (1.26) gives $|\gamma_L/2\pi| = 14 \text{ GHz/T}$ (1.4 MHz/G) for orbital angular momentum.

As discussed in Section 1.1.1, the application of a magnetic field will always induce a small perturbation in the orbital angular momentum giving rise to a diamagnetic contribution to the susceptibility. If the atom or ion under consideration has no intrinsic net magnetic moment, this induced moment represents the total magnetic response and the material is diamagnetic. If an intrinsic net moment does exist, then the induced moment will typically be much weaker and can be treated as a small perturbation. In either case, the frequency of precession is given by (1.17) with $\gamma = \gamma_L = q/2m_q$, since the frequency is independent of the strength of the moment. This is called the *Larmor precession frequency*.

Although the preceding calculations were entirely classical, it is fortunate that the results are also correct quantum mechanically. The situation is somewhat different for spin angular momentum. When the appropriate quantum

mechanical calculation is performed, the gyromagnetic ratio for spin is different by a factor of 2:

$$\gamma_S = q/m_q. \quad (1.27)$$

Thus, for spin, $|\gamma_S/2\pi| = 28 \text{ GHz/T}$ (2.8 MHz/G).

In the presence of both spin and orbital angular momenta, we can write

$$\boldsymbol{\mu} = \gamma_L(\mathbf{L} + 2\mathbf{S}). \quad (1.28)$$

Strictly speaking, then, $\boldsymbol{\mu}$ and \mathbf{J} are no longer parallel or antiparallel when both \mathbf{L} and \mathbf{S} contribute to \mathbf{J} (cf. Eq. (1.20)). However, it can be shown that only the component of $\boldsymbol{\mu}$ parallel to \mathbf{J} has a well-defined measurable value. Because of this, it is possible to write

$$\boldsymbol{\mu} = \gamma\mathbf{J}, \quad (1.29)$$

where

$$\gamma = g \frac{q}{2m_q} \quad (1.30)$$

and g is called the *Landé g factor*. It has the value 2 for pure spin and 1 for pure orbital angular momenta. For mixtures of \mathbf{L} and \mathbf{S} , it takes on other values to represent the projection of $\boldsymbol{\mu}$ along the direction of \mathbf{J} . To obtain a general expression for g , first dot \mathbf{J} into both sides of (1.29) giving

$$\boldsymbol{\mu} \cdot \mathbf{J} = g\gamma_L J^2. \quad (1.31)$$

Substituting (1.20) and (1.28) for \mathbf{J} and $\boldsymbol{\mu}$, respectively, into the left side of (1.31) gives

$$L^2 + 3\mathbf{L} \cdot \mathbf{S} + 2S^2 = gJ^2. \quad (1.32)$$

An expression for $\mathbf{L} \cdot \mathbf{S}$ in terms of L^2 , S^2 , and J^2 can be obtained by squaring (1.20):

$$\mathbf{L} \cdot \mathbf{S} = \frac{1}{2} (J^2 - L^2 - S^2). \quad (1.33)$$

Substituting this result into (1.32) and solving for g gives

$$g = \frac{3}{2} + \frac{S^2 - L^2}{2J^2}. \quad (1.34)$$

This result, obtained by treating \mathbf{J} , \mathbf{L} , and \mathbf{S} as classical vectors, is in agreement with the quantum mechanical result only when S^2 , L^2 , and J^2 are very large. In Section 1.4, we consider some of the basic postulates of quantum mechanics that lead us to a more accurate expression for the Landé g factor.

1.4 Angular Momentum in Quantum Mechanics

It is helpful in our study of magnetism to briefly discuss those aspects of the quantum theory of angular momentum that have the greatest impact on the properties of magnetic materials. Specifically, we are interested in the difference between spin and orbital angular momenta and the way that these two sources of magnetic moments combine to yield the Landé g factor.

1.4.1 Basic Postulates of Quantum Mechanics

In quantum mechanics the description of a particle is given by specifying a continuous function of position called the *wave function*.⁶ Estimates of the physical parameters such as position, momentum, and energy are obtained by applying appropriate operators to the wave function. The operators corresponding to position and momentum are listed in Table 1.1. Here \hbar is Planck's constant divided by 2π ($\hbar = 1.0546 \times 10^{-34}$ J s). The operators corresponding to other quantities dependent on \mathbf{r} and \mathbf{p} can be obtained by substituting the appropriate operator in the classical expression for that quantity. For example, the potential and kinetic energy operators are given by

$$\text{Potential:} \quad V(\mathbf{r}) \rightarrow V(\mathbf{r}), \quad (1.35a)$$

$$\text{Kinetic:} \quad \frac{\mathbf{p}^2}{2m_q} \rightarrow \frac{-\hbar^2 \nabla^2}{2m_q}, \quad (1.35b)$$

where m_q is the mass of the particle (assumed to have charge q). The operator for the total energy would then be, of course, the sum of the potential and kinetic energy operators.

According to quantum theory, both the position and the momentum of a particle cannot be simultaneously specified with arbitrary precision. This is known as the *Heisenberg uncertainty principle*. As a consequence, precise values for physical quantities cannot be calculated. Only their statistical expectation, or mean, values can be obtained. The expectation value of a physical quantity represented by the operator \mathcal{A} is given by

$$\langle \mathcal{A} \rangle = \int \psi^* \mathcal{A} \psi dv, \quad (1.36)$$

where the integral is over all space, the asterisk denotes complex conjugation and the wavefunction ψ is normalized such that

$$\int \psi^* \psi dv = 1. \quad (1.37)$$

Table 1.1. Quantum mechanical operators corresponding to classical quantities.

Quantity	Operator
position \mathbf{r}	\mathbf{r}
momentum \mathbf{p}	$\frac{\hbar}{i} \nabla$

⁶ The wavefunction may also depend on other generalized coordinates such as those describing spin.

1.4.2 Eigenvalue Equations

Consider the class of equations of the form

$$\mathcal{A}\psi = \alpha\psi, \quad (1.38)$$

where \mathcal{A} is an operator and α is a scalar. The function $\psi(r)$ that satisfies this equation is called an eigenfunction of the operator \mathcal{A} , and α is called the eigenvalue associated with that eigenfunction. Equations in the form of (1.38) are called eigenvalue equations.

Evaluation of the expectation value of an operator is especially easy if the wave function is an eigenfunction of the operator:

$$\langle \mathcal{A} \rangle = \int \psi^* \mathcal{A}\psi dv \quad (1.39)$$

$$= \int \psi^* \alpha\psi dv \quad (1.40)$$

$$= \alpha \int \psi^* \psi dv, \quad (1.41)$$

$$\implies \langle \mathcal{A} \rangle = \alpha. \quad (1.42)$$

Thus, the expectation values of an operator are equal to its eigenvalues.

In classical mechanics, the expression for the total energy of a system is often called the *Hamiltonian*, and is given by

$$\mathcal{H} = \frac{p^2}{2m_q} + V(\mathbf{r}) \quad (1.43)$$

for a particle moving in a potential field. The corresponding quantum mechanical Hamiltonian operator is therefore

$$\mathcal{H} = -\frac{\hbar^2 \nabla^2}{2m_q} + V(\mathbf{r}). \quad (1.44)$$

The eigenvalue equation for the Hamiltonian operator is

$$\mathcal{H}\psi = \mathcal{E}\psi \quad (1.45)$$

or

$$-\frac{\hbar^2}{2m_q} \nabla^2 \psi + V(\mathbf{r})\psi = \mathcal{E}\psi. \quad (1.46)$$

This differential equation governing the behavior of ψ is the time independent form of *Schrödinger's equation*.

1.4.3 Angular Momentum

Angular momentum in classical physics is the cross-product of the radial vector and the linear momentum, i.e., $\mathbf{L} = \mathbf{r} \times \mathbf{p}$. Thus, the quantum mechanical angular momentum operator is

$$\mathbf{L} = \mathbf{r} \times \frac{\hbar}{i} \nabla, \quad (1.47)$$

or, in rectangular coordinates,

$$L_x = \frac{\hbar}{i} \left[y \frac{\partial}{\partial z} - z \frac{\partial}{\partial y} \right], \quad (1.48a)$$

$$L_y = \frac{\hbar}{i} \left[z \frac{\partial}{\partial x} - x \frac{\partial}{\partial z} \right], \quad (1.48b)$$

$$L_z = \frac{\hbar}{i} \left[x \frac{\partial}{\partial y} - y \frac{\partial}{\partial x} \right]. \quad (1.48c)$$

Although it is obvious that scalar multiplication is commutative, i.e. $ab = ba$, operators do not generally commute. This has important consequences regarding our ability to obtain the expectation values for more than one operator for a given system. As an example, consider two operators, A and B , such that

$$A\psi = \alpha\psi \quad (1.49)$$

and

$$B\psi = \beta\psi + \varphi, \quad (1.50)$$

where α and β are scalars and ψ and φ are linearly independent functions. For ψ to simultaneously be an eigenfunction of A and B , we need to determine the conditions under which φ vanishes. The difference in the result when A and B are applied in opposite order is given by

$$\begin{aligned} AB\psi - BA\psi &= A(\beta\psi + \varphi) - B\alpha\psi \\ &= \alpha\beta\psi + A\varphi - \alpha(\beta\psi + \varphi) \\ &= A\varphi - \alpha\varphi. \end{aligned} \quad (1.51)$$

If φ is not an eigenfunction of A , the right-hand side can only be zero when $\varphi = 0$. However, if $\varphi = 0$ then ψ is an eigenfunction of A and B (cf. Eqs. (1.49) and (1.50)). Thus, a requirement for ψ to be an eigenfunction of both A and B is that the order of the operators must not matter, i.e., the operators must commute. As an example, let us consider whether or not the operators for position and momentum commute:

$$\begin{aligned} (xp - px)\psi &= x \frac{\hbar}{i} \frac{\partial \psi}{\partial x} - \frac{\hbar}{i} \frac{\partial}{\partial x} (x\psi) \\ &= x \frac{\hbar}{i} \frac{\partial \psi}{\partial x} - \frac{\hbar}{i} \psi - x \frac{\hbar}{i} \frac{\partial \psi}{\partial x} \\ &= i\hbar\psi. \end{aligned} \quad (1.52)$$

This result can be summarized by the *commutation relation*

$$xp - px \equiv [x, p] = i\hbar, \quad (1.53)$$

where $[x, p]$ is referred to as the *commutator* of x and p . We conclude that the position and momentum operators do not commute, so that we cannot

have an eigenfunction of both position and momentum. Thus, in the quantum domain, it is not possible to simultaneously specify the precise position and momentum of a particle.⁷

Returning to the discussion on angular momentum, let us see if $L_x L_y \psi$ is the same as $L_y L_x \psi$; i.e., we want to evaluate

$$(L_x L_y - L_y L_x) \psi \equiv [L_x, L_y] \psi. \quad (1.54)$$

After substituting Eqs. (1.48) into (1.54) and simplifying we obtain

$$[L_x, L_y] = i\hbar L_z, \quad (1.55a)$$

and similarly, by cyclic permutation ($x \rightarrow y \rightarrow z \rightarrow x$)

$$[L_y, L_z] = i\hbar L_x, \quad (1.55b)$$

$$[L_z, L_x] = i\hbar L_y. \quad (1.55c)$$

Thus, the components of the angular momentum operator do not commute with one another and we cannot, in general, assign definite values to all the angular momentum components simultaneously. These commutation relationships can be represented conveniently by the vector cross-product

$$\mathbf{L} \times \mathbf{L} = i\hbar \mathbf{L}. \quad (1.56)$$

Unlike the cross-product of classical vectors, $\mathbf{L} \times \mathbf{L}$ does not vanish because the components of \mathbf{L} are operators rather than scalars and the operators do not commute.

Equation (1.56) has been obtained starting with the classical expression $\mathbf{L} = \mathbf{r} \times \mathbf{p}$ for orbital angular momentum.⁸ However, operators can be constructed that satisfy (1.56) but cannot be represented by a term of the form $\mathbf{r} \times \mathbf{p}$. Thus, in general, we will consider any vector that satisfies an equation of the same form as (1.56) to be a genuine angular momentum vector operator whether or not it can be expressed as $\mathbf{r} \times \mathbf{p}$. Let us define three more operators that will be useful in future discussions:

$$L_+ = L_x + iL_y, \quad (1.57a)$$

$$L_- = L_x - iL_y, \quad (1.57b)$$

$$L^2 = \mathbf{L} \cdot \mathbf{L} = L_x^2 + L_y^2 + L_z^2. \quad (1.57c)$$

These operators obey the following commutators:

$$[L_z, L_+] = \hbar L_+, \quad (1.58a)$$

⁷ This uncertainty in position and momentum leads to the Heisenberg uncertainty principle $\Delta x \Delta p \geq \hbar$.

⁸ Classically speaking, orbital angular momentum is the only kind of angular momentum.

$$[L_z, L_-] = -\hbar L_-, \quad (1.58b)$$

$$[L_+, L_-] = 2\hbar L_z, \quad (1.58c)$$

and

$$[L^2, L_x] = [L^2, L_y] = [L^2, L_z] = [L^2, L_+] = [L^2, L_-] = 0. \quad (1.58d)$$

Let ψ_m be an eigenfunction of L_z with eigenvalue $m\hbar$ such that

$$L_z \psi_m = m\hbar \psi_m. \quad (1.59)$$

Using the commutator (1.58a), we can write

$$(L_z L_+ - L_+ L_z) \psi_m = \hbar L_+ \psi_m \quad (1.60)$$

or, using (1.59)

$$L_z (L_+ \psi_m) = \hbar(m+1)(L_+ \psi_m). \quad (1.61)$$

Thus, $(L_+ \psi_m)$ is an eigenfunction of L_z , with eigenvalue $\hbar(m+1)$. Similarly, $(L_- \psi_m)$ is found to have the eigenvalue $\hbar(m-1)$. Because of these properties, L_+ and L_- are called “raising” and “lowering” operators, respectively.

Referring to Eqs. (1.55) and (1.58d), we conclude that a wave function can be constructed that simultaneously has definite expectation values for L^2 and one (but only one) of the components of \mathbf{L} . Because of this, the eigenvalues of these two operators are sometimes referred to as *good quantum numbers*. This result is in sharp contrast with classical mechanics, where definite values can be assigned to all the components of \mathbf{L} . For definiteness, let us assume that ψ is an eigenfunction of both L^2 and L_z :

$$L_z \psi = m\hbar \psi, \quad (1.62a)$$

$$L^2 \psi = \hbar^2 \lambda \psi, \quad (1.62b)$$

where λ is a constant to be determined. Equation (1.57c) for L^2 is not convenient for finding λ , since we cannot obtain definite expectation values for L_x and L_y . A more convenient form can be obtained using the definitions of the raising and lowering operators (1.57a) and (1.57b), and the commutator (1.58c):

$$\begin{aligned} L^2 &= L_x^2 + L_y^2 + L_z^2 \\ &= \frac{1}{2}(L_+ L_- + L_- L_+) + L_z^2 \\ &= L_- L_+ + L_z(L_z + \hbar). \end{aligned} \quad (1.63)$$

We have previously shown that application of the operator L_+ increases the expectation value of the z -component of angular momentum. Thinking

classically for a moment, the projection of a vector along a given axis will reach a maximum value when the vector is parallel to that axis. Thus, it is reasonable to expect that the quantum number m also possesses a maximum value, since it represents the projection of the angular momentum along the z -axis. We can therefore write $m \leq l$, where l is the maximum value of m . If ψ is a wave function with $m = l$, then

$$L_+\psi = 0. \quad (1.64)$$

Application of (1.63) then gives

$$L^2\psi = \hbar^2 l(l+1)\psi. \quad (1.65)$$

Comparison of (1.62b) and (1.65) gives

$$\lambda = l(l+1). \quad (1.66)$$

We would now like to find λ when $m \neq l$. The value of m can be lowered by applying the operator L_- :

$$L_z(L_-\psi) = \hbar(l-1)(L_-\psi). \quad (1.67)$$

The eigenvalue of L^2 associated with $(L_-\psi)$ can be found as follows:

$$\begin{aligned} L^2(L_-\psi) &= [L_-L_+ + L_z(L_z + \hbar)](L_-\psi) \\ &= [L_-L_+ + \hbar(l-1)(\hbar(l-1) + \hbar)](L_-\psi) \\ &= [L_-L_+ + \hbar^2 l(l-1)](L_-\psi). \end{aligned} \quad (1.68)$$

Using the commutator $[L_+, L_-] = 2\hbar L_z$, this becomes

$$L^2(L_-\psi) = L_-(L_-L_+ + 2\hbar L_z)\psi + \hbar^2 l(l-1)(L_-\psi). \quad (1.69)$$

Since ψ is already associated with the maximum value of m , we observe that $L_+\psi = 0$ and Eq. (1.69) can be written as

$$\begin{aligned} L^2(L_-\psi) &= 2\hbar^2 l(L_-\psi) + \hbar^2 l(l-1)(L_-\psi), \\ &= \hbar^2 l(l+1)(L_-\psi). \end{aligned} \quad (1.70)$$

Comparing Eqs. (1.65) and (1.70), we see that $(L_-\psi)$ and ψ have the same eigenvalues of L^2 , though they have different eigenvalues of L_z . This can be visualized as rotating a classical vector (Figure 1.7). As the vector is rotated, the length will remain constant but the projection along the z -axis may vary. Classically, however, if the maximum z -component is $\hbar l$, then the total length of the vector should also be $\hbar l$, rather than $\hbar[l(l+1)]^{1/2}$. This difference as well as the discrete nature of the z -component are essential differences between the quantum and classical descriptions of angular momentum. The classical result is recovered in the limit of large l .

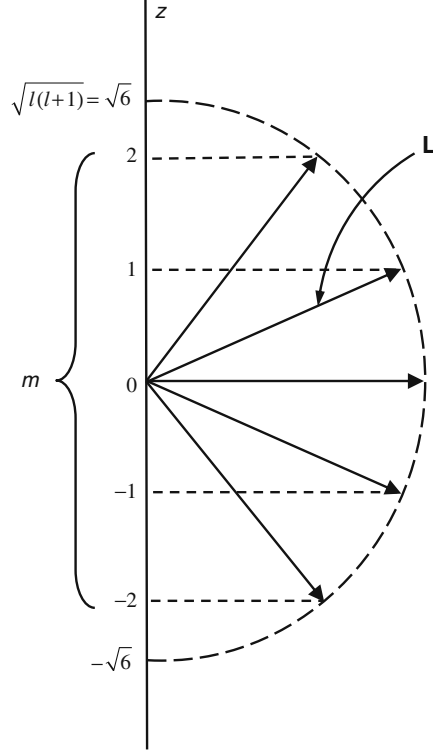


Fig. 1.7. Vector interpretation of the discrete nature of the projection of L along the z -axis for $l = 2$.

Keeping in mind this picture of a vector making different angles with the z -axis, it follows that the minimum value of m must be $-l$. Thus

$$-l \leq m \leq l. \quad (1.71)$$

Application of the lowering operator $2l$ times will, therefore, take us from the maximum to the minimum value of m . Also, $2l$ must be an integer since each application of L_- lowers m by 1. Thus, l must be an integer or half integer.

For orbital angular momentum, i.e. angular momentum arising from the motion of particles, we have seen that L_z can be expressed as a differential operator. In spherical coordinates, we have

$$L_z \psi = \frac{\hbar}{i} \frac{\partial \psi}{\partial \phi} = \hbar l \psi. \quad (1.72)$$

The solution of this equation is

$$\psi = e^{il\phi}. \quad (1.73)$$

For this to be a single-valued function of position (and hence independent of our choice of coordinate system), we require

$$e^{il\phi} = e^{il(\phi+2\pi)}. \quad (1.74)$$

Thus, l must be an integer for orbital angular momentum. The number of possible m values is therefore $2l + 1$ which is always an odd integer.

However, experiments performed on Ag atoms by Gerlach and Stern in 1922 [11] revealed the presence of only two discrete values of m . This suggested $l = 1/2$ and a source of angular momentum fundamentally different from that arising from the motion of particles. Many elementary particles have since been found to possess this intrinsic source of angular momentum, called spin. The most common spin $1/2$ particles are protons, neutrons, and electrons.

Although the term “spin” suggests a source of intrinsic angular momentum similar to a planet spinning about its axis, caution is in order since quantum mechanical spin has no classical analog. This is because a spinning planet (or top) can be analyzed in terms of the motion of differential mass elements and is therefore a form of orbital angular momentum. Thus, such a motion should cause integer rather than half-integer l .

We showed earlier that well-defined values could only be simultaneously assigned to the magnitude and one component of the angular momentum vector (such as L_z). This can be visualized as a rigid vector precessing about the z -axis but without definite phase.

1.4.4 Addition of Angular Momenta

If in a physical system, we have two separate sources of angular momentum that when isolated from one another can be described by functions $\psi_{j_1 m_1}$ and $\psi_{j_2 m_2}$, then we can construct a set of basis functions for describing the composite system by multiplying the two functions together:

$$\psi_{j_1 m_1 j_2 m_2} = \psi_{j_1 m_1} \psi_{j_2 m_2}. \quad (1.75)$$

Here, the z -component and magnitude squared of the angular momentum are given by $m_{1,2}$ and $j_{1,2}(j_{1,2} + 1)$, respectively. The angular momentum can be due to either spin or orbital motion. This approach is similar to constructing a trial product-form-solution to a multivariate partial differential equation using the separation of variables technique. Since for a given value of j , m can take on $2j+1$ values (cf. Eq. (1.71)), Eq. (1.75) represents a total of $(2j_1+1)(2j_2+1)$ basis functions for specified values of j_1 and j_2 . It is important to note that any one of these functions by itself may or may not be an adequate representation for a given physical system; construction of a satisfactory wave function may require a suitable linear combination of these basis functions.

Taking a clue from classical physics, we write the total angular momentum operator as

$$\mathbf{J} = \mathbf{J}_1 + \mathbf{J}_2. \quad (1.76)$$

Since \mathbf{J}_1 and \mathbf{J}_2 operate on different parts of the total system (i.e., they belong to different vector spaces), the components of these vectors commute:

$$[\mathbf{J}_1, \mathbf{J}_2] = 0. \quad (1.77)$$

Using this result, it can be verified that $\mathbf{J} \times \mathbf{J} = i\hbar\mathbf{J}$ demonstrating that \mathbf{J} is a properly defined angular momentum operator.

Since J_{1z} , J_1^2 , J_{2z} , and J_2^2 all commute, the quantum numbers $j_1 m_1 j_2 m_2$ can be used to describe the states in this product space representation. However, we would like to be able to also describe the state in terms of the eigenvalues and eigenvectors of the *total angular momentum* operators J_z and J^2 , since we expect the net magnetization to depend on the net total angular momentum. In this new representation, we again need four quantum numbers, so we need two more operators that commute with J_z and J^2 as well as with each other. Two additional operators are suggested by the following commutation relations:

$$[J_z, J_1^2] = 0, \quad (1.78a)$$

$$[J_z, J_2^2] = 0, \quad (1.78b)$$

$$[J^2, J_1^2] = 0, \quad (1.78c)$$

$$[J^2, J_2^2] = 0. \quad (1.78d)$$

Thus, the four operators J_z , J^2 , J_1^2 , and J_2^2 can be simultaneously diagonalized to obtain the states $\psi_{j_1 j_2 j m}$.

Since J^2 has the eigenvalue $\hbar^2 j(j+1)$, the length of J can be taken as $\hbar[j(j+1)]^{1/2}$. However, the largest z -component is j , so we can visualize \mathbf{J} precessing randomly about the z -axis and making an angle θ such that $\cos \theta = j/[j(j+1)]^{1/2}$. In a similar fashion, we can visualize the relationships among \mathbf{J} , \mathbf{J}_1 , and \mathbf{J}_2 as shown in Figure 1.8. Note that \mathbf{J}_1 and \mathbf{J}_2 do not have definite projections along z . This is an illustration of the result that J_{1z} and J_{2z} are not good quantum numbers for the state $\psi_{j_1 j_2 j m}$.

Goudsmit and Uhlenbeck correctly interpreted the results of the Stern–Gerlach experiment and introduced the possibility of half-integer spin

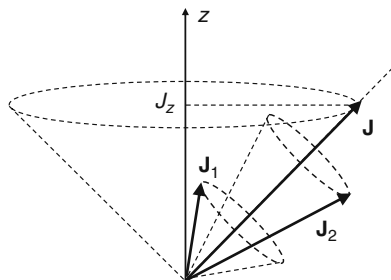


Fig. 1.8. Vector model for visualizing the random precession of \mathbf{J} , \mathbf{J}_1 , and \mathbf{J}_2 .

particles [12]. The spin operator \mathbf{S} for an electron is a true angular momentum operator (cf. Problem 1.5) with the properties

$$S^2 \chi_{s,m_s} = \hbar^2 s(s+1) \chi_{s,m_s} \quad (1.79)$$

$$S_z \chi_{s,m_s} = \hbar m_s \chi_{s,m_s} \quad (1.80)$$

where χ_{s,m_s} is the spin state with $s = 1/2$ and $m_s = \pm 1/2$. Thus, there are two potential sources of electron angular momentum (\mathbf{L} and \mathbf{S}) in a single electron atom. Since the number of sources of angular momentum increases as twice the number of electrons, a rigorous treatment of the net angular momentum rapidly becomes unwieldy in multi-electron atoms. Fortunately, in most cases the ground state can be obtained using a relatively simple approximation called the L-S coupling scheme or Russell-Saunders coupling scheme [13]. In this approximation, all of the electron spins combine to form a single spin vector $\mathbf{S} = \sum_i \mathbf{S}_i$ and all of the orbital angular momenta combine to form a single vector $\mathbf{L} = \sum_i \mathbf{L}_i$. The two vectors \mathbf{L} and \mathbf{S} are identified as \mathbf{J}_1 and \mathbf{J}_2 , respectively, and then combined to form \mathbf{J} , as was discussed in this section and shown schematically in Figure 1.9.

For our present purpose, we argue that under the L-S coupling scheme, the eigenvalues of the squares of the total spin vector, S^2 , and the total orbital angular momentum, L^2 , are $\hbar^2 S(S+1)$ and $\hbar^2 L(L+1)$, respectively, along with the eigenvalues $\hbar^2 J(J+1)$ for the square of the total angular momentum J^2 . Thus, the correct expression for the Landé g factor, from Eq. (1.34), is

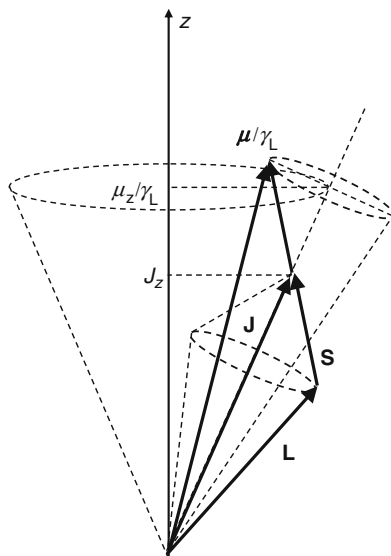


Fig. 1.9. Vector model showing the relationship between the moment normalized by the gyromagnetic ratio $\mu/\gamma_L = (\mathbf{L} + 2\mathbf{S})$ and the angular momentum $\mathbf{J} = \mathbf{L} + \mathbf{S}$.

$$g = \frac{3}{2} + \frac{S(S+1) - L(L+1)}{2J(J+1)}, \quad (1.81)$$

where we use the eigenvalues for the different angular momentum operators instead of the classical magnitudes S^2 , L^2 , and J^2 . The use of the L–S coupling scheme along with Hund’s rule, under the approximation of weak spin–orbit interactions, is further discussed in Section 1.5. The reader is also referred to one of the many texts on this topic [4, 14–17].

In yttrium iron garnet (YIG), the magnetic moment comes from Fe^{3+} ions, which have no net orbital angular momentum in their ground state. Thus, the magnetic properties of YIG are due entirely to spin and the gyromagnetic ratio $|\gamma/2\pi| = |\gamma_S/2\pi| = 28 \text{ GHz/T}$ (2.8 MHz/G).

1.5 Magnetic Moments of Atoms and Ions

The ground states of various ions and atoms to get some insight into why certain elements are more prominent in magnetism than others. Let us first summarize the key differences between the quantum operators and the classical vectors described in the previous sections.

- (a) It is not possible to precisely specify all three components of an angular momentum vector simultaneously. It is possible, however, to specify the average values of the magnitude squared (J^2) and one component (usually J_z) simultaneously.
- (b) The average values of J^2 and J_z are given by

$$\langle J^2 \rangle = \hbar^2 j(j+1), \quad (1.82a)$$

$$\langle J_z \rangle = m\hbar, \quad (1.82b)$$

where

$$m = -j, -j+1, -j+2, \dots, j-1, j,$$

\hbar is Planck’s constant divided by 2π ($\hbar = 1.055 \times 10^{-34} \text{ J s}$) and m and j must be either integers or half-integers for orbital or spin angular momentum, respectively. Quantization of angular momentum leads also to discrete values of the magnetic moment through (1.29). Substitution of (1.82b) into (1.29) shows that μ_z is quantized in units of $\mu_B = |q|\hbar/2m_q$ for both spin and orbital moments. The magnetic moment μ_B is called the *Bohr magneton* and has the value $9.274 \times 10^{-24} \text{ J/T}$.

1.5.1 Construction of Ground States of Atoms and Ions⁹

As we discussed in Section 1.4.1, the Heisenberg uncertainty principle does not allow us to simultaneously determine both the position and the momentum of

⁹ This section draws heavily from D. H. Martin, pp. 114–128 [3].

an electron with arbitrary precision. Instead, the electron is represented by a continuous function of position or a wave function, $\psi(r)$. The absolute square of the wave function $\psi^*(\mathbf{r})\psi(\mathbf{r})$ is proportional to the probability of finding the electron at position \mathbf{r} . Consider the electronic states of a hydrogen atom. The wave functions describing these states have appreciable amplitudes only in a limited region surrounding the nucleus and are labeled by the following four quantum numbers:

1. n is the principal quantum number; the number of radial nodes in the wave function $\psi(\mathbf{r})$ is given by $n - 1$,
2. l is the orbital angular momentum in units of \hbar ; $l \leq n - 1$,
3. m_l is the z -component of orbital angular momentum in units of \hbar ; $-l \leq m_l \leq l$, and
4. m_s is the z -component of spin angular momentum in units of \hbar ; $m_s = \pm 1/2$.

States with the same principal quantum number n are said to belong to the same *shell*; states with the same values of both n and l are said to belong to the same *subshell*; and states with the same n, l , and m_l values are said to belong to the same *orbital*. Since m_s can assume only two values, there are two allowed electrons in each orbital.

Subshells are often denoted as nX , where n is the principal quantum number and X is either s , p , d , or f , depending on whether the angular momentum quantum number l has the value 0, 1, 2, or 3, respectively. For example, the subshell for $n = 2$, $l = 1$ is denoted as $2p$.

Although all four quantum numbers are necessary to specify the electronic state, the energy depends only on the principal quantum number n for an isolated atom with no externally applied fields:

$$E = -\frac{q^4 m_q}{2(4\pi\epsilon_0 \hbar n)^2}, \quad (1.83)$$

where q and m_q are the charge and mass of an electron, respectively, and ϵ_0 is the permittivity of free space ($\epsilon_0 = 8.85 \text{ pF/m}$). This is a result of the particular form of the central coulomb potential. If the potential were to fall off with a form other than $1/r$, the energy would depend on l as well as n . This is precisely what happens in multiple electron atoms, since the inner electrons tend to screen the nucleus for the outer electrons. Close to the nucleus, the full charge of Zq is experienced, but far away the apparent charge is $(Z - N)q$, where Z is the number of positive charges in the nucleus and N is the number of electrons already present around the ion. For a given value of n , an electron with a lower value of l spends more time close to the nucleus. As the l value increases, the electron tends to spend more time away from the nucleus and therefore “sees” a weaker central charge due to the screening. Within a given shell, the energy therefore increases (becomes less negative) with increasing l . This effect is so large in the $n = 3$ shell that the $3d$ orbitals ($n = 3$, $l = 2$) of a multi-electron atom can have higher energies than the $4s$ orbitals ($n = 4$,

$l = 0$). Thus, if we imagine building up an atom by adding electrons one by one, the $4s$ subshell will be filled before the $3d$ subshell. However, an outer subshell with a lower energy than an inner subshell seems to violate our shielding argument! To resolve this paradox, more careful consideration must be given to the radial distributions of the orbital wave functions. In particular, the $4s$ wave function is spread out in such a way that it significantly penetrates the inner subshells, while also extending to larger radii than the $3d$ wave function.¹⁰ We will find that elements with incomplete inner d and f shells are very important to the study of magnetism.

Towards the end of Section 1.4.4, we introduced the notion that the spin of an electron interacts more strongly with other spins than it does with its own orbital angular momentum or the orbital angular momenta of other electrons. Similarly, the orbital angular momentum interacts most strongly with other orbital angular momenta. As a result, the spins combine to give a total spin vector $\mathbf{S} = \sum \mathbf{S}_i$, the orbital moments combine to give a total orbital angular momentum vector $\mathbf{L} = \sum \mathbf{L}_i$ and we obtain the total angular momentum vector $\mathbf{J} = \mathbf{L} + \mathbf{S}$. This approximation, called L-S coupling or Russell-Saunders coupling [13], is valid when spin-orbit interactions are weak. Within this approximation, we will use the quantum numbers L , M_L , S , and M_S to label the angular momentum state of the entire atom, where

$$M_L = \sum_{i=1}^N m_l^{(i)}, \quad (1.84)$$

$$M_S = \sum_{i=1}^N m_s^{(i)}, \quad (1.85)$$

and

$$-L \leq M_L \leq L, \quad (1.86)$$

$$-S \leq M_S \leq S, \quad (1.87)$$

where $m_l^{(i)}$ and $m_s^{(i)}$ are the quantum numbers for the i th electron and the sums are over all electrons in the atom. (Note that when specifying the state of a single electron, the total spin \mathbf{S} is usually omitted since it must always be $1/2$.)

As suggested earlier, let us consider further the buildup of an atom by adding one electron at a time. To do this, we will need to make use of the exclusion principle that states that no two electrons can occupy precisely the same state at the same time. In the present situation, this means that no two

¹⁰ A detailed account of how the orbitals are filled must also consider direct electron-electron interactions.

electrons can have the same four quantum numbers. Since the energy increases with both n and l , we begin with $n = 1$, $l = 0$:

- (a) The first electron goes into the lowest energy orbital ($n = 1$, $l = 0$) to form the configuration $1s^1$, where the principal quantum number n forms the prefix and the superscript indicates the number of electrons in the subshell. Since there is only one electron, $M_L = m_l = 0$ and $M_S = m_s = \pm 1/2$. Noting that L and S are the maximum values of M_L and M_S , we conclude that this state is characterized by $L = 0$ and $S = 1/2$.
- (b) Because m_s can take on two values corresponding to the “up” and “down” spin states, s subshells may contain two and only two electrons. Thus, the addition of the second electron gives the configuration $1s^2$ and fills the $1s$ subshell. The atomic state is now characterized by $L = 0$ and $S = 1/2 - 1/2 = 0$. The vanishing of the total angular momentum is, in fact, a general result for any filled subshell, since for every electron with $m_s = +1/2$ there is one with $m_s = -1/2$, and for every electron with $m_l = +m'$ there is one with $m_l = -m'$. Hence, filled subshells contribute nothing to the permanent magnetic moment of atoms and ions. (In the present case, of course, the only possible value for m_l is zero.)
- (c) Continuing the buildup of electronic states, the third electron goes into the $2s$ subshell to give the atomic state $L = 0$ and $S = 1/2$.
- (d) The fourth electron fills the $2s$ subshell and again we have $S=0$ and $L=0$.
- (e) The fifth electron goes into the $2p$ subshell with $n=2$ and $l=1$, yielding the atomic state $S=1/2$ and $L=1$.
- (f) With the sixth electron, we first encounter the situation with more than one electron in an unfilled subshell. We can determine the electronic configuration in the ground state using *Hund’s rules*. These rules were first determined empirically by spectroscopic studies, but are also confirmed by detailed calculations. When the atom is in the ground state, the electrons will occupy the orbitals so that S takes on the maximum possible value and L takes on the maximum possible value for this S . This is equivalent to saying that the interactions among spins and among orbital momenta are both ferromagnetic in sign, but that the spin interaction is stronger. The total angular momentum is then $J = |L - S|$ when the shell is less than half-full, and $J = L + S$ when the shell is more than half-full. This difference in computing the total angular momentum is caused by a relatively weak interaction between the spin and orbital angular momenta, called the spin-orbit coupling. When the subshell is exactly half-full, maximizing S results in $L=0$ so that $J = S$. For the present case, the application of Hund’s rules yields the ground state with $S=1$, $L=1$, and $J=0$, as explained later.

Let us now consider the application of Hund’s rules to the six-electron atom in detail. The maximum value of M_S that can be obtained with the two electrons in the p subshell is $1/2 + 1/2 = 1$, so the ground state must correspond to a total spin of $S=1$. Without considering other constraints, the

maximum value of M_L is $1 + 1 = 2$, where the possible values of m_l are $\{-1, 0, 1\}$. But we cannot have simultaneously two electrons with the *same* four quantum numbers n, l, m_l and m_s , so if $m_{s1} = m_{s2}$, we cannot also have $m_{l1} = m_{l2}$. The next highest value of M_L is $1 + 0 = 1$. Since this is the maximum value of M_L for $S=1$, the total orbital angular momentum of the state is $L = M_L = 1$. Finally, since a p subshell will hold six electrons, the shell is less than half-full and $J = |L - S| = 0$.

The ground states of atoms and ions are often indicated with the notation $^{2S+1}X_J$, where $2S + 1$ is the number of states with a given S (called the multiplicity) and X is a letter corresponding to the value of L according to the convention shown in Table 1.2. Thus, the ground state of our six-electron atom would be 3P_0 .

Table 1.2. Symbols used to denote total orbital angular momentum in the Hund-rule ground state.

L	Symbol
0	S
1	P
2	D
3	F
4	G
5	H
6	I

As a further example of the use of Hund's rules, consider the ground state of the ion Fe^{2+} with an electronic configuration $3d^6$. For d subshells, $l = 2$, and m_l can assume the values 2, 1, 0, -1 , -2 . Two spin states are allowed for each m_l value, so the subshell can accommodate 10 electrons. The application of Hund's rules is illustrated in Figure 1.10. The top row lists the possible m_l values for the d subshell and is divided into half, representing the two spin states. The highest M_S value is achieved by requiring as many electrons as possible to have parallel spins. The maximum M_L state for this M_S is obtained by filling the states with largest m_l first; i.e., by filling in the electrons from left to right in the diagram. The ground state is thus characterized by $L = \max\{M_L\} = 2$, $S = \max\{M_S\} = 2$, and $J = L + S = 4$, since the shell is more than half-full. This state is denoted by 5D_4 .

m_l	:	2	1	0	-1	-2		2	1	0	-1	-2
m_s	:	\uparrow	\uparrow	\uparrow	\uparrow	\uparrow		\downarrow				
		spin-up states						spin-down states				
		$J = L - S $						$J = L + S$				

Fig. 1.10. Hund-rule ground state for Fe^{2+} .

1.6 Elements Important to Magnetism

Using Hund's rules, we can calculate what the ground state of an isolated atom or ion will be. If the ground state has non-zero angular momentum, J , the atom will possess a magnetic moment. Such a calculation is useful for understanding magnetism in solids arising from incomplete inner subshells that tend to become involved in bonding much less than the outer, or valence, electrons. Consequently, an atom that possesses such a magnetic moment when isolated can often retain a moment after becoming part of a solid. Such is the case for the *transition elements*, which are especially important in magnetism. The five transition series are listed in Table 1.3. The two best known are the *iron group* and the rare earths.

Table 1.3. The five transition series. The two best known are the iron group and the rare earths.

Series	Elements	Incomplete shell
Iron group	Sc–Cu	$3d$
Palladium group	Y–Ag	$4d$
Platinum group	La–Au	$5d$
Rare earths	Ce–Lu	$4f$
Actinides	Ac–Lr	$5f$

Measured moments in solids are often different from those of an isolated ion or atom as calculated with Hund's rules, however. As an example, elements in the iron group exhibit reasonable agreement when S is calculated with Hund's rules, but with $L = 0$. The orbital angular momentum is said to be *quenched*. Quenching of orbital angular momentum results from the effects of the strong electric fields from neighboring ions. The presence of these fields causes the orbitals to continually change orientation so that the expected value of orbital angular momentum along any particular direction is zero.

The three most important elements for materials with permanent magnetic moments are Fe, Co, and Ni. The magnetic moment of an isolated Ni atom with electronic structure $4s^2 3d^8$ will have a ground state $S = 1, L = 3$, or 3F_4 . Likewise, the magnetic moment of yttrium iron garnet, $Y_3Fe_5O_{12}$, comes from the ion Fe^{3+} whose ground state is given by $S = 5/2, L = 0$, or $^6S_{5/2}$.

Problems

1.1. Consider a top in the shape of a right circular cone with height h and maximum radius R .

- (a) Show that the mass moment of inertia about the symmetry axis of the top is given by

$$I = \frac{3mR^2}{10}, \quad (1.88)$$

and that the center of mass is located on the axis of the cone a distance $d = 3h/4$ from the apex.

- (b) Using the results of part (a), show that the angular precession frequency is given by

$$\omega_P = \frac{5hg}{2R^2\omega_0}. \quad (1.89)$$

- (c) If $h = 0.016$ m and $R = 0.020$ m, and the top is spinning at 1500 RPM, calculate $f_P = \omega_P/2\pi$.
 (d) How will the precession frequency change as the top slows down? What will be the effect of spinning the top in the opposite direction?

1.2. Using Eq. (1.55) verify Eqs. (1.58a), (1.58b), (1.58c), and (1.58d).

1.3. If

$$L^2\psi = \hbar^2 l(l+1)\psi$$

and

$$L_-(L_-)^n\psi = 0,$$

show that $n = 2l$ and thus Eq. (1.71) follows.

1.4. Show that $[J^2, J_{1z}] \neq 0$ and $[J^2, J_{2z}] \neq 0$, so that eigenvectors specified by the numbers m_1, m_2, j , and m *cannot* be constructed.

1.5. Consider the spin eigenvalue equation

$$S_z\chi_{s,m_s} = \hbar m_s\chi_{s,m_s}. \quad (1.90)$$

For a single electron, m_s can only take on the two values $\pm 1/2$. Since there are, in general, n eigenvalues and eigenvectors for an $n \times n$ matrix, S_z can be represented by a 2×2 matrix. In such a matrix representation, the total spin operator is defined by

$$\mathbf{S} = \frac{\hbar}{2}\boldsymbol{\sigma}, \quad (1.91)$$

where

$$\boldsymbol{\sigma} = \hat{\mathbf{x}}\sigma_x + \hat{\mathbf{y}}\sigma_y + \hat{\mathbf{z}}\sigma_z, \quad (1.92)$$

and σ_x , σ_y , and σ_z are the *Pauli spin matrices*:

$$\sigma_x = \begin{bmatrix} 0 & 1 \\ 1 & 0 \end{bmatrix}, \quad \sigma_y = \begin{bmatrix} 0 & -i \\ i & 0 \end{bmatrix}, \quad \sigma_z = \begin{bmatrix} 1 & 0 \\ 0 & -1 \end{bmatrix}. \quad (1.93)$$

(a) Verify that \mathbf{S} is a true angular momentum operator by showing that

$$\mathbf{S} \times \mathbf{S} = i\hbar\mathbf{S}. \quad (1.94)$$

(b) Let

$$\chi_{\uparrow} = \begin{bmatrix} 1 \\ 0 \end{bmatrix}, \quad \chi_{\downarrow} = \begin{bmatrix} 0 \\ 1 \end{bmatrix}.$$

Show that χ_{\uparrow} and χ_{\downarrow} satisfy

$$S_z \chi_{\uparrow} = \frac{\hbar}{2} \chi_{\uparrow}, \quad (1.95a)$$

$$S_z \chi_{\downarrow} = -\frac{\hbar}{2} \chi_{\downarrow}, \quad (1.95b)$$

and thus represent “spin-up” and “spin-down” states, respectively. These vectors are called *spinors*.

(c) Since spin coordinates are discrete, evaluating the expectation values of spin operators involves summations rather than integrals. Evaluate the following expectation values:

$$\langle S^2 \rangle = \chi_{\downarrow}^T S^2 \chi_{\downarrow}, \quad (1.96a)$$

$$\langle S_z \rangle = \chi_{\downarrow}^T S_z \chi_{\downarrow}, \quad (1.96b)$$

and

$$\langle S^2 \rangle = \chi_{\uparrow}^T S^2 \chi_{\uparrow}, \quad (1.96c)$$

$$\langle S_z \rangle = \chi_{\uparrow}^T S_z \chi_{\uparrow}, \quad (1.96d)$$

where the superscript T indicates the matrix transpose.

1.6. Rare earth ions tend to first lose their $6s$ electrons, then their $4f$ electrons. The incomplete $4f$ subshell is shielded from the crystal fields by the outer $5s$ and $5p$ subshells so that the orbital angular momentum in these ions is not quenched. Calculate the Hund-rule ground states of the following ions and express the states in the spectroscopic notation $^{2S+1}X_J$: Ce^{3+} , Pr^{3+} , Nd^{3+} , Sm^{3+} , Eu^{3+} , Gd^{3+} , Tb^{3+} , Er^{3+} , and Lu^{3+} . Also calculate the Landé g factor for each state.

1.7. Iron group ions lose their $4s$ electrons before losing $3d$ electrons. Unlike the Rare Earths, there are no outer filled subshells to shield the $3d$ orbitals from the crystal fields of a host crystal. As a consequence, the orbital angular momentum of these ions is usually quenched in solids. Assuming that the orbital angular momentum is quenched, calculate the Hund-rule ground states of the following ions and express the states in the spectroscopic notation $^{2S+1}X_J$: Cr^{2+} , Mn^{3+} , Fe^{3+} , Fe^{4+} , Co^{2+} , Ni^{2+} , Cu^{2+} , and Cu^{3+} . Also calculate the Landé g factor for each state.

1.8. The magnetic oxide yttrium iron garnet $\text{Y}_3\text{Fe}_5\text{O}_{12}$ is often used in microwave devices. This material has a complicated cubic crystal structure with eight formula units per cell. The five Fe^{3+} ions per formula unit are distributed between antiparallel sublattices, giving the material its ferrimagnetic structure. The net difference is one Fe^{3+} ion per formula unit. The edge of the cubic cell is 12.38 Å. Calculate the maximum value of the magnetization M , i.e., its value at $T = 0\text{ K}$.

References

- [1] F. Brailsford, *Physical Principles of Magnetism*. London: Van Nostrand, 1966.
- [2] S. Chikazumi and S. H. Charap, *Physics of Magnetism*. Huntington, NY: R. E. Krieger Publishing Co., 1978.
- [3] D. H. Martin, *Magnetism in Solids*. Cambridge, MA: M.I.T. Press, 1967.
- [4] D. C. Mattis, *The Theory of Magnetism I: Statics and Dynamics*. New York: Springer-Verlag, Berlin, 1981.
- [5] N. Ashcroft and N. D. Mermin, *Solid State Physics*. New York: Holt, Rinehart and Winston, 1976.
- [6] C. Kittel, *Introduction to Solid State Physics*, 8th ed. New York: John Wiley & Sons, 2005.
- [7] N. Bohr, *Studies on the Electron Theory of Metals*. Doctoral thesis, University of Copenhagen, 1911.
- [8] H.-J. van Leeuwen, Doctoral thesis, University of Leiden, 1911. *Summary in* Hendrika Johanna van Leeuwen, “Problèmes de la théorie électronique du magnétisme”, *Journal de Physique et le Radium*, vol. 2 No. 12 p. 361 (1921).
- [9] R. P. Feynman, R. B. Leighton, and M. Sands, *The Feynman Lectures on Physics*. Reading, MA: Addison-Wesley, 1964, vol. I.
- [10] H. Goldstein, C. P. Poole, and J. L. Safko, *Classical Mechanics*, 3rd ed. Cambridge, MA: Addison-Wesley, 2001.
- [11] W. Gerlach and O. Stern, *Z. Phys.*, vol. 9, p. 349, 1922.
- [12] G. E. Uhlenbeck and S. Goudsmit, *Naturwiss.*, vol. 19, p. 953, 1925.
- [13] H. N. Russell and F. A. Saunders, “New regularities in the spectra of the alkaline earths,” *Astrophys. J.*, vol. 61, p. 38, 1925.
- [14] R. M. Eisberg, *Fundamentals of Modern Physics*. New York: John Wiley & Sons, 1961.
- [15] R. P. Feynman, R. B. Leighton, and M. Sands, *The Feynman Lectures on Physics*. Reading, MA: Addison-Wesley, 1964, vol. III.
- [16] L. I. Schiff, *Quantum Mechanics*. New York: McGraw-Hill, 1968.
- [17] E. Merzbacher, *Quantum Mechanics*, 3rd ed. New York: John Wiley & Sons, 1998.

Quantum Theory of Spin Waves

In Chapter 1, we discussed the angular momenta and magnetic moments of individual atoms and ions. When these atoms or ions are constituents of a solid, it is important to take into consideration the ways in which the angular momenta on different sites interact with one another. For simplicity, we will restrict our attention to the case when the angular momentum on each site is entirely due to spin.

The elementary excitations of coupled spin systems in solids are called *spin waves*. In this chapter, we will introduce the quantum theory of these excitations at low temperatures. The two primary interaction mechanisms for spins are magnetic dipole–dipole coupling and a mechanism of quantum mechanical origin referred to as the *exchange interaction*. The dipolar interactions are of importance when the spin wavelength is very long compared to the spacing between spins, and the exchange interaction dominates when the spacing between spins becomes significant on the scale of a wavelength. In this chapter, we focus on exchange-dominated spin waves, while dipolar spin waves are the primary topic of subsequent chapters.

We begin this chapter with a quantum mechanical treatment of a single electron in a uniform field and follow it with the derivations of Zeeman energy and Larmor precession. We then consider one of the simplest exchange-coupled spin systems, molecular hydrogen. Exchange plays a crucial role in the existence of ordered spin systems. The ground state of H_2 is a two-electron exchange-coupled system in an embryonic antiferromagnetic state. It serves to illustrate the origins of the exchange interaction and also provides a vehicle for our discussion on the Heisenberg spin Hamiltonian in ferromagnetic solids.

2.1 Charged Particle in an Electromagnetic Field

We obtained the time-independent Schrödinger equation (1.46) by quantizing the total energy of a particle moving in an electrostatic potential. Since we also want to understand the effects of a magnetic field, we now concern

ourselves with understanding the interactions of a charged particle in a general electromagnetic field. Maxwell's equation from Gauss' Law specifies the divergence of the magnetic flux density as

$$\nabla \cdot \mathbf{B} = 0. \quad (2.1)$$

This allows us to express \mathbf{B} as the curl of a vector

$$\mathbf{B} = \nabla \times \mathbf{A}, \quad (2.2)$$

where \mathbf{A} is known as the vector potential.¹ If we substitute this into Maxwell's equation from Faraday's law

$$\nabla \times \mathbf{E} = -\frac{\partial \mathbf{B}}{\partial t}, \quad (2.3)$$

we obtain

$$\nabla \times \left(\mathbf{E} + \frac{\partial \mathbf{A}}{\partial t} \right) = 0. \quad (2.4)$$

Thus, we can set

$$\mathbf{E} = -\frac{\partial \mathbf{A}}{\partial t} - \nabla \phi, \quad (2.5)$$

where ϕ is known as the scalar potential.

Now, consider the motion of a particle with charge q in an electromagnetic field. The force acting on the particle is given by

$$\mathbf{F} = q[\mathbf{E} + \mathbf{v} \times \mathbf{B}] \quad (2.6)$$

or

$$m \frac{d\mathbf{v}}{dt} = q \left(-\frac{\partial \mathbf{A}}{\partial t} - \nabla \phi + \mathbf{v} \times (\nabla \times \mathbf{A}) \right). \quad (2.7)$$

Since

$$\frac{dA_x}{dt} = \frac{\partial A_x}{\partial t} + \left(v_x \frac{\partial A_x}{\partial x} + v_y \frac{\partial A_x}{\partial y} + v_z \frac{\partial A_x}{\partial z} \right), \quad (2.8)$$

we can write

$$\begin{aligned} (\mathbf{v} \times \nabla \times \mathbf{A})_x &= v_y \left(\frac{\partial A_y}{\partial x} - \frac{\partial A_x}{\partial y} \right) - v_z \left(\frac{\partial A_x}{\partial z} - \frac{\partial A_z}{\partial x} \right) \\ &= \frac{\partial}{\partial x} (\mathbf{v} \cdot \mathbf{A}) - \frac{dA_x}{dt} + \frac{\partial A_x}{\partial t}. \end{aligned} \quad (2.9)$$

¹ Note that (2.2) gives us the freedom to write $\mathbf{A} = \mathbf{A}' + \nabla \phi$, since $\nabla \times (\nabla \phi) = 0$ for any scalar function ϕ . Further, we must specify the divergence as well as the curl to uniquely define a vector function. Generally, the choice of $\nabla \cdot \mathbf{A}$ is made for convenience. The choice $\nabla \cdot \mathbf{A} = 0$ is known as the *Coulomb gauge* [1].

With some simple algebra, we simplify Eq. (2.7) to

$$\frac{d}{dt}[m\mathbf{v} + q\mathbf{A}] = \nabla[-q\phi + q(\mathbf{v} \cdot \mathbf{A})]. \quad (2.10)$$

Let us borrow the concept of a *Lagrangian* from classical mechanics, to aid us in the interpretation of Eq. (2.10). Consider the motion of a particle, in three dimensions, in a potential $V(\mathbf{x})$. The Lagrangian for the particle is defined as the difference between the kinetic and potential energies:

$$\begin{aligned} \mathcal{L} &= T - V \\ &= \frac{1}{2}m|\dot{\mathbf{x}}|^2 - V(\mathbf{x}). \end{aligned} \quad (2.11)$$

The motion of the particle is given by the *Euler–Lagrange* equation (cf. Goldstein [2])

$$\frac{d}{dt} \left(\frac{\partial \mathcal{L}}{\partial \dot{\mathbf{x}}} \right) = \frac{\partial \mathcal{L}}{\partial \mathbf{x}}. \quad (2.12)$$

Substituting (2.11) into (2.12) yields $m\ddot{\mathbf{x}} + \nabla V = 0$. If we define the force exerted on the particle as $\mathbf{F} = -\nabla V$, we recover the first law of Newtonian mechanics, $\mathbf{F} = m\ddot{\mathbf{x}}$. We can also identify the *canonical variable* $\mathbf{p} = m\dot{\mathbf{x}}$ as the momentum of the particle in consonance with Newton’s second law $\mathbf{F} = d\mathbf{p}/dt$.

Returning to our discussion of a charged particle in an electromagnetic field, consider the x component of (2.10),

$$\frac{d}{dt}[m\mathbf{v}_x + q\mathbf{A}_x] = \frac{\partial}{\partial x} [-q\phi + q(\mathbf{v} \cdot \mathbf{A})]. \quad (2.13)$$

If we identify the Lagrangian as

$$\mathcal{L} = \frac{1}{2}m\mathbf{v} \cdot \mathbf{v} - q\phi + q\mathbf{A} \cdot \mathbf{v}, \quad (2.14)$$

we observe that (2.13) is the Euler–Lagrange equation in one dimension,

$$\frac{d}{dt} \left(\frac{\partial \mathcal{L}}{\partial \dot{x}} \right) = \frac{\partial \mathcal{L}}{\partial x}. \quad (2.15)$$

We can also identify the conjugate momentum variable for x ,

$$p_x = \frac{\partial \mathcal{L}}{\partial \dot{x}} = mv_x + qA_x. \quad (2.16)$$

Performing a similar analysis for the y and z -components of (2.12) leads to

$$\mathbf{p} = m\mathbf{v} + q\mathbf{A}. \quad (2.17)$$

A reformulation of Lagrangian mechanics, introduced by the Irish mathematician W. R. Hamilton, allows us to express the equations of motion as first

order differential equations in a phase space defined by \mathbf{x} and \mathbf{p} . The Hamiltonian of a system, introduced in Eq. (1.43), is defined as the sum of the kinetic and potential energies. A particle with velocity \mathbf{v} has kinetic energy $T = (\mathbf{p} \cdot \mathbf{v})/2$. To study the interaction of the particle with an electromagnetic field, we use (2.11) and rewrite the Hamiltonian as

$$\begin{aligned}\mathcal{H} &= T + V \\ &= \mathbf{p} \cdot \mathbf{v} - \mathcal{L} \\ &= \mathbf{p} \cdot \left[\frac{1}{m}(\mathbf{p} - q\mathbf{A}) \right] - \frac{m}{2} \left[\frac{1}{m}(\mathbf{p} - q\mathbf{A}) \right]^2 + q\phi - q\mathbf{A} \cdot \frac{1}{m}(\mathbf{p} - q\mathbf{A}) \\ &= \frac{1}{2m}[\mathbf{p} - q\mathbf{A}]^2 + q\phi,\end{aligned}\tag{2.18}$$

where we have used (2.17) to eliminate \mathbf{v} . We make the transition to quantum mechanics, following the procedure adopted in Section 1.4.2, by replacing the operator \mathbf{p} with $(\hbar/i)\nabla$ to yield

$$\mathcal{H} = \frac{1}{2m} \left[\frac{\hbar}{i}\nabla - q\mathbf{A} \right]^2 + q\phi.\tag{2.19}$$

Finally, we postulate that the particle is described by a wavefunction $\Psi(\mathbf{r}, t)$, which is a solution to the *time-dependent Schrödinger equation*

$$i\hbar \frac{\partial \Psi}{\partial t} = \mathcal{H}\Psi.\tag{2.20}$$

The Schrödinger equation (2.20) is an operator equation that describes how the wavefunction Ψ evolves with time, while \mathcal{H} is time independent. Other interpretations of time evolution in quantum mechanics, such as the Heisenberg and the interaction pictures [3], allow operators like \mathcal{H} to become time dependent. We shall confine our present discussions to the Schrödinger picture of quantum mechanics.

2.2 Zeeman Energy

Let us write the wavefunction of the particle in a static electromagnetic field as

$$\Psi(\mathbf{r}, t) = \psi(\mathbf{r})e^{-i\mathcal{E}t/\hbar}.\tag{2.21}$$

Substituting $\Psi(\mathbf{r}, t)$ into Eq. (2.20), we find that $\psi(\mathbf{r})$ must satisfy the equation

$$\frac{1}{2m} \left[\frac{\hbar}{i}\nabla - q\mathbf{A} \right]^2 \psi + q\phi\psi = \mathcal{E}\psi\tag{2.22}$$

or

$$-\frac{\hbar^2}{2m}\nabla^2\psi - \frac{\hbar}{i}\frac{q}{2m}[\nabla \cdot (\mathbf{A}\psi) + \mathbf{A} \cdot \nabla\psi] + \left[\frac{q^2}{2m}A^2 + q\phi\right]\psi = \mathcal{E}\psi. \quad (2.23)$$

Recall that we had some flexibility in our definition of the vector potential \mathbf{A} , and in particular we can specify $\nabla \cdot \mathbf{A}$ to our convenience. A common choice is $\nabla \cdot \mathbf{A} = 0$, referred to as the Coulomb gauge. Hence,

$$\nabla \cdot (\mathbf{A}\psi) = (\nabla \cdot \mathbf{A})\psi + \mathbf{A} \cdot \nabla\psi = \mathbf{A} \cdot \nabla\psi. \quad (2.24)$$

Furthermore, for a uniform magnetic field, since

$$\begin{aligned} \nabla \times (\mathbf{B} \times \mathbf{r}) &= \mathbf{B} \nabla \cdot \mathbf{r} - \mathbf{r} \nabla \cdot \mathbf{B} + (\mathbf{r} \cdot \nabla)\mathbf{B} - (\mathbf{B} \cdot \nabla)\mathbf{r} \\ &= (\nabla \cdot \mathbf{r})\mathbf{B} - (\mathbf{B} \cdot \nabla)\mathbf{r} \\ &= [3\mathbf{B} - \mathbf{B}] \\ &= 2\mathbf{B}, \end{aligned} \quad (2.25)$$

we can write

$$\nabla \times \mathbf{A} = \frac{1}{2}\nabla \times (\mathbf{B} \times \mathbf{r}). \quad (2.26)$$

Using Eqs. (2.24) and (2.26), we find that the second term on the left of Eq. (2.23) can be simplified and written as²

$$\begin{aligned} -\frac{\hbar}{i}\frac{q}{m}\mathbf{A} \cdot \nabla\psi &= -\frac{\hbar}{i}\frac{q}{2m}(\mathbf{B} \times \mathbf{r}) \cdot \nabla\psi \\ &= -\frac{q}{2m}\mathbf{B} \cdot \left[\mathbf{r} \times \left(\frac{\hbar}{i}\nabla\right)\right]\psi \\ &= -\frac{q}{2m}\mathbf{B} \cdot (\mathbf{r} \times \mathbf{p})\psi \\ &= -\frac{q}{2m}(\mathbf{B} \cdot \mathbf{L})\psi \\ &= -\boldsymbol{\mu} \cdot \mathbf{B}\psi, \end{aligned} \quad (2.27)$$

where we have used the classical definition of angular momentum $\mathbf{L} = \mathbf{r} \times \mathbf{p}$. We define the *Zeeman energy* as

$$\mathcal{E}_z = -\boldsymbol{\mu} \cdot \mathbf{B}, \quad (2.28)$$

and note that it yields a lower energy when the magnetic moment $\boldsymbol{\mu}$ is parallel to the applied magnetic field.

The term proportional to $q^2 A^2$ in Eq. (2.23) is often ignored since, for typical magnetic field values, it makes a negligible contribution to the total energy. In the absence of an electric field, the Hamiltonian thus reduces to

$$\mathcal{H} = -\frac{\hbar^2}{2m}\nabla^2 - \frac{q}{2m}(\mathbf{L} \cdot \mathbf{B}). \quad (2.29)$$

² The *scalar triple product* of three vectors has the identity $\mathbf{a} \cdot (\mathbf{b} \times \mathbf{c}) = (\mathbf{a} \times \mathbf{b}) \cdot \mathbf{c}$.

2.3 Larmor Precession

Let us concentrate on the specific problem of an electron in a uniform magnetic field assumed to be along the $\hat{\mathbf{z}}$ direction. Recall, from Section 1.4.4, that in the presence of both spin and orbital angular momentum, the total angular momentum $\mathbf{J} = \mathbf{L} + \mathbf{S}$. If we neglect all orbital motion, the Hamiltonian representing the interaction of the magnetic field with the magnetic moment of the electron is

$$\mathcal{H}^{\text{spin}} = -\frac{gq}{2m} \mathbf{S} \cdot \mathbf{B}, \quad (2.30)$$

where we have used the Landé g -factor of Eq. (1.81) with $L = 0$. Writing \mathbf{S} in terms of the Pauli spin matrices (cf. Problem 1.5), we have

$$\mathcal{H}^{\text{spin}} = \frac{1}{2} \hbar \omega_0 \sigma_z, \quad (2.31)$$

where we have defined the Larmor precession frequency

$$\omega_0 = -\frac{gqB_0}{2m} = \frac{g\mu_B B_0}{\hbar}, \quad (2.32)$$

for a single electron in a magnetic field of magnitude B_0 . The eigenvalues of σ_z are ± 1 yielding the corresponding eigenvalues $\pm \frac{1}{2} \hbar \omega_0$ for $\mathcal{H}^{\text{spin}}$ with the spinor eigenstates $\chi_{\uparrow\downarrow}$, respectively. Thus, the general solution to the time-dependent Schrödinger equation (2.20) is

$$\Psi(t) = c_1 e^{-i\omega_0 t/2} \chi_{\uparrow} + c_2 e^{+i\omega_0 t/2} \chi_{\downarrow}, \quad (2.33)$$

where

$$\chi_{\uparrow} = \begin{bmatrix} 1 \\ 0 \end{bmatrix}, \quad \chi_{\downarrow} = \begin{bmatrix} 0 \\ 1 \end{bmatrix}. \quad (2.34)$$

A particularly interesting case results when we choose $c_1 = \cos(\theta/2)$ and $c_2 = \sin(\theta/2)$ to yield

$$\Psi(t) = \cos \frac{\theta}{2} e^{-i\omega_0 t/2} \chi_{\uparrow} + \sin \frac{\theta}{2} e^{i\omega_0 t/2} \chi_{\downarrow}. \quad (2.35)$$

To interpret this wavefunction, let us first find the expected value of the x -component of spin using the operator

$$S_x = \frac{\hbar}{2} \sigma_x, \quad (2.36)$$

where (cf. Eq. (1.93))

$$\sigma_x = \begin{bmatrix} 0 & 1 \\ 1 & 0 \end{bmatrix}. \quad (2.37)$$

The expected value of this operator is

$$\begin{aligned}\langle S_x \rangle &= \psi^\dagger S_x \psi \\ &= \left(\cos \frac{\theta}{2} e^{i\omega_0 t/2} \chi_\uparrow^\dagger + \sin \frac{\theta}{2} e^{-i\omega_0 t/2} \chi_\downarrow^\dagger \right) \\ &\quad \times \frac{\hbar}{2} \sigma_x \left(\cos \frac{\theta}{2} e^{-i\omega_0 t/2} \chi_\uparrow + \sin \frac{\theta}{2} e^{i\omega_0 t/2} \chi_\downarrow \right).\end{aligned}\tag{2.38}$$

Performing the required matrix multiplication and simplifying gives

$$\langle S_x \rangle = \frac{\hbar}{2} \sin \theta \cos(\omega_0 t).\tag{2.39}$$

In a similar manner, we find

$$\langle S_y \rangle = \frac{\hbar}{2} \sin \theta \sin(\omega_0 t),\tag{2.40}$$

$$\langle S_z \rangle = \frac{\hbar}{2} \cos \theta.\tag{2.41}$$

This solution represents a spin making an angle θ with the $\hat{\mathbf{z}}$ axis and precessing about it with angular velocity, ω_0 . Thus, we find that a measurement on the quantum mechanical system yields a result analogous to the semi-classical description of a precessing moment adopted in Chapter 1.

2.4 Origins of Exchange: The Heisenberg Hamiltonian³

To be independent of any coordinate system, the energy of interaction between two spins should depend on \mathbf{S}_1 and \mathbf{S}_2 only through their relative orientation. Thus, the interaction should be a function of $\mathbf{S}_1 \cdot \mathbf{S}_2$. The simplest form is that of the *Heisenberg Hamiltonian*:

$$\mathcal{H} = -2 \frac{\mathcal{J}}{\hbar^2} \mathbf{S}_1 \cdot \mathbf{S}_2.\tag{2.42}$$

Here, \mathbf{S}_1 and \mathbf{S}_2 are angular momentum operators (see Section 1.4 and Problem 1.5) and \mathcal{J} is referred to as the exchange constant for reasons that will become apparent shortly.

To begin to get an understanding of the origin and meaning of the Heisenberg Hamiltonian, we consider the simplest system of coupled atoms whose spins interact: molecular hydrogen. We would like to calculate the expected energy of the hydrogen molecule, illustrated in Figure 2.1, to gain an understanding of how the energy is affected by the spins of the electrons.

³ This section follows a discussion in Mattis [4, Chapter 2]. Treatments of exchange can also be found in Martin [5] and Rado and Suhl [6]. The approach taken here was introduced by Heitler and London [7].

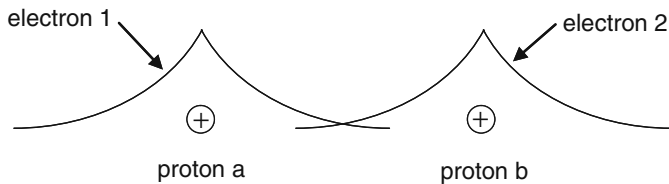


Fig. 2.1. The hydrogen molecule consists of two protons, each with a bound electron. The protons are sufficiently close that the electronic orbitals overlap.

As discussed in Section 1.4.2, we can obtain such an estimate by computing the expectation of the Hamiltonian operator. This operator is obtained by writing down an expression for the total energy of the system (kinetic plus potential), and making the operator substitutions indicated in Table 1.1. The total energy of this system can be written

$$\mathcal{H} = \underbrace{\frac{p_1^2}{2m} + \frac{p_2^2}{2m}}_{\text{electron kinetic energy}} - \underbrace{\frac{q^2}{cr_{1a}} - \frac{q^2}{cr_{2b}} - \frac{q^2}{cr_{1b}} - \frac{q^2}{cr_{2a}}}_{\text{potential energy between opposite charges (attractive)}} + \underbrace{\frac{q^2}{cr_{12}} + \frac{q^2}{cR_{ab}}}_{\text{potential energy between like charges (repulsive)}}, \quad (2.43)$$

where $c = 4\pi\epsilon_0$, p_i are the electron momenta, m is the electron mass, and r_{ij} is the distance between particles i, j . The separation between the protons R_{ab} , will be considered fixed, as we are primarily interested in how the energy is affected by the electron dynamics. As indicated in the equation, the total energy consists of the kinetic energy associated with the electron motion, the attractive potential energy between each electron and both protons, and the repulsive potential energy between the electrons and between the protons. We have neglected the kinetic energy associated with the motion of the protons, assuming that they are relatively stationary because of their large mass. We have also neglected the magnetic interaction between the electron spins, as this interaction is much weaker than the electrostatic interactions contained in (2.43).

If ψ is the wave function for the system, then the expectation of the energy can be obtained from Schrödinger's equation (1.46) generalized to two particles:

$$\langle \mathcal{E} \rangle = \frac{\int \psi^* \mathcal{H} \psi d^3r_1 d^3r_2}{\int \psi^* \psi d^3r_1 d^3r_2}. \quad (2.44)$$

Here, two volume integrations are necessary – one for the coordinate of each electron. Since the correct answer will be the minimum value of this expression, a small error in the wave function will result in an error in the energy that is second order in small quantities. Consequently, we should obtain a satisfactory answer with a reasonable approximation to the wave function. Because of

this tolerance to errors in the wave function, this expression is said to be *stationary*.⁴ If the atoms are far apart compared to the atomic diameter, we should be able to construct a reasonable wave function using the unperturbed hydrogen atom wave functions φ_a and φ_b . The unperturbed wave functions satisfy the equations

$$\left(\frac{p_1^2}{2m} - \frac{q^2}{cr_{1a}} \right) \varphi_a(\mathbf{r}_1) = \mathcal{E}_0 \varphi_a(\mathbf{r}_1), \quad (2.45)$$

$$\left(\frac{p_2^2}{2m} - \frac{q^2}{cr_{2b}} \right) \varphi_b(\mathbf{r}_2) = \mathcal{E}_0 \varphi_b(\mathbf{r}_2). \quad (2.46)$$

Using these as basis functions, or building blocks, we can construct symmetric and antisymmetric two particle wave functions as follows:

$$\psi_S = \frac{1}{\sqrt{2}} [\varphi_a(\mathbf{r}_1) \varphi_b(\mathbf{r}_2) + \varphi_a(\mathbf{r}_2) \varphi_b(\mathbf{r}_1)], \quad (2.47)$$

$$\psi_A = \frac{1}{\sqrt{2}} [\varphi_a(\mathbf{r}_1) \varphi_b(\mathbf{r}_2) - \varphi_a(\mathbf{r}_2) \varphi_b(\mathbf{r}_1)], \quad (2.48)$$

or

$$\psi_{\pm} = \frac{1}{\sqrt{2}} [\varphi_a(\mathbf{r}_1) \varphi_b(\mathbf{r}_2) \pm \varphi_a(\mathbf{r}_2) \varphi_b(\mathbf{r}_1)]. \quad (2.49)$$

We first calculate the normalization integral in the denominator of (2.44). For the two-particle wave functions, we must perform a double integration over the coordinates of both electrons:

$$\iint \psi_{\pm}^*(\mathbf{r}_1, \mathbf{r}_2) \psi_{\pm}(\mathbf{r}_1, \mathbf{r}_2) d^3r_1 d^3r_2 = 1 \pm \alpha^2, \quad (2.50)$$

where we have used

$$\int |\varphi_a(\mathbf{r})| d^3r = \int |\varphi_b(\mathbf{r})| d^3r = 1, \quad (2.51)$$

and α is defined to be the overlap integral

$$\alpha = \int \varphi_a^*(\mathbf{r}) \varphi_b(\mathbf{r}) d^3r. \quad (2.52)$$

After some manipulation, the numerator of Eq. (2.44) is found in a similar manner to be

$$\int \psi_{\pm}^*(\mathbf{r}_1, \mathbf{r}_2) \mathcal{H}(\mathbf{r}_1, \mathbf{r}_2) \psi_{\pm}(\mathbf{r}_1, \mathbf{r}_2) d^3r_1 d^3r_2 = 2\mathcal{E}_0(1 \pm \alpha^2) + V \pm U \quad (2.53)$$

where V and U are a “coulomb integral” and an “exchange integral”, respectively, defined by

⁴ We provide a more detailed discussion of stationary formulas and variational formulations in Chapter 7.

$$V = \int \varphi_a^*(\mathbf{r}_1) \varphi_b^*(\mathbf{r}_2) \mathcal{H}_i(\mathbf{r}_1, \mathbf{r}_2) \varphi_a(\mathbf{r}_1) \varphi_b(\mathbf{r}_2) d^3r_1 d^3r_2, \quad (2.54)$$

$$U = \int \varphi_a^*(\mathbf{r}_2) \varphi_b^*(\mathbf{r}_1) \mathcal{H}_i(\mathbf{r}_1, \mathbf{r}_2) \varphi_a(\mathbf{r}_1) \varphi_b(\mathbf{r}_2) d^3r_1 d^3r_2, \quad (2.55)$$

and \mathcal{H}_i is the interaction part of the Hamiltonian given by

$$\mathcal{H}_i = \frac{q^2}{cr_{12}} + \frac{q^2}{cR_{ab}} - \frac{q^2}{cr_{1b}} - \frac{q^2}{cr_{2a}}. \quad (2.56)$$

To understand why U is called the exchange integral, note that it gives the probability of the system making a transition from the state $\varphi_a(\mathbf{r}_1) \varphi_b(\mathbf{r}_2)$ to the state $\varphi_a(\mathbf{r}_2) \varphi_b(\mathbf{r}_1)$ owing to the presence of the interaction Hamiltonian. Since these two states differ only by the interchange of the electrons, this integral is a measure of the rate at which the electrons will exchange places. The energies of the symmetric and antisymmetric states are, therefore,

$$\mathcal{E}_{\pm} = 2\mathcal{E}_0 + \frac{V \pm U}{1 \pm \alpha^2}. \quad (2.57)$$

The difference in energy between the two states is

$$\mathcal{E}_S - \mathcal{E}_A = -2 \frac{V\alpha^2 - U}{1 - \alpha^4}. \quad (2.58)$$

The actual value of this difference will clearly depend on the relative magnitudes of α , V , and U .

So far so good, but what about spin? None of these calculations has explicitly taken spin into account, so how can the spin affect the energy? We have seen that the energy difference between the symmetric and antisymmetric states can be thought of as arising from the overlap of electronic wave functions along with the possibility of the electrons exchanging positions. It can also be thought of as depending on the spin orientations through the *Pauli exclusion principle*, as we will now show.

First, we need to show that the complete two-particle wave function (by complete we mean including spin) must be antisymmetric. This follows from the Pauli exclusion principle: no two electrons can be in the same state at the same time. To see that this principle requires an antisymmetric wave function, consider what would happen if we interchanged the electrons.

- If the wave function is antisymmetric, then interchanging them should give the negative of the wave function ($-\psi$).
- If the electrons were in the same state, then interchanging them will leave the wave function (ψ) unchanged.

The only way that both conditions can be satisfied is for the trivial case of $\psi = 0$. Consequently, we conclude that the use of antisymmetric wave functions ensures that no two electrons can be in the same state, and the

Pauli exclusion principle is satisfied. In statistical mechanics, the behavior of particles that obey the Pauli exclusion principle is described by the *Fermi–Dirac statistics*, and are referred to as *fermions*. In contrast, a moment’s consideration of the same interchange operation on a symmetric wave function would again leave the wave function ψ_S unchanged, but ψ_S would not have to vanish. Consequently, symmetric wave functions *do* allow multiple particles to be in the same state. Particles that do not obey the Pauli exclusion principle obey *Bose–Einstein statistics*, and are called *bosons*. We will return to the topic of bosons in a later section.

Having established that the complete wave function for a multiple electron system must be antisymmetric, we must assign a symmetric spin function to ψ_A , and an antisymmetric spin function to ψ_S . The possibilities are shown in Table 2.1. As discussed in Section 1.4, the angular momentum (in this case spin only) can be characterized by the total angular momentum and the component along a single direction. Consequently, we have also listed the total spin and the z -component of spin for the corresponding states in Table 2.1.

Since any of the three symmetric spin eigenfunctions could be used without changing the energy (the energy is determined by ψ_A), we will use the symbols χ_A and χ_S to represent antisymmetric and symmetric spin eigenfunctions, respectively.

At this point, we note that the singlet state $\psi_S \chi_A$ has a total spin 0, whereas each of the triplet states $\psi_A \chi_S$ has spin 1. Since these two states have different energy, we should be able to construct an operator that could give us the energy of the state by “sniffing out” the spin orientations without regard to spatial coordinate symmetries. Before considering such operators, let us consider how the spin orientation affects the energy.

If the two spins are lined up, the Pauli exclusion principle requires them to stay away from each other thereby reducing the Coulomb repulsion energy between them. Based on this argument alone, one would conclude that the ground state of H_2 should be the triplet state. However, in hydrogen, the increase in kinetic energy associated with the parallel spin configuration outweighs the decrease in coulomb potential energy and the antiparallel configuration turns out to be more favorable. The result is that the difference in energy may be viewed as depending on the spin orientations through the

Table 2.1. Two electron spin eigenfunctions.

Function	Parity	Total spin	z -Component of spin
$\frac{1}{\sqrt{2}} [\chi_{\uparrow\downarrow} - \chi_{\downarrow\uparrow}]$	antisymm	0	0
$\chi_{\uparrow\uparrow}$	symm	1	1
$\frac{1}{\sqrt{2}} [\chi_{\uparrow\downarrow} + \chi_{\downarrow\uparrow}]$	symm	1	0
$\chi_{\downarrow\downarrow}$	symm	1	–1

exclusion principle. Thus, although the hydrogen molecule exhibits antiferromagnetic rather than ferromagnetic order, it does illustrate how energy can depend on spin orientation, and hence helps to motivate the form of the Heisenberg Hamiltonian. It is interesting that the interactions that give rise to magnetic ordering are actually electrostatic in origin!

The task at hand, then, is to find an operator that can sense the spin orientations and thereby give us the energy of the state. Clearly, one choice would be the square of the total spin operator S^2 since it has the properties (see Section 1.4)⁵

$$S^2\psi_S\chi_A = \hbar^2 s(s+1)\psi_S\chi_A = 0, \quad (2.59)$$

$$S^2\psi_A\chi_S = \hbar^2 s(s+1)\psi_A\chi_S = 2\hbar^2\psi_A\chi_S. \quad (2.60)$$

A suitable operator would be

$$\mathcal{H}^{\text{spin}} = \mathcal{E}_S + \frac{1}{2\hbar^2} [\mathcal{E}_T - \mathcal{E}_S] S^2, \quad (2.61)$$

where the subscripts now indicate singlet and triplet states rather than symmetric and antisymmetric (e.g., $\mathcal{E}_T = \mathcal{E}_A$), respectively. The dependence on the relative orientations of the two electron spins can be made more apparent by expanding the operator as $S^2 = (\mathbf{S}_1 + \mathbf{S}_2) \cdot (\mathbf{S}_1 + \mathbf{S}_2)$ such that

$$\begin{aligned} \mathcal{H}^{\text{spin}} &= \mathcal{E}_S + \frac{1}{2\hbar^2} [\mathcal{E}_T - \mathcal{E}_S] [S_1^2 + S_2^2 + 2\mathbf{S}_1 \cdot \mathbf{S}_2] \\ &= \mathcal{E}_S + \frac{1}{2\hbar^2} [\mathcal{E}_T - \mathcal{E}_S] [2\hbar^2 s(s+1) + 2\mathbf{S}_1 \cdot \mathbf{S}_2] \\ &= \frac{1}{4} [\mathcal{E}_S + 3\mathcal{E}_T] + \frac{1}{\hbar^2} [\mathcal{E}_T - \mathcal{E}_S] \mathbf{S}_1 \cdot \mathbf{S}_2. \end{aligned} \quad (2.62)$$

In the last line, we have made use of the fact that $s = 1/2$ for an electron.⁶

Since we are interested in low-lying excitations above the ground state, the zero of energy is not important. We can, therefore, write Eq. (2.62) in the form of a Heisenberg spin Hamiltonian (cf. Eq. (2.42))

$$\mathcal{H} = -2\frac{\mathcal{J}}{\hbar^2} \mathbf{S}_1 \cdot \mathbf{S}_2, \quad (2.63)$$

where

$$\mathcal{J} = \frac{1}{2} (\mathcal{E}_S - \mathcal{E}_T) = \frac{U - V\alpha^2}{1 - \alpha^4}. \quad (2.64)$$

⁵ Note that the spin operator only operates on the spin eigenfunction χ_A or χ_S .

⁶ In (2.62), $s = 1/2$ since it results from the single electron operators $S_{1,2}^2$. In contrast, $s = 1$ in (2.60), since it results from the square of the total spin operator \mathbf{S} .

One last item and we will be over the hump of hydrogen molecule Hamiltonians and we can go on to bigger and better things.

The exchange phenomenon can be further clarified by introducing the Pauli spin exchange operator P . This operator simply interchanges the two electron spins: $P\chi_{\uparrow\downarrow} = \chi_{\downarrow\uparrow}$. Using this property, it is apparent that

$$P\chi_S = \chi_S, \quad P\chi_A = -\chi_A. \quad (2.65)$$

Since this operator obviously senses the spin orientations, it should be no surprise that the Hamiltonian can also be written in terms of it:

$$\mathcal{H}^P = -\frac{\mathcal{J}}{2} (2P - 1). \quad (2.66)$$

To verify the equivalence, we first need to find the expected value of the Hamiltonian (2.63), then compare with the expected value of (2.66). From (2.62) we have

$$\frac{1}{\hbar^2} [\mathcal{E}_T - \mathcal{E}_S] \mathbf{S}_1 \cdot \mathbf{S}_2 = -2\frac{\mathcal{J}}{\hbar^2} \mathbf{S}_1 \cdot \mathbf{S}_2 = \mathcal{H}^{\text{spin}} - \frac{1}{4} [\mathcal{E}_S + 3\mathcal{E}_T]. \quad (2.67)$$

Applying this operator to the singlet state gives

$$\begin{aligned} -2\frac{\mathcal{J}}{\hbar^2} \mathbf{S}_1 \cdot \mathbf{S}_2 \psi_S \chi_A &= \left(\mathcal{H}^{\text{spin}} - \frac{1}{4} [\mathcal{E}_S + 3\mathcal{E}_T] \right) \psi_S \chi_A \\ &= \left(\mathcal{E}_S - \frac{1}{4} [\mathcal{E}_S + 3\mathcal{E}_T] \right) \psi_S \chi_A \\ &= \frac{3}{4} (\mathcal{E}_S - \mathcal{E}_T) \psi_S \chi_A \\ &= \frac{3}{2} \mathcal{J} \psi_S \chi_A. \end{aligned} \quad (2.68)$$

Examination of the Hamiltonian expressed in terms of the spin exchange operator (2.66) shows that it gives the identical result:

$$\begin{aligned} \mathcal{H}^P \psi_S \chi_A &= -\frac{\mathcal{J}}{2} (2P - 1) \psi_S \chi_A = -\frac{\mathcal{J}}{2} (-2 - 1) \psi_S \chi_A \\ &= \frac{3}{2} \mathcal{J} \psi_S \chi_A. \end{aligned} \quad (2.69)$$

Following a similar procedure for the triplet state, we find that

$$\mathcal{H}^P \psi_A \chi_S = \mathcal{H} \psi_A \chi_S = -\frac{1}{2} \mathcal{J} \psi_A \chi_S \quad (2.70)$$

from both the Heisenberg form (2.63) and the spin exchange form (2.66) (see Problem 2.1). Thus, we have established the equivalence between the Heisenberg and the Pauli spin exchange operator forms of the Hamiltonian.

2.5 Spin Wave on a Linear Ferromagnetic Chain: Spin Exchange Operator Method⁷

It is a great leap from the hydrogen molecule to a linear chain of coupled spins. The fact that a Heisenberg Hamiltonian can be written for two coupled spins is no guarantee that the Hamiltonian for N -coupled spins can be written in a similar form. It is an even greater leap to postulate a Heisenberg Hamiltonian for a 3D solid. In actual solids, the interactions are often so complex that the concept of an exchange interaction ceases to be well defined. Nevertheless, it turns out that many phenomena described by the Heisenberg Hamiltonian are observed in magnetic materials so that it has been found to be a simple model rich in physical insight. We, therefore, postulate the Hamiltonian for a chain of N spins to be

$$\mathcal{H} = -2\frac{\mathcal{J}}{\hbar^2} \sum_n \mathbf{S}_n \cdot \mathbf{S}_{n+1}, \quad (2.71)$$

where we have made the additional assumptions that only nearest neighbor interactions are important, and all nearest neighbor exchange interactions are equal. We will further assume $s = 1/2$ and $\mathcal{J} > 0$.

Using the Pauli spin exchange operator introduced in Section 2.4 we can also write this Hamiltonian in the form

$$\mathcal{H}^P = -\frac{\mathcal{J}}{2} \sum_n (2P_{n,n+1} - 1). \quad (2.72)$$

Before continuing with the calculation of the expected energy, it is convenient to introduce a compact notation introduced by Dirac. Instead of representing a state with a wave function, the state is represented by the symbol

$$\psi \leftrightarrow |\psi\rangle. \quad (2.73)$$

The Hermitian transpose (simply the complex conjugate for a scalar function) is written

$$\psi^* \leftrightarrow \langle\psi|. \quad (2.74)$$

When the symbols are juxtaposed, an *inner product* is indicated. If the state is represented by a vector, then the inner product is simply the vector dot product. If the state is represented by a continuous function, then the inner product implies integration:

$$\langle\psi|\psi\rangle = \int \psi^* \psi d^3r. \quad (2.75)$$

As a joke on the word “bracket,” the symbol $\langle\psi|$ is called a “bra” and the symbol $|\psi\rangle$ is called a “ket” (note that the terminology does *not* refer to any

⁷ This section draws heavily on [8, Section 15-2].

articles of clothing!). The inner product between two states represents the probability amplitude that the system will transition between the states:

$$\langle \varphi | \psi \rangle = \int \varphi^* \psi d^3 r. \quad (2.76)$$

Finally, if an operator is placed between a “bra” and a “ket,” it represents the expected value of the operator if the bra and ket represent the same state, and a transition probability amplitude if the bra and ket states are different:

$$\langle \varphi | A | \psi \rangle = \int \varphi^* A \psi d^3 r. \quad (2.77)$$

Returning now to the linear chain of spins, with $\mathcal{J} > 0$, the lowest energy will clearly be that with all spins aligned. We will call this the ground state and denote it $|G\rangle$. The spin exchange operator leaves the ground state unchanged, so that

$$\langle G | \mathcal{H}^P | G \rangle = -\mathcal{J}N/2. \quad (2.78)$$

As before, we are not interested in the constant energy offset, so we can subtract this energy and refer all excitation energies to the ground state. The Hamiltonian (2.72) then becomes

$$\mathcal{H}^P = -\mathcal{J} \sum_n (P_{n,n+1} - 1). \quad (2.79)$$

This clearly gives zero for the ground state energy.

The lowest excited states of this system are those for which one spin is flipped. One possible choice of basis states to use is the set of all possible states in which only one spin is flipped. We will denote the state in which the spin on the m th site is flipped by $|m\rangle$. The actual state of the system $|\psi\rangle$ can be expressed as a sum over all possible states with one flipped spin

$$|\psi\rangle = \sum_m |m\rangle \langle m | \psi \rangle, \quad (2.80)$$

where $\langle m | \psi \rangle$ is the probability amplitude that the system is in the state with a flipped spin at location m . The Schrödinger equation can be written

$$\begin{aligned} \mathcal{H} |\psi\rangle &= \mathcal{E} |\psi\rangle, \\ \langle n | \mathcal{H} |\psi\rangle &= \mathcal{E} \langle n | \psi \rangle, \\ \sum_m \langle n | \mathcal{H} | m \rangle \langle m | \psi \rangle &= \mathcal{E} \langle n | \psi \rangle, \\ -\mathcal{J} \sum_i \sum_m \langle n | (P_{i,i+1} - 1) | m \rangle \langle m | \psi \rangle &= \mathcal{E} \langle n | \psi \rangle. \end{aligned} \quad (2.81)$$

Now consider what happens when the spin exchange operator is applied to the state $|m\rangle$. If neither i nor $i+1$ are equal to m , then two parallel spins

are flipped leaving the state unchanged and $(P_{i,i+1} - 1) |m\rangle = 0$. However, if $i = m$, then the flipped spin at location m is transferred to location $m + 1$ so that

$$(P_{m,m+1} - 1) |m\rangle = |m + 1\rangle - |m\rangle. \quad (2.82)$$

Similarly, if $i + 1 = m$, then the flipped spin is transferred to location $m - 1$:

$$(P_{m-1,m} - 1) |m\rangle = |m - 1\rangle - |m\rangle. \quad (2.83)$$

Substitution of Eqs. (2.82) and (2.83) into (2.81) leads to

$$-\mathcal{J} \sum_m \langle n | (|m + 1\rangle - |m\rangle + |m - 1\rangle - |m\rangle) \langle m | \psi \rangle = \mathcal{E} \langle n | \psi \rangle. \quad (2.84)$$

To simplify this, we use the fact that the state with a flipped spin at location m is orthogonal to the state with a flipped spin at location n unless $m = n$. We further take the states to be normalized so that

$$\langle m | n \rangle = \delta_{m,n}, \quad (2.85)$$

and $\delta_{m,n}$ is the Kronecker delta. Consider the first term on the left-hand side of (2.84):

$$\begin{aligned} -\mathcal{J} \sum_m \langle n | m + 1 \rangle \langle m | \psi \rangle &= -\mathcal{J} \sum_m \delta_{n,m+1} \langle m | \psi \rangle \\ &= -\mathcal{J} \langle n - 1 | \psi \rangle. \end{aligned} \quad (2.86)$$

Simplifying the remaining terms in (2.84) in a similar manner gives

$$-\mathcal{J} (\langle n - 1 | \psi \rangle + \langle n + 1 | \psi \rangle - 2 \langle n | \psi \rangle) = \mathcal{E} \langle n | \psi \rangle. \quad (2.87)$$

If the location of the n th spin is x_n and the spacing between spins is a , let us write

$$\langle n | \psi \rangle \equiv C(x_n), \quad (2.88a)$$

$$\langle n \pm 1 | \psi \rangle \equiv C(x_n \pm a). \quad (2.88b)$$

Equation (2.87) can now be written as

$$-\frac{\mathcal{E}}{\mathcal{J}} C(x_n) = C(x_n - a) + C(x_n + a) - 2C(x_n) \quad (2.89)$$

which is a difference equation with a solution of the form

$$C(x_n) = e^{ikx_n}. \quad (2.90)$$

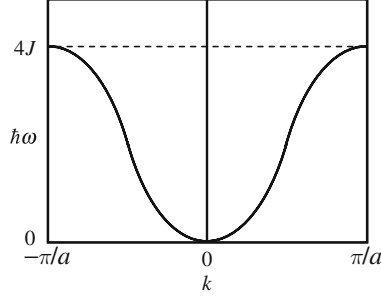


Fig. 2.2. Dispersion relation for a spin wave on a linear chain of spins. The points $k = \pm\pi/a$ represent the edges of the *Brillouin zone*. Because the spacing between spins is a , any value of k outside this range is indistinguishable from the point within this range obtained by adding or subtracting an integer multiple of $G = 2\pi/a$, referred to as a *reciprocal lattice vector*.

Substituting this trial solution into (2.89) and simplifying yields

$$\begin{aligned} -\frac{\mathcal{E}}{\mathcal{J}}e^{ikx_n} &= e^{ik(x_n-a)} + e^{ik(x_n+a)} - 2e^{ikx_n}, \\ -\frac{\mathcal{E}}{\mathcal{J}} &= 2\left(\frac{e^{ika} + e^{-ika}}{2}\right) - 2, \\ \mathcal{E} &= 2\mathcal{J}(1 - \cos ka). \end{aligned} \quad (2.91)$$

Associating the energy \mathcal{E} with the frequency $\hbar\omega$ gives the *dispersion relation* (Figure 2.2)

$$\omega = \frac{2\mathcal{J}}{\hbar}(1 - \cos ka). \quad (2.92)$$

If the wavelength is long compared to the spacing between spins so that $ka \ll 1$, the dispersion relation reduces to

$$\omega \approx \frac{\mathcal{J}a^2}{\hbar}k^2. \quad (2.93)$$

Recall that $\langle n | \psi \rangle \equiv C(x_n) = \exp(ikx_n)$ represents the probability amplitude that the flipped spin is located on site n . Referring to the semi-classical picture of a precessing spin introduced in Section 1.4, we can interpret the spin wave as an excitation in which the precession phase varies linearly from site-to-site as illustrated in Figure 2.3.

If we were to add together several closely spaced frequency components, we can form a “wave packet” that moves along the chain in the same manner as a particle. Comparing $\hbar^2k^2/(2m^*)$ with $\mathcal{J}a^2k^2$ suggests a particle with an effective mass

$$m^* = \frac{\hbar^2}{2\mathcal{J}a^2}. \quad (2.94)$$

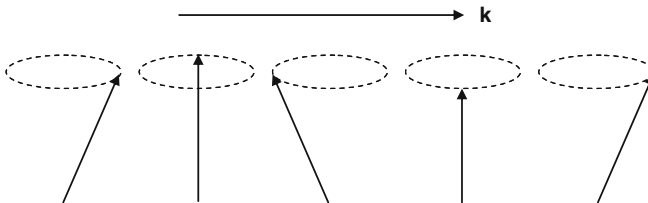


Fig. 2.3. Visualization of a spin wave as a disturbance in which the angle of precession varies linearly from spin-to-spin in the direction of propagation.

This “particle” is sometimes called a *magnon*, and represents the movement along the chain of a region where the likelihood of a flipped spin is high. The movement is enabled by the probability that spins will exchange places with a nearest neighbor, effectively moving the location of the flipped spin.

2.6 Harmonic Oscillator⁸

In Section 2.5, we considered the properties of a single spin wave on a linear chain. Clearly, we would like to be able to discuss the properties of multiple spin waves in 3D solids. To enable this more ambitious discussion, it is helpful to briefly make a side trip into a very important model in quantum mechanics: the *harmonic oscillator*. We will see that the concepts introduced by the model play an important role in the description of magnons.

2.6.1 Harmonic Oscillator Eigenfunctions

We begin by considering the solution to the Schrödinger equation for a charged particle in one dimension (cf. Eq. (1.46)):

$$-\frac{\hbar^2}{2m} \frac{d^2\psi}{dx^2} + V(x)\psi(x) = \mathcal{E}\psi(x). \quad (2.95)$$

The classical harmonic oscillator consists of a mass on the end of a spring. In this case, the potential energy is that of a stretched spring, or $V = Kx^2/2$, where K is the spring constant. We know from the classical problem that there is a natural resonant frequency of oscillation of the spring given by $\omega = \sqrt{K/m}$. In terms of the resonant frequency, the potential energy can be expressed $V = m\omega^2 x^2/2$. Substituting this expression for the potential into Schrödinger’s equation (2.95) gives the equation describing the quantum mechanical harmonic oscillator:

⁸ For a more detailed discussion of the quantum mechanical harmonic oscillator, see [3, Chapter 5].

$$-\frac{\hbar^2}{2m} \frac{d^2\psi}{dx^2} + \frac{1}{2}m\omega^2 x^2 \psi = \mathcal{E}\psi. \quad (2.96)$$

To obtain solutions to this equation, it is helpful to make the change of variables

$$\xi = \sqrt{\frac{m\omega}{\hbar}} x. \quad (2.97)$$

After making this substitution, Schrödinger's equation becomes

$$\frac{d^2\psi'}{d\xi^2} + \left(\frac{2\mathcal{E}}{\hbar\omega} - \xi^2 \right) \psi' = 0. \quad (2.98)$$

Next, we introduce a new function f such that

$$\psi'(\xi) = e^{-\xi^2/2} f(\xi). \quad (2.99)$$

The equation for f is found to be

$$\frac{d^2 f}{d\xi^2} - 2\xi \frac{df}{d\xi} + 2nf = 0, \quad (2.100)$$

where $2n \equiv 2\mathcal{E}/\hbar\omega - 1$ or

$$\mathcal{E} = \hbar\omega \left(n + \frac{1}{2} \right). \quad (2.101)$$

It turns out that the solutions to (2.100) diverge as $\xi \rightarrow \infty$ in such a way that ψ' also diverges unless n is a positive integer. Since the wave function for a real particle must be bounded, we conclude that physically meaningful solutions only exist when n is a positive integer. In this case, the solutions to (2.100) are given by the *Hermite polynomials* $H_n(\xi)$. The first few polynomials are

$$\begin{aligned} H_0(\xi) &= 1, \\ H_1(\xi) &= 2\xi, \\ H_2(\xi) &= -2 + 4\xi^2. \end{aligned} \quad (2.102)$$

These polynomials have the following useful recurrence relations:

$$\frac{dH_n}{d\xi} = 2nH_{n-1}, \quad (2.103)$$

$$H_{n+1} = 2\xi H_n - 2nH_{n-1}. \quad (2.104)$$

The eigenfunctions for the original harmonic oscillator problem are, therefore

$$\psi_n(x) = C_n \exp\left(-\frac{x^2}{2\alpha^2}\right) H_n\left(\frac{x}{\alpha}\right), \quad (2.105)$$

where α is a characteristic length given by $\alpha = \sqrt{\hbar/(m\omega)}$. The constant C_n is normally chosen so that the eigenfunctions are orthonormal, i.e.,

$$\int_{-\infty}^{\infty} \psi_n(x) \psi_m(x) dx = \delta_{m,n}. \quad (2.106)$$

Using the integral

$$\int_{-\infty}^{\infty} H_m(\xi) H_n(\xi) e^{-\xi^2} d\xi = 2^n n! \sqrt{\pi} \delta_{m,n}, \quad (2.107)$$

the normalization coefficient is found to be

$$C_n = (\alpha 2^n n! \sqrt{\pi})^{-1/2}. \quad (2.108)$$

The normalized eigenfunctions are finally

$$\psi_n(x) = \frac{e^{-x^2/(2\alpha^2)} H_n\left(\frac{x}{\alpha}\right)}{\sqrt{\alpha 2^n n! \sqrt{\pi}}}. \quad (2.109)$$

Using this expression along with the recurrence relations (2.103) and (2.104) leads to a property that we will need in the next section:

$$\frac{d\psi_n}{dx} = \frac{1}{\alpha} \left(\psi_{n-1} \sqrt{\frac{n}{2}} - \psi_{n+1} \sqrt{\frac{n+1}{2}} \right). \quad (2.110)$$

2.6.2 Raising and Lowering Operators

It is convenient to introduce a new operator defined by

$$a = \sqrt{\frac{m\omega}{2\hbar}} \left(x + i \frac{p}{m\omega} \right), \quad (2.111)$$

where $p = (\hbar/i)d/dx$ is the 1D momentum operator from Table 1.1. Making this substitution and again introducing the characteristic length α , the operator can be expressed as

$$a = \frac{1}{\sqrt{2}} \left(\frac{x}{\alpha} + \alpha \frac{d}{dx} \right). \quad (2.112)$$

To understand the significance of this operator, we apply it to the n th harmonic oscillator eigenfunction:

$$\begin{aligned} a\psi_n &= \frac{1}{\sqrt{2}} \left(\frac{x}{\alpha} + \alpha \frac{d}{dx} \right) \psi_n \\ &= \frac{1}{\sqrt{2}} \left(\frac{x}{\alpha} \psi_n + \psi_{n-1} \sqrt{\frac{n}{2}} - \psi_{n+1} \sqrt{\frac{n+1}{2}} \right). \end{aligned} \quad (2.113)$$

Here, we have expanded the derivative using (2.110). Using the recurrence relation (2.104) along with the normalized eigenfunctions (2.109), we can show that

$$\frac{x}{\alpha} \psi_n - \sqrt{\frac{n+1}{2}} \psi_{n+1} = \sqrt{\frac{n}{2}} \psi_{n-1}. \quad (2.114)$$

Making this substitution into (2.113) gives

$$a \psi_n = \sqrt{n} \psi_{n-1}. \quad (2.115)$$

We see that the effect of the operator a is to lower the state from n to $n-1$. For this reason, a is referred to as a *lowering operator*. Similarly, let us define the operator

$$a^\dagger = \sqrt{\frac{m\omega}{2\hbar}} \left(x - i \frac{p}{m\omega} \right) = \frac{1}{\sqrt{2}} \left(\frac{x}{\alpha} - \alpha \frac{d}{dx} \right). \quad (2.116)$$

Following a similar procedure as before, we find that (Problem 2.2)

$$a^\dagger \psi_n = \sqrt{n+1} \psi_{n+1}. \quad (2.117)$$

We refer to a^\dagger as a *raising operator* since it raises the state n to $n+1$. It is also interesting to consider the effect of consecutively applying the operators:

$$a^\dagger a \psi_n = a^\dagger \sqrt{n} \psi_{n-1} = \sqrt{n} a^\dagger \psi_{n-1} = n \psi_n. \quad (2.118)$$

We observe that the expected value of the operator $a^\dagger a$ is simply the state number n . What if we were to apply the operators in the reverse order? We have:

$$a a^\dagger \psi_n = a \sqrt{n+1} \psi_{n+1} = \sqrt{n+1} a \psi_{n+1} = (n+1) \psi_n. \quad (2.119)$$

It is clear, then, that the operators do not commute. We encountered non-commuting operators when we discussed angular momentum in Section 1.4, and we found it useful to specify their properties with commutators. In the present case, (2.118) and (2.119) imply

$$[a, a^\dagger] \psi_n \equiv (a a^\dagger - a^\dagger a) \psi_n = \psi_n, \quad (2.120)$$

or equivalently

$$[a, a^\dagger] = 1. \quad (2.121)$$

It is often useful to generalize the notion from the specific case of a charged particle in a quadratic potential well to an abstract state labeled by n for which raising and lowering operators can be defined. In this case, we define

$$a = \sqrt{\frac{m\omega}{2\hbar}} \left(q + i \frac{p}{m\omega} \right), \quad (2.122)$$

$$a^\dagger = \sqrt{\frac{m\omega}{2\hbar}} \left(q - i \frac{p}{m\omega} \right), \quad (2.123)$$

where q and p are canonical position and momentum operators, respectively, and m is a canonical effective mass. The Hamiltonian expressed in terms of these canonical variables takes the form

$$\mathcal{H} = \frac{|p|^2}{2m} + \frac{m\omega^2}{2} |q|^2. \quad (2.124)$$

The canonical variables can also be expressed in terms of the raising and lowering operators:

$$q = \sqrt{\frac{\hbar}{2m\omega}} (a + a^\dagger), \quad (2.125)$$

$$p = -i\sqrt{\frac{m\omega\hbar}{2}} (a - a^\dagger). \quad (2.126)$$

Substituting these relations into (2.124) leads to the Hamiltonian expressed in terms of raising and lowering operators:

$$\begin{aligned} H &= \frac{|p|^2}{2m} + \frac{m\omega^2}{2} |q|^2 \\ &= \frac{1}{2m} \frac{m\omega\hbar}{2} (a - a^\dagger) (a^\dagger - a) + \frac{m\omega^2}{2} \frac{\hbar}{2m\omega} (a + a^\dagger) (a^\dagger + a) \\ &= \frac{\hbar\omega}{2} (aa^\dagger + a^\dagger a). \end{aligned} \quad (2.127)$$

Using the commutation relation (2.121), this can be written as

$$\mathcal{H} = \hbar\omega \left(a^\dagger a + \frac{1}{2} \right). \quad (2.128)$$

Let $|n\rangle$ represent an abstract state with state number n . The actions of the raising and lowering operators on these states are given by

$$\begin{aligned} a|n\rangle &= \sqrt{n}|n-1\rangle, \\ a^\dagger|n\rangle &= \sqrt{n+1}|n+1\rangle, \\ a^\dagger a|n\rangle &= n|n\rangle, \\ \mathcal{H}|n\rangle &= \hbar\omega \left(a^\dagger a + \frac{1}{2} \right) |n\rangle = \hbar\omega \left(n + \frac{1}{2} \right) |n\rangle. \end{aligned} \quad (2.129)$$

Note that the action of the Hamiltonian operator on the state $|n\rangle$ gives the energy of the state as given in Eq. (2.101).

2.7 Magnons in a 3D Ferromagnet: Method of Holstein and Primakoff⁹

For our discussion of a 3D ferromagnet, we will again assume that only nearest-neighbor interactions are important. We will also add the Zeeman energy from a static bias magnetic field. The Hamiltonian in this case can be expressed

$$\mathcal{H} = -2\frac{\mathcal{J}}{\hbar^2} \sum_{j,\delta} \mathbf{S}_j \cdot \mathbf{S}_{j+\delta} - \frac{g\mu_B B_0}{\hbar} \sum_j S_{jz}. \quad (2.130)$$

In this expression, j represents a specific spin site in the crystal, δ represents a vector to one of the nearest-neighbors of j , and we have chosen the sign of B_0 so that the lowest energy configuration occurs when all spins are “up.”

2.7.1 Magnon Dispersion Relation

It is computationally convenient to re-express the first term of (2.130) in terms of the spin raising and lowering operators introduced in Section 1.4.3. For the j th spin site, we define

$$S_j^+ = S_{jx} + iS_{jy}, \quad (2.131a)$$

$$S_j^- = S_{jx} - iS_{jy}. \quad (2.131b)$$

In terms of these operators, the Hamiltonian (2.130) can be written as

$$\mathcal{H} = -2\frac{\mathcal{J}}{\hbar^2} \sum_{j,\delta} \left[\frac{1}{2} \left(S_j^- S_{j+\delta}^+ + S_j^+ S_{j+\delta}^- \right) + S_{jz} S_{j+\delta,z} \right] - \frac{g\mu_B B_0}{\hbar} \sum_j S_{jz}. \quad (2.132)$$

Now consider a state $|s_{jz}\rangle$, where the z -quantum number on site j is s_{jz} . We know that (cf. Eq. (1.62))

$$S_{jz} |s_{jz}\rangle = s_{jz} |s_{jz}\rangle, \quad (2.133)$$

but we need to evaluate

$$S_j^\pm |s_{jz}\rangle = \lambda |s_{jz} \pm 1\rangle, \quad (2.134)$$

or its Hermitian adjoint

$$\langle s_{jz} | S_j^\mp = \langle s_{jz} \pm 1 | \lambda^*. \quad (2.135)$$

Taking the inner product of (2.134) and (2.135) gives

$$\langle s_{jz} | S_j^\mp S_j^\pm |s_{jz}\rangle = \langle s_{jz} \pm 1 | \lambda^* \lambda |s_{jz} \pm 1\rangle = |\lambda|^2, \quad (2.136)$$

⁹ In addition to the original paper [9], discussions of this topic can be found in Sparks [10, Section 3.2] and Kittel [11, Chapter 4].

where we have assumed the states are normalized so that $\langle s_{jz} | s_{jz} \rangle = 1$. To find λ , we make use of the relation

$$S_j^2 = \frac{1}{2} (S_j^+ S_j^- + S_j^- S_j^+) + S_{jz}^2. \quad (2.137)$$

The quantity $S_j^+ S_j^-$ can be eliminated from (2.137) using the commutator (cf. Eq. (1.58c))

$$[S_j^+, S_j^-] = S_j^+ S_j^- - S_j^- S_j^+ = 2\hbar S_{jz}. \quad (2.138)$$

The result is

$$S_j^- S_j^+ = S_j^2 - S_{jz} (S_{jz} + \hbar). \quad (2.139)$$

The inner product can now be evaluated:

$$\begin{aligned} \langle s_{jz} | S_j^- S_j^+ | s_{jz} \rangle &= \langle s_{jz} | (S_j^2 - S_{jz} (S_{jz} + \hbar)) | s_{jz} \rangle \\ &= \langle s_{jz} | (\hbar^2 s(s+1) - \hbar^2 s_{jz} (s_{jz} + 1)) | s_{jz} \rangle \\ &= \hbar^2 (s(s+1) - s_{jz} (s_{jz} + 1)) \\ &= |\lambda|^2. \end{aligned} \quad (2.140)$$

We conclude that

$$\lambda = \hbar (s(s+1) - s_{jz} (s_{jz} + 1))^{1/2} \quad (2.141)$$

and

$$S_j^+ |s_{jz}\rangle = \lambda |s_{jz} + 1\rangle = \hbar (s(s+1) - s_{jz} (s_{jz} + 1))^{1/2} |s_{jz} + 1\rangle. \quad (2.142)$$

Following a similar procedure, we find (Problem 2.3)

$$S_j^- |s_{jz}\rangle = \hbar (s(s+1) - s_{jz} (s_{jz} - 1))^{1/2} |s_{jz} - 1\rangle. \quad (2.143)$$

We next introduce the basis states $|n_j\rangle$, where n_j is the number of spin deviations (flipped spins) at site j . Increasing n_j by 1 decreases s_{jz} by 1. We also introduce raising and lowering operators similar to those for the harmonic oscillator with the properties

$$\begin{aligned} [a_i, a_j^+] &= \delta_{i,j}, \\ [a_i^\pm, a_j^\pm] &= 0. \end{aligned} \quad (2.144)$$

When these operators are applied to the basis states, we obtain (cf. Eq. (2.129))

$$\begin{aligned} a_j |n_j\rangle &= \sqrt{n_j} |n_j - 1\rangle, \\ a_j^+ |n_j\rangle &= \sqrt{n_j + 1} |n_j + 1\rangle, \\ a_j^+ a_j |n_j\rangle &= n_j |n_j\rangle. \end{aligned} \quad (2.145)$$

Since flipping a spin reduces the z -component of the spin on the site, we have

$$S_{jz}|s_{jz}\rangle = \hbar(s - n_j)|s_{jz}\rangle \quad (2.146)$$

or

$$s_{jz} = s - n_j, \quad (2.147)$$

where s is the total spin on the site. Since we saw previously that a flipped spin distributed over a group of sites corresponds to a quasi-particle called a magnon, the operators a_j^+ and a_j can also be viewed as magnon (or spin deviation) *creation* and *annihilation* operators, respectively. Since more than one flipped spin can exist on a site (depending on the total spin), it is possible for multiple magnons to exist at the same location, and we conclude that the quasi-particles do not obey the Pauli exclusion principle. This means that magnons behave as bosons.

Using Eqs. (2.147) and (2.142), the effect of the raising operator on the new basis states can be written as

$$\begin{aligned} S_j^+ |n_j\rangle &= \hbar(s(s+1) - (s - n_j)(s - n_j + 1))^{1/2} |n_j - 1\rangle \\ &= \hbar(2sn_j - n_j^2 + n_j)^{1/2} |n_j - 1\rangle \\ &= \hbar\sqrt{2s} \left(1 - \frac{(n_j - 1)}{2s}\right) \sqrt{n_j} |n_j - 1\rangle. \end{aligned} \quad (2.148)$$

Comparison with (2.145) suggests that the spin raising operator S_j^+ can be expressed in terms of the new harmonic oscillator raising and lowering operators as follows:

$$S_j^+ = \hbar\sqrt{2s} \left(1 - \frac{a_j^+ a_j}{2s}\right)^{1/2} a_j. \quad (2.149)$$

Following a similar procedure, we find that

$$S_j^- = \hbar\sqrt{2s} a_j^+ \left(1 - \frac{a_j^+ a_j}{2s}\right)^{1/2}. \quad (2.150)$$

Equations (2.149) and (2.150) are known as the *Holstein–Primakoff transformation* [9].

We now make the low-temperature approximation that makes this problem solvable. Specifically, we assume that the total number of flipped spins in the system is small compared to the total number of spins. In this case

$$\left\langle \sum_j \left(1 - \frac{a_j^+ a_j}{2s}\right)^{1/2} \right\rangle \approx N, \quad (2.151)$$

where the brackets indicate the expected value. This suggests that we can approximate the radical by

$$\left(1 - \frac{a_j^\dagger a_j}{2s}\right)^{1/2} \approx 1. \quad (2.152)$$

If s is small, this may introduce considerable error in the term for the j th site, but since the operator is averaged over the entire sample, the overall error in the energy will be small provided

$$\frac{\langle \sum_j (a_j^\dagger a_j) \rangle}{2Ns} \ll 1. \quad (2.153)$$

We can then approximate the spin raising and lowering operators as

$$S_j^+ \approx \hbar \sqrt{2s} a_j, \quad (2.154)$$

$$S_j^- \approx \hbar \sqrt{2s} a_j^\dagger. \quad (2.155)$$

Substituting these approximations into the Hamiltonian (2.132) and keeping terms up to second-order in creation/annihilation operators gives

$$\begin{aligned} \mathcal{H} = & -2\mathcal{J}s \sum_{j,\delta} \left[a_j^\dagger a_{j+\delta} + a_j a_{j+\delta}^\dagger - a_j^\dagger a_j - a_{j+\delta}^\dagger a_{j+\delta} + s \right] \\ & - g\mu_B B_0 \sum_j (s - a_j^\dagger a_j). \end{aligned} \quad (2.156)$$

We would now like to diagonalize this Hamiltonian. Since the form of Eq. (2.156) clearly shows the coupling between adjacent spins, we suspect the basis states that will diagonalize the Hamiltonian will involve collective excitations of all the spins in the system. The transformation to collective excitations can be made through the use of the *Fourier transforms* of the a_j 's. We therefore introduce the operators¹⁰ $a_{\mathbf{k}}^\dagger$ and $a_{\mathbf{k}}$ which create and annihilate magnons of wavevector \mathbf{k} , respectively:

$$\begin{aligned} a_{\mathbf{k}}^\dagger &= N^{-1/2} \sum_j e^{i\mathbf{k} \cdot \mathbf{r}_j} a_j^\dagger, \\ a_{\mathbf{k}} &= N^{-1/2} \sum_j e^{-i\mathbf{k} \cdot \mathbf{r}_j} a_j. \end{aligned} \quad (2.157)$$

Here, \mathbf{r}_j is the vector locating the j th site in the crystal. The inverse transform is

$$\begin{aligned} a_j^\dagger &= N^{-1/2} \sum_{\mathbf{k}} e^{-i\mathbf{k} \cdot \mathbf{r}_j} a_{\mathbf{k}}^\dagger \\ a_j &= N^{-1/2} \sum_{\mathbf{k}} e^{i\mathbf{k} \cdot \mathbf{r}_j} a_{\mathbf{k}}. \end{aligned} \quad (2.158)$$

¹⁰ Our choice of sign convention in the exponent is that of Oguchi [12] and opposite to that of Holstein and Primakoff [9].

The commutation relation for the new operators is

$$\begin{aligned}
 [a_{\mathbf{k}}, a_{\mathbf{k}'}^+] &= \frac{1}{N} \sum_{j,l} e^{-i\mathbf{k} \cdot \mathbf{r}_j} e^{i\mathbf{k}' \cdot \mathbf{r}_l} [a_j, a_l^+] \\
 &= \frac{1}{N} \sum_{j,l} e^{-i\mathbf{k} \cdot \mathbf{r}_j} e^{i\mathbf{k}' \cdot \mathbf{r}_l} \delta_{j,l} \\
 &= \frac{1}{N} \sum_j e^{i(\mathbf{k}' - \mathbf{k}) \cdot \mathbf{r}_j} \\
 &= \delta_{\mathbf{k}, \mathbf{k}'} .
 \end{aligned} \tag{2.159}$$

The last step results from the periodicity of the crystal (Problem 2.4). If the site j has Z -nearest neighbors, the Hamiltonian then becomes

$$\mathcal{H} = -2\mathcal{J}NZs^2 - g\mu_B B_0 Ns + \mathcal{H}_0, \tag{2.160}$$

where

$$\begin{aligned}
 \mathcal{H}_0 &= -\frac{2\mathcal{J}s}{N} \sum_{j\delta\mathbf{k}\mathbf{k}'} \left(e^{-i(\mathbf{k}-\mathbf{k}') \cdot \mathbf{r}_j} e^{i\mathbf{k}' \cdot \delta} a_{\mathbf{k}}^+ a_{\mathbf{k}'} + e^{i(\mathbf{k}-\mathbf{k}') \cdot \mathbf{r}_j} e^{-i\mathbf{k}' \cdot \delta} a_{\mathbf{k}} a_{\mathbf{k}'}^+ \right. \\
 &\quad \left. - e^{-i(\mathbf{k}-\mathbf{k}') \cdot \mathbf{r}_j} a_{\mathbf{k}}^+ a_{\mathbf{k}'} - e^{-i(\mathbf{k}-\mathbf{k}') \cdot (\mathbf{r}_j + \delta)} a_{\mathbf{k}}^+ a_{\mathbf{k}'} \right) \\
 &\quad + \frac{g\mu_B B_0}{N} \sum_{j\mathbf{k}\mathbf{k}'} e^{-i(\mathbf{k}-\mathbf{k}') \cdot \mathbf{r}_j} a_{\mathbf{k}}^+ a_{\mathbf{k}'} .
 \end{aligned} \tag{2.161}$$

As before, the sums over j will cause all of the terms to vanish unless $\mathbf{k} = \mathbf{k}'$. We now have

$$\begin{aligned}
 \mathcal{H}_0 &= -2\mathcal{J}s \sum_{\delta\mathbf{k}} \left(e^{i\mathbf{k} \cdot \delta} a_{\mathbf{k}}^+ a_{\mathbf{k}} + e^{-i\mathbf{k} \cdot \delta} a_{\mathbf{k}} a_{\mathbf{k}}^+ - 2a_{\mathbf{k}}^+ a_{\mathbf{k}} \right) + g\mu_B B_0 \sum_{\mathbf{k}} a_{\mathbf{k}}^+ a_{\mathbf{k}} \\
 &= -2\mathcal{J}sZ \sum_{\mathbf{k}} \left(\gamma_{\mathbf{k}} a_{\mathbf{k}}^+ a_{\mathbf{k}} + \gamma_{-\mathbf{k}} a_{\mathbf{k}} a_{\mathbf{k}}^+ - 2a_{\mathbf{k}}^+ a_{\mathbf{k}} \right) + g\mu_B B_0 \sum_{\mathbf{k}} a_{\mathbf{k}}^+ a_{\mathbf{k}},
 \end{aligned} \tag{2.162}$$

where we have defined

$$\gamma_{\mathbf{k}} = \frac{1}{Z} \sum_{\delta} e^{i\mathbf{k} \cdot \delta}. \tag{2.163}$$

For crystals with a center of symmetry $\gamma_{\mathbf{k}} = \gamma_{-\mathbf{k}}$ and \mathcal{H}_0 can be further simplified with the commutation relation (2.159):

$$\begin{aligned}
 \mathcal{H}_0 &= -2\mathcal{J}sZ \sum_{\mathbf{k}} \left(\gamma_{\mathbf{k}} a_{\mathbf{k}}^+ a_{\mathbf{k}} + \gamma_{\mathbf{k}} (1 + a_{\mathbf{k}}^+ a_{\mathbf{k}}) - 2a_{\mathbf{k}}^+ a_{\mathbf{k}} \right) + g\mu_B B_0 \sum_{\mathbf{k}} a_{\mathbf{k}}^+ a_{\mathbf{k}} \\
 &= -4\mathcal{J}sZ \sum_{\mathbf{k}} (\gamma_{\mathbf{k}} - 1) a_{\mathbf{k}}^+ a_{\mathbf{k}} + g\mu_B B_0 \sum_{\mathbf{k}} a_{\mathbf{k}}^+ a_{\mathbf{k}} \\
 &= \sum_{\mathbf{k}} (4\mathcal{J}sZ (1 - \gamma_{\mathbf{k}}) + g\mu_B B_0) a_{\mathbf{k}}^+ a_{\mathbf{k}} .
 \end{aligned} \tag{2.164}$$

One last simplification allows us to write

$$\mathcal{H}_0 = \sum_{\mathbf{k}} \hat{n}_{\mathbf{k}} \hbar \omega_{\mathbf{k}}, \quad (2.165)$$

where $\hat{n}_{\mathbf{k}} = a_{\mathbf{k}}^+ a_{\mathbf{k}}$ is the operator for the number of magnons with wavevector \mathbf{k} , and the frequency is given by

$$\hbar \omega_{\mathbf{k}} = 4\mathcal{J}sZ(1 - \gamma_{\mathbf{k}}) + g\mu_B B_0. \quad (2.166)$$

As an example, consider the case of a simple cubic lattice. In this case, the nearest neighbors are along the $\pm x$, $\pm y$, and $\pm z$ axes at a distance a and we have

$$\begin{aligned} \gamma_{\mathbf{k}} &= \frac{1}{Z} \sum_{\boldsymbol{\delta}} e^{i\mathbf{k} \cdot \boldsymbol{\delta}} \\ &= \frac{1}{6} (e^{ik_x a} + e^{-ik_x a} + e^{ik_y a} + e^{-ik_y a} + e^{ik_z a} + e^{-ik_z a}) \\ &= \frac{1}{3} (\cos k_x a + \cos k_y a + \cos k_z a). \end{aligned} \quad (2.167)$$

The dispersion relation becomes finally

$$\hbar \omega_{\mathbf{k}} = 24\mathcal{J}s \left(1 - \frac{1}{3} (\cos k_x a + \cos k_y a + \cos k_z a) \right) + g\mu_B B_0. \quad (2.168)$$

For small k , this reduces to approximately

$$\hbar \omega_k = g\mu_B B_0 + 4\mathcal{J}s a^2 k^2. \quad (2.169)$$

2.7.2 Magnon Interactions

The first rigorous calculation of spin wave interactions was done by Dyson [13, 14]. However, in the words of Oguchi [12], “Although Dyson’s paper is rigorous, it is not so easy to understand.” Consequently, to obtain an understanding of these interactions, we follow Oguchi’s approach, which is based on a further expansion of the Holstein–Primakoff transformation. We therefore need to expand the square root in Eq. (2.152) to higher order:

$$\left(1 - \frac{a_j^+ a_j}{2s} \right)^{1/2} \approx 1 - \frac{a_j^+ a_j}{4s}. \quad (2.170)$$

The spin raising and lowering operators then become

$$S_j^+ \approx \hbar \sqrt{2s} \left(a_j - \frac{a_j^+ a_j a_j}{4s} + \dots \right), \quad (2.171)$$

$$S_j^- \approx \hbar \sqrt{2s} \left(a_j^+ - \frac{a_j^+ a_j^+ a_j}{4s} + \dots \right). \quad (2.172)$$

Substituting these expressions into (2.132) and keeping terms to fourth order in creation/annihilation operators gives

$$\mathcal{H} = -2\mathcal{J}NZs^2 - g\mu_B B_0 N s + \mathcal{H}_0 + \mathcal{H}_1 \quad (2.173)$$

where

$$\begin{aligned} \mathcal{H}_1 = \frac{\mathcal{J}}{2} \sum_{j,\delta} & \left(a_j^+ a_{j+\delta}^+ a_{j+\delta} a_{j+\delta} + a_j^+ a_j^+ a_j a_{j+\delta} + a_j a_{j+\delta}^+ a_{j+\delta}^+ a_{j+\delta} \right. \\ & \left. + a_j^+ a_j a_j a_{j+\delta}^+ - 4a_j^+ a_j a_{j+\delta}^+ a_{j+\delta} \right). \end{aligned} \quad (2.174)$$

At this point, we again transform this expression to one in terms of $a_{\mathbf{k}}^+$ and $a_{\mathbf{k}}$. The ensuing calculation quickly becomes very tedious, so let us consider the transformation of only the first term to get an idea for what happens:

$$\begin{aligned} \mathcal{H}_1^{(1)} &= \frac{\mathcal{J}}{2} \sum_{j,\delta} a_j^+ a_{j+\delta}^+ a_{j+\delta} a_{j+\delta} \\ &= \frac{\mathcal{J}}{2N^2} \sum_{\mathbf{k}_1 \mathbf{k}_2 \mathbf{k}_3 \mathbf{k}_4} \sum_{j,\delta} e^{-i(\mathbf{k}_1 + \mathbf{k}_2 - \mathbf{k}_3 - \mathbf{k}_4) \cdot \mathbf{r}_j} e^{-i(\mathbf{k}_2 - \mathbf{k}_3 - \mathbf{k}_4) \cdot \delta} a_{\mathbf{k}_1}^+ a_{\mathbf{k}_2}^+ a_{\mathbf{k}_3} a_{\mathbf{k}_4}. \end{aligned} \quad (2.175)$$

As before, owing to the periodicity of the crystal, the sum over j gives

$$\sum_j e^{-i(\mathbf{k}_1 + \mathbf{k}_2 - \mathbf{k}_3 - \mathbf{k}_4) \cdot \mathbf{r}_j} = N \Delta(\mathbf{k}_1 + \mathbf{k}_2 - \mathbf{k}_3 - \mathbf{k}_4), \quad (2.176)$$

where $\Delta(0) = 1$ and $\Delta(x \neq 0) = 0$ (i.e., it is equivalent to the Kronecker delta $\Delta(x) = \delta_{x,0}$). Consequently, the term vanishes unless *momentum is conserved*:

$$\mathbf{k}_1 + \mathbf{k}_2 = \mathbf{k}_3 + \mathbf{k}_4. \quad (2.177)$$

The sum over nearest neighbors can then be written

$$\sum_{\delta} e^{-i(\mathbf{k}_2 - \mathbf{k}_3 - \mathbf{k}_4) \cdot \delta} = \sum_{\delta} e^{i\mathbf{k}_1 \cdot \delta} = Z \gamma_{\mathbf{k}_1}, \quad (2.178)$$

where $\gamma_{\mathbf{k}_1}$ is given by (2.163). The first term in the Hamiltonian (i.e., Eq. (2.175)) can now be written

$$\mathcal{H}_1^{(1)} = \frac{\mathcal{J}Z}{2N} \sum_{\mathbf{k}_1 \mathbf{k}_2 \mathbf{k}_3 \mathbf{k}_4} \Delta(\mathbf{k}_1 + \mathbf{k}_2 - \mathbf{k}_3 - \mathbf{k}_4) \gamma_{\mathbf{k}_1} a_{\mathbf{k}_1}^+ a_{\mathbf{k}_2}^+ a_{\mathbf{k}_3} a_{\mathbf{k}_4}. \quad (2.179)$$

When all of the terms are collected, the interaction Hamiltonian becomes

$$\mathcal{H}_1 = \frac{\mathcal{J}Z}{N} \sum_{\mathbf{k}_1 \mathbf{k}_2 \mathbf{k}_3 \mathbf{k}_4} \Delta(\mathbf{k}_1 + \mathbf{k}_2 - \mathbf{k}_3 - \mathbf{k}_4) (\gamma_{\mathbf{k}_1} + \gamma_{\mathbf{k}_3} - 2\gamma_{\mathbf{k}_1 - \mathbf{k}_3}) a_{\mathbf{k}_1}^+ a_{\mathbf{k}_2}^+ a_{\mathbf{k}_3} a_{\mathbf{k}_4}. \quad (2.180)$$

For a simple cubic lattice at long wavelengths ($ka \ll 1$), $\gamma_{\mathbf{k}}$ can be approximated from (2.167) to be

$$\gamma_{\mathbf{k}} \approx 1 - (ka)^2/6, \quad (2.181)$$

and

$$\gamma_{\mathbf{k}_1 - \mathbf{k}_3} \approx 1 - \frac{(k_1 a)^2}{6} - \frac{(k_3 a)^2}{6} + \frac{\mathbf{k}_1 \cdot \mathbf{k}_3 a^2}{3}. \quad (2.182)$$

The magnitude of the interaction Hamiltonian is therefore proportional to

$$\gamma_{\mathbf{k}_1} + \gamma_{\mathbf{k}_3} - 2\gamma_{\mathbf{k}_1 - \mathbf{k}_3} \approx \frac{1}{6} (k_1^2 a^2 + k_3^2 a^2 - 4\mathbf{k}_1 \cdot \mathbf{k}_3 a^2). \quad (2.183)$$

The transition probability from a state with magnons $\mathbf{k}_1, \mathbf{k}_2$ to a state with magnons $\mathbf{k}_3, \mathbf{k}_4$ is proportional to $|\langle 3, 4 | \mathcal{H}_1 | 1, 2 \rangle|^2 \sim (ka)^4$, so that the interactions are very weak for long-wavelength magnons.

In the case of the spin eigenstates $|s_{jz}\rangle$, the z -component of spin can only be raised or lowered until the z -component is equal to the total spin. Further applications of the raising or lowering operators, S_j^\pm , will give zero. In contrast, the states $|n_j\rangle$ have a harmonic oscillator on each site, so that the number of spin deviations is unlimited. The fact that in reality not more than $2s_j$ spin deviations can exist on a given site gives rise to what Dyson calls the *kinematical interaction*. As we have mentioned, a spin wave is actually a collective excitation; a single spin deviation does not appear on a particular site, but is rather distributed over all of the sites in the crystal. Because of this, the expectation value of the z -component of spin for one spin deviation in a lattice of N sites is of order $s - 1/N$ instead of $s - 1$ (taking the ground state to be all spins up). Speaking classically, the kinematical interaction is caused by the fact that the cone angle of the spin precession can only be opened to π . However, the above z -component of spin suggests a cone angle on the order of $\sqrt{2/(Ns)} \ll 1$ for N large (Problem 2.5). Hence, we expect the effects of the kinematical interaction to be small at low temperatures where the number of magnons present is small compared to the number of sites in the crystal.

In Dyson's analysis, there is another interaction that results from the fact that the spin wave states $|s_j, s_{jz}\rangle$ are not eigenfunctions of the Hamiltonian (2.132). Dyson calls this the *dynamical interaction*. The effects of the simultaneous presence of two spin waves can be modeled by applying two rotations to a given spin vector. The fact that rotations do not commute results in a mutual disturbance that is the dynamical interaction. However, since two very small rotations almost commute, we expect the dynamical interaction to likewise be very small.

The effects of these interactions can be grouped into three categories, namely those due to

- (1) the dynamical interaction only,
- (2) the kinematical interaction only, and
- (3) more complicated effects involving both interactions.

Dyson [14] shows that the contributions from (2) and (3) exactly cancel for all non-negative powers of temperature T . For negative powers of T , he shows that the contribution of the kinematical interaction to the free energy is less than $\exp(-T_c/T)$, where T_c is the Curie temperature. This interaction, therefore, makes a rigorously negligible contribution for $T \rightarrow 0$ when the number of magnons is small. The net result is the following very significant conclusion: the kinematical interaction has no effect on the spin wave scattering probability amplitudes at low temperatures. These processes are governed entirely by the dynamical interaction. Therefore, the scattering probability amplitudes given by our harmonic oscillator model (that does not contain the kinematical interaction) should be entirely satisfactory.

Finally, we note that our Hamiltonian (2.173) does not contain any three wave processes; i.e., terms involving three creation/annihilation operators. This is because we have neglected the magnetic dipole-dipole interactions between the spins in an effort to simplify the discussion. When dipole-dipole interactions are included, it is possible to have magnon splitting and magnon confluence processes as illustrated in Figure 2.4(b),(c). These processes are represented by terms in the Hamiltonian of form

$$\mathcal{H}'_1 = \sum_{\mathbf{k}_1, \mathbf{k}_2, \mathbf{k}_3} \Delta(\mathbf{k}_1 + \mathbf{k}_2 - \mathbf{k}_3) (V(\mathbf{k}_1, \mathbf{k}_2, \mathbf{k}_3) a_{\mathbf{k}_1}^+ a_{\mathbf{k}_2}^+ a_{\mathbf{k}_3} + h.c.) \quad (2.184)$$

where $h.c.$ indicates the Hermitian conjugate.

Dipole-dipole interactions also affect the magnon dispersion relation in the absence of magnon interactions. The net result is to make the dispersion

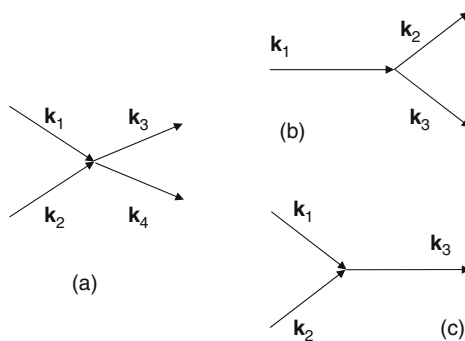


Fig. 2.4. Representative 3- and 4-magnon interactions. Part (a) depicts the scattering process indicated by (2.180), (b) depicts the magnon splitting process described by the first term in (2.184), and (c) illustrates the magnon confluence process described by the Hermitian conjugate term in (2.184).

relation anisotropic even for long-wavelength excitations. To understand the origin of the anisotropy, recall that there is a null in the field from a dipole in directions along its axis, while the field is strongest perpendicular to the axis. If we define θ to be the angle between the direction of propagation and the spin axis, then we expect the shift from dipole coupling to be zero for propagation in the direction $\theta = 0$, and for the shift to be greatest for the direction $\theta = \pi/2$. This spreads the dispersion relation into a band of frequencies for $ka \ll 1$ as illustrated in Figure 2.5. This band of frequencies is referred to as the *spin wave manifold*. Calculations of the effects of dipole–dipole interactions are simpler in a classical formulation for continuous media, so we will defer a more detailed treatment until Chapter 5.

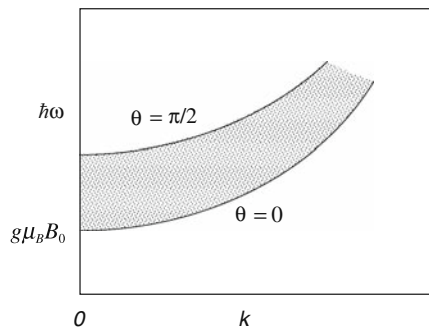


Fig. 2.5. Spin wave dispersion diagram near $k = 0$ with dipolar interactions. The dipole–dipole interactions spread the range of frequencies into a band depending on the direction of propagation with respect to the spin orientation. For $\theta = 0$ the dipolar coupling is zero, and the dispersion relation is given by (2.169). Compared with Figure 2.2, the presence of a bias field raises the frequency for $k = 0$ spin waves.

Problems

2.1. In this problem, we will verify the equivalence of the Heisenberg Hamiltonian and the alternative form expressed in terms of the Pauli spin exchange operator when applied to the hydrogen triplet state $\psi_{\text{A}\chi\text{S}}$.

(a) Calculate the expected value of the Heisenberg Hamiltonian by evaluating

$$-2\frac{\mathcal{J}}{\hbar^2}\mathbf{S}_1 \cdot \mathbf{S}_2 \psi_{\text{A}\chi\text{S}} = \left(\mathcal{H}^{\text{spin}} - \frac{1}{4} [\mathcal{E}_{\text{S}} + 3\mathcal{E}_{\text{T}}] \right) \psi_{\text{A}\chi\text{S}}, \quad (2.185)$$

where $\mathcal{J} = (\mathcal{E}_{\text{S}} - \mathcal{E}_{\text{T}})/2$.

(b) Calculate the expected value of the alternative Hamiltonian by evaluating

$$\mathcal{H}^P \psi_A \chi_S = -\frac{\mathcal{J}}{2}(2P-1) \psi_A \chi_S. \quad (2.186)$$

2.2. Show that

$$a^\dagger \psi_n = \sqrt{n+1} \psi_{n+1}, \quad (2.187)$$

where

$$a^\dagger = \frac{1}{\sqrt{2}} \left(\frac{x}{\alpha} - \alpha \frac{d}{dx} \right) \quad (2.188)$$

and

$$\psi_n(x) = \frac{e^{-\frac{x^2}{2\alpha^2}} H_n\left(\frac{x}{\alpha}\right)}{\sqrt{\alpha 2^n n! \sqrt{\pi}}}. \quad (2.189)$$

2.3. Referring to Section 2.7.1, show that

$$S_j^- |s_{jz}\rangle = \hbar (s(s+1) - s_{jz}(s_{jz}-1))^{1/2} |s_{jz}-1\rangle. \quad (2.190)$$

2.4. Consider a linear chain of N spins. The exact solution on a finite chain will depend on the boundary conditions at the ends. A common choice in solid-state physics is the periodic boundary condition, i.e., $\psi(x_1) = \psi(x_{1+N})$.

- (a) If $x_n = na$ and $\psi(x) = e^{ikx}$, show that the allowed values of k are $k_m = 2\pi m/Na$, where $m = 0, \pm 1, \pm 2, \dots, \pm N/2$ (assuming N is even).
 (b) With the definitions from Part (a), show that

$$\sum_{j=0}^{N-1} e^{ik_m x_j} = 0, \quad k_m \neq 0 \quad (2.191)$$

$$\sum_{j=0}^{N-1} e^{ik_m x_j} = N, \quad k_m = 0. \quad (2.192)$$

$$(2.193)$$

2.5. Consider a classical vector of length s precessing about the z axis. If the z -component of \mathbf{s} is $s-1/N$ with $s \ll N$, show that the cone angle of the precession (i.e., the angle of s with respect to the z -axis) is approximately $\sqrt{2/(Ns)}$.

References

- [1] J. D. Jackson, *Classical Electrodynamics*, 3rd ed. Singapore: John Wiley and Sons, 1999.

- [2] H. Goldstein, C. P. Poole, and J. L. Safko, *Classical Mechanics*, 3rd ed. Cambridge, MA: Addison-Wesley, 2001.
- [3] E. Merzbacher, *Quantum Mechanics*, 3rd ed. New York: John Wiley & Sons, 1998.
- [4] D. C. Mattis, *The Theory of Magnetism I: Statics and Dynamics*. New York: Springer-Verlag, Berlin, 1981.
- [5] D. H. Martin, *Magnetism in Solids*. Cambridge, MA: M.I.T. Press, 1967.
- [6] G. T. Rado and H. Suhl, Eds., *Magnetism I*. New York: Academic Press, 1963.
- [7] W. Heitler and F. London, "Reciprocal action of neutral atoms and homopolar combination according to quantum mechanics," *Z. Physik*, vol. 44, pp. 455–472, 1927.
- [8] R. P. Feynman, R. B. Leighton, and M. Sands, *The Feynman Lectures on Physics*. Reading, MA: Addison-Wesley, 1964, vol. III.
- [9] T. Holstein and H. Primakoff, "Field dependence of the intrinsic domain magnetization of a ferromagnet," *Phys. Rev.*, vol. 58, no. 12, pp. 1098–1113, Dec 1940.
- [10] M. Sparks, *Ferromagnetic Relaxation Theory*. New York: McGraw-Hill, 1964.
- [11] C. Kittel, *Quantum Theory of Solids*. New York: John Wiley & Sons, 1963.
- [12] T. Oguchi, "Theory of spin wave interactions in ferro- and antiferromagnetism," *Phys. Rev.*, vol. 117, pp. 117–123, 1960.
- [13] F. J. Dyson, "General theory of spin-wave interactions," *Phys. Rev.*, vol. 102, pp. 1217–1230, 1956.
- [14] F. J. Dyson, "Thermodynamic behavior of an ideal ferro-magnet," *Phys. Rev.*, vol. 102, pp. 1230–1244, 1956.

Magnetic Susceptibilities

The previous chapters concentrated on the origins of magnetic moments in individual ions or atoms and collective excitations of spin systems coupled by the exchange interaction. In this chapter, we will discuss the magnetic properties of macroscopic media composed of very large numbers of individual moments and the dependence of these properties on the magnetic field.¹ Specifically, we are interested in the net *magnetization* (magnetic dipole moment per unit volume) that exists either spontaneously or in response to an applied magnetic field. If the relationship between the induced magnetization and the applied field is linear, we can write

$$\mathbf{M} = \mathbf{M}_0 + \bar{\chi} \cdot \mathbf{H}, \quad (3.1)$$

where $\bar{\chi}$ is called the magnetic susceptibility tensor of the medium. For isotropic media, the susceptibility reduces to a scalar constant times the identity matrix, and \mathbf{M} and \mathbf{H} are collinear.

3.1 Diamagnetism

According to Lenz's law, currents are induced in conductors when a magnetic field is applied. These currents persist only as long as the applied field is changing and circulate in such a way as to produce a magnetic field that opposes the applied field. In addition to these currents from the conduction electrons, the application of a magnetic field produces perturbations in the orbitals of bound electrons resulting in microscopic currents opposing the applied field. In contrast to the macroscopic currents, however, the microscopic currents persist as long as the field is applied.

¹ General introductory treatments of the theory of magnetism and magnetic susceptibilities are given by Brailsford [1], Ashcroft and Mermin [2], and Kittel [3]. Effective field theories in magnetism are discussed in detail by Smart [4].

To estimate the magnetic moment from these induced microscopic currents, we first calculate the induced electric field caused by a buildup of the applied magnetic field. This can be done by applying Faraday's law to the electron path shown in Figure 3.1:

$$\oint \mathbf{E} \cdot d\mathbf{l} = - \int_S \frac{\partial \mathbf{B}}{\partial t} \cdot d\mathbf{s},$$

therefore,

$$E 2\pi R = -\pi R^2 \frac{dB}{dt}$$

or

$$E = -\frac{R}{2} \frac{dB}{dt}. \quad (3.2)$$

Here, we have assumed $\partial \mathbf{B}/\partial t = d\mathbf{B}/dt$, since the field is assumed to be spatially uniform. This \mathbf{E} field exerts a force on the electron giving rise to the torque $q \mathbf{R} \times \mathbf{E}$. Referring to Figure 3.1, this torque has only a z -component given by

$$\tau = \frac{dL}{dt} = qRE$$

or

$$E = \frac{1}{qR} \frac{dL}{dt}, \quad (3.3)$$

where L is the orbital angular momentum. Equating (3.2) and (3.3) and solving for dL/dt gives

$$\frac{dL}{dt} = -\frac{qR^2}{2} \frac{dB}{dt}. \quad (3.4)$$

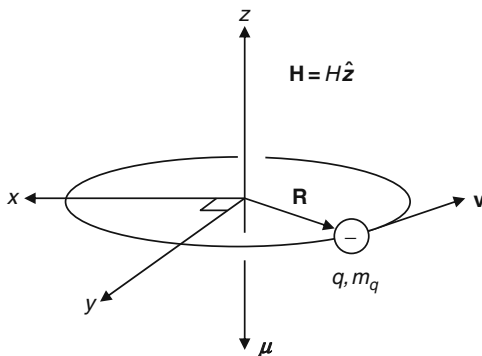


Fig. 3.1. The induced magnetic moment due to the applied field \mathbf{H} . The counter-clockwise circulation of the negative charge q is equivalent to a clockwise current that generates a magnetic field opposing the applied field.

Integrating both sides over the time interval required to apply a magnetic field B gives

$$\begin{aligned}\int_0^T \frac{dL}{dt} dt &= -\frac{qR^2}{2} \int_0^T \frac{dB}{dt} dt, \\ \int_0^L dL' &= -\frac{qR^2}{2} \int_0^B dB', \\ L &= -\frac{\mu_0 q R^2}{2} H.\end{aligned}\tag{3.5}$$

Multiplying this by the gyromagnetic ratio for orbital angular momentum (1.25) yields the induced magnetic moment:

$$\mu = -\frac{\mu_0 q^2 R^2}{4m_q} H.\tag{3.6}$$

If there are n electrons per ion and N ions per unit volume, the total magnetic moment per unit volume, or *magnetization*, is

$$M = -\frac{\mu_0 N q^2}{4m_q} \sum_{i=1}^n R_i^2 H,\tag{3.7}$$

where R_i is the orbital radius of the i th electron. Here, we have assumed a planar circular orbit perpendicular to the field where $R_i^2 = x_i^2 + y_i^2$. We can still use these results for non-circular orbits, if we replace R_i^2 with its mean value $\langle R_i^2 \rangle = \langle x_i^2 \rangle + \langle y_i^2 \rangle$.

For a spherically symmetric orbital (such as an s orbital), the average spherical radius is $\langle r_i^2 \rangle = \langle x_i^2 \rangle + \langle y_i^2 \rangle + \langle z_i^2 \rangle$, where $\langle x_i^2 \rangle = \langle y_i^2 \rangle = \langle z_i^2 \rangle$ because of the orbital symmetry. It follows that

$$\langle R_i^2 \rangle = \frac{2}{3} \langle r_i^2 \rangle.\tag{3.8}$$

and (3.7) becomes

$$M = -\frac{\mu_0 N q^2}{6m_q} \sum_{i=1}^n \langle r_i^2 \rangle H.\tag{3.9}$$

Comparing this with Eq. (3.1) gives the diamagnetic susceptibility for spherically symmetric orbitals as

$$\chi_{\text{dia}} = -\frac{\mu_0 N q^2}{6m_q} \sum_{i=1}^n \langle r_i^2 \rangle.\tag{3.10}$$

This is called the *Langevin diamagnetism* formula.

3.2 Paramagnetism

In a paramagnetic material, thermal vibrations tending to randomize the orientations of the elementary moments overcome any magnetic- or quantum mechanical-coupling effects. Thus, the net magnetic moment of the material is zero in thermal equilibrium and zero applied field. Application of an external field, however, does cause a partial alignment of the moments and the material exhibits an induced net magnetization. The strength of the induced magnetization depends on the temperature as well as the strength of the applied field.

The change in energy of a magnetic moment $\boldsymbol{\mu}$ caused by the presence of a magnetic field \mathbf{H} is called the Zeeman energy (see Section 2.2) and is given by

$$\mathcal{E}_{zm} = -\boldsymbol{\mu} \cdot \mathbf{B}. \quad (3.11)$$

This expression simply indicates that the energy is lowest (most negative) when the moment is aligned with the field. This can be expressed in terms of the angular momentum using Eqs. (1.29) and (1.30):

$$\mathcal{E}_{zm} = +\frac{g\mu_0\mu_B}{\hbar} \mathbf{J} \cdot \mathbf{H}, \quad (3.12)$$

where $\mu_B = |q|\hbar/2m_q$ is the Bohr magneton (Section 1.5). Assuming the magnetic field is along the $\hat{\mathbf{z}}$ direction, this becomes

$$\mathcal{E}_{zm} = g\mu_0\mu_B J_z H / \hbar. \quad (3.13)$$

If the angular momentum is treated quantum mechanically, then J_z is given by $J_z = \hbar m$, where m can only take on the discrete values $-J, -J+1, \dots, J-1, J$, where J is an integer or half-integer. Thus, the z -component of the magnetic moment and the Zeeman energy are also restricted to discrete values:

$$\mu_z(m) = -g\mu_B m, \quad (3.14)$$

$$\mathcal{E}_{zm}(m) = +g\mu_0\mu_B m H. \quad (3.15)$$

According to statistical mechanics, the probability that an electron is in a state with energy \mathcal{E} is proportional to the *Boltzmann factor* $\exp(-\mathcal{E}/k_B T)$ where $k_B = 1.38 \times 10^{-23}$ J/K is Boltzmann's constant and T is the absolute temperature in Kelvins. The probability of an electron occupying the m th angular momentum state in the presence of a magnetic field can therefore be written

$$P(m) = A e^{-\mathcal{E}_{zm}(m)/k_B T}. \quad (3.16)$$

The constant A can be determined by requiring the sum of probabilities to add up to unity:

$$\sum_{m=-J}^J P(m) = A \sum_{m=-J}^J e^{-\mathcal{E}_{zm}(m)/k_B T} = 1, \quad (3.17)$$

or

$$A = \left[\sum_{m=-J}^J e^{-\mathcal{E}_{zm}(m)/k_B T} \right]^{-1}. \quad (3.18)$$

At a given temperature, the *thermal average* of the $\hat{\mathbf{z}}$ component of the magnetic moment $\langle\langle\mu_z\rangle\rangle$ is given by the product of $\mu_z(m)$ times the probability that the m th state is occupied, summed over all possible values of m :

$$\begin{aligned} \langle\langle\mu_z\rangle\rangle &= \frac{\sum_{m=-J}^J \mu_z(m) e^{-\mathcal{E}_{zm}(m)/k_B T}}{\sum_{m=-J}^J e^{-\mathcal{E}_{zm}(m)/k_B T}} \\ &= - \frac{g\mu_B \sum_{m=-J}^J m e^{-g\mu_0\mu_B m H/k_B T}}{\sum_{m=-J}^J e^{-g\mu_0\mu_B m H/k_B T}}. \end{aligned} \quad (3.19)$$

If there are N moments per unit volume, the thermal average of the magnetization is

$$\langle\langle M \rangle\rangle = -g\mu_B N \frac{\sum_{m=-J}^J m e^{-mx}}{\sum_{m=-J}^J e^{-mx}}, \quad (3.20)$$

where $x = g\mu_0\mu_B H/k_B T$. Using the properties of the natural logarithm, Eq. (3.20) can be written in terms of a single summation:

$$\langle\langle M \rangle\rangle = g\mu_B N \frac{d}{dx} \left[\ln \left(\sum_{m=-J}^J e^{-mx} \right) \right]. \quad (3.21)$$

The summation is a finite geometric series that can be summed in closed form:

$$\sum_{m=-J}^J z^m = \frac{z^{J+1/2} - z^{-(J+1/2)}}{z^{1/2} - z^{-1/2}}, \quad (3.22)$$

where $z = \exp(-x)$. The summation in (3.21) can thus be written

$$\begin{aligned} \sum_{m=-J}^J e^{-mx} &= \frac{e^{-(J+1/2)x} - e^{(J+1/2)x}}{e^{-x/2} - e^{x/2}} \\ &= \frac{\sinh[(J+1/2)x]}{\sinh(x/2)}. \end{aligned} \quad (3.23)$$

Substituting this result into (3.21) and carrying out the indicated differentiation gives

$$\langle\langle M \rangle\rangle = M_{\max} B_J(\mu_0 \mu_{\max} H / k_B T), \quad (3.24)$$

where $B_J(y)$ is the *Brillouin function*

$$B_J(y) = \frac{2J+1}{2J} \coth\left(\frac{2J+1}{2J}y\right) - \frac{1}{2J} \coth\left(\frac{y}{2J}\right), \quad (3.25)$$

and

$$\mu_{\max} = g\mu_B J, \quad (3.26)$$

$$M_{\max} = g\mu_B N J. \quad (3.27)$$

Equations (3.24) and (3.25) are plotted in Figure 3.2 for several values of J . For small values of y , $B_J(y)$ is approximated by

$$B_J(y) \approx \frac{J+1}{3J}y - \frac{[(J+1)^2 + J^2](J+1)}{90J^3}y^3 + \dots \quad (3.28)$$

Thus, to lowest order in H/T we can write

$$\langle\langle M \rangle\rangle = \frac{\mu_0 N g^2 J(J+1) \mu_B^2}{3k_B T} H. \quad (3.29)$$

The paramagnetic susceptibility is, therefore

$$\chi_{\text{para}} = \frac{\langle\langle M \rangle\rangle}{H} = \frac{\mu_0 N g^2 J(J+1) \mu_B^2}{3k_B T} = \frac{C}{T}. \quad (3.30a)$$

This $1/T$ dependence of the susceptibility is called the *Curie Law*. Equation (3.30a) is sometimes written as

$$\chi_{\text{para}} = \frac{\mu_0 N p^2 \mu_B^2}{3k_B T}, \quad (3.30b)$$

where $p = g[J(J+1)]^{1/2}$ is called the *effective magneton number*.

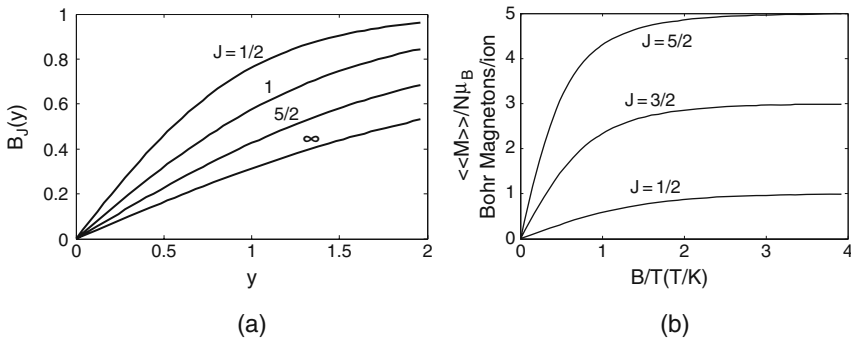


Fig. 3.2. (a) The Brillouin function $B_J(y)$ for several values of J . (b) Thermal average of the induced moment per atom or ion as a function of the ratio B/T . The Landé g factor is taken to be 2 for definiteness.

3.3 Weiss Theory of Ferromagnetism

According to the theory of Section 3.2, paramagnetic materials only exhibit a net moment when an external field is applied. This suggests that materials that exhibit net spontaneous magnetic moments could be modeled with a similar theory if the total magnetic field had an additional component present independent of an external field. Thus, according to the *Weiss molecular field theory*, the total field is equal to the applied field plus the *molecular field* \mathbf{H}_m :

$$\mathbf{H}_{\text{tot}} = \mathbf{H} + \mathbf{H}_m, \quad (3.31)$$

where the molecular field is assumed to be proportional to the thermally averaged magnetization:²

$$\mathbf{H}_m = \lambda \mathbf{M}. \quad (3.32)$$

This field was originally thought to be the magnetostatic field experienced by a moment due to neighboring moments, but order-of-magnitude calculations show that this cannot possibly account for the effective fields observed. We will return to this topic in a later section.

For high-temperature and small fields, we can again expand the Brillouin function to lowest order in H_{tot}/T . Substituting the total field (3.31) into the constitutive relation (3.29) gives

$$M = \frac{C}{T}(H + \lambda M), \quad (3.33)$$

where

$$C = \frac{\mu_0 N p^2 \mu_B^2}{3k_B}. \quad (3.34)$$

The susceptibility is obtained by solving for M/H :

$$\chi = \frac{M}{H} = \frac{C}{T - T_c}, \quad (3.35)$$

where T_c is called the *Curie temperature* and is given by

$$T_c = \lambda C = \frac{\lambda \mu_0 N p^2 \mu_B^2}{3k_B}. \quad (3.36)$$

Equation (3.35) is called the *Curie–Weiss law* and is valid for small H and $T \gg T_c$.

For low temperatures ($T < T_c$), we clearly cannot expand $B_J(y)$ and keep only the lowest-order term; we must use the entire function. We are particularly interested in the case $H = 0$, since ferromagnetic materials exhibit

² For the rest of the text, M rather than $\langle\langle M \rangle\rangle$ will be used to refer to the thermal average of the magnetization for simplicity.

spontaneous magnetization even in the absence of external fields. Thus, we are interested in solutions to the equation

$$M(T) = M_{\max} B_J(\mu_0 \mu_{\max} \lambda M(T) / k_B T). \quad (3.37)$$

For simplicity, let us define

$$m = \frac{M(T)}{M_{\max}} \quad (3.38)$$

and

$$t = \frac{J(J+1)}{3J^2} \frac{T}{T_c}. \quad (3.39)$$

In terms of these normalized magnetization and temperature variables, the equation for the magnetization (3.37) becomes

$$m = B_J(m/t). \quad (3.40)$$

This equation can be solved graphically as shown in Figure 3.3. From part (a) of the figure, it is apparent that $B_J(m/t)$ has an initial slope of unity when $T = T_c$.

Experimentally, T_c can be obtained by determining the temperature at which the magnetization vanishes. The molecular field parameter λ can then be estimated from the Curie temperature expression (3.36).

As an example, consider the simple ferromagnet EuO. The Hund-rule ground state for Eu^{2+} is calculated with the aid of Figure 3.4. The ground state is characterized by $L = 0$, $S = 7/2$, $J = 7/2$, and $g = 2$, since the angular momentum is due entirely to spin. In spectroscopic notation, this state is denoted $^8S_{7/2}$.

EuO has a face-centered cubic crystal structure with lattice constant 5.141 Å [5]. In this structure, there are four EuO molecules per unit cell. Thus, from

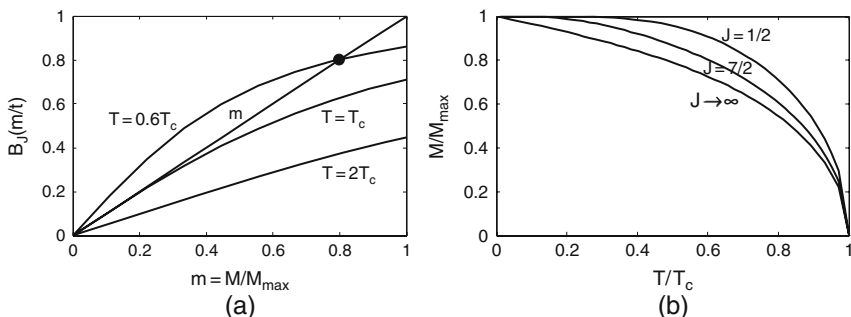


Fig. 3.3. (a) Graphical solution of Eq. (3.40) with $J = 7/2$ for several temperatures. (b) The resulting magnetization as a function of temperature. Note that $M(0) = M_{\max}$. This calculation neglects the change in N caused by thermal expansion and contraction of the lattice.

m_l	:	3	2	1	0	-1	-2	-3		3	2	1	0	-1	-2	-3
m_s	:	↑	↑	↑	↑	↑	↑	↑								
"spin-up" states									"spin-down" states							
$J = L - S $									$J = L + S$							

Fig. 3.4. The $^8S_{7/2}$ Hund-rule ground state for Eu^{2+} ($L=0$, $S=7/2$, and $J=7/2$).

the moment and magnetization given in Eqs. (3.26) and (3.27), each molecule should exhibit a maximum moment of $\mu_{\text{max}} = 7\mu_B$ and the magnetization at 0 K should be $M(0) = M_{\text{max}} = 1911 \text{ kA/m}$ ($4\pi M = 24 \text{ kG}$). The Curie–Weiss constant is calculated from (3.34) to be $C = 4.84$. The experimental inverse susceptibility along with the theoretical expression (3.35) are shown in Figure 3.5 for $T_c = 69.2 \text{ K}$. The experimental magnetization along with the theoretical expression (3.40) are shown in Figure 3.6. The agreement is striking in both cases.

Thus far, the Curie–Weiss theory appears to give a satisfactory description of this simple ferromagnet. Difficulties appear, however, when we attempt to evaluate the molecular field H_m . The molecular field constant λ can be obtained by comparing the experimental Curie temperature of 69.2 K with the theoretical expression (3.36). The strength of the molecular field for $M = M_{\text{max}}$ can then be obtained from Eq. (3.32). Using this procedure, we find $\lambda = 14.3$ and $H_m = 2.73 \times 10^7 \text{ A/m}$ (343 kOe). For comparison, let us estimate the magnetostatic dipole field from the surrounding moments. The magnitude of the field from a magnetic dipole depends on direction, but is of order [6, p. 189]

$$H_{\text{dip}} = \frac{\mu}{4\pi R^3}. \quad (3.41)$$

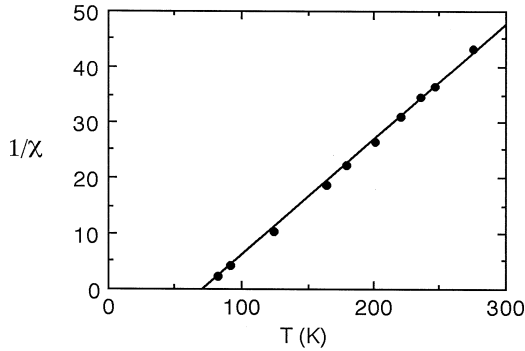


Fig. 3.5. Reciprocal susceptibility of EuO . Circles represent experimental points and the theoretical line corresponds to Eq. (3.35) with $C=4.84$ ($Jg = 7$) and $T_c = 69.2 \text{ K}$ (measurements from Matthias and Bozorth [5]).

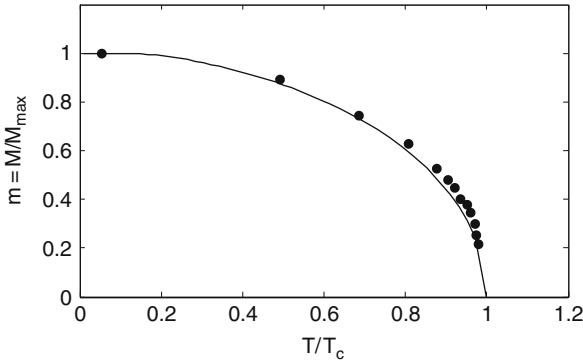


Fig. 3.6. Magnetization of EuO as a function of temperature. Circles are experimental points and the theoretical line corresponds to Eq. (3.40) with $J = 7/2$, $T_c = 69.2$ K (measurements from Als-Nielsen et al. [7]).

In the face-centered cubic structure, there are 12 nearest-neighbors at a distance $a\sqrt{2}$, where a is the lattice constant. Using $R = a/\sqrt{2}$, $\mu = 7\mu_B$, and multiplying the dipole field (3.41) by the number of nearest-neighbors (12) gives a total field of $H_{\text{dip}} = 1.29 \times 10^6$ A/m (16.2 kOe).³ This is more than an order of magnitude smaller than the effective field indicated by T_c . This discrepancy is even greater for materials with higher Curie temperatures. The origin of this effective field can be clarified by a quantum-mechanical treatment of the interaction between electrons on different lattice sites. This interaction is none other than the exchange interaction discussed in Section 2.4. We will return to this topic in Section 3.5.

3.4 Néel Theory of Ferrimagnetism

In some materials, the interactions between the atomic moments are such that in equilibrium some “point up” and some “point down.” As discussed in Chapter 1, such materials are called ferrimagnets. The analysis of ferrimagnets can be facilitated by breaking the pattern of magnetic order into two *sublattices* – an “up” sublattice labeled a and a “down” sublattice labeled b , for example. In keeping with the spirit of the molecular field model, this situation can be described by introducing the molecular fields

$$\begin{aligned}\mathbf{H}_a &= -\lambda_{aa}\mathbf{M}_a - \lambda_{ab}\mathbf{M}_b, \\ \mathbf{H}_b &= -\lambda_{ba}\mathbf{M}_a - \lambda_{bb}\mathbf{M}_b.\end{aligned}\tag{3.42}$$

Here, $\mathbf{H}_{a,b}$ is the effective field seen by a moment on an a or b sublattice site, respectively, and $\mathbf{M}_{a,b}$ is the respective sublattice magnetization. Note that we

³ This is a generous estimate; in reality, the dipolar fields cancel in a cubic lattice!

have chosen the signs to favor antiparallel alignment of the spins within each sublattice, as well as between the sublattices (cf. Eq. (3.32)). The sublattice magnetizations at temperature T are determined from the coupled nonlinear equations

$$M_a = M_{a,\max} B_{J_a} \left[\frac{\mu_{a,\max} \mu_0}{k_B T} (H - \lambda_{aa} M_a - \lambda_{ab} M_b) \right], \quad (3.43a)$$

$$M_b = M_{b,\max} B_{J_b} \left[\frac{\mu_{b,\max} \mu_0}{k_B T} (H - \lambda_{ba} M_a - \lambda_{bb} M_b) \right]. \quad (3.43b)$$

In the calculations to follow, we will assume that the symmetry of the interactions is such that $\lambda_{ab} = \lambda_{ba}$. Also, because of the way in which the sublattices are interleaved, the nearest-neighbor of a given ion will generally belong to the opposite sublattice. Since the strength of interaction between moments decreases rapidly with their separation, the dominant molecular fields will be proportional to λ_{ab} . Thus, assuming nearest-neighbor interactions to dominate, the equations for the magnetization (3.43a,b) become:

$$M_a = M_{a,\max} B_{J_a} \left[\frac{\mu_{a,\max} \mu_0}{k_B T} (H - \lambda_{ab} M_b) \right], \quad (3.44a)$$

$$M_b = M_{b,\max} B_{J_b} \left[\frac{\mu_{b,\max} \mu_0}{k_B T} (H - \lambda_{ab} M_a) \right]. \quad (3.44b)$$

At high temperatures, the thermal fluctuations are strong enough to destroy the long-range magnetic order, and ferrimagnets exhibit a paramagnetic susceptibility. Expanding the Brillouin functions to lowest order gives

$$M_a = \frac{C_a}{T} (H - \lambda_{ab} M_b), \quad (3.45a)$$

$$M_b = \frac{C_b}{T} (H - \lambda_{ab} M_a), \quad (3.45b)$$

where

$$C_{a,b} = \frac{\mu_0 N_{a,b} p_{a,b}^2 \mu_B^2}{2k_B}. \quad (3.46)$$

These equations can be written in matrix form as

$$\begin{bmatrix} T & \lambda_{ab} C_a \\ \lambda_{ab} C_b & T \end{bmatrix} \begin{bmatrix} M_a \\ M_b \end{bmatrix} = \begin{bmatrix} C_a \\ C_b \end{bmatrix} H. \quad (3.47)$$

Solving for $[M_a \ M_b]^T$ gives

$$\begin{bmatrix} M_a \\ M_b \end{bmatrix} = \frac{H}{T^2 - T_c^2} \begin{bmatrix} T & -\lambda_{ab} C_a \\ -\lambda_{ab} C_b & T \end{bmatrix} \begin{bmatrix} C_a \\ C_b \end{bmatrix}, \quad (3.48)$$

where

$$T_c = \lambda_{ab} [C_a C_b]^{1/2}. \quad (3.49)$$

The singularity in the linearized equations at $T = T_c$ indicates the onset of ferrimagnetic order. The paramagnetic susceptibility for a ferrimagnet is thus

$$\chi = \frac{M_a + M_b}{H} = \frac{(C_a + C_b)T - 2\lambda_{ab}C_aC_b}{T^2 - T_c^2}. \quad (3.50)$$

The magnetization below T_c can be obtained by solving the two nonlinear coupled equations

$$M_a = M_{a,\max} B_{J_a}(-\mu_0 \mu_{a,\max} \lambda_{ab} M_b / k_B T), \quad (3.51a)$$

$$M_b = M_{b,\max} B_{J_b}(-\mu_0 \mu_{b,\max} \lambda_{ab} M_a / k_B T). \quad (3.51b)$$

The graphical solution of these equations is illustrated in Figure 3.7. The net magnetization can be obtained by adding $M_a + M_b$. The net magnetization from (3.51a,b) monotonically decreases with increasing temperature. However, if λ_{aa} and λ_{bb} are not negligible, the net magnetization may exhibit a peaked behavior or possess an additional zero for $T < T_c$. In the latter case, the temperature at which the net magnetization goes to zero without destroying magnetic order is called the *compensation point*. Examples of these various possible magnetization curves are shown in Figure 3.8.

The magnetizations of both sublattices in yttrium iron garnet (YIG) are due to Fe^{3+} ions in the ground state ${}^6S_{5/2}$ (Section 1.6). Other parameters are listed in Appendix A.⁴ Next-nearest-neighbor interactions cannot be neglected in this case, so the general Eqs. (3.43a,b) must be solved. The result is shown in Figure 3.9. The molecular field constants used (Appendix) were obtained by fitting (3.43a,b) to experimental data [8].

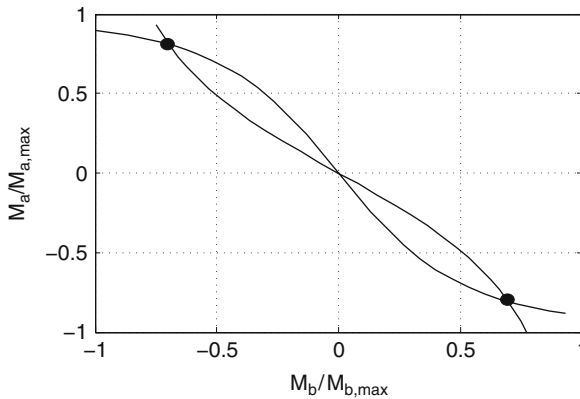


Fig. 3.7. Graphical solution of the nonlinear-coupled equations for ferrimagnetic order (3.51a,b). The symmetric solutions reflect the arbitrariness of choosing the directions “up” and “down.”

⁴ The properties of YIG and other ferrites are well documented in [9–11].

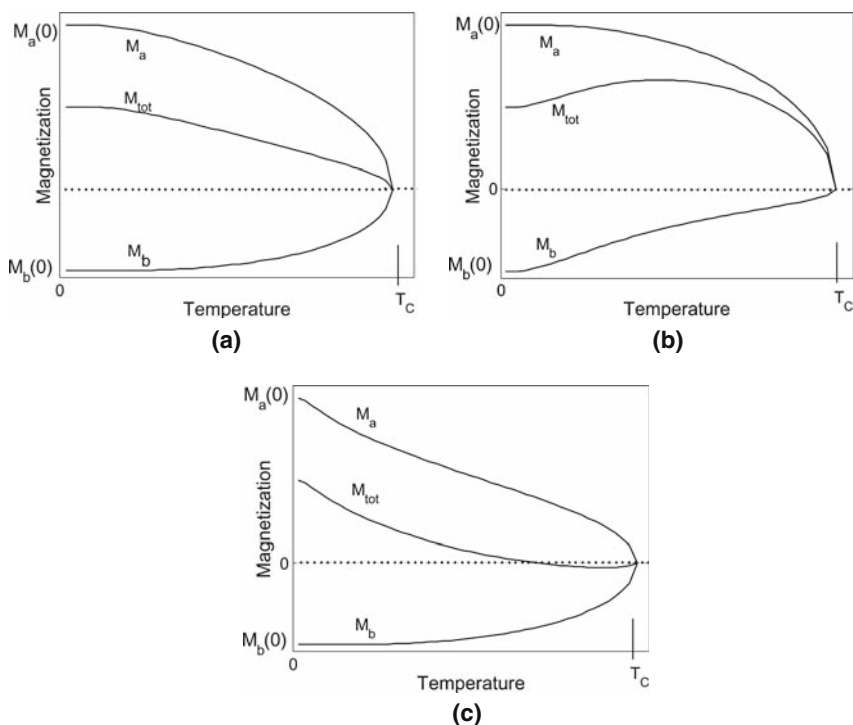


Fig. 3.8. Possible forms of the temperature dependence of the total magnetization M_{tot} of a ferrimagnet: (a) monotonic, (b) peaked, and (c) existence of a compensation point.

The behavior of an *antiferromagnet* can be obtained by setting $C_a = C_b = C$, since the sublattices are assumed to be identical. The critical temperature marking the onset of magnetic order is here called the *Néel temperature* and is given by (cf. Eq. (3.49))

$$T_N = \lambda_{ab}C, \quad (3.52)$$

if next-nearest-neighbor interactions can be neglected. The susceptibility becomes

$$\begin{aligned} \chi &= \frac{2CT - 2\lambda_{ab}C^2}{T^2 - T_N^2} \\ &= \frac{2C(T - T_N)}{(T + T_N)(T - T_N)} \\ &= \frac{2C}{T + T_N}. \end{aligned} \quad (3.53)$$

Note that the singularity at $T = T_N$ has been removed.

Equation (3.53) for the susceptibility of an antiferromagnet is only valid for $T > T_N$, since it was obtained using the linearized Brillouin functions.

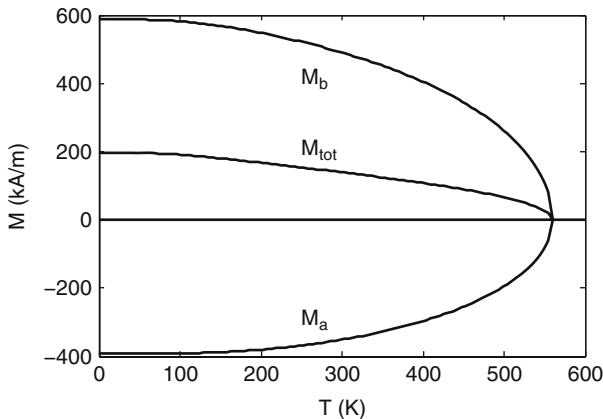


Fig. 3.9. Magnetization as a function of temperature for $\text{Y}_3\text{Fe}_5\text{O}_{12}$. Parameters used are listed in Appendix A.

Below T_N , where the material becomes magnetically ordered, there is no net spontaneous magnetization since $\mathbf{M}_a = -\mathbf{M}_b$ and $\mathbf{M}_{\text{tot}} = \mathbf{M}_a + \mathbf{M}_b = 0$. There will still be a susceptibility below T_N , but it will depend on the *direction* of \mathbf{H} . At very low temperatures, the spins of the two sublattices are almost exactly antiparallel. Application of a field collinear with the sublattice magnetizations results in no net torque and consequently no induced magnetization (Figure 3.10(a)). As the temperature increases, however, \mathbf{M}_a and \mathbf{M}_b fluctuate away from equilibrium and a small net moment can be induced. In contrast, application of a field perpendicular to the sublattice magnetizations can induce a comparatively large moment by tipping the moments away from equilibrium (Figure 3.10(b)). For comparison, paramagnetic, ferromagnetic,

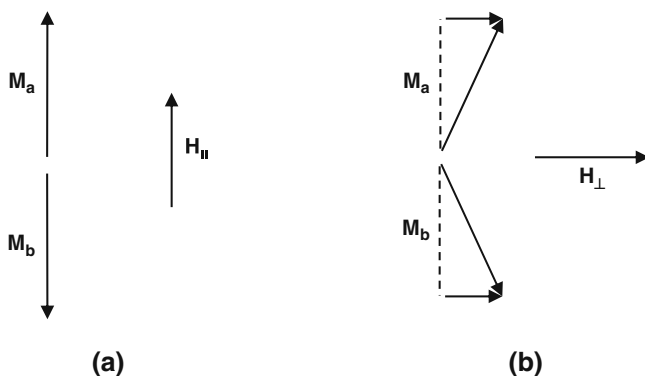


Fig. 3.10. Antiferromagnetic susceptibilities: (a) except for overcoming thermal deviations from collinear alignment, \mathbf{H}_{\parallel} has no effect; (b) application of \mathbf{H}_{\perp} can induce comparatively large moments.

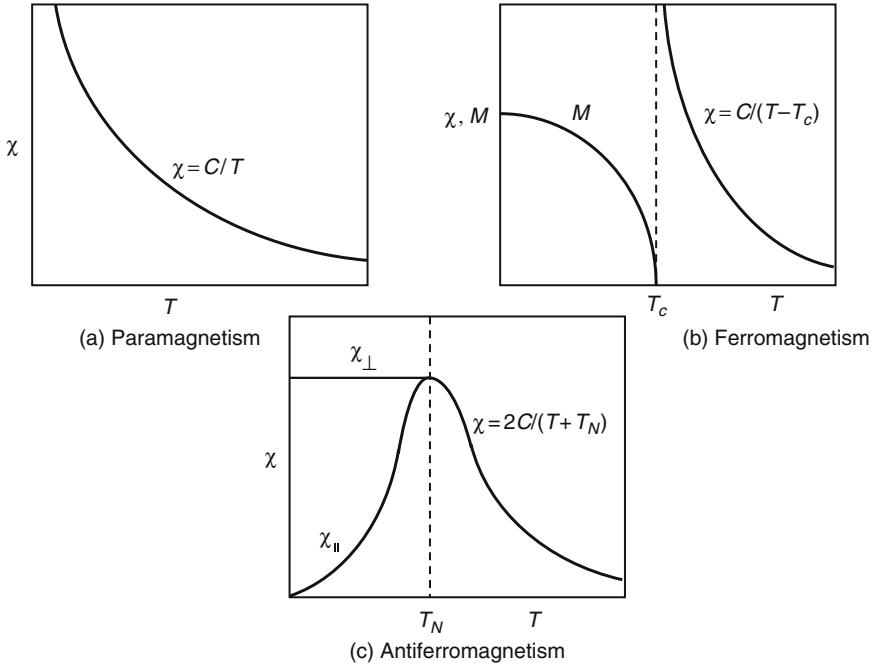


Fig. 3.11. Comparison of magnetic susceptibilities. Ferrimagnets without compensation points exhibit the same qualitative behavior as ferromagnets.

and antiferromagnetic susceptibilities are sketched in Figure 3.11. The behavior of those ferrimagnets that do not have compensation points is very similar to that of ferromagnets (Figure 3.11(b)).

3.5 Exchange Field

Although the molecular field theories of the previous sections successfully describe the main features of ferromagnetism and ferrimagnetism, they are not complete because the origin of the necessary molecular fields is not explained. To begin to understand how these effective fields come about, we must return to the exchange interaction introduced in Chapter 2.

As we did in Sections 2.5 and 2.7, let us assume that the interaction is significant only with nearest neighbors. The total exchange energy of the i th spin interacting with its neighbors is

$$\begin{aligned}
 \mathcal{E}_i^{(\text{ex})} &= -2 \sum_{j=n.n.} \mathcal{J}_{ij} \mathbf{S}_i \cdot \mathbf{S}_j \\
 &= -2 \mathbf{S}_i \cdot \sum_j' \mathcal{J}_{ij} \mathbf{S}_j.
 \end{aligned} \tag{3.54}$$

Here, the prime on the summation sign indicates a sum only over the nearest-neighbors of i .

The magnetic moment associated with the spin \mathbf{S} is

$$\boldsymbol{\mu} = -g\mu_B \mathbf{S}. \quad (3.55)$$

Thus, the exchange energy can be written

$$\mathcal{E}_i^{(\text{ex})} = \frac{2\mu_i}{g\mu_B} \cdot \sum_j' \mathcal{J}_{ij} \mathbf{S}_j. \quad (3.56)$$

Recalling the form of the Zeeman energy (3.11), Eq. (3.56) can be interpreted as the interaction of the i th moment with an effective magnetic field:⁵

$$\mathbf{H}_{\text{ex}} = -\frac{2}{g\mu_0\mu_B} \sum_j' \mathcal{J}_{ij} \mathbf{S}_j. \quad (3.57)$$

3.5.1 Uniform Magnetization

The simplest case to consider is that for which the spins on the nearest-neighbor sites are either exactly parallel or antiparallel. In this case, the magnetization will be spatially uniform. If there are Z nearest-neighbors and the interaction is the same with all ($\mathcal{J}_{ij} = \mathcal{J}$), the exchange field (3.57) can be written

$$\mathbf{H}_{\text{ex}} = -\frac{2Z\mathcal{J}}{g\mu_0\mu_B} \mathbf{S}, \quad (3.58)$$

where \mathbf{S} is the spin on any one site and all sites are assumed to be equivalent. This effective field can be related to the molecular field coefficient λ of a ferromagnet by noting that $\mathbf{M} = N\boldsymbol{\mu}$, where N is the density of moments (m^{-3}). Thus

$$\mathbf{H}_{\text{ex}} = \frac{2Z\mathcal{J}}{\mu_0 N g^2 \mu_B^2} \mathbf{M} = \lambda \mathbf{M} \quad (3.59)$$

and

$$\lambda = \frac{2Z\mathcal{J}}{\mu_0 N g^2 \mu_B^2}. \quad (3.60)$$

The exchange parameter \mathcal{J} can also be related to the Curie temperature using (3.36):⁶

$$\mathcal{J} = \frac{3k_B T_c}{2ZS(S+1)}. \quad (3.61)$$

⁵ In general, the i th component of the effective magnetic field is defined as $H_{\text{eff},i} = -(\delta\mathcal{E}/\delta\mu_i)/\mu_0$, where $\delta\mathcal{E}/\delta\mu_i$ is the variational derivative defined by Eq. (7.8).

⁶ Here, we have assumed $L=0$ so that $J = S$ in Eq. (3.36).

For EuO ($T_c = 69.2$ K, $Z = 12$, and $S = 7/2$), we obtain $\mathcal{J} = 7.58 \times 10^{-24}$ J, or $\mathcal{J}/k_B = 0.55$ K. This is in reasonable agreement with more sophisticated analyses [12] yielding $\mathcal{J}/k_B = 0.61$ K. The error in our result is caused by the neglect of next-nearest-neighbor interactions and intrinsic limitations of the molecular field theory.

3.5.2 Non-uniform Magnetization

If nearest-neighbor spins are not precisely parallel, then additional care must be taken in evaluating the sum over nearest-neighbors in the exchange field expression (3.57). Let us consider a continuous vector function $\mathbf{S}(\mathbf{r})$ that gives the spin on the i th site when evaluated at $\mathbf{r} = \mathbf{r}_i$. The sum over nearest-neighbors can thus be written (again assuming the \mathcal{J}_{ij} are equal)

$$\sum_j' \mathbf{S}_j = \sum_j' \mathbf{S}(\mathbf{r}_i + \boldsymbol{\delta}_j), \quad (3.62)$$

where $\boldsymbol{\delta}_j$ is the position vector from the i th to the j th site. As an example, consider a simple cubic lattice with six nearest-neighbors. The sum over nearest-neighbors (3.62) becomes

$$\begin{aligned} \sum_j' \mathbf{S}(\mathbf{r}_i + \boldsymbol{\delta}_j) &= \mathbf{S}(\mathbf{r}_i + a\hat{\mathbf{x}}) + \mathbf{S}(\mathbf{r}_i - a\hat{\mathbf{x}}) \\ &\quad + \mathbf{S}(\mathbf{r}_i + a\hat{\mathbf{y}}) + \mathbf{S}(\mathbf{r}_i - a\hat{\mathbf{y}}) \\ &\quad + \mathbf{S}(\mathbf{r}_i + a\hat{\mathbf{z}}) + \mathbf{S}(\mathbf{r}_i - a\hat{\mathbf{z}}), \end{aligned} \quad (3.63)$$

where a is the nearest-neighbor distance. If the function \mathbf{S} is slowly varying over the distance a , the second derivative with respect to x can be approximated by

$$\frac{\partial^2 \mathbf{S}(\mathbf{r}_i)}{\partial x^2} \approx \frac{1}{a^2} [\mathbf{S}(\mathbf{r}_i + a\hat{\mathbf{x}}) - 2\mathbf{S}(\mathbf{r}_i) + \mathbf{S}(\mathbf{r}_i - a\hat{\mathbf{x}})]. \quad (3.64)$$

Using this result in the sum over nearest-neighbors (3.63) permits us to write

$$\begin{aligned} \sum_j' \mathbf{S}(\mathbf{r}_i + \boldsymbol{\delta}_j) &\approx a^2 \left[\frac{\partial^2 \mathbf{S}}{\partial x^2} + \frac{\partial^2 \mathbf{S}}{\partial y^2} + \frac{\partial^2 \mathbf{S}}{\partial z^2} \right]_{\mathbf{r}=\mathbf{r}_i} + 6\mathbf{S}(\mathbf{r}_i) \\ &= a^2 \nabla^2 \mathbf{S}(\mathbf{r}_i) + 6\mathbf{S}(\mathbf{r}_i). \end{aligned} \quad (3.65)$$

The result for any of the three cubic lattices (simple cubic, face-centered cubic, and body-centered cubic) is

$$\sum_j' \mathbf{S}(\mathbf{r}_i + \boldsymbol{\delta}_j) = Z\mathbf{S}(\mathbf{r}_i) + \frac{ZR_n^2}{6} \nabla^2 \mathbf{S}(\mathbf{r}_i), \quad (3.66)$$

where Z is the number of nearest-neighbors and R_n is the nearest-neighbor distance. Substituting this result into the effective field expression (3.57) gives

$$\mathbf{H}_{\text{ex}} = \frac{2Z\mathcal{J}}{\mu_0 N g^2 \mu_B^2} \left[\mathbf{M} + \frac{R_n^2}{6} \nabla^2 \mathbf{M} \right]. \quad (3.67)$$

The first term is the effective field found in the previous section. The second term is a new contribution arising from the non-uniformity of the magnetization.

3.6 Magnetocrystalline Anisotropy

If the orbital of an electron is not spherically symmetric, the energy of the state will depend on the orientation of the orbital with respect to surrounding ions in the crystal. Interaction between the spin and orbital magnetic moments (spin-orbit coupling) will then cause the energy of the net moment of the ion to depend on its orientation with respect to the major axes of the crystal. The orientation-dependent contribution to the total energy is called the *magnetocrystalline anisotropy* energy, \mathcal{E}_a .

In YIG, the magnetic moment comes from Fe^{3+} ions in the ground state ${}^6S_{5/2}$. Since the ground state has no orbital angular momentum, there should be no spin-orbit coupling and hence no anisotropy. Experimentally, however, a small anisotropy energy contribution is present. This is probably due to small spin-orbit interactions among the electronic substates neglected in the Russell-Saunders coupling scheme [13] (this coupling scheme is used to construct the Hund-rule ground state; see Section 1.5).

3.6.1 Uniaxial Anisotropy

Uniaxial anisotropy can result from growth-induced stress in thin films and occurs naturally in hexagonal crystals. It is characterized by a single axis corresponding to either a maximum or minimum of energy. If the axis corresponds to maximum energy it is referred to as a “hard” axis; if it corresponds to minimum energy it is called an “easy” axis.

The crystal is assumed to appear the same, regardless of which way you look along the hard or easy axis. Because of this symmetry, the energy should be the same whether the magnetization is up or down along the axis. Conventionally, an even power series in $\sin \theta$ is used:

$$W_{au} = K_{u1} \sin^2 \theta + K_{u2} \sin^4 \theta + \cdots \quad (3.68)$$

It is often convenient to express the *anisotropy energy density* in terms of direction cosines, α_i , as defined in Figure 3.12, where the symmetry axis is taken

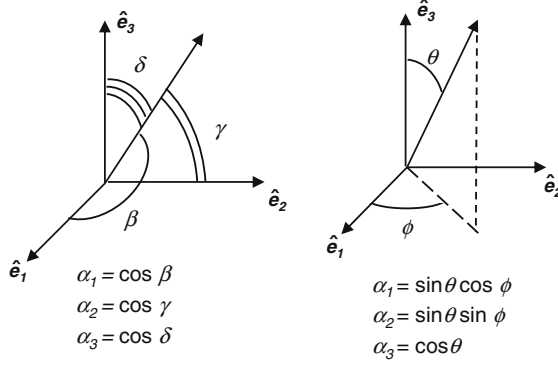


Fig. 3.12. Definitions of direction cosines.

to be along $\hat{\mathbf{e}}_3$. The magnetization components are related to the direction cosines by

$$\alpha_1 = \frac{M_1}{M_S}, \quad \alpha_2 = \frac{M_2}{M_S}, \quad \alpha_3 = \frac{M_3}{M_S}, \quad (3.69)$$

where M_i is the component of \mathbf{M} along the i th axis and M_S is the magnitude of the total magnetization vector. (M_S is sometimes called the *saturation magnetization* since it is the value of net magnetization exhibited when an external field is applied that is strong enough to completely orient all magnetic domains.) The anisotropy energy density can be written explicitly in terms of the magnetization components using the direction cosine definitions (3.69):

$$W_{au} = K_{u1}(1 - M_3^2/M_S^2) + K_{u2}(1 - M_3^2/M_S^2)^2 + \dots \quad (3.70)$$

Since the presence of a magnetic field also causes an orientation-dependent energy, we can model the effects of anisotropy by introducing an *effective anisotropy field*, \mathbf{H}_k . In analogy with (3.11) and (3.57), we define

$$\mathbf{H}_k = -\frac{1}{\mu_0} \frac{\partial W_a}{\partial \mathbf{M}}. \quad (3.71)$$

To lowest order, the effective uniaxial anisotropy field is, therefore,

$$\begin{aligned}\mathbf{H}_{ku} &= -\frac{K_{u1}}{\mu_0} \left[\hat{\mathbf{e}}_1 \frac{\partial}{\partial M_1} + \hat{\mathbf{e}}_2 \frac{\partial}{\partial M_2} + \hat{\mathbf{e}}_3 \frac{\partial}{\partial M_3} \right] \left[1 - \frac{M_3^2}{M_S^2} \right] \\ &= \frac{2K_{u1}M_3}{\mu_0 M_S^2} \hat{\mathbf{e}}_3.\end{aligned} \quad (3.72)$$

In the case of magnetic resonance and spin waves, the total instantaneous magnetization can be expressed as the sum of a large equilibrium component and a small time-varying component:

$$\mathbf{M} = \mathbf{M}_0 + \mathbf{m}(t). \quad (3.73)$$

If \mathbf{M}_0 is parallel to the $\hat{\mathbf{e}}_3$ axis, we have

$$\mathbf{M} \approx M_S \hat{\mathbf{e}}_3 + \mathbf{m}(t), \quad (3.74)$$

where $\mathbf{m}(t)$ is perpendicular to $\hat{\mathbf{e}}_3$ to lowest order. The anisotropy field, is therefore,

$$\mathbf{H}_{ku} = \frac{2K_{u1}}{\mu_0 M_S} \hat{\mathbf{e}}_3. \quad (3.75)$$

On the other hand, if \mathbf{M}_0 is perpendicular to $\hat{\mathbf{e}}_3$, only the time-varying component contributes to \mathbf{H}_{ku} . For definiteness, let

$$\mathbf{M} \approx M_S \hat{\mathbf{e}}_1 + m_2(t) \hat{\mathbf{e}}_2 + m_3(t) \hat{\mathbf{e}}_3. \quad (3.76)$$

The anisotropy field in this case is

$$\mathbf{h}_{ku}(t) = \frac{2K_{u1}m_3(t)}{\mu_0 M_S^2} \hat{\mathbf{e}}_3. \quad (3.77)$$

3.6.2 Cubic Anisotropy

Because of symmetry, the general form for the anisotropy energy density of cubic crystals must satisfy the following requirements:

- (a) Reversal of \mathbf{M} must not affect the anisotropy energy density. It follows that W_a must be a function of even powers of the direction cosines, α_i .
- (b) W_a must be invariant under the interchange of any two axes.

A function that satisfies these two conditions to sixth order is

$$W_{ac} = K_{c1}(\alpha_1^2\alpha_2^2 + \alpha_2^2\alpha_3^2 + \alpha_3^2\alpha_1^2) + K_{c2}\alpha_1^2\alpha_2^2\alpha_3^2 + \dots \quad (3.78)$$

This can also be expressed in terms of the components of the magnetization:

$$W_{ac} = \frac{K_{c1}}{M_S^4}[M_1^2M_2^2 + M_2^2M_3^2 + M_3^2M_1^2] + \frac{K_{c2}}{M_S^6}M_1^2M_2^2M_3^2 + \dots \quad (3.79)$$

To lowest order, the effective anisotropy field is

$$\begin{aligned} H_{kc} &= -\frac{K_{c1}}{\mu_0 M_S^4} \frac{\partial}{\partial \mathbf{M}} [M_1^2M_2^2 + M_2^2M_3^2 + M_3^2M_1^2] \\ &= -\frac{2K_{c1}}{\mu_0 M_S^4} \begin{bmatrix} M_1(M_2^2 + M_3^2) \\ M_2(M_3^2 + M_1^2) \\ M_3(M_1^2 + M_2^2) \end{bmatrix}. \end{aligned} \quad (3.80)$$

Again assuming \mathbf{M} can be expressed as the sum of a static equilibrium component and a small time-dependent perturbation (cf. (3.73)) and keeping terms to lowest order in the perturbation \mathbf{m} gives [14]

$$H_{kc} = -\frac{2K_{c1}}{\mu_0 M_S^4} \begin{bmatrix} M_{01}(M_{02}^2 + M_{03}^2) \\ M_{02}(M_{03}^2 + M_{01}^2) \\ M_{03}(M_{01}^2 + M_{02}^2) \end{bmatrix} + \bar{\mathbf{N}}^a \cdot \mathbf{m}, \quad (3.81)$$

where the off-diagonal elements of the anisotropy tensor $\bar{\mathbf{N}}^a$ are

$$N_{ij}^a = -\frac{4K_{c1}}{\mu_0 M_S^4} M_{0i} M_{0j}; \quad i \neq j \quad (3.82a)$$

and the diagonal elements are

$$N_{ii}^a = -\frac{4K_{c1}}{\mu_0 M_S^4} [M_S^2 - M_{0i}^2]. \quad (3.82b)$$

3.6.3 Coordinate Transformations⁷

It is important to note that the anisotropy fields given in the previous section are expressed in terms of the principal coordinate system of the crystal. This may not always correspond to the most convenient coordinate system for problem analysis. In particular, it is often convenient to choose a coordinate system for which the external applied field is oriented along the $\hat{\mathbf{e}}'_3$ axis and the $\hat{\mathbf{e}}'_1$ or $\hat{\mathbf{e}}'_2$ axis has a convenient orientation with respect to the sample shape. We will now show how to transform vectors and tensors between the two coordinate systems.

Clearly, a vector \mathbf{a} can be expressed in terms of the basis vectors in either coordinate system:

$$\mathbf{a} = a_i \hat{\mathbf{e}}_i = a'_j \hat{\mathbf{e}}'_j, \quad (3.83)$$

where summation over repeated indices is assumed.⁸ In particular, the basis vectors in one system can be expressed in terms of the basis vectors in the other system. Let

$$\hat{\mathbf{e}}'_j = T_{jk} \hat{\mathbf{e}}_k. \quad (3.84)$$

⁷ Coordinate transformations are described in detail by Goldstein et al. [15] and Matthews and Walker [16].

⁸ In repeated index notation, a sum over any index that appears twice in a given term is implied. Thus, $a_i b_j$ is one term, but $a_i b_i \equiv \sum_{i=1}^3 a_i b_i$ is the sum of three terms.

To find the elements of the transformation matrix T_{jk} , dot $\hat{\mathbf{e}}_i$ into both sides of (3.84):

$$\begin{aligned}\hat{\mathbf{e}}'_j \cdot \hat{\mathbf{e}}_i &= T_{jk} \hat{\mathbf{e}}_k \cdot \hat{\mathbf{e}}_i \\ &= T_{jk} \delta_{ki}\end{aligned}$$

or

$$T_{ji} = \hat{\mathbf{e}}'_j \cdot \hat{\mathbf{e}}_i. \quad (3.85)$$

Here, δ_{ij} is the *Kronecker delta* and is equal to 1 when $i = j$ and 0 otherwise. This symbol conveniently expresses the orthogonality between the basis vectors in the crystal system, $\hat{\mathbf{e}}_i$. If both sets of basis vectors are required to be orthogonal, then

$$\begin{aligned}\hat{\mathbf{e}}'_i \cdot \hat{\mathbf{e}}'_j &= (T_{il} \hat{\mathbf{e}}_l) \cdot (T_{jk} \hat{\mathbf{e}}_k) \\ &= T_{il} \hat{\mathbf{e}}_l \cdot \hat{\mathbf{e}}_k T_{jk} \\ &= T_{il} T_{jk} \delta_{lk} \\ \delta_{ij} &= T_{ik} T_{jk} = T_{ik} T_{kj}^T.\end{aligned} \quad (3.86)$$

The Kronecker delta on the left side describes the elements of the identity matrix, while the right side describes the matrix multiplication between $\bar{\mathbf{T}}$ and its transpose $\bar{\mathbf{T}}^T$. If $\bar{\mathbf{T}} \cdot \bar{\mathbf{T}}^T = \bar{\mathbf{I}}$, then

$$\bar{\mathbf{T}}^T = \bar{\mathbf{T}}^{-1}. \quad (3.87)$$

A real matrix with this property is said to be *orthogonal*.

To transform a vector, we write

$$\begin{aligned}a_i \hat{\mathbf{e}}_i &= a'_j \hat{\mathbf{e}}'_j \\ &= a'_j T_{jk} \hat{\mathbf{e}}_k.\end{aligned} \quad (3.88)$$

Next, pick out the l th component by dotting $\hat{\mathbf{e}}_l$ into both sides:

$$\begin{aligned}a_i \hat{\mathbf{e}}_l \cdot \hat{\mathbf{e}}_i &= a'_j T_{jk} \hat{\mathbf{e}}_l \cdot \hat{\mathbf{e}}_k \\ a_i \delta_{li} &= a'_j T_{jk} \delta_{lk} \\ a_l &= a'_j T_{jl} = T_{lj}^T a'_j,\end{aligned} \quad (3.89a)$$

or, in vector notation:

$$\mathbf{a} = \bar{\mathbf{T}}^T \cdot \mathbf{a}' \quad (3.89b)$$

and

$$\mathbf{a}' = \bar{\mathbf{T}} \cdot \mathbf{a}. \quad (3.89c)$$

The transformation of tensors such as $\bar{\mathbf{N}}^a$ is accomplished as follows:

$$\begin{aligned}
 \mathbf{h}_k &= \bar{\mathbf{N}}^a \cdot \mathbf{m} \\
 \bar{\mathbf{T}} \cdot \mathbf{h}_k &= \bar{\mathbf{T}} \cdot \bar{\mathbf{N}}^a \cdot \bar{\mathbf{T}}^{-1} \cdot \bar{\mathbf{T}} \cdot \mathbf{m} \\
 \mathbf{h}'_k &= [\bar{\mathbf{T}} \cdot \bar{\mathbf{N}}^a \cdot \bar{\mathbf{T}}^{-1}] \cdot \mathbf{m}' \\
 \mathbf{h}'_k &= \bar{\mathbf{N}}^{a'} \cdot \mathbf{m}',
 \end{aligned} \tag{3.90}$$

where

$$\bar{\mathbf{N}}^{a'} = \bar{\mathbf{T}} \cdot \bar{\mathbf{N}}^a \cdot \bar{\mathbf{T}}^T \tag{3.91}$$

and $\bar{\mathbf{T}}^T = \bar{\mathbf{T}}^{-1}$.

When discussing coordinate systems in crystals, it is convenient to specify a direction using the notation $[lmn]$, where l , m , and n are integers. A vector pointing in the desired direction is then given by $l\mathbf{a} + m\mathbf{b} + n\mathbf{c}$, where \mathbf{a} , \mathbf{b} , and \mathbf{c} are the basis vectors for the particular lattice type. Negative integers are denoted by placing a minus sign above the index. Thus, the direction $[\bar{1}10]$ corresponds to $-\mathbf{a} + \mathbf{b}$.

As an example of the use of coordinate transformations, let us find the cubic anisotropy field for an equilibrium magnetization along the $[111]$ direction. YIG films are commonly grown with this axis perpendicular to the film plane, as shown in Figure 3.13. Referring to the sample geometry in Figure 3.13, let us consider conversion to the following laboratory system:

$$\hat{\mathbf{e}}'_1 = \frac{1}{\sqrt{2}} [-\hat{\mathbf{e}}_1 + \hat{\mathbf{e}}_2], \tag{3.92}$$

$$\hat{\mathbf{e}}'_2 = \frac{1}{\sqrt{6}} [-\hat{\mathbf{e}}_1 - \hat{\mathbf{e}}_2 + 2\hat{\mathbf{e}}_3], \tag{3.93}$$

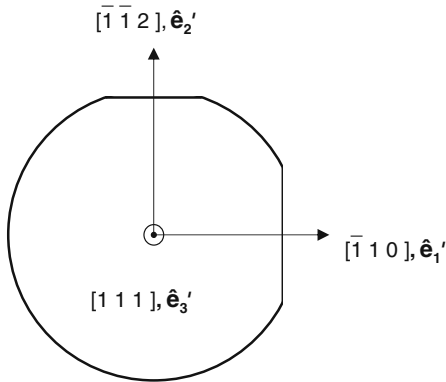


Fig. 3.13. Common geometry and orientation of gadolinium gallium garnet (GGG) substrates used to grow epitaxial YIG films. The $[\bar{1}10]$ and $[\bar{1}\bar{1}2]$ directions are perpendicular to the large and small flats, respectively.

$$\hat{\mathbf{e}}'_3 = \frac{1}{\sqrt{3}} [\hat{\mathbf{e}}_1 + \hat{\mathbf{e}}_2 + \hat{\mathbf{e}}_3]. \quad (3.94)$$

Using Eq. (3.85) for the elements of the transformation matrix gives

$$\bar{\mathbf{T}} = \begin{bmatrix} -\frac{1}{\sqrt{2}} & \frac{1}{\sqrt{2}} & 0 \\ -\frac{1}{\sqrt{6}} & -\frac{1}{\sqrt{6}} & \frac{2}{\sqrt{6}} \\ \frac{1}{\sqrt{3}} & \frac{1}{\sqrt{3}} & \frac{1}{\sqrt{3}} \end{bmatrix}. \quad (3.95)$$

For $\mathbf{M}_0 \parallel [111]$, the components of \mathbf{M}_0 are $M_{01} = M_{02} = M_{03} = M_0/\sqrt{3}$. Substituting these values in the expressions for the effective anisotropy field (3.81) and (3.82) gives

$$\mathbf{H}_k = \mathbf{H}_{0k} + \bar{\mathbf{N}}^a \cdot \mathbf{m}, \quad (3.96)$$

where

$$\mathbf{H}_{0k} = -\frac{4K_{c1}}{2\mu_0 M_S} \frac{1}{\sqrt{3}} \begin{bmatrix} 1 \\ 1 \\ 1 \end{bmatrix} \quad (3.97)$$

and

$$\bar{\mathbf{N}}^a = -\frac{4K_{c1}}{3\mu_0 M_S^2} \begin{bmatrix} 1 & 1 & 1 \\ 1 & 1 & 1 \\ 1 & 1 & 1 \end{bmatrix}. \quad (3.98)$$

In the transformed coordinate system, we have

$$\mathbf{H}'_{0k} = \bar{\mathbf{T}} \cdot \mathbf{H}_{0k} = -\frac{4K_{c1}}{3\mu_0 M_S} \begin{bmatrix} 0 \\ 0 \\ 1 \end{bmatrix} \quad (3.99)$$

and

$$\bar{\mathbf{N}}^{a'} = \bar{\mathbf{T}} \cdot \bar{\mathbf{N}}^a \cdot \bar{\mathbf{T}}^T = -\frac{4K_{c1}}{\mu_0 M_S^2} \begin{bmatrix} 0 & 0 & 0 \\ 0 & 0 & 0 \\ 0 & 0 & 1 \end{bmatrix}. \quad (3.100)$$

Thus, the static anisotropy field is parallel or antiparallel to the equilibrium magnetization, depending on the sign of K_{c1} . Likewise, the time-varying anisotropy field is also parallel or antiparallel to \mathbf{M}_0 . However, $m_z(t)$ is a second-order quantity (proportional to θ^2 for small θ) and hence can be neglected to first order. For YIG, $K_{c1} = -610 \text{ J/m}^3$ at room temperature (Appendix A). Thus, the first-order anisotropy field for magnetization along the $[111]$ direction is $H_{0k} = +4.62 \text{ kA/m}$ (58 Oe). Since K_{c1} is negative and $\mathbf{H}_{0k} \parallel \mathbf{M}_0$, the $[111]$ direction corresponds to an easy axis. The second-order cubic anisotropy term may not be negligible in all cases, however. The contribution of the second-order term to the anisotropy field along the $[111]$ direction is found to be

$$\mathbf{H}_{0k}^{(2)'} = -\frac{2K_{c2}}{9\mu_0 M_S} \begin{bmatrix} 0 \\ 0 \\ 1 \end{bmatrix}, \quad (3.101)$$

expressed in the laboratory coordinate system.

3.7 Polder Susceptibility Tensor⁹

We now turn our attention to obtaining the magnetic response of a ferro- or ferrimagnet to small time-varying magnetic fields. The goal will be to obtain a small-signal susceptibility that can be used in the presence of the rf and microwave fields associated with magnetic resonance and the propagation of magnetostatic waves. We begin by discussing the nonlinear equation of motion for the magnetization. The equation of motion is then linearized for small perturbations about an equilibrium (saturated) state.

3.7.1 Equation of Motion for the Magnetization

The equation of motion for the angular momentum \mathbf{J} in the presence of a magnetic field was found in Section 1.3.1 to be (cf. Eq. (1.14)):

$$\frac{d\mathbf{J}}{dt} = \gamma\mu_0\mathbf{J} \times \mathbf{H}_{\text{eff}}. \quad (3.102)$$

Here, \mathbf{H}_{eff} represents the sum of all torque-producing effective fields:

$$\mathbf{H}_{\text{eff}} = \mathbf{H} + \mathbf{H}_{\text{ex}} + \mathbf{H}_k, \quad (3.103)$$

where \mathbf{H} is the Maxwellian field and \mathbf{H}_{ex} and \mathbf{H}_k are effective fields due to exchange and anisotropy, respectively. Multiplying both sides of the equation of motion (3.102) by γN and noting that $\mathbf{M} = \gamma N\mathbf{J}$, we obtain

$$\frac{d\mathbf{M}}{dt} = \gamma\mu_0\mathbf{M} \times \mathbf{H}_{\text{eff}}. \quad (3.104)$$

This is the lossless form of the *Landau-Lifshitz* equation of motion for the magnetization. Note that although Eq. (3.67) for \mathbf{H}_{ex} contains terms proportional to both \mathbf{M} and $\nabla^2\mathbf{M}$, only the $\nabla^2\mathbf{M}$ term contributes to the torque since $\mathbf{M} \times \mathbf{M} \equiv 0$. Thus, in the present context (and in the rest of the text), we may take

$$\mathbf{H}_{\text{ex}} = \lambda_{\text{ex}}\nabla^2\mathbf{M} \quad (3.105)$$

without loss of generality, where $\lambda_{\text{ex}} = 2ZJR_n^2/(6\mu_0Ng^2\mu_B^2)$ for a simple ferromagnet¹⁰ (cf. Eq. (3.67)). The effective anisotropy field \mathbf{H}_k is obtained for a given geometry and crystal structure as discussed in the previous section.

3.7.2 Susceptibility Without Exchange or Anisotropy

Let us assume that the motion of the fields can be described as a small time-dependent perturbation added to a static equilibrium configuration. For simplicity, we first neglect \mathbf{H}_{ex} and \mathbf{H}_k . The remaining fields can be divided into static and time-varying parts as follows:

⁹ The reader may also refer to similar treatment in [17–19].

¹⁰ Equation (3.105) is also applicable to a cubic ferrimagnet, but the relationship between λ_{ex} and the microscopic parameters is more complicated.

$$\mathbf{M} = \mathbf{M}_0 + \mathbf{m}(t), \quad (3.106)$$

$$\mathbf{H} = \mathbf{H}_0 + \mathbf{h}(t). \quad (3.107)$$

Substituting these equations into the equation of motion (3.104) gives

$$\frac{d\mathbf{m}}{dt} = \gamma\mu_0[\mathbf{M}_0 \times \mathbf{H}_0 + \mathbf{M}_0 \times \mathbf{h} + \mathbf{m} \times \mathbf{H}_0 + \mathbf{m} \times \mathbf{h}]. \quad (3.108)$$

For the study of magnetic resonance and magnetostatic waves, we are primarily interested in saturated single-domain materials. Under this circumstance and with the neglect of anisotropy, the static magnetization \mathbf{M}_0 will lie parallel to the net static field \mathbf{H}_0 causing the first term on the right-hand side of the equation of motion (3.108) to vanish. Since \mathbf{m} and \mathbf{h} are both assumed to be small in magnitude when compared with the static field components, the last term in (3.108) is of second-order in small quantities and will be neglected.

For definiteness, let us assume that the static equilibrium fields lie along the $\hat{\mathbf{z}}$ direction. Also, for small deviations from equilibrium, the $\hat{\mathbf{z}}$ component of the magnetization is unchanged to first-order in small quantities so that $M_0 \approx M_S$. If the time dependence is taken to be of the form $\exp(-i\omega t)$, the linearized equation of motion for the small-signal magnetization can be written

$$-i\omega\mathbf{m} = \hat{\mathbf{z}} \times [-\omega_M\mathbf{h} + \omega_0\mathbf{m}], \quad (3.109)$$

where

$$\omega_M \equiv -\gamma\mu_0 M_S \quad (3.110)$$

and

$$\omega_0 \equiv -\gamma\mu_0 H_0. \quad (3.111)$$

Solving the linearized *torque equation* (3.109) for \mathbf{h} gives

$$\begin{bmatrix} h_x \\ h_y \end{bmatrix} = \frac{1}{\omega_M} \begin{bmatrix} \omega_0 & i\omega \\ -i\omega & \omega_0 \end{bmatrix} \begin{bmatrix} m_x \\ m_y \end{bmatrix}. \quad (3.112)$$

The susceptibility tensor can be identified by inverting this equation to obtain

$$\mathbf{m} = \bar{\chi} \cdot \mathbf{h}, \quad (3.113)$$

where the *Polder susceptibility tensor* is given by

$$\bar{\chi} = \begin{bmatrix} \chi & -i\kappa \\ i\kappa & \chi \end{bmatrix} \quad (3.114)$$

and

$$\chi = \frac{\omega_0\omega_M}{\omega_0^2 - \omega^2}, \quad (3.115)$$

$$\kappa = \frac{\omega\omega_M}{\omega_0^2 - \omega^2}. \quad (3.116)$$

ω_0 is also referred to as the ferromagnetic *resonance frequency*. We observe that the elements of $\bar{\chi}$ can become infinite as $\omega \rightarrow \omega_0$. This mathematical anomaly is typical of idealized lossless systems subject to periodic excitations. The introduction of energy dissipation or damping will address the singularity but will not change the value of the resonance frequency to lowest order (cf. Section 3.8).

3.7.3 Susceptibility with Exchange and Anisotropy

To include exchange and anisotropy in the linearized torque equation, we must also separate \mathbf{H}_{ex} and \mathbf{H}_k in terms of static and time-varying components:

$$\mathbf{H}_k = \mathbf{H}_{0k} + \mathbf{h}_k(t), \quad (3.117)$$

$$\mathbf{H}_{\text{ex}} = \mathbf{H}_{0\text{ex}} + \mathbf{h}_{\text{ex}}(t). \quad (3.118)$$

Including these fields along with \mathbf{H} and \mathbf{M} from (3.106) and (3.107) in the torque equation (3.104) gives

$$\begin{aligned} \frac{1}{\gamma\mu_0} \frac{d\mathbf{m}}{dt} = & \mathbf{M}_0 \times [\mathbf{H}_0 + \mathbf{H}_{0k} + \mathbf{H}_{0\text{ex}}] + \mathbf{M}_0 \times [\mathbf{h} + \mathbf{h}_k + \mathbf{h}_{\text{ex}}] \\ & + \mathbf{m} \times [\mathbf{H}_0 + \mathbf{H}_{0k} + \mathbf{H}_{0\text{ex}}] + \mathbf{m} \times [\mathbf{h} + \mathbf{h}_k + \mathbf{h}_{\text{ex}}]. \end{aligned} \quad (3.119)$$

As previously mentioned, we are primarily interested in single-domain materials; i.e., configurations for which \mathbf{M}_0 is spatially uniform. In such cases, $\mathbf{H}_{0\text{ex}}$ vanishes according to the exchange field expression (3.105). The remainder of the first term on the right-hand side also vanishes since the equilibrium configuration is characterized by the condition $\mathbf{M}_0 \times (\mathbf{H}_0 + \mathbf{H}_{0k}) = 0$. However, it is convenient to assume $\mathbf{M}_0 \parallel \mathbf{H}_0$. This is rigorously true only for directions of high-crystal symmetry, where \mathbf{H}_{0k} is also parallel to \mathbf{M}_0 and \mathbf{H}_0 . It is a good approximation, however, whenever $|\mathbf{H}_0| \gg |\mathbf{H}_{0k}|$. Making these assumptions, neglecting terms of second-order in small quantities, and assuming harmonic time dependence enables us to write the torque equation (3.119) in the linearized form

$$i\Omega\mathbf{m} = \hat{\mathbf{z}} \times \left[\mathbf{h} + \lambda_{\text{ex}} \nabla^2 \mathbf{m} + \bar{\mathbf{N}}^a \cdot \mathbf{m} - (Z_0 + Z_k) \mathbf{m} \right], \quad (3.120)$$

where we have introduced several new quantities:

$$\Omega = \omega/\omega_M, \quad (3.121)$$

$$Z_0 = H_0/M_S, \quad (3.122)$$

and

$$Z_k = \mathbf{H}_{0k} \cdot \hat{\mathbf{z}}/M_S. \quad (3.123)$$

Here, we have again chosen the coordinate system so that the equilibrium magnetization points along the $\hat{\mathbf{z}}$ direction. Keeping only the $\hat{\mathbf{z}}$ component of

\mathbf{H}_{0k} is justified since the other components give rise to m_z , which we neglect as a second-order quantity. The inclusion of higher order terms leads to nonlinear excitations which are described in further detail in Chapter 9.

Solving for \mathbf{h} in the linearized equation (3.120) gives

$$\mathbf{h} = \bar{\mathbf{A}}_{\text{op}} \cdot \mathbf{m}, \quad (3.124)$$

where

$$\bar{\mathbf{A}}_{\text{op}} = \begin{bmatrix} Z_0 + Z_k - N_{xx}^a - \lambda_{\text{ex}} \nabla^2 & i\Omega - N_{xy}^a \\ -i\Omega - N_{yx}^a & Z_0 + Z_k - N_{yy}^a - \lambda_{\text{ex}} \nabla^2 \end{bmatrix}. \quad (3.125)$$

The presence of the differential operators significantly complicates the process of taking the inverse to obtain the susceptibility. An alternative approach to mode analysis that can be taken in this case is to expand the small-signal magnetization in the eigenvectors of $\bar{\mathbf{A}}_{\text{op}}$ [20–22]. If exchange is neglected, the operator (3.125) can be inverted to obtain the generalized Polder tensor with anisotropy:

$$\bar{\chi} = \frac{1}{D} \begin{bmatrix} Z_0 + Z_k - N_{yy}^a & -i\Omega + N_{xy}^a \\ i\Omega + N_{yx}^a & Z_0 + Z_k - N_{xx}^a \end{bmatrix}, \quad (3.126a)$$

where

$$D = [Z_0 + Z_k - N_{yy}^a][Z_0 + Z_k - N_{xx}^a] - [i\Omega + N_{yx}^a][-i\Omega + N_{xy}^a]. \quad (3.126b)$$

Resonant uniform precession in systems with crystalline anisotropy will occur when $D = 0$. As an example, consider a magnetic system with uniaxial anisotropy and an easy axis transverse to \mathbf{H}_0 . For definiteness, let $\mathbf{H}_0 = H_0 \hat{\mathbf{z}}$ and let the easy axis be along $\hat{\mathbf{x}}$. Following an analysis similar to that in Section 3.6.1, we find that the anisotropy field is $\mathbf{h}_{ku} = H_{ku} m_x / M_S \hat{\mathbf{x}}$. It follows that $N_{xx}^a = H_k / M_S$, $N_{xy}^a = N_{yx}^a = N_{yy}^a = Z_k = 0$, and the resonant frequency found by setting (3.126b) to zero is $\omega_R = -\gamma \mu_0 \sqrt{H_0(H_0 - H_k)}$, where $H_k \triangleq 2K_{u1} / (\mu_0 M_S)$ [23, p. 255]. This is a typical configuration considered for measurements of *transverse susceptibility* of fine particles where we sweep the DC-applied field and measure the variation in the magnetization along the direction of an applied small signal AC field. The peaks observed are in fact associated with a ferromagnetic resonance at zero frequency which occur when $H_0 = H_k$ [24].

3.8 Magnetic Damping

According to the equation of motion (3.104), once the magnetization is misaligned, it forever precesses about an applied magnetic field; it is never able to achieve the lowest energy configuration with \mathbf{M} parallel to \mathbf{H} . This rather

unintuitive result is obtained because no sources of magnetic damping have been included in the model.

Physically, damping results from a transfer of energy from the precessing spin system to lattice vibrations. The energy transfer can occur directly or involve intermediate spin wave states. One mechanism of direct coupling between the magnetic system and lattice vibrations can be visualized in the following way [19, p. 118]. Spins located in different parts of a crystal interact via their dipolar fields. Since the strength of this interaction depends on the distance between the spins, lattice vibrations will modulate the dipolar interaction giving rise to spin–lattice coupling. Direct coupling to the lattice can also be mediated by spin–orbit interactions.

To phenomenologically introduce loss into the torque equation, we need a component of $d\mathbf{M}/dt$ in the $-\theta$ direction; i.e., in a direction seeking to minimize the cone angle and drive the magnetization toward an equilibrium state with \mathbf{M} parallel to \mathbf{H} . One possible choice introduced by Landau and Lifshitz [25] is a term proportional to $-(\mathbf{M} \times \mathbf{M} \times \mathbf{H}_{\text{eff}})$ (Figure 3.14):

$$\frac{d\mathbf{M}}{dt} = \gamma\mu_0(\mathbf{M} \times \mathbf{H}_{\text{eff}}) + \frac{\lambda\gamma\mu_0}{M_S}\mathbf{M} \times (\mathbf{M} \times \mathbf{H}_{\text{eff}}). \quad (3.127)$$

An alternate damping term suggested by Gilbert [26] is

$$\frac{d\mathbf{M}}{dt} = \gamma\mu_0(\mathbf{M} \times \mathbf{H}_{\text{eff}}) + \frac{\alpha}{M_S}\left(\mathbf{M} \times \frac{d\mathbf{M}}{dt}\right). \quad (3.128)$$

If both λ and α are small so that the direction of $d\mathbf{M}/dt$ is only slightly perturbed by the presence of the loss terms, the Landau–Lifshitz and Gilbert forms are equivalent. The Gilbert form is particularly convenient mathematically as we will now demonstrate. Following the linearization procedure introduced in the previous section and neglecting exchange and anisotropy gives

$$i\omega\mathbf{m} = \hat{\mathbf{z}} \times [\omega_M\mathbf{h} - (\omega_0 - i\alpha\omega)\mathbf{m}]. \quad (3.129)$$

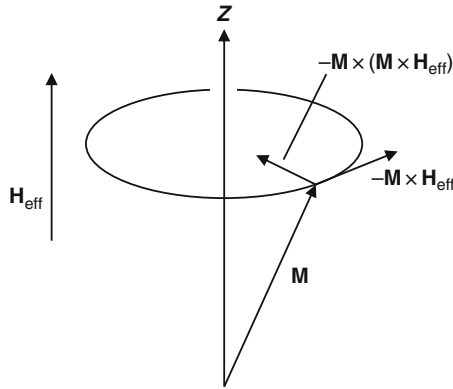


Fig. 3.14. Illustration of the damping torque introduced by Landau and Lifshitz.

Comparison with the linearized equation without loss (3.109) shows that the effect of loss is simply to add an imaginary part to the normalized field. Thus, loss can be introduced into the Polder tensor (3.114) by making the substitution $\omega_0 \rightarrow (\omega_0 - i\omega\alpha)$.

To investigate the effects of damping, let us consider the response to an external excitation of the form

$$\mathbf{h}_{\text{ext}}(t) = \hat{\mathbf{x}} \delta(t). \quad (3.130)$$

Since the susceptibility tensor (3.114) relating \mathbf{m} and \mathbf{h} is given in the frequency domain, let us relate $\mathbf{h}_{\text{ext}}(t)$ and $\mathbf{h}_{\text{ext}}(\omega)$ with the Fourier transform pair

$$f(t) = \int_{-\infty}^{\infty} \frac{d\omega}{2\pi} e^{i\omega t} f(\omega), \quad (3.131)$$

$$f(\omega) = \int_{-\infty}^{\infty} dt e^{i\omega t} f(t). \quad (3.132)$$

Using (3.132) to take the Fourier transform of the excitation (3.130) gives

$$\mathbf{h}_{\text{ext}}(\omega) = \begin{bmatrix} 1 \\ 0 \end{bmatrix}. \quad (3.133)$$

The magnetic response is, therefore

$$\begin{bmatrix} m_x \\ m_y \end{bmatrix} = \begin{bmatrix} \chi & -i\kappa \\ i\kappa & \chi \end{bmatrix} \begin{bmatrix} 1 \\ 0 \end{bmatrix} \quad (3.134a)$$

or

$$m_x = \chi, \quad (3.134b)$$

$$m_y = i\kappa. \quad (3.134c)$$

The time-domain response of m_x is given by

$$m_x(t) = \int_{-\infty}^{\infty} \frac{d\omega}{2\pi} e^{-i\omega t} \frac{\omega_0 \omega_M}{\omega_0^2 - \omega^2}. \quad (3.135)$$

Performing a partial fraction expansion of χ and introducing loss gives

$$m_x(t) = \frac{\omega_M}{2} \int_{-\infty}^{\infty} \frac{d\omega}{2\pi} e^{i\omega t} \left[\frac{1}{\omega_0 + \omega(1 - i\alpha)} + \frac{1}{\omega_0 - \omega(1 + i\alpha)} \right]. \quad (3.136)$$

Multiplying and dividing the first term by $1 + i\alpha$ and the second term by $1 - i\alpha$ and keeping only terms linear in α gives

$$m_x(t) \approx \frac{\omega_M}{2} \int_{-\infty}^{\infty} \frac{d\omega}{2\pi} e^{i\omega t} \left[\frac{1+i\alpha}{\omega + \omega_0(1+i\alpha)} - \frac{1-i\alpha}{\omega - \omega_0(1-i\alpha)} \right]. \quad (3.137)$$

The integrand has poles at $\omega = -\omega_0 - i\alpha\omega_0$ and $\omega = \omega_0 - i\alpha\omega_0$ as shown in Figure 3.15. The path of integration is along the real axis from $-\infty$ to ∞ . However, for $t < 0$, the integration contour can be closed in the upper half-plane at a very large radius without affecting the value of the integral since the integrand vanishes as $\exp(-\text{Im}\{\omega\}|t|)/|\omega|$ along this contour. Similarly, for $t > 0$ the contour can be closed at a large radius in the lower half-plane since the integrand vanishes according to the same factor along this contour. Having constructed these auxiliary closed integration contours, the integral in the expression for $m_x(t)$ (3.137) can be evaluated using the method of residues. In particular,

$$\oint_C f(z)dz = 2\pi i \sum_k \text{Res}(f(z_k)), \quad (3.138)$$

where $\text{Res} f(z_k)$ is the residue of the pole located at $z = z_k$. For simple first-order poles we have

$$\text{Res} f(z_k) = \lim_{z \rightarrow z_k} (z - z_k) f(z). \quad (3.139)$$

Applying the residue theorem from Eqs. (3.138) and (3.139) to the evaluation of Eq. (3.137) for $m_x(t)$ gives

$$m_x(t) = -\frac{i\omega_M}{2} \left[(1+i\alpha)e^{i\omega_0(1+i\alpha)t} - (1-i\alpha)e^{-i\omega_0(1-i\alpha)t} \right] u(t), \quad (3.140)$$

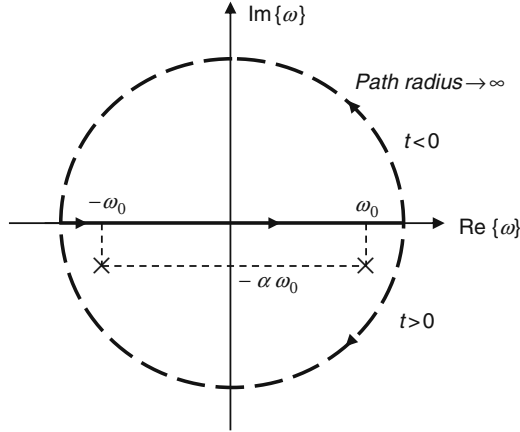


Fig. 3.15. Complex integration contours used in the evaluation of the impulse response (3.137). (Reprinted with permission from [27]. Copyright 1996, American Institute of Physics.)

where $u(t)$ is the unit step function and there is an overall minus sign since the integration contour is clockwise and hence opposite to that assumed in the residue theorem (3.138). After rearranging terms, Eq. (3.140) for $m_x(t)$ can be written

$$m_x(t) = \omega_M e^{-\alpha\omega_0 t} [\sin(\omega_0 t) + \alpha \cos(\omega_0 t)] u(t). \quad (3.141)$$

For α sufficiently small, this is approximately

$$m_x(t) \approx \omega_M e^{-\alpha\omega_0 t} \sin(\omega_0 t) u(t). \quad (3.142)$$

A similar analysis for $m_y(t)$ yields

$$m_y(t) \approx -\omega_M e^{-\alpha\omega_0 t} \cos(\omega_0 t) u(t). \quad (3.143)$$

The motion described by Eqs. (3.142) and (3.143) for $m_x(t)$ and $m_y(t)$, respectively, is shown in Figure 3.16. In response to the impulse, the magnetization tilts away from the $\hat{\mathbf{z}}$ axis in the direction of $-\mathbf{M} \times \mathbf{h}_{\text{ext}}$ and then spirals back to equilibrium, with the transverse component decaying in amplitude according to the factor $\exp(-\alpha\omega_0 t)$.

Experimentally, the magnetic damping parameters of magnetic materials used in microwave devices are commonly determined from *ferromagnetic resonance* measurements. In these measurements, a small sample is placed in a microwave cavity and an applied field is swept through the resonance ($\omega_0 = \omega$)

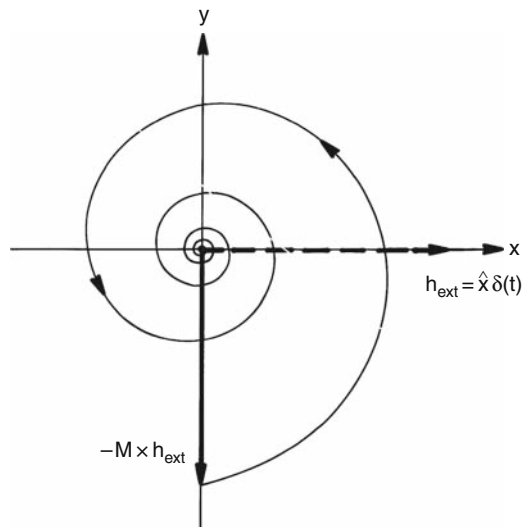


Fig. 3.16. The response of the small-signal magnetization to an impulse driving the field along the $\hat{\mathbf{x}}$ axis. (Reprinted with permission from [27]. Copyright 1996, American Institute of Physics.)

of the susceptibility (3.114). The microwave power absorbed by the cavity exhibits a peak when the resonance condition is satisfied. The width of this peak is proportional to the damping parameter α , as we shall now show.

It is convenient to first find the eigenvalues Λ and eigenvectors \mathbf{C} of $\bar{\chi}$, i.e., we want to solve

$$\bar{\chi} \cdot \mathbf{C} = \Lambda \mathbf{C}. \quad (3.144)$$

The possible values of Λ are determined by

$$\det [\bar{\chi} - \Lambda \mathbf{I}] = \begin{vmatrix} \chi - \Lambda & -i\kappa \\ i\kappa & \chi - \Lambda \end{vmatrix} = 0 \quad (3.145)$$

or

$$(\chi - \Lambda)^2 - \kappa^2 = 0. \quad (3.146)$$

Solving for Λ gives

$$\begin{aligned} \Lambda_{\pm} &= \chi \pm \kappa \\ &= \frac{Z}{Z^2 - \Omega^2} \pm \frac{\Omega}{Z^2 - \Omega^2} \\ &= \frac{1}{Z \mp \Omega}. \end{aligned} \quad (3.147)$$

The normalized eigenvectors corresponding to these eigenvalues are found to be

$$\mathbf{C}_{\pm} = \frac{1}{\sqrt{2}} \begin{bmatrix} 1 \\ \pm i \end{bmatrix}. \quad (3.148)$$

Assuming a time dependence of the form $\exp(-i\omega t)$ and taking the real parts of the complex eigenvector expressions (3.148) gives the instantaneous expressions

$$\mathbf{C}_{\pm} = \frac{1}{\sqrt{2}} [\hat{\mathbf{x}} \cos \omega t \pm \hat{\mathbf{y}} \sin \omega t]. \quad (3.149)$$

These vectors represent resonant and nonresonant precession as shown in Figure 3.17.

If we now choose $\mathbf{h}_{\pm} = h_0 \mathbf{C}_{\pm}$, then the magnetization is

$$\begin{aligned} \mathbf{m}_{\pm} &= \bar{\chi} \cdot \mathbf{h}_{\pm} \\ &= h_0 \bar{\chi} \cdot \mathbf{C}_{\pm} \\ &= h_0 \Lambda_{\pm} \mathbf{C}_{\pm} \\ \therefore \mathbf{m}_{\pm} &= \Lambda_{\pm} \mathbf{h}_{\pm} \equiv \chi_{\pm} \mathbf{h}_{\pm}. \end{aligned} \quad (3.150)$$

Thus, the eigenvector representation permits the use of the scalar susceptibility χ_{\pm} in place of the more complicated tensor susceptibility $\bar{\chi}$.

Consider the behavior of the resonant susceptibility with loss:

$$\begin{aligned} \chi_{+} &= \frac{1}{Z - i\Omega\alpha - \Omega}, \\ &= \chi'_{+} + i\chi''_{+}, \end{aligned} \quad (3.151)$$

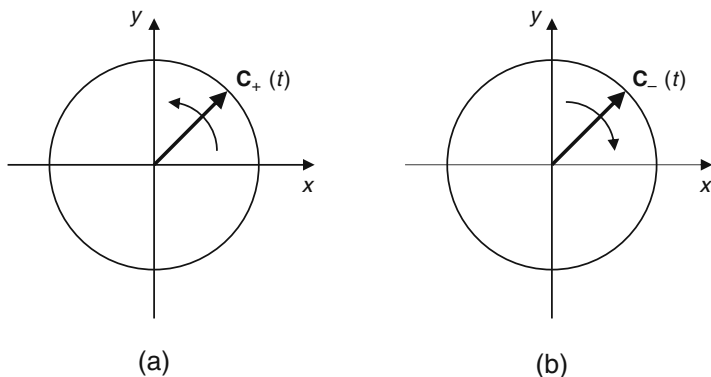


Fig. 3.17. Eigenvectors of the susceptibility tensor representing (a) resonant and (b) non-resonant circular precession.

where

$$\chi'_+ = \text{Re}\{\chi_+\} = \frac{Z - \Omega}{(Z - \Omega)^2 + \Omega^2 \alpha^2}, \quad (3.152)$$

$$\chi''_+ = \text{Im}\{\chi_+\} = \frac{\Omega \alpha}{(Z - \Omega)^2 + \Omega^2 \alpha^2}. \quad (3.153)$$

These functions are plotted in Figure 3.18. The imaginary part of χ_+ is responsible for damping. The maximum value of χ''_+ as the field Z is varied is $1/(\Omega \alpha)$ and occurs when $Z - \Omega = 0$. The full width at half-maximum ΔZ is obtained as follows:

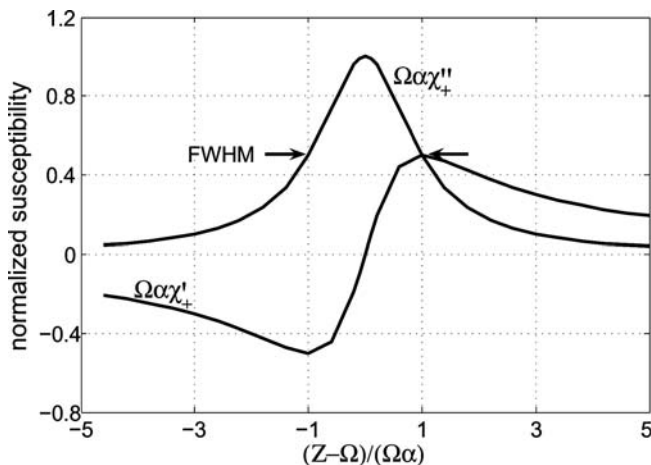


Fig. 3.18. Real and imaginary parts of the resonant susceptibility χ_r in the presence of damping.

$$\frac{\Omega\alpha}{(\Delta Z/2)^2 + \alpha^2\Omega^2} = \frac{1}{2\Omega\alpha}. \quad (3.154)$$

Solving for ΔZ gives

$$\Delta Z = 2\Omega\alpha, \quad (3.155a)$$

$$\Delta B = -\frac{2\omega\alpha}{\gamma}, \quad (3.155b)$$

or

$$\Delta H = -\frac{2\omega\alpha}{\gamma\mu_0}, \quad (3.155c)$$

where ΔZ , ΔB , and ΔH correspond to the full resonance line width at half-maximum.

Recalling Eqs. (3.142) and (3.143), the amplitude of the small-signal magnetization is of the form

$$|\mathbf{m}| = m_0 e^{-\alpha\omega_0 t}. \quad (3.156)$$

Substituting the full width at half maximum from (3.155b) and using the fact that $\omega = \omega_0$ at resonance gives

$$|\mathbf{m}| = m_0 e^{\frac{\gamma\Delta B t}{2}}. \quad (3.157)$$

The normalized magnitude expressed in dB is

$$\frac{|\mathbf{m}|}{m_0}(\text{dB}) = 20 \log e^{\frac{\gamma\Delta B t}{2}}$$

or

$$\frac{|\mathbf{m}|}{m_0}(\text{dB}) = -76.4 \times 10^{10} \Delta B t, \quad (3.158)$$

where ΔB is in Teslas and t is in seconds. We define the loss parameter L as the attenuation in dB/ns:¹¹

$$L = 764\Delta B \text{ (dB/ns)}, \quad (3.159)$$

where ΔB is again given in Teslas.

Although this analysis has specifically treated the decay of the uniform precession of the magnetization in an infinite medium, the loss parameter given by (3.159) is also a good approximation for the attenuation of propagating waves in finite samples under certain conditions. In the context of traveling waves, Eq. (3.159) for the attenuation indicates that the attenuation is not fundamentally dependent on the path *length*, but on the propagation *delay* along a given path. We will examine the attenuation of propagating waves in more detail in Chapter 6.

¹¹ The analogous cgs expression is $L = 76.4 \Delta H \text{ (dB/}\mu\text{s)}$, with ΔH given in Oe.

3.9 Magnetic Switching

The susceptibilities described in earlier sections of this chapter quantify the response of a magnet to a small-signal magnetic excitation. But what would happen to \mathbf{M} if the externally applied field was large and not along the direction of \mathbf{M} ? It is natural to ask “what causes the magnetization to be oriented along a particular direction?” and “how can we control and reverse that orientation?” A popular quasi-static model for the switching of magnetic particles was introduced by Stoner and Wohlfarth [28]. While the *Stoner–Wohlfarth model* provides us with the energy landscape that favors switching, we need to solve the Landau–Lifshitz–Gilbert equation (3.128) to obtain the trajectory traced by the tip of the magnetization vector.

3.9.1 Stoner–Wohlfarth Particle

Consider a uniformly magnetized particle in the shape of a prolate ellipsoid. We further assume, as shown in Figure 3.19 that the particle has its major axis and its “easy axis” along $\hat{\mathbf{x}}$ and we apply an external field H_0 at an angle ϕ relative to $\hat{\mathbf{x}}$. As a result, the magnetization of the particle orients itself at an angle θ relative to $\hat{\mathbf{x}}$. The total energy density is the sum of the Zeeman and anisotropic contribution

$$W = -\mu_0 M_S H_x \cos \theta - \mu_0 M_S H_y \sin \theta + K \sin^2 \theta, \quad (3.160)$$

where $H_x = H_0 \cos \phi$, $H_y = H_0 \sin \phi$, and we assume a saturation magnetization M_S and an anisotropy constant K (cf. Eq. (3.68)).¹² The direction of the equilibrium magnetization is determined by the condition

$$\frac{\partial W}{\partial \theta} = 0 \quad (3.161)$$

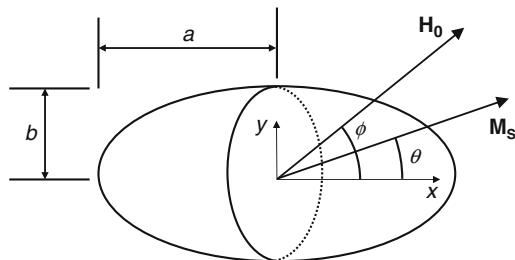


Fig. 3.19. Single domain prolate ellipsoid with a field \mathbf{H} applied at an angle ϕ with respect to the major axis.

¹² Here, K contains contributions from demagnetizing fields as well as magnetocrystalline anisotropy. Demagnetizing fields are discussed in Chapter 5, but all we need for the present discussion is that they contribute to uniaxial anisotropy in an ellipsoidal particle.

or

$$H_x \sin \theta - H_y \cos \theta + H_k \sin \theta \cos \theta = 0, \quad (3.162)$$

where we have defined

$$H_k = \frac{2K}{\mu_0 M_S}$$

analogous to Eq. (3.75). However, stability is ensured only when we also satisfy

$$\left. \frac{\partial^2 W}{\partial \theta^2} \right|_{\theta_0} > 0, \quad (3.163)$$

evaluated at angles θ_0 that satisfy (3.162). Setting the second derivative to zero yields

$$H_x \cos \theta + H_y \sin \theta + H_k \cos 2\theta = 0. \quad (3.164)$$

Equations (3.162) and (3.164) yield

$$H_x = -H_k \cos^3 \theta \quad (3.165a)$$

and

$$H_y = H_k \sin^3 \theta, \quad (3.165b)$$

which can be combined to yield the equation of an *asteroid*

$$H_x^{2/3} + H_y^{2/3} = H_k^{2/3}. \quad (3.166)$$

The Stoner–Wohlfarth asteroid separates the region where the system has two stable minima from that with a single stable minimum. We see this by applying the chain rule to calculate the slope of the asteroid curve. We find

$$\frac{dH_y}{dH_x} = \frac{dH_y}{d\theta} \frac{d\theta}{dH_x} = \tan \theta, \quad (3.167)$$

where we used Eqs. (3.165) to calculate the derivatives with respect to θ . Recall that θ also represents the direction of \mathbf{M} with respect to the easy axis. Thus, the tangent to the asteroid can be used to determine the direction of the magnetization in the presence of an applied field (cf. Problem 3.11). If the field has a magnitude and direction that lies outside the asteroid (e.g., point B), then we can draw a single tangent to the asteroid. This is seen geometrically in Figure 3.20 where we draw tangents to the upper half of the asteroid. However, if the field has a smaller magnitude and direction (e.g., point A), then the two tangents to the asteroid mark two equally stable magnetization directions that the particle can oscillate between.

To switch the magnetization of a particle from $-\hat{\mathbf{x}}$ to $\hat{\mathbf{y}}$, we must clearly apply a field that lies outside the asteroid curve, similar to that marked by point B. However, the calculations outlined here are rather simplistic as the actual task of switching a collection of magnetic particles will depend on the minima in the total energy of the system. The small signal ferromagnetic response of a collection of such particles can be estimated using expressions for the complex transverse and parallel susceptibilities [24].

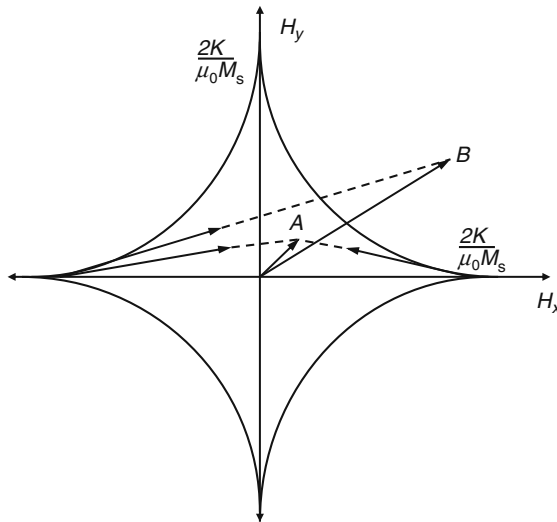


Fig. 3.20. Tangents to the Stoner–Wohlfarth asteroid (in the upper half plane) can be used to determine the stability of the resulting magnetic orientation.

3.9.2 Damped Precession

The Landau–Lifshitz equation of motion is popular among researchers involved in computational *micromagnetics*. Seminal work by Brown describes the basic physics of micromagnetics [29]. With the advent of faster computers and specialized algorithms, Eq. (3.127) has been solved for many magnetic microstructures and materials particularly useful in the data storage industry [30, 31]. The Landau–Lifshitz equation, for each micromagnetic cell, is written in discrete form as

$$\mathbf{M}_{i+1} = \mathbf{M}_i + f(\mathbf{M}_i, \mathbf{H}_i)\Delta t, \quad (3.168)$$

where $f(\mathbf{M}_i, \mathbf{H}_i)$ is merely the right-hand side of (3.127) for the i th cell at the time instant t_i , $\Delta t = t_{i+1} - t_i$ is the time step used and \mathbf{H}_i represents the effective field acting on the cell. From our previous discussion on the precession of the magnetization, we realize that Δt must be chosen smaller than $T = 2\pi/\omega_0$, where ω_0 is the Larmor precession frequency for that cell. Thus, the smallest time step allowed in a dynamic micromagnetic simulation is often determined by cells experiencing the highest effective fields. In a typical thin-film structure, these are the *stiff* cells at the boundaries with minimal contributions to the dynamic $\mathbf{M} - \mathbf{H}$ response curve. An understanding of the precessional motion can thus lead to improved algorithms suitable for use in large simulations. We also note that the use of discrete time stepping algorithms (see, e.g., Euler and Runge–Kutta methods described in [32]) have errors that accumulate and manifest themselves in long simulations. Similarly,

the damping term in (3.127) requires that we renormalize the magnetization after every time step or adopt other advanced approaches such as the *mid-point rule* which ensures stability and second-order accuracy in the numerical integration [33].

For the rest of our discussion, we consider a single magnetic moment \mathbf{M} and focus our attention on understanding the role of the damping coefficient α in the Gilbert equation

$$\frac{d\mathbf{M}}{dt} = \gamma\mu_0\mathbf{M} \times \mathbf{H}_{\text{eff}} + \frac{\alpha}{M_S}\mathbf{M} \times \frac{d\mathbf{M}}{dt}. \quad (3.169)$$

We choose a single-domain, spherical grain made of magnetic material that has uniaxial magneto-crystalline anisotropy. A constant magnetic field $\mathbf{H} = -H_0 \hat{\mathbf{z}}$ is applied coaxial with the easy axis as shown in Figure 3.21. Given an initial magnetization making an angle θ with respect to $\hat{\mathbf{z}}$, we expect that \mathbf{M} will undergo gyroscopic revolutions and finally align itself to the applied magnetic field. The energy density for our geometry is

$$W = \mu_0 M_S H_0 \cos \theta + K \sin^2 \theta, \quad (3.170)$$

with the magnetocrystalline anisotropy initially opposing the switching of \mathbf{M} . Since

$$\frac{dW}{d\theta} = \mu_0 M_S (-H_0 + H_k \cos \theta) \sin \theta, \quad (3.171)$$

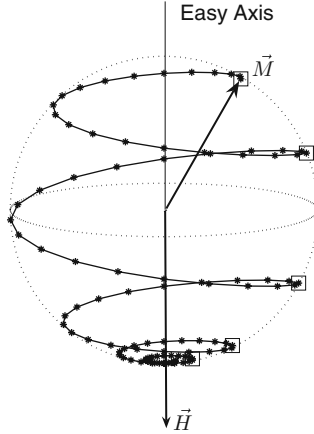


Fig. 3.21. Trajectory of the magnetization vector as it undergoes gyroscopic revolution and aligns itself to the applied field. θ is the angle between the easy axis and the magnetization vector. The points where \mathbf{M} crosses the median plane after one rotation are marked inside squares. \mathbf{M} is the initial magnetization, \mathbf{H} is the applied field, $\alpha = 0.15$ and $|\gamma| = 2\pi(28 \text{ GHz/T})$.

we can identify two opposing field components that contribute to the torque:¹³ $\mathbf{H} = -H_0 \hat{\mathbf{z}}$ and a fictitious field $\mathbf{H}_f = H_k \cos \theta \hat{\mathbf{z}}$. It becomes easier to understand the change in the polar angle θ of the magnetization if we switch to spherical coordinates, write

$$\mathbf{M} = M_S \hat{\mathbf{r}}, \quad (3.172)$$

$$\begin{aligned} \mathbf{H} &= -[H_0 - H_k \cos \theta] \hat{\mathbf{z}} \\ &= -[H_0 - H_k \cos \theta] [\cos \theta \hat{\mathbf{r}} - \sin \theta \hat{\boldsymbol{\theta}}], \end{aligned} \quad (3.173)$$

and describe the precessional motion of \mathbf{M} in spherical coordinates as

$$\dot{\mathbf{M}} = C_1 \hat{\boldsymbol{\theta}} + C_2 \hat{\boldsymbol{\phi}}, \quad (3.174)$$

where C_1 and C_2 are yet to be determined. Substituting (3.174) into both sides of (3.128), and equating terms along $\hat{\boldsymbol{\theta}}$ and $\hat{\boldsymbol{\phi}}$, we obtain

$$C_1 = \left(\frac{d\mathbf{M}}{dt} \right)_{\boldsymbol{\theta}} = \omega_M \left(\frac{\alpha}{1 + \alpha^2} \right) (H_0 \sin \theta - H_k \sin \theta \cos \theta). \quad (3.175)$$

Note that the crystallographic anisotropy opposes an increase in θ when $\theta < \pi/2$ but aids it once \mathbf{M} crosses the equatorial ($z = 0$) plane. In Figure 3.21, we visualize the gyroscopic motion by choosing an artificially large value for α in Figure 3.21. For typical values of $\alpha \lesssim 0.01$, the magnetization vector will cross the median plane at the locations marked by the square boxes approximately every $T = 2\pi/\omega_0$ seconds.

Mallinson [34] provides a detailed explanation on the role played by α on the switching characteristics of a single particle. We observe from Eq. (3.175) that for small values of α the change in azimuthal angle θ is linearly proportional to α , i.e., a reduced switching time is favored by increasing α . However, as Mallinson points out [35], the fastest switching occurs when $\alpha = 1$, out of the reach of common materials that typically exhibit damped precession with $\alpha < 0.1$. The effect of finite damping can be negated by externally inducing a torque, a technique proposed by Berger [36] and Slonzewski [37] (described further in Chapter 10) to achieve steady-state precession of magnetic moments in ferromagnets.

Problems

3.1. Estimate the diamagnetic susceptibility for the two $1s$ electrons in helium using the Langevin diamagnetism formula (3.10). Use the Bohr radius

¹³ In Chapter 5 we will introduce the concept of a demagnetizing field. For now, it is sufficient to note that the demagnetizing field for a spherical particle acts opposite to \mathbf{M} and does not contribute to the torque.

$r_0 = 4\pi\epsilon_0\hbar^2/m_q q^2$ and $N = 2.7 \times 10^{27} \text{ m}^3$ at STP. Compare your result with the experimental value -1.1×10^{-7} (from Kubo and Nagamiya [38, p. 439] converted to SI units).

3.2. Show that for the special case of $J=1/2$, the Brillouin function (3.25) can be reduced to

$$B_{1/2}(y) = \tanh y. \quad (3.176)$$

Expand this result for small y and show that the paramagnetic susceptibility for $J = 1/2$ is given by

$$\chi_{\text{para}} = \frac{\mu_0 N \mu_B^2}{k_B T}. \quad (3.177)$$

3.3. Show that if λ_{aa} and λ_{bb} are not neglected, the Curie temperature of a two-sublattice ferrimagnet is given by

$$T_c = -\frac{1}{2}(\lambda_{aa}C_a + \lambda_{bb}C_b) + \frac{1}{2}[(\lambda_{aa}C_a - \lambda_{bb}C_b)^2 + 4C_aC_b\lambda_{ab}^2]^{1/2}. \quad (3.178)$$

3.4. Verify (3.66) for face-centered and body-centered cubic lattices.

3.5. Verify that the second-order cubic anisotropy field along the $[111]$ direction is given by Eq. (3.101).

3.6. A cubic crystal is magnetized along the $[\bar{1}10]$ direction.

- (a) Show that the first-order static anisotropy field is also along the $[\bar{1}10]$ direction with magnitude $-K_{c1}/\mu_0 M_S$.
- (b) Show that the first-order anisotropy tensor in the crystal coordinate system is given by

$$\bar{\mathbf{N}}^a = \frac{K_{c1}}{\mu_0 M_S^2} \begin{bmatrix} -1 & 2 & 0 \\ 2 & -1 & 0 \\ 0 & 0 & -2 \end{bmatrix}. \quad (3.179)$$

- (c) Transform the anisotropy tensor of part (b) into a coordinate system where $\hat{\mathbf{z}} \parallel [\bar{1}10]$ and $\hat{\mathbf{y}} \parallel [111]$. Show that the result is

$$\bar{\mathbf{N}}^{a'} = \frac{K_{c1}}{\mu_0 M_S^2} \begin{bmatrix} -1 & \sqrt{2} & 0 \\ -\sqrt{2} & 0 & 0 \\ 0 & 0 & -3 \end{bmatrix}. \quad (3.180)$$

3.7. Consider a ferrite magnetized in the plane perpendicular to the $[111]$ direction.

- (a) Show that the magnetization vector making the angle ψ with the $[\bar{1}10]$ direction is

$$\mathbf{M} = M_S \begin{bmatrix} -\frac{1}{\sqrt{2}} \cos \psi - \frac{1}{\sqrt{6}} \sin \psi \\ \frac{1}{\sqrt{2}} \cos \psi - \frac{1}{\sqrt{6}} \sin \psi \\ +\sqrt{\frac{2}{3}} \sin \psi \end{bmatrix} \quad (3.181)$$

in the crystal coordinate system.

- (b) Show that the first-order cubic anisotropy energy is independent of the angle ψ .

3.8. Find γ' and the relationship between λ and α that allow the Landau–Lifshitz equation to be cast into the same form as the Gilbert equation even if α and λ are not small:

$$\text{LL: } \frac{d\mathbf{M}}{dt} = \gamma'\mu_0(\mathbf{M} \times \mathbf{H}_{\text{eff}}) + \frac{\lambda\gamma'\mu_0}{M_S}\mathbf{M} \times (\mathbf{M} \times \mathbf{H}_{\text{eff}}), \quad (3.182)$$

$$\text{G: } \frac{d\mathbf{M}}{dt} = \gamma\mu_0(\mathbf{M} \times \mathbf{H}_{\text{eff}}) + \frac{\alpha}{M_S}\left(\mathbf{M} \times \frac{d\mathbf{M}}{dt}\right). \quad (3.183)$$

Although the equations can be cast into the same form, they describe different physics since the dependence on the loss parameter differs between the two cases (e.g., consider what happens when loss becomes large in both cases [35]).

3.9. A low-loss ferrite is found to have a ferromagnetic resonance (FMR) line width of $\Delta B = 50\text{ }\mu\text{T}$ at 9.3 GHz. If the external field driving the resonance is removed at $t = 0$, how long will it take for the small-signal magnetization to decay by 10 dB relative to its magnitude at $t = 0$?

3.10. Most ferromagnetic resonance spectrometers measure the derivative of the absorption with respect to the bias field H_0 rather than the absorption curve itself. The peak-to-peak resonance line width ΔH_{pp} is obtained from this curve. Find the separation between the peaks of the derivative of the imaginary part of the susceptibility (3.153) and show that $\Delta H_{\text{FWHM}} = \sqrt{3}\Delta H_{\text{pp}}$, where ΔH_{FWHM} is the full width at half-maximum of the absorption curve and is given by (3.155c).

3.11. A field $\mathbf{H} = H_a \hat{\mathbf{x}} + H_b \hat{\mathbf{y}}$ is applied to a Stoner–Wohlfarth particle. According to the discussion in Section 3.9.1, the magnetization of the particle is stable when it makes an angle θ with respect to the x -axis. Show that a line with slope $\tan\theta$, tangential to the asteroid at a point (H_1, H_2) and passing through the point (H_a, H_b) , satisfies the equation (cf. Eq. (3.162)):

$$H_a \sin\theta - H_b \cos\theta + H_k \sin\theta \cos\theta = 0. \quad (3.184)$$

References

- [1] F. Brailsford, *Physical Principles of Magnetism*. London: Van Nostrand, 1966.
- [2] N. Ashcroft and N. D. Mermin, *Solid State Physics*. New York: Holt, Rinehart and Winston, 1976.
- [3] C. Kittel, *Introduction to Solid State Physics*, 8th ed. New York: John Wiley & Sons, 2005.

- [4] J. S. Smart, *Effective Field Theories of Magnetism*. Philadelphia: W. B. Saunders, 1966.
- [5] B. T. Matthias and R. M. Bozorth, "Ferromagnetic interaction in EuO," *Phys. Rev. Lett.*, vol. 7, p. 160, 1961.
- [6] D. K. Cheng, *Fundamentals of Engineering Electromagnetics*. Reading, MA: Addison Wesley, 1993.
- [7] J. Als-Nielsen, O. W. Dietrich, and L. Passell, "Neutron scattering from the Heisenberg ferromagnets EuO and EuS. II. Static critical properties," *Phys. Rev. B*, vol. 14, p. 4908, 1976.
- [8] E. E. Anderson, "Molecular field model and magnetization of YIG," *Phys. Rev.*, vol. 134, p. A1581, 1964.
- [9] W. H. von Aulock and A. S. Boxer, Eds., *Handbook of Microwave Ferrite Materials*. New York: Academic Press, 1965.
- [10] G. Winkler, *Magnetic Garnets*. Braunschweig: Vieweg and Sohn, 1981.
- [11] E. P. Wolfarth, Ed., *Ferro-magnetic Materials*. New York: North-Holland, 1980, vol. 2.
- [12] L. Passell, O. W. Dietrich, and J. Als-Nielsen, "Neutron scattering from the Heisenberg ferromagnets EuO and EuS I. The exchange constants," *Phys. Rev. B*, vol. 14, p. 4897, 1976.
- [13] J. H. Van Vleck and W. G. Penney, "The theory of the paramagnetic rotation and susceptibility in manganous and ferric salts," *Phil. Mag.*, vol. 17, p. 961, 1934.
- [14] C. Vittoria, G. C. Bailey, R. C. Barker, and A. Yelon, "Ferromagnetic resonance field and linewidth in an anisotropic magnetic metallic medium," *Phys. Rev. B*, vol. 7, p. 2112, 1973.
- [15] H. Goldstein, C. P. Poole, and J. L. Safko, *Classical Mechanics*, 3rd ed. Cambridge, MA: Addison-Wesley, 2001.
- [16] J. Matthews and R. L. Walker, *Mathematical Methods of Physics*. Menlo Park, CA: W. A. Benjamin Inc., 1970.
- [17] B. Lax and K. J. Button, *Microwave Ferrites and Ferrimagnetics*. New York: McGraw-Hill, 1962.
- [18] M. S. Sodha and N. C. Srivastava, *Microwave Propagation in Ferrimagnetics*. New York: Harper and Row, 1981.
- [19] R. F. Sooho, *Microwave Magnetics*. New York: Harper and Row, 1985.
- [20] O. G. Vendik, B. A. Kalinikos, and D. N. Chortorizhski, "Instability of spin waves in tangentially magnetized ferromagnetic films," *Soviet Phys. Solid State*, vol. 19, p. 222, 1977.
- [21] O. G. Vendik and D. N. Chortorizhski, "Spin-wave spectrum in a thin ferromagnetic film in a rectangular waveguide," *Soviet Phys. Solid State*, vol. 11, p. 1957, 1970.
- [22] D. D. Stancil, "Magnetostatic waves in non-uniform bias fields including exchange effects," *IEEE Trans. Mag.*, vol. MAG-16, p. 1153, 1980.
- [23] A. Morrish, *The Physical Principles of Magnetism*. New York: IEEE Press, 2001.

- [24] L. Spinu, I. Dumitru, A. Stancu, and D. Cimpoesu, "Transverse susceptibility as the low-frequency limit of ferromagnetic resonance," *J. Magn. Magn. Mater.*, vol. 296, pp. 1–8, 2006.
- [25] L. Landau and L. Lifshitz, *Phys. Zeit. Sowjetunion*, vol. 8, p. 153, 1935.
- [26] T. A. Gilbert, "Equation of motion of magnetization," Armor Research Foundation, Chicago, IL, Tech. Rep. 11, January 1955.
- [27] D. D. Stancil, "Phenomenological propagation loss theory for the magnetostatic waves in thin ferrite films," *J. Appl. Phys.*, vol. 59, p. 218, 1986.
- [28] E. C. Stoner and E. P. Wohlfarth, "A mechanism of magnetic hysteresis in heterogeneous alloys," *Philos. Trans. Soc. London*, 240A, pp. 599–642, 1948.
- [29] W. F. Brown Jr., *Micromagnetics*, ser. Interscience Tracts on Physics and Astronomy. New York: Interscience Publishers, 1963, vol. 18.
- [30] J.-G. Zhu and H. N. Bertram, "Micromagnetic studies of thin metallic films," *J. Appl. Phys.*, vol. 63, p. 3248, 1988.
- [31] S. W. Yuan and H. N. Bertram, "Magnetoresistive heads for ultra high density recording," *IEEE Trans. Mag.*, vol. 29, no. 6, p. 3811, Nov. 1993.
- [32] S. C. Chapra and R. P. Canale, *Numerical Methods for Engineers*, 5th ed. McGraw-Hill, 2005.
- [33] M. d'Aquino, C. Serpico, and G. Miano, "Geometrical integration of Landau - Lifshitz - Gilbert equation based on the mid-point rule," *J. Comput. Phys.*, vol. 209, pp. 730–753, 2005.
- [34] J. C. Mallinson, "Damped gyromagnetic switching," *IEEE Trans. Magn.*, vol. 36, p. 1976, 2000.
- [35] J. C. Mallinson, "On damped gyromagnetic precession," *IEEE Trans. Mag.*, vol. MAG-23, no. 4, p. 2003, 1987.
- [36] L. Berger, "Emission of spin waves by a magnetic multilayer traversed by a current," *Phys. Rev. B*, vol. 54, p. 9353, 1996.
- [37] J. C. Slonczewski, "Excitation of spin waves by an electric current," *J. Magn. Magn. Mat.*, vol. 195, p. L261, 1999.
- [38] R. Kubo and T. Nagamiya, *Solid State Physics*. New York: McGraw-Hill, 1969.

Electromagnetic Waves in Anisotropic-Dispersive Media

In Chapters 1 and 3, we examined the basic theory of magnetism and developed a model for the magnetic susceptibility tensor of a saturated ferro- or ferrimagnetic insulator. In this chapter, we will examine the properties of electromagnetic waves traveling in media characterized by frequency-dependent electric and magnetic susceptibilities. We then combine this formalism with the Polder susceptibility tensor to obtain the properties of electromagnetic waves in saturated magnetic insulators.

4.1 Maxwell's Equations¹

The fundamental equations governing electromagnetic fields are Maxwell's equations:

$$\nabla \times \mathbf{H} = \frac{\partial \mathbf{D}}{\partial t} + \mathbf{J}, \quad (4.1)$$

$$\nabla \times \mathbf{E} = -\frac{\partial \mathbf{B}}{\partial t}, \quad (4.2)$$

$$\nabla \cdot \mathbf{D} = \rho, \quad (4.3)$$

$$\nabla \cdot \mathbf{B} = 0. \quad (4.4)$$

Here, all of the field quantities are assumed to depend explicitly on time. Although we have encountered some of these quantities in previous chapters, we define them all here for convenience:

\mathbf{H} is the magnetic field intensity (A/m);

\mathbf{D} is the electric flux density (C/m²);

\mathbf{J} is the electric volume current density (A/m²);

\mathbf{E} is the electric field intensity (V/m);

¹ Standard text books by Jordan and Balmain [1], Kraus and Fleisch [2], and Cheng [3] serve as good sources of introductory material on Maxwell's equations.

\mathbf{B} is the magnetic flux density (Wb/m² or T); and
 ρ is the electric volume charge density (C/m³).

We are often interested in fields that are varying sinusoidally at a single frequency. In such cases, we can write

$$\mathbf{E}(t) = \text{Re}\{\mathbf{E}(\omega)e^{-i\omega t}\}, \quad (4.5)$$

where $\mathbf{E}(\omega)$ is a complex quantity containing the amplitude and phase information of the field. Since in this notation all time dependence is of the form $\exp(-i\omega t)$, time derivatives can be replaced by $-i\omega$. Thus, in the frequency domain, Maxwell's equations can be written

$$\nabla \times \mathbf{H} = -i\omega \mathbf{D} + \mathbf{J}, \quad (4.6)$$

$$\nabla \times \mathbf{E} = i\omega \mathbf{B}, \quad (4.7)$$

$$\nabla \cdot \mathbf{D} = \rho, \quad (4.8)$$

$$\nabla \cdot \mathbf{B} = 0, \quad (4.9)$$

where all of the field quantities are assumed to be complex functions of frequency. We will generally use the same notation for both time- and frequency-domain quantities. Where the context does not make the distinction clear, the dependence will be explicitly shown.

4.2 Constitutive Relations

The flux densities in free space are related to the field intensities by the linear relations

$$\mathbf{D} = \varepsilon_0 \mathbf{E}, \quad (4.10)$$

$$\mathbf{B} = \mu_0 \mathbf{H}, \quad (4.11)$$

where ε_0 and μ_0 are the permittivity and permeability of free space, respectively:

$$\varepsilon_0 \approx \frac{1}{36\pi} \times 10^{-9} \text{ (F/m)}, \quad (4.12)$$

$$\mu_0 \equiv 4\pi \times 10^{-7} \text{ (H/m)}. \quad (4.13)$$

In a material medium, however, additional terms appear because of the response of the medium to the presence of the fields. The general expressions are

$$\mathbf{D} = \varepsilon_0 \mathbf{E} + \mathbf{P}, \quad (4.14)$$

$$\mathbf{B} = \mu_0 (\mathbf{H} + \mathbf{M}), \quad (4.15)$$

where

\mathbf{P} is the electric dipole moment per unit volume $((\text{C m})/\text{m}^3 = \text{C}/\text{m}^2)$ and \mathbf{M} is the magnetic dipole moment per unit volume $((\text{A m}^2)/\text{m}^3 = \text{A}/\text{m})$, also commonly referred to as the polarization and magnetization respectively. Media in which \mathbf{P} and \mathbf{M} depend only on the first power of the field quantities are said to be *linear*. If the response of a linear medium to an applied field is instantaneous, the polarization density and magnetization are related to the field intensities by

$$\mathbf{P}(t) = \varepsilon_0 \overline{\chi}_e \cdot \mathbf{E}(t), \quad (4.16)$$

$$\mathbf{M}(t) = \overline{\chi}_m \cdot \mathbf{H}(t), \quad (4.17)$$

where $\overline{\chi}_e$ and $\overline{\chi}_m$ are the electric and magnetic susceptibility tensors, respectively, and are assumed to be constant in time. If the response is *not* instantaneous, then in effect the medium has “memory” and the present response must be obtained by integrating over all past excitations. Such a medium is said to be *dispersive*.

In the frequency domain, however, the response to a sinusoid always reaches a steady state that is determined by the amplitude of the excitation. In terms of these steady-state quantities, integration is not necessary and we can write

$$\mathbf{P}(\omega) = \varepsilon_0 \overline{\chi}_e(\omega) \cdot \mathbf{E}(\omega), \quad (4.18)$$

$$\mathbf{M}(\omega) = \overline{\chi}_m(\omega) \cdot \mathbf{H}(\omega). \quad (4.19)$$

Substituting these expressions into the constitutive relations (4.14) and (4.15) allows us to write

$$\mathbf{D} = \overline{\varepsilon} \cdot \mathbf{E}, \quad (4.20)$$

$$\mathbf{B} = \overline{\mu} \cdot \mathbf{H}, \quad (4.21)$$

where

$$\overline{\varepsilon} = \varepsilon_0(\overline{\mathbf{I}} + \overline{\chi}_e) \quad (4.22)$$

and

$$\overline{\mu} = \mu_0(\overline{\mathbf{I}} + \overline{\chi}_m) \quad (4.23)$$

are the permittivity and permeability tensors, respectively, and $\overline{\mathbf{I}}$ is the unit matrix. Equations (4.20), (4.21), (4.22), and (4.23) are general forms of the *constitutive relations*. If either $\overline{\varepsilon}$ or $\overline{\mu}$ reduces to a scalar constant times the unit matrix, the material is said to be electrically or magnetically *isotropic*, respectively. Alternatively, media requiring $\overline{\varepsilon}$ or $\overline{\mu}$ to be represented by a 3×3 matrix are called electrically or magnetically *anisotropic*. Of course, it is possible for a medium to be both electrically and magnetically isotropic or anisotropic [4–6].

4.3 Instantaneous Poynting Theorem

Consider the finite volume V bounded by the surface S as shown in Figure 4.1. Let the power leaving this volume per unit area at the point \mathbf{r}_S on the surface be $\mathbf{P}(\mathbf{r}_S) \cdot \hat{\mathbf{n}}$, where $\hat{\mathbf{n}}$ is the surface normal at \mathbf{r}_S . The net power leaving the volume is, therefore,

$$\oint_S \mathbf{P} \cdot \hat{\mathbf{n}} ds \equiv \oint_S \mathbf{P} \cdot d\mathbf{s}. \quad (4.24)$$

By conservation of energy, the net power entering the volume may either be stored or dissipated. Thus

$$-\oint_S \mathbf{P} \cdot d\mathbf{s} = \int_V \frac{\partial w}{\partial t} dv + \int_V P_d dv, \quad (4.25a)$$

where

$$-\oint_S \mathbf{P} \cdot d\mathbf{s} = \text{net power entering } V, \quad (4.25b)$$

$$\int_V \frac{\partial w}{\partial t} dv = \text{power stored (rate at which energy is increasing)}, \quad (4.25c)$$

$$\int_V P_d dv = \text{power dissipated}, \quad (4.25d)$$

w is the stored energy density (J/m^3) and P_d is the density of power dissipated (W/m^3).

The surface integral on the left-hand side of the energy conservation Eq. (4.25a) can be expressed as a volume integral using the divergence theorem valid for any differentiable vector function \mathbf{A} :

$$\oint_S \mathbf{A} \cdot d\mathbf{s} = \int_V \nabla \cdot \mathbf{A} dv. \quad (4.26)$$

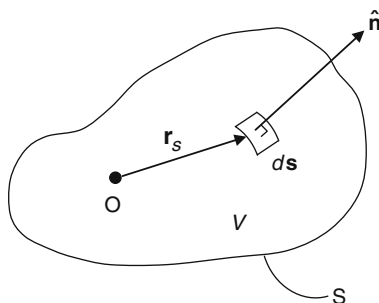


Fig. 4.1. Finite volume V enclosed by the surface S .

Thus, Eq. (4.25a) can be written

$$\int_V \nabla \cdot \mathbf{P} \, dv + \int_V \frac{\partial w}{\partial t} \, dv + \int_V P_d \, dv = 0. \quad (4.27)$$

Since this equation must be true for any volume V , we require the sum of the integrands to vanish:

$$\nabla \cdot \mathbf{P} + \frac{\partial w}{\partial t} + P_d = 0. \quad (4.28)$$

This is called the *continuity equation* and expresses conservation of energy at a point.

To obtain an equation expressing conservation of electromagnetic energy, we need to manipulate Maxwell's equations to look like the continuity equation (4.28). This can be done in the following way. First, take the dot product between \mathbf{H} and both sides of Eq. (4.2), the dot product between \mathbf{E} and both sides of Eq. (4.1), and form the difference of the resulting equations. The result is

$$\mathbf{H} \cdot (\nabla \times \mathbf{E}) - \mathbf{E} \cdot (\nabla \times \mathbf{H}) + \mathbf{H} \cdot \frac{\partial \mathbf{B}}{\partial t} + \mathbf{E} \cdot \frac{\partial \mathbf{D}}{\partial t} + \mathbf{E} \cdot \mathbf{J} = 0. \quad (4.29)$$

The first two terms can be combined using the vector identity

$$\nabla \cdot (\mathbf{A} \times \mathbf{B}) = \mathbf{B} \cdot (\nabla \times \mathbf{A}) - \mathbf{A} \cdot (\nabla \times \mathbf{B}) \quad (4.30)$$

to obtain the *Poynting theorem*:

$$\nabla \cdot (\mathbf{E} \times \mathbf{H}) + \mathbf{H} \cdot \frac{\partial \mathbf{B}}{\partial t} + \mathbf{E} \cdot \frac{\partial \mathbf{D}}{\partial t} + \mathbf{E} \cdot \mathbf{J} = 0. \quad (4.31)$$

For isotropic non-dispersive media, we note that

$$\mathbf{H} \cdot \frac{\partial \mathbf{B}}{\partial t} = \mu \mathbf{H} \cdot \frac{\partial \mathbf{H}}{\partial t} = \frac{\mu}{2} \frac{\partial (H^2)}{\partial t}, \quad (4.32)$$

and similarly for the electric field term $\mathbf{E} \cdot \partial \mathbf{D} / \partial t$. Thus, the Poynting theorem (4.31) can be written

$$\nabla \cdot (\mathbf{E} \times \mathbf{H}) + \frac{\partial}{\partial t} \left[\frac{1}{2} \varepsilon E^2 + \frac{1}{2} \mu H^2 \right] + \mathbf{E} \cdot \mathbf{J} = 0. \quad (4.33)$$

Comparison with the continuity equation (4.28) suggests the following identifications:

$\mathbf{P} = \mathbf{E} \times \mathbf{H}$ is the instantaneous power per unit area, or the *Poynting vector* (W/m^2),

$w_e = \frac{1}{2} \varepsilon E^2$ is the instantaneous stored energy density in the electric field (J/m^3),

$w_m = \frac{1}{2} \mu H^2$ is the instantaneous stored energy density in the magnetic field (J/m^3),

$w = w_e + w_m$ is the total instantaneous energy density (J/m^3), and

$P_d = \mathbf{E} \cdot \mathbf{J}$ is the dissipated power density (W/m^3).

4.4 Complex Poynting Theorem

To understand the convenience of complex notation, let us examine the time average of the product of two harmonically varying quantities. As an example, let the voltage and current in a circuit element be

$$V(t) = V_0 \cos \omega t, \quad (4.34)$$

$$I(t) = I_0 \cos(\omega t + \phi). \quad (4.35)$$

The time-averaged power dissipated in the element is

$$\begin{aligned} \langle V(t)I(t) \rangle &= \frac{1}{T} \int_0^T dt V_0 I_0 \cos \omega t \cos(\omega t + \phi) \\ &= \frac{V_0 I_0}{2T} \int_0^T dt [\cos \phi + \cos(2\omega t + \phi)], \end{aligned} \quad (4.36)$$

where we have used the trigonometric identity

$$2 \cos \alpha \cos \beta = \cos(\alpha + \beta) + \cos(\alpha - \beta). \quad (4.37)$$

Since the integral of a sinusoid over an integral number of cycles is zero, the second term in the integrand of Eq. (4.36) does not contribute. The integral reduces to

$$\langle V(t)I(t) \rangle = \frac{1}{2} V_0 I_0 \cos \phi. \quad (4.38)$$

In complex phasor notation, the voltage and current can be written

$$V(t) = \text{Re}\{V e^{-i\omega t}\}, \quad (4.39)$$

$$I(t) = \text{Re}\{I e^{-i\omega t}\}, \quad (4.40)$$

where $V = V_0$ and $I = I_0 \exp(-i\phi)$. Consider the following calculation:

$$\begin{aligned} \frac{1}{2} V I^* &= \frac{1}{2} V_0 I_0 e^{i\phi} \\ &= \frac{1}{2} V_0 I_0 [\cos \phi + i \sin \phi]. \end{aligned} \quad (4.41)$$

Comparison with the time-averaged expression (4.38) shows

$$\langle V(t)I(t) \rangle = \frac{1}{2} \text{Re}\{V I^*\}. \quad (4.42)$$

Thus, the time average of the product of two sinusoidally varying quantities can be easily obtained in complex notation as half the real part of the product of one times the complex conjugate of the other.

With this understanding, let us consider the complex form of Maxwell's equations. Dot multiplying the complex conjugate of Eq. (4.6) by \mathbf{E} , dot multiplying Eq. (4.7) by \mathbf{H}^* , and forming the difference of the resulting equations gives

$$\mathbf{H}^* \cdot (\nabla \times \mathbf{E}) - \mathbf{E} \cdot (\nabla \times \mathbf{H}^*) + i\omega \mathbf{E} \cdot \mathbf{D}^* - i\omega \mathbf{H}^* \cdot \mathbf{B} + \mathbf{E} \cdot \mathbf{J}^* = 0. \quad (4.43)$$

Using the vector identity (4.30), we obtain the complex form of the Poynting theorem:

$$\nabla \cdot (\mathbf{E} \times \mathbf{H}^*) + i\omega (\mathbf{E} \cdot \mathbf{D}^* - \mathbf{H}^* \cdot \mathbf{B}) + \mathbf{E} \cdot \mathbf{J}^* = 0. \quad (4.44)$$

The time-averaged quantities can be obtained by taking the real part of this equation. If this equation is then integrated over a sample volume V as in Figure 4.1, then the first term will yield the net power leaving the volume during one period of the oscillation. If the material is lossless, then all the power that enters must leave (on average) and the real part of the first term must vanish. It follows that the real parts of either of the other two terms represent loss for a passive medium. Thus, for a lossless medium we require

$$\text{Re}\{i\omega (\mathbf{E} \cdot \mathbf{D}^* - \mathbf{H}^* \cdot \mathbf{B}) + \mathbf{E} \cdot \mathbf{J}^*\} = 0. \quad (4.45)$$

In the absence of sources, $\mathbf{E} \cdot \mathbf{J}^*$ is identically zero for non-conducting media. Using the constitutive relations (4.20) and (4.21) and noting that $\text{Re}\{z\} = (z + z^*)/2$ allows us to write Eq. (4.45) in the form (Problem 4.1)

$$\text{Re}\{i\omega (\mathbf{E} \cdot \mathbf{D}^* - \mathbf{H}^* \cdot \mathbf{B})\} = \frac{i\omega}{2} [\mathbf{E}^* \cdot (\bar{\epsilon}^\dagger - \bar{\epsilon}) \cdot \mathbf{E} + \mathbf{H}^* \cdot (\bar{\mu}^\dagger - \bar{\mu}) \cdot \mathbf{H}] = 0, \quad (4.46)$$

where $\bar{\epsilon}^\dagger = (\bar{\epsilon}^*)^T$ and the superscript T refers to the matrix transpose. Since \mathbf{E} and \mathbf{H} represent arbitrary solutions to Maxwell's equations, the lossless condition requires

$$\bar{\epsilon}^\dagger = \bar{\epsilon} \quad (4.47)$$

and

$$\bar{\mu}^\dagger = \bar{\mu}. \quad (4.48)$$

Matrices satisfying these conditions are said to be Hermitian.

4.5 Energy Densities in Lossless Dispersive Media

To obtain energy expressions that are valid for lossless dispersive media, let us return to the general instantaneous Poynting theorem given by Eq. (4.31) with $\mathbf{J} = 0$. Let us assume that for $t \rightarrow -\infty$, all fields were zero. We then define the energy stored in the electromagnetic fields as the energy absorbed by the medium during the buildup of the fields. Thus, the total instantaneous energy density is

$$\begin{aligned}
w(t) &= \int_{-\infty}^t \frac{\partial w}{\partial t'} dt' \\
&= \int_{-\infty}^t \left[\mathbf{E} \cdot \frac{\partial \mathbf{D}}{\partial t'} + \mathbf{H} \cdot \frac{\partial \mathbf{B}}{\partial t'} \right] dt' \\
&= w_e(t) + w_m(t),
\end{aligned} \tag{4.49}$$

where

$$w_e(t) = \int_{-\infty}^t \mathbf{E} \cdot \frac{\partial \mathbf{D}}{\partial t'} dt', \tag{4.50}$$

$$w_m(t) = \int_{-\infty}^t \mathbf{H} \cdot \frac{\partial \mathbf{B}}{\partial t'} dt'. \tag{4.51}$$

Let us consider the evaluation of the electric energy density (4.50) for slowly varying fields of the form

$$\mathbf{E}(t) = \text{Re}\{\mathbf{E}(s)e^{-ist}\}, \tag{4.52}$$

$$\mathbf{D}(t) = \text{Re}\{\mathbf{D}(s)e^{-ist}\}, \tag{4.53}$$

where $s = \omega + i\alpha$ and $\alpha \ll \omega$. The small imaginary shift in the frequency causes the fields to build up slowly in time while vanishing for $t \rightarrow -\infty$. Since $\alpha \ll \omega$, we assume that the amplitudes do not change appreciably during a single period of oscillation. The frequency-domain quantities $\mathbf{D}(s)$ and $\mathbf{E}(s)$ are related through the constitutive law (cf. Eq. (4.20)):

$$\mathbf{D}(s) = \bar{\epsilon}(s) \cdot \mathbf{E}(s). \tag{4.54}$$

These complex quantities can be used to aid in the evaluation of the time average of Eq. (4.50) over a single period. We have

$$\langle w_e(t) \rangle = \int_{-\infty}^t \langle \mathbf{E} \cdot \frac{\partial \mathbf{D}}{\partial t'} \rangle dt'. \tag{4.55}$$

In terms of the complex fields, the integrand can be written

$$\langle \mathbf{E} \cdot \frac{\partial \mathbf{D}}{\partial t} \rangle = \frac{1}{2} \text{Re}\{\mathbf{E}^*(s) \cdot (-is)\bar{\epsilon}(s) \cdot \mathbf{E}(s)\}e^{2\alpha t}. \tag{4.56}$$

Since α is assumed to be small, we can approximate $s\bar{\epsilon}(s)$ by the first two terms of a Taylor series expansion:

$$s\bar{\epsilon}(s) \approx \omega\bar{\epsilon}(\omega) + i\alpha \frac{\partial}{\partial\omega} [\omega\bar{\epsilon}(\omega)]. \quad (4.57)$$

Substituting this result into Eq. (4.56) gives

$$\begin{aligned} \langle \mathbf{E} \cdot \frac{\partial \mathbf{D}}{\partial t} \rangle &= \frac{1}{2} \text{Re} \left\{ -i\omega \mathbf{E}^*(s) \cdot \bar{\epsilon}(\omega) \cdot \mathbf{E}(s) + \alpha \mathbf{E}^*(s) \cdot \frac{\partial}{\partial\omega} [\omega\bar{\epsilon}(\omega)] \cdot \mathbf{E}(s) \right\} e^{2\alpha t} \\ &= \frac{\alpha}{2} \mathbf{E}^*(s) \cdot \frac{\partial}{\partial\omega} [\omega\bar{\epsilon}(\omega)] \cdot \mathbf{E}(s) e^{2\alpha t}, \end{aligned} \quad (4.58)$$

where we have used the fact that $\mathbf{E}^*(s) \cdot \bar{\epsilon} \cdot \mathbf{E}(s)$ is real, since $\bar{\epsilon}(\omega)$ is Hermitian for a lossless medium. This result can now be used with Eq. (4.55) to find the total time average electric energy density at time t :

$$\begin{aligned} \langle w_e(t) \rangle &= \frac{\alpha}{2} \mathbf{E}^*(s) \cdot \frac{\partial}{\partial\omega} [\omega\bar{\epsilon}(\omega)] \cdot \mathbf{E}(s) \int_{-\infty}^t e^{2\alpha t'} dt' \\ &= \frac{1}{4} \mathbf{E}^*(\omega) \cdot \frac{\partial}{\partial\omega} [\omega\bar{\epsilon}(\omega)] \cdot \mathbf{E}(\omega), \end{aligned} \quad (4.59)$$

where we have taken the limit $\alpha \rightarrow 0$ after evaluating the integral. Similarly, the time-averaged magnetic energy density is

$$\langle w_m(t) \rangle = \frac{1}{4} \mathbf{H}^*(\omega) \cdot \frac{\partial}{\partial\omega} [\omega\bar{\mu}(\omega)] \cdot \mathbf{H}(\omega). \quad (4.60)$$

For non-dispersive media, neither $\bar{\epsilon}$ nor $\bar{\mu}$ depends on frequency and the energy densities (4.59) and (4.60) reduce to the complex forms of the expressions following (4.33).

4.6 Wave Equations

Let us consider the properties of fields with space and time dependence of the form $\exp(i\mathbf{k} \cdot \mathbf{r} - i\omega t)$. At a particular time t_0 , the surface on which the phase remains constant is given by

$$\mathbf{k} \cdot \mathbf{r} - \omega t_0 = \phi_0 \quad (4.61a)$$

or

$$\hat{\mathbf{k}} \cdot \mathbf{r} = \frac{\omega t_0 + \phi_0}{k} \equiv C_0, \quad (4.61b)$$

where $\hat{\mathbf{k}} = \mathbf{k}/|\mathbf{k}|$ is a unit vector parallel to \mathbf{k} . Equation (4.61b) is the equation for a plane perpendicular to the vector \mathbf{k} as shown in Figure 4.2.²

² We here assume that \mathbf{k} is a constant vector, i.e., \mathbf{k} does not vary in magnitude or direction with \mathbf{r} .

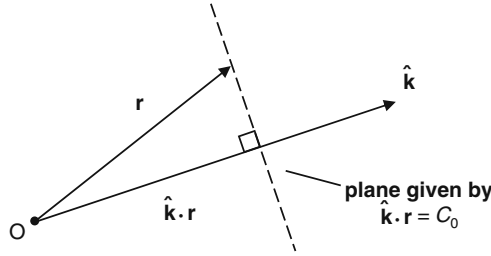


Fig. 4.2. The plane surface described by $\hat{\mathbf{k}} \cdot \mathbf{r} = C_0$.

Note that according to Eq. (4.61a), the phase increases along the direction of \mathbf{k} with t_0 constant. The distance along $\hat{\mathbf{k}}$ corresponding to a phase shift of 2π is called the *wavelength*, λ . Thus, from Eq. (4.61a), we have

$$k = \frac{2\pi}{\lambda}. \quad (4.62)$$

The quantity k is called the *wave number* since it is proportional to the number of wavelengths per unit distance.

Referring to Eq. (4.61b), we see that the constant C_0 increases as time increases. Thus, the constant phase plane moves in the direction of $\hat{\mathbf{k}}$. The velocity of this motion is called the *phase velocity* v_p and is given by

$$v_p = \frac{\partial C_0}{\partial t_0} = \frac{\omega}{k}. \quad (4.63)$$

Because of the shape and motion of the constant phase surface, solutions of the form $\exp(i\mathbf{k} \cdot \mathbf{r} - i\omega t)$ are called *uniform plane waves*.

Just as assuming a time dependence of the form $\exp(-i\omega t)$ allowed us to replace the time derivatives in Maxwell's equations with $-i\omega$, assuming a space dependence of the form $\exp(i\mathbf{k} \cdot \mathbf{r})$ allows us to replace the ∇ operator with $i\mathbf{k}$. As an example, consider the following:

$$\begin{aligned} \nabla e^{i\mathbf{k} \cdot \mathbf{r}} &= \left[\hat{\mathbf{x}} \frac{\partial}{\partial x} + \hat{\mathbf{y}} \frac{\partial}{\partial y} + \hat{\mathbf{z}} \frac{\partial}{\partial z} \right] e^{i\mathbf{k} \cdot \mathbf{r}} \\ &= [\hat{\mathbf{x}} i k_x + \hat{\mathbf{y}} i k_y + \hat{\mathbf{z}} i k_z] e^{i\mathbf{k} \cdot \mathbf{r}} \\ &= i\mathbf{k} e^{i\mathbf{k} \cdot \mathbf{r}}. \end{aligned} \quad (4.64)$$

Thus, for plane wave solutions, Maxwell's equations become:

$$i\mathbf{k} \times \mathbf{H} = -i\omega \mathbf{D} + \mathbf{J}, \quad (4.65)$$

$$\mathbf{k} \times \mathbf{E} = \omega \mathbf{B}, \quad (4.66)$$

$$i\mathbf{k} \cdot \mathbf{D} = \rho, \quad (4.67)$$

$$\mathbf{k} \cdot \mathbf{B} = 0. \quad (4.68)$$

Note that Eq. (4.68) follows from dotting \mathbf{k} into both sides of Eq. (4.66), since $\mathbf{k} \cdot (\mathbf{k} \times \mathbf{E}) \equiv 0$. Similarly, dotting \mathbf{k} into both sides of Eq. (4.65) gives (4.67) provided ρ and \mathbf{J} are related by

$$\mathbf{k} \cdot \mathbf{J} = \omega \rho. \quad (4.69)$$

This is a form of the continuity equation, and it expresses conservation of charge. It is generally true that Maxwell's two divergence equations (in this case (4.67) and (4.68)) are redundant provided we separately postulate charge conservation.

Let us consider Maxwell's first two equations, (4.65) and (4.66), for the case of source-free non-conducting media. These equations can be expressed entirely in terms of \mathbf{E} and \mathbf{H} with the use of the constitutive relations (4.20) and (4.21). The result is

$$\mathbf{k} \times \mathbf{H} = -\omega \bar{\epsilon} \cdot \mathbf{E}, \quad (4.70)$$

$$\mathbf{k} \times \mathbf{E} = \omega \bar{\mu} \cdot \mathbf{H}. \quad (4.71)$$

It is convenient to define the antisymmetric matrix $\bar{\mathbf{k}}$ such that

$$\bar{\mathbf{k}} \equiv \mathbf{k} \times \bar{\mathbf{I}} = \begin{bmatrix} 0 & -k_z & k_y \\ k_z & 0 & -k_x \\ -k_y & k_x & 0 \end{bmatrix}. \quad (4.72)$$

This matrix has the following property:

$$\mathbf{k} \times \mathbf{A} = \bar{\mathbf{k}} \cdot \mathbf{A}, \quad (4.73)$$

where \mathbf{A} is an arbitrary vector. Thus, it permits a vector cross product to be replaced with a matrix dot product. Maxwell's equations (4.70) and (4.71) can now be written

$$\bar{\mathbf{k}} \cdot \mathbf{H} = -\omega \bar{\epsilon} \cdot \mathbf{E}, \quad (4.74)$$

$$\bar{\mathbf{k}} \cdot \mathbf{E} = \omega \bar{\mu} \cdot \mathbf{H}. \quad (4.75)$$

Multiplying Eq. (4.74) from the left by the inverse of the permittivity tensor and dotting $\bar{\mathbf{k}}$ into both sides from the left gives

$$\bar{\mathbf{k}} \cdot \bar{\epsilon}^{-1} \cdot \bar{\mathbf{k}} \cdot \mathbf{H} = -\omega \bar{\mathbf{k}} \cdot \mathbf{E}. \quad (4.76)$$

Substituting Eq. (4.75) for $\bar{\mathbf{k}} \cdot \mathbf{E}$ gives

$$[\bar{\mathbf{k}} \cdot \bar{\epsilon}^{-1} \cdot \bar{\mathbf{k}} + \omega^2 \bar{\mu}] \cdot \mathbf{H} = 0. \quad (4.77)$$

Following a similar procedure to eliminate \mathbf{H} gives

$$[\bar{\mathbf{k}} \cdot \bar{\mu}^{-1} \cdot \bar{\mathbf{k}} + \omega^2 \bar{\epsilon}] \cdot \mathbf{E} = 0. \quad (4.78)$$

Equations (4.77) and (4.78) are the *complex wave equations* for the fields \mathbf{H} and \mathbf{E} , respectively. From linear algebra, we know that for non-trivial solutions to exist (i.e., solutions for which \mathbf{E} and \mathbf{H} do not vanish), the determinants of the coefficient matrices in Eqs. (4.77) and (4.78) must vanish. We therefore require

$$\det [\bar{\mathbf{k}} \cdot \bar{\boldsymbol{\varepsilon}}^{-1} \cdot \bar{\mathbf{k}} + \omega^2 \bar{\boldsymbol{\mu}}] = 0, \quad (4.79)$$

$$\det [\bar{\mathbf{k}} \cdot \bar{\boldsymbol{\mu}}^{-1} \cdot \bar{\mathbf{k}} + \omega^2 \bar{\boldsymbol{\varepsilon}}] = 0. \quad (4.80)$$

These equations give the allowed relationships between ω and \mathbf{k} for plane wave solutions to exist in the medium described by $\bar{\boldsymbol{\mu}}$ and $\bar{\boldsymbol{\varepsilon}}$. The resulting function $\omega(\mathbf{k})$ is called the dispersion relation for the waves. Since both \mathbf{E} and \mathbf{H} exist simultaneously in an electromagnetic wave, Eqs. (4.79) and (4.80) must be equivalent. The choice regarding which to use is usually determined by which constitutive tensor is easiest to invert.

As a simple example, consider the case of an isotropic medium. In this case, the wave equations (4.77) and (4.78) can be written as

$$[\bar{\mathbf{k}} \cdot \bar{\mathbf{k}} + \omega^2 \mu \varepsilon \bar{\mathbf{I}}] \cdot \mathbf{H} = 0, \quad (4.81)$$

$$[\bar{\mathbf{k}} \cdot \bar{\mathbf{k}} + \omega^2 \mu \varepsilon \bar{\mathbf{I}}] \cdot \mathbf{E} = 0, \quad (4.82)$$

where $\bar{\mathbf{I}}$ is the identity matrix. These equations can be simplified using the identity

$$\bar{\mathbf{k}} \cdot \bar{\mathbf{k}} = \mathbf{k}\mathbf{k} - k^2 \bar{\mathbf{I}}, \quad (4.83)$$

where the dyadic product \mathbf{uv} between two vectors \mathbf{u} and \mathbf{v} is defined as

$$\mathbf{uv} = \begin{bmatrix} u_x v_x & u_x v_y & u_x v_z \\ u_y v_x & u_y v_y & u_y v_z \\ u_z v_x & u_z v_y & u_z v_z \end{bmatrix}. \quad (4.84)$$

Substituting the vector identity (4.83) into the wave equation (4.81) gives

$$\mathbf{k}\mathbf{k} \cdot \mathbf{H} - k^2 \mathbf{H} + \omega^2 \mu \varepsilon \mathbf{H} = 0. \quad (4.85)$$

The first term vanishes by virtue of Maxwell's equation (4.68) in an isotropic medium. Considering the remaining terms, the only way for non-trivial solutions to exist is to require

$$k^2 = \omega^2 \mu \varepsilon. \quad (4.86)$$

This is the dispersion relation for plane waves in an isotropic medium.

4.7 Polarization of the Electromagnetic Fields

The polarization of a field is determined by the shape of the curve traced by the tip of the instantaneous field vector. Three cases are of primary interest:

- (a) The field is *linearly polarized* if the tip of the vector oscillates along a fixed direction. An example of a linearly polarized field expressed in both real and complex notations is

$$\mathbf{E}(t) = \hat{\mathbf{x}}E_0 \cos \omega t, \quad (4.87a)$$

$$\mathbf{E}(t) = \text{Re}\{\hat{\mathbf{x}}E_0 e^{-i\omega t}\}. \quad (4.87b)$$

- (b) If the tip of the field vector traces out an ellipse, the field is said to be *elliptically polarized*:

$$\mathbf{E}(t) = \hat{\mathbf{x}}E_x \cos \omega t + \hat{\mathbf{y}}E_y \sin \omega t, \quad (4.88a)$$

$$\mathbf{E}(t) = \text{Re}\{(\hat{\mathbf{x}}E_x + i\hat{\mathbf{y}}E_y)e^{-i\omega t}\}. \quad (4.88b)$$

It is also important to specify the rotation direction of the field. For plane waves, this is done in terms of the directions of \mathbf{k} and $d\mathbf{E}/dt$ (see Figure 4.3). The sense of rotation is specified as either right- or left-hand according to the following definitions:

Right-hand polarization:

$$\hat{\mathbf{k}} \cdot \left(\mathbf{E} \times \frac{d\mathbf{E}}{dt} \right) > 0, \quad (4.89)$$

Left-hand polarization:

$$\hat{\mathbf{k}} \cdot \left(\mathbf{E} \times \frac{d\mathbf{E}}{dt} \right) < 0. \quad (4.90)$$

These definitions are such that the fields of a right-hand polarized wave follow the threads of a right-hand screw. Another way of saying this is that the fingers of your right hand will point in the direction of the motion of the field for a right-hand polarized wave when your thumb points along $\hat{\mathbf{k}}$.

- (c) Circular polarization is a special case of elliptical polarization with both transverse components of the field equal in magnitude. Right- and left-hand circularly polarized waves are illustrated in Figure 4.4.

In complex notation, circularly and elliptically polarized waves can be written as

$$\mathbf{E}_{\text{RHP}}(t) = \text{Re}\{(\hat{\mathbf{x}}E_x + i\hat{\mathbf{y}}E_y)e^{i(kz - \omega t)}\}, \quad (4.91)$$

$$\mathbf{E}_{\text{LHP}}(t) = \text{Re}\{(\hat{\mathbf{x}}E_x - i\hat{\mathbf{y}}E_y)e^{i(kz - \omega t)}\}, \quad (4.92)$$

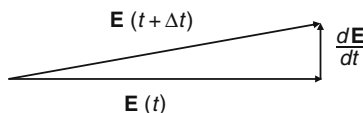


Fig. 4.3. Definition of the vector $d\mathbf{E}/dt$.

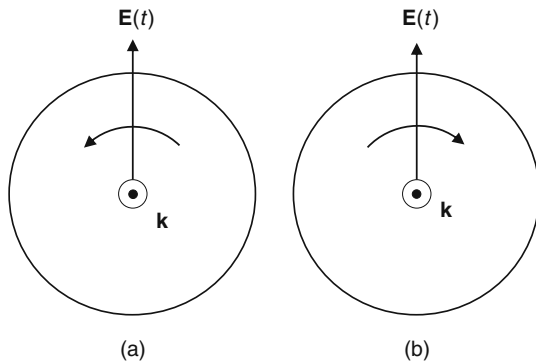


Fig. 4.4. Circular polarization states: (a) right-hand circular and (b) left-hand circular.

where the propagation direction is taken to be along $\hat{\mathbf{z}}$. Equations (4.91) and (4.92) can also be written

$$\mathbf{E}_{\pm} = \frac{E_0}{\sqrt{1 + \alpha^2}} \begin{bmatrix} 1 \\ \pm i\alpha \\ 0 \end{bmatrix} e^{i(kz - \omega t)}, \quad (4.93)$$

where $+$ and $-$ correspond to right- and left-hand polarizations, respectively, and α is a positive real parameter that determines the ellipticity of the polarization.

Examination of Eqs. (4.91), (4.92), and (4.93) shows that elliptical polarization can be viewed as the sum of two orthogonal linear polarizations that are 90° out-of-phase. Similarly, the complex sum of suitable right- and left-hand polarized waves can generate any other polarization – elliptical or linear.

4.8 Group and Energy Velocities

Although plane waves are very useful idealizations, physical fields are of finite duration and extent. Such a field can be represented by the general Fourier integral:

$$\mathbf{H}(\mathbf{r}, t) = \int_{-\infty}^{\infty} \frac{d\omega}{2\pi} \int_{-\infty}^{\infty} \frac{d^3k}{(2\pi)^3} \mathbf{H}(\mathbf{k}, \omega) e^{i(\mathbf{k} \cdot \mathbf{r} - \omega t)}, \quad (4.94)$$

where the integral over k is 3D and $d^3k = dk_x dk_y dk_z$ is a volume element in k -space. This integral, formed by summing individual plane waves, can represent any well-behaved function of \mathbf{r} and t . However, constraints placed by Maxwell's equations and the constitutive tensors do not permit plane waves with arbitrary ω and \mathbf{k} ; only those waves that satisfy the dispersion relation

$\omega = \omega(\mathbf{k})$ can contribute. Imposing this condition effectively clears the ω integral and we can write

$$\mathbf{H}(\mathbf{r}, t) = \text{Re} \int_{-\infty}^{\infty} \frac{d^3 k}{(2\pi)^3} \mathbf{H}(\mathbf{k}) e^{i(\mathbf{k} \cdot \mathbf{r} - \omega(\mathbf{k})t)}. \quad (4.95)$$

Now consider a wave packet similar to that shown in Figure 4.5. If this packet contains a large number of oscillations with wavelength λ_0 , then we expect the function $\mathbf{H}(\mathbf{k})$ to be sharply peaked about $\mathbf{k} = \mathbf{k}_0 = (2\pi/\lambda_0)\hat{\mathbf{k}}$. Thus, the dominant contributions to the integral will occur for \mathbf{k} near \mathbf{k}_0 . If the contributing interval is sufficiently small, we can approximate $\omega(\mathbf{k})$ by the first two terms of a Taylor series³

$$\omega(\mathbf{k}) \approx \omega(\mathbf{k}_0) + \left. \frac{\partial \omega}{\partial \mathbf{k}} \right|_{\mathbf{k}_0} \cdot (\mathbf{k} - \mathbf{k}_0) + \cdots, \quad (4.96)$$

where

$$\frac{\partial \omega}{\partial \mathbf{k}} = \hat{\mathbf{x}} \frac{\partial \omega}{\partial k_x} + \hat{\mathbf{y}} \frac{\partial \omega}{\partial k_y} + \hat{\mathbf{z}} \frac{\partial \omega}{\partial k_z} \equiv \nabla_{\mathbf{k}} \omega. \quad (4.97)$$

Substituting this expansion into the Fourier integral (4.95) and writing $\mathbf{k} = \mathbf{k}_0 + (\mathbf{k} - \mathbf{k}_0)$ gives

$$\mathbf{H}(\mathbf{r}, t) = \text{Re} \left\{ e^{i(\mathbf{k}_0 \cdot \mathbf{r} - \omega(\mathbf{k}_0)t)} \int_{-\infty}^{\infty} \frac{d^3 k}{(2\pi)^3} \mathbf{H}(\mathbf{k}) \exp[i(\mathbf{k} - \mathbf{k}_0) \cdot (\mathbf{r} - \nabla_{\mathbf{k}} \omega|_{\mathbf{k}_0} t)] \right\} \quad (4.98)$$

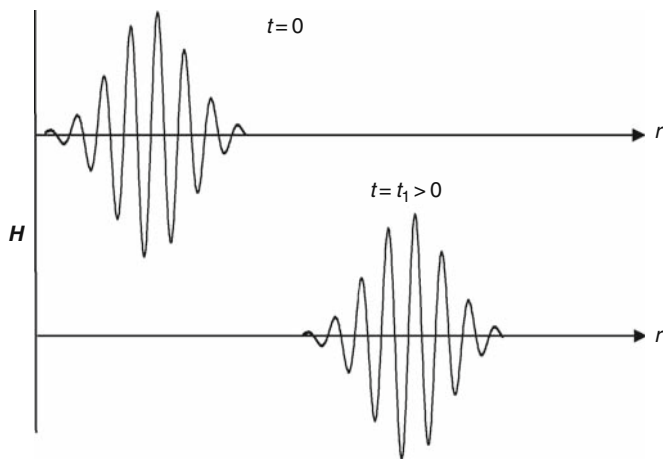


Fig. 4.5. Propagation of a wave packet. The field oscillations are shown at two instants of time.

³ The second-order term in the Taylor series expansion is the *dispersion coefficient*, which is discussed in Section 9.4.

The factor outside the integral is simply a plane wave characterized by (ω_0, \mathbf{k}_0) . The integral is slowly varying in space compared with the plane wave factor, since $|\mathbf{k} - \mathbf{k}_0| \ll |\mathbf{k}_0|$ by assumption. This integral, therefore, represents the envelope of the wave packet shown in Figure 4.5. To examine the motion of a particular point on the envelope function, we require

$$\mathbf{r} - \nabla_{\mathbf{k}}\omega|_{\mathbf{k}_0}t = \text{constant}. \quad (4.99)$$

The velocity at which the envelope moves is called the *group velocity* \mathbf{v}_g and is obtained by taking the derivative of Eq. (4.99) with respect to time:

$$\mathbf{v}_g \equiv \nabla_{\mathbf{k}}\omega. \quad (4.100)$$

In general, the phase and group velocities of a wave are not equal. The difference between the two velocities can be illustrated geometrically as follows. Consider the surface in \mathbf{k} -space defined by the equation

$$\omega(\mathbf{k}) = \text{constant}. \quad (4.101)$$

The phase velocity v_p at a particular point on this surface is parallel to the vector \mathbf{k} from the origin to the point under consideration and has the magnitude $v_p = \omega/k$. This is illustrated in Figure 4.6. In contrast, the group velocity is given by $\nabla_{\mathbf{k}}\omega$, which yields a vector normal to the constant-omega surface. Thus, v_g and v_p in general may differ both in magnitude and direction.

If the medium is isotropic, v_p and v_g will be parallel, but may have different magnitudes. The difference between v_p and v_g in this case is illustrated in Figure 4.7.

A third kind of velocity is obtained by dividing the time-averaged Poynting vector by the average energy density:

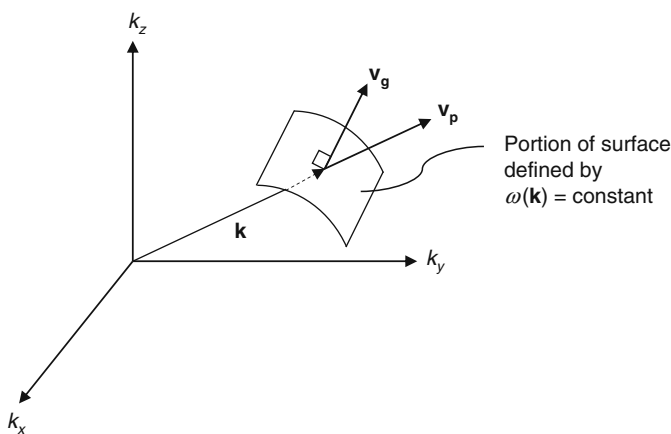


Fig. 4.6. Geometrical interpretation of phase and group velocities for anisotropic media.

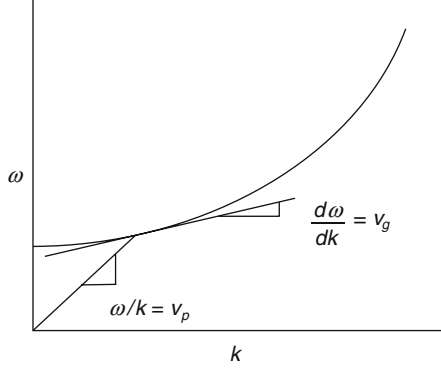


Fig. 4.7. Phase and group velocities for isotropic media.

$$\mathbf{v}_e \equiv \frac{\langle \mathbf{P}(t) \rangle}{\langle w(t) \rangle}. \quad (4.102)$$

This is the velocity at which the energy in the wave propagates. Since it is intuitively reasonable for the energy associated with a packet to have the same location as the packet itself, it should not be surprising that $\mathbf{v}_e = \mathbf{v}_g$ for lossless media.

4.9 Plane Waves in a Magnetized Ferrite

Consider plane wave propagation in a magnetized ferrite with the magnetic field \mathbf{H}_0 along the $\hat{\mathbf{z}}$ direction. If the ferrite is assumed to be electrically isotropic, then $\bar{\epsilon}^{-1} = (1/\epsilon)\bar{\mathbf{I}}$ and Eq. (4.77) for the magnetic field can be written as

$$[\mathbf{k}\mathbf{k} - k^2\bar{\mathbf{I}} + \omega^2\bar{\boldsymbol{\mu}}\epsilon] \cdot \mathbf{H} = 0, \quad (4.103)$$

where we have used Eq. (4.83) to expand the quantity $\bar{\mathbf{k}} \cdot \bar{\mathbf{k}}$. The permeability $\bar{\boldsymbol{\mu}}$ is given by

$$\bar{\boldsymbol{\mu}} = \mu_0 \begin{bmatrix} 1 + \chi & -i\kappa & 0 \\ i\kappa & 1 + \chi & 0 \\ 0 & 0 & 1 \end{bmatrix} \quad (4.104)$$

where χ and κ are given by Eqs. (3.115) and (3.116), respectively.

For a non-trivial solution, the determinant of the coefficient matrix in Eq. (4.103) must vanish. Hence, we require (cf. Eq. (4.79))

$$\det [\mathbf{k}\mathbf{k} - k^2\bar{\mathbf{I}} + \omega^2\bar{\boldsymbol{\mu}}\epsilon] = 0. \quad (4.105)$$

Carrying out the indicated matrix multiplication and addition, the coefficient matrix can be written as

$$\mathbf{k} \mathbf{k} - k^2 \bar{\mathbf{I}} + \omega^2 \bar{\boldsymbol{\mu}} \boldsymbol{\varepsilon} = \begin{bmatrix} k_0^2(1 + \chi) - k_y^2 - k_z^2 & k_x k_y - i k_0^2 \kappa & k_x k_z \\ k_y k_x + i k_0^2 \kappa & k_0^2(1 + \chi) - k_x^2 - k_z^2 & k_y k_z \\ k_z k_x & k_z k_y & k_0^2 - k_x^2 - k_y^2 \end{bmatrix}, \quad (4.106)$$

where $k_0^2 = \omega^2 \mu_0 \varepsilon$. Let us consider in detail the cases where \mathbf{k} is parallel or perpendicular to the applied field.

4.9.1 Propagation Parallel to the Applied Field

Assuming $\mathbf{k} = k \hat{\mathbf{z}}$, Eq. (4.106) simplifies to

$$\mathbf{k} \mathbf{k} - k^2 \bar{\mathbf{I}} + \omega^2 \bar{\boldsymbol{\mu}} \boldsymbol{\varepsilon} = \begin{bmatrix} k_0^2(1 + \chi) - k^2 & -i k_0^2 \kappa & 0 \\ +i k_0^2 \kappa & k_0^2(1 + \chi) - k^2 & 0 \\ 0 & 0 & k_0^2 \end{bmatrix}. \quad (4.107)$$

Evaluating the determinant and neglecting solutions with $\omega = 0$ gives

$$k_+^2 = k_0^2(1 + \chi + \kappa), \quad (4.108)$$

$$k_-^2 = k_0^2(1 + \chi - \kappa). \quad (4.109)$$

With the aid of Eqs. (3.115) and (3.116) for χ and κ , these dispersion relations can be expressed

$$k_+^2 = k_0^2 \left[\frac{\omega_0 + \omega_M - \omega}{\omega_0 - \omega} \right], \quad (4.110)$$

$$k_-^2 = k_0^2 \left[\frac{\omega_0 + \omega_M + \omega}{\omega_0 + \omega} \right]. \quad (4.111)$$

These dispersion relations are plotted in Figure 4.8. Note that the k_+ wave is perturbed much more strongly by the medium than is the k_- wave. We will return to this observation after finding the field vectors for the two modes.

Let us assume the magnetic field is of the form

$$\mathbf{H} = H_0 \hat{\mathbf{z}} + \mathbf{h}, \quad (4.112)$$

where H_0 is the magnitude of the static bias field and \mathbf{h} is the field component associated with the propagating wave. According to Eqs. (4.103) and (4.107), the magnetic field \mathbf{h} must satisfy

$$\begin{bmatrix} k_0^2(1 + \chi) - k^2 & -i k_0^2 \kappa & 0 \\ +i k_0^2 \kappa & k_0^2(1 + \chi) - k^2 & 0 \\ 0 & 0 & k_0^2 \end{bmatrix} \begin{bmatrix} h_x \\ h_y \\ h_z \end{bmatrix} = 0. \quad (4.113)$$

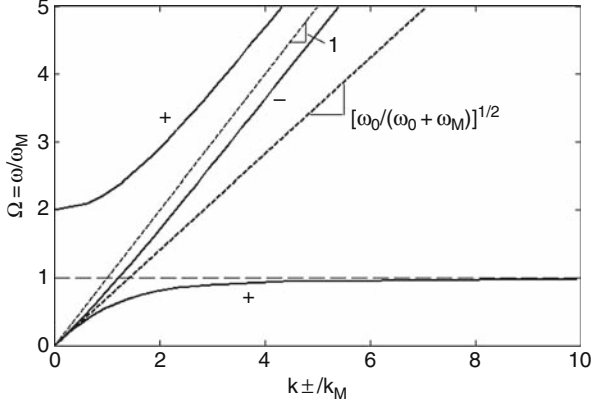


Fig. 4.8. Dispersion relations for propagation parallel to the applied field in a magnetized ferrite. Between ω_0 and $\omega_0 + \omega_M$, k_+ is imaginary and this mode does not propagate. The wave number is normalized to $k_M = \omega_M \sqrt{\mu_0 \epsilon}$ and calculations are for $\omega_0/\omega_M = 1$.

Examination of the last row leads us to the conclusion that $h_z = 0$ for all finite frequency excitations. To find the other components, we substitute $k^2 = k_\pm^2$ from Eq. (4.108) or (4.109). For $k^2 = k_+^2$ we have

$$k_0^2 \kappa \begin{bmatrix} -1 & -i \\ i & -1 \end{bmatrix} \begin{bmatrix} h_x \\ h_y \end{bmatrix} = 0 \quad (4.114)$$

or

$$\frac{h_y}{h_x} = i. \quad (4.115)$$

Thus, the magnetic field is right circularly polarized and can be written as

$$\mathbf{h}_+ = \frac{h_0}{\sqrt{2}} \begin{bmatrix} 1 \\ i \\ 0 \end{bmatrix} e^{i(k_+ z - \omega t)}. \quad (4.116)$$

The electric field \mathbf{e} associated with the wave can be obtained from Maxwell's equation (cf. Eq. (4.65))

$$\mathbf{e} = -\frac{1}{\omega \epsilon} \mathbf{k} \times \mathbf{h}. \quad (4.117)$$

For the k_+ wave we have

$$\begin{aligned} \mathbf{e} &= -\frac{k_+}{\omega \epsilon} \hat{\mathbf{z}} \times \mathbf{h} \\ &= \frac{i h_0 k_+}{\omega \epsilon \sqrt{2}} \begin{bmatrix} 1 \\ i \\ 0 \end{bmatrix} e^{i(k_+ z - \omega t)}. \end{aligned} \quad (4.118)$$

Thus, both the electric and magnetic fields are right circularly polarized.

Following a similar procedure for the k_- wave gives

$$\mathbf{h}_- = \frac{h_0}{\sqrt{2}} \begin{bmatrix} 1 \\ -i \\ 0 \end{bmatrix} e^{i(k_- z - \omega t)}, \quad (4.119)$$

$$\mathbf{e}_- = -\frac{ih_0 k_-}{\omega \varepsilon \sqrt{2}} \begin{bmatrix} 1 \\ -i \\ 0 \end{bmatrix} e^{i(k_- z - \omega t)}. \quad (4.120)$$

The fields of the k_- wave are, therefore, left circularly polarized.

Referring again to Figure 4.8, we note that the strong interaction of the k_+ wave with the medium is caused by the fact that the right circularly polarized fields of a wave propagating along the $+\hat{\mathbf{z}}$ direction rotate in the same sense as the natural precession of the magnetization (cf. Figure 3.16). The interaction is greatest when the fields also rotate with the same frequency as the natural precession ($\omega = \omega_0$).

4.9.2 Propagation Perpendicular to the Applied Field

Let us next consider the case $\mathbf{k} = k\hat{\mathbf{y}}$. The coefficient matrix for \mathbf{h} can be obtained as before by substituting this form for \mathbf{k} into Eq. (4.106). We find that the \mathbf{h} field must satisfy the equation

$$\begin{bmatrix} k_0^2(1 + \chi) - k^2 & -ik_0^2\kappa & 0 \\ +ik_0^2\kappa & k_0^2(1 + \chi) & 0 \\ 0 & 0 & k_0^2 - k^2 \end{bmatrix} \begin{bmatrix} h_x \\ h_y \\ h_z \end{bmatrix} = 0. \quad (4.121)$$

Setting the determinant of the coefficient matrix to zero gives the results

$$k_a^2 = k_0^2 = \omega^2 \mu_0 \varepsilon, \quad (4.122)$$

$$k_b^2 = k_0^2 \left[\frac{(1 + \chi)^2 - \kappa^2}{1 + \chi} \right]. \quad (4.123)$$

Substituting Eqs. (3.115) and (3.116) for χ and κ and simplifying allows us to write the dispersion relation (4.123) in the form

$$k_b^2 = k_0^2 \left[\frac{(\omega_0 + \omega_M)^2 - \omega^2}{\omega_0(\omega_0 + \omega_M) - \omega^2} \right]. \quad (4.124)$$

These dispersion relations are plotted in Figure 4.9.

The magnetic fields for the waves can be obtained by substituting the dispersion relations in Eqs. (4.122) and (4.123) into the wave equation (4.121). Substituting $k^2 = k_0^2$ immediately allows an arbitrary field component along the $\hat{\mathbf{z}}$ direction. However, examination of the remaining 2×2 system of equations for h_x and h_y , shows that the only solution for finite ω is $h_x = h_y = 0$ (Problem 4.5). The field is thus linearly polarized:

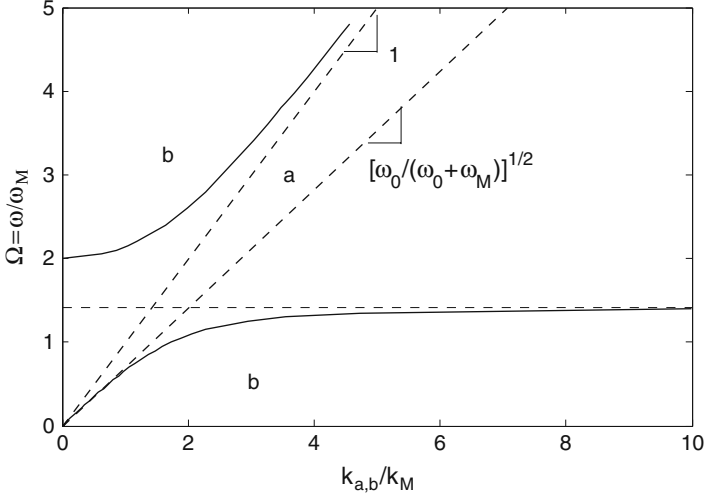


Fig. 4.9. Dispersion relations for propagation perpendicular to the applied field in a magnetized ferrite. Between $[\omega_0(\omega_0 + \omega_M)]^{1/2}$ and $\omega_0 + \omega_M$, k_b is imaginary and the mode does not propagate. The wave number is normalized to $k_M = \omega_M \sqrt{\mu_0 \epsilon}$, and calculations are for $\omega_0/\omega_M = 1$.

$$\mathbf{h}_a = h_0 \begin{bmatrix} 0 \\ 0 \\ 1 \end{bmatrix} e^{i(k_a y - \omega t)}. \quad (4.125)$$

Substituting this field into equation (4.117) for the electric field shows that \mathbf{e} is also linearly polarized:

$$\mathbf{e}_a = -\frac{h_0 k_a}{\omega \epsilon} \begin{bmatrix} 1 \\ 0 \\ 0 \end{bmatrix} e^{i(k_a y - \omega t)}. \quad (4.126)$$

An examination of the permeability tensor (4.104) shows that there is no material susceptibility along the $\hat{\mathbf{z}}$ direction. Since the only component of \mathbf{h} is along $\hat{\mathbf{z}}$, there is no magnetic interaction with the medium and the wave properties are the same as in a non-magnetic material with identical dielectric properties.

Substituting $k^2 = k_b^2$ from the dispersion relation (4.123) into the wave equation (4.121) gives

$$k_0^2 \begin{bmatrix} \kappa^2/(1 + \chi) & -i\kappa & 0 \\ +i\kappa & 1 + \chi & 0 \\ 0 & 0 & -[\chi - \kappa^2/(1 + \chi)] \end{bmatrix} \begin{bmatrix} h_x \\ h_y \\ h_z \end{bmatrix} = 0. \quad (4.127)$$

Careful examination shows that the coefficient of h_z does not vanish for finite ω other than $\omega = \omega_0$. At this point, the susceptibility elements are singular

and $\mathbf{h} = 0$ for finite \mathbf{m} . Thus, we conclude $h_z = 0$. Solving the remaining 2×2 system for h_x and h_y gives

$$\frac{h_y}{h_x} = -\frac{i\kappa}{1 + \chi} = -\frac{i\omega\omega_M}{\omega_0(\omega_0 + \omega_M) - \omega^2}. \quad (4.128)$$

The field can therefore be written

$$\mathbf{h}_b = C \begin{bmatrix} 1 + \chi \\ -i\kappa \\ 0 \end{bmatrix} e^{i(k_b y - \omega t)}, \quad (4.129)$$

where C is an arbitrary constant. Following the same procedure as before to obtain the electric field gives

$$\mathbf{e}_b = \frac{k_b C}{\omega \varepsilon} \begin{bmatrix} 0 \\ 0 \\ 1 + \chi \end{bmatrix} e^{i(k_b y - \omega t)}. \quad (4.130)$$

This result is unusual compared to the previous cases because the polarizations of \mathbf{e}_b and \mathbf{h}_b are different. The electric field is linearly polarized, whereas the magnetic field is elliptically polarized. Further, \mathbf{k}_b is parallel rather than perpendicular to the plane of the ellipse. It is interesting to note that at $\omega^2 = \omega_0(\omega_0 + \omega_M)$, Eq. (4.128) shows that h_y is the only nonzero component of \mathbf{h} ; the field is *entirely parallel* to \mathbf{k}_b ! It follows that, in this limit, $\nabla \times \mathbf{h} \approx 0$. This is an example of what is known as the *magnetostatic limit* and will be discussed in more detail in Section 4.10.

Comparison of Figures 4.8 and 4.9 shows that the $k = 0$ limit of the upper branch occurs at $\omega = \omega_0 + \omega_M$ for both directions of propagation. On the other hand, the $k \rightarrow \infty$ limit on the lower branch occurs when $\omega = \omega_0$ for $\mathbf{k} \parallel \mathbf{H}_0$ and when $\omega = \omega_0(\omega_0 + \omega_M)^{1/2}$ for $\mathbf{k} \perp \mathbf{H}_0$. A complete analysis shows that the frequency of this asymptote varies continuously between these two limits for intermediate orientations of \mathbf{k} (see Problem 4.6).

4.10 The Magnetostatic Approximation⁴

Let us consider uniform plane waves propagating in an arbitrary direction in a magnetized ferrite. From Eqs. (4.15), (4.70), and (4.71), Maxwell's equations can be written:

$$\mathbf{k} \times \mathbf{h} = -\omega \varepsilon \mathbf{e}, \quad (4.131)$$

$$\mathbf{k} \times \mathbf{e} = \omega \mu_0 (\mathbf{h} + \mathbf{m}). \quad (4.132)$$

⁴ This section draws heavily from "Waves in Ferrites," by F. R. Morgenthaler (1967, unpublished), which was used as course notes for M.I.T. courses 6.58, "Electrodynamics of Waves, Media, and Interactions," and 6.753, "Microwave Magnetics."

Crossing \mathbf{k} into both sides of Eq. (4.131) gives

$$\mathbf{k}\mathbf{k} \cdot \mathbf{h} - k^2\mathbf{h} = -\omega^2\mu_0\varepsilon(\mathbf{h} + \mathbf{m}), \quad (4.133)$$

where we have used the identity (4.83) and substituted Eq. (4.132) for $\mathbf{k} \times \mathbf{e}$. Since $\mathbf{k} \cdot \mathbf{b} = \mu_0\mathbf{k} \cdot (\mathbf{h} + \mathbf{m}) = 0$, it follows that

$$\mathbf{k} \cdot \mathbf{h} = -\mathbf{k} \cdot \mathbf{m}. \quad (4.134)$$

Substituting this result into Eq. (4.133) and solving for \mathbf{h} gives

$$\mathbf{h} = \frac{k_0^2\mathbf{m} - \mathbf{k}\mathbf{k} \cdot \mathbf{m}}{k^2 - k_0^2}, \quad (4.135)$$

where $k_0^2 = \omega^2\mu_0\varepsilon$.

Following a similar procedure, we can find \mathbf{e} in terms of \mathbf{m} . Crossing \mathbf{k} into both sides of Eq. (4.132) gives

$$-k^2\mathbf{e} = -\omega^2\mu_0\varepsilon\mathbf{e} + \omega\mu_0\mathbf{k} \times \mathbf{m}. \quad (4.136)$$

Here we have used the fact that $\mathbf{k} \cdot \mathbf{e} = 0$ and substituted Eq. (4.131) for $\mathbf{k} \times \mathbf{h}$. Solving for \mathbf{e} gives

$$\mathbf{e} = \frac{\omega\mu_0\mathbf{k} \times \mathbf{m}}{k_0^2 - k^2}. \quad (4.137)$$

Finally, since $\nabla \times \mathbf{h} = -\omega\varepsilon\mathbf{e}$, we can write

$$\nabla \times \mathbf{h} = -\frac{k_0^2\mathbf{k} \times \mathbf{m}}{k_0^2 - k^2}. \quad (4.138)$$

We found in Section 4.9 that $|\mathbf{k}| \gg |\mathbf{k}_0|$ for certain frequencies. Let us examine Eqs. (4.135), (4.137), and (4.138) in this limit. Since both the numerator and denominator of (4.135) contain terms quadratic in \mathbf{k} , we conclude that \mathbf{h} remains finite for large $|\mathbf{k}|$ provided $\mathbf{k} \cdot \mathbf{m} \neq 0$. In contrast, Eqs. (4.137) and (4.138) for \mathbf{e} and $\nabla \times \mathbf{h}$, respectively, vanish as $1/k$ for large $|\mathbf{k}|$. Thus to lowest order, the waves are described by the magnetostatic equations

$$\nabla \times \mathbf{h} = 0, \quad (4.139)$$

$$\nabla \cdot \mathbf{b} = 0. \quad (4.140)$$

After solving these equations for \mathbf{b} and \mathbf{h} , an approximation to the electric field may be obtained from

$$\nabla \times \mathbf{e} = i\omega\mathbf{b}. \quad (4.141)$$

Equations (4.139), (4.140), and (4.141) comprise the magnetoquasistatic approximation to Maxwell's equations.⁵ Waves that are described by these

⁵ Examination of Eqs. (4.135), (4.137), and (4.138) shows that the magnetoquasistatic approximation is also valid in the limit $|\mathbf{k}| \ll |\mathbf{k}_0|$.

equations can be called magnetoquasistatic waves, or more commonly, *magnetostatic waves*. Because precessing spins are responsible for the form of the permeability tensor (4.104), these waves can also be viewed as a type of spin wave. However, unlike the spin waves in Chapter 2, the coupling between the spins is dominated by the dipolar fields from the magnetic moments rather than the exchange interaction. This occurs when $k_0 \ll k \ll \pi/a$, where a is the spacing between spins. Consequently, these waves are also known as *dipolar spin waves*. Dipolar spin waves or magnetostatic waves propagating in various geometries are discussed in more detail in the next two chapters.

Before leaving this topic, let us return to the case $\mathbf{k} \cdot \mathbf{m} = 0$ which was excluded in the previous discussion. In this case we find that both \mathbf{e} and \mathbf{h} vanish for large k so that the magnetostatic approximation $\nabla \times \mathbf{h} = 0$ is still valid. This does not represent a trivial solution, however, since \mathbf{m} does not vanish. This situation results from the resonance in the susceptibility at $\omega = \omega_0$.

Problems

4.1. Derive the lossless condition (4.46) by showing that

$$\operatorname{Re}\{i\omega \mathbf{E} \cdot \mathbf{D}^*\} = \frac{i\omega}{2} \mathbf{E}^* \cdot (\bar{\boldsymbol{\epsilon}}^\dagger - \bar{\boldsymbol{\epsilon}}) \cdot \mathbf{E} \quad (4.142)$$

and

$$\operatorname{Re}\{-i\omega \mathbf{H}^* \cdot \mathbf{B}\} = \frac{i\omega}{2} \mathbf{H}^* \cdot (\bar{\boldsymbol{\mu}}^\dagger - \bar{\boldsymbol{\mu}}) \cdot \mathbf{H}. \quad (4.143)$$

4.2. The electric field of a plane wave propagating in free space is given by

$$\mathbf{E} = \hat{\mathbf{y}} E_0 e^{ikz - i\omega t}. \quad (4.144)$$

- (a) Using Maxwell's equations, find \mathbf{H} .
- (b) Calculate the time-averaged electric and magnetic energy densities and show that

$$\langle w_m(t) \rangle = \langle w_e(t) \rangle. \quad (4.145)$$

- (c) Calculate the energy velocity defined by Eq. (4.102) and show that

$$\mathbf{v}_e = \mathbf{v}_p = \frac{\omega}{k} \hat{\mathbf{z}}. \quad (4.146)$$

- (d) Find an expression for the *intrinsic wave impedance* of the medium defined as

$$Z_0 \equiv \frac{|\mathbf{E}|}{|\mathbf{H}|}. \quad (4.147)$$

Use the dispersion relation to express this in a form independent of ω and k .

4.3. The permittivity tensor of a uniaxial dielectric is of the form

$$\bar{\epsilon} = \begin{bmatrix} \epsilon & 0 & 0 \\ 0 & \epsilon & 0 \\ 0 & 0 & \epsilon_z \end{bmatrix} \quad (4.148)$$

The $\hat{\mathbf{z}}$ -direction is called the *optic axis*.

- (a) Assuming uniform plane wave propagation and a non-magnetic medium, show that the electric field must satisfy the equation

$$\bar{\mathbf{W}}(\omega, \mathbf{k}) \cdot \mathbf{E} = 0, \quad (4.149)$$

where $\bar{\mathbf{W}}(\omega, \mathbf{k})$ is a 3×3 matrix whose elements are functions of (ω, \mathbf{k}) . $\bar{\mathbf{W}}(\omega, \mathbf{k})$ is sometimes called the *wave matrix* or *dispersion matrix*.

- (b) By setting the determinant of $\bar{\mathbf{W}}(\omega, \mathbf{k})$ to zero, show that Eq. (4.149) can be satisfied by two different waves with the dispersion relations

$$k^2 = \omega^2 \mu_0 \epsilon, \quad (4.150)$$

$$k_x^2 + k_y^2 + \frac{\epsilon_z}{\epsilon} k_z^2 = \omega^2 \mu_0 \epsilon_z. \quad (4.151)$$

The wave governed by (4.151) is called the *extraordinary* electromagnetic wave since the relation between ω and \mathbf{k} depends on the direction of \mathbf{k} . In contrast, the wave governed by (4.150) is isotropic and is called the *ordinary* electromagnetic wave.

- (c) Assume the direction of \mathbf{k} makes an angle θ with respect to the optic axis $\hat{\mathbf{z}}$. Find the magnitudes of the phase velocities for these two waves for arbitrary θ .
- (d) Using the results of parts (a) and (b), find the electric field polarizations of both waves.

4.4. Consider wave propagation along the direction of an applied magnetic field in a ferrite, as discussed in Section 4.9.1. If propagation occurs along the $\hat{\mathbf{z}}$ direction, assume the total electric field at $z = 0$ is linearly polarized along the $\hat{\mathbf{x}}$ direction.

- (a) Show that the linearly polarized field can be expressed as the sum of left and right circularly polarized waves propagating with wave numbers k_- and k_+ , respectively.
- (b) Show that after propagating a distance d , the linear polarization of the total field will be rotated through the angle (Figure 4.10)

$$\theta_F = (k_+ - k_-) \frac{d}{2}. \quad (4.152)$$

This phenomenon is called *Faraday rotation*.

- (c) Show that the polarization continues to rotate in the same direction if the propagation direction reverses.

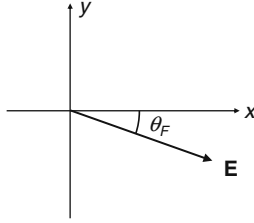


Fig. 4.10. Faraday rotation angle for a wave initially polarized along the x -axis.

- (d) Using Eqs. (4.110) and (4.111) for k_+ and k_- show that the direction of rotation for $\omega > \omega_0 + \omega_M$ is opposite to that for $\omega < \omega_0$.

4.5. In Section 4.9.2, wave propagation perpendicular to the applied field in a ferrite was considered. The equation for the x and y magnetic field components of the wave associated with the wave number k_a is obtained by substituting Eq. (4.122) into Eq. (4.121).

- (a) Show that the x and y components of the magnetic fields for the k_a wave must satisfy

$$\begin{bmatrix} \chi & -i\kappa \\ i\kappa & 1 + \chi \end{bmatrix} \begin{bmatrix} h_x \\ h_y \end{bmatrix} = 0. \quad (4.153)$$

- (b) Using the definitions for χ and κ (Eqs. (3.115) and (3.116)) show that the only solution for finite ω is $h_x = h_y = 0$. (Hint: If the elements of $\bar{\chi}$ are singular, $\mathbf{h} = 0$ for any finite \mathbf{m} since $\mathbf{m} = \bar{\chi} \cdot \mathbf{h}$.)

4.6. Consider plane waves propagating in a magnetized ferrite.

- (a) Show that the magnetic field in the $|\mathbf{k}| \gg |\mathbf{k}_0|$ magnetostatic limit is given by

$$\mathbf{h} = -\frac{\mathbf{k}\mathbf{k} \cdot \mathbf{m}}{k^2}. \quad (4.154)$$

- (b) Using the constitutive relation between \mathbf{m} and \mathbf{h} along with the results of part (a), show that \mathbf{h} must satisfy

$$(k^2 \bar{\mathbf{I}} + \mathbf{k}\mathbf{k} \cdot \bar{\chi}) \cdot \mathbf{h} = 0, \quad (4.155)$$

where $\bar{\chi}$ is the Polder susceptibility tensor (Eq. 3.114).

- (c) Assume $\mathbf{k} = k(\hat{\mathbf{y}} \sin \theta + \hat{\mathbf{z}} \cos \theta)$, where θ is the angle between \mathbf{k} and the applied field direction (taken to be $\hat{\mathbf{z}}$). Substitute this into the result of part (b) and show that the existence of a non-trivial solution requires

$$\omega^2 = \omega_0(\omega_0 + \omega_M \sin^2 \theta). \quad (4.156)$$

This expression gives the correct frequencies for the $k \rightarrow \infty$ asymptotes for the limiting cases of $\theta = 0, \pi/2$ discussed in Section 4.9. The present result shows that the frequency of the asymptote lies between these two limits for intermediate angles.

References

- [1] E. C. Jordan and K. G. Balmain, *Electromagnetic Waves and Radiating Systems*. Englewood Cliffs, NJ: Prentice Hall, 1968.
- [2] J. D. Kraus and D. Fleisch, *Electromagnetics with Applications*. New York: McGraw-Hill, 1999.
- [3] D. K. Cheng, *Fundamentals of Engineering Electromagnetics*. Reading, MA: Addison Wesley, 1993.
- [4] H. C. Chen, *Theory of Electromagnetic Waves: A Coordinate-Free Approach*. New York: McGraw-Hill, 1983.
- [5] H. A. Haus, *Waves and Fields in Optoelectronics*. Englewood Cliffs, NJ: Prentice-Hall, 1984.
- [6] J. A. Kong, *Electromagnetic Wave Theory*. Cambridge, MA: EMW Publishing, 2005.

Magnetostatic Modes

We saw in Chapter 4 that the equations of magneto-quasi-statics are useful for describing waves when the wavelength in the medium is very different from that of an ordinary electromagnetic wave at the same frequency. We will now elaborate on this idea and show how the magneto-quasi-static approximation can be used to analyze modes in a variety of geometries.¹

5.1 Walker's Equation

The equations of magneto-quasi-statics were shown in Section 4.10 to be (cf. Eqs. (4.139), (4.140), and (4.141))

$$\nabla \times \mathbf{h} = 0, \quad (5.1)$$

$$\nabla \cdot \mathbf{b} = 0, \quad (5.2)$$

$$\nabla \times \mathbf{e} = i\omega \mathbf{b}. \quad (5.3)$$

To uniquely determine the field quantities, we must also specify the constitutive relations. For a magnetized ferrite, we have (cf. (4.21) and (4.23))

$$\mathbf{b} = \bar{\boldsymbol{\mu}} \cdot \mathbf{h}, \quad (5.4)$$

where²

$$\bar{\boldsymbol{\mu}} = \mu_0(\bar{\mathbf{I}} + \bar{\boldsymbol{\chi}}). \quad (5.5)$$

The permeability tensor in the absence of exchange and anisotropy is (cf. (4.104))

¹ Additional general references on these topics include Lax and Button [1], Soohoo [2], and Sodha and Srivastava [3].

² The subscript m on the magnetic susceptibility tensor will be omitted when there is no possibility of confusion between the electric and magnetic susceptibilities.

$$\bar{\boldsymbol{\mu}} = \mu_0 \begin{bmatrix} 1 + \chi & -i\kappa & 0 \\ i\kappa & 1 + \chi & 0 \\ 0 & 0 & 1 \end{bmatrix}, \quad (5.6)$$

where the bias field is assumed to lie along the $\hat{\mathbf{z}}$ -direction. Since $\nabla \times (\nabla \psi) \equiv 0$ for any analytic function ψ , (5.1) implies that we can write

$$\mathbf{h} = -\nabla \psi. \quad (5.7)$$

where ψ is a magnetostatic scalar potential.³ Combining Eqs. (5.2), (5.4), and (5.7) gives

$$\nabla \cdot (\bar{\boldsymbol{\mu}} \cdot \nabla \psi) = 0. \quad (5.8)$$

This can be expanded using (5.5) and (5.6) to obtain

$$(1 + \chi) \left[\frac{\partial^2 \psi}{\partial x^2} + \frac{\partial^2 \psi}{\partial y^2} \right] + \frac{\partial^2 \psi}{\partial z^2} = 0, \quad (5.9)$$

where χ and κ are assumed to be independent of position. Since Eq. (5.9) is based only on the magnetostatic equations (5.1) and (5.2), solutions are commonly referred to as *magnetostatic modes* [4–6]. It is important to keep in mind, however, that the solutions are not rigorously magnetostatic since time variations at microwave frequencies are assumed. Equation (5.9) is called *Walker's equation* and is the basic equation for magnetostatic modes in homogeneous media.

As an example of the use of Walker's equation, let us again consider uniform plane wave propagation in an infinite medium. Assuming $\psi \propto \exp(i\mathbf{k} \cdot \mathbf{r})$, Eq. (5.9) becomes

$$(1 + \chi)(k_x^2 + k_y^2) + k_z^2 = 0. \quad (5.10)$$

If the propagation angle with respect to the $\hat{\mathbf{z}}$ axis (also the direction of the DC bias field) is θ , then

$$k_x^2 + k_y^2 = k^2 \sin^2 \theta, \quad (5.11)$$

$$k_z^2 = k^2 \cos^2 \theta. \quad (5.12)$$

Substituting these equations into Eq. (5.10) and simplifying yields

$$\chi \sin^2 \theta = -1. \quad (5.13)$$

This can be expressed explicitly in terms of frequency using Eq. (3.115) for χ . The result is (cf. Problem 4.6)

$$\omega = [\omega_0(\omega_0 + \omega_M \sin^2 \theta)]^{1/2}. \quad (5.14)$$

Note that this result is independent of the magnitude of k ; waves at this frequency can have any wavelength! This can be understood by referring to the

³ The choice of sign in (5.7) is arbitrary. The minus sign is usually chosen, however, in analogy with the electrostatic equation $\mathbf{E} = -\nabla V$.

dispersion relations for electromagnetic waves shown in Figures 4.8 and 4.9. For $\theta = 0$, the frequency given by Eq. (5.14) corresponds to the large- k asymptote for propagation parallel to the bias field (lowest dispersion branch in Figure 4.8). Similarly, $\theta = \pi/2$ gives the large- k asymptote for propagation perpendicular to the bias field (lowest branch in Figure 4.9). Thus, for sufficiently large k , the magnetostatic solution approximates the complete electromagnetic analysis. The frequency degeneracy in the magnetostatic approximation is removed by considering the effects of either finite sample boundaries or the exchange interaction. Both of these possibilities are considered in the following sections.

5.2 Spin Waves

In the presence of exchange, \mathbf{h} is obtained from \mathbf{m} using the matrix differential $\bar{\mathbf{A}}_{\text{op}}$ (cf. Eqs. (3.124) and (3.125)):

$$\mathbf{h} = \bar{\mathbf{A}}_{\text{op}} \cdot \mathbf{m}, \quad (5.15)$$

where

$$\bar{\mathbf{A}}_{\text{op}} = \frac{1}{\omega_{\text{M}}} \begin{bmatrix} \omega_0 - \omega_{\text{M}}\lambda_{\text{ex}}\nabla^2 & i\omega \\ -i\omega & \omega_0 - \omega_{\text{M}}\lambda_{\text{ex}}\nabla^2 \end{bmatrix}, \quad (5.16)$$

and magnetocrystalline anisotropy has been neglected. For uniform plane wave propagation, the spatial dependence of \mathbf{m} and \mathbf{h} is taken to be of the form $\exp(i\mathbf{k} \cdot \mathbf{r})$. Thus, the operator ∇^2 can be replaced by the factor $-k^2$. Equation (5.15) then becomes

$$\mathbf{h} = \bar{\mathbf{A}}_{\text{op}} \cdot \mathbf{m} = \frac{1}{\omega_{\text{M}}} \begin{bmatrix} \omega_0 + \omega_{\text{M}}\lambda_{\text{ex}}k^2 & i\omega \\ -i\omega & \omega_0 + \omega_{\text{M}}\lambda_{\text{ex}}k^2 \end{bmatrix} \begin{bmatrix} m_x \\ m_y \end{bmatrix}. \quad (5.17)$$

Since the exchange term $\omega_{\text{M}}\lambda_{\text{ex}}k^2$ appears everywhere with ω_0 , it follows that the effects of exchange can be added to the previous magnetostatic plane wave analysis by simply replacing ω_0 with $\omega_0 + \omega_{\text{M}}\lambda_{\text{ex}}k^2$. The dispersion relation (5.14) thus becomes

$$\omega = [(\omega_0 + \omega_{\text{M}}\lambda_{\text{ex}}k^2)(\omega_0 + \omega_{\text{M}}(\lambda_{\text{ex}}k^2 + \sin^2 \theta))]^{1/2}. \quad (5.18)$$

We see that the consideration of exchange has restored the one-to-one correspondence between frequency and wave number. Equation (5.18) is graphed in Figure 5.1 for the two cases $\theta = 0, \pi/2$. The same behavior was illustrated qualitatively in Figure 2.5.

As the magnitude of k increases, the exchange term $\lambda_{\text{ex}}k^2$ eventually becomes large when compared with unity. When this occurs, the excitations are traditionally called spin waves or *exchange spin waves*. In contrast, when

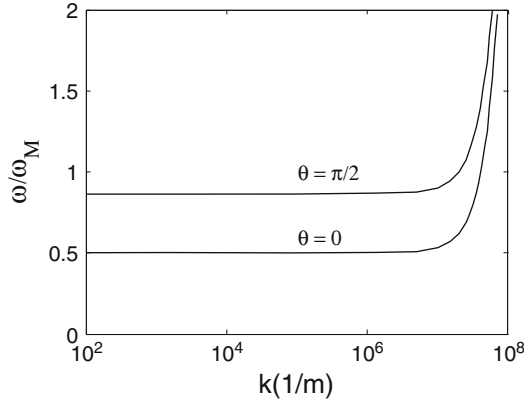


Fig. 5.1. Magnetostatic wave dispersion relations including exchange for propagation parallel and perpendicular to the applied bias field. An infinite YIG medium is assumed with $\omega_0/\omega_M = 0.5$, $\lambda_{\text{ex}} = 3 \times 10^{-16} \text{ m}^2$.

$\lambda_{\text{ex}} k^2 \ll 1$, the excitations are called *dipolar spin waves* or *magnetostatic waves*. The wave therefore evolves continuously in character as k increases; we use the term *electromagnetic wave* when both electric and magnetic dipolar interactions are important but exchange interactions are negligible, *magnetostatic wave* or *dipolar spin wave* when magnetic dipolar interactions dominate both electric and exchange interactions, and *exchange spin wave* when only the exchange interaction is important. The general term *spin wave* is used for both dipolar- and exchange-dominated excitations. The value of the exchange constant determined from spin wave measurements at microwave frequencies in YIG is $\lambda_{\text{ex}} = 3 \times 10^{-16} \text{ m}^2$ [7].

Experimentally, it is observed that the spins near the surfaces of magnetic thin films often behave as if they are “pinned” and not allowed to precess. This behavior may result from spins near the surface experiencing different anisotropy fields from those in the bulk. Reflections at the top and bottom surfaces cause *spin wave resonances*, whenever the film thickness equals an integral number of half wavelengths (Figure 5.2). As a result of the pinning effect, uniform RF drive fields can be used to excite spin wave resonances corresponding to an odd number of half wavelengths through the film thickness [8]. The resonant frequencies can be obtained from (5.18) with $k = n\pi/d$, where d is the film thickness and n is an integer. The result for a normally magnetized film ($\theta = 0$) is

$$\omega_n = \omega_0 + \omega_M \lambda_{\text{ex}} \left(\frac{\pi n}{d} \right)^2, \quad (5.19)$$

where $\omega_0 = -\gamma\mu_0(H_{\text{DC}} - M_S)$ and H_{DC} and M_S are the externally applied field and the saturation magnetization of the film, respectively. The applied

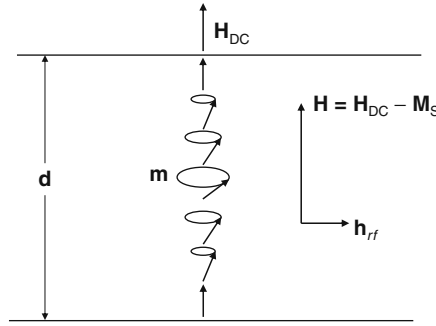


Fig. 5.2. Standing spin wave resonance in a magnetic thin film. The precession cone angle of the magnetization has been exaggerated for clarity.

field is reduced in the film by the presence of the demagnetizing field, $-M_S$, generated by effective magnetic charges on the film surfaces. This will be discussed in more detail in Section 5.3.

Spin wave resonances in thin films were first observed by Seavey and Tannenwald [9]. In their experiment on permalloy films, they used a microwave cavity which required that they fix the microwave frequency and vary the bias field. The spin wave resonance absorption peaks observed in their measurements are shown in Figure 5.3.

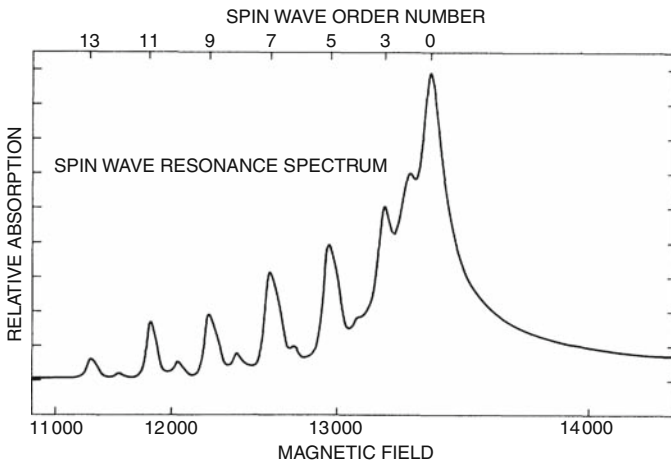


Fig. 5.3. One of the earliest observations of spin wave resonances. Seavey and Tannenwald conducted their experiments on a $0.56\text{ }\mu\text{m}$ thin film of permalloy placed inside a microwave cavity in the presence of an external magnetic field. (Reprinted with permission from [9]. Copyright 1998 by the American Physical Society.)

5.3 Uniform Precession Modes

For a plane wave in an infinite medium, we have shown that the magnetostatic approximation is valid when k is large compared with the free-space wave number. For finite media, the magnetostatic approximation can be extended to $k = 0$ if the sample dimensions are small when compared with a free-space wavelength. Such modes are called *uniform precession modes* since the magnetization precesses in-phase throughout the entire sample.⁴

5.3.1 Normally Magnetized Ferrite⁵ Film

Consider a thin ferrite film with a DC bias field applied perpendicular to its plane as shown in Figure 5.4. We first need to determine what the field inside the film is for a given applied field H_{DC} as measured outside the ferrite. This is because the internal field H_0 is the field quantity that enters the permeability tensor elements. Here and in the following sections, we assume that the applied field is strong enough to saturate the ferrite so that \mathbf{M}_S is everywhere parallel to \mathbf{H}_{DC} .

In the ferrite, the pertinent constitutive relation is

$$\mathbf{B}_f = \mu_0(\mathbf{H}_0 + \mathbf{M}_S), \quad (5.20)$$

whereas in the non-magnetic region external to the ferrite, we have

$$\mathbf{B}_{ext} = \mu_0 \mathbf{H}_{DC}. \quad (5.21)$$

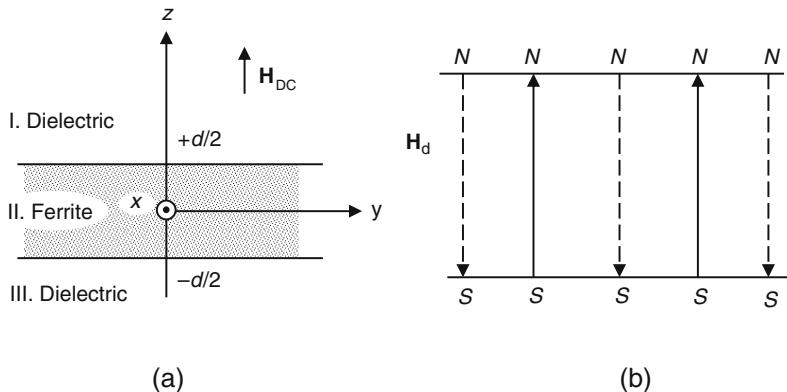


Fig. 5.4. (a) Geometry for the uniform precession mode analysis of a normally magnetized ferrite film. (b) The demagnetizing field generated by effective magnetic surface charges.

⁴ See, e.g., Lax and Button [1], Soohoo [2], and Walker [6].

⁵ Although we use the term ferrite, the analysis applies equally well to other materials with low-magnetic loss, such as magnetic garnets (e.g., YIG).

The boundary conditions require that the normal component of \mathbf{B} be continuous. In the present case, the entire field is normal, so we require

$$\mu_0 \mathbf{H}_{\text{DC}} = \mu_0 (\mathbf{H}_0 + \mathbf{M}_S)$$

or

$$\mathbf{H}_0 = \mathbf{H}_{\text{DC}} - \mathbf{M}_S. \quad (5.22)$$

Thus, the field in the film is reduced by the amount M_S . This is called the *demagnetizing field* \mathbf{H}_d and is due to effective magnetic poles on the top and bottom surfaces of the film (Figure 5.4(b)).

Since the RF fields of interest are also uniform, surface poles can be used to describe the RF demagnetizing fields as well. However, the small-signal magnetization will be in the plane of the film and thus will not induce magnetic poles on the top and bottom surfaces. If the width of the film is much larger than its thickness, the effects of induced poles on the film edges will be small and can be neglected. We conclude that there will be no RF demagnetizing field for the uniform precession mode in this geometry. Thus, we require $\mathbf{h} = 0$.

The relationship between the small-signal magnetization and field intensity must also be consistent with the linearized torque equation. From (5.17) with $k = 0$ we have

$$\mathbf{h} = \bar{\chi}^{-1} \cdot \mathbf{m} = \frac{1}{\omega_M} \begin{bmatrix} \omega_0 & i\omega \\ -i\omega & \omega_0 \end{bmatrix} \cdot \begin{bmatrix} m_x \\ m_y \end{bmatrix} \quad (5.23)$$

Applying the additional requirement $\mathbf{h} = 0$, the non-trivial solution is obtained by setting the determinate of the coefficient matrix to zero. The result is

$$\omega = \omega_0 = -\gamma\mu_0(H_{\text{DC}} - M_S). \quad (5.24)$$

This frequency corresponds to the resonance in the permeability tensor.

As the small-signal amplitude $m_\rho = \sqrt{m_x^2 + m_y^2}$ increases, there is a reduction in the $\hat{\mathbf{z}}$ component of the magnetization such that

$$M_z = \sqrt{M_S^2 - m_\rho^2} \approx M_S \left(1 - \frac{1}{2} \frac{m_\rho^2}{M_S^2} \right). \quad (5.25)$$

This causes a reduction in ω_0 when the spin wave amplitude is large. This nonlinear effect is described in greater detail in Chapter 9.

5.3.2 Tangentially Magnetized Ferrite Film

The geometry for the tangentially magnetized film is shown in Figure 5.5. The determination of the DC field inside the film is much easier than before. Since the tangential components of \mathbf{H} must be continuous, we have $\mathbf{H}_0 = \mathbf{H}_{\text{DC}}$; there is no static demagnetizing field when the applied field is in the plane of an infinite film.

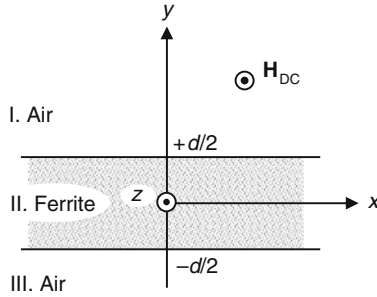


Fig. 5.5. Geometry for the analysis of the uniform precession mode in a tangentially magnetized ferrite film.

There will, in general, be two components to the small-signal magnetization: m_x and m_y . However, only m_y will give rise to an RF demagnetizing field since m_x is parallel to the top and bottom surfaces. The small-signal field generated by the induced surface poles can thus be written

$$\mathbf{h} = -\bar{\mathbf{N}}_d \cdot \mathbf{m} = - \begin{bmatrix} 0 & 0 \\ 0 & 1 \end{bmatrix} \begin{bmatrix} m_x \\ m_y \end{bmatrix}, \quad (5.26)$$

where $\bar{\mathbf{N}}_d$ is the demagnetizing tensor. Combining the requirements of Eqs. (5.23) and (5.26) gives

$$[\bar{\mathbf{N}}_d + \bar{\chi}^{-1}] \cdot \mathbf{m} = 0, \quad (5.27a)$$

which can be written:

$$\begin{bmatrix} \omega_0 & i\omega \\ -i\omega & \omega_0 + \omega_M \end{bmatrix} \begin{bmatrix} m_x \\ m_y \end{bmatrix} = 0. \quad (5.27b)$$

Non-trivial solutions are obtained when

$$\omega = [\omega_0(\omega_0 + \omega_M)]^{1/2}. \quad (5.28)$$

5.3.3 Ferrite Sphere

Consider a ferrite sphere of radius r_0 in a uniform DC field as shown in Figure 5.6. Again, we must find the field inside the sphere to calculate the components of the permeability tensor.

Because of the symmetry of the problem, it is most convenient to use spherical coordinates. Outside the sphere, Walker's equation reduces to Laplace's equation ($\nabla^2 \psi = 0$) written as [6]

$$\left[\frac{1}{r^2} \frac{\partial}{\partial r} \left(r^2 \frac{\partial}{\partial r} \right) + \frac{1}{r^2 \sin \theta} \frac{\partial}{\partial \theta} \left(\sin \theta \frac{\partial}{\partial \theta} \right) + \frac{1}{r^2 \sin^2 \theta} \frac{\partial^2}{\partial \phi^2} \right] \psi = 0. \quad (5.29)$$

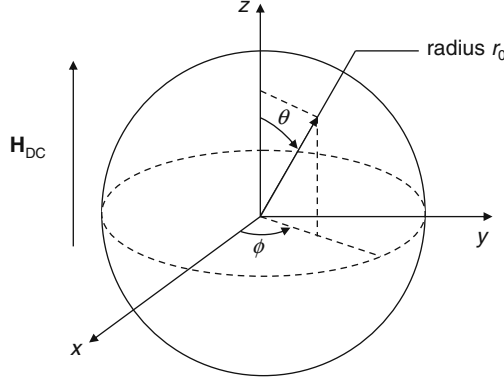


Fig. 5.6. Ferrite sphere placed in a uniform DC bias field.

Since a uniformly magnetized sphere exhibits perfect rotational symmetry about the direction of the bias field, neither the magnetization nor the potential function ψ will depend on ϕ . Thus, the ϕ derivatives in Eq. (5.29) can be set to zero. Using the separation-of-variables technique, we substitute

$$\psi = R(r)\Theta(\theta) \quad (5.30)$$

into Eq. (5.29) and multiply by $1/(R\Theta)$ from the left to obtain

$$\frac{1}{R} \frac{d}{dr} \left(r^2 \frac{dR}{dr} \right) + \frac{1}{\Theta \sin \theta} \frac{d}{d\theta} \left(\sin \theta \frac{d\Theta}{d\theta} \right) = 0. \quad (5.31)$$

For these two terms to always sum to zero, each must be equal to a constant. By convention, we set the first term equal to $+n(n+1)$ and the second equal to $-n(n+1)$, where n is an arbitrary constant. The resulting equation governing Θ is

$$\frac{1}{\sin \theta} \frac{d}{d\theta} \left(\sin \theta \frac{d\Theta}{d\theta} \right) + n(n+1)\Theta = 0. \quad (5.32)$$

Let us now make the change of variable

$$\begin{aligned} x &= \cos \theta \\ dx &= -\sin \theta d\theta \\ \sin \theta &= \sqrt{1 - x^2} \end{aligned} \quad (5.33)$$

where $-1 \leq x \leq 1$ for angles between 0 and π . This allows Eq. (5.32) to be written as

$$(1 - x^2) \frac{d^2 \Theta}{dx^2} - 2x \frac{d\Theta}{dx} + n(n+1)\Theta = 0. \quad (5.34)$$

This is *Legendre's equation* and is known to have finite solutions on the interval $-1 \leq x \leq +1$ when n is an integer [10, pp. 14–16, 167–169]. The

resulting normalized solutions are the *Legendre polynomials* $P_n(x)$. The first few polynomials are

$$\begin{aligned} P_0(x) &= 1 \\ P_1(x) &= x = \cos \theta \\ P_2(x) &= (3x^2 - 1)/2 = (3 \cos^2 \theta - 1)/2. \end{aligned} \quad (5.35)$$

The equation for R is obtained by equating the first term in Eq. (5.31) with $+n(n+1)$. After expanding the derivatives we obtain

$$r^2 \frac{d^2 R}{dr^2} + 2r \frac{dR}{dr} - n(n+1)R = 0. \quad (5.36)$$

It is easily verified that this has solutions

$$R = \begin{cases} r^n, \\ r^{-(n+1)}. \end{cases} \quad (5.37)$$

Outside the sphere, we want the fields caused by the surface poles to decay as we go to infinity, so we choose the second solution. Our complete trial solutions are obtained by combining Eqs. (5.35) and (5.37):

$$\begin{aligned} \psi_0 &= \frac{A}{r}, \\ \psi_1 &= \frac{A}{r^2} \cos \theta, \\ \psi_2 &= \frac{A}{r^3} (3 \cos^2 \theta - 1), \end{aligned} \quad (5.38)$$

where A is an arbitrary constant to be determined by matching the boundary conditions at the surface of the sphere. We want to choose the simplest solution that is appropriate to our problem. The first solution ($n = 0$) will give an entirely radial field like that of a monopole. We know, however, that there will be north poles on one side of a uniformly magnetized sphere and south poles on the other. Thus, $n = 0$ is unsatisfactory. For $n = 1$, the potential changes sign from $\theta = 0$ to π and hence is a possibility. The resulting fringing fields of the sphere are

$$(\mathbf{H}_{\text{fr}})_r = -\frac{\partial \psi}{\partial r} = \frac{2A}{r^3} \cos \theta, \quad (5.39a)$$

$$(\mathbf{H}_{\text{fr}})_\theta = -\frac{1}{r} \frac{\partial \psi}{\partial \theta} = \frac{A}{r^3} \sin \theta, \quad (5.39b)$$

for $r \geq r_0$.

To proceed with matching the boundary conditions, we must now obtain expressions in spherical coordinates for the uniform internal and external fields. We can do this with the aid of the coordinate transformation

$$\hat{\mathbf{z}} = \hat{\mathbf{r}} \cos \theta - \hat{\boldsymbol{\theta}} \sin \theta. \quad (5.40)$$

Thus, the uniform applied field is given by

$$\mathbf{H}_{\text{DC}} = H_{\text{DC}}(\hat{\mathbf{r}} \cos \theta - \hat{\boldsymbol{\theta}} \sin \theta) \quad (5.41)$$

for all r . Similarly, inside the sphere ($r \leq r_0$) we assume the magnetization and demagnetizing field are given by⁶

$$\mathbf{M}_0 = M_S(\hat{\mathbf{r}} \cos \theta - \hat{\boldsymbol{\theta}} \sin \theta) \quad (5.42)$$

$$\mathbf{H}_d = -H_d(\hat{\mathbf{r}} \cos \theta - \hat{\boldsymbol{\theta}} \sin \theta). \quad (5.43)$$

We are now in a position to consider the boundary conditions. For the present geometry, $\hat{\mathbf{r}}$ is normal to the boundary and $\hat{\boldsymbol{\theta}}$ is tangential. We first require the tangential components of \mathbf{H} to be continuous at $r = r_0$:

$$\begin{aligned} [(\mathbf{H}_{\text{fr}})_\theta + (\mathbf{H}_{\text{DC}})_\theta]_{r=r_0} &= [(\mathbf{H}_d)_\theta + (\mathbf{H}_{\text{DC}})_\theta]_{r=r_0} \\ \frac{A}{r_0^3} \sin \theta - H_{\text{DC}} \sin \theta &= H_d \sin \theta - H_{\text{DC}} \sin \theta \\ \frac{A}{r_0^3} &= H_d. \end{aligned} \quad (5.44)$$

Similarly, requiring the normal components of \mathbf{B} to be continuous at $r = r_0$ gives

$$\begin{aligned} [(\mathbf{H}_{\text{fr}})_r + (\mathbf{H}_{\text{DC}})_r]_{r=r_0} &= [(\mathbf{H}_d)_r + (\mathbf{H}_{\text{DC}})_r + (\mathbf{M}_0)_r]_{r=r_0} \\ \frac{2A}{r_0^3} \cos \theta + H_{\text{DC}} \cos \theta &= -H_d \cos \theta + H_{\text{DC}} \cos \theta + M_0 \cos \theta \\ \frac{2A}{r_0^3} &= -H_d + M_S. \end{aligned} \quad (5.45)$$

Combining Eqs. (5.44) and (5.45) gives the demagnetizing field in terms of the saturation magnetization:

$$H_d = \frac{1}{3} M_S. \quad (5.46)$$

Thus, the total internal field of the ferrite sphere is

$$H_0 = H_{\text{DC}} - \frac{1}{3} M_S. \quad (5.47)$$

Owing to the symmetry of the sphere, it is clear that the magnitude of the internal field is given by Eq. (5.47) regardless of the direction of \mathbf{H}_{DC} , provided only that H_0 is positive.⁷ Thus, this result can be generalized by introducing an appropriate demagnetizing tensor $\bar{\mathbf{N}}_d$:

⁶ The internal demagnetizing field of an arbitrarily shaped sample (e.g., a cube or rectangular prism) is *not* uniform. A uniform demagnetizing field is a special property of *ellipsoidal* samples of which a sphere is a special case.

⁷ This is necessary to ensure that the magnetization of the sphere is saturated.

$$\mathbf{H}_0 = \mathbf{H}_{\text{DC}} - \bar{\mathbf{N}}_{\text{d}} \cdot \mathbf{M}_{\text{S}}, \quad (5.48)$$

where

$$\bar{\mathbf{N}}_{\text{d}} = \begin{bmatrix} 1/3 & 0 & 0 \\ 0 & 1/3 & 0 \\ 0 & 0 & 1/3 \end{bmatrix}. \quad (5.49)$$

Comparison of Eqs. (5.49) and (5.26) shows the demagnetizing tensor to be strongly geometry-dependent. It can be shown, however, that the trace of the demagnetizing tensor is always equal to unity. For sample shapes in which the demagnetizing field is non-uniform, the trace of the tensor at each position inside the sample is still unity, although the tensor elements will vary from point to point [11].

As before, the static demagnetizing tensor can also be used to obtain the RF magnetic field intensity induced by the small-signal magnetization since we are interested in the uniform precession mode of the sphere (cf. Eq. (5.26)). Combining this requirement with that of the linearized torque equation (Eq. (5.23)) again gives Eq. (5.27a) but with $\bar{\mathbf{N}}_{\text{d}}$ given by Eq. (5.49). The frequency for a non-trivial solution is given by

$$\det [\bar{\mathbf{N}}_{\text{d}} + \bar{\chi}^{-1}] = 0. \quad (5.50a)$$

After multiplying through by ω_{M} , and using the fact that $m_z = 0$, this can be written as

$$\begin{vmatrix} \omega_0 + \omega_{\text{M}}/3 & i\omega \\ -i\omega & \omega_0 + \omega_{\text{M}}/3 \end{vmatrix} = 0. \quad (5.50b)$$

The result is

$$\omega = \omega_0 + \omega_{\text{M}}/3 \quad (5.51)$$

or, using Eq. (5.47):

$$\begin{aligned} \omega &= -\gamma\mu_0 \left[H_{\text{DC}} - \frac{1}{3}M_{\text{S}} + \frac{1}{3}M_{\text{S}} \right] \\ &= -\gamma\mu_0 H_{\text{DC}}. \end{aligned} \quad (5.52)$$

We see that the effects of the static and RF demagnetizing fields exactly cancel and the resonant frequency is independent of the magnitude of the saturation magnetization. This is an important point for device applications, since we showed in Chapter 3 that the saturation magnetization depends strongly on temperature. Thus, resonators made with spheres will not be as sensitive to temperature as those made with thin films.⁸ On the other hand, the planar geometry of thin films lends itself more readily to mass production.

⁸ The resonant frequency of a sphere does depend on temperature through the magnetocrystalline anisotropy field, which we have neglected in the present analysis. This dependence can be minimized by proper orientation of the sphere with respect to the bias field.

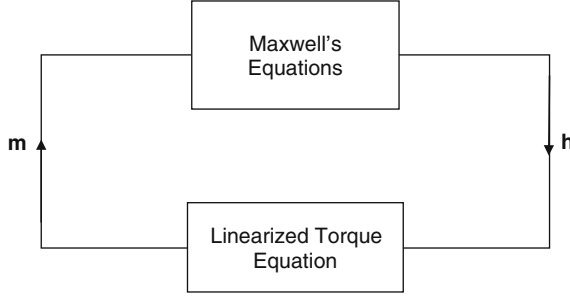


Fig. 5.7. The correct solution to an electromagnetics problem must simultaneously satisfy both the material constitutive relations and Maxwell's equations.

The method of analysis used in this section may be diagrammed as in Figure 5.7. According to Maxwell's equations, the presence of \mathbf{m} acts as a source creating \mathbf{h} . For the uniform precession modes, the sources are always surface poles, although for higher-order modes volume pole densities $\nabla \cdot \mathbf{m}$ will contribute. From the Landau–Lifshitz equation (or torque equation), however, \mathbf{m} can be viewed as the response of the medium to the excitation \mathbf{h} . The complete solution requires both of these equations to be satisfied by the same \mathbf{m} and \mathbf{h} , as indicated by the closed loop in Figure 5.7.

5.4 Normally Magnetized Film: Forward Volume Waves⁹

Let us return to the geometry of Figure 5.4 and consider excitations with nonzero k . Recall from Section 5.1 that magnetostatic plane waves can propagate in the ferrite whenever the frequency lies in the range

$$\omega_0 \leq \omega \leq \sqrt{\omega_0(\omega_0 + \omega_M)}. \quad (5.53)$$

Because of the multiplicity of propagating waves over this range, this band of frequencies is sometimes called the magnetostatic wave or spin wave *manifold*.

Suppose we launch such a plane wave in the ferrite with wave vector

$$\mathbf{k} = \mathbf{k}_t + \hat{\mathbf{z}}k_z, \quad (5.54)$$

where

$$\mathbf{k}_t = \hat{\mathbf{x}}k_x + \hat{\mathbf{y}}k_y. \quad (5.55)$$

We expect that reflections will occur when this wave hits the upper film boundary as suggested in Figure 5.8. The reflected wave vector will be

$$\mathbf{k} = \mathbf{k}_t - \hat{\mathbf{z}}k_z. \quad (5.56)$$

⁹ See, e.g., Damon and van de Vaart [5] and Parekh et al. [12].

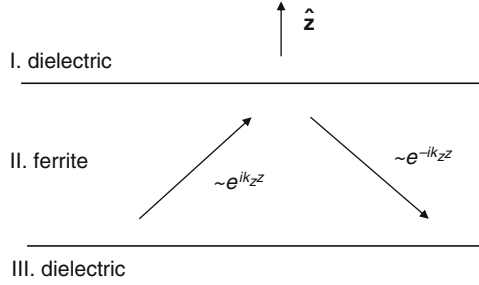


Fig. 5.8. A guided wave in the film can be analyzed as plane waves bouncing back and forth from the upper and lower film boundaries.

This wave will subsequently reflect from the bottom surface, again reversing the sign of the z -component of \mathbf{k} . Eventually, a steady-state field distribution will be formed that can be decomposed into plane waves bouncing back and forth in the film.

As a trial solution for the magnetostatic potential in the ferrite (Region II), we assume a symmetric superposition of bouncing plane waves of the form

$$\begin{aligned}\psi_{\text{II}} &= \psi_0 e^{i\mathbf{k}_t \cdot \mathbf{r}} \left[\frac{e^{ik_z z} + e^{-ik_z z}}{2} \right] \\ &= \psi_0 \cos(k_z z) e^{i\mathbf{k}_t \cdot \mathbf{r}},\end{aligned}\tag{5.57}$$

where ψ_0 is an arbitrary constant determining the mode amplitude.

In the dielectric, $\chi = 0$, and Walker's equation reduces to Laplace's equation. From Eq. (5.10), we have

$$k_{t,d}^2 + k_{z,d}^2 = 0 \implies k_{z,d} = \pm i k_{t,d},\tag{5.58}$$

where the subscript d refers to the dielectric regions. This suggests trial solutions of the form

$$\psi_a(\mathbf{r}) = C e^{i\mathbf{k}_{t,d} \cdot \mathbf{r} \pm k_{t,d} z}.\tag{5.59}$$

To ensure that the mode is localized to the film, we choose the signs in the exponent so that the potential vanishes as $z \rightarrow \pm\infty$:

$$\psi_{\text{I}}(\mathbf{r}) = C e^{i\mathbf{k}_{t,d} \cdot \mathbf{r} - k_{t,d} z},\tag{5.60}$$

$$\psi_{\text{III}}(\mathbf{r}) = D e^{i\mathbf{k}_{t,d} \cdot \mathbf{r} + k_{t,d} z}.\tag{5.61}$$

Next we must consider the boundary conditions for the RF fields:

- (a) tangential \mathbf{h} must be continuous and
- (b) normal \mathbf{b} must be continuous.

The first boundary condition assumes the absence of current sheets since the ferrite is an electrical insulator.

The tangential components of \mathbf{h} are given by (cf. Eq. (5.7))

$$\mathbf{h}_t = -\nabla_t \psi, \quad (5.62)$$

where

$$\nabla_t = \hat{\mathbf{x}} \frac{\partial}{\partial x} + \hat{\mathbf{y}} \frac{\partial}{\partial y}. \quad (5.63)$$

Requiring \mathbf{h}_t to be continuous at $z = \pm d/2$ gives

$$-i\mathbf{k}_{t,d} \psi_I(z = d/2) = -i\mathbf{k}_t \psi_{II}(z = d/2) \quad (5.64)$$

and

$$-i\mathbf{k}_{t,d} \psi_{III}(z = -d/2) = -i\mathbf{k}_t \psi_{II}(z = -d/2). \quad (5.65)$$

Since $\psi_{I,III} \sim \exp(i\mathbf{k}_{t,d} \cdot \mathbf{r})$ and $\psi_{II} \sim \exp(i\mathbf{k}_t \cdot \mathbf{r})$, the only way these equalities can be satisfied *for all* (x, y) is for $\mathbf{k}_{t,d} = \mathbf{k}_t$. Making this assignment, we see from (5.64) and (5.65) that the boundary condition on tangential \mathbf{h} is equivalent to requiring the potential function ψ to be continuous. Equations (5.64) and (5.65) become

$$C e^{-k_t d/2} = \psi_0 \cos(k_z d/2), \quad (5.66)$$

$$D e^{-k_t d/2} = \psi_0 \cos(k_z d/2), \quad (5.67)$$

from which we conclude $C = D$.

Next we require normal \mathbf{b} to be continuous at $z = \pm d/2$. We have

$$k_t C e^{-k_t d/2} = \psi_0 k_z \sin(k_z d/2), \quad (5.68)$$

$$-k_t D e^{-k_t d/2} = -\psi_0 k_z \sin(k_z d/2). \quad (5.69)$$

With $C = D$, it is clear that these two equations are identical. Thus Eqs. (5.66), (5.67), (5.68), and (5.69) give us only two linearly independent equations that can be combined to give

$$\psi_0 k_t \cos(k_z d/2) = \psi_0 k_z \sin(k_z d/2)$$

or

$$\tan(k_z d/2) = \frac{k_t}{k_z}. \quad (5.70)$$

The wave vector components k_t , k_z can be related using Eq. (5.10):

$$\frac{k_t}{k_z} = \frac{1}{\sqrt{-(1+\chi)}}. \quad (5.71)$$

This expression is real since $1 + \chi < 0$ in the spin wave manifold. Substituting Eq. (5.71) into (5.70) and eliminating k_z gives

$$\tan \left[\frac{k_t d}{2} \sqrt{-(1 + \chi)} \right] = \frac{1}{\sqrt{-(1 + \chi)}}. \quad (5.72)$$

This equation relates the wave number in the film k_t to the radian frequency ω (contained in χ). This is the dispersion relation for magnetostatic waves with symmetric potential functions. The dispersion relation in Eq. (5.72) can be solved graphically by plotting both sides of the equation against $[-(1 + \chi)]^{1/2}$ as shown in Figure 5.9. Intersections of the curves represent solutions to the dispersion relation. Note that there are multiple solutions owing to the periodicity of the tangent function. These solutions have even potential functions of the form given by Eq. (5.57) and differ by the number of zeros through the thickness of the film. The solution labeled $n = 0$ in Figure 5.9 is the lowest-order mode and has no zeros. The solution labeled $n = 2$ has two zeros, and so on.

Solutions corresponding to odd numbers of zeros can be obtained using the trial potential function

$$\psi_{II}(\mathbf{r}) = \psi_0 \sin(k_z z) e^{i\mathbf{k}_t \cdot \mathbf{r}} \quad (5.73)$$

and repeating the preceding analysis. The resulting dispersion relation is

$$-\cot \left[\frac{k_t d}{2} \sqrt{-(1 + \chi)} \right] = \frac{1}{\sqrt{-(1 + \chi)}}. \quad (5.74)$$

The even and odd mode dispersion relations can be combined into a single equation using the identity

$$\tan(\theta - \pi/2) = -\cot \theta. \quad (5.75)$$

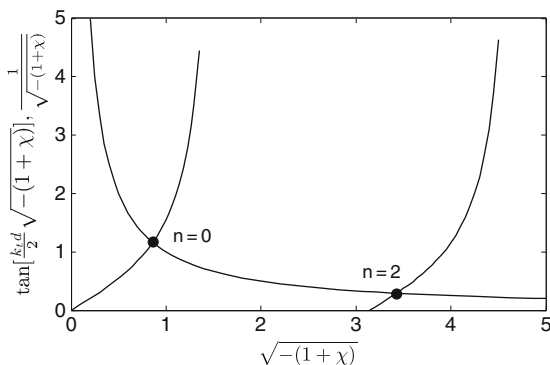


Fig. 5.9. Graphical solution to the dispersion relation for forward volume modes with even potential functions ($k_t d = 2$).

The result is

$$\tan \left[\frac{k_t d}{2} \sqrt{-(1+\chi)} - \frac{n\pi}{2} \right] = \frac{1}{\sqrt{-(1+\chi)}}. \quad (5.76a)$$

A useful approximation to the dispersion relation (5.76a) that can be solved explicitly for ω has been derived by Kalinikos [13]. For the lowest-order mode ($n = 0$), the result is

$$\omega^2 = \omega_0 \left[\omega_0 + \omega_M \left(1 - \frac{1 - e^{-k_t d}}{k_t d} \right) \right]. \quad (5.76b)$$

The solutions to (5.76a) are plotted in Figure 5.10. Note that the mode frequencies correspond to the bottom of the magnetostatic wave manifold for $k_t = 0$. Since there is no in-plane component to \mathbf{k} in this limit, the mode can be decomposed into plane waves bouncing back and forth along the $\hat{\mathbf{z}}$ direction. This is consistent with the $\theta = 0$ limit shown in Figure 5.1. As k_t increases, the angle of the total \mathbf{k} vector of the constituent plane waves also increases. In the limit of large k_t , the frequency corresponds to the upper band edge consistent with $\theta = \pi/2$.

The group velocity is defined to be (cf. Eq. (4.100)):

$$v_g = \frac{\partial \omega}{\partial k}. \quad (5.77)$$

Differentiating the dispersion relation (5.76a) with respect to ω gives

$$\frac{1}{v_g} = \frac{\chi \kappa}{(1+\chi)\omega_M d} \left[\frac{2}{\chi} - k_t d \right]. \quad (5.78a)$$

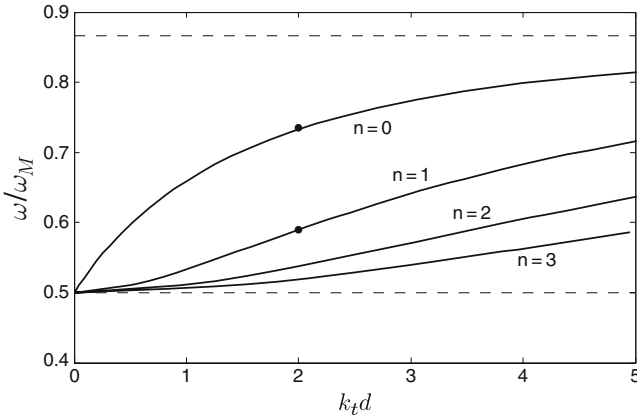


Fig. 5.10. Dispersion diagram for forward volume waves with $\omega_0/\omega_M = 0.5$.

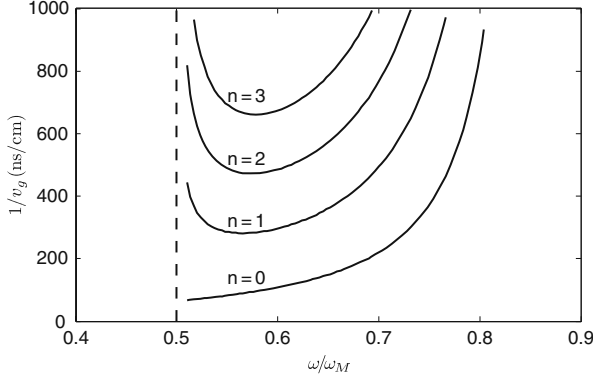


Fig. 5.11. Inverse group velocity (delay/length) for the first four forward volume wave thickness modes ($M_S = 140$ kA/m, $H_0 = 70$ kA/m).

This equation is plotted for $n = 0 \dots 3$ in Figure 5.11. For $n = 0$, $k_t d \ll 1$, Eq. (5.78a) reduces to

$$\left. \frac{1}{v_g} \right|_{kd=0} = \frac{4}{\omega_M d}. \quad (5.78b)$$

It is interesting to note that the initial group velocity is independent of frequency or field and depends only on geometrical and material parameters. This suggests a novel way to characterize the saturation magnetization or thickness of thin-film samples.

For modes with even potential functions, the potential in the film is given by Eq. (5.57). The coefficients for the dielectric regions are given by Eqs. (5.66) and (5.67):

$$C = D = \psi_0 e^{k_t d/2} \cos(k_z d/2). \quad (5.79)$$

The potential function is, therefore

$$\psi^{(e)}(\mathbf{r}) = \begin{cases} \psi_0 e^{k_t d/2} \cos(\sqrt{-(1+\chi)} k_t d/2) e^{i\mathbf{k}_t \cdot \mathbf{r} - k_t z}, & z > d/2 \\ \psi_0 \cos(\sqrt{-(1+\chi)} k_t z) e^{i\mathbf{k}_t \cdot \mathbf{r}}, & |z| \leq d/2 \\ \psi_0 e^{k_t d/2} \cos(\sqrt{-(1+\chi)} k_t d/2) e^{i\mathbf{k}_t \cdot \mathbf{r} + k_t z}, & z < -d/2. \end{cases} \quad (5.80)$$

Following a similar procedure, the odd mode potential is given by:

$$\psi^{(o)}(\mathbf{r}) = \begin{cases} \psi_0 e^{k_t d/2} \sin(\sqrt{-(1+\chi)} k_t d/2) e^{i\mathbf{k}_t \cdot \mathbf{r} - k_t z}, & z > d/2 \\ \psi_0 \sin(\sqrt{-(1+\chi)} k_t z) e^{i\mathbf{k}_t \cdot \mathbf{r}}, & |z| \leq d/2 \\ -\psi_0 e^{k_t d/2} \sin(\sqrt{-(1+\chi)} k_t d/2) e^{i\mathbf{k}_t \cdot \mathbf{r} + k_t z}, & z < -d/2. \end{cases} \quad (5.81)$$

Expressions for the amplitude ψ_0 for various normalization conditions are given in Section 6.3. The potential functions for the lowest-order even and odd forward volume wave modes are shown in Figure 5.12.

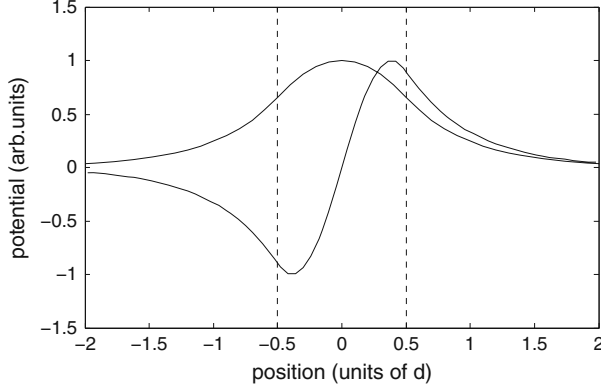


Fig. 5.12. Potential profiles for the lowest-order even and odd forward volume wave modes at the points indicated on the dispersion curves in Figure 5.10 ($\omega_0/\omega_M = 0.5$, $k_t d = 2$, $d = 20 \mu\text{m}$).

An attractive feature of the magnetostatic approximation is that all of the mode fields can be obtained from the potential function. The quantities \mathbf{h} , \mathbf{m} , and \mathbf{b} are found from the following relations:

$$\mathbf{h} = -\nabla\psi, \quad (5.82)$$

$$\mathbf{m} = \overline{\chi} \cdot \mathbf{h}, \quad (5.83)$$

$$\mathbf{b} = \mu_0(\mathbf{h} + \mathbf{m}). \quad (5.84)$$

Several important observations can be made regarding the nature of these modes:

- Unlike other examples of guided electromagnetic waves, all modes have the same cutoff frequency. Thus, there is no frequency range where only a single mode propagates. (This degeneracy is lifted by the exchange interaction in thin films.)
- The dispersion relation depends on the magnitude but not the direction of \mathbf{k}_t . Therefore, the wave propagation is isotropic in the plane of the film. (The presence of magnetocrystalline anisotropy can give rise to anisotropy in the propagation characteristics, however.)
- Although the phase and group velocities have different magnitudes, they are both in the same direction. Waves with this characteristic are called *forward waves*.
- The wave amplitude is distributed sinusoidally through the volume of the film.

Because of the last two characteristics and the use of the magnetostatic approximation, these modes are collectively called *magnetostatic forward volume waves* or *forward volume spin waves*.

5.5 Tangentially Magnetized Film: Backward Volume Waves¹⁰

Because of the symmetry, when a field is applied normal to the film plane, we found that the propagation characteristics of forward volume waves are independent of direction in the plane of the film. This symmetry is no longer present when a field is applied in the film plane. In general, the propagation characteristics for waves in a tangentially magnetized film depend on the angle between \mathbf{k} and \mathbf{H}_{DC} . We will consider only the two special cases: $\mathbf{k} \parallel \mathbf{H}_{\text{DC}}$ and $\mathbf{k} \perp \mathbf{H}_{\text{DC}}$. When \mathbf{k} is parallel to \mathbf{H}_{DC} , modes known as *magnetostatic backward volume waves* propagate. When \mathbf{k} is perpendicular to \mathbf{H}_{DC} , *magnetostatic surface waves* propagate. In this section, we consider the case of backward volume waves.

Let us consider the propagation of guided waves along the $\pm \hat{\mathbf{z}}$ directions in the geometry of Figure 5.5. Thus, we assume the potential to be proportional to $\exp(i\nu k_z z)$, where $\nu = \pm 1$. Trial potential functions in each region can be written as follows:

$$\psi_{\text{I}}(\mathbf{r}) = C e^{-k_z y + i\nu k_z z}, \quad (5.85)$$

$$\psi_{\text{II}}(\mathbf{r}) = \psi_0 \sin(k_y y) e^{i\nu k_z z}, \quad (5.86)$$

$$\psi_{\text{III}}(\mathbf{r}) = D e^{k_z y + i\nu k_z z}. \quad (5.87)$$

In writing down these expressions, we have made use of two facts learned from the forward volume wave analysis. First, Laplace's equation in the dielectric regions requires $k_{y,d} = \pm k_{z,d}$, and second, the component of \mathbf{k} tangent to the boundaries must be the same in each region: $k_{z,d} = k_z$. The choice of the odd potential function will serve to illustrate the analysis of odd modes to complement the previous forward volume wave discussion. Also, we shall discover that this choice yields the lowest-order backward volume wave mode.

In the ferrite, k_z and k_y are related by Walker's equation:

$$(1 + \chi)k_y^2 + k_z^2 = 0. \quad (5.88)$$

As before, we see that solutions for real k_y , k_z require $(1 + \chi) < 0$. Thus, guided modes, which can be decomposed into plane waves bouncing back and forth in the ferrite film, can only occur for frequencies within the volume wave manifold.

Next we apply the boundary conditions at $y = \pm d/2$. First, we require ψ to be continuous (recall this is equivalent to tangential \mathbf{h} continuous). This gives

$$C e^{-k_z d/2} = \psi_0 \sin(k_y d/2), \quad (5.89)$$

$$D e^{-k_z d/2} = -\psi_0 \sin(k_y d/2). \quad (5.90)$$

¹⁰ The reader may also refer to Damon and Eshbach [4] and Parekh et al. [12].

Thus, we see that $C = -D$, as expected for an odd function.

The remaining boundary condition is that normal \mathbf{b} must be continuous at $y = \pm d/2$. The normal component of \mathbf{b} in this geometry is b_y . From the constitutive relation (5.4), we have

$$b_y = i\mu_0\kappa h_x + \mu_0(1 + \chi)h_y. \quad (5.91)$$

The first term vanishes since the potential is independent of x . Thus, requiring b_y to be continuous at $y = \pm d/2$ gives

$$-k_z C e^{-k_z d/2} = k_y(1 + \chi)\psi_0 \cos(k_y d/2), \quad (5.92)$$

$$k_z D e^{-k_z d/2} = k_y(1 + \chi)\psi_0 \cos(k_y d/2). \quad (5.93)$$

Since $C = -D$, these two equations are equivalent. Combining with the previous boundary conditions, Eqs. (5.89) and (5.90), gives

$$\tan(k_y d/2) = -(1 + \chi)k_y/k_z. \quad (5.94)$$

Walker's equation (5.88) can now be used to eliminate k_y . The result is

$$\tan \left[\frac{k_z d}{2\sqrt{-(1 + \chi)}} \right] = \sqrt{-(1 + \chi)}. \quad (5.95)$$

This is the dispersion relation for modes with odd potential functions. Following a similar procedure for an even potential yields

$$-\cot \left[\frac{k_z d}{2\sqrt{-(1 + \chi)}} \right] = \sqrt{-(1 + \chi)}. \quad (5.96)$$

As before, the even and odd mode solutions can be combined using the identity (5.75) to obtain

$$\tan \left[\frac{k_z d}{2\sqrt{-(1 + \chi)}} - \frac{(n - 1)\pi}{2} \right] = \sqrt{-(1 + \chi)}, \quad n = 1, 2, 3, \dots \quad (5.97a)$$

Kalinikos [13] has also obtained an approximation to (5.97a) that can be solved explicitly for ω . For the lowest-order mode ($n = 1$), the result is

$$\omega^2 = \omega_0 \left[\omega_0 + \omega_M \left(\frac{1 - e^{-k_z d}}{k_z d} \right) \right]. \quad (5.97b)$$

The solutions to Eq. (5.97a) are shown in Figure 5.13. As with forward volume waves, these modes can be decomposed into plane waves bouncing back and forth between the top and bottom surfaces of the film while propagating along the z -direction. When $k_z = 0$, the plane waves are propagating perpendicular to the applied field. Referring to Figure 5.1, this corresponds

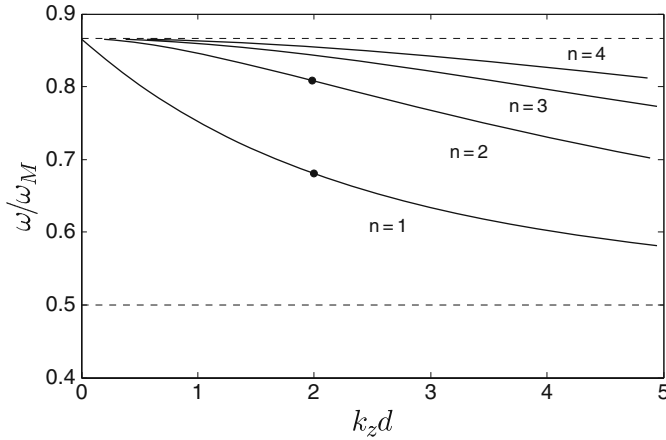


Fig. 5.13. Dispersion diagram for backward volume waves with $\omega_0/\omega_M=0.5$.

to the limit $\theta = \pi/2$ so that the frequency is that of the top of the magnetostatic wave manifold. As k_z increases, the angle of the total \mathbf{k} vector of the constituent plane waves decreases. In the limit of large k_z , the plane waves are propagating parallel to the applied field ($\theta = 0$) and the frequency approaches the lower manifold edge.

The group velocity is obtained by differentiating the dispersion relation (5.97a) with respect to ω . The result is

$$\frac{1}{v_g} = \frac{\chi\kappa}{\omega_M d} \left[\frac{2}{\chi} + \frac{k_z d}{1 + \chi} \right]. \quad (5.98a)$$

For $n = 1$, $k_z d \ll 1$, this reduces to

$$\left. \frac{1}{v_g} \right|_{k_d=0} = -\frac{4}{\omega_M d} \frac{\sqrt{\omega_0(\omega_0 + \omega_M)}}{\omega_0}. \quad (5.98b)$$

Unlike forward volume waves, the initial slope of the present dispersion relation depends on the field as well as geometrical and material parameters. The magnitude of the inverse group velocity from Eq. (5.98a) is plotted in Figure 5.14 for $n = 1 \cdots 4$.

The odd and even mode potential functions are given by

$$\psi^{(o)}(\mathbf{r}) = \begin{cases} \psi_0 e^{k_z d/2} \sin(k_y d/2) e^{i\nu k_z z - k_z y}, & y > d/2, \\ \psi_0 \sin(k_y y) e^{i\nu k_z z}, & |y| \leq d/2, \\ -\psi_0 e^{k_z d/2} \sin(k_y d/2) e^{i\nu k_z z + k_z y}, & y < -d/2 \end{cases} \quad (5.99)$$

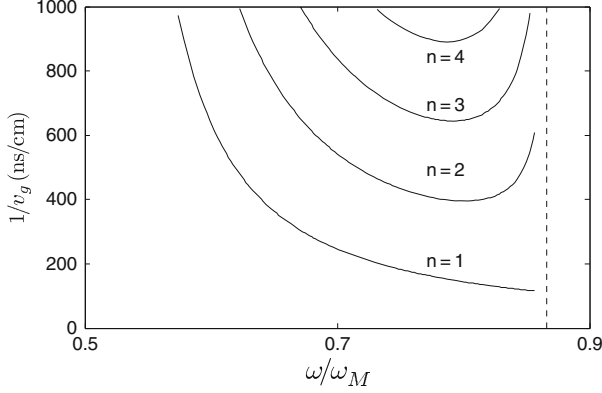


Fig. 5.14. Magnitude of the inverse group velocity (delay/length) for the first four backward volume wave thickness modes ($M_S = 140 \text{ kA/m}$, $H_0 = 70 \text{ kA/m}$, $d = 20 \mu\text{m}$).

and

$$\psi^{(e)}(\mathbf{r}) = \begin{cases} \psi_0 e^{k_z d/2} \cos(k_y d/2) e^{i\nu k_z z - k_z y}, & y > d/2, \\ \psi_0 \cos(k_y y) e^{i\nu k_z z}, & |y| \leq d/2, \\ \psi_0 e^{k_z d/2} \cos(k_y d/2) e^{i\nu k_z z + k_z y}, & y < -d/2, \end{cases} \quad (5.100)$$

where Walker's equation (5.88) relates k_y and k_z . Expressions for ψ_0 for various normalization conditions are given in Section 6.3. The potential functions for the lowest-order odd and even modes are shown in Figure 5.15.

The following observations can be made regarding the nature of these modes:

- As with forward volume waves, all modes have the same cutoff frequency in the absence of exchange. There is no frequency range where only a single mode propagates.
- The dispersion relation is independent of the direction parameter ν . Thus, reversing the direction of propagation does not change the properties of the mode. (The present analysis is only valid for \mathbf{k} parallel or antiparallel to \mathbf{H}_{DC} , however.)
- The phase velocity of a given mode at a point (ω_1, k_{z1}) in Figure 5.13 is $v_p = \omega_1/k_{z1}$ and is positive. In contrast, the group velocity is given by the slope $v_g = \partial\omega/\partial k_z$ and is negative. Thus, the phase and group velocities are pointing in opposite directions. A wave with this property is called a *backward wave*.
- The wave amplitude is distributed sinusoidally through the volume of the film.

The terms *magnetostatic backward volume wave* or *backward volume spin wave* follow from the last two observations. The *backward* nature of these

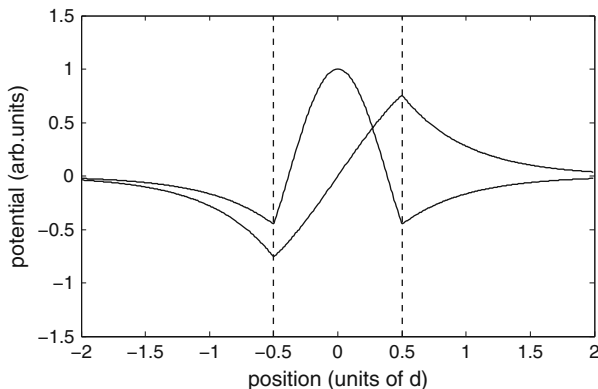


Fig. 5.15. Potential profiles for the lowest-order odd and even backward volume wave modes at the points indicated on the dispersion curves in Figure 5.13 ($\omega_0/\omega_M = 0.5$, $k_z d = 2$, $d = 20 \mu\text{m}$).

waves can be exploited to illustrate novel wave properties such as the inverse Doppler effect, described in further detail in Chapter 10.

5.6 Tangentially Magnetized Film: Surface Waves¹¹

We now consider propagation perpendicular to an in-plane bias field, or along the $\pm x$ direction of Figure 5.5. As a trial solution, let us assume a potential of similar form to the previous volume wave modes:

$$\psi_{\text{I}}(\mathbf{r}) = C e^{-k_x y + i\nu k_x x}, \quad (5.101)$$

$$\psi_{\text{II}}(\mathbf{r}) = \psi_0 \cos(k_y y) e^{i\nu k_x x}, \quad (5.102)$$

$$\psi_{\text{III}}(\mathbf{r}) = D e^{k_x y + i\nu k_x x} \quad (5.103)$$

In the ferrite (Region II), Walker's equation (5.10) reduces to

$$(1 + \chi)(k_x^2 + k_y^2) = 0. \quad (5.104)$$

One possible solution to this equation is $1 + \chi = 0$. However, this only occurs for one specific frequency. Such a solution would not give a band of solutions similar to what we have previously encountered. The alternative is to require $k_y^2 = -k_x^2$. If we require k_x to be real for propagating waves, then k_y must be imaginary. Hence, ψ_{II} will not be oscillatory as we have assumed, but must consist of growing and decaying exponentials. We therefore replace the potential in Region II (5.102) with

$$\psi_{\text{II}} = [\psi_{0+} e^{k_y y} + \psi_{0-} e^{-k_y y}] e^{i\nu k_x x}. \quad (5.105)$$

¹¹ The reader may also refer to Damon and Eshbach [4] and Parekh et al. [12].

Note that we have dropped the wave number subscripts since $|k_y| = k_x \equiv k$.

We must next apply the boundary conditions at $y = \pm d/2$. Requiring ψ to be continuous gives

$$C e^{-kd/2} = \psi_{0+} e^{kd/2} + \psi_{0-} e^{-kd/2}, \quad (5.106)$$

$$D e^{-kd/2} = \psi_{0+} e^{-kd/2} + \psi_{0-} e^{kd/2}. \quad (5.107)$$

Note that these two equations imply neither even nor odd mode symmetry, in contrast to the previous modes.

The final boundary condition requires b_y to be continuous. From (5.91) for b_y and the present potential functions (5.101), (5.103), and (5.105), we have

$$C e^{-kd/2} = \nu \kappa \left[\psi_{0+} e^{kd/2} + \psi_{0-} e^{-kd/2} \right] - (1 + \chi) \left[\psi_{0+} e^{kd/2} - \psi_{0-} e^{-kd/2} \right], \quad (5.108)$$

$$D e^{-kd/2} = -\nu \kappa \left[\psi_{0+} e^{-kd/2} + \psi_{0-} e^{kd/2} \right] + (1 + \chi) \left[\psi_{0+} e^{-kd/2} - \psi_{0-} e^{kd/2} \right]. \quad (5.109)$$

Substituting the previous boundary conditions (5.106) and (5.107) for the left sides of (5.108) and (5.109) and collecting terms gives

$$\begin{bmatrix} (\chi + 2 - \nu \kappa) e^{kd/2} & -(\chi + \nu \kappa) e^{-kd/2} \\ -(\chi - \nu \kappa) e^{-kd/2} & (\chi + 2 + \nu \kappa) e^{kd/2} \end{bmatrix} \begin{bmatrix} \psi_{0+} \\ \psi_{0-} \end{bmatrix} = 0. \quad (5.110)$$

The dispersion relation is obtained by setting the determinant of the coefficient matrix to zero and simplifying. The result is

$$e^{-2kd} = \frac{(\chi + 2)^2 - \kappa^2}{\chi^2 - \kappa^2}. \quad (5.111a)$$

Note that the dependence on ν has vanished, showing that the dispersion relation is unchanged if the direction of propagation is reversed. Substituting for χ and κ from Eqs. (3.115) and (3.116), respectively, and solving for ω^2 gives

$$\omega^2 = \omega_0(\omega_0 + \omega_M) + \frac{\omega_M^2}{4} [1 - e^{-2kd}]. \quad (5.111b)$$

Solving instead for k gives

$$k = -\frac{1}{2d} \ln \left[1 + \frac{4}{\omega_M^2} [\omega_0(\omega_0 + \omega_M) - \omega^2] \right]. \quad (5.111c)$$

It is important to remember that k can only take on positive values in either of these equations. The dispersion relation is plotted in Figure 5.16.

The group velocity is obtained by differentiating Eq. (5.111b). The result is

$$\frac{1}{v_g} = \frac{4\omega}{\omega_M^2 d} e^{2kd}. \quad (5.112a)$$

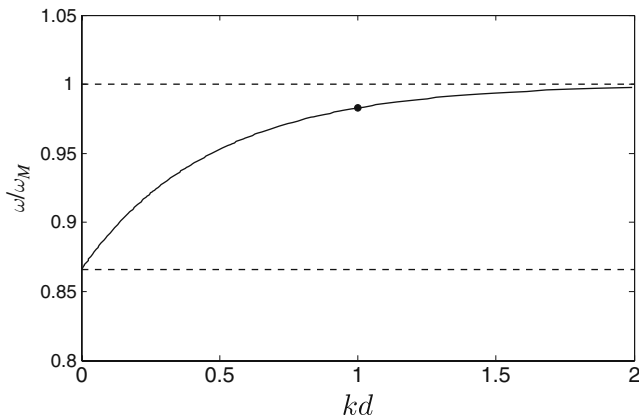


Fig. 5.16. Dispersion diagram for surface waves with $\omega_0/\omega_M = 0.5$.

The group velocity near $kd = 0$ is given by

$$\left. \frac{1}{v_g} \right|_{kd=0} = \frac{4}{\omega_M d} \frac{\sqrt{\omega_0(\omega_0 + \omega_M)}}{\omega_M}. \quad (5.112b)$$

Again the initial group velocity is found to depend on the field as well as on geometrical and material parameters. The delay per unit length from (5.112a) is plotted in Figure 5.17.

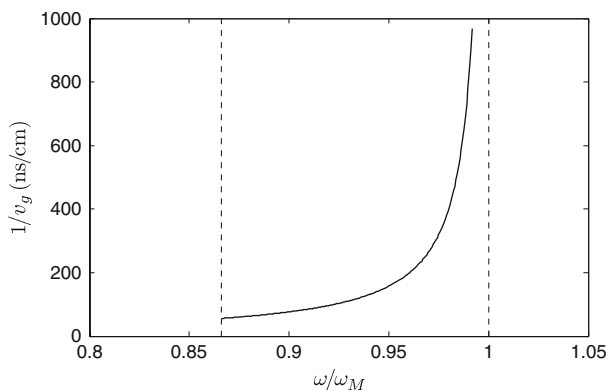


Fig. 5.17. Inverse group velocity (delay/length) for magnetostatic surface waves ($M_S = 140$ kA/m, $H_0 = 70$ kA/m, $d = 20$ μ m).

Since the potential function is not periodic through the thickness of the film, surface waves do not exhibit multiple thickness modes. The potential can be expressed

$$\psi_\nu(\mathbf{r}) = \begin{cases} \psi_0 (e^{kd} + p(\nu)) e^{-ky + i\nu kx}, & y > d/2, \\ \psi_0 (e^{ky} + p(\nu)e^{-ky}) e^{i\nu kx}, & |y| \leq d/2, \\ \psi_0 (1 + p(\nu)e^{kd}) e^{ky + i\nu kx}, & y < -d/2, \end{cases} \quad (5.113)$$

where $p(\nu) \equiv \psi_{0-}/\psi_{0+}$ and is given equivalently by the following two expressions from (5.110):

$$p(\nu) \equiv \frac{\psi_{0-}}{\psi_{0+}} = \frac{\chi - \nu\kappa}{\chi + 2 + \nu\kappa} e^{-kd}, \quad (5.114a)$$

$$p(\nu) = \frac{\chi + 2 - \nu\kappa}{\chi + \nu\kappa} e^{kd}, \quad (5.114b)$$

and ψ_0 is an arbitrary amplitude factor that can be chosen according to the normalization condition discussed in Section 6.3.

The potential functions for $\nu = \pm 1$ are shown in Figure 5.18. It is important to note that although the dispersion relation is independent of ν , the mode fields are not. When the direction of propagation is reversed, the mode shifts from one surface to the other. This phenomenon is called *field displacement non-reciprocity*.

Let us summarize several important properties of these modes:

- There is only a single propagating mode instead of a series of modes with different thickness variations, as found with forward and backward volume waves.
- Although the dispersion relation is independent of ν , the mode fields are not. The fields shift from one side of the film to the other when the direction of propagation is reversed. The fact that the dispersion relation is not

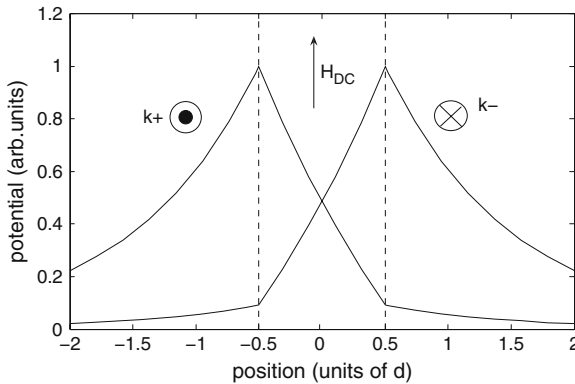


Fig. 5.18. Potential profiles for surface waves with $\nu = \pm 1$ at the point indicated on the dispersion curve of Figure 5.16 ($\omega_0/\omega_M = 0.5$, $kd = 1$, $d = 20\mu\text{m}$).

affected by this field shift is due to the symmetry of the boundary conditions on either side of the film. The dispersion relation will also depend on ν if, as an example, conducting planes are placed asymmetrically about the film. The present analysis is only valid for \mathbf{k} perpendicular to \mathbf{H}_{DC} , however.

- The phase and group velocities point in the same direction. Thus, this mode is a *forward wave*.
- The wave amplitude is not distributed periodically through the film thickness but decays exponentially from the surfaces of the film.

Because of this last observation, these modes are called *magnetostatic surface waves* or *surface spin waves*.

Problems

5.1. Calculate the frequencies of the spin wave resonance modes for $n = 1, 3, 5, 7, 9$ in a $0.5\text{ }\mu\text{m}$ YIG film if the field $H_{\text{DC}} = 240\text{ kA/m}$ is applied normal to the film plane. For YIG, $M_{\text{S}} = 140\text{ kA/m}$, $|\gamma|/2\pi = 28\text{ GHz/T}$, and $\lambda_{\text{ex}} = 3 \times 10^{-16}\text{ m}^2$.

5.2. Calculate the uniform precession frequency for a YIG film in the applied field $B_{\text{DC}} = 0.5\text{ T}$ if the field is

- parallel to the film and
- perpendicular to the film.

Use the parameters for YIG in Problem 5.1.

5.3. The uniform precession mode of ferrite spheres is widely used to make tunable microwave filters. What field B_{DC} is required to obtain a resonance at 10 GHz in YIG?

5.4. Using the image theorem, find the forward volume wave dispersion relation for a ferrite film with one side in contact with a perfect conductor. Show that your result is identical to the even mode dispersion relation of an isolated film twice as thick.

5.5. The most common magnetostatic wave device geometry consists of a YIG film above a ground plane. Consider a layered geometry consisting of a perfect conductor for $z \leq -t$, a non-magnetic dielectric for $-t < z \leq 0$, a ferrite film for $0 < z \leq d$, and a non-magnetic dielectric for $z > d$. Show that the dispersion relation for forward volume waves can be written

$$-\tan\left[kd\sqrt{-(1+\chi)}\right] = \frac{2\sqrt{-(1+\chi)}}{2+\chi(1+e^{-2kt})}, \quad (5.115)$$

where k is the wave number in the plane of the film (the subscript t has been omitted for clarity).

5.6. Consider magnetostatic backward volume waves in a ferrite film with an adjacent ground plane. The geometry consists of a perfect conductor for $y \leq -t$, a non-magnetic dielectric for $-t < y \leq 0$, a ferrite film for $0 < y \leq d$, and a non-magnetic dielectric for $y > d$. Show that the dispersion relation for backward volume waves can be written

$$\tan \left[\frac{kd}{\sqrt{-(1+\chi)}} \right] = \frac{2\sqrt{-(1+\chi)}}{2 + \chi(1 + e^{-2kt})}, \quad (5.116)$$

where k is the wave number along the direction of propagation (the subscript z has been omitted for clarity).

5.7. Consider magnetostatic surface waves in a ferrite film above a ground plane. Use the geometry of Problem 5.6 and show that the dispersion relation can be written

$$e^{2kd} = \frac{\chi + \nu\kappa}{2 + \chi - \nu\kappa} \left[\frac{\chi - \nu\kappa + e^{-2kt}(2 + \chi - \nu\kappa)}{2 + \chi + \nu\kappa + e^{-2kt}(\chi + \nu\kappa)} \right]. \quad (5.117)$$

References

- [1] B. Lax and K. J. Button, *Microwave Ferrites and Ferrimagnetics*. New York: McGraw-Hill, 1962.
- [2] R. F. Soohoo, *Microwave Magnetics*. New York: Harper and Row, 1985.
- [3] M. S. Sodha and N. C. Srivastava, *Microwave Propagation in Ferrimagnetics*. New York: Harper and Row, 1981.
- [4] R. W. Damon and J. R. Eshbach, "Magnetostatic modes of a ferromagnet slab," *J. Phys. Chem. Solids*, vol. 19, p. 308, 1961.
- [5] R. W. Damon and H. van de Vaart, "Propagation of magnetostatic spin waves at microwave frequencies in a normally magnetized disk," *J. Appl. Phys.*, vol. 36, p. 3453, 1965.
- [6] L. R. Walker, "Resonant modes of ferromagnetic spheroids," *J. Appl. Phys.*, vol. 2, p. 318, 1958.
- [7] E. H. Turner, "Interaction of phonons and spin waves in yttrium iron garnet," *Phys. Rev. Lett.*, vol. 5, p. 100, 1960.
- [8] C. Kittel, "Excitation of spin waves in a ferromagnet by a uniform rf field," *Phys. Rev.*, vol. 110, p. 1295, 1958.
- [9] M. H. Seavey and P. E. Tannenwald, "Direct observation of spin-wave resonance," *Phys. Rev. Lett.*, vol. 1, pp. 168–169, 1958.
- [10] J. Matthews and R. L. Walker, *Mathematical Methods of Physics*. Menlo Park, CA: W. A. Benjamin Inc., 1970.
- [11] E. Schlömann, "A sum rule concerning the inhomogeneous demagnetizing field in nonellipsoidal samples," *J. Appl. Phys.*, vol. 33, p. 2825, 1962.

- [12] J. P. Parekh, K. W. Chang, and H. S. Tuan, "Propagation characteristics of magnetostatic waves," *Circ. Syst. Signal Process*, vol. 4, p. 9, 1985.
- [13] B. A. Kalinikos, "Excitation of propagating spin waves in ferromagnetic films," *IEE Proc.*, vol. 127, no. H, pp. 4–10, 1980.

Propagation Characteristics and Excitation of Dipolar Spin Waves

Chapter 5 treated the resonant frequencies, dispersion relations, and mode fields for various dipolar spin modes. In this chapter, we expand on the properties of dipolar spin waves in thin films and describe how to excite them. We first establish approximate expressions for the Poynting vector and energy velocity valid in the magnetostatic approximation. Next, we apply the phenomenological description of magnetic damping introduced in Chapter 3 to the problem of dipolar spin wave attenuation. Finally, we derive orthogonality and normalization conditions and use these relations to calculate the excitation of dipolar spin waves by thin wires and conducting strips.

6.1 Energy Velocities for Dipolar Spin Waves

The energy velocity for uniform plane waves was defined in Chapter 4 as (cf. Eq. (4.102))

$$\mathbf{v}_e = \frac{\langle \mathbf{P}(t) \rangle}{\langle w(t) \rangle}. \quad (6.1)$$

For guided waves, however, $\langle \mathbf{P}(t) \rangle$ and $\langle w(t) \rangle$ are functions of position. Because of this, the expression for energy velocity for guided waves is modified by integrating the Poynting vector and energy density over the cross section of the guide. The general expression for the component of \mathbf{v}_e perpendicular to the surface S is

$$v_{e,s} = \frac{\int_S \langle \mathbf{P}(t) \rangle \cdot d\mathbf{s}}{\int_S \langle w(t) \rangle ds}. \quad (6.2)$$

We will now seek simplified expressions for $\langle \mathbf{P}(t) \rangle$ and $\langle w(t) \rangle$ valid within the magnetostatic approximation. We begin by considering the Poynting theorem for time-harmonic fields with slowly varying amplitudes of the form considered in Section 4.5. Averaging the Poynting theorem (Eq. (4.31)) over a period of the oscillation and assuming a lossless medium yields

$$\nabla \cdot \langle \mathbf{P}(t) \rangle + \frac{\partial \langle w(t) \rangle}{\partial t} = 0, \quad (6.3)$$

where

$$\langle \mathbf{P}(t) \rangle = \frac{1}{2} \text{Re}(\mathbf{e} \times \mathbf{h}^*) \quad (6.4)$$

and

$$\langle w(t) \rangle = \frac{1}{4} \mathbf{h}^* \cdot \frac{\partial}{\partial \omega} [\omega \bar{\boldsymbol{\mu}}(\omega)] \cdot \mathbf{h} + \frac{1}{4} \varepsilon \mathbf{e}^* \cdot \mathbf{e}. \quad (6.5)$$

The magnetostatic approximation to the total energy density (6.5) can be obtained by neglecting the electric energy density. To obtain an approximation to the Poynting vector (6.4), we first expand the divergence of the time-averaged Poynting vector:

$$\nabla \cdot (\mathbf{e} \times \mathbf{h}^*) = \mathbf{h}^* \cdot (\nabla \times \mathbf{e}) - \mathbf{e} \cdot (\nabla \times \mathbf{h}^*). \quad (6.6)$$

In the magnetostatic approximation, $\nabla \times \mathbf{h} = 0$, so the last term vanishes. Further, \mathbf{e} can be eliminated using Maxwell's equation from Faraday's law (5.3). The result is

$$\nabla \cdot (\mathbf{e} \times \mathbf{h}^*) = -i\omega \nabla \psi^* \cdot \mathbf{b}. \quad (6.7)$$

The right-hand side can be written as a divergence using the vector identity

$$\nabla \cdot (\psi^* \mathbf{b}) = \mathbf{b} \cdot (\nabla \psi^*) + \psi^* (\nabla \cdot \mathbf{b}) \quad (6.8)$$

and the fact that $\nabla \cdot \mathbf{b} = 0$. This gives

$$\nabla \cdot (\mathbf{e} \times \mathbf{h}^*) = -i\omega \nabla \cdot (\psi^* \mathbf{b}). \quad (6.9)$$

This suggests the following form for the Poynting vector in the magneto-quasistatic approximation:

$$\langle \mathbf{P}(t) \rangle = \frac{1}{2} \text{Re}(-i\omega \psi^* \mathbf{b}). \quad (6.10)$$

Note that this vector is not the same as Eq. (6.4), but it has the same divergence from Eq. (6.9). It therefore satisfies the Poynting theorem and can be used in energy flow calculations just as well.¹

For propagation along the $\hat{\mathbf{k}}$ direction in a uniform infinite film, the energy velocity in Eq. (6.2) becomes

$$v_e = \frac{-2 \text{Re} \int_{-\infty}^{\infty} i\omega \psi^* \mathbf{b} \cdot \hat{\mathbf{k}} d\zeta}{\int_{-\infty}^{\infty} \mathbf{h}^* \cdot \frac{\partial}{\partial \omega} [\omega \bar{\boldsymbol{\mu}}(\omega)] \cdot \mathbf{h} d\zeta}, \quad (6.11)$$

where ζ is the coordinate normal to the film plane. The energy velocity has been calculated in this way by Gupta and Srivastava [1, 2] for each of the

¹ It is generally true that the Poynting vector is not a uniquely defined quantity; any vector with zero divergence can be added to Eq. (6.4) or (6.10) to obtain a new Poynting vector that also satisfies the Poynting theorem.

three dipolar spin modes of a thin film and was shown in each case to be identical to the group velocity. The equivalence of group and energy velocities for electromagnetic waves in lossless media is well established. The fact that the equivalence is also found in a magnetostatic analysis is evidence of the self-consistency of the magnetostatic approximation.

6.2 Propagation Loss²

Up to this point, we have assumed that dipolar spin waves propagate without attenuation. We will now build on the discussion of magnetic damping in Chapter 3 and develop a phenomenological model to describe propagation loss.

6.2.1 Relaxation Time for Propagating Modes

The equation of motion for the magnetization including the Gilbert form of the damping term is (cf. Eq. (3.128))

$$\frac{d\mathbf{M}}{dt} = \gamma\mu_0\mathbf{M} \times \mathbf{H}_{\text{eff}} + \frac{\alpha}{M_S}\mathbf{M} \times \frac{d\mathbf{M}}{dt}, \quad (6.12)$$

where \mathbf{H}_{eff} is the total effective internal magnetic field intensity. We will assume in the following that \mathbf{H}_{eff} is given completely by the applied field plus the demagnetizing field (exchange and magnetocrystalline anisotropy will be neglected for simplicity). As shown in Chapter 3, the effect of the damping term in Eq. (6.12) on the magnetic susceptibility tensor is simply to replace ω_0 with $\omega_0 - i\alpha\omega$, where $\omega_0 = -\gamma\mu_0 H_{\text{eff}}$ and a time dependence of the form $\exp(-i\omega t)$ is assumed. Let us define the *relaxation time* of a mode as the time required for the amplitude of the small-signal magnetization to decay by the factor $1/e$ after removal of an excitation. The relaxation time T_0 of the uniform precession mode in an infinite medium is related to the damping parameter α by (cf. Eq. (3.156))

$$\frac{1}{T_0} = \omega\alpha, \quad (6.13)$$

where ω is the resonant frequency of the uniform precession mode. Alternatively, T_0 is related to the full FMR line width ΔH of the uniform precession mode by (cf. Eqs. (3.155))

$$\frac{1}{T_0} = -\frac{\gamma\mu_0\Delta H}{2}. \quad (6.14)$$

The relationship between α and ΔH is, therefore,

² The discussion in this section follows Stancil [3]. Magnetostatic wave propagation loss has also been discussed by Vittoria and Wilsey [4].

$$\alpha = -\frac{\gamma\mu_0\Delta H}{2\omega}. \quad (6.15)$$

Assuming the small-signal magnetization in the general case decays according to the factor $\exp(-t/T_k)$, where T_k is a relaxation time appropriate for the particular mode and geometry, we can define the loss per unit time as

$$\begin{aligned} L &= -\frac{20 \log e^{-t/T_k}}{t \times 10^6} \\ &= \frac{8.686}{T_k} \times 10^{-6} (\text{dB}/\mu\text{s}), \end{aligned} \quad (6.16)$$

where t and T_k are given in seconds. Substituting from Eq. (6.14) for the relaxation time into Eq. (6.16) shows that the decay of the uniform precession mode in an infinite ferrite occurs at the rate of $0.960 \Delta H$ (dB/ μs), as discussed in Chapter 3. The decay rate is more complex for propagating waves in a thin-film geometry, as we will now show.

Damping of dipolar spin waves can be modeled by allowing the frequency ω to be complex. Thus, if the time dependence is of the form $\exp(-i\omega t)$, the amplitude will decay according to the factor $\exp(\text{Im}\{\omega\}t)$, where $\text{Im}\{\omega\} < 0$. Comparison with the loss parameter in Eq. (6.16) suggests the relaxation time T_k be defined as

$$\frac{1}{T_k} = -\text{Im}\{\omega\}. \quad (6.17)$$

Since ω generally depends on ω_0 , ω can be represented by the Taylor series:

$$\omega(\omega_0 + \Delta\omega_0) = \omega(\omega_0) + \frac{\partial\omega}{\partial\omega_0}\Delta\omega_0 + \cdots \quad (6.18)$$

In the presence of loss, we set $\Delta\omega_0 = -i/T_0$ to obtain

$$\omega(\omega_0 - i/T_0) \approx \omega(\omega_0) - \frac{\partial\omega}{\partial\omega_0} \frac{i}{T_0}, \quad (6.19)$$

to lowest-order in $1/T_0$. Note that $\omega(\omega_0)$ is the frequency in the absence of loss and is therefore real. The imaginary part of ω is thus approximated by

$$\text{Im}\{\omega\} \approx \frac{-1}{T_0} \frac{\partial\omega}{\partial\omega_0}. \quad (6.20)$$

Combining this result with Eq. (6.17) gives

$$\frac{1}{T_k} = \frac{1}{T_0} \frac{\partial\omega}{\partial\omega_0}. \quad (6.21)$$

For the uniform precession mode in a sphere as well as an infinite medium, $\omega = \omega_0$ and T_k reduces to T_0 as expected. Although Eq. (6.21) clearly shows that the mode relaxation time will generally depend on the sample geometry

through $\partial\omega/\partial\omega_0$, it is interesting to note that the relationship between α and ΔH given by Eq. (6.15) can be shown to be geometry independent provided the damping term is of the Landau–Lifshitz type [5]. It can also be shown that Eq. (6.15) is not limited to the uniform precession mode, but is valid regardless of the value of k [3].

In general, however, spin wave dispersion relations are transcendental and of the form

$$F(\omega, k, \omega_0) = 0. \quad (6.22)$$

When it is not possible to solve explicitly for $\omega(k, \omega_0)$, the derivative in Eq. (6.21) is best obtained by implicit differentiation. The result is

$$\frac{1}{T_k} = -\frac{1}{T_0} \frac{\partial F/\partial\omega_0}{\partial F/\partial\omega}, \quad (6.23)$$

where the right-hand side is understood to be evaluated at $\omega_0 = -\gamma\mu_0 H_{\text{eff}}$.

6.2.2 Surface Waves

The dispersion relation for surface dipolar spin waves in an isolated slab is given by Eq. (5.111b). Even though it is possible to solve for ω in this case, it is computationally convenient to use Eq. (6.23) and rewrite Eq. (5.111b) as

$$F = \Gamma - \frac{\omega_M^2}{4} (1 - e^{-2kd}) = 0, \quad (6.24)$$

where

$$\Gamma = \omega^2 - \omega_0(\omega_0 + \omega_M). \quad (6.25)$$

Since Γ contains all the explicit dependence on ω and ω_0 , we have

$$\begin{aligned} \frac{1}{T_k} &= -\frac{1}{T_0} \frac{\partial\Gamma/\partial\omega_0}{\partial\Gamma/\partial\omega} \\ &= \frac{1}{T_0} \left[\frac{2\omega_0 + \omega_M}{2\omega} \right]. \end{aligned} \quad (6.26a)$$

Alternatively, this can be written in terms of α or ΔH :

$$\frac{1}{T_k} = \alpha \left(\omega_0 + \frac{\omega_M}{2} \right), \quad (6.26b)$$

$$\frac{1}{T_k} = \frac{|\gamma|\mu_0\Delta H}{4\omega} (2\omega_0 + \omega_M). \quad (6.26c)$$

Assuming α is frequency independent, Eq. (6.26b) shows that for a fixed field, the relaxation time will be constant across the surface wave passband.

The field necessary to place the low-frequency band edge at the frequency ω is given by $H_{0l} = \omega_{0l}/|\gamma|\mu_0$, where ω_{0l} is obtained from Eq. (5.111b) in the limit $k \rightarrow 0$. The result is

$$\omega_{0l} = -\frac{\omega_M}{2} + \omega \left[1 + \frac{\omega_M^2}{4\omega^2} \right]^{1/2}. \quad (6.27)$$

Substituting this result into Eqs. (6.26b) and (6.26c) gives

$$\frac{1}{T_{kl}} = \alpha\omega \left[1 + \frac{\omega_M^2}{4\omega^2} \right]^{1/2}, \quad (6.28a)$$

$$\frac{1}{T_{kl}} = \frac{|\gamma|\mu_0\Delta H}{2} \left[1 + \frac{\omega_M^2}{4\omega^2} \right]^{1/2}. \quad (6.28b)$$

Similarly, the field necessary to place the high-frequency band edge at the frequency ω is obtained from Eq. (5.111b) with $k \rightarrow \infty$. The result is $H_{0h} = \omega_{0h}/|\gamma|\mu_0$, where ω_{0h} is given by

$$\omega_{0h} = \omega - \frac{\omega_M}{2}. \quad (6.29)$$

Substituting this into Eqs. (6.26b) and (6.26c) gives

$$\frac{1}{T_{kh}} = \alpha\omega, \quad (6.30a)$$

$$\frac{1}{T_{kh}} = \frac{|\gamma|\mu_0\Delta H}{2}. \quad (6.30b)$$

Equations (6.30a) and (6.30b) are identical to (6.13) and (6.14) and thus the loss at the high-frequency band edge is the same as that of the uniform precession mode. Equations (6.28a) and (6.28b) show, however, that the loss at the low-frequency band edge is higher than that of the uniform precession mode. The corresponding losses per unit time can be obtained by replacing $1/T_k$ in Eq. (6.16) with Eq. (6.26), (6.28), or (6.30). These equations are illustrated in Figure 6.1 for $\alpha = 1.5 \times 10^{-4}$ ($\Delta H = 79.6$ A/m (1 Oe) at 9.3 GHz) and several values of applied field [3]. The dashed lines represent the limits given by Eqs. (6.28) and (6.30). The loss for a given value of field is simply a horizontal line drawn between these two limits according to Eq. (6.26b). The loss per unit time for the low-frequency ($k=0$) surface wave band edge is

$$L = 0.960 \left[1 + \frac{\omega_M^2}{4\omega^2} \right] \Delta H \quad (\text{dB}/\mu\text{s}). \quad (6.31)$$

6.2.3 Volume Waves

The dispersion relations for forward and backward volume waves are given by Eqs. (5.76) and (5.97), respectively. A significant point to notice about both of these equations is that the dependence on ω and ω_0 enters only through χ . Because of this, we can write

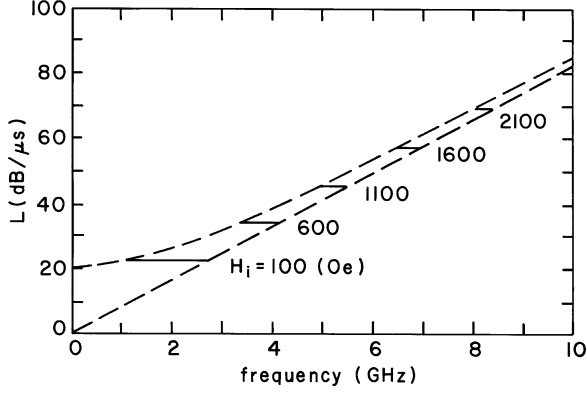


Fig. 6.1. Variations of surface wave loss with frequency for several different values of bias field. The dashed lines represent the limits given by Eqs. (6.28) and (6.30), and the solid lines give the propagation loss parameter L according to Eqs. (6.16) and (6.26b). Parameters used are $M_S = 141.6 \text{ kA/m}$ and $\alpha = 1.5 \times 10^{-4}$ ($\Delta H = 79.6 \text{ A/m}$ (1 Oe) at 9.3 GHz). Reprinted with permission from [3]. Copyright 1986, American Institute of Physics.

$$\frac{\partial F}{\partial \omega} = \frac{\partial F}{\partial \chi} \frac{\partial \chi}{\partial \omega}, \quad (6.32)$$

$$\frac{\partial F}{\partial \omega_0} = \frac{\partial F}{\partial \chi} \frac{\partial \chi}{\partial \omega_0}. \quad (6.33)$$

Fortunately, the complicated quantity $\partial F / \partial \chi$ divides out of Eq. (6.23), leaving us with the much simpler result

$$\frac{1}{T_k} = -\frac{1}{T_0} \frac{\partial \chi / \partial \omega_0}{\partial \chi / \partial \omega}. \quad (6.34)$$

Evaluating the indicated derivatives in Eq. (6.34) using the definition of χ from Eq. (3.115) gives

$$\frac{1}{T_k} = \frac{1}{T_0} \left[\frac{\omega_0^2 + \omega^2}{2\omega_0\omega} \right]. \quad (6.35a)$$

As before, the frequency dependence can be emphasized using Eq. (6.13) to obtain

$$\frac{1}{T_k} = \alpha \frac{\omega_0^2 + \omega^2}{2\omega_0}, \quad (6.35b)$$

while the line width dependence can be emphasized using Eq. (6.14):

$$\frac{1}{T_k} = |\gamma| \mu_0 \Delta H \frac{\omega_0^2 + \omega^2}{4\omega_0\omega}. \quad (6.35c)$$

Note that these equations are valid for both forward and backward volume waves.

As in the surface wave case, let us find the limits imposed by the volume wave band edges. The field necessary to place the low-frequency band edge at ω is obtained by letting $k \rightarrow \infty$ in Eq. (5.97), or $k = 0$ in Eq. (5.76), and solving for ω_0 . The result is

$$\omega_{0l} = \omega. \quad (6.36)$$

Thus,

$$\frac{1}{T_{kl}} = \alpha\omega = \frac{|\gamma|\mu_0\Delta H}{2}. \quad (6.37)$$

This is the same result obtained for the high-frequency surface wave band edge (cf. Eqs. (6.30a) and (6.30b)) and again leads to the same loss as the uniform precession mode. The field necessary to place the high-frequency band edge at ω is given by Eq. (6.27) and leads to

$$\frac{1}{T_{kh}} = \alpha\omega \left[1 + \frac{\omega_M^2}{4\omega^2}\right]^{1/2} = \frac{|\gamma|\mu_0\Delta H}{2} \left[1 + \frac{\omega_M^2}{4\omega^2}\right]^{1/2}. \quad (6.38)$$

This is identical to the result obtained for the low-frequency surface wave band edge (cf. Eq. (6.28)). Thus, we see that the loss for any of the three principal dipolar spin wave modes must lie between the limits given by Eqs. (6.37) and (6.38), or (6.28) and (6.30). Within these limits, $1/T_k$ is a quadratic function of frequency for volume waves according to Eq. (6.35b), whereas the surface wave relaxation time is constant for fixed ω_0 .

Equations (6.35), (6.37), and (6.38) are illustrated in Figure 6.2 for $\alpha = 1.5 \times 10^{-4}$ ($\Delta H = 79.6$ A/m (1 Oe) at 9.3 GHz) and several values of internal field. The curve for each internal field can be interpreted as applying to either forward or backward volume waves, although the necessary external fields would differ for the two cases because of demagnetizing effects. The upper frequency limit (high loss) thus corresponds to the $k = 0$ band edge for backward volume waves and the $k \rightarrow \infty$ band edge for forward volume waves. Since the $k = 0$ band edge corresponds to the high loss limit for both surface and backward volume waves, we see that if the $k = 0$ band edge is to be set at a specified frequency, forward volume waves will always exhibit the lowest propagation loss per unit time. The loss for other values of line width can be easily scaled from the figures.

6.2.4 Summary of the Phenomenological Loss Theory

The theory described in this section represents a simple application of the Gilbert form of the Landau–Lifshitz equation to the damping of dipolar spin waves. The damping parameter, α , has been assumed to be frequency independent. The key features of the theory can be summarized as follows:

- (a) At a given frequency, the propagation loss per unit time L for any one of the three principal modes lies between the limits

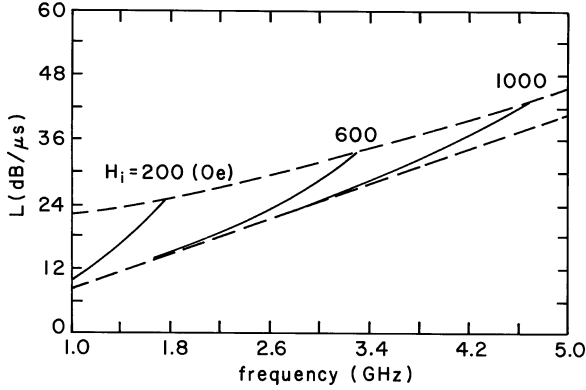


Fig. 6.2. Variations of volume wave losses per unit time with frequency for several different values of bias field. The dashed lines represent the same limits shown in Figure 6.1 and the solid lines give the propagation loss parameter L according to (6.16) and (6.35b). For a given internal field, the solid curves apply to either forward or backward volume waves. The low-frequency limit corresponds to the $k=0$ band edge for forward volume waves and the $k \rightarrow \infty$ band edge for backward volume waves. Parameters used are the same as in Figure 6.1. Reprinted with permission from [3]. Copyright 1986, American Institute of Physics.

$$0.960 \Delta H \leq L \leq 0.960 \left[1 + \frac{\omega_M^2}{4\omega^2} \right]^{1/2} \Delta H, \quad (6.39)$$

where ΔH is the full FMR line width in A/m at the frequency ω , and L is in dB/ μ s.

- (b) The propagation loss parameter L for dipolar surface spin waves is independent of frequency within the passband for a constant bias field. At the low-frequency ($k=0$) band edge the value of L coincides with the upper limit in Eq. (6.39), and at the high-frequency ($k \rightarrow \infty$) band edge the value of L coincides with the lower limit. For a constant frequency, L increases with bias field.
- (c) The loss parameter L for volume waves increases quadratically with frequency for a given bias field and progresses from one limit in Eq. (6.39) to the other across the passband. The value of L at the forward volume wave $k=0$ band edge is given by the lower limit in Eq. (6.39), whereas the value of L at the backward volume wave $k=0$ band edge is given by the upper limit.
- (d) It follows from these conclusions that the uniform precession loss estimate of $0.960 \Delta H$ dB/ μ s should be accurate for forward volume waves with small k , but should always underestimate the losses per unit time of surface and backward volume waves.

Existing measurements of dipolar spin wave propagation losses are in reasonable agreement with this theory for surface and forward volume waves

above 3 GHz. However, substantial discrepancies exist between the theory and backward volume wave measurements [6]. Consequently, additional loss measurements are needed to adequately test the applicability of the phenomenological loss theory.

6.3 Mode Orthogonality and Normalization

When the excitation of dipolar spin waves is considered, it is often the case that a given excitation structure will couple to multiple propagating modes. When decomposing the total potential into its constituent modes, it is useful to establish the *orthogonality* of the modes. In the following sections, we will derive the orthogonality properties of the three principal modes and illustrate their use in the calculation of the total power carried by a multimode film [7]. The discussion allows variations of the material properties through the thickness of the film, but assumes the film is uniform in the plane.

6.3.1 Forward Volume Waves

Consider two forward volume wave modes with wave numbers k_a and k_b propagating with the same frequency ω . The potential functions are of the form

$$\psi_{a,b}(\mathbf{r}) = \phi_{a,b}(y)e^{i\mathbf{k}_{a,b}\cdot\mathbf{r}}, \quad (6.40)$$

where $\mathbf{k}_{a,b}$ are vectors in the $x-y$ plane. From Walker's equation (Eq. (5.9)), the functions $\phi_{a,b}(z)$ must satisfy the equations

$$\frac{\partial^2 \phi_a}{\partial z^2} - k_a^2(1 + \chi)\phi_a = 0, \quad (6.41)$$

$$\frac{\partial^2 \phi_b}{\partial z^2} - k_b^2(1 + \chi)\phi_b = 0. \quad (6.42)$$

To obtain the orthogonality relation, we first multiply Eq. (6.41) by $\phi_b(z)$ and integrate over z :

$$\int_{-\infty}^{\infty} \frac{\partial^2 \phi_a}{\partial z^2} \phi_b \, dz = k_a^2 \int_{-\infty}^{\infty} (1 + \chi) \phi_a \phi_b \, dz. \quad (6.43)$$

Integrating the left-hand side by parts gives

$$\int_{-\infty}^{\infty} \frac{\partial^2 \phi_a}{\partial z^2} \phi_b \, dz = \left. \frac{\partial \phi_a}{\partial z} \phi_b \right|_{-\infty}^{\infty} - \int_{-\infty}^{\infty} \frac{\partial \phi_a}{\partial z} \frac{\partial \phi_b}{\partial z} dz. \quad (6.44)$$

The potential functions decay exponentially away from the film, so that the first term on the right-hand side vanishes. Integrating by parts a second time yields

$$\begin{aligned}
\int_{-\infty}^{\infty} \frac{\partial^2 \phi_a}{\partial z^2} \phi_b \, dz &= -\phi_a \left. \frac{\partial \phi_b}{\partial z} \right|_{-\infty}^{\infty} + \int_{-\infty}^{\infty} \phi_a \frac{\partial^2 \phi_b}{\partial z^2} \, dz \\
&= \int_{-\infty}^{\infty} \phi_a \frac{\partial^2 \phi_b}{\partial z^2} \, dz \\
&= k_b^2 \int_{-\infty}^{\infty} (1 + \chi) \phi_a \phi_b \, dz.
\end{aligned} \tag{6.45}$$

The last step follows from Eq. (6.42). Thus

$$(k_a^2 - k_b^2) \int_{-\infty}^{\infty} (1 + \chi) \phi_a(z) \phi_b(z) \, dz = 0. \tag{6.46}$$

If $k_a^2 \neq k_b^2$, then the integral must vanish:

$$\int_{-\infty}^{\infty} (1 + \chi) \phi_a(z) \phi_b(z) \, dz = 0, \quad a \neq b. \tag{6.47}$$

This is the orthogonality property of forward volume wave modes. Note that when evaluating this integral, χ must be set to zero in the dielectric regions.

To illustrate the use of the orthogonality property, consider the total power carried by a multimode film. If multiple thickness modes are excited, the total potential can be written as

$$\psi(\mathbf{r}) = \sum_{n=0}^{\infty} a_n \phi_n(z) e^{i\mathbf{k}_n \cdot \mathbf{r}}. \tag{6.48}$$

The total power carried by the waveguide is

$$P = \frac{1}{2} \text{Re} \int_{-\infty}^{\infty} (-i\omega \psi^*) \mathbf{b} \cdot \hat{\mathbf{k}} \, dz, \tag{6.49}$$

where P (mW/mm) is the power per unit length in the plane of the film perpendicular to the direction of propagation. For multiple forward volume wave modes, $\mathbf{b} \cdot \hat{\mathbf{k}}$ is given by

$$\mathbf{b} \cdot \hat{\mathbf{k}} = -i\mu_0 \sum_{m=0}^{\infty} a_m k_m (1 + \chi) \psi_m. \tag{6.50}$$

Substituting this expression along with Eq. (6.48) for the potential into the integral for total power in Eq. (6.49) gives

$$P = -\frac{\omega\mu_0}{2} \operatorname{Re} \left\{ \sum_{m,n} a_n^* a_m k_m e^{i(\mathbf{k}_m - \mathbf{k}_n) \cdot \mathbf{r}} \int_{-\infty}^{\infty} (1 + \chi) \phi_n(z) \phi_m(z) dz \right\}. \quad (6.51)$$

The orthogonality relation (6.47) causes the terms in the sum over m to vanish unless $m = n$. The expression therefore simplifies to

$$P = -\frac{\omega\mu_0}{2} \sum_n |a_n|^2 k_n \int_{-\infty}^{\infty} (1 + \chi) \phi_n(z) \phi_n(z) dz. \quad (6.52)$$

Since the cross terms between modes have vanished, we conclude that the total power is simply the sum of the powers carried in the individual modes.

The preceding discussions of orthogonality and mode power suggest two ways to normalize the mode amplitude ψ_0 in Eqs. (5.80) and (5.81). The simplest condition is to require the normalization integral in Eq. (6.47) to have unity magnitude when $m = n$:

$$-\int_{-\infty}^{\infty} (1 + \chi) \phi_a(z) \phi_b(z) dz = \delta_{a,b}, \quad (6.53)$$

where $\delta_{a,b}$ is the Kronecker delta and is equal to 1 if $a = b$ and 0 otherwise. With this normalization condition, the coefficient ψ_0 is found to be

$$\psi_0 = \sqrt{\frac{2}{-(1 + \chi)d}} \quad (6.54)$$

for all modes (even and odd).

Alternatively, the mode functions can be normalized so that if $a_n = 1$ in Eq. (6.52), the power in the n th mode is P_n (mW/mm). In this case, the coefficient is found to be

$$\psi_{0n} = \sqrt{\frac{4P_n}{-(1 + \chi)\omega\mu_0 k_n d}}. \quad (6.55)$$

6.3.2 Backward Volume Waves

Mode orthogonality relations can be derived for backward volume waves in a similar manner. We consider two modes with wave numbers k_a and k_b propagating with the same frequency ω . The potential functions are of the form:

$$\psi_{a,b}(\mathbf{r}) = \phi_{a,b}(y) e^{i\nu k_{a,b} z}. \quad (6.56)$$

The functions $\phi_{a,b}(y)$ are determined by Walker's equation (5.9). Allowing for inhomogeneities through the thickness (note that the boundaries of the film can be viewed as limiting cases of thickness inhomogeneities) yields

$$\frac{\partial}{\partial y} \left[(1 + \chi) \frac{\partial \phi_{a,b}}{\partial y} \right] - k_{a,b}^2 \phi_{a,b} = 0. \quad (6.57)$$

As before, multiply both sides of the equation for ϕ_a by ϕ_b and integrate through the thickness to obtain

$$\int_{-\infty}^{\infty} \phi_b \frac{\partial}{\partial y} \left[(1 + \chi) \frac{\partial \phi_a}{\partial y} \right] dy = k_a^2 \int_{-\infty}^{\infty} \phi_a \phi_b dy. \quad (6.58)$$

Integrating the left-hand side by parts twice leads to the result

$$(k_a^2 - k_b^2) \int_{-\infty}^{\infty} \phi_a(y) \phi_b(y) dy = 0. \quad (6.59)$$

If $k_a^2 \neq k_b^2$, the integral must vanish:

$$\int_{-\infty}^{\infty} \phi_a(y) \phi_b(y) dy = 0. \quad (6.60)$$

This is the orthogonality property of backward volume wave modes.

For multimode propagation, the total potential is

$$\psi(\mathbf{r}) = \sum_{n=1}^{\infty} a_n \phi_n(y) e^{i\nu k_n z}. \quad (6.61)$$

Note that the sum begins with $n=1$ since the lowest-order backward volume wave mode is odd. The component of \mathbf{b} along the direction of $\hat{\mathbf{k}}$ is

$$\mathbf{b} \cdot \hat{\mathbf{k}} = -i\mu_0 \sum_{m=1}^{\infty} a_m k_m \psi_m. \quad (6.62)$$

Substituting these expressions for the potential and $\mathbf{b} \cdot \hat{\mathbf{k}}$ into the integral for total mode power (Eq. (6.49) but with the integration over y instead of z) and using the orthogonality property (6.60) leads to the waveguide power

$$P = -\frac{\omega\mu_0}{2} \sum_n |a_n|^2 k_n \int_{-\infty}^{\infty} \phi_n(y) \phi_n(y) dy. \quad (6.63)$$

As before, the total power is just the sum of the powers carried by the individual modes. In contrast with the forward volume wave case, however, the minus sign along with the absence of the factor $(1 + \chi)$ implies energy flow in the direction opposite to $\hat{\mathbf{k}}$.

Applying the simple normalization condition

$$\int_{-\infty}^{\infty} \phi_a(y) \phi_b(y) dy = \delta_{a,b} \quad (6.64)$$

requires the mode coefficient in Eqs. (5.99) and (5.100) to be

$$\psi_0 = \sqrt{\frac{2}{d}}. \quad (6.65)$$

Similarly, normalizing so that $a_n = 1$ in Eq. (6.63) represents P_n (mW/mm along the $\hat{\mathbf{x}}$ direction) gives

$$\psi_{0n} = \sqrt{\frac{4P_n}{\omega\mu_0 k_n d}}. \quad (6.66)$$

6.3.3 Surface Waves

Since multiple thickness modes are not present for a given direction of surface wave propagation, we consider modes traveling in opposite directions at the same frequency. The mode potentials take the form

$$\psi_{a,b}(\mathbf{r}) = \phi_{a,b}(y) e^{i\nu_{a,b} k x}, \quad (6.67)$$

where $\nu_{a,b} = \pm 1$ and k is positive definite. The function $\phi_{a,b}$ satisfies Walker's equation for a general medium with inhomogeneities along $\hat{\mathbf{y}}$:

$$\frac{\partial}{\partial y} \left[(1 + \chi) \frac{\partial \phi_{a,b}}{\partial y} \right] - \left[(1 + \chi) k^2 + \nu_{a,b} k \frac{\partial \kappa}{\partial y} \right] \phi_{a,b} = 0. \quad (6.68)$$

Multiplying Walker's equation for ϕ_a by ϕ_b and integrating over all y gives

$$\int_{-\infty}^{\infty} \frac{\partial}{\partial y} \left[(1 + \chi) \frac{\partial \phi_a}{\partial y} \right] \phi_b dy = \int_{-\infty}^{\infty} \left[(1 + \chi) k^2 + \nu_a k \frac{\partial \kappa}{\partial y} \right] \phi_a \phi_b dy. \quad (6.69)$$

Integrating the left-hand side of Eq. (6.69) by parts twice and using Walker's equation for ϕ_b leads to

$$(\nu_a - \nu_b) \int_{-\infty}^{\infty} \frac{\partial \kappa}{\partial y} \phi_a(y) \phi_b(y) dy = 0. \quad (6.70)$$

If $\nu_a \neq \nu_b$, then the waves are oppositely directed and we obtain the orthogonality relation for surface waves:

$$\int_{-\infty}^{\infty} \frac{\partial \kappa}{\partial y} \phi_+(y) \phi_-(y) dy = 0. \quad (6.71)$$

The absence of thickness modes along with the fact that this integral is not the same as that appearing in the mode power expression (Eq. (6.49) but integrated over y instead of z) makes this result less useful than in the case of volume waves. Nevertheless, it can be used to derive an interesting symmetry property of surface wave potential functions, as we will now show.

For a uniform film of thickness d , κ can be expressed

$$\kappa = \kappa_0 [u(y + d/2) - u(y - d/2)], \quad (6.72)$$

where $u(y)$ is the unit step function. It follows that

$$\frac{\partial \kappa}{\partial y} = \kappa_0 [\delta(y + d/2) - \delta(y - d/2)]. \quad (6.73)$$

Substituting this result into Eq. (6.71) gives the symmetry relation

$$\phi_+(-d/2)\phi_-(-d/2) = \phi_+(d/2)\phi_-(d/2). \quad (6.74)$$

The validity of this expression is readily seen from the potential functions Eq. (5.113) and Figure 5.18.

The surface wave power can be found from Eq. (6.49) but integrated over y instead of z . After some rather tedious manipulations involving the dispersion relation in Eq. (5.111a) and the definition of p from Eq. (5.114), the normalization for a power P (mW/mm along z) can be cast in the form

$$\psi_{0\nu} = \sqrt{\frac{P}{-(1 + \chi)\omega\mu_0 p(\nu)kd}}. \quad (6.75)$$

6.4 Excitation of Dipolar Spin Waves

Experimentally, it is surprisingly easy to excite dipolar spin waves in thin films; all that is required is to place a current-carrying wire near the film. In practice, such a structure is readily made with microstrip transmission line techniques [8–20]. In this section, we describe a simple excitation structure and use the mode orthogonality relations to obtain the coupling to forward and backward volume waves. The mode orthogonality approach is not as well suited to surface waves, however, so we simply quote the results from the literature for completeness [11].

6.4.1 Common Excitation Structures

Two common microstrip structures for the excitation of dipolar spin waves are shown in Figure 6.3. In both cases, the sample consists of a thin single-crystal film of YIG grown by liquid phase epitaxy on a gadolinium gallium

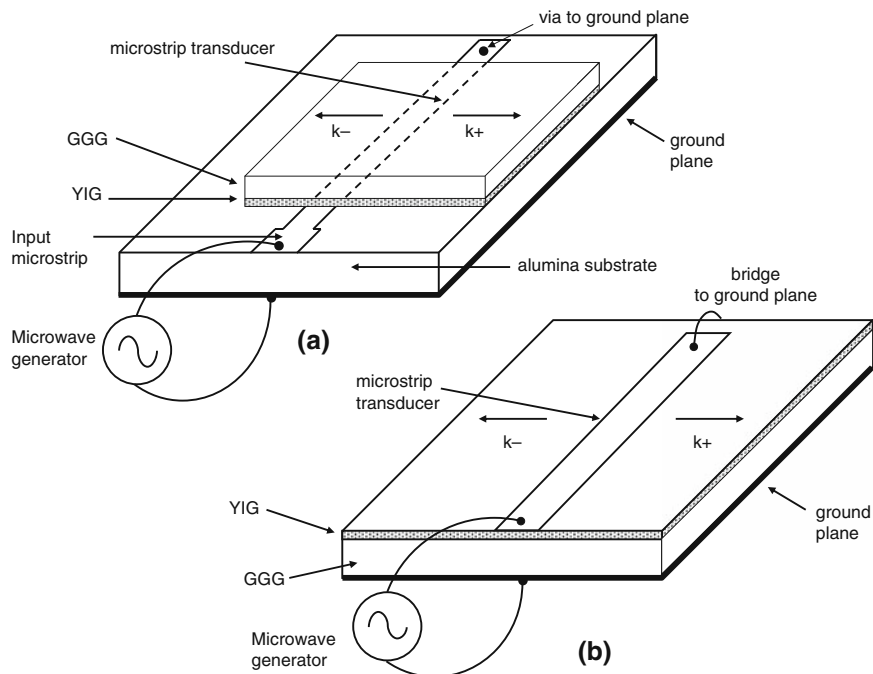


Fig. 6.3. Microstrip excitation geometries: (a) YIG sample is placed in contact with a microstrip transducer made on an alumina substrate and (b) YIG/GGG sample is used as the substrate for the microstrip.

garnet (GGG) substrate. In part (a), the microstrip circuit is made on an alumina substrate and the sample is placed YIG side down over the thin portion of the microstrip lines. A ground plane completely covers the bottom side of the alumina substrate. The conductors on both sides of the alumina are usually sputtered gold, although aluminum (evaporated or sputtered) can also be used with somewhat greater resistive losses. The width of the input line and the alumina substrate thickness are chosen so that the resulting microstrip transmission line has the same characteristic impedance as the source (usually $50\ \Omega$). For an alumina substrate with relative permittivity of about 10, this is achieved when the width of the strip is approximately equal to the thickness of the substrate.

At low-microwave frequencies where the length of the radiating portion of the microstrip is short compared to a wavelength along the transmission line, best results are obtained if the far end of the microstrip is shorted to the ground plane either with a via through the substrate or with a conducting wraparound at the edge of the substrate. The radiating portion of the microstrip is referred to as the *transducer*. Shorting the end creates the maximum current through the microstrip and therefore the maximum coupling. At frequencies approaching 10 GHz, however, a microstrip antenna of even a few millimeters becomes an appreciable fraction of a wavelength and better

results are obtained by terminating the transducer with a segment of open-circuited transmission line whose length has been selected to reflect a short (or current maximum) near the center of the transducer.

The configuration in Figure 6.3(b) differs in that the YIG/GGG sample is used as the microstrip substrate. In both cases the strength of coupling decreases exponentially with separation between the transducer and the YIG film.

The width of the transducer determines the range of wavelengths that can be easily excited. As long as the width is small compared to a spin wavelength, radiation will be efficient. However, when the width becomes a half wavelength, waves launched from one edge of the transducer will be exactly out of phase with waves launched from the other edge and no net radiation will occur. This will be discussed in more detail in the following sections.

As the incident wave propagates along the transducer, energy is lost to dipolar spin waves. This can be included in a transmission line model as an effective radiation resistance per unit length r_r . An equivalent transmission line model is shown in Figure 6.4. The transducer can be modeled as a lossy transmission line with characteristic impedance and propagation constant given by³

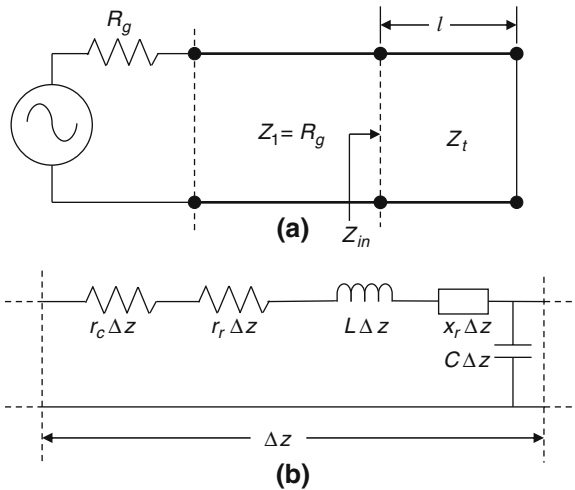


Fig. 6.4. Transducer circuit models: (a) transmission line model for a shortened transducer. Z_t is the complex impedance of the transducer and Z_1 is the impedance of the input transmission line. (b) Equivalent lumped element model for an incremental length Δz of the transducer.

³ While discussing impedances, we will switch to the time convention $\exp(j\omega t)$ rather than $\exp(-i\omega t)$ used in the rest of the book. This ensures that capacitive and inductive reactances have the proper signs. To convert a formula containing j s to i s and vice versa, use the relation $j = -i$.

$$Z_t = \sqrt{\frac{r_c + r_r + j(\omega L + x_r)}{j\omega C}}, \quad (6.76)$$

$$\gamma_t = \sqrt{(r_c + r_r + j(\omega L + x_r))j\omega C}, \quad (6.77)$$

where r_c is the resistance per unit length from the finite conductivity of the transducer, r_r and x_r are the radiation resistance and reactance per unit length resulting from coupling to dipolar spin waves, and L and C are the inductance and capacitance per unit length, respectively, of the microstrip transducer in the absence of dipolar spin wave coupling. The input impedance of a length l of the transducer terminated in the impedance Z_L is given by the standard lossy transmission line relation

$$Z_{in} = Z_t \frac{Z_L + Z_t \tanh(\gamma_t l)}{Z_t + Z_L \tanh(\gamma_t l)}. \quad (6.78)$$

For a shorted transducer as shown in Figures 6.3 and 6.4, the input impedance reduces to

$$Z_{in} = Z_t \tanh(\gamma_t l). \quad (6.79)$$

For an electrically short transducer, $|\gamma_t l| \ll 1$ and the input impedance (6.79) reduces to

$$Z_{in} = Z_t \gamma_t l. \quad (6.80)$$

Substituting Eqs. (6.76) and (6.77) for Z_t and γ_t gives⁴

$$Z_{in} = R_c + R_r + j(X_l + X_r), \quad (6.81)$$

where $R_c = r_c l$, $R_r = r_r l$, $X_l = \omega L l$ and $X_r = x_r l$. Since energy is radiated in both directions away from the transducer, R_r may be subdivided into $R_r = R_r^+ + R_r^-$. The resulting lumped equivalent circuit for an electrically short transducer is shown in Figure 6.5.

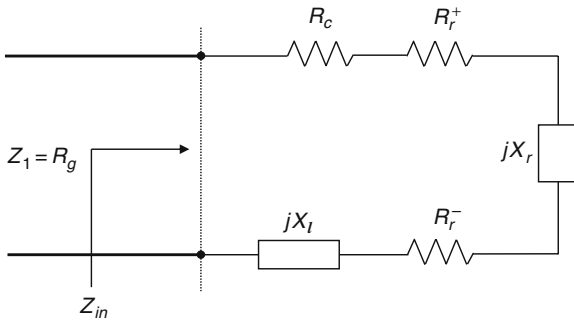


Fig. 6.5. Lumped element model for an electrically short transducer terminated in a short circuit.

⁴ When loss and reactances are neglected, Eq. (6.81) reduces to $Z_{in} = R_r$. Unfortunately, the incorrect result $Z_{in} = R_r/2$ has been widely used in the literature.

The reflection coefficient at the input of the transducer is given by

$$\Gamma = \frac{Z_{\text{in}} - R_g}{Z_{\text{in}} + R_g}. \quad (6.82)$$

The return loss RL from the transducer is, therefore

$$RL = -10 \log |\Gamma|^2 = -10 \log \left[\frac{(R_c + R_r - R_g)^2 + (X_l + X_r)^2}{(R_c + R_r + R_g)^2 + (X_l + X_r)^2} \right]. \quad (6.83)$$

It follows that the total power coupled into the transducer is $1 - |\Gamma|^2$, and the fraction of this power that is coupled into dipolar spin waves propagating in a single direction is $R_r^\pm / (R_c + R_r)$. Thus, the transduction loss TL^\pm for coupling into the (\pm) wave is

$$\begin{aligned} TL^\pm &= -10 \log \left[\frac{(1 - |\Gamma|^2) R_r^\pm}{R_c + R_r} \right] \\ &= -10 \log \left[\frac{4 R_r^\pm R_g}{(R_c + R_r + R_g)^2 + (X_l + X_r)^2} \right]. \end{aligned} \quad (6.84)$$

Assuming an identical transduction loss at the receiving transducer, the total insertion loss IL^\pm through a simple delay line with group delay $\tau^\pm (\mu\text{s})$ is

$$IL^\pm = 2TL^\pm + L\tau^\pm, \quad (6.85)$$

where L is the appropriate loss parameter from Section 6.2 in $(\text{dB}/\mu\text{s})$. More general expressions for transducers that are not electrically short and terminated in arbitrary impedances may be obtained by using the general expression for Z_{in} (6.78) when computing the reflection coefficient (6.82).

As with standard antenna theory, the radiation reactance results from energy stored in the fringing fields near the transducer. The model we will consider permits the direct calculation of R_r , but not X_r . However, the real and imaginary parts of the response function of a system that is causal, linear, and bounded are not independent. Consequently, it is possible to obtain X_r from R_r and vice versa. The transformations relating these two quantities are known to electrical engineers as *Hilbert transforms* and to physicists as the *Kramers–Kronig relations*. In particular, after we have obtained R_r , the radiation reactance may then be obtained from the Hilbert transform

$$X_r(\omega) = \frac{1}{\pi} \int_{-\infty}^{\infty} \frac{R_r(\omega') - R_r(\omega)}{\omega' - \omega} d\omega'. \quad (6.86a)$$

Since dipolar spin waves propagate only over a finite range of frequencies $\omega_1 < \omega < \omega_2$, $R_r(\omega) = 0$ for $0 < \omega < \omega_1$ and $\omega > \omega_2$. For volume waves

$$\begin{aligned}\omega_1 &= \omega_0, \\ \omega_2 &= [\omega_0(\omega_0 + \omega_M)]^{1/2},\end{aligned}$$

and for surface waves

$$\begin{aligned}\omega_1 &= [\omega_0(\omega_0 + \omega_M)]^{1/2}, \\ \omega_2 &= \omega_0 + \frac{\omega_M}{2}.\end{aligned}$$

Further, to ensure a real response in the time domain, $R_r(\omega) = R_r(-\omega)$. Using these properties, Eq. (6.86a) can be transformed into [12]

$$\begin{aligned}X_r &= \frac{R_r(\omega)}{\pi} \ln \left[\frac{(\omega_2 - \omega)(\omega + \omega_1)}{(\omega_2 + \omega)(\omega - \omega_1)} \right] \\ &+ \frac{2\omega}{\pi\omega_1} \int_1^{\omega_2/\omega_1} \frac{R_r(x\omega_1) - R_r(\omega)}{x^2 - (\omega/\omega_1)^2} dx.\end{aligned}\quad (6.86b)$$

This form is well suited to direct numerical integration. In the following sections, we turn our attention to the computation of the radiation resistance R_r for various modes.

6.4.2 Forward Volume Waves

To obtain an approximation to the radiation resistance per unit length, we will assume the current distribution in the wire or microstrip is known and is not affected by coupling to the dipolar spin waves. We further neglect any alteration of the spin wave mode fields and velocity beneath the current element caused by the conducting boundary of the element.

With these approximations in mind, consider the geometry shown in Figure 6.6. We begin by considering excitation by a current filament I spaced a distance s above the surface of the film and displaced a distance ξ along the negative y -direction. The current filament imposes a magneto-quasi-static potential, which we will then expand in a series of orthogonal functions that includes the forward volume wave thickness modes.

To obtain the potential created by the filament, consider an auxiliary coordinate system with its origin centered on the current filament as shown in Figure 6.7. By an elementary application of Ampere's law in integral form, the field created by the filament is

$$\mathbf{H}_I = \hat{\mathbf{e}}_{\phi'} \frac{1}{2\pi r'}.\quad (6.87)$$

At all points in the plane except where the filament is located, it is possible to define a magneto-quasi-static potential in the usual manner:

$$\mathbf{H}_I = -\nabla\psi_I = -\hat{\mathbf{e}}_{\phi'} \frac{1}{r'} \frac{\partial\psi_I}{\partial\phi'}.\quad (6.88)$$

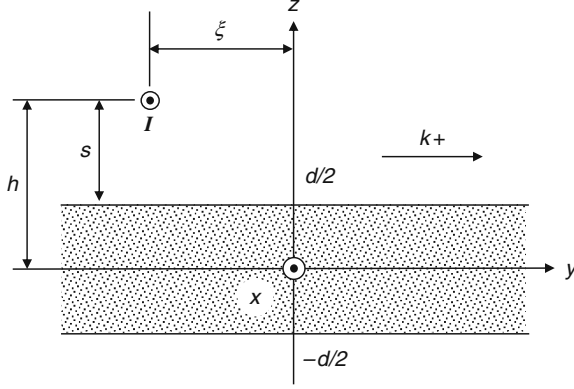


Fig. 6.6. Current element above a ferrite film. The structure is uniform along the x -direction.

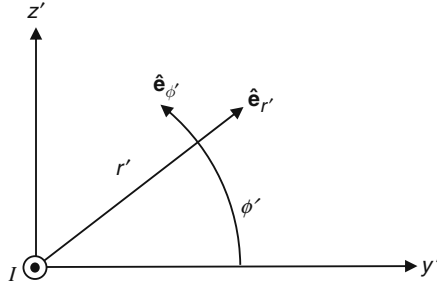


Fig. 6.7. Local coordinate system around the current filament in Figure 6.6.

Equating (6.87) and (6.88) and integrating gives the following expression for the potential:

$$\psi_I = -\frac{I}{2\pi}\phi' + C, \quad (6.89)$$

where C is a constant of integration that can be taken to be zero without loss of generality. Consider the behavior of this potential in the plane $y' = 0$. For $z' < 0$, $\phi' = -\pi/2$ while for $z' > 0$, $\phi' = +\pi/2$. The potential therefore changes abruptly from $-I/4$ to $+I/4$ at the origin. This can be expressed in the original problem coordinate system as

$$\psi_I(y = -\xi, z) = \frac{I}{4} [1 - 2u(z - h)], \quad (6.90)$$

where $u(z)$ is the unit step function. This potential we will take as an imposed boundary condition at the plane $y = -\xi$.

To the right of $y = -\xi$, we assume the potential can be expanded in a sum of complete orthogonal functions. To solve the problem of excitation of forward volume waves, we choose the set of functions so as to include the forward

volume wave mode potentials as a subset. Solving for the coefficients of these functions in the expansion will then give the strength of mode excitation. The mode expansion can be written⁵

$$\psi_I(y = -\xi, z) = \sum_{n=0}^{\infty} g_n \phi_n(z) e^{jk_n \xi} + \sum_{n=0}^{\infty} d_n f_n(z), \quad (6.91)$$

where the first summation is over forward volume mode functions of the form given in Eq. (6.40), and the second summation is over any additional functions needed to make the set complete. We leave these functions unspecified except for the requirement that they be orthogonal to the forward volume mode functions in the sense described by the orthogonality integral (6.47). To find the coefficient g_m , we multiply both sides of the expansion (6.91) by $(1+\chi)\phi_m$ and integrate over all z :

$$\begin{aligned} \int_{-\infty}^{\infty} (1+\chi)\phi_m \psi_I(y = -\xi, z) dz = \\ \sum_{n=0}^{\infty} g_n e^{jk_n \xi} \int_{-\infty}^{\infty} (1+\chi)\phi_m \phi_n dz + \sum_{n=0}^{\infty} d_n \int_{-\infty}^{\infty} (1+\chi)\phi_m f_n dz. \end{aligned} \quad (6.92)$$

All of the terms in the second summation vanish as a consequence of our orthogonality requirement on the functions f_n . Similarly, only the term $n = m$ survives from the first sum. Using the normalization condition (6.53), the coefficient of the m th mode is given by

$$g_m = -e^{-jk_m \xi} \int_{-\infty}^{\infty} (1+\chi)\phi_m(z) \psi_I(y = -\xi, z) dz. \quad (6.93)$$

Substituting the potential for even modes from (5.80), carrying out the indicated integrations, and simplifying using the dispersion relation (5.72) leads to

$$g_m = \frac{I}{2k_m} \sqrt{\frac{2}{-(1+\chi)d}} \cos \left[\frac{k_m d}{2} \sqrt{-(1+\chi)} \right] e^{-k_m s - jk_m \xi}. \quad (6.94)$$

By superposition, the net amplitude from N current filaments is

$$\begin{aligned} a_m &= \sum_{q=1}^N g_m(I_q, h_q, \xi_q) \\ &= \frac{I}{2k_m} \sqrt{\frac{2}{-(1+\chi)d}} \cos \left[\frac{k_m d}{2} \sqrt{-(1+\chi)} \right] \sum_{q=1}^N I_q e^{-k_m s_q - jk_m \xi_q}. \end{aligned} \quad (6.95)$$

⁵ Remember, $j = -i$!

The summation in Eq. (6.95) is called the *array factor* F . To obtain the array factor for a microstrip transducer, we consider an array of current filaments having the same spacing from the film s with amplitudes $I_q = K_q \Delta\xi$, where K_q is a surface current density (A/m). In the limit $N \rightarrow \infty$, $\Delta\xi \rightarrow 0$, the array factor becomes

$$F = e^{-k_m s} \int_{\xi_1}^{\xi_2} K(\xi) e^{-j k_m \xi} d\xi. \quad (6.96)$$

The limits on this integral can be extended to $\pm\infty$ if the current density K is set to zero for regions outside the width of the microstrip. The integral in (6.96) then takes the form of the Fourier transform of the current density. As a simple example, consider a uniform current distribution described by $K(\xi) = I/w$ for $-w/2 \leq \xi \leq w/2$ and $K = 0$ elsewhere. The resulting array factor is

$$F = I e^{-k_m s} \frac{\sin(k_m w/2)}{k_m w/2}. \quad (6.97)$$

In an actual microstrip, the current is peaked at the edges of the conductor. A more accurate approximation to the current that includes this effect is [12]

$$K(\xi) = \frac{2I}{\pi w \sqrt{1 - (2\xi/w)^2}}. \quad (6.98)$$

Taking the Fourier transform of this current density leads to the array factor

$$F = I e^{-k_m s} J_0(k_m w/2), \quad (6.99)$$

where J_0 is the Bessel function of order 0.

From Eq. (6.52), the power per unit length in the m th even mode is given by

$$\begin{aligned} P_m^+ &= \frac{1}{2} \omega \mu_0 k_m |a_m|^2 \\ &= \frac{\omega \mu_0}{4[-(1 + \chi)] k_m d} \cos^2 \left[\frac{k_m d}{2} \sqrt{-(1 + \chi)} \right] |F|^2. \end{aligned} \quad (6.100)$$

The corresponding radiation resistance per unit length is given by

$$\begin{aligned} r_{rm}^+ &= \frac{2P_m^+}{I^2} \\ &= \frac{\omega \mu_0}{2[-(1 + \chi)] k_m d} \cos^2 \left[\frac{k_m d}{2} \sqrt{-(1 + \chi)} \right] \left| \frac{F}{I} \right|^2. \end{aligned} \quad (6.101)$$

Since forward volume waves are reciprocal, the total radiation resistance per unit length from the m th even mode is simply twice this expression:

$$r_{rm} = \frac{\omega\mu_0}{[-(1+\chi)]k_md} \cos^2 \left[\frac{k_md}{2} \sqrt{-(1+\chi)} \right] \left| \frac{F}{I} \right|^2, \quad m = 0, 2, 4, \dots \quad (6.102)$$

A similar calculation for the odd modes using the potential functions of Eq. (5.81) gives

$$r_{rm} = \frac{\omega\mu_0}{[-(1+\chi)]k_md} \sin^2 \left[\frac{k_md}{2} \sqrt{-(1+\chi)} \right] \left| \frac{F}{I} \right|^2, \quad m = 1, 3, 5, \dots \quad (6.103)$$

To compute the return loss and insertion loss, we need the total radiation resistance from all the modes

$$R_r = \sum_{m=0}^{\infty} R_{rm} = \sum_{m=0}^{\infty} r_{rm}l, \quad (6.104)$$

although it is often a good approximation to take $R_r \approx R_{r0}$.

The radiation resistances for the first three forward volume wave modes computed from Eqs. (6.102) and (6.103) using the uniform current expression (6.97) are shown in Figure 6.8. The dispersion relations were computed using Eq. (5.76). Clearly, the excitation of higher-order thickness modes is inefficient in this case, so $R_r \approx R_{r0}$ is a good approximation. The return loss and insertion loss are shown in Figures 6.9 and 6.10. These curves were obtained using Eqs. (6.83), (6.84), and (6.85) along with the approximation $R_r \approx R_{r0}$, and $X_r = X_l = 0$. This last approximation would be valid if a series reactance was used to tune the transducer.

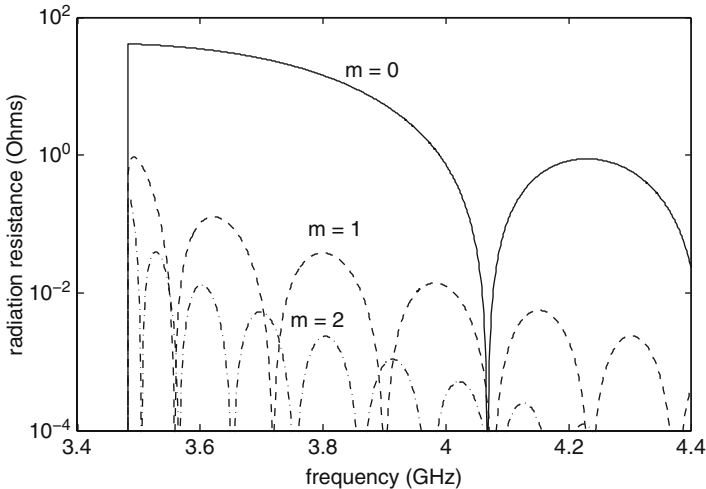


Fig. 6.8. Radiation resistances for the three lowest-order forward volume wave thickness modes. Parameters used are $H_{DC} = 239$ kA/m (3000 Oe), $M_S = 140$ kA/m ($4\pi M_S = 1760$ G), film thickness $d = 5\mu\text{m}$, transducer width $w = 50\mu\text{m}$, YIG-transducer spacing $s = 2\mu\text{m}$, and transducer length $l = 3$ mm.

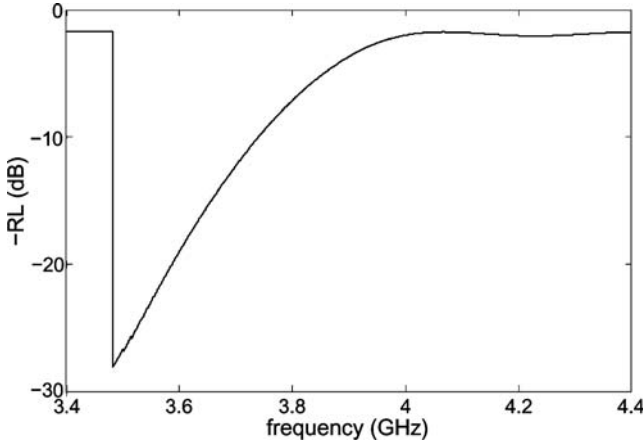


Fig. 6.9. Return loss for a spin wave transducer, considering only the lowest order mode. Parameters for the calculation are the same as in Figure 6.8.

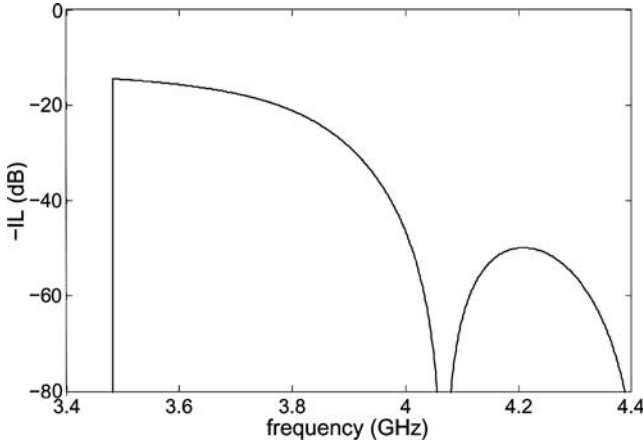


Fig. 6.10. Insertion loss for the lowest-order forward volume spin wave mode. Parameters are propagation path length = 10 mm, $\Delta H = 79.6$ A/m (1 Oe) at 9.3 GHz, and $R_c = 5 \Omega$. The remaining parameters are the same as in Figure 6.8.

Note that our model for R_r neglects the presence of the ground plane shown in Figure 6.3. This is a good approximation so long as the dipolar spin wave potential decays away from the film so rapidly that it is not significantly perturbed by the ground plane. At long wavelengths ($k \times$ ground plane distance ~ 1), the ground plane has a significant effect and the present approximation fails. In this case, both growing and decaying exponential terms must be included in the potential for the region between the ground plane and the film (see Problem 5.5). Expressions valid for long wavelengths can be obtained by using the appropriately modified potential functions in the integral Eq. (6.93).

6.4.3 Backward Volume Waves

Now that we have carefully worked through the excitation model for forward volume waves, the backward volume wave case will be straightforward. The film geometry differs from Figure 6.6 only in that the y and z axes are interchanged and the x direction is into the page. The potential imposed by the current filament at $z = -\xi$ is now given by (cf. Eq. (6.90))

$$\psi_I(z = -\xi, y) = \frac{I}{4} [1 - 2u(y - h)]. \quad (6.105)$$

We now expand this potential in a series of orthogonal modes that includes the backward volume wave thickness modes as a subset:

$$\psi_I(z = -\xi, y) = \sum_{n=1}^{\infty} g_n \phi_n(y) e^{ik_n \xi} + \sum_{n=0}^{\infty} d_n f_n(y). \quad (6.106)$$

The first summation is over backward volume wave functions of the form given in Eq. (6.56) and the second summation is over any additional functions needed to make the set complete. Note that these additional functions will not be the same, in general, as those required for the forward volume wave mode expansion. As before, we leave these functions unspecified except for the requirement that they be orthogonal to the backward volume mode functions according to the integral in Eq. (6.60). To find the coefficient g_m , we multiply both sides of the expansion in Eq. (6.106) by ϕ_m and integrate over all y . Using the normalization condition (6.64) gives

$$g_m = e^{-jk_m \xi} \int_{-\infty}^{\infty} \phi_m(y) \psi_I(z = -\xi, y) dy. \quad (6.107)$$

Substituting the potential for odd modes from Eq. (5.99), carrying out the indicated integrations, and simplifying leads to

$$g_m = -\frac{I}{2k_m} \sqrt{\frac{2}{d}} \sin \left[\frac{k_m d}{2\sqrt{-(1+\chi)}} \right] e^{-k_m s - jk_m \xi}. \quad (6.108)$$

Summing up the contributions from infinitesimally spaced current filaments gives the excitation amplitude from a microstrip transducer:

$$a_m = -\frac{1}{2k_m} \sqrt{\frac{2}{d}} \sin \left[\frac{k_m d}{2\sqrt{-(1+\chi)}} \right] F, \quad (6.109)$$

where F is the array factor given by Eq. (6.96).

From Eq. (6.63), the magnitude of the power per unit length in the m th odd mode is given by

$$\begin{aligned}
P_m^+ &= \frac{1}{2} \omega \mu_0 k_m |a_m|^2 \\
&= \frac{\omega \mu_0}{4 k_m d} \sin^2 \left[\frac{k_m d}{2 \sqrt{-(1 + \chi)}} \right] |F|^2,
\end{aligned} \tag{6.110}$$

with a corresponding radiation resistance per unit length

$$\begin{aligned}
r_{rm}^+ &= \frac{2P_m^+}{I^2} \\
&= \frac{\omega \mu_0}{2 k_m d} \sin^2 \left[\frac{k_m d}{2 \sqrt{-(1 + \chi)}} \right] \left| \frac{F}{I} \right|^2.
\end{aligned} \tag{6.111}$$

Backward volume waves are also reciprocal, so the total radiation resistance per unit length for the m th odd mode is obtained by multiplying this expression by 2:

$$r_{rm} = \frac{\omega \mu_0}{k_m d} \sin^2 \left[\frac{k_m d}{2 \sqrt{-(1 + \chi)}} \right] \left| \frac{F}{I} \right|^2, \quad m = 1, 3, 5, \dots \tag{6.112}$$

A similar calculation for the even modes using the potential functions in Eq. (5.100) gives

$$r_{rm} = \frac{\omega \mu_0}{k_m d} \cos^2 \left[\frac{k_m d}{2 \sqrt{-(1 + \chi)}} \right] \left| \frac{F}{I} \right|^2, \quad m = 2, 4, 6, \dots \tag{6.113}$$

Finally, the total radiation resistance from all modes is given by

$$R_r = \sum_{m=1}^{\infty} R_{rm} = \sum_{m=1}^{\infty} r_{rm} l. \tag{6.114}$$

The radiation resistances for the first three backward volume wave modes computed from Eqs. (6.112) and (6.113) using the uniform current expression (6.97) are shown in Figure 6.11. The dispersion relation was computed using Eq. (5.97). Again we see that the excitation of higher-order thickness modes is inefficient so that $R_r \approx R_{r1}$ is a good approximation. The return loss and insertion loss are shown in Figures 6.12 and 6.13. As before, these curves were obtained using Eqs. (6.83), (6.84), and (6.85) along with the approximation $R_r \approx R_{r1}$ and $X_r = X_l = 0$.

6.4.4 Surface Waves

Since multiple thickness modes do not exist in the surface wave geometry, the orthogonal function expansion method is not well suited to the treatment of surface wave excitation. Instead, the method commonly used is to treat the

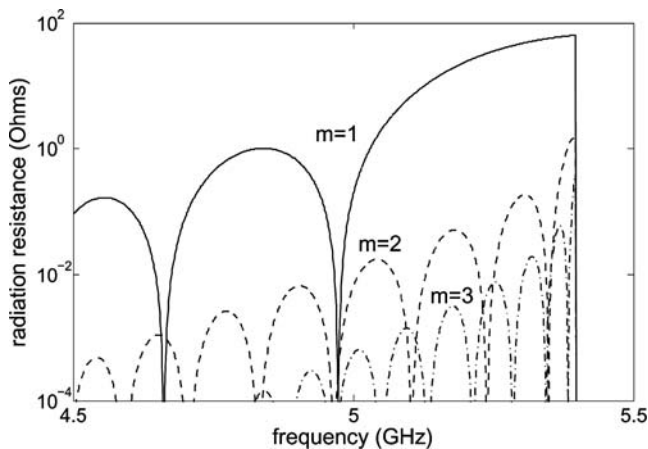


Fig. 6.11. Radiation resistances for the three lowest-order backward volume wave thickness modes. Parameters used are $H_{DC} = 98.7$ kA/m (1240 Oe), $M_S = 140$ kA/m ($4\pi M_S = 1760$ G), film thickness $d = 5$ μm , transducer width $w = 50$ μm , YIG-transducer spacing $s = 2$ μm , and transducer length $l = 3$ mm.

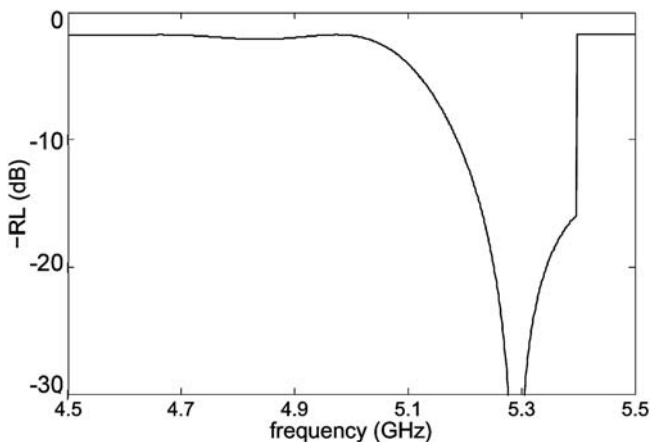


Fig. 6.12. Return loss for a backward volume wave transducer, considering only the lowest-order mode. Parameters are the same as Figure 6.11.

presence of the current-carrying strip as an inhomogeneous boundary condition on the in-plane magnetic field, h , in the plane containing the strip. The details of this method can be found in [9, 11, 12, 16, 18]. For completeness, however, we will quote the results from the literature and briefly discuss the unique features of surface wave excitation.

The radiation resistance per unit length for surface waves traveling in the ν direction (where $\nu = \pm 1$) is given by [9]

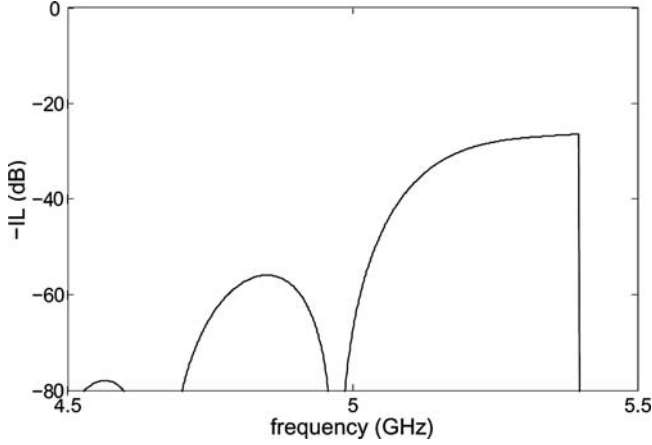


Fig. 6.13. Insertion loss for the lowest-order backward volume spin wave mode. Parameters are propagation path length = 10 mm, $\Delta H = 79.6$ A/m (1 Oe) at 9.3 GHz, and $R_c = 5 \Omega$. The remaining parameters are the same as in Figure 6.11.

$$r_r^{(\nu)} = \frac{\mu_0 \omega}{2kd} \left[\frac{1 + \chi}{(1 + \nu\kappa)^2 - (1 + \chi)^2} \right] \left| \frac{F}{I} \right|^2. \quad (6.115)$$

Because the surface waves exhibit field–displacement non-reciprocity (cf. Figure 5.18), the radiation resistance is different for the two directions of propagation. The excitation is strongest for the mode localized at the surface nearest the transducer. Thus, unlike volume waves, the radiation of surface waves tends to be unidirectional. Typical radiation resistances are shown in Figure 6.14 for a uniform current distribution as described by Eq. (6.97). The parameters for the calculation are given in Figure 6.14. The corresponding return loss is shown in Figure 6.15 and the insertion loss for a 10 mm long delay line is shown in Figure 6.16. Note the strongly non-reciprocal transmission characteristics. The transmission characteristics suggest that the device could be used as an isolator. Practical difficulties for such an application, however, include a relatively high insertion loss and low power handling capabilities.

6.4.5 Discussion of Excitation Calculations

The method we have used to calculate the excitation of volume waves serves as another illustration of the use of spin wave orthogonality relations. The technique is similar in principle to a Fourier series decomposition and consists of finding a particular mode component of an imposed boundary condition.

In the interest of simplicity, however, several important issues have not been discussed. In particular, we have not shown that suitable auxiliary functions exist, and we have not shown that the orthogonal function series is complete. The nature of the expansion ensures continuity of the potential across

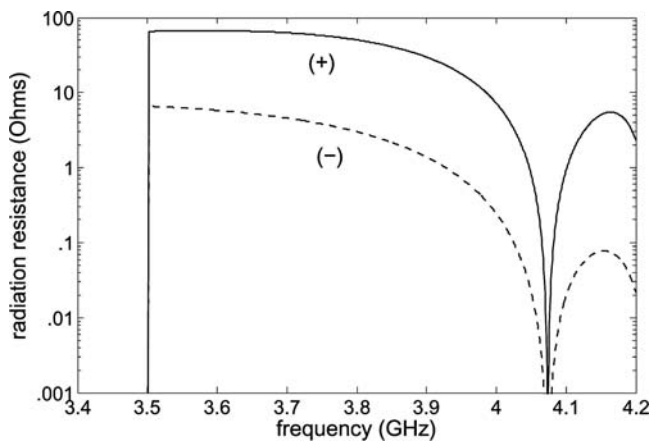


Fig. 6.14. Radiation resistances for both directions of surface wave propagation. Parameters used are $H_{DC} = 51.7$ kA/m (650 Oe), $M_S = 140$ kA/m ($4\pi M_S = 1760$ G), film thickness $d = 5$ μm , transducer width $w = 50$ μm , YIG-transducer spacing $s = 2$ μm , and transducer length $l = 3$ mm.

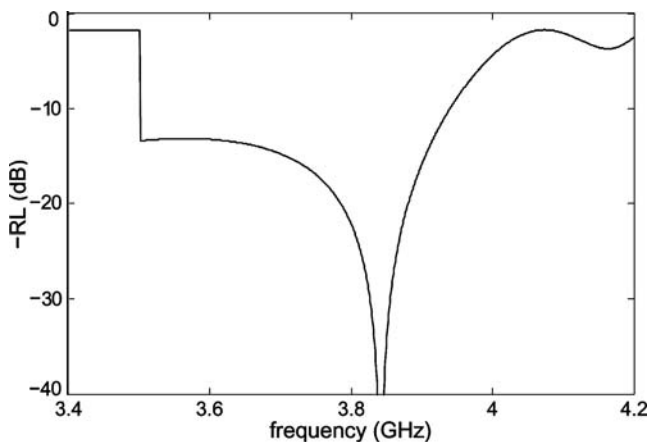


Fig. 6.15. Return loss for a surface wave transducer. Parameters are the same as in Figure 6.14.

the boundary plane containing a current filament, but the continuity of the normal derivative of the total potential in this plane has not been considered.

The most common approach to the calculation of dipolar spin wave excitation involves modeling the current in the microstrip transducer with an inhomogeneous boundary condition near one surface of the film. The fact that the present model agrees well with the more common approach is offered as a weak substitute for rigorous discussions of these issues!

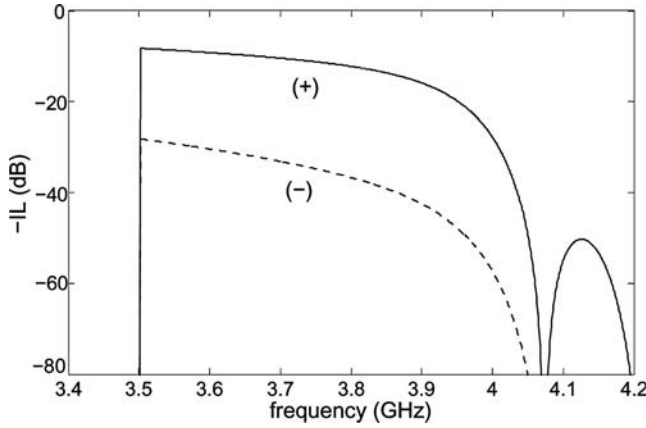


Fig. 6.16. Insertion loss for surface spin waves. Parameters are as follows: propagation path length = 10 mm, $\Delta H = 79.6$ A/m (1 Oe) at 9.3 GHz, and $R_c = 5 \Omega$. The remaining parameters are the same as in Figure 6.14.

Finally, it is interesting to comment on the presence of the weaker peaks in the transmission passbands (Figures 6.10, 6.13, and 6.16). Although present in the model calculations, these subsidiary peaks are not observed experimentally. These peaks do not appear in more rigorous calculations that also include the influence of the dipolar spin waves back on the current in a self-consistent way [13, 14].

Problems

6.1. A surface spin wave propagates in an isolated YIG film with $f = 6.3$ GHz and $B_{DC} = 0.15$ T. The ferromagnetic resonance line width (full width, half maximum) is $\Delta H = 80$ A/m at 9.3 GHz. The gyromagnetic ratio for the film is 2.8 MHz/G.

- Find the Gilbert damping parameter, α .
- Calculate the loss per unit time, L , in dB/ μ s.

6.2. The ferromagnetic resonance line width (full width, half maximum) of a particular YIG film is $\Delta H = 60$ A/m at 9.3 GHz. Consider a forward volume spin wave propagating with $f = 3.9$ GHz and $H_{DC} = 239$ kA/m. The gyromagnetic ratio for the film is 2.8 MHz/G.

- Find the Gilbert damping parameter, α .
- Calculate the loss per unit time, L , in dB/ μ s.

6.3. Repeat Problem 6.2 but for backward volume spin waves at 5.4 GHz and $H_{DC} = 98.7$ kA/m in the same film.

6.4. Perform the integration in Eqs. (6.52) and (6.53) using the forward volume mode functions (5.80) and (5.81). Verify that the mode normalizations are given by (6.54) and (6.55) for both even and odd modes. (Hint: some expressions can be simplified using the dispersion relations (5.72) and (5.74).)

6.5. Perform the integration in Eqs. (6.63) and (6.64) using the backward volume mode functions (5.99) and (5.100). Verify that the mode normalizations are given by Eqs. (6.65) and (6.66) for both even and odd modes. (Hint: some expressions can be simplified using the dispersion relations (5.95) and (5.96).)

6.6. The power carried by surface spin waves is given by Eq. (6.49) but integrated over y instead of z . Evaluate this integral using the mode functions (5.113) and verify the normalization constant (6.75). Remember that \mathbf{b} has both y and x components. (Hint: some expressions can be simplified using the dispersion relation (5.111a) and the definitions of the parameter p from (5.114). This calculation is rather tedious; be forewarned!)

6.7. Consider the radiation resistance for the lowest-order forward volume wave mode in the limit $k \rightarrow 0$ [9].

- (a) Using the dispersion relation (5.72), show that $kd[-(1 + \chi)] \approx 2$ for small k .
- (b) Using the result of part (a), take the limit of the radiation resistance in Eq. (6.102) as $k \rightarrow 0$ and show that

$$\lim_{k \rightarrow 0} r_{r0} = \frac{\omega\mu_0}{2}. \quad (6.116)$$

6.8. Consider the radiation resistance for the lowest-order backward volume wave mode in the limit $k \rightarrow 0$ [9].

- (a) Using the dispersion relation (5.95), show that $kd/[-(1 + \chi)] \approx 2$ for small k .
- (b) Using the result of part (a), take the limit of the radiation resistance (6.112) as $k \rightarrow 0$ and show that the result is the same as that for forward volume waves; i.e.,

$$\lim_{k \rightarrow 0} r_{r1} = \frac{\omega\mu_0}{2}. \quad (6.117)$$

6.9. Repeat Problem 6.8 for surface waves.

- (a) Expand the dispersion relation (5.111b) for small k and show that

$$kd \approx 2 [\omega^2 - \omega_0(\omega_0 + \omega_M)] / \omega_M^2. \quad (6.118)$$

- (b) Using the result of part (a) along with the fact that $\omega^2 = \omega_0(\omega_0 + \omega_M)$ at the $k = 0$ band edge, take the limit of the radiation resistance (6.115) as $k \rightarrow 0$ and show that the result can be expressed

$$\lim_{k \rightarrow 0} r_r^{(\nu)} = \frac{\omega\mu_0}{4} \frac{\omega\omega_M}{[\omega_0 - \nu\omega]^2}. \quad (6.119)$$

References

- [1] S. S. Gupta and N. C. Srivastava, "Power flow and energy distribution of magnetostatic bulk waves in dielectric layered structure," *J. Appl. Phys.*, vol. 50, p. 6697, 1979.
- [2] S. S. Gupta, "Power flow and energy distribution of magnetostatic bulk and surface waves in dielectric layered structure," *IEEE Trans. Mag.*, vol. MAG-18, p. 1639, 1982.
- [3] D. D. Stancil, "Phenomenological propagation loss theory for the magnetostatic waves in thin ferrite films," *J. Appl. Phys.*, vol. 59, p. 218, 1986.
- [4] C. Vittoria and N. D. Wilsey, "Magnetostatic wave propagation loss in an anisotropic insulator," *J. Appl. Phys.*, vol. 45, p. 414, 1974.
- [5] A. D. Berk, "Dependence of the ferromagnetic resonance line width on the shape of the specimen," *J. Appl. Phys.*, vol. 28, p. 190, 1957.
- [6] D. J. Halchin, "Characterization of thin ferrite films using magnetostatic wave propagation," Ph.D. dissertation, North Carolina State University, 1987.
- [7] N. E. Buris, "Magnetostatic wave propagation in inhomogeneous and anisotropic ferrite thin films," Ph.D. dissertation, North Carolina State University, 1986.
- [8] J. D. Adam and S. N. Bajpai, "Magnetostatic forward volume wave propagation in YIG strips," *IEEE Trans. Magn.*, vol. 18, p. 1598, 1982.
- [9] P. R. Emtage, "Interaction of magnetostatic waves with a current," *J. Appl. Phys.*, vol. 49, p. 4475, 1978.
- [10] M. Cottam, Ed., *Linear and Nonlinear Spin Waves in Magnetic Films and Superlattices*. Singapore: World Scientific, 1994.
- [11] A. K. Ganguly and D. C. Webb, "Microstrip excitation of magnetostatic surface waves, theory and experiment," *IEEE Microw. Theory Tech.*, vol. MTT-23, p. 998, 1975.
- [12] A. K. Ganguly, D. C. Webb, and C. Banks, "Complex radiation impedance of microstrip-excited magnetostatic-surface waves," *IEEE Trans. Microw. Theory Tech.*, vol. 26, p. 444, 1978.
- [13] B. A. Kalinikos and V. F. Dmitriev, "Self-consistent calculation of radiation resistance of microstrip transducer of spin waves in a perpendicularly magnetized ferromagnetic film," *Zh. Tech. Fiz.*, vol. 58, p. 248, 1988.
- [14] B. A. Kalinikos and V. F. Dmitriev, "Self-consistent theory of excitation of spin waves by microstrip transducer in tangentially magnetized layered structure," *Radiotekhnika Electronica*, vol. 33, p. 2248, 1988.
- [15] J. P. Parekh, "Theory of magnetostatic forward volume wave excitation," *J. Appl. Phys.*, vol. 50, p. 2452, 1979.
- [16] J. C. Sethares, "Magnetostatic surface wave transducers," *IEEE Trans. Microw. Theory Tech.*, vol. 27, p. 902, 1979.
- [17] J. C. Sethares and I. J. Weinberg, "Apodization of variable coupling MSSW transducers," *J. Appl. Phys.*, vol. 50, p. 2458, 1979.

- [18] J. C. Sethares and I. J. Weinberg, "Theory of MSW transducers," *Circ. Syst. Signal Process*, vol. 4, p. 41, 1985.
- [19] J. H. Wu, C. V. Smith, J. H. Collins, and J. M. Owens, "Bandpass filtering with multibar magnetostatic surface wave microstrip transducers," *Electron. Lett.*, vol. 13, p. 610, 1977.
- [20] J. H. Wu, C. V. Smith, and J. M. Owens, "Bandpass filtering and input impedance characterization for driven multielement transducer pair-delay line magnetostatic wave devices," *J. Appl. Phys.*, vol. 50, p. 2455, 1979.

Variational Formulation for Magnetostatic Modes

In Chapter 5, we solved for the magnetostatic modes in a variety of geometries. These geometries were characterized by simple boundary shapes, uniform bias fields, and uniform materials. In some cases, however, material and field non-uniformities may be needed to control the dispersion or to guide and localize the magnetostatic mode energy. In other cases, the effects of undesired inhomogeneities need to be assessed. Such problems are not easily attacked by the classical boundary value techniques used in Chapter 5. Consequently, this chapter is devoted to a *variational approach* capable of treating arbitrary inhomogeneities in a relatively simple and elegant way.

7.1 General Problem Statement

As applied to magnetostatic modes, the general inhomogeneous medium problem could be said to include:

- (a) non-uniform bias fields,
- (b) non-uniform material parameters,
- (c) irregular boundary conditions, and
- (d) finite width effects in thin films.

The last two items concern themselves with boundaries and may not at first seem appropriate for inclusion in inhomogeneous media problems. They are included, however, because any boundary value problem can be viewed as the limiting case of a corresponding inhomogeneous medium problem.

Problems of this type can be treated effectively using a variational approach. The basic steps in such an approach can be summarized as follows:

- (a) Formulate the problem as an integral expression whose minimum (or maximum) gives the exact solution. Boundary conditions generally enter such an expression through the limits of integration, and material inhomogeneities through the integrand.

- (b) Using a knowledge of existing solutions and physical insight, “guess” the form of the potential function ψ .
- (c) Modify the guess for ψ so that the integral is minimized (or maximized).

This approach can be very powerful – especially when coupled with numerical methods such as finite elements. For example, the region of interest could be broken up into arbitrarily small subdivisions with the material properties and/or boundary conditions for each subdivision individually specified. Thus, a single computer software package could be envisioned that would be capable of solving virtually any of these inhomogeneous medium problems.

In this chapter, we first review the underlying calculus of variations, describe and interpret the integral to be minimized for magnetostatic modes, and present some simple examples. The approach used in this chapter is based on [1–5]. Other variational formulations for dipolar spin waves in thin films have been described by Tsutsumi et al. [6] and Sawado and Chang [7].

7.2 Calculus of Variations

In this section, we introduce the methods and terminology used with the calculus of variations. We start with the case of one independent variable then extend the results to three independent variables.

7.2.1 Formulation for One Independent Variable¹

We begin by considering the expression $L(\psi, d\psi/dx, x)$ and the integral

$$L = \int_a^b \mathcal{L}(\psi, d\psi/dx, x) dx \equiv L[\psi(x)]. \quad (7.1)$$

Note that this integral yields a number whose value depends on the function $\psi(x)$. Recall that a *function* maps one number onto another number. In an analogous way, we define a *functional* as an entity such as L that maps a *function* onto a number. Our goal is to find a function $\psi(x)$ that maximizes or minimizes L or (more generally) makes L stationary. Specifically, we want to determine $\psi(x)$ such that

$$L[\psi(x) + \xi(x)] = L[\psi(x)] + \text{Order}(\xi^2) \quad (7.2)$$

for $\xi^2(x)$ small but otherwise arbitrary. To aid computation, let

$$\xi(x) = \alpha \eta(x), \quad (7.3)$$

¹ This section draws heavily from Matthews and Walker [8, Chapter 12]. The calculus of variations is also discussed in Goldstein et al. [9].

where α is small and $\eta(x)$ is an arbitrary function of x (not necessarily small). The stationary condition for L can now be written as

$$\left. \frac{dL}{d\alpha} \right|_{\alpha=0} = 0 \quad \forall \eta(x). \quad (7.4)$$

Substituting $\psi(x) + \alpha\eta(x)$ into Eq. (7.1) and expanding in a Taylor series gives

$$\begin{aligned} L(\alpha) &= \int_a^b \mathcal{L}(\psi + \alpha\eta, \psi' + \alpha\eta', x) dx \\ &= L(0) + \alpha \int_a^b \left[\frac{\partial \mathcal{L}}{\partial \psi} \eta + \frac{\partial \mathcal{L}}{\partial \psi'} \eta' \right] dx + \text{Order}(\alpha^2), \end{aligned} \quad (7.5)$$

where the prime denotes a total derivative with respect to x . For the functional L to be stationary, we require the coefficient of α to vanish for all η :

$$\int_a^b \left[\frac{\partial \mathcal{L}}{\partial \psi} \eta + \frac{\partial \mathcal{L}}{\partial \psi'} \eta' \right] dx = 0. \quad (7.6)$$

After integrating the second term in the integrand by parts, Eq. (7.6) becomes

$$\int_a^b \left[\frac{\partial \mathcal{L}}{\partial \psi} - \frac{d}{dx} \frac{\partial \mathcal{L}}{\partial \psi'} \right] \eta dx + \left. \frac{\partial \mathcal{L}}{\partial \psi'} \eta \right|_a^b = 0. \quad (7.7)$$

Since η is arbitrary, the equation can only be satisfied if

$$\frac{\partial \mathcal{L}}{\partial \psi} - \frac{d}{dx} \frac{\partial \mathcal{L}}{\partial \psi'} \equiv \frac{\delta \mathcal{L}}{\delta \psi} = 0 \quad (7.8)$$

and

$$\left. \frac{\partial \mathcal{L}}{\partial \psi'} \right|_b = \left. \frac{\partial \mathcal{L}}{\partial \psi'} \right|_a = 0. \quad (7.9)$$

The quantity $\delta \mathcal{L} / \delta \psi$ is called the *variational* or *functional* derivative of \mathcal{L} and the differential Eq. (7.8) is called the *Euler–Lagrange* equation. Equation (7.9) specifies the boundary conditions for the Euler–Lagrange equation. Thus minimizing the functional L is equivalent to solving the differential Eq. (7.8) subject to the boundary conditions (7.9).

To further illustrate this equivalence, consider the following expression associated with longitudinal acoustic waves with frequency ω :

$$\mathcal{L} = \frac{1}{2}\rho\omega^2 u^2 - \frac{B}{2} \left(\frac{du}{dx} \right)^2. \quad (7.10)$$

Here, ρ and B are the density and bulk modulus of the medium, respectively, and $u(x)$ is the displacement of the wave. Equation (7.10) can be interpreted as the difference between the kinetic and potential energy densities associated with the displacement and is called the Lagrangian density.

The derivatives needed for Eq. (7.8) are

$$\frac{\partial \mathcal{L}}{\partial u} = \rho\omega^2 u \quad (7.11)$$

and

$$\frac{\partial \mathcal{L}}{\partial u'} = -B \frac{du}{dx}. \quad (7.12)$$

The Euler–Lagrange equation can therefore be written

$$\frac{d^2 u}{dx^2} + \left(\frac{\omega}{v_s} \right)^2 u = 0. \quad (7.13)$$

where $v_s = [B/\rho]^{1/2}$ is the velocity of sound in the medium. The boundary condition (7.9) is

$$\left. \frac{du}{dx} \right|_a = \left. \frac{du}{dx} \right|_b = 0. \quad (7.14)$$

The solutions to Eqs. (7.13) and (7.14) describe standing waves through the thickness of an elastic plate with unconstrained boundaries.

The standing wave modes can therefore be obtained either by solving the differential Eq. (7.13) subject to the boundary conditions (7.14), or by finding u such that the integral of \mathcal{L} over the interval $[a, b]$ is minimized.

The boundary conditions described by Eq. (7.14) are the *natural boundary conditions* of the functional given by the integral of \mathcal{L} from Eq. (7.10). It is possible to impose other boundary conditions by adding additional terms to the functional.

7.2.2 Extensions to Three Independent Variables

In general, the potential function for magnetostatic waves may depend on all three spatial coordinates. The functional in this case can be written as an integral over the volume of interest V (cf. Eq. (7.1)):

$$L = \int_a^b \mathcal{L}(\psi, \psi_x, \psi_y, \psi_z, x, y, z) dx dy dz, \quad (7.15)$$

where $\psi_q = \partial\psi/\partial q$ and $q = x, y, z$. If ψ is perturbed to $\psi + \delta\psi$, then to lowest order in the variation $\delta\psi$, we have

$$\begin{aligned}
\mathcal{L} + \delta\mathcal{L} &= \mathcal{L}(\psi, \psi_x, \psi_y, \psi_z, x, y, z) \\
&+ \frac{\partial\mathcal{L}}{\partial\psi}\delta\psi + \frac{\partial\mathcal{L}}{\partial\psi_x}\delta\psi_x + \frac{\partial\mathcal{L}}{\partial\psi_y}\delta\psi_y + \frac{\partial\mathcal{L}}{\partial\psi_z}\delta\psi_z.
\end{aligned} \tag{7.16}$$

This can be written in a more compact notation by defining

$$\frac{\partial\mathcal{L}}{\partial(\nabla\psi)} \equiv \hat{\mathbf{x}} \frac{\partial\mathcal{L}}{\partial\psi_x} + \hat{\mathbf{y}} \frac{\partial\mathcal{L}}{\partial\psi_y} + \hat{\mathbf{z}} \frac{\partial\mathcal{L}}{\partial\psi_z}. \tag{7.17}$$

The variation $\delta\mathcal{L}$ can now be written as

$$\delta\mathcal{L} = \frac{\partial\mathcal{L}}{\partial\psi}\delta\psi + \frac{\partial\mathcal{L}}{\partial(\nabla\psi)} \cdot \nabla(\delta\psi). \tag{7.18}$$

Taking the volume integral of this equation yields the variation of the functional δL , which is required to vanish:

$$\delta L = \int_V \left[\frac{\partial\mathcal{L}}{\partial\psi}\delta\psi + \frac{\partial\mathcal{L}}{\partial(\nabla\psi)} \cdot \nabla(\delta\psi) \right] dv = 0. \tag{7.19}$$

Using the vector identity

$$\nabla \cdot (f\mathbf{G}) = \mathbf{G} \cdot (\nabla f) + f(\nabla \cdot \mathbf{G}), \tag{7.20}$$

we can write the second term in Eq. (7.19) as

$$\int_V \left[\frac{\partial\mathcal{L}}{\partial(\nabla\psi)} \cdot \nabla(\delta\psi) \right] dv = \int_V \left\{ \nabla \cdot \left[\frac{\partial\mathcal{L}}{\partial(\nabla\psi)} \delta\psi \right] - \left[\nabla \cdot \frac{\partial\mathcal{L}}{\partial(\nabla\psi)} \right] \delta\psi \right\} dv. \tag{7.21}$$

Furthermore, the first term on the right-hand side of Eq. (7.21) can be expressed as a surface integral using the divergence theorem:

$$\int_V \nabla \cdot \mathbf{A} dv = \oint_S \mathbf{A} \cdot d\mathbf{s}, \tag{7.22}$$

where the surface S encloses the volume V and $d\mathbf{s} \equiv \hat{\mathbf{n}} ds$, where $\hat{\mathbf{n}}$ is an outward surface normal. Equation (7.21) becomes

$$\int_V \left[\frac{\partial\mathcal{L}}{\partial(\nabla\psi)} \cdot \nabla(\delta\psi) \right] dv = \oint_S \delta\psi \frac{\partial\mathcal{L}}{\partial(\nabla\psi)} \cdot d\mathbf{s} - \int_V \left[\nabla \cdot \frac{\partial\mathcal{L}}{\partial(\nabla\psi)} \right] \delta\psi dv. \tag{7.23}$$

This result is equivalent to integration by parts in three dimensions. Substituting Eq. (7.23) into the expression for δL in (7.19) gives

$$\delta L = \oint_S \delta\psi \frac{\partial\mathcal{L}}{\partial(\nabla\psi)} \cdot d\mathbf{s} + \int_V \left[\frac{\partial\mathcal{L}}{\partial\psi} - \nabla \cdot \frac{\partial\mathcal{L}}{\partial(\nabla\psi)} \right] \delta\psi dv = 0. \tag{7.24}$$

For δL to vanish for an arbitrary $\delta\psi$, we require

$$\frac{\partial \mathcal{L}}{\partial \psi} - \nabla \cdot \frac{\partial \mathcal{L}}{\partial (\nabla \psi)} = 0, \quad (7.25)$$

$$\hat{\mathbf{n}} \cdot \frac{\partial \mathcal{L}}{\partial (\nabla \psi)} \Big|_S = 0. \quad (7.26)$$

Equation (7.25) is the generalized Euler–Lagrange equation for three dimensions and Eq. (7.26) expresses the natural boundary conditions on the surface S .

7.3 Small-Signal Functional for Ferrites

Let us now consider a region of space filled with an inhomogeneous ferrite and bounded by a perfectly conducting surface as shown in Figure 7.1. The medium is magnetically saturated and is characterized by the permeability tensor $\bar{\boldsymbol{\mu}}(\mathbf{r})$.

We are interested in finding the magnetostatic modes that can exist in this structure. These modes are characterized by the time-harmonic small-signal fields \mathbf{b} and \mathbf{h} . With this in mind, consider the functional

$$L = \int_V \mathbf{b} \cdot \mathbf{h}^* dv. \quad (7.27)$$

We first show that this functional is stationary for perturbations about fields that satisfy $\nabla \cdot \mathbf{b} = 0$ in the volume and $\hat{\mathbf{n}} \cdot \mathbf{b} = 0$ on the boundary, where $\hat{\mathbf{n}}$ is an outward surface normal. It follows that the Euler–Lagrange equation corresponding to this functional is Walker’s equation (5.8).

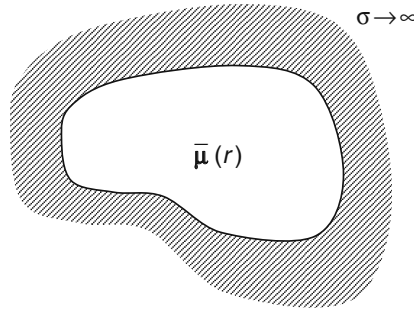


Fig. 7.1. Cross section of a region of space bounded on all sides by a perfectly conducting surface. The cavity is filled by an inhomogeneous ferrite described by $\bar{\boldsymbol{\mu}}(\mathbf{r})$. (Adapted from [2]. © 1983 IEEE.)

Since $\mathbf{h} = -\nabla\psi$ in the magnetostatic limit and $\mathbf{b} = \bar{\boldsymbol{\mu}} \cdot \mathbf{h}$, we see that L depends on both $\nabla\psi$ and $\nabla\psi^*$, but not directly on the potential or its complex conjugate. Requiring δL to vanish therefore yields

$$\delta L = \int_V \left[\frac{\partial \mathcal{L}}{\partial(\nabla\psi)} \cdot \nabla(\delta\psi) + \frac{\partial \mathcal{L}}{\partial(\nabla\psi^*)} \cdot \nabla(\delta\psi^*) \right] dv = 0. \quad (7.28)$$

Integrating the second term by parts and requiring δL to vanish for arbitrary $\delta\psi^*$ as before leads to equations similar to (7.25) and (7.26) but with $\partial\mathcal{L}/\partial\psi^* = 0$. Writing $\mathcal{L} = -\mathbf{b} \cdot \nabla\psi^*$ and taking the partial derivative with respect to $\nabla\psi^*$ gives

$$\frac{\partial \mathcal{L}}{\partial(\nabla\psi^*)} = -\mathbf{b}. \quad (7.29)$$

Using this equation in (7.25) and (7.26) expressed in terms of ψ^* leads to the desired results:

$$\nabla \cdot \mathbf{b} = 0. \quad (7.30)$$

$$\hat{\mathbf{n}} \cdot \mathbf{b}|_S = 0. \quad (7.31)$$

Similarly, integration of the first term in (7.28) leads to the complex conjugates of (7.30) and (7.31) since \mathcal{L} is real. Substituting $\mathbf{b} = \bar{\boldsymbol{\mu}} \cdot \mathbf{h}$ and $\mathbf{h} = -\nabla\psi$ into (7.30) gives Walker's equation (5.8), and the natural boundary condition given by Eq. (7.31) is appropriate for time-varying fields at the surface of a perfect conductor.

A second important property is that the stationary value of L is zero. To show this, we write the functional in the form

$$L = - \int_V \mathbf{b} \cdot \nabla\psi^* dv \quad (7.32)$$

and integrate by parts to obtain

$$L = - \oint_S \psi^* \mathbf{b} \cdot \hat{\mathbf{n}} ds + \int_V \psi^* \nabla \cdot \mathbf{b} dv. \quad (7.33)$$

The first term vanishes because of the boundary condition $\mathbf{b} \cdot \hat{\mathbf{n}} = 0$ on S , and the Maxwell equation $\nabla \cdot \mathbf{b} = 0$ causes the last term to vanish, yielding the desired result, $L = 0$.

It may seem surprising that one would obtain anything but a trivial solution by setting L equal to zero in the absence of source currents, since the integrand looks like an energy density. If the medium were characterized by a constant scalar permeability, it would be a simple matter to show that the integrand must be positive definite if different from zero. Consequently, the integral over the volume would vanish only if $\mathbf{b} = \mathbf{h} = 0$. In a ferrite, however, resonances in the permeability tensor can cause some of the elements to

change sign. Thus, the integrand of (7.27) need not be positive definite, and non-trivial solutions can be found. The difficulty is further resolved by noting that $\mathbf{b} \cdot \mathbf{h}^*$ is not the modal energy density in a dispersive medium, as shown in Chapter 4. This point is discussed in greater detail in Section 7.4.

7.4 Interpretation of the Functional

Using the constitutive relation $\mathbf{b} = \mu_o(\mathbf{h} + \mathbf{m})$, the Lagrangian density \mathcal{L} can be expressed

$$\mathcal{L} = \mu_o |\mathbf{h}|^2 + \mu_o \mathbf{m} \cdot \mathbf{h}^*. \quad (7.34)$$

An expansion for $\mathbf{m} \cdot \mathbf{h}^*$ can be obtained from the linearized torque Eq. (3.109). Neglecting exchange and magnetocrystalline anisotropy gives

$$\mathbf{m} = -i \frac{\omega_M}{\omega} \hat{\mathbf{z}} \times \left(\mathbf{h} - \frac{H_0}{M_0} \mathbf{m} \right). \quad (7.35)$$

Crossing \mathbf{m} into the complex conjugate of (7.35) to construct $\mathbf{m} \times \mathbf{m}^*$ and using the vector identity

$$\mathbf{A} \times (\mathbf{B} \times \mathbf{C}) = (\mathbf{A} \cdot \mathbf{C})\mathbf{B} - (\mathbf{A} \cdot \mathbf{B})\mathbf{C} \quad (7.36)$$

leads to the expression

$$-i \frac{\omega}{\omega_M} \mathbf{m} \times \mathbf{m}^* = \mathbf{m} \cdot \left(\mathbf{h}^* - \frac{H_0}{M_0} \mathbf{m}^* \right) \hat{\mathbf{z}} - (\mathbf{m} \cdot \hat{\mathbf{z}}) \left(\mathbf{h}^* - \frac{H_0}{M_0} \mathbf{m}^* \right). \quad (7.37)$$

The second term on the right-hand side vanishes because the small signal magnetization is perpendicular to $\hat{\mathbf{z}}$. Dotting $\hat{\mathbf{z}}$ into both sides of the remainder of the expression and solving for $\mathbf{m} \cdot \mathbf{h}^*$ gives the desired result:

$$\mathbf{m} \cdot \mathbf{h}^* = \frac{H_0}{M_0} |\mathbf{m}|^2 - i \frac{\omega}{\omega_M} (\mathbf{m} \times \mathbf{m}^*) \cdot \hat{\mathbf{z}}. \quad (7.38)$$

The Lagrangian density \mathcal{L} can now be expressed

$$\mathcal{L} = \mathbf{b} \cdot \mathbf{h}^* = 4 \left[\frac{\mu_o}{4} |\mathbf{h}|^2 + \frac{\mu_o}{4} \frac{H_0}{M_0} |\mathbf{m}|^2 - i \frac{\mu_o}{4} \frac{\omega}{\omega_M} (\mathbf{m} \times \mathbf{m}^*) \cdot \hat{\mathbf{z}} \right]. \quad (7.39)$$

The first two terms in (7.39) represent the small-signal magnetostatic and Zeeman energy densities, respectively. The last term is always real and can be viewed as resulting from the time-averaged expression $\langle \mathbf{m} \times d\mathbf{m}/dt \rangle$. The dependence on the time derivative of \mathbf{m} suggests that the last term be interpreted as a small-signal pseudo-kinetic energy density associated with the precession of the magnetization. (The reason for the use of the term “pseudo-kinetic” rather than simply “kinetic” will become apparent shortly.) Thus, the Lagrangian density consists of the difference between the potential and

pseudo-kinetic energy densities of the mode. Since $L = \int \mathbf{b} \cdot \mathbf{h}^* dv = 0$, we conclude that the net potential and pseudo-kinetic energies of the mode are equal.

We noted in Sections 7.3 and 4.5 that $\mathbf{b} \cdot \mathbf{h}^*$ is not the correct expression for the time-averaged magnetic energy density in a dispersive medium. The correct expression is given by Eq. (4.60):

$$\begin{aligned} \langle w_m(t) \rangle &= \frac{1}{4} \mathbf{h}^* \cdot \frac{\partial(\omega \bar{\boldsymbol{\mu}})}{\partial \omega} \cdot \mathbf{h} \\ &= \frac{1}{4} \mathbf{b} \cdot \mathbf{h}^* + \frac{\omega}{4} \mathbf{h}^* \cdot \frac{\partial \bar{\boldsymbol{\mu}}}{\partial \omega} \cdot \mathbf{h}. \end{aligned} \quad (7.40)$$

Using the permeability tensor (5.6) and the tensor elements given by (3.115) and (3.116), the last term in the energy expression (7.40) can be expressed

$$\frac{\omega}{4} \mathbf{h}^* \cdot \frac{\partial \bar{\boldsymbol{\mu}}}{\partial \omega} \cdot \mathbf{h} = i \frac{\mu_0}{4} \frac{\omega}{\omega_M} (\mathbf{m} \times \mathbf{m}^*) \cdot \hat{\mathbf{z}}. \quad (7.41)$$

The first and second terms in the magnetic energy density (7.40) are sometimes called the *pseudo-energy density* and the *dispersion energy density*, respectively. In plasmas and ionic crystals, the electric dispersion energy density is associated with the kinetic energy of the ions or charge carriers. Similarly, Eq. (7.41) identifies the dispersion energy density with the pseudo-kinetic energy density associated with the magnetic precession.

However, the precession of the magnetization does not contribute to the total energy of the system (hence our choice of the term pseudo-kinetic). Substituting the pseudo-energy density (7.39) and the dispersion energy (7.41) into the total magnetic energy density expression (7.40) gives

$$\langle w_m(t) \rangle = \frac{\mu_0}{4} |\mathbf{h}|^2 + \frac{\mu_0}{4} \frac{H_0}{M_0} |\mathbf{m}|^2, \quad (7.42)$$

verifying that the pseudo-kinetic energy term does not contribute to the total mode energy density. It is a general result that gyroscopic motion does not contribute to the total energy of a system.

An interesting and useful result follows from the fact that $L = 0$ and therefore the potential and pseudo-kinetic energies of a mode are equal. To find the total energy of a mode, the potential energy (7.42) can be integrated over all of space, or the pseudo-kinetic energy (7.41) can be integrated only over the volume of the sample (\mathbf{m} vanishes outside the sample). This result was first shown by Fishman and Morgenthaler [10] and can simplify calculations in many geometries.

Morgenthaler has also interpreted the pseudo-kinetic energy density in terms of a quasi-particle density [11, 12]. The linear dependence of (7.41) on ω suggests the possibility of writing

$$\langle w_m(t) \rangle = n_{\text{eff}} \hbar \omega, \quad (7.43)$$

where the effective *quasi-particle number density* is defined by

$$n_{\text{eff}} = i \frac{\mu_0}{4\hbar\omega_M} (\mathbf{m} \times \mathbf{m}^*) \cdot \hat{\mathbf{z}}. \quad (7.44)$$

The notion of a Lagrangian is also useful in identifying the canonical variables suitable for field quantization. This idea is explored in further detail in Chapter 9.

7.5 Stationary Formulas

Expanding the integrand of the functional (7.27) and imposing the condition $L = 0$ gives

$$\int_V dv \{ (1 + \chi) [\psi_x^* \psi_x + \psi_y^* \psi_y] + \psi_z^* \psi_z - i\kappa [\psi_x^* \psi_y - \psi_y^* \psi_x] \} = 0, \quad (7.45)$$

where we have used the short-hand $\psi_q = \partial\psi/\partial q$, and χ and κ are the susceptibility tensor elements given by Eqs. (3.115) and (3.116), respectively. Equation (7.45) can be used to estimate the magnetostatic mode resonant frequencies of a ferrite-filled cavity using reasonable approximations for the potential function. The cavity can be of arbitrary shape, and χ and κ can be functions of position.

It is also possible to obtain stationary formulas for the wave numbers of propagating modes from (7.45) by continuously distorting the cavity into an arbitrarily long waveguide of uniform cross section. For a sufficiently long cavity, the longitudinal modes will be so closely spaced that we can approximate the wave number as a continuous variable.

For a z -directed bias field and propagation along the $\pm x$ direction, either forward volume or surface waves can propagate depending on the orientation of the film (see Figure 7.2). For either mode, the wave number k is given by the quadratic equation

$$\begin{aligned} k^2 \int_S (1 + \chi) \psi^* \psi \, ds - k\nu \int_S \kappa [\psi_y^* \psi + \psi^* \psi_y] \, ds \\ + \int_S [(1 + \chi) \psi_y^* \psi_y + \psi_z^* \psi_z] \, ds = 0, \end{aligned} \quad (7.46)$$

where $\psi \propto \exp(i\nu kx)$, $\nu = \pm 1$, k is positive definite, and the integrals are over the cross section of the waveguide. The integral over x omitted from Eq. (7.46) simply multiplies the equation by a constant proportional to the integration path length along the propagation direction.

If variations are present only along the z -direction (as in the case of forward volume waves in an infinite slab), Eq. (7.46) reduces to

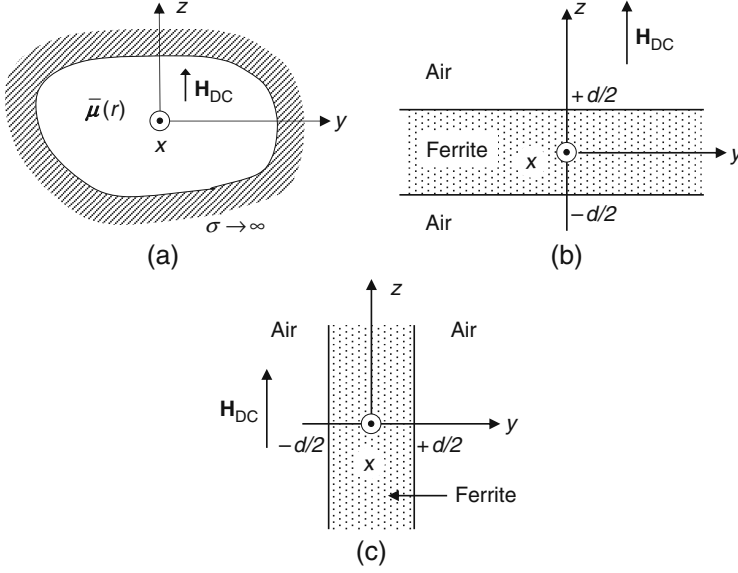


Fig. 7.2. Cross sections of a cylindrical ferrite-filled waveguide in the configuration for propagation of surface waves or forward volume waves, depending on the form of $\bar{\mu}(\mathbf{r})$: (a) general configuration; (b) geometry for forward volume waves as discussed in Chapter 5; (c) geometry for surface waves as discussed in Chapter 5. The geometries shown in (b) and (c) are special cases of that shown in (a). (Adapted from [2]. © 1983 IEEE.)

$$k^2 = \frac{\int \psi_z^* \psi_z dz}{\int [-(1 + \chi)] \psi^* \psi dz}, \quad (7.47)$$

where the integration paths extend between conducting planes on either side of the film.

Backward volume waves propagate in a z -directed bias field if $\psi \propto \exp(i\nu kz)$ (Figure 7.3). For these modes the wave number is given by

$$k^2 = \int_S \frac{\{[-(1 + \chi)][\psi_x^* \psi_x + \psi_y^* \psi_y] + i\kappa[\psi_x^* \psi_y - \psi_y^* \psi_x]\} ds}{\int_S \psi^* \psi ds}. \quad (7.48)$$

If variations are only present through the thickness of the film (y -direction), a simplified expression analogous with (7.47) is obtained:

$$k^2 = \frac{\int [-(1 + \chi)] \psi_y^* \psi_y dy}{\int \psi^* \psi dy}. \quad (7.49)$$

It is interesting to note that the direction of propagation (indicated by ν) only enters the volume/surface wave expression (7.46) if the potential varies

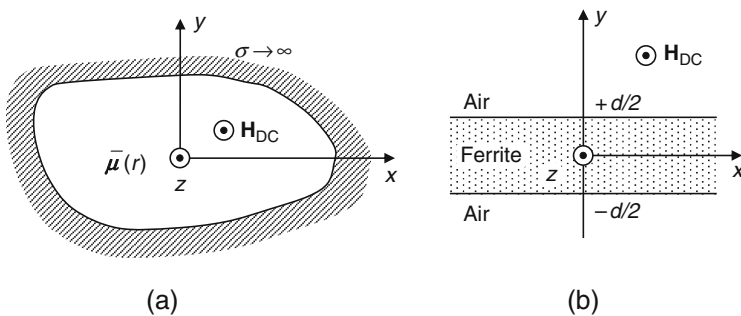


Fig. 7.3. Cross section of a cylindrical ferrite-filled waveguide in the configuration for propagation of backward volume waves: (a) general configuration; (b) geometry for backward volume waves as discussed in Chapter 5 and obtained as a special case of the geometry shown in (a). (Adapted from [2]. © 1983 IEEE.)

with y . The simplest surface wave geometry consists of an infinite slab parallel to the z -axis for which the potential has rapid variations with y . The dependence on ν manifests itself in this case as field displacement non-reciprocity. On the other hand, the simplest forward volume wave geometry consists of an infinite slab parallel to the y -axis for which there is no y variation. Hence this mode is reciprocal. Note, however, that any variation in the y -direction, such as caused by inhomogeneities or finite width, will induce non-reciprocal behavior in the forward volume wave modes.

In contrast, the general equation for backward volume waves (7.48) does not depend explicitly on ν . We conclude that backward volume waves do not exhibit non-reciprocal behavior. (This conclusion rests on the assumption of propagation along the z -axis. If the wave is traveling at some angle relative to the z -axis so that $\psi \propto \exp(i\nu(k_x x + k_z z))$, then $\psi_x = i\nu k_x \psi$ and the mode can again exhibit non-reciprocal characteristics.)

7.6 Stationary Formula Examples with Forward Volume Waves

As an example of the use of the stationary formulas, consider the effects of the ground plane shown in Figure 7.4 on the propagation characteristics of forward volume waves. This geometry can be analyzed exactly² and therefore allows us to evaluate the accuracy of the stationary formulas. The exact solution is given by

$$-\tan \left[kd\sqrt{-(1+\chi)} \right] = \frac{2\sqrt{-(1+\chi)}}{2+\chi(1+e^{-2kt})}. \quad (7.50)$$

² See Problem 5.5.

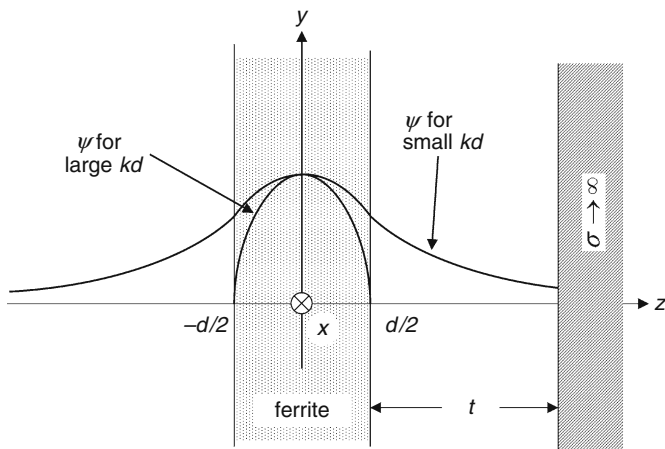


Fig. 7.4. Ferrite film with an adjacent ground plane. Approximate potential functions for the small kd and large kd limits are also shown. The film is magnetized along the z -direction for forward volume wave propagation.

We first obtain a simple solution valid for large k , then discuss an improved approximation that does not have this restriction.

7.6.1 Large k -limit

Referring to the even mode potential function given by Eqs. (5.80) and Figure 5.12, we recall that the potential for forward volume waves varies sinusoidally through the film and decays exponentially outside of the film. In the presence of the ground plane, both growing and decaying exponential terms are required for $z > d/2$. However, in the limit of large k , we expect the potential to decay quickly away from the surface of the film so that the presence of the ground plane will have a negligible effect on the modes. In this limit, the mode fields are tightly confined to the film and the following approximation to the potential is reasonable:

$$\psi = \begin{cases} \cos(\pi z/d), & |z| < d/2 \\ 0, & |z| > d/2 \end{cases} \quad (7.51)$$

Substituting this expression into the variational formula (7.47) and performing the indicated integrations gives

$$kd = \frac{\pi}{\sqrt{-(1+\chi)}}. \quad (7.52)$$

Both the exact solution with a ground plane (7.50) and without a ground plane (5.72) reduce to Eq. (7.52) in the limit $[-(1+\chi)] \ll 1$, which is appropriate for

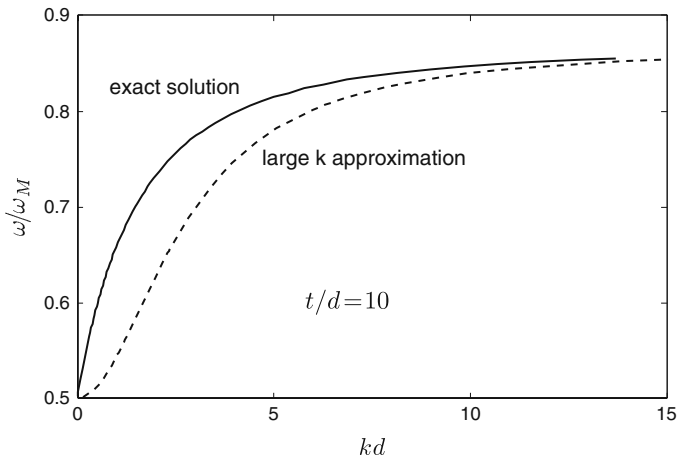


Fig. 7.5. Comparison of the large- k expression (7.52) with the exact solution (7.50) for $\omega_o/\omega_M = 0.5$. The curves are in reasonable agreement for kd greater than about 10.

large k . Equation (7.52) is compared with the exact result (7.50) for $t/d = 10$ in Figure 7.5. The expressions are in reasonable agreement for kd greater than about 10.

7.6.2 Improved Approximation

Let us now consider the case when k is sufficiently small that we can no longer neglect the potential outside the film. This would be the situation when either kt or kd is of the order of unity or smaller. We expect the potential to be peaked about the ferrite film as before, but we cannot set it to zero outside the film. If we assume the ground plane causes only a minor perturbation in the shape of the potential function, we can approximate ψ by the isolated film expressions (5.80) for $z < t + d/2$. The variational approximation for k^2 (7.47) then becomes

$$k^2 = \frac{\int_{-\infty}^{d/2+t} \psi_z^* \psi_z dz}{\int_{-\infty}^{d/2+t} [-(1 + \chi)] \psi^* \psi dz}, \quad (7.53)$$

where ψ and ψ_z are obtained from the isolated film expressions (5.80). Using the form of the potential in the region $z > d/2 + t$ along with the fact that χ vanishes outside the film, Eq. (7.53) can also be written in the form

$$k^2 = \frac{\int_{-\infty}^{\infty} \psi_z^* \psi_z dz - k_0^2 \int_{d/2+t}^{\infty} \psi^* \psi dz}{\int_{-\infty}^{\infty} [-(1 + \chi)] \psi^* \psi dz + \int_{d/2+t}^{\infty} \psi^* \psi dz}. \quad (7.54)$$

where k_0 is the wavenumber of an isolated film. Note that Eq. (7.54) will simply give k_0^2 if the ground plane spacing t is allowed to be arbitrarily large.

This observation can be used to rearrange Eq. (7.54) so that the evaluation of only one integral is required:

$$k^2 = k_0^2 \left[\frac{1 - \eta}{1 + \eta} \right], \quad (7.55)$$

where

$$\eta = \int_{d/2+t}^{\infty} \psi^* \psi dz, \quad (7.56)$$

and we have assumed the normalization condition given by Eq. (6.53). Evaluating Eq. (7.56) using the potential functions (5.80) and the normalization constants (6.54) gives

$$\eta = \frac{e^{-2k_0 d(t/d)}}{-(1 + \chi)k_0 d} \cos^2 \left[\frac{k_0 d}{2} \sqrt{-(1 + \chi)} \right]. \quad (7.57)$$

The variational approximation given by Eqs. (7.55) and (7.57) is compared with the exact solutions with and without a ground plane in Figure 7.6. The variational approximation gives better accuracy than neglecting the ground plane, although differences with the exact solution are still apparent. All three curves converge for large k since the ground plane perturbation becomes negligible in this limit. To further improve the variational approximation, the slope of the potential should be required to vanish at the surface of the conductor, and the potential function must be allowed to be asymmetrical about the center of the film.

Before leaving this discussion, it is interesting to evaluate Eqs. (7.55) and (7.57) in the limit of vanishing $k_0 d$. In this limit, $k_0 d[-(1 + \chi)] \approx 2$ (see

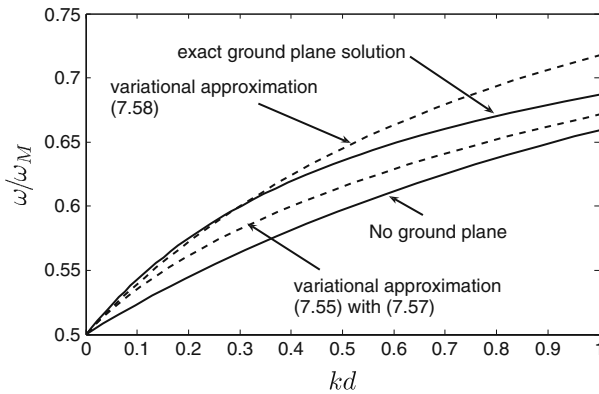


Fig. 7.6. Comparison between the improved variational approximations (Eqs. (7.55) and (7.58)) and the exact solutions with and without the ground plane (Eqs. (7.50) and (5.76), respectively, with $\omega_0/\omega_M = 0.5$) and $t/d = 0.5$.

Problem 6.7), and Eq. (7.57) reduces to $\eta = 1/2$. The variational dispersion relation (7.55) then becomes

$$k = k_0/\sqrt{3}. \quad (7.58)$$

Although this differs from the exact result³ $k = k_0/2$, Figure 7.6 shows that it is more accurate than the previous variational approximation for $kd \leq 0.5$.

7.6.3 Effect of Medium Inhomogeneity

Of course, stationary formulas are of greatest interest for problems that cannot be solved in closed form. As an example of such a problem, consider forward volume waves propagating in the presence of a material inhomogeneity. For simplicity, we assume the inhomogeneity exists only through the thickness of the film (z -direction) and is uniform along the in-plane directions (x and y). As a result of this inhomogeneity, the small-signal susceptibility can be written

$$\chi = \chi_0 + \Delta\chi, \quad (7.59)$$

where $\Delta\chi \ll \chi_0$. Substituting this expression into the variational expression (7.47) and keeping only terms linear in the perturbation ($\Delta\chi$) leads to the result

$$\Delta k = \frac{k_0}{2} \frac{\int_{-\infty}^{\infty} \Delta\chi \psi^* \psi \, dz}{\int_{-\infty}^{\infty} [-(1 + \chi_0)] \psi^* \psi \, dz}. \quad (7.60)$$

From the form of Δk given in Eq. (7.60), we can reach the following general conclusions: (1) the sign of Δk will be the same as the sign of $\Delta\chi$ and (2) the inhomogeneity has the greatest effect (i.e., $\Delta k/k_0$ is largest) near the top of the band where $[-(1 + \chi_0)] \rightarrow 0$.

7.7 Finite Element Analysis

We have seen that the correct field solution for spin waves in thin films minimizes certain functionals. This suggests a general method for solving such problems numerically. Specifically, suppose that we choose a set of points distributed throughout the volume of the geometry at which we want to find the values of the magnetostatic potential. If there are N such points, then it is possible to write a set of N simultaneous linear equations whose solution minimizes the desired functional. This solution will be a discrete approximation to the actual solution. Values of the field at intermediate points can be estimated using interpolation. For 2D problems, the points are selected by dividing the geometry into triangles that completely cover the geometry of the problem, and choosing the vertices of the triangles. For 3D problems, the

³ This result follows from Problem 5.4.

space is filled with tetrahedra. The material properties within the triangles or tetrahedra are assumed to be uniform, so changes in material are represented by choosing the triangles or tetrahedra to follow the shapes of the different regions. Continuous variations can be approximated by allowing the properties to vary slightly from element to element.

The general approach that we have described is known as finite element analysis (FEA) and was introduced by R. Courant in 1943 [13]. FEA has found applications in all areas of engineering and is often used to simulate electromagnetic wave propagation and scattering phenomena. In particular, FEA has been successfully used to analyze dipolar spin waves in inhomogeneous films [14], films with finite dimensions [15], and nonlinear dipolar spin waves [16].

Problems

7.1. Show that the function ϕ that minimizes the functional

$$I[\phi(x)] = \frac{1}{2} \int_V (\nabla \phi)^2 dv \quad (7.61)$$

also satisfies Laplace's equation, $\nabla^2 \phi = 0$.

7.2. According to the method of Lagrange multipliers (see, e.g., Matthews and Walker [8, Chapter 12]), minimizing the functional $I[\psi(x)]$ subject to the constraint $J[\psi(x)] = \text{constant}$ is equivalent to minimizing the composite functional $I - \lambda J$, where λ is called the Lagrange multiplier.

- (a) Consider forward volume waves propagating in an infinite film as shown in Figure 7.2(b). In this geometry, the only transverse component of the small-signal field \mathbf{h} is $\mathbf{h} \cdot \hat{\mathbf{z}} = -\partial\psi/\partial z \equiv -\psi_z$. Show that minimizing the functional

$$I[\psi(z)] = \int_{-\infty}^{\infty} \psi_z^* \psi_z dz \quad (7.62)$$

is the same as requiring ψ to satisfy the 1D Laplace equation $\partial^2 \psi / \partial z^2 = 0$.

- (b) Consider the constraint

$$J[\psi(z)] = \int_{-\infty}^{\infty} [-(1 + \chi)] \psi^* \psi dz = \text{constant}, \quad (7.63)$$

which is simply a normalization condition derived from the orthogonality relation (6.53) applied to a single mode. Find the Lagrange multiplier λ that makes the composite functional $\mu_0(I - \lambda J)$ identical with L from Eq. (7.27)

specialized to the present geometry. This leads us to the alternate interpretation of the variational formulation for forward volume waves: *the transverse variations of the potential must satisfy Laplace's equation subject to the normalization constraint (7.63).*

7.3. This problem applies the Lagrange multiplier analysis of Problem 7.2 to the case of backward volume waves in the geometry of Figure 7.3(a).

(a) Show that minimizing the functional

$$I[\psi(x, y)] = \int_S \{ [-(1 + \chi)] [\psi_x^* \psi_x + \psi_y^* \psi_y] + i\kappa [\psi_x^* \psi_y - \psi_y^* \psi_x] \} ds \quad (7.64)$$

is the same as requiring ψ to satisfy the 2D Walker equation

$$\frac{\partial}{\partial x} [(1 + \chi)\psi_x] + \frac{\partial}{\partial y} [(1 + \chi)\psi_y] - i\frac{\partial}{\partial x} [\kappa\psi_y] + i\frac{\partial}{\partial y} [\kappa\psi_x] = 0. \quad (7.65)$$

(b) Consider the constraint

$$J[\psi(z)] = \int_S \psi^* \psi ds = \text{constant}, \quad (7.66)$$

which is simply a normalization condition derived from the orthogonality relation (6.64) applied to a single mode. Find the Lagrange multiplier λ that makes the composite functional $\mu_0(I - \lambda J)$ identical with L from Eq. (7.27) specialized to the present geometry. This leads us to the alternate interpretation of the variational formulation for backward volume waves: *the transverse variations of the potential must satisfy the 2D Walker equation (7.65) subject to the normalization constraint (7.66).*

7.4. The instantaneous Zeeman energy density is given by

$$W_z(t) = -\mu_0 H_0 M_0 \cos \theta(t), \quad (7.67)$$

where $\theta(t)$ is the time-varying angle between the magnetization vector and the applied bias field.

- (a) Expand $W_z(t)$ for small $\theta(t)$ and show that $W_z(t) = W_0 + w_z(t)$, where W_0 and $w_z(t)$ are static and time-varying components, respectively.
 (b) Show that the time average of $w_z(t)$ from part (a) can be expressed

$$\langle w_z(t) \rangle = \frac{\mu_0}{4} \frac{H_0}{M_0} |\mathbf{m}|^2, \quad (7.68)$$

as discussed in the text following the Lagrangian density (7.39).

7.5. Using the permeability tensor (5.6) and the tensor elements given by (3.115) and (3.116), show that the last term in the energy expression (7.40) can be expressed

$$\frac{\omega}{4} \mathbf{h}^* \cdot \frac{\partial \bar{\boldsymbol{\mu}}}{\partial \omega} \cdot \mathbf{h} = i \frac{\mu_0}{4} \frac{\omega}{\omega_M} (\mathbf{m} \times \mathbf{m}^*) \cdot \hat{\mathbf{z}}. \quad (7.69)$$

7.6. Substitute the trial potential function (7.51) into the variational formula (7.47) and perform the necessary integrations to obtain the approximate dispersion relation (7.52).

7.7. Show that the exact forward volume wave dispersion relations with and without a ground plane, (7.50) and (5.72) respectively, reduce to Eq. (7.52) in the limit $[-(1 + \chi)] \rightarrow 0$.

References

- [1] W. F. Brown Jr., *Micromagnetics*, ser. Interscience Tracts on Physics and Astronomy. New York: Interscience Publishers, 1963, vol. 18.
- [2] D. D. Stancil, "Variational formulation of magnetostatic wave dispersion relations," *IEEE Trans. Magn.*, vol. 19, p. 1865, 1983.
- [3] N. E. Buris and D. D. Stancil, "Magnetostatic surface-wave propagation in ferrite thin films with arbitrary variations of the magnetization through the film thickness," *IEEE Trans. Microwave Theory Tech.*, vol. MTT-33, p. 484, 1985.
- [4] N. E. Buris and D. D. Stancil, "Magnetostatic volume modes of ferrite thin films with magnetization inhomogeneities through the film thickness," *IEEE Trans. Microwave Theory Tech.*, vol. MTT-33, p. 1089, 1985.
- [5] N. E. Buris and D. D. Stancil, "Magnetostatic backward waves in low dose ion implanted YIG films," *IEEE Trans. Magn.*, vol. 22, p. 859, 1986.
- [6] M. Tsutsumi, Y. Masaoka, T. Ohira, and N. Kumagai, "A new technique for magnetostatic wave delay lines," *IEEE Trans. Microwave Theory Tech.*, vol. 29, p. 583, 1981.
- [7] E. Sawado and N. S. Chang, "Variational approach to analysis of propagation of magnetostatic waves in highly inhomogeneously magnetized media," *J. Appl. Phys.*, vol. 55, p. 1062, 1984.
- [8] J. Matthews and R. L. Walker, *Mathematical Methods of Physics*. Menlo Park, CA: W. A. Benjamin Inc., 1970.
- [9] H. Goldstein, C. P. Poole, and J. L. Safko, *Classical Mechanics*, 3rd ed. Cambridge, MA: Addison-Wesley, 2001.
- [10] D. A. Fishman and F. R. Morgenthaler, "Investigation of the velocity of energy circulation of magnetostatic modes in ferrites," *J. Appl. Phys.*, vol. 54, p. 3387, 1983.
- [11] F. R. Morgenthaler, "Dynamic magnetoelastic coupling in ferromagnets and antiferromagnets," *IEEE Trans. Magn.*, vol. 8, p. 130, 1972.

- [12] F. R. Morgenthaler, "Control of magnetostatic waves in thin films by means of spatially nonuniform bias fields," *Circ. Syst. Signal Pr.*, vol. 4, p. 63, 1985.
- [13] R. Courant, "Variational methods for the solution of problems of equilibrium and vibrations," *Bull. Amer. Math. Soc.*, vol. 49, p. 123, 1943.
- [14] Y. Long, M. Koshiba, and M. Suzuki, "Finite-element solution of planar inhomogeneous waveguides for magnetostatic waves," *IEEE Trans. Microwave Theory Tech.*, vol. 35, p. 731, 1987.
- [15] M. Koshiba and Y. Long, "Finite-element analysis of magnetostatic wave propagation in a YIG film of finite dimensions," *IEEE Trans. Microwave Theory Tech.*, vol. 37, p. 1768, 1989.
- [16] T. Ueda, Y. Ueda, H. Shimasaki, and M. Tsutsumi, "Numerical analysis of nonlinear magnetostatic wave propagation by finite-element method," *IEEE Trans. Mag.*, vol. 39, pp. 3157–3159, 2003.

Optical-Spin Wave Interactions

It is fortunate that the garnet films that support dipolar spin wave propagation are also transparent to infrared light in the range of wavelengths between 1 and $5\mu\text{m}$. This includes wavelengths of 1.3 and $1.5\mu\text{m}$, which are of particular interest for optical fiber communication systems. Since a single film can be used simultaneously as a waveguide for optical and spin wave modes, interactions between these modes can be exploited for devices such as microwave spectrum analyzers, optical frequency shifters, tunable optical filters, and optical beam deflectors.

The two dominant interaction mechanisms are Faraday rotation and the Cotton–Mouton effect. Faraday rotation occurs in a bulk medium when the normal modes of optical propagation along the direction of magnetization are right- and left-circularly polarized (see Problem 4.4). Since these waves travel with different velocities, Faraday rotation is sometimes referred to as *magnetic circular birefringence* and gives rise to non-reciprocal effects. In contrast, the Cotton–Mouton effect results in *linearly* polarized normal modes whose velocities depend on the direction of the magnetization. This phenomenon is sometimes referred to as *magnetic linear birefringence* and is a purely reciprocal effect. Faraday rotation is usually the larger of the two effects, while the Cotton–Mouton effect will add or subtract from the Faraday effect depending on the interaction geometry.

In this chapter, we first treat the optical modes of a thin-film waveguide consisting of a non-magnetic isotropic dielectric. We next discuss the nature of the magneto-optic interaction and how it affects the constitutive tensors. Finally, we consider the perturbation to the optical tensors caused by the presence of a dipolar spin wave and the resulting optical scattering and mode conversion. We will theoretically describe scattering from forward volume spin waves and will detail experiments using both the co-propagating and transverse spin wave (SW)-optical interaction geometries.

8.1 Symmetric Dielectric Waveguides¹

The geometry for a symmetric *dielectric waveguide* is shown in Figure 8.1. For wave guiding to occur, the permittivity of the film ϵ_f must be larger than that of the surrounding dielectric ϵ_c . For definiteness, we assume the propagation to occur along the direction of the $+\hat{\mathbf{z}}$ axis. It is convenient to divide the waves that can be guided by this structure into two classes: those with the \mathbf{E} field transverse to the propagation direction (called TE for Transverse Electric) and those with the \mathbf{H} field transverse to the propagation direction (called TM for Transverse Magnetic). Because the structure is symmetric about the $x = 0$ plane, we expect solutions that are either even or odd in x .

It is worth noting that not all waveguiding structures permit these classifications; sometimes longitudinal components of *both* \mathbf{E} and \mathbf{H} are required to match the boundary conditions. Such modes are called *hybrid* modes.

As we found when considering volume spin wave modes, we can visualize a guided mode as a plane wave undergoing multiple total internal reflections at the dielectric boundary. Taking the polarization either in or out of the plane of the paper gives rise to the two possibilities shown in Figure 8.2. Note that the TE/TM terminology is consistent with that used in discussing reflection from plane interfaces.²

8.1.1 TE Modes

First, let us consider TE modes that are symmetric about the x -axis. The \mathbf{E} field is composed of a single component along the $\hat{\mathbf{y}}$ direction:

$$E_y = e_y(x)e^{ik_z z}, \quad (8.1)$$

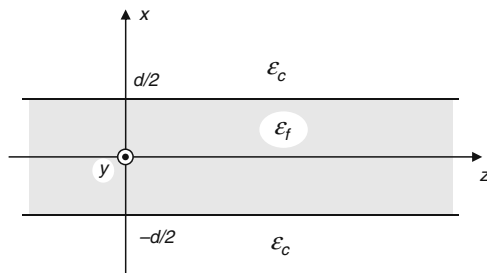


Fig. 8.1. Geometry for a symmetric dielectric waveguide.

¹ This section draws heavily from H. A. Haus [1].

² When considering a plane wave incident on a plane boundary between two media, the *plane of incidence* is defined as the plane containing both the incident \mathbf{k} vector and the surface normal. Referring to Figure 8.2, the plane of incidence is clearly parallel to the direction of propagation. Consequently, an electric field that is transverse to the propagation direction will also be transverse to the plane of incidence defined for the boundaries of the waveguide.

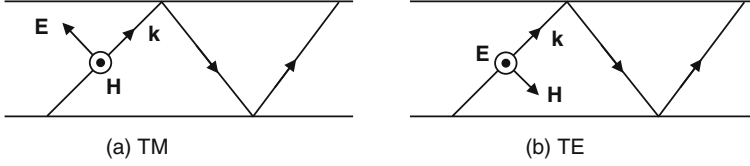


Fig. 8.2. Visualization of (a) TM and (b) TE modes as plane waves undergoing total internal reflection.

where

$$e_y(x) = \begin{cases} C e^{-\alpha_x x}, & x > d/2, \\ A \cos(k_x x), & |x| \leq d/2, \\ C e^{+\alpha_x x}, & x < -d/2. \end{cases} \quad (8.2)$$

From Figure 8.2, there will be two components of the \mathbf{H} field. These components can be obtained from the electric field (8.1) using Maxwell's equation from Faraday's law (4.7). However, for matching boundary conditions, all we need is H_z :

$$H_z = -\frac{i}{\omega\mu_0} \frac{\partial E_y}{\partial x}, \quad (8.3)$$

where

$$H_z = h_z(x) e^{ik_z z} \quad (8.4)$$

and

$$h_z(x) = \begin{cases} \frac{iC\alpha_x}{\omega\mu_0} e^{-\alpha_x x}, & x > d/2, \\ \frac{iAk_x}{\omega\mu_0} \sin(k_x x), & |x| \leq d/2, \\ -\frac{iC\alpha_x}{\omega\mu_0} e^{+\alpha_x x}, & x < -d/2. \end{cases} \quad (8.5)$$

We now take advantage of the symmetry in the the assumed mode fields to only match boundary conditions at one interface. Requiring E_y and H_z to be continuous at $x = d/2$ leads to

$$\tan\left[\frac{k_x d}{2}\right] = \frac{\alpha_x}{k_x} \quad (8.6)$$

and

$$C = A e^{\alpha_x d/2} \cos(k_x d/2). \quad (8.7)$$

The parameters α_x and k_x can be related to each other and to the wave number k_z using the dispersion relations for plane waves in each medium (cf. Eq. (4.86)):

$$\omega^2 \mu_0 \varepsilon_c = k_z^2 - \alpha_x^2, \quad (8.8)$$

$$\omega^2 \mu_0 \varepsilon_f = k_z^2 + k_x^2. \quad (8.9)$$

Eliminating k_z^2 gives

$$\alpha_x^2 = \omega^2 \mu_0 (\varepsilon_f - \varepsilon_c) - k_x^2. \quad (8.10)$$

Thus,

$$\frac{\alpha_x}{k_x} = \sqrt{\frac{\omega^2 \mu_0 (\varepsilon_f - \varepsilon_c)}{k_x^2} - 1}, \quad (8.11)$$

and (8.6) becomes

$$\tan \left[\frac{k_x d}{2} \right] = \sqrt{\frac{\omega^2 \mu_0 (\varepsilon_f - \varepsilon_c)}{k_x^2} - 1}. \quad (8.12)$$

Equation (8.12) is a transcendental equation for k_x . Once k_x is found for a given ω , the wave number k_z can be obtained from (8.9).

A given mode is confined to the waveguide so long as $\alpha_x > 0$. When $\alpha_x = 0$, the fields no longer decay away from the surfaces of the film. At this point, the right-hand side of (8.12) vanishes and we have the relationship

$$k_x^2 = \omega^2 \mu_0 (\varepsilon_f - \varepsilon_c). \quad (8.13)$$

To satisfy the dispersion relation, the left-hand side of (8.12) must also vanish. This occurs when $k_x d / 2 = n\pi$. Substituting this result into (8.13) gives the cutoff frequencies for the even modes:

$$f_{c,m} = \frac{m}{2d\sqrt{\mu_0(\varepsilon_f - \varepsilon_c)}}, \quad (8.14)$$

where $f_{c,m} = \omega_{c,m}/2\pi$ is the cutoff frequency for the m th mode and $m = 2n$. Note that the lowest-order mode ($m=0$) has a zero cutoff frequency!³ However, (8.10) shows that α_x must also go to zero in the limit of vanishing k_x and ω . Thus, the mode energy is increasingly less confined as the frequency decreases. The electric field for the TE₀ mode is shown in Figure 8.3 for two values of the free-space wavelength λ (equivalent to two values of ω).

For modes with finite cutoff frequencies, (8.10) also implies that α_x becomes imaginary for $\omega < \omega_c$. This means that the fields in the regions $|x| > d/2$ represent propagating waves rather than exponentially decaying waves, and energy leaks away from the guide.

Near cutoff, the dispersion relation for each mode approaches (Problem 8.1)

$$k_z^2 \approx \omega \mu_0 \varepsilon_c, \quad (8.15)$$

and the propagation is dominated by the properties of the outer medium. This is because most of the energy is in the outer region, since α_x is small. On the other hand, for $\omega \rightarrow \infty$, each of the mode dispersion relations approaches (Problem 8.2)

³ If the permittivity is different above and below the film, the cutoff frequency of the lowest-order mode is no longer zero.

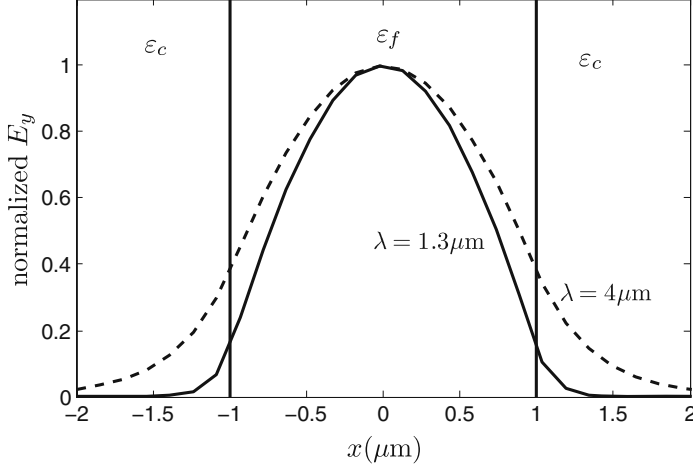


Fig. 8.3. Normalized electric field profiles for the TE_0 mode in a symmetric dielectric film waveguide for (free space) optical wavelengths of $1.3\mu\text{m}$ (*solid*) and $4\mu\text{m}$ (*dashed*). The film thickness is $d = 2\mu\text{m}$, and the permittivities are $\varepsilon_c = 1$ and $\varepsilon_f = 4.84$.

$$k_z^2 \approx \omega^2 \mu_0 \varepsilon_f, \quad (8.16)$$

and the propagation is dominated by the properties of the film. In this limit, α_x is large and the mode is highly localized to the film.

The TE modes with antisymmetric thickness variations can be analyzed in a similar fashion. The dispersion relation is found to be

$$\cot \left[\frac{k_x d}{2} \right] = - \sqrt{\frac{\omega^2 \mu_0 (\varepsilon_f - \varepsilon_c)}{k_x^2}} - 1. \quad (8.17)$$

The odd-mode cutoff frequencies are again given by (8.14), but with m odd; thus (8.14) is valid for both even and odd modes if $m = 0, 1, 2, 3, \dots$

8.1.2 TM Modes

In the case of TM modes, the \mathbf{H} field is composed of a single component along the $\hat{\mathbf{y}}$ -axis. For symmetric modes, the magnetic field intensity can be written:

$$H_y = h_y(x) e^{ik_z z}, \quad (8.18)$$

where

$$h_y(x) = \begin{cases} C e^{-\alpha_x x}, & x > d/2, \\ A \cos(k_x x), & |x| \leq d/2, \\ C e^{+\alpha_x x}, & x < -d/2. \end{cases} \quad (8.19)$$

Again referring to Figure 8.2, we see that there will be two components of the electric field for TM modes. However, to match boundary conditions, only E_z is needed. The desired component can be obtained from Ampere's law (4.6):

$$E_z = \frac{i}{\omega\epsilon} \frac{\partial H_y}{\partial x}, \quad (8.20)$$

where

$$E_z = e_z(x)e^{ik_z z}. \quad (8.21)$$

The mode function e_z for the electric field is found to be

$$e_z(x) = \begin{cases} -\frac{iC\alpha_x}{\omega\epsilon_c} e^{-\alpha_x x}, & x > d/2, \\ -\frac{iAk_x}{\omega\epsilon_f} \sin(k_x x), & |x| \leq d/2, \\ \frac{iC\alpha_x}{\omega\epsilon_c} e^{+\alpha_x x}, & x < -d/2. \end{cases} \quad (8.22)$$

Matching the boundary conditions at $x = d/2$ gives (8.7) relating A and C , and the dispersion relation:

$$\tan \left[\frac{k_x d}{2} \right] = \frac{\epsilon_f \alpha_x}{\epsilon_c k_x} = \frac{\epsilon_f}{\epsilon_c} \sqrt{\frac{\omega^2 \mu_0 (\epsilon_f - \epsilon_c)}{k_x^2} - 1}. \quad (8.23)$$

The magnetic field intensity for the TM_0 mode is shown in Figure 8.4 for two values of free-space wavelength λ .

Following a similar analysis for odd modes leads to the dispersion relation:

$$\cot \left[\frac{k_x d}{2} \right] = -\frac{\epsilon_f}{\epsilon_c} \sqrt{\frac{\omega^2 \mu_0 (\epsilon_f - \epsilon_c)}{k_x^2} - 1}. \quad (8.24)$$

A comparison of the dispersion relations for TE modes, (8.12) and (8.17), with those for TM modes, (8.23) and (8.24), shows that they only differ by the ratio of permittivities on the right-hand sides. It follows that the TE and TM modes have the same cutoff frequencies in a symmetric dielectric waveguide. Since $\epsilon_f/\epsilon_c > 1$, k_x is larger for TM modes than for TE modes of the same mode order m . It follows from (8.9) that the longitudinal wave number k_z is smaller for TM modes than for TE modes of the same order. This may not be true if the cladding and/or film layers have anisotropic permittivities.

8.1.3 Optical Mode Orthogonality and Normalization

To determine the coupling between optical modes in the presence of a magneto-optical perturbation, we will need orthogonality relations between

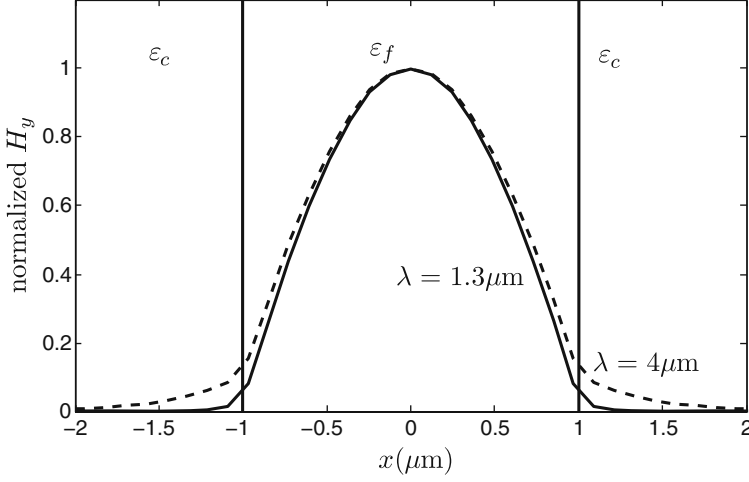


Fig. 8.4. Normalized magnetic field intensity profiles for the TM_0 mode in a symmetric dielectric film waveguide for (free space) optical wavelengths of $1.3\text{ }\mu\text{m}$ (*solid*) and $4\text{ }\mu\text{m}$ (*dashed*). Other parameters are the same as in Figure 8.3.

the optical modes. The necessary relations can be obtained using the *Lorentz reciprocity theorem*, which we will now derive for lossless source-free media.

Consider the fields associated with two independent solutions to Maxwell's equations, $(\mathbf{E}_1, \mathbf{H}_1)$ and $(\mathbf{E}_2, \mathbf{H}_2)$. Using the vector identity (4.30), we can write

$$\nabla \cdot (\mathbf{E}_1 \times \mathbf{H}_2) = i\omega\mu_0 \mathbf{H}_2 \cdot \mathbf{H}_1 + i\omega\varepsilon \mathbf{E}_1 \cdot \mathbf{E}_2. \quad (8.25)$$

Subtracting from this the equation obtained by interchanging subscripts 1 and 2 gives

$$\nabla \cdot (\mathbf{E}_1 \times \mathbf{H}_2 - \mathbf{E}_2 \times \mathbf{H}_1) = i\omega\mu_0 \mathbf{H}_2 \cdot \mathbf{H}_1 + i\omega\varepsilon \mathbf{E}_1 \cdot \mathbf{E}_2 - i\omega\mu_0 \mathbf{H}_1 \cdot \mathbf{H}_2 - i\omega\varepsilon \mathbf{E}_2 \cdot \mathbf{E}_1$$

or

$$\nabla \cdot (\mathbf{E}_1 \times \mathbf{H}_2 - \mathbf{E}_2 \times \mathbf{H}_1) = 0. \quad (8.26)$$

This is the Lorentz reciprocity theorem for lossless media. Using the assumed z dependence for the thin-film waveguide modes, e.g. (8.1), the reciprocity theorem can be written as

$$\nabla_t \cdot (\mathbf{E}_1 \times \mathbf{H}_2 - \mathbf{E}_2 \times \mathbf{H}_1) + i(k_z^{(1)} + k_z^{(2)})\hat{\mathbf{z}} \cdot (\mathbf{E}_1 \times \mathbf{H}_2 - \mathbf{E}_2 \times \mathbf{H}_1) = 0, \quad (8.27)$$

where ∇_t is the transverse component of the ∇ operator. Integrating over an arbitrary surface S in the xy plane and making use of the 2D divergence theorem gives

$$\begin{aligned}
\int_S \nabla_t \cdot (\mathbf{E}_1 \times \mathbf{H}_2 - \mathbf{E}_2 \times \mathbf{H}_1) ds &= \oint_C \hat{\mathbf{n}} \cdot (\mathbf{E}_1 \times \mathbf{H}_2 - \mathbf{E}_2 \times \mathbf{H}_1) dl \\
&= -i(k_z^{(1)} + k_z^{(2)}) \int_S \hat{\mathbf{z}} \cdot (\mathbf{E}_1 \times \mathbf{H}_2 - \mathbf{E}_2 \times \mathbf{H}_1) ds,
\end{aligned} \tag{8.28}$$

where C is a contour around the surface S and $\hat{\mathbf{n}}$ is normal to C . Consider a rectangular contour with top and bottom edges parallel to the film and sides perpendicular to the film. If we stretch the surface S along the direction perpendicular to the plane of the film, then the fields on the top and bottom segments of the contour C will vanish as C goes to infinity for all modes localized to the film. Since there is no variation of the thin-film modes along the in-plane direction perpendicular to the direction of propagation, the integrals along the side segments will exactly cancel each other. Thus, the contour integral will vanish around this surface. The integral over the guide cross section (8.28) then becomes

$$(k_z^{(1)} + k_z^{(2)}) \int_S \hat{\mathbf{z}} \cdot (\mathbf{E}_1 \times \mathbf{H}_2 - \mathbf{E}_2 \times \mathbf{H}_1) ds = 0. \tag{8.29}$$

Since the waveguide under consideration is bidirectional, we can replace mode 2 with an identical one traveling in the opposite direction. To do this, we make the substitutions $k_z^{(2)} \rightarrow -k_z^{(2)}$, $\mathbf{H}_2 \rightarrow -\mathbf{H}_2$, and $\mathbf{E}_2 \rightarrow \mathbf{E}_2$ to obtain

$$(k_z^{(1)} - k_z^{(2)}) \int_S \hat{\mathbf{z}} \cdot (-\mathbf{E}_1 \times \mathbf{H}_2 - \mathbf{E}_2 \times \mathbf{H}_1) ds = 0. \tag{8.30}$$

Adding and subtracting (8.29) and (8.30) gives the orthogonality relation:

$$\int_S \hat{\mathbf{z}} \cdot (\mathbf{E}_1 \times \mathbf{H}_2) ds = 0, \quad \left[k_z^{(1)} \right]^2 \neq \left[k_z^{(2)} \right]^2. \tag{8.31}$$

This relation can be related to mode power if we identify solutions 1 and 2 with the m th and n th waveguide modes: $\mathbf{E}_1 = \mathbf{E}_m$ and $\mathbf{H}_2 = \mathbf{H}_n^*$. Normalizing to 1 W per unit length along the y -direction gives the orthonormality relation

$$\frac{1}{2} \int_{-\infty}^{\infty} \hat{\mathbf{z}} \cdot (\mathbf{E}_m \times \mathbf{H}_n^*) dx = \delta_{m,n}, \tag{8.32}$$

where $\delta_{m,n}$ is the Kronecker delta (cf. Eq. (6.53)). Applying this relation to the TE and TM modes of the thin-film dielectric waveguide gives:

$$\int_{-\infty}^{\infty} e_y^{(m)}(x) e_y^{(n)}(x) dx = \delta_{m,n} \frac{2\omega\mu_0}{k_z^{(m)}} \quad (\text{TE}), \quad (8.33)$$

$$\int_{-\infty}^{\infty} \frac{1}{\varepsilon} h_y^{(m)}(x) h_y^{(n)}(x) dx = \delta_{m,n} \frac{2\omega}{k_z^{(m)}} \quad (\text{TM}). \quad (8.34)$$

In (8.34), note that the permittivity ε is different in the various layers and is therefore a function of x .

8.2 Magneto-Optical Interactions

In our analysis of thin-film waveguides, the permittivity and permeability were taken to be isotropic. In this case, the normal modes were found to separate cleanly into TE and TM polarizations. However, if either $\bar{\mu}$ or $\bar{\varepsilon}$ contains off-diagonal elements, then coupling will occur between orthogonal linear polarization components and the normal modes will no longer be pure TE and TM. Rigorously, the normal modes of such an anisotropic waveguide should be found by solving the boundary value problem again using the appropriate $\bar{\mu}$ and $\bar{\varepsilon}$. On the other hand, if the off-diagonal elements are small compared with the diagonal elements, then a perturbation approach can be taken to obtain the new propagation behavior from the unperturbed TE and TM modes. Fortunately, this is the case with magneto-optical interactions, so we will proceed with the somewhat simpler perturbation approach in discussing the optical-magnetostatic wave interactions. Our goal in this section is to motivate appropriate forms for $\bar{\mu}$ and $\bar{\varepsilon}$.

8.2.1 Can You Tell the Difference Between $\bar{\mu}$ and $\bar{\varepsilon}$?

Although we are used to thinking of $\bar{\mu}$ and $\bar{\varepsilon}$ as distinct physical quantities, we will now show that from a phenomenological point of view, the effects of the material can be contained in either an effective permittivity or an effective permeability for time-varying fields in an infinite medium. For simplicity, we will show how this comes about in isotropic media [2]. (The derivation of an effective permittivity is extended to anisotropic media in Problem 8.7.) For this purpose, Maxwell's equations can be written

$$\nabla \times \mathbf{E} = -\frac{\partial \mathbf{B}}{\partial t}, \quad (8.35)$$

$$\nabla \times \mathbf{B} = \frac{1}{c^2} \frac{\partial \mathbf{E}}{\partial t} + \mu_0 \mathbf{J}, \quad (8.36)$$

where

$$\mathbf{J} = \frac{\partial \mathbf{P}}{\partial t} + \nabla \times \mathbf{M}. \quad (8.37)$$

Note that Ampere's law (8.36) differs from (4.1) in that we have explicitly shown the polarization current and have represented \mathbf{M} by a circulating current. We will now show that with suitable substitutions, the current (8.37) can be expressed entirely in terms of either \mathbf{E} or \mathbf{B} ; hence, it is not possible to phenomenologically distinguish between the contributions of \mathbf{P} and \mathbf{M} . Let us define (cf. Eqs. (4.18) and (4.19))

$$\mathbf{P} = \varepsilon_0 \chi_e \mathbf{E}, \quad (8.38)$$

$$\mathbf{M} = \frac{1}{\mu_0} \chi'_m \mathbf{B}, \quad (8.39)$$

where

$$\chi'_m = \frac{\chi_m}{1 + \chi_m}, \quad (8.40)$$

and χ_m is defined as in (4.19). These expressions allow us to write the current \mathbf{J} in terms of the electric and magnetic susceptibilities:

$$\mathbf{J} = \varepsilon \chi_e \frac{\partial \mathbf{E}}{\partial t} + \frac{1}{\mu_0} \chi'_m \nabla \times \mathbf{B}. \quad (8.41)$$

Ampere's law (8.36) can now be used to eliminate $\nabla \times \mathbf{B}$ from the current (8.41). After simplification, the current can be written entirely in terms of an effective electric susceptibility:

$$\mathbf{J} = \varepsilon_0 \frac{(\chi_e + \chi'_m)}{(1 - \chi'_m)} \frac{\partial \mathbf{E}}{\partial t} \equiv \varepsilon_0 \chi_e^{(\text{eff})} \frac{\partial \mathbf{E}}{\partial t}. \quad (8.42)$$

Alternatively, (8.36) can be used to eliminate $\partial \mathbf{E} / \partial t$. In this case, the current can be written entirely in terms of an effective magnetic susceptibility:

$$\mathbf{J} = \frac{1}{\mu_0} \frac{(\chi_e + \chi'_m)}{(1 + \chi_e)} \nabla \times \mathbf{B} \equiv \frac{1}{\mu_0} \chi_m^{(\text{eff})} \nabla \times \mathbf{B}. \quad (8.43)$$

Thus, the properties of the medium can be modeled either with an effective electric *or* magnetic susceptibility!

The situation is somewhat more complicated if the boundary conditions of a finite region are considered. For example, let us consider the case where the magnetic effects are included in an effective electric susceptibility as in (8.42). In this case, the relation between \mathbf{B} and the effective magnetic field intensity \mathbf{H}' is simply $\mathbf{B} = \mu_0 \mathbf{H}'$. Ampere's law becomes

$$\nabla \times \mathbf{H}' = \varepsilon_0 \frac{\partial \mathbf{E}}{\partial t} + \frac{\partial \mathbf{P}}{\partial t} + \nabla \times \mathbf{M}. \quad (8.44)$$

To obtain the boundary conditions on \mathbf{H}' , we integrate (8.44) over a small surface S crossing the boundary between two media as shown in Figure 8.5. This gives

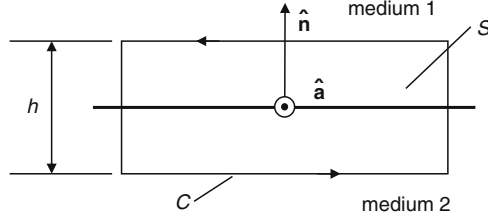


Fig. 8.5. Geometry for finding the boundary conditions on \mathbf{H}' from Ampere's law.

$$\oint_C \mathbf{H}' \cdot d\mathbf{l} = \int_S \left[\epsilon_0 \frac{\partial \mathbf{E}}{\partial t} + \frac{\partial \mathbf{P}}{\partial t} \right] \cdot d\mathbf{s} + \oint_C \mathbf{M} \cdot d\mathbf{l}, \quad (8.45)$$

where we have used *Stoke's theorem*:

$$\int_S [\nabla \times \mathbf{A}] \cdot d\mathbf{s} = \oint_C \mathbf{A} \cdot d\mathbf{l} \quad (8.46)$$

valid for any analytic vector function \mathbf{A} if the contour C bounds the surface S . For finite fields \mathbf{E} and \mathbf{P} , the surface integral on the right-hand side of (8.45) vanishes in the limit $h \rightarrow 0$. If we further assume that the width of the contour parallel to the boundary is arbitrarily small, then the loop integrals in (8.45) become approximately

$$-(\hat{\mathbf{n}} \times \hat{\mathbf{a}}) \cdot \mathbf{H}'_1 + (\hat{\mathbf{n}} \times \hat{\mathbf{a}}) \cdot \mathbf{H}'_2 = -(\hat{\mathbf{n}} \times \hat{\mathbf{a}}) \cdot \mathbf{M}_1 + (\hat{\mathbf{n}} \times \hat{\mathbf{a}}) \cdot \mathbf{M}_2. \quad (8.47)$$

Reversing the order of the cross products and using the vector identity $(\mathbf{A} \times \mathbf{B}) \cdot \mathbf{C} = \mathbf{A} \cdot (\mathbf{B} \times \mathbf{C})$ gives

$$\hat{\mathbf{a}} \cdot [\hat{\mathbf{n}} \times (\mathbf{H}'_1 - \mathbf{H}'_2)] = \hat{\mathbf{a}} \cdot [\hat{\mathbf{n}} \times (\mathbf{M}_1 - \mathbf{M}_2)]. \quad (8.48)$$

It is important to note that this analysis is equally valid for any other surface S' obtained by rotating S about the surface normal $\hat{\mathbf{n}}$. Thus, (8.48) must be true for any vector $\hat{\mathbf{a}}$ in the plane of the boundary. It follows that the quantities in the square brackets in (8.48) must also be equal:

$$\hat{\mathbf{n}} \times (\mathbf{H}'_1 - \mathbf{H}'_2) = \hat{\mathbf{n}} \times (\mathbf{M}_1 - \mathbf{M}_2). \quad (8.49)$$

We conclude that although the tangential components of \mathbf{H} are continuous at a boundary between two insulating media, there is a discontinuity in the tangential components of the effective field \mathbf{H}' .

In an infinite medium, we cannot phenomenologically distinguish between electric and magnetic susceptibilities; in boundary value problems, however, the introduction of effective electric or magnetic susceptibilities as we have done will generally change the boundary conditions. It would seem, then, that for boundary value problems we are just as well off with the conventional separation of electric and magnetic effects. However, at optical frequencies,

it is difficult to give \mathbf{M} , and therefore the magnetic susceptibility, a clear physical interpretation. For this reason, it is often argued⁴ that it is better to describe the fields with an effective permittivity and current density than to introduce \mathbf{M} . This topic is discussed in more detail in Section 8.2.2.

8.2.2 Definition of Magnetization at High Frequencies

At low frequencies, the magnetization is physically interpreted to be the magnetic dipole moment per unit volume. To understand the difficulty with interpreting \mathbf{M} at high frequencies, consider the classical magnetic moment of a finite volume of magnetic material:

$$\boldsymbol{\mu} = \frac{1}{2} \int_V \mathbf{r} \times \mathbf{J} dv, \quad (8.50)$$

where \mathbf{J} is given by (8.37), and the volume V is larger than the volume of the sample V_0 . Substituting from (8.37) for \mathbf{J} gives

$$\boldsymbol{\mu} = \frac{1}{2} \int_V \mathbf{r} \times \frac{\partial \mathbf{P}}{\partial t} dv + \frac{1}{2} \int_V \mathbf{r} \times (\nabla \times \mathbf{M}) dv. \quad (8.51)$$

The second term on the right can be integrated by parts as follows:

$$\int_V \mathbf{r} \times (\nabla \times \mathbf{M}) dv = - \oint_S \mathbf{r} \times (\mathbf{M} \times d\mathbf{s}) - \int_V (\mathbf{M} \times \nabla) \times \mathbf{r} dv. \quad (8.52)$$

The integral over the surface S surrounding V vanishes since $\mathbf{M} = 0$ outside the material and the surface is completely outside the volume of the sample V_0 . The second integral on the right-hand side can be simplified using the vector identity (Problem 8.8):

$$(\mathbf{M} \times \nabla) \times \mathbf{r} = -2\mathbf{M}. \quad (8.53)$$

Making this substitution into (8.52) and using the result in (8.51) leads to

$$\boldsymbol{\mu} = \frac{1}{2} \int_V \mathbf{r} \times \frac{\partial \mathbf{P}}{\partial t} dv + \int_V \mathbf{M} dv. \quad (8.54)$$

We see that \mathbf{M} can be interpreted cleanly as the magnetic dipole moment density only when the second term dominates the first. As shown in Problem 8.9, this requirement is satisfied when the sample dimensions are small compared to a wavelength. Since this is not satisfied at optical frequencies, the magnetization – and hence the magnetic susceptibility – do not have clear physical interpretations.

⁴ See, for example, Landau and Lifshitz [3, pp. 251–253] or Pershan [2].

We have seen in Chapters 3–5 that the presence of dipolar spin waves in a magnetic garnet film causes small time-varying perturbations in the direction of the magnetization. These perturbations can affect both the optical permittivity and permeability of the material, in principle. However, we have shown that the polarization \mathbf{P} and magnetization \mathbf{M} cannot be uniquely defined in the presence of time-varying fields. Consequently, magneto-optical effects can be modeled either with an effective permittivity, an effective permeability, or a combination of both (although modifications of the electromagnetic boundary conditions may be required). The most common approach is to model the effects with an effective permittivity, set the permeability to that of free space, and use the standard electromagnetic boundary conditions. This is equivalent to neglecting the direct interaction of the magnetic field of the wave with the medium. It is possible that careful experiments may eventually identify inadequacies with this approach to describing magneto-optical waveguide phenomena [4, 5]. In the absence of such experiments – and in the interest of simplicity – we will proceed with the common approach.

8.2.3 Symmetry Requirements on the Permittivity

Having decided to phenomenologically model magneto-optical effects with an effective permittivity, let us consider the symmetry requirements that the permittivity must satisfy. First, we know from Eq. (4.47) that the permittivity must be Hermitian for a lossless medium. Thus, if the permittivity is given by

$$\bar{\epsilon} = \bar{\epsilon}_1 + i\bar{\epsilon}_2, \quad (8.55)$$

where $\bar{\epsilon}_1$ and $\bar{\epsilon}_2$ are real, we require

$$\bar{\epsilon}^\dagger = \bar{\epsilon}_1^\dagger - i\bar{\epsilon}_2^\dagger = \bar{\epsilon}_1 + i\bar{\epsilon}_2 = \bar{\epsilon}. \quad (8.56)$$

We conclude that $\bar{\epsilon}_1$ must be symmetric and $\bar{\epsilon}_2$ must be antisymmetric.

Second, we must consider the effects of time-reversal symmetry, or reciprocity. For a reciprocal medium

$$\epsilon_{ij} = \epsilon_{ji}, \quad (8.57)$$

i.e., the coupling from $i \rightarrow j$ is the same as from $j \rightarrow i$. We know, however, that magnetic materials are *not* reciprocal. To get complete time-reversal symmetry we must also invert \mathbf{M} . Thus, we also require

$$\epsilon_{ij}(\mathbf{M}) = \epsilon_{ji}(-\mathbf{M}). \quad (8.58)$$

(This property can be rigorously shown thermodynamically and follows from what are known as the *Onsager reciprocity relations*.) Since we have gone to some length to argue that the magnetization is not well defined at optical frequencies, we must be careful to say what is meant by \mathbf{M} in (8.58) and subsequent discussions. What we mean is that the *optical* permittivity is influenced

by the direction of the *static* magnetization. Even microwave precessions of \mathbf{M} can be considered “static” when compared to the optical field oscillations. Further, \mathbf{M} is well defined at microwave frequencies since the film dimensions are small compared to microwave wavelengths.

Combining the requirements of (8.56) and (8.58), we conclude that the symmetric component $\bar{\epsilon}_1$ must depend on even powers of \mathbf{M} , and the anti-symmetric component $\bar{\epsilon}_2$ must depend on odd powers of \mathbf{M} . To lowest order in \mathbf{M} , and assuming an otherwise isotropic dielectric, the permittivity takes the form

$$\bar{\epsilon} = \epsilon_0 [\epsilon_r \bar{\mathbf{I}} + if \mathbf{M} \times \bar{\mathbf{I}}], \quad (8.59)$$

where ϵ_r is the relative permittivity of an otherwise identical non-magnetic dielectric, and the term $\mathbf{M} \times \bar{\mathbf{I}}$ is defined as in (4.72). Tensors containing the antisymmetric second term are said to be *gyrotropic*. Using matrix notation and rectangular coordinates, the permittivity (8.59) can also be written

$$\bar{\epsilon} = \epsilon_0 \begin{bmatrix} \epsilon_r & -ifM_z & ifM_y \\ ifM_z & \epsilon_r & -ifM_x \\ -ifM_y & ifM_x & \epsilon_r \end{bmatrix}. \quad (8.60)$$

The off-diagonal elements give rise to Faraday rotation in a manner analogous to that of a magnetically gyrotropic medium (Problem 4.4). If the magnetization is saturated and parallel to the direction of light propagation, the Faraday rotation (rotation angle per unit length of propagation) is found to be (Problem 8.10)

$$\phi_F = \frac{k_0 M_S f}{2\sqrt{\epsilon_r}}, \quad (8.61)$$

where k_0 is the free-space wave number and M_S is the saturation magnetization of the medium. (Note that the Faraday rotation ϕ_F as defined here differs from the total rotation angle $\theta_F = \phi_F d$, where d is the propagation distance.) Alternatively, (8.61) can be used to determine the phenomenological parameter f from measurements of ϕ_F .

8.3 Coupled-Mode Theory

As discussed in the previous section, the off-diagonal elements of the permittivity tensor (8.60) give rise to a rotation in the polarization of an electromagnetic wave as it propagates in the medium. As the polarization rotates, the energy in the mode is transferred between two orthogonal polarization states. The off-diagonal elements can be viewed as coupling the modes characterized by these polarization states. In this section, we will expand on this point of view and describe Faraday rotation using the language of coupled-mode theory [1, 6, 7].

8.3.1 Coupled-Mode Equations

For an insulating dielectric medium, Maxwell's curl equations (4.1) and (4.2) can be written as

$$\nabla \times \mathbf{E} = -\mu_0 \frac{\partial \mathbf{H}}{\partial t}, \quad (8.62)$$

$$\nabla \times \mathbf{H} = \frac{\partial \mathbf{D}}{\partial t}. \quad (8.63)$$

To better illustrate the coupled-mode formalism, we will assume that the medium is birefringent in the absence of the magnetic perturbation, and that the optic axis is parallel to the x -coordinate axis. We will further assume that the magnetization is static and saturated along the z -direction. The permittivity then takes the form

$$\bar{\epsilon} = \epsilon_0 \begin{bmatrix} \epsilon_{rx} & -ifM_S & 0 \\ ifM_S & \epsilon_r & 0 \\ 0 & 0 & \epsilon_r \end{bmatrix}. \quad (8.64)$$

Taking the curl of (8.62) and substituting (8.63) gives the wave equation for \mathbf{E} :

$$\nabla(\nabla \cdot \mathbf{E}) - \nabla^2 \mathbf{E} + \mu_0 \frac{\partial^2}{\partial t^2} (\bar{\epsilon} \cdot \mathbf{E}) = 0. \quad (8.65)$$

Let us now consider an electric field comprised of two orthogonally polarized uniform plane waves:

$$\mathbf{E} = \hat{\mathbf{x}}B\sqrt{\frac{2\omega\mu_0}{k_B}}e^{i(k_B z - \omega t)} + \hat{\mathbf{y}}A\sqrt{\frac{2\omega\mu_0}{k_A}}e^{i(k_A z - \omega t)}. \quad (8.66)$$

This represents an exact solution to the wave equation (8.65) in the absence of the magnetic perturbation if A and B are constants. The fields are normalized so that the Poynting flux (W/m^2) in the y or x polarization components is A^2 or B^2 , respectively. The dispersion relations for these two modes are (cf. Problem 4.3):

$$k_B^2 = \omega^2 \mu_0 \epsilon_0 \epsilon_{rx}, \quad (8.67)$$

$$k_A^2 = \omega^2 \mu_0 \epsilon_0 \epsilon_r. \quad (8.68)$$

In the presence of the perturbation, mode conversion can be represented by allowing A and B to be functions of z . Substituting the field (8.66) into the wave equation (8.65) and simplifying using the dispersion relations (8.67) and (8.68) leads to the equation

$$\begin{aligned} & \left[\sqrt{\frac{2\omega\mu_0}{k_B}} \left(\frac{\partial^2 B}{\partial z^2} + i2k_B \frac{\partial B}{\partial z} \right) e^{i(k_B z - \omega t)} - ik_0^2 f M_S \sqrt{\frac{2\omega\mu_0}{k_A}} A e^{i(k_A z - \omega t)} \right] \hat{\mathbf{x}} \\ & + \left[\sqrt{\frac{2\omega\mu_0}{k_A}} \left(\frac{\partial^2 A}{\partial z^2} + i2k_A \frac{\partial A}{\partial z} \right) e^{i(k_A z - \omega t)} + ik_0^2 f M_S \sqrt{\frac{2\omega\mu_0}{k_B}} B e^{i(k_B z - \omega t)} \right] \hat{\mathbf{y}} \\ & = 0. \end{aligned} \quad (8.69)$$

This can be further simplified if we assume the coefficients A and B are slowly varying on the scale of an electromagnetic wavelength. In this case

$$\left| \frac{\partial^2 A}{\partial z^2} \right| \ll \left| k_A \frac{\partial A}{\partial z} \right|, \quad \left| \frac{\partial^2 B}{\partial z^2} \right| \ll \left| k_B \frac{\partial B}{\partial z} \right|, \quad (8.70)$$

and the second derivatives in (8.69) can be neglected. Equation (8.69) can be split into two independent scalar equations using the orthogonality of the unit vectors; i.e., $\hat{\mathbf{x}} \cdot \hat{\mathbf{y}} = 0$. Alternately, dot-multiplying (8.69) with $\hat{\mathbf{y}}$ and $\hat{\mathbf{x}}$ gives the *coupled-mode equations*:

$$\frac{\partial A}{\partial z} = \kappa_{ab} B e^{-i\Delta z}, \quad (8.71)$$

$$\frac{\partial B}{\partial z} = \kappa_{ba} A e^{+i\Delta z}, \quad (8.72)$$

where

$$\kappa_{ab} = -\frac{k_0 f M_S}{2[\varepsilon_{rx} \varepsilon_r]^{1/4}} = -\kappa_{ba} \quad (8.73)$$

and

$$\Delta = k_A - k_B. \quad (8.74)$$

Coupled mode theory assumes that the two orthogonally polarized plane waves that form the solution in (8.66) continue to be eigenmodes in the presence of a perturbation in the medium. As mentioned at the beginning of Section 8.2, this is a good approximation as long as the off-diagonal elements of $\bar{\varepsilon}$ are small. For a more accurate solution, we should adopt the non-orthogonal coupled mode theory described by Haus [8, Section VI], where each eigenvector of the perturbed medium is expressed as a linear combination of the orthogonal eigenmodes of the unperturbed medium.

8.3.2 Energy Conservation

In general, the mode amplitudes A and B can be complex. In this case, the amplitudes of the modes can be normalized so that the mode powers are $|A|^2$ and $|B|^2$. By “mode power,” we mean the Poynting flux (W/m^2) for infinite uniform plane waves, the power per unit width (W/m) for planar waveguides, or the total power (W) for waveguides confined in two dimensions. For energy to be conserved, the sum of the powers in both modes must be constant with z :

$$\frac{d}{dz} (|A|^2 + |B|^2) = 0. \quad (8.75)$$

Expanding the derivatives gives

$$A \frac{dA^*}{dz} + A^* \frac{dA}{dz} + B \frac{dB^*}{dz} + B^* \frac{dB}{dz} = 0. \quad (8.76)$$

After substituting the coupled-mode equations (8.71) and (8.72) in place of the derivatives and collecting terms we obtain

$$AB^* e^{i\Delta z} (\kappa_{ab}^* + \kappa_{ba}) + c.c. = 0. \quad (8.77)$$

Since the initial mode amplitudes A, B are arbitrary, we arrive at the following constraint for the coupling constants:

$$\kappa_{ab} = -\kappa_{ba}^*. \quad (8.78)$$

The coupling constant for Faraday rotation (8.73) is a special case of this relation for κ_{ab} real.

8.3.3 Solutions to the Coupled-Mode Equations

To find general solutions to the coupled-mode equations (8.71) and (8.72), we assume trial functions of the form

$$A = [C_1 e^{i\beta_0 z} + C_2 e^{-i\beta_0 z}] e^{-i\Delta z/2}, \quad (8.79)$$

$$B = [D_1 e^{i\beta_0 z} + D_2 e^{-i\beta_0 z}] e^{i\Delta z/2}. \quad (8.80)$$

Substituting these trial functions into (8.71) and (8.72) and regrouping terms leads to

$$e^{i\beta_0 z} [(i\beta_0 - i\Delta/2)C_1 - \kappa_{ab}D_1] - e^{-i\beta_0 z} [(i\beta_0 + i\Delta/2)C_2 + \kappa_{ab}D_2] = 0, \quad (8.81)$$

$$e^{i\beta_0 z} [(i\beta_0 + i\Delta/2)D_1 - \kappa_{ba}C_1] - e^{-i\beta_0 z} [(i\beta_0 - i\Delta/2)D_2 + \kappa_{ba}C_2] = 0. \quad (8.82)$$

Since these equations must be valid for all z , the terms inside each of the brackets must vanish. Combining the four resulting equations to eliminate C_1, C_2, D_1 , and D_2 gives

$$\beta_0 = \pm \sqrt{|\kappa|^2 + (\Delta/2)^2}, \quad (8.83)$$

where

$$|\kappa| = |\kappa_{ab}| = |\kappa_{ba}|. \quad (8.84)$$

The complete solutions are found to be (Problem 8.11)

$$A(z) = e^{-i\Delta z/2} \left[A(0) \cos \beta_0 z + \frac{\kappa_{ab}B(0) + (i\Delta/2)A(0)}{\beta_0} \sin \beta_0 z \right], \quad (8.85a)$$

$$B(z) = e^{i\Delta z/2} \left[B(0) \cos \beta_0 z + \frac{\kappa_{ba}A(0) - (i\Delta/2)B(0)}{\beta_0} \sin \beta_0 z \right], \quad (8.85b)$$

where $A(0)$ and $B(0)$ are the initial mode amplitudes at $z = 0$.

As an example, consider the case $A(0) = 1$, $B(0) = 0$. The mode powers are

$$|A|^2 = \cos^2 \left[z \sqrt{|\kappa|^2 + (\Delta/2)^2} \right] + \frac{(\Delta/2)^2}{|\kappa|^2 + (\Delta/2)^2} \sin^2 \left[z \sqrt{|\kappa|^2 + (\Delta/2)^2} \right], \quad (8.86a)$$

$$|B|^2 = \frac{|\kappa|^2}{|\kappa|^2 + (\Delta/2)^2} \sin^2 \left[z \sqrt{|\kappa|^2 + (\Delta/2)^2} \right]. \quad (8.86b)$$

These equations are graphed as functions of propagation distance in Figure 8.6 for different values of the phase-matching parameter Δ . It can be easily verified that $|A|^2 + |B|^2 = 1$ and the energy conservation equation (8.75) is satisfied.

It is clear from Figure 8.6 that complete mode conversion can only occur when the modes are *phase matched*, i.e., when $\Delta = 0$. In this case, the converted mode amplitude is simply $B = \sin(|\kappa|z)$. For the case of Faraday rotation, the argument of the sine is just the angle of polarization rotation, so we conclude

$$\phi_F = |\kappa| = \frac{k_0 f M_S}{2\sqrt{\epsilon_r}}, \quad (8.87)$$

in agreement with (8.61). When the modes are phase matched, the power will be transferred completely from one mode to the other in a length

$$L_c = \frac{\pi}{2|\kappa|}. \quad (8.88)$$

If the wavelength of the light is varied instead of the propagation distance, then the phase-matching parameter Δ will change because of the dispersion

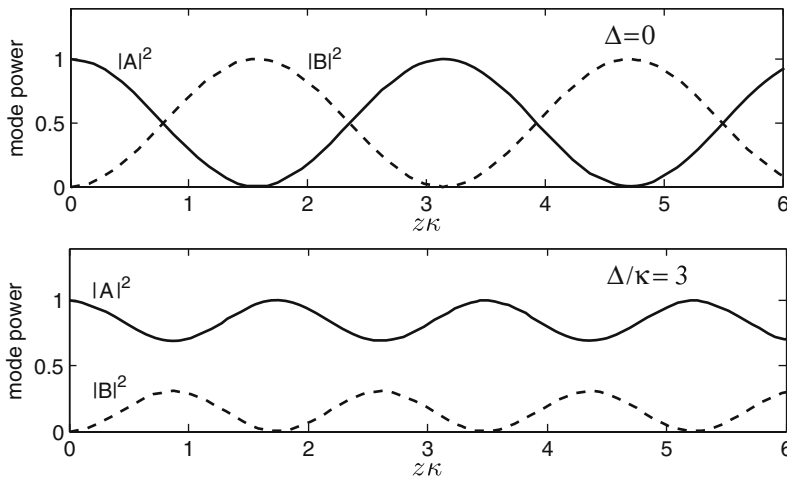


Fig. 8.6. Mode power as a function of propagation distance z for two values of the phase-matching parameter $\Delta = 0$ and $\Delta/\kappa = 3$.

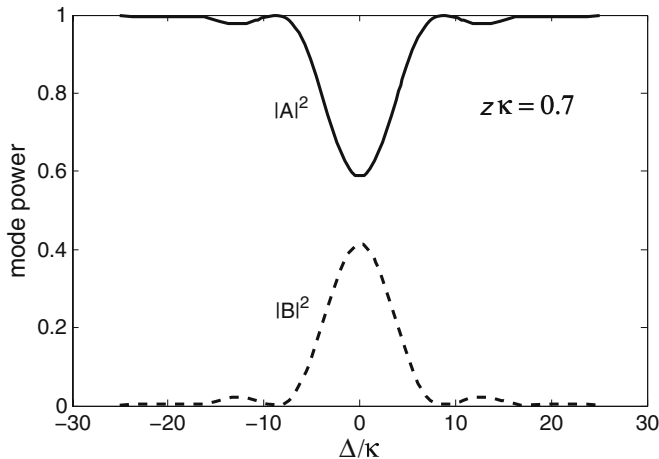


Fig. 8.7. Power in the two coupled modes as functions of the phase mismatch with a fixed propagation distance.

of the optical modes. In addition, if the coupling between the optical modes is caused by the presence of dipolar spin waves, Δ can also be varied by changing the SW wavelength. This is because the phase-matching parameter Δ depends on the SW wave number as well as the difference between the two optical wave numbers, as we will see in Section 8.4 (cf. Eq. (8.120)). In these cases, we are interested in the behavior of (8.86a) and (8.86b) as functions of the phase-matching parameter with fixed propagation distance, as shown in Figure 8.7. We see that when the wavelength is varied, the coupled-mode system can be used as either an optical notch or bandpass filter.

8.4 Scattering of Optical-Guided Modes by Forward Volume Spin Waves

We now turn our attention to obtaining the coupled-mode equations and coupling coefficients for optical modes coupled by dipolar spin waves. This is somewhat more complicated than the static magneto-optical coupling discussed earlier, since the permittivity is now a slowly varying function of time [9, 10].

8.4.1 Coupled-Mode Equations

In the presence of dipolar spin waves, the permittivity will have time-varying components with microwave frequencies. Since these variations are slow compared to optical frequencies, we can write the dielectric constitutive relation in a mixed-domain representation:

$$D_m(\omega_L) = \varepsilon_0 \varepsilon_{mn}(\omega_L, t) E_n(\omega_L), \quad (8.89)$$

where ω_L is an optical frequency, the time variations described by t are slow compared with the optical period, and summation over repeated indices is assumed.

When light is scattered from dipolar spin waves, the frequency of the light is shifted by that of the spin waves. This shift results from the nonlinear interaction between the microwave and optical fields. This nonlinear interaction is best described by Maxwell's equations in the time domain. Consequently, we need to transform the constitutive relation (8.89) from a mixed-domain representation into the time domain. To do this, we first define the Fourier transform pair:

$$F(\omega) = \int_{-\infty}^{\infty} dt e^{i\omega t} f(t), \quad (8.90)$$

$$f(t) = \int_{-\infty}^{\infty} \frac{d\omega}{2\pi} e^{-i\omega t} F(\omega). \quad (8.91)$$

Applying (8.91) to the constitutive law (8.89) gives

$$D_m(t) = \varepsilon_0 \int_{-\infty}^{\infty} \frac{d\omega}{2\pi} e^{-i\omega t} \varepsilon_{mn}(\omega, t) E_n(\omega). \quad (8.92)$$

For a monochromatic light source such as a laser, $E_n(\omega)$ will be sharply peaked about $\omega = \pm\omega_L$ and can be represented by

$$E_n(\omega) = \pi E_n [\delta(\omega + \omega_L) + \delta(\omega - \omega_L)]. \quad (8.93)$$

Substituting this into Eq. (8.92) gives the following approximate time-domain expression for $D_m(t)$:

$$D_m(t) = \frac{1}{2} \varepsilon_0 \varepsilon_{mn}(\omega_L, t) E_n e^{-i\omega_L t} + c.c. \quad (8.94)$$

Here we have used the fact that $\varepsilon_{mn}(-\omega_L, t) = \varepsilon_{mn}^*(\omega_L, t)$ as required for a real response function in time. If ε_{mn} is real, then this can be written as

$$D_m(t) = \varepsilon_0 \varepsilon_{mn}(\omega_L, t) E_n(t), \quad (8.95)$$

where $E_n(t) = E_n \cos \omega_L t$. These expressions are valid provided the time variations of ε_{mn} are slow compared with the optical period $2\pi/\omega_L$.

It is convenient to separate the non-magnetic and magnetic components of the permittivity. If the non-magnetic part of the permittivity is given by $\varepsilon_{mn}^{(0)}$, then we define the magneto-optical polarization P_m^{MO} as

$$P_m^{\text{MO}}(t) = D_m(t) - \varepsilon_0 \varepsilon_{mn}^{(0)} E_n(t), \quad (8.96)$$

where we have assumed $\varepsilon_{mn}^{(0)}$ to be real. For an insulating dielectric medium, Maxwell's curl equations (4.1) and (4.2) can be written

$$\nabla \times \mathbf{E} = -\mu_0 \frac{\partial \mathbf{H}}{\partial t}, \quad (8.97)$$

$$\nabla \times \mathbf{H} = \frac{\partial \mathbf{D}}{\partial t}. \quad (8.98)$$

Taking the curl of Eq. (8.97) and substituting (8.98) and (8.96) gives the wave equation for \mathbf{E} :

$$\nabla(\nabla \cdot \mathbf{E}) - \nabla^2 \mathbf{E} + \mu_0 \varepsilon_0 \frac{\partial^2}{\partial t^2} (\bar{\varepsilon}^{(0)} \cdot \mathbf{E}) = -\mu_0 \frac{\partial^2}{\partial t^2} \mathbf{P}^{\text{MO}}. \quad (8.99)$$

Equation (8.99) suggests that the magneto-optical polarization can be interpreted as a source that radiates the scattered field.

Note that $\nabla \cdot \mathbf{E}$ may not vanish if the dielectric is inhomogeneous or anisotropic. For example, the electric field for TM modes in a thin-film waveguide is discontinuous at the boundaries of the film. In contrast, the electric field is continuous for TE modes, and there are no field variations in the direction of the electric field. Consequently, $\nabla \cdot \mathbf{E} = 0$ is always satisfied. As a result, we will find that the coupling constant for TM \rightarrow TE conversion is more easily obtained from (8.99) than the coupling constant for TE \rightarrow TM conversion. However, because the two coupling constants are related for a lossless system by (8.78), only one of the coupling constants need be explicitly derived. We will therefore concentrate on the case of TM \rightarrow TE conversion.

The mode conversion geometry that we will consider is shown in Figure 8.8. The region of interaction is assumed to have a length L along the z -axis, but to be infinite in extent along the y -axis. Here \mathbf{k}_{TE} is the in-plane wave vector

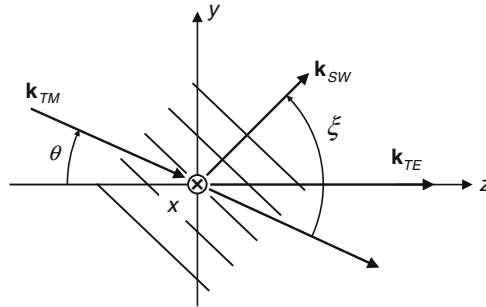


Fig. 8.8. Geometry for noncollinear SW-optical interaction. The relative magnitudes of the vectors and the angle θ are exaggerated for clarity. (Adapted with permission from [10]. © 1999 IEEE.)

for the scattered TE mode with the same magnitude as k_z determined by (8.9) along with (8.12) or (8.17). Similarly, the magnitude of \mathbf{k}_{TM} is the same as k_z determined by (8.9) along with (8.23) or (8.24). Finally, for forward volume spin waves, the magnitude of \mathbf{k}_{SW} is the same as k_t in (5.76). In the following, we assume that the deflection angle θ is small, but the angle ξ between the incident optical mode and the SW wave vector is unrestricted.

The field for an unperturbed m th order TE mode is (cf. Eq. (8.1))

$$\mathbf{E}_m(\mathbf{r}, t) = \frac{1}{2} \hat{\mathbf{y}} e_y^{(m)}(x) e^{-i(\omega_{\text{TE}} t - \mathbf{k}_{\text{TE}}^{(m)} \cdot \mathbf{r})} + \text{c.c.} \quad (8.100)$$

In the presence of the perturbation, multiple modes may be diffracted, so we take the diffracted TE field to be of the form

$$E_{y,\text{TE}}(\mathbf{r}, t) = \frac{1}{2} \sum_{m=0}^{\infty} A_m(z) e_y^{(m)}(x) e^{-i(\omega_{\text{TE}} t - \mathbf{k}_{\text{TE}}^{(m)} \cdot \mathbf{r})} + \text{c.c.} \quad (8.101)$$

where $A_m(z)$ is a slowly varying amplitude on the scale of the optical wavelength.

The total electric field is the sum of the incident and diffracted fields and must satisfy Eq. (8.99). If the two fields are at different frequencies, then Eq. (8.99) must be satisfied independently by each frequency component. The equation for the component at the frequency ω_{TE} of the diffracted field is

$$\nabla^2 E_{y,\text{TE}} + \omega_{\text{TE}}^2 \mu_0 \varepsilon_0 \varepsilon(x) E_{y,\text{TE}} = \mu_0 \frac{\partial^2}{\partial t^2} [P_y^{\text{MO}}]^{(\omega_{\text{TE}})}, \quad (8.102)$$

since there is only one component of the diffracted electric field and $\nabla \cdot \mathbf{E}_{\text{TE}}$ vanishes because the fields have no y dependence. Here, the superscript ω_{TE} on the right-hand side denotes those parts of the magneto-optical polarization synchronous with the frequency of the diffracted wave. Using the field expression (8.101), the first term in Eq. (8.102) can be written

$$\begin{aligned} \nabla^2 E_{y,\text{TE}} = & \frac{1}{2} \sum_{m=0}^{\infty} \left[A_m \nabla^2 \left(e_y^{(m)} e^{-i(\omega_{\text{TE}} t - \mathbf{k}_{\text{TE}}^{(m)} \cdot \mathbf{r})} \right) \right. \\ & \left. + \left(\frac{\partial^2 A_m}{\partial t^2} + i 2 k_{\text{TE}}^{(m)} \frac{\partial A_m}{\partial z} \right) e_y^{(m)} e^{-i(\omega_{\text{TE}} t - \mathbf{k}_{\text{TE}}^{(m)} \cdot \mathbf{r})} \right] + \text{c.c.} \end{aligned} \quad (8.103)$$

Because $A_m(z)$ is slowly varying we assume

$$\left| \frac{\partial^2 A_m}{\partial z^2} \right| \ll \left| k_{\text{TE}}^{(m)} \frac{\partial A_m}{\partial z} \right| \quad (8.104)$$

and neglect the second derivative of A_m in (8.103). Substituting (8.103) into (8.102) and using the fact that $e_y^{(m)} \exp(-i\omega_{\text{TE}}t + i\mathbf{k}_{\text{TE}}^{(m)} \cdot \mathbf{r})$ satisfies the homogeneous wave equation ((8.102) with the right-hand side set to zero) yields

$$\sum_{m=0}^{\infty} ik_{\text{TE}}^{(m)} \frac{\partial A_m}{\partial z} e_y^{(m)} e^{-i(\omega_{\text{TE}}t - \mathbf{k}_{\text{TE}}^{(m)} \cdot \mathbf{r})} + \text{c.c.} = \mu_0 \frac{\partial^2}{\partial t^2} [P_y^{\text{MO}}]^{(\omega_{\text{TE}})}. \quad (8.105)$$

The amplitude of the n th mode can be selected out of the sum by multiplying both sides of the equation by the TE mode function $e_y^{(n)}$, integrating over all x , and using the orthogonality relation (8.33). The resulting coupling equation is

$$2i\omega_{\text{TE}} \frac{\partial A_n}{\partial z} e^{-i\omega_{\text{TE}}t + i\mathbf{k}_{\text{TE}}^{(n)} \cdot \mathbf{r}} + \text{c.c.} = \frac{\partial^2}{\partial t^2} \int_{-\infty}^{\infty} e_y^{(n)}(x) [P_y^{\text{MO}}]^{(\omega_{\text{TE}})} dx. \quad (8.106)$$

8.4.2 Coupling Coefficients

We now turn our attention to evaluating the source integral on the right-hand side of (8.106). The y -component of the polarization is obtained from (8.96) using the permittivity (8.60):

$$P_y^{\text{MO}}(\mathbf{r}, t) = \frac{\varepsilon_0}{2} [ifM_z(t)E_x - ifM_x(t)E_z] + \text{c.c.} \quad (8.107)$$

The electric field components in this equation are obtained from the sum of the incident and diffracted fields. The diffracted field has only a single component along the y -direction, whereas the incident field is given in complex form by

$$\mathbf{E}_{\text{TM}}(\mathbf{r}, t) = B_m e^{-i\omega_{\text{TM}}t + i\mathbf{k}_{\text{TM}}^{(m)} \cdot \mathbf{r}} \left[\hat{\mathbf{x}}e_x^{(m)} - \hat{\mathbf{y}}\sin\theta e_z^{(m)} + \hat{\mathbf{z}}\cos\theta e_z^{(m)} \right]. \quad (8.108)$$

Here, the subscripts on the mode functions $e_x^{(m)}$ and $e_z^{(m)}$ refer to the case of propagation purely along the z -axis ($\theta = 0$), and $\mathbf{k}_{\text{TM}}^{(m)}$ is given by

$$\mathbf{k}_{\text{TM}}^{(m)} = k_{\text{TM}}^{(m)} [-\hat{\mathbf{y}}\sin\theta + \hat{\mathbf{z}}\cos\theta]. \quad (8.109)$$

Thus, the x - and z -components of the electric field are determined completely by the incident field.

For forward volume spin waves in the present coordinate system, the magnetization is of the form

$$\mathbf{M}(t) = M_S \hat{\mathbf{x}} + m_y(t) \hat{\mathbf{y}} + m_z(t) \hat{\mathbf{z}}, \quad (8.110)$$

where

$$m_i(t) = \frac{1}{2} m_{0i}(x) e^{-i\omega_{\text{SW}}t + i\mathbf{k}_{\text{SW}} \cdot \mathbf{r}} + \text{c.c.}, \quad (8.111)$$

$m_{0i}(x)$ is the mode function determined by (5.83), and $i = y, z$. Substituting the magnetization (8.110) into the polarization (8.107) gives

$$P_y^{\text{MO}}(\mathbf{r}, t) = \frac{\varepsilon_0}{2} [ifm_z(t)E_x - ifM_S E_z] + \text{c.c.} \quad (8.112)$$

The coefficient of E_x contains a time-varying magnetization component with frequency ω_{SW} . The product of this quantity with E_x will generate sum and difference frequencies that may be synchronous with ω_{TE} and contribute to mode conversion.

In contrast, the coefficient of E_z is entirely static (to lowest order in the small-signal magnetization). The static term could result in significant mode conversion at the frequency ω_{TM} if the incident and diffracted modes were properly phase matched. We will assume, however, that the mismatch $k_{\text{TE}} - k_{\text{TM}}$ is sufficiently large that significant mode conversion cannot occur without SW assistance. We will therefore neglect the static term.

The polarization component synchronous with ω_{TE} and contributing to mode conversion is, therefore

$$[P_y^{\text{MO}}(\mathbf{r}, t)]^{(\omega_{\text{TE}})} = \frac{\varepsilon_0}{2} ifm_z(t)E_x + \text{c.c.} \quad (8.113)$$

Combining Eqs. (8.106), (8.108), (8.111), and (8.113) allows us to write the coupling equation as

$$\begin{aligned} i \frac{\partial A_n}{\partial z} e^{-i\omega_{\text{TE}}t + i\mathbf{k}_{\text{TE}}^{(n)} \cdot \mathbf{r}} + \text{c.c.} = & -\frac{i\varepsilon_0\omega_{\text{TM}}B_m}{8} \int_{-\infty}^{\infty} dx f e_y^{(n)}(x) e_x^{(m)}(x) \\ & \times \left[m_{0z}(x) e^{-i(\omega_{\text{TM}} + \omega_{\text{SW}})t + i(\mathbf{k}_{\text{TM}} + \mathbf{k}_{\text{SW}}) \cdot \mathbf{r}} \right. \\ & \left. + m_{0z}^*(x) e^{-i(\omega_{\text{TM}} - \omega_{\text{SW}})t + i(\mathbf{k}_{\text{TM}} - \mathbf{k}_{\text{SW}}) \cdot \mathbf{r}} \right] + \text{c.c.} \end{aligned} \quad (8.114)$$

To obtain this result, the time derivatives on the right-hand side of the coupled-mode equation (8.106) were evaluated using the approximation $\omega_{\text{TE}} \approx \omega_{\text{TM}} \approx \omega_{\text{TM}} \pm \omega_{\text{SW}}$, which is valid to about 1 part in 10^4 . The distinctions between the frequencies are retained in the exponential arguments, however.

Both of the terms on the right-hand side of (8.114) cannot be at the frequency ω_{TE} simultaneously. To know which term to select, we must consider wave vector constraints arising from the dependence on position. Dropping the complex conjugate terms from both sides, dividing through by the factor $i \exp(i\mathbf{k}_{\text{TE}}^{(n)} \cdot \mathbf{r})$, and integrating over a length W along y gives

$$\begin{aligned}
W \frac{\partial A_n}{\partial z} e^{-i\omega_{\text{TE}} t} = & -\frac{\varepsilon_0 \omega_{\text{TM}} B_m}{8} \int_{-\infty}^{\infty} dx f e_y^{(n)}(x) e_x^{(m)}(x) \\
& \times \left[m_{0z}(x) e^{-i(\omega_{\text{TM}} + \omega_{\text{SW}})t + i(\mathbf{k}_{\text{TM}}^{(m)} - \mathbf{k}_{\text{TE}}^{(n)} + \mathbf{k}_{\text{SW}}) \cdot \hat{\mathbf{z}} z} \int_{-W/2}^{W/2} e^{i(\mathbf{k}_{\text{TM}}^{(m)} - \mathbf{k}_{\text{TE}}^{(n)} + \mathbf{k}_{\text{SW}}) \cdot \hat{\mathbf{y}} y} dy \right. \\
& \left. + m_{0z}^*(x) e^{-i(\omega_{\text{TM}} - \omega_{\text{SW}})t + i(\mathbf{k}_{\text{TM}}^{(m)} - \mathbf{k}_{\text{TE}}^{(n)} - \mathbf{k}_{\text{SW}}) \cdot \hat{\mathbf{z}} z} \int_{-W/2}^{W/2} e^{i(\mathbf{k}_{\text{TM}}^{(m)} - \mathbf{k}_{\text{TE}}^{(n)} - \mathbf{k}_{\text{SW}}) \cdot \hat{\mathbf{y}} y} dy \right]. \quad (8.115)
\end{aligned}$$

In the limit $W \rightarrow \infty$, the y integrals on the right-hand side vanish because of the oscillating integrands unless

$$(\mathbf{k}_{\text{TM}}^{(m)} - \mathbf{k}_{\text{TE}}^{(n)} \pm \mathbf{k}_{\text{SW}}) \cdot \hat{\mathbf{y}} = 0. \quad (8.116)$$

For a given interaction geometry, this condition will be satisfied by only one of the terms on the right-hand side of (8.115). Selecting out the appropriate term and using

$$e_x^{(m)}(x) = \frac{k_{\text{TM}}^{(m)}}{\omega_{\text{TM}} \varepsilon_0 \varepsilon_r(x)} h_y^{(m)}(x) \quad (8.117)$$

leads to the complex coupling equation

$$\frac{\partial A_n}{\partial z} = \kappa_{ab} B_m e^{-i\Delta z}, \quad (8.118)$$

where

$$\kappa_{ab} = -\frac{k_{\text{TM}}^{(m)}}{8} \int_{-\infty}^{\infty} dx \frac{f(x) e_y^{(n)}(x) h_y^{(m)}(x)}{\varepsilon_r(x)} \left\{ m_{0z}(x) \right\}, \quad (8.119)$$

$$\Delta = (\mathbf{k}_{\text{TE}}^{(n)} - \mathbf{k}_{\text{TM}}^{(m)} \mp \mathbf{k}_{\text{SW}}) \cdot \hat{\mathbf{z}}, \quad (8.120)$$

and

$$\omega_{\text{TE}} = \omega_{\text{TM}} \pm \omega_{\text{SW}}. \quad (8.121)$$

The upper term in the curly brackets in (8.119) goes with the upper signs in (8.120) and (8.121). In the coupling coefficient (8.119), we have explicitly shown that the relative permittivity ε and the Faraday rotation coefficient f vary with x .

From our previous discussion of coupled-mode theory, we know that maximum conversion will occur when $\Delta = 0$. Putting together the constraints on the components of the wave vectors (8.116) and (8.120) leads to the requirement

$$\mathbf{k}_{\text{TE}}^{(n)} = \mathbf{k}_{\text{TM}}^{(m)} \pm \mathbf{k}_{\text{SW}}, \quad (8.122)$$

where the upper sign goes with the upper sign in (8.121).

As an example, consider the common case of coupling between TE and TM modes of the same order ($m = n$). Usually, for an isotropic dielectric waveguide, $k_{\text{TE}} > k_{\text{TM}}$ for modes of the same order. Consequently, the coupling is via the first term on the right-hand side of (8.115) when $\mathbf{k}_{\text{TE}} \cdot \mathbf{k}_{\text{SW}} > 0$. In this case, maximum coupling occurs when the SW wave vector is adjusted so that

$$\mathbf{k}_{\text{TE}}^{(n)} = \mathbf{k}_{\text{TM}}^{(n)} + \mathbf{k}_{\text{SW}}, \quad (8.123a)$$

and the frequency of the diffracted beam will be shifted to

$$\omega_{\text{TE}} = \omega_{\text{TM}} + \omega_{\text{SW}}. \quad (8.123b)$$

Similarly, the coupling is via the second term in (8.115) when $\mathbf{k}_{\text{TE}} \cdot \mathbf{k}_{\text{SW}} < 0$. In this case, we have

$$\mathbf{k}_{\text{TE}}^{(n)} = \mathbf{k}_{\text{TM}}^{(n)} - \mathbf{k}_{\text{SW}}, \quad (8.124a)$$

$$\omega_{\text{TE}} = \omega_{\text{TM}} - \omega_{\text{SW}}. \quad (8.124b)$$

Note that the phase-matching condition in Eq. (8.122) cannot be satisfied when $\mathbf{k}_{\text{TE}} \cdot \mathbf{k}_{\text{SW}} = 0$ if $k_{\text{TE}} > k_{\text{TM}}$ as is the case for $\text{TM} \rightarrow \text{TE}$ conversion between modes of the same order. The relation between the wave vectors is discussed in more detail in Section 8.4.3.

The magnetization \mathbf{m} is related to the small-signal field \mathbf{h} by (cf. Eq. (5.83)):

$$\begin{bmatrix} m_y \\ m_z \end{bmatrix} = \begin{bmatrix} \chi & -i\kappa \\ i\kappa & \chi \end{bmatrix} \begin{bmatrix} h_y \\ h_z \end{bmatrix}. \quad (8.125)$$

Using Eq. (5.7) to relate \mathbf{h} to the magnetostatic potential ψ , the z -component of the small-signal magnetization is found to be

$$m_{0z}(x) = -ik_{\text{SW}} \phi(x) [i\kappa \sin(\xi - \theta) + \chi \cos(\xi - \theta)], \quad |x| < d/2, \quad (8.126)$$

where the transverse mode function $\phi(x)$ for the lowest-order forward volume wave mode is given by (cf. Eq. (5.80))

$$\phi(x) = \psi_0 \cos \left(\sqrt{-(1 + \chi)} k_{\text{SW}} x \right), \quad |x| < d/2, \quad (8.127)$$

and the SW wave vector is given by

$$\mathbf{k}_{\text{SW}} = k_{\text{SW}} [\hat{\mathbf{y}} \sin(\xi - \theta) + \hat{\mathbf{z}} \cos(\xi - \theta)]. \quad (8.128)$$

Examination of m_{0z} from (8.126) shows that κ_{ab} is proportional to χ in the collinear configuration ($\xi = \theta = 0$) and is proportional to κ in the transverse configuration ($\xi \approx \pi/2$). The relative coupling strength for the two configurations is therefore given by $\kappa/\chi = \omega/\omega_0$. Since $\omega > \omega_0$ when

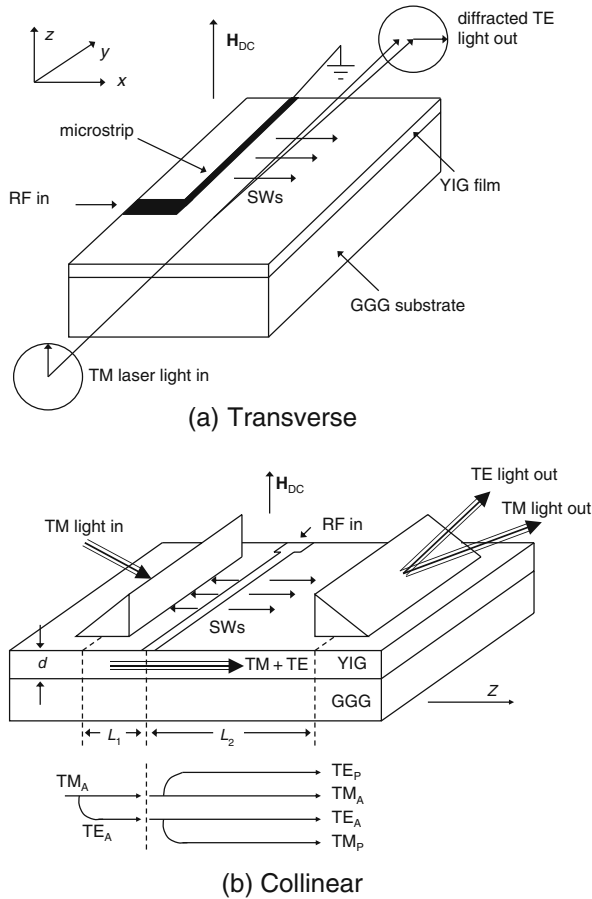


Fig. 8.9. Typical interaction geometries between dipolar spin waves, or magneto-static waves (MSWs) [12, 13]. (© 1996 IEEE.)

dipolar spin waves propagate, the coupling will be somewhat greater in the transverse configuration, although the difference is usually less than 1 %. The experimental geometry for these configurations is shown in Figure 8.9. Coupling to the optical modes can be through the edge as in Figure 8.9(a), or through the top surface using prism coupling as in Figure 8.9(b).⁵

The collinear configuration has the advantage of a longer possible interaction length, as determined by the separation between the prisms. However, the amplitude of the small signal magnetization decays along the interaction length. Very often, the optical beam in this configuration is launched into the film a short distance before the transducer. This causes multiple $\text{TM} \rightarrow \text{TE} \rightarrow \text{TM} + \text{TE}$ conversions, shown schematically in Figure 8.9(b) due

⁵ See, e.g., [11] for a discussion on coupling to optical-guided modes using prisms.

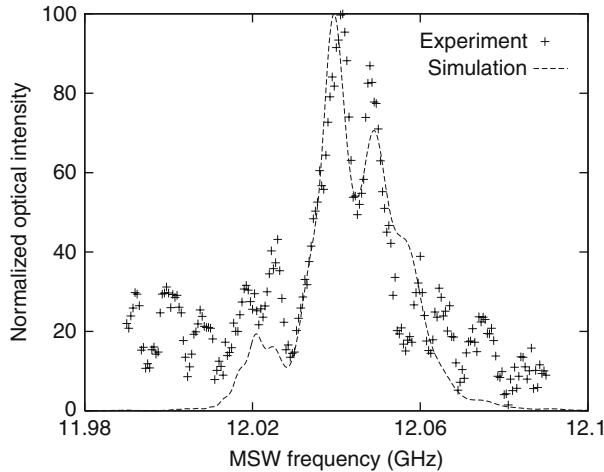


Fig. 8.10. Experimental and simulated results of multiple interaction peaks due to the effects of counter and co-propagating dipolar spin waves, or magnetostatic waves (MSWs) [13]. (© 1996 IEEE.)

to counter and co-propagating SWs relative to the direction of the optical beam [13]. Such interactions can lead to multiple SW–optical interaction peaks, as shown in Figure 8.10. The SW–optical interaction in the presence of a bidirectional parallel/antiparallel coupling coefficient has been discussed in some detail by Butler [14].

In the transverse interaction geometry, the optical beam can be focused near, or even beneath, the microstrip transducer. This yields maximum coupling between TE and TM modes. However, the length of the transducer cannot be made arbitrarily long due to practical considerations of impedance matching and propagation delays of the RF signal along the length of the microstrip. The transverse geometry is, however, advantageous when the SW–optical interaction is being used to study nonlinear spin wave excitations, discussed in Chapter 9, as these will be predominant in spatial regions close to the microstrip transducer.

8.4.3 Tightly Bound Optical Mode Approximation

As an example, let us consider the collinear geometry with $\mathbf{k}_{\text{TE}} \cdot \mathbf{k}_{\text{SW}} > 0$. Since the magnetization is nonzero only inside the film, the coupling coefficient (8.119) can be written as

$$\kappa_{ab} = -\frac{k_{\text{TM}}^{(m)} f}{8\varepsilon_r} \int_{-d/2}^{d/2} dx e_y^{(n)}(x) h_y^{(m)}(x) m_{0z}(x). \quad (8.129)$$

This can be further simplified if we assume the optical wavelength to be smaller than the film thickness and the SW wavelength to be much larger than the film thickness. Reference to Figures 8.3 and 8.4 shows that when $k_{\text{TE,TM}}d \gg 1$, the mode fields e_y and h_y almost go to zero on the film boundaries. Using the normalization conditions (8.33) and (8.34), the mode fields (8.2) and (8.19) can be approximated by

$$e_y^{(0)}(x) = 2\sqrt{\frac{\omega\mu_0}{k_{\text{TE}}^{(0)}d}} \cos\left(\frac{\pi x}{d}\right), \quad |x| \leq d/2, \quad (8.130)$$

$$h_y^{(0)}(x) = 2\sqrt{\frac{\omega\varepsilon_f}{k_{\text{TM}}^{(0)}d}} \cos\left(\frac{\pi x}{d}\right), \quad |x| \leq d/2, \quad (8.131)$$

for the lowest-order optical modes ($m = n = 0$). In contrast, if $k_{\text{SW}}d \ll 1$, then $m_{0z}(x) \approx m_{0z}$ is approximately constant through the thickness of the film. Substituting the field expressions (8.130) and (8.131) into the coupling equation (8.129) and simplifying gives (Problem 8.13)

$$\kappa_{ab} = -\frac{1}{2}\phi_F \frac{m_{0z}}{M_S}. \quad (8.132)$$

In obtaining this result, we have made the approximation $k_{\text{TM}}/k_{\text{TE}} \approx 1$. Aside from the factor of $1/2$ arising from the thickness variations of the optical mode fields, this is just the same as the static conversion coefficient (cf. Eq. (8.87)) reduced by the actual fraction of M_S pointing along the z direction.

From (8.126) and (8.127), the magnetization for $k_{\text{SW}}d \ll 1$ is approximately given by

$$m_{0z} = -ik_{\text{SW}} \chi \psi_0. \quad (8.133)$$

This can be expressed in terms of the SW power per unit width P using the normalization condition (6.55) (Problem 8.14):

$$m_{0z} = i\frac{2}{d}\sqrt{\frac{2P}{\omega\mu_0}}. \quad (8.134)$$

In deriving (8.134), we have used the approximations $k_{\text{SW}}d = -2/(1 + \chi)$ and $|\chi| \gg 1$. The coupling coefficient (8.132) can now be written

$$\kappa_{ab} = -i\frac{\phi_F}{M_S d} \sqrt{\frac{2P}{\omega\mu_0}}, \quad (8.135)$$

and the *conversion length* (8.88) becomes

$$L_c = \frac{\pi M_S d}{|\phi_F|} \sqrt{\frac{\omega\mu_0}{8P}}. \quad (8.136)$$

Although this expression was derived assuming the collinear interaction, it is also a good approximation for the transverse configuration since $\omega \approx \omega_0$ (and hence $\chi \approx \kappa$) when $k_{\text{SW}}d \ll 1$.

8.4.4 Cotton–Mouton Effect

The Cotton–Mouton (CM) effect was discovered in 1907 and refers to the interaction of light with a transverse magnetic field. It differs from the Faraday effect in that it results in *magnetic linear birefringence*. It is the magnetic analog of the *Kerr effect* familiar to most students of optics where the change in refractive index is proportional to the square of the applied field. In our case [15],

$$\Delta n \propto B^2. \quad (8.137)$$

If we consider the non-collinear SW–optical interaction geometry shown in Figure 8.8, we expect to obtain a coupling coefficient term similar to Eq. (8.119) for the Cotton–Mouton interaction. The CM tensor in magnetic films was worked out by Prokhorov and co-workers [4]. For the coordinate system shown in Figure 8.11, the CM tensor in cubic materials takes the form

$$\varepsilon_{\text{CM}} = \begin{bmatrix} g_{12} + \frac{\Delta g}{3} + 2g_{44} & 2(g_{44} + \frac{\Delta g}{3})m_y & 2(g_{44} + \frac{\Delta g}{3})m_z \\ 2(g_{44} + \frac{\Delta g}{3})m_y & g_{12} + \frac{\Delta g}{3}(1 - \sqrt{2}m_y) & \sqrt{2}\frac{\Delta g}{3}m_z \\ 2(g_{44} + \frac{\Delta g}{3})m_z & \sqrt{2}\frac{\Delta g}{3}m_z & g_{12} + \frac{\Delta g}{3}(1 + \sqrt{2}m_y) \end{bmatrix} M_S, \quad (8.138)$$

where the three independent components of the Cotton–Mouton tensor are g_{11} , g_{12} , and g_{44} and $\Delta g = g_{11} - g_{12} - 2g_{44}$. The generalized permittivity tensor (up to second-order magneto-optic effects) is the sum of ε_{CM} and the permittivity in Eq. (8.60) which describes Faraday rotation.

For long-wavelength volume spin waves with nearly circular precession ($|m_{0y}| \approx |m_{0z}| = m$), the total coupling including the Cotton–Mouton effect can be written as

$$\kappa_{ab}^{\pm} = \frac{m}{2M_S} [-\phi_F \pm \phi_{\text{CM}}] \quad (8.139)$$

where (+) or (−) correspond to the up- or down-shifted light, respectively and ϕ_{CM} is the first-order Cotton–Mouton coefficient given by

$$\phi_{\text{CM}} = \frac{2\pi g_{44} M_S^2}{\lambda \sqrt{\varepsilon_r}}, \quad (8.140)$$

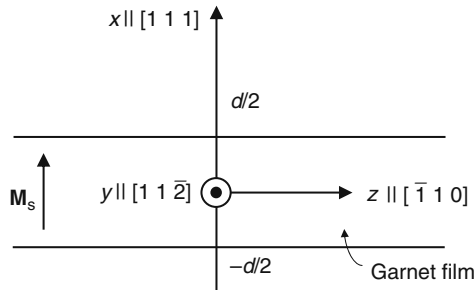


Fig. 8.11. Coordinate system for the Cotton–Mouton tensor (8.138).

where λ is the free space optical wavelength. $|\phi_{\text{CM}}| \sim 0.6|\phi_{\text{F}}|$ for YIG and depending on the interaction angle between the incident TM mode and the scattered TE mode, the Cotton–Mouton effect could aid or hamper the $\text{TM} \rightarrow \text{TE}$ mode conversion [10].

8.5 Anisotropic Bragg Diffraction

The coupling between the TE and TM modes that we have been discussing can also be viewed as a type of *Bragg diffraction* [16]. In ordinary (isotropic) Bragg diffraction, light is scattered from periodic partially reflecting planes and the wave number of the diffracted wave is equal to that of the incident wave. This leads to the familiar result that the angle of the incident wave with respect to the diffracting planes is equal to the angle of the diffracted wave. A familiar example of Bragg diffraction in solid-state physics is X-ray diffraction from crystal planes.

In the case of TE–TM mode coupling by dipolar spin waves, the incident and diffracted wave numbers differ. As a consequence, the relation between the angles of the incident and diffracted waves is more complicated. This is referred to as *anisotropic Bragg diffraction*.

While deriving expressions for the coupling coefficient, we restricted ourselves to small angular deflections. This is reasonable since accessible SW wave numbers are about two orders of magnitude smaller than the optical wave numbers. However, the frequency and wave vector sum rules (8.121) and (8.122) are not restricted to small angles. If the mode coupling is viewed as a photon-scattering process, then (8.121) is a statement of conservation of energy, and (8.122) is a statement of momentum conservation. Although the coupled-mode equations of the previous sections are needed to obtain the amplitudes of the coupled waves, the possible diffraction angles are completely described by (8.122).

The solutions of the *phase matching* (or momentum conservation) condition (8.122) can be visualized with the aid of a wave vector diagram as shown in Figure 8.12. Since both TE and TM modes propagate isotropically in the film plane, the possible TE and TM wave vectors must lie on concentric circles. The phase-matching condition (8.122) is satisfied by connecting the tips of the TE and TM wave vectors with the SW wave vector. The resulting two possible directions for \mathbf{k}_{SW} correspond to the two signs in (8.121) and (8.122) and determine whether the diffracted mode is up-shifted or down-shifted in frequency.

To obtain explicit expressions for the angles between the wave vectors, it is convenient to consider the components of (8.122) parallel and perpendicular to \mathbf{k}_{SW} . To this end, let us introduce the unit vectors $\hat{\mathbf{k}}_{\text{SW}} = \mathbf{k}_{\text{SW}}/k_{\text{SW}}$ and $\hat{\mathbf{n}} = \hat{\mathbf{x}} \times \hat{\mathbf{k}}_{\text{SW}}$. Dotting $\hat{\mathbf{n}}$ into both sides of Eq. (8.122) gives the relation between the diffraction angle, θ , and the angle of the spin wave, ξ , both referred to the TM wave vector:

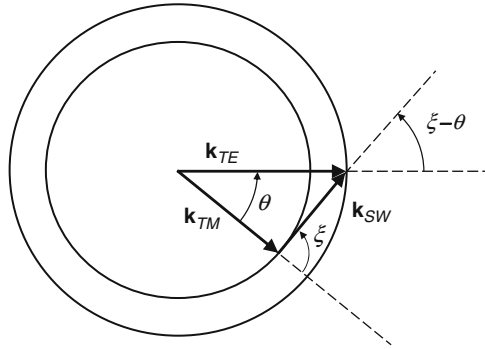


Fig. 8.12. Wave vector diagram for anisotropic Bragg diffraction. The difference between the TE and TM wave vectors has been exaggerated for clarity.

$$k_{TE} \sin(\xi - \theta_{\pm}) = k_{TM} \sin(\xi). \quad (8.141)$$

For a given ξ , there are two solutions of this equation for $-\pi < \theta < \pi$. These solutions are labeled by the subscripts \pm and correspond to the two possible signs in the phase-matching condition (8.122). The solutions to (8.141) for the lowest-order ($n = 0$) TE and TM modes in a $5\mu\text{m}$ YIG film on a GGG substrate are shown in Figure 8.13. As previously mentioned, θ is usually limited to a few degrees by the accessible range of k_{SW} . The vertical axis is expanded in Figure 8.13(b) to show this region more clearly. The greatest deflection is obtained when $\xi \approx \pi/2$ (transverse configuration) and this configuration has been used by many researchers [12, 17, 18].

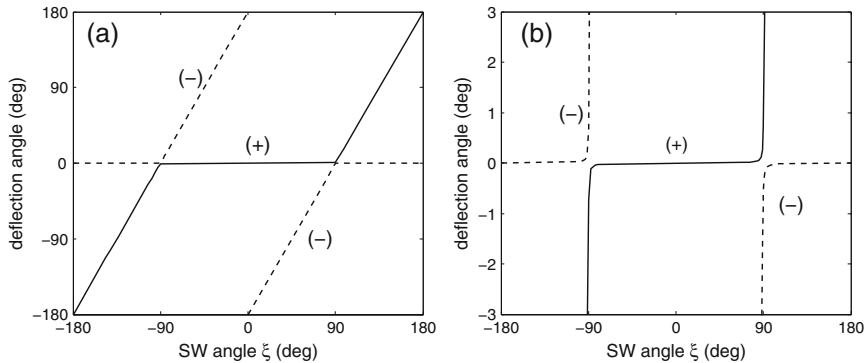


Fig. 8.13. Deflection angle θ versus spin wave angle ξ referenced to the TM beam angle. The vertical axis is expanded in part (b) to more clearly show the behavior for small deflection angles. Wave numbers used are $k_{TE}=105,204.31$ (1/cm) and $k_{TM}=105,195.86$ (1/cm). The wave numbers were calculated using the dispersion relation in Problem 8.5 using the parameters: $d = 5\mu\text{m}$, $\epsilon_c = 1$, $\epsilon_f = 4.893$, $\epsilon_s=3.783$, an optical free-space wave length of $\lambda=1.319\mu\text{m}$, and assuming lowest-order modes ($n=0$).

The required SW wave number given (θ, ξ) can be obtained by dotting $\hat{\mathbf{k}}_{\text{SW}}$ into both sides of (8.122):

$$k_{\text{SW}} = \pm[k_{\text{TE}} \cos(\xi - \theta_{\pm}) - k_{\text{TM}} \cos(\xi)]. \quad (8.142)$$

The solutions of this equation for the parameters in Figure 8.13 are shown in Figure 8.14. The required values of k_{SW} are limited to the range

$$k_{\text{TE}} - k_{\text{TM}} \leq k_{\text{SW}} \leq k_{\text{TE}} + k_{\text{TM}}. \quad (8.143)$$

In most experiments, only wave numbers corresponding to the lower half of Figure 8.13 are accessible. Thus, for the collinear interaction ($\xi = \theta = 0$), only the (+) solution is realizable and $\omega_{\text{TE}} > \omega_{\text{TM}}$. Similarly, for the antiparallel geometry ($\xi = \pi, \theta = 0$), only the (−) solution is realizable and $\omega_{\text{TE}} < \omega_{\text{TM}}$. In general, $\omega_{\text{TE}} > \omega_{\text{TM}}$ for $|\xi| < \pi/2$, and $\omega_{\text{TE}} < \omega_{\text{TM}}$ for $|\xi| > \pi/2$.

For a given SW angle ξ , Figure 8.13 gives the resulting deflection angle and Figure 8.14 gives the required SW wave number. Although this is a convenient way to display the information for experimental purposes, when discussing Bragg diffraction it is common to refer angles to the diffracting planes rather than to one of the optical beams. We can do a similar thing by defining the optical beam angles

$$\theta_{\text{TM}} = -\xi, \quad (8.144)$$

$$\theta_{\text{TE}} = \theta - \xi. \quad (8.145)$$

Note, however, that these angles are referenced to the direction of SW propagation rather than the SW constant phase planes (see Figure 8.8). These optical mode angles are plotted against SW wave number in Figure 8.15 (equivalent to combining Figures 8.13 and 8.14). Close examination of the

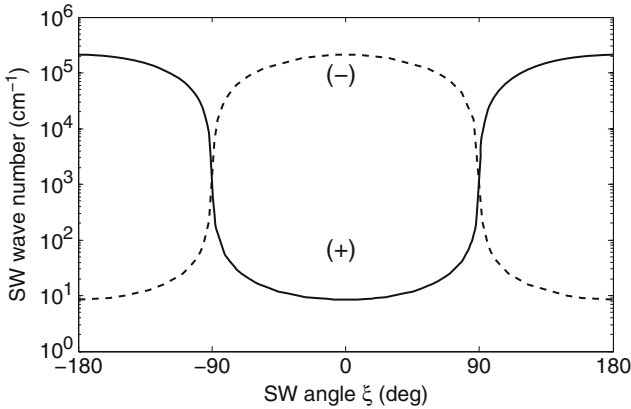


Fig. 8.14. Required SW wavelength as a function of angle with respect to the TM beam. Parameters are the same as in Figure 8.13.

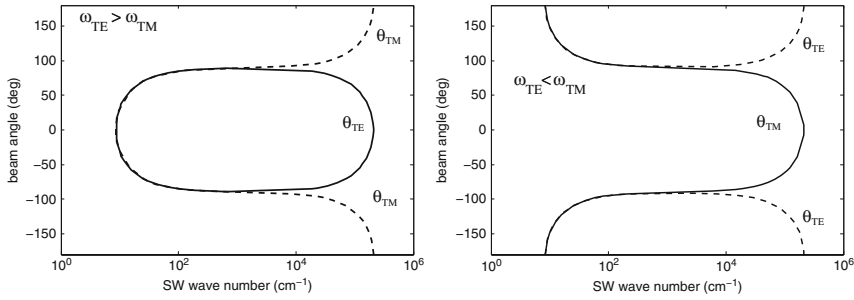


Fig. 8.15. TM and TE beam angles measured with respect to the SW propagation direction. Parameters are the same as in Figure 8.13.

figure shows that in the transverse configuration ($\theta_{TE}, \theta_{TM} \approx \pm\pi/2$), θ_{TM} varies approximately linearly with k_{SW} , while θ_{TE} is approximately independent of k_{SW} . This suggests that for TE \rightarrow TM conversion, the input angle would not need to be adjusted for a wide range of k_{SW} resulting in a wider interaction bandwidth.

Problems

8.1. Near cutoff, the propagation characteristics of guided modes in a symmetric dielectric waveguide are dominated by the outside medium as indicated by Eq. (8.15). Starting with the requirement that $\alpha_x \rightarrow 0$, show that Eq. (8.15) is valid for both even and odd TE and TM modes near cutoff.

8.2. Each branch of the tangent function in the dispersion relation (8.12) yields a separate mode solution. On each positive branch, the tangent ranges from 0 to ∞ , while $k_x d/2$ is bounded between $n\pi$ and $(n + 1/2)\pi$. If k_x is bounded, the right-hand side of (8.12) can be singular only if $\omega \rightarrow \infty$. Take the limit $\omega \rightarrow \infty$ with k_x finite in (8.9) to obtain the dispersion relation far from cutoff (8.16). Is this conclusion limited to symmetric TE modes, or does it apply to both TE and TM modes regardless of symmetry? Explain your answer.

8.3. Derive the antisymmetric TE mode dispersion relation (8.17) starting with the TE mode function

$$e_y(x) = \begin{cases} C e^{-\alpha_x x}, & x > d/2, \\ A \sin(k_x x), & |x| \leq d/2, \\ -C e^{+\alpha_x x}, & x < -d/2. \end{cases} \quad (8.146)$$

8.4. Derive the antisymmetric TM mode dispersion relation (8.24) starting with a TM mode function h_y with the same functional form as e_y in (8.146).

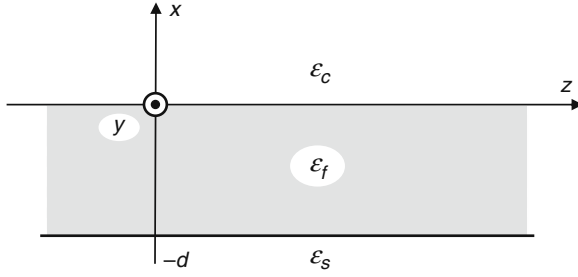


Fig. 8.16. General three-layer dielectric waveguide consisting of a cover, a film, and a substrate.

8.5. Most thin-film waveguides encountered in optical devices are not symmetric about the guiding layer. The general three-layer geometry consists of a cover, a film, and a substrate as shown in Figure 8.16.

The mode fields in this structure will be neither symmetric nor antisymmetric. Consequently, we choose a trial TE mode function of the form

$$e_y(x) = \begin{cases} A e^{-\alpha_c x}, & x > 0, \\ B \cos(k_x x) + C \sin(k_x x), & -d \leq |x| \leq 0, \\ D e^{+\alpha_s x}, & x < -d. \end{cases} \quad (8.147)$$

- Find the mode function for the z -component of the magnetic field intensity h_z .
- By requiring that e_y and h_z be continuous at $x = 0, -d$, show that the TE mode dispersion relation is

$$\tan(k_x d) = \frac{k_x(\alpha_c + \alpha_s)}{k_x^2 - \alpha_c \alpha_s}, \quad (8.148)$$

where

$$\alpha_c = \sqrt{k_z^2 - \omega^2 \mu_0 \epsilon_c}, \quad (8.149)$$

$$\alpha_s = \sqrt{k_z^2 - \omega^2 \mu_0 \epsilon_s}, \quad (8.150)$$

and k_x is defined by (8.9).

8.6. Consider the TM modes of the general dielectric waveguide shown in Figure 8.16. A suitable trial mode function is

$$h_y(x) = \begin{cases} A e^{-\alpha_c x}, & x > 0, \\ B \cos(k_x x) + C \sin(k_x x), & -d \leq |x| \leq 0, \\ D e^{+\alpha_s x}, & x < -d. \end{cases} \quad (8.151)$$

- (a) Find the mode function for the z -component of the electric field intensity e_z .
- (b) By requiring that h_y and e_z be continuous at $x = 0, -d$, show that the TM mode dispersion relation is

$$\tan(k_x d) = \frac{k_x(\tilde{\alpha}_c + \tilde{\alpha}_s)}{k_x^2 - \tilde{\alpha}_c \tilde{\alpha}_s}, \quad (8.152)$$

where

$$\tilde{\alpha}_c = \frac{\varepsilon_f}{\varepsilon_c} \alpha_c, \quad (8.153)$$

$$\tilde{\alpha}_s = \frac{\varepsilon_f}{\varepsilon_s} \alpha_s, \quad (8.154)$$

and α_c , α_s , and k_x are defined as in Problem 8.5.

8.7. In this problem, we will show that an infinite medium that is both electrically and magnetically anisotropic can be alternatively modeled with a single effective permittivity tensor for uniform plane waves.

- (a) Starting with the constitutive relations (4.19), (4.21), and (4.23), show that the relation between \mathbf{M} and \mathbf{B} is

$$\mathbf{M} = \frac{1}{\mu_0} \overline{\chi}'_m \cdot \mathbf{B}, \quad (8.155)$$

where

$$\overline{\chi}'_m = \overline{\chi}_m \cdot [\overline{\mathbf{I}} + \overline{\chi}_m]^{-1}. \quad (8.156)$$

- (b) From the discussion in Section 4.6, we know that for uniform plane waves, Maxwell's equations (8.35) and (8.36) can be written

$$\overline{\mathbf{k}} \cdot \mathbf{E} = \omega \mathbf{B}, \quad (8.157)$$

$$\overline{\mathbf{k}} \cdot \mathbf{B} = -\frac{\omega}{c^2} \mathbf{E} - i\mu_0 \mathbf{J}, \quad (8.158)$$

where

$$\mathbf{J} = -i\omega \mathbf{P} + i\overline{\mathbf{k}} \cdot \mathbf{M}, \quad (8.159)$$

and $\overline{\mathbf{k}}$ is defined by (4.72). Use Eqs. (8.155), (8.157), and (8.158) to eliminate \mathbf{M} and \mathbf{B} from the current (8.159). Finally, use the constitutive relation (4.18) to express \mathbf{J} entirely in terms of \mathbf{E} . Show that \mathbf{J} can be obtained from an effective susceptibility tensor defined as

$$\mathbf{J} = -i\omega \varepsilon_0 \overline{\chi}_e^{\text{eff}} \cdot \mathbf{E}, \quad (8.160)$$

where

$$\overline{\chi}_e^{\text{eff}} = \overline{\chi}_e - \frac{c^2}{\omega^2} \overline{\mathbf{k}} \cdot \overline{\chi}'_m \cdot \overline{\mathbf{k}}. \quad (8.161)$$

- (c) Show that Eq. (8.160) reduces to (8.42) for an electrically and magnetically isotropic medium. (Hint: Use Eq. (8.158) along with (8.157) to show that $\mathbf{k} \mathbf{k} \cdot \mathbf{E} = -i\omega\mu_0\mathbf{J}$.)

8.8. Prove the vector identity (8.53).

8.9. Consider a sphere of a magnetic-insulating material with radius R . The material is electrically isotropic with susceptibility $\chi_e = 3$. The time-varying magnetization is directed along the z -axis and is of the form

$$\mathbf{M} = M_0 e^{-i\omega t} \hat{\mathbf{z}}. \quad (8.162)$$

- (a) Using Faraday's law (8.35), show that the oscillating magnetization induces an electric field

$$E_\phi = \frac{1}{2} i\omega\mu_0 M_0 r. \quad (8.163)$$

- (b) Using the field found in part (a), evaluate the first integral on the right-hand side of the magnetic moment expression (8.54). Show that it is negligible compared to the second term only if $R \ll \lambda$.

8.10. Consider light propagation in a medium magnetized along the z -direction. From (8.60), the permittivity is of the form

$$\bar{\epsilon} = \epsilon_0 \begin{bmatrix} \epsilon_r & -i\epsilon_g & 0 \\ i\epsilon_g & \epsilon_r & 0 \\ 0 & 0 & \epsilon_r \end{bmatrix}. \quad (8.164)$$

- (a) Assuming the permeability is that of free space, evaluate (4.80) for $\mathbf{k} = k\hat{\mathbf{z}}$ and show that the normal mode dispersion relations are

$$k_\pm^2 = \omega^2 \mu_0 \epsilon_0 (\epsilon_r \pm \epsilon_g). \quad (8.165)$$

- (b) The Faraday rotation is given by (cf. Problem 4.4)

$$\phi_F = \frac{1}{2}(k_+ - k_-). \quad (8.166)$$

Find an approximation to the Faraday rotation in the limit $\epsilon_g \ll \epsilon_r$ and show that your result agrees with (8.61) if $\epsilon_g = fM_S$.

8.11. Derive the general solutions (8.85a) and (8.85b) to the coupled-mode equations (8.71) and (8.72). The following steps will assist you.

- (a) Obtain two boundary condition equations by imposing the initial values $A(0)$ and $B(0)$ on the trial solutions (8.79) and (8.80).
 (b) Using (8.81), find expressions for the ratios D_1/C_1 and D_2/C_2 . Use these ratios to eliminate D_1 and D_2 from the boundary condition equations obtained in part (a). The result is a set of two simultaneous equations for C_1 and C_2 .

- (c) Solve the equations for C_1 and C_2 obtained in part (b). Substitute the result into the trial solution (8.79), group terms, and simplify to obtain the general solution (8.85a).
- (d) Next, find expressions for the ratios C_1/D_1 and C_2/D_2 using (8.82). Use these ratios to eliminate C_1 and C_2 from the boundary condition equations obtained in part (a). The result is a set of two simultaneous equations for D_1 and D_2 .
- (e) Solve the equations for D_1 and D_2 obtained in part (d). Substitute the result into the trial solution (8.80), group terms, and simplify to obtain the general solution (8.85b).

8.12. Verify that the general coupled-mode solutions (8.85a) and (8.85b) satisfy the energy conservation relation (8.75).

8.13. Derive the expression for the coupling coefficient (8.132) by substituting the field expressions (8.130) and (8.131) into the coupling equation (8.129) and simplifying. Take m_{0z} to be approximately constant through the film thickness.

8.14. Consider the z -component of the small-signal magnetization in the limit $k_{\text{SW}}d \ll 1$.

- (a) Starting with the dispersion relation for forward volume waves (5.76), take $n = 0$ and show that

$$k_{\text{SW}}d \approx \frac{2}{-(1 + \chi)}. \quad (8.167)$$

- (b) Show that $|\chi| \gg 1$.
- (c) Using the results of parts (a) and (b), show that the normalization constant (6.55) reduces to

$$\psi_0 \approx \sqrt{\frac{2P}{\omega\mu_0}}, \quad (8.168)$$

and the small-signal magnetization (8.133) is approximated by (8.134).

8.15. Calculate the conversion length (8.136) if $M_S = 140 \text{ kA/m}$, $d = 5 \mu\text{m}$, $\omega/(2\pi) = 6 \text{ GHz}$, $P = 30 \text{ mW/mm}$, and $|\phi_F| = 0.17^\circ/\mu\text{m}$.

References

- [1] H. A. Haus, *Waves and Fields in Optoelectronics*. Englewood Cliffs, NJ: Prentice-Hall, 1984.
- [2] P. S. Pershan, "Magneto-optical effects," *J. Appl. Phys.*, vol. 38, p. 1482, 1967.
- [3] L. D. Landau and E. M. Lifshitz, *Electrodynamics of Continuous Media*. New York: Pergamon, 1960.

- [4] A. M. Prokhorov, G. A. Smolenskii, and A. N. Ageev, "Optical phenomena in thin-film magnetic waveguides and their technical application," *Sov. Phys. Usp.*, vol. 27, p. 339, 1984.
- [5] A. A. Stashkevich, "Waveguide interaction of light with spin waves in a ferromagnetic film," *Sov. Phys. J.*, vol. 32, p. 241, 1989.
- [6] A. Yariv, "Coupled-mode theory for guided-wave optics," *IEEE J. Quant. Elect.*, vol. QE-9, p. 919, 1973.
- [7] A. Yariv and P. Yeh, *Optical Waves in Crystals*. New York: John Wiley, 1984.
- [8] H. A. Haus, "Coupled mode theory," *Proc. IEEE*, vol. 79, no. 10, p. 1505, July 1991.
- [9] A. D. Fisher, "Optical signal processing with magnetostatic waves," *Circ., Syst. Signal Process.*, vol. 4, p. 265, 1985.
- [10] D. D. Stancil, "Optical-magnetostatic wave coupled-mode interactions in garnet heterostructures," *IEEE J. Quant. Elect.*, vol. QE-27, p. 61, 1991.
- [11] P. K. Tien, "Light waves in thin films and integrated optics," *Appl. Optics*, vol. 10, pp. 2395–2413, 1971.
- [12] A. Cash and D. D. Stancil, "Measurement of magnetostatic wave profiles using the interaction with transverse optical guided modes," *IEEE Trans. Mag.*, vol. 32, p. 5188, 1996.
- [13] A. Prabhakar and D. D. Stancil, "Effects of high microwave power on collinear magnetostatic – optical wave interactions," *IEEE Trans. Mag.*, vol. 32, p. 1919, 1996.
- [14] J. C. Butler, "Coupling between guided-wave optical modes – a dynamical system model," *Opt. Eng.*, vol. 46, no. 12, p. 127203, 2007.
- [15] R. V. Pisarev, I. G. Sinii, N. N. Kolpakova, and Y. M. Yakovlev, "Magnetic birefringence of light in iron garnets," *Sov. Phys. JETP*, vol. 33, p. 1175, 1971.
- [16] C. Tsai and D. Young, "Magnetostatic-forward-volume-wave-based guided-wave magneto-optic bragg cells and applications to communications and signal processing," *IEEE Trans. Microw. Theory Tech.*, vol. 38, no. 5, p. 560, 1990.
- [17] C. S. Tsai, D. Young, W. Chen, L. Adkins, C. C. Lee, and H. Glass, "Noncollinear coplanar magneto-optic interaction of guided optical wave and magnetostatic surface waves in yttrium iron garnet – gadolinium gallium garnet waveguide," *Appl. Phys. Lett.*, vol. 47, p. 651, 1985.
- [18] H. Tamada, M. Kaneko, and T. Okamoto, "TM-TE optical-mode conversion induced by a transversely propagating magnetostatic wave in a $[\text{BiLu}]_3\text{Fe}_5\text{O}_{12}$ garnet film," *J. Appl. Phys.*, vol. 64, p. 554, 1988.

Nonlinear Interactions

In Chapter 2, we introduced the Lagrangian and the Hamiltonian equations of motion. The variational formulation of Chapter 7 describes the Lagrangian as an energy density functional from which it is possible to derive the equations of motion. In the case of wave propagation, the physics of nonlinear wave interactions becomes mathematically tractable when we use the Hamiltonian formalism with the understanding that the classical spin waves can be represented by their complex amplitudes instead of Bose operators that would represent magnons. The Hamiltonian method is specifically suitable for the analysis of weakly interacting and weakly dissipative wave systems, where nonlinear interactions can be treated as higher order corrections to the lowest order wave solutions. The Hamiltonian yields first-order differential equations which are easier to solve than Lagrange's equations.

The latter part of this chapter deals with the notion of low-dimensional chaos caused by the simultaneous interactions of two or more spin wave excitations. We describe some of the basic mathematical tools used to analyze a system of nonlinear equations as well as those required to quantify experimental observations.

9.1 Large-Amplitude Spin Waves

Before we launch into the seemingly complicated world of nonlinear spin wave interactions, it is instructive to explore the lowest-order nonlinear effect that we can experimentally observe. For a film magnetized perpendicular to the plane, the internal field is reduced by a demagnetizing field numerically equal to the saturation magnetization M_S (cf. Section 5.3.1). However, spin waves with $k = 0$ are associated with a nearly circular precession of the magnetization about the film normal. As the cone angle of precession θ increases, the z -component of the magnetization is reduced by the factor $\cos \theta$ such that the total magnetization

$$M_S^2 = m_x^2 + m_y^2 + M_z^2 \quad (9.1)$$

remains constant and the amplitude of the precession is given by

$$\begin{aligned} m_\rho^2 &= m_x^2 + m_y^2 \\ &= M_S^2 \sin^2 \theta. \end{aligned} \quad (9.2)$$

Thus, as θ increases, the demagnetizing field $(-M_S \cos \theta)\hat{z}$ decreases which causes a corresponding increase in the frequency of the $k = 0$ band edge by the amount

$$\Delta\omega = \omega_M(1 - \cos \theta) \approx \omega_M \frac{\theta^2}{2}. \quad (9.3)$$

Using the normalization condition in Eq. (6.55) (cf. Problem 8.14), the small cone angle of precession¹ can be related to the power in the uniform precession spin waves as

$$|\theta| = \frac{2}{M_S d} \sqrt{\frac{2P}{\omega\mu_0}}, \quad (9.4)$$

where d is the film thickness. Combining Eqs. (9.3) and (9.4), we estimate the shift in the lower edge of the passband as

$$\frac{\Delta\omega}{P} = \frac{\omega_M}{\omega} \frac{4}{M_S^2 d^2 \mu_0}. \quad (9.5)$$

According to Eq. (9.3), the edge of the passband is expected to shift linearly towards higher frequencies as the cone angle of the uniform precession mode increases. The shift in the edge of the passband is easily visible in SW–optical interaction in the transverse geometry (cf. Figure 8.9). Figure 9.1 shows the location of the spin wave passband as a function of microwave power sampled below the transducer. In this case, the observed shift in the passband would be a combination of both nonlinear as well as thermal effects [2, 3]. However, the latter effect can be mitigated by using pulsed high-power microwave experiments with a low-duty cycle [4].

The SW–optical interaction provides a spatially accurate estimate of the precession cone angle. However, if we are primarily interested in the edge of the passband, it is possible to monitor the RF transmission characteristics and focus on the low-frequency edge of the microwave passband. A typical passband obtained for forward volume spin waves, captured using a RF scalar network analyzer, is shown in Figure 9.2. A series of similar measurements were captured at different input power levels, using the setup shown in Figure 9.3. The high-power microwave passband is measured by sweeping f , feeding the output from the device into a low-barrier Schottky diode detector (with a 10 MHz–26.5 GHz frequency response) and capturing a trace of the

¹ $\sin \theta \approx \theta$ is often referred to as being valid for *small angles*. However, by requiring that the next term in the series expansion $\theta^3/6 \lesssim 0.1\theta$ we see that $\sin \theta \approx \theta$ holds true to within a 10% error, for angles as large as 40° .

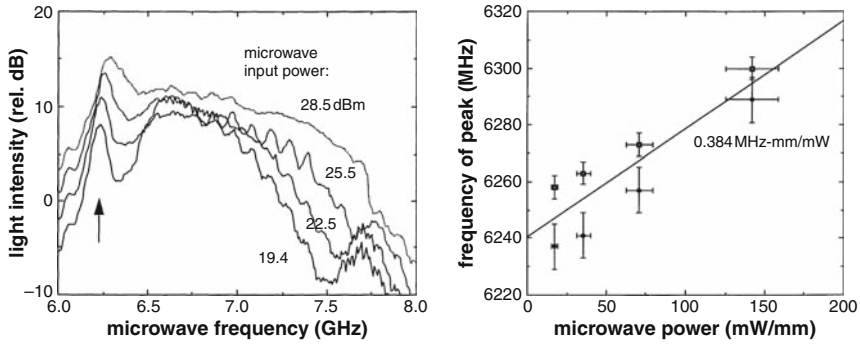


Fig. 9.1. SW-optical interaction spectra with the optical beam directly beneath the transducer for various values of total microwave input power. The arrow in (a) marks the edge of the microwave passband at low power, which shifts towards higher frequencies as the cone angle of precession increases. The external bias field was 0.457 T (4.57 kG) [1]. (© 1996 IEEE.)

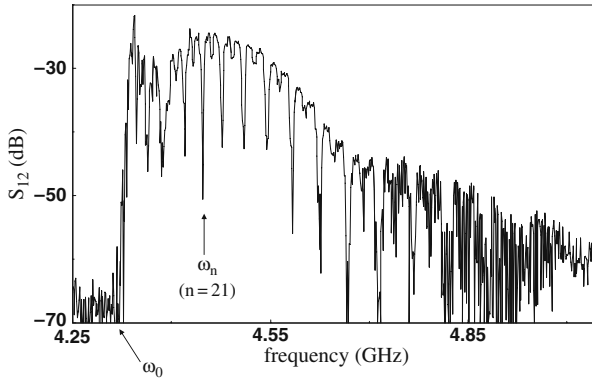


Fig. 9.2. Microwave passband for forward volume spin waves in a film with thickness $d = 5.9 \mu\text{m}$ and $M_S = 140 \text{ kA/m}$. The arrow at ω_n is the location of a *dipole gap*, described further in Section 9.4.3. (Data from [5].)

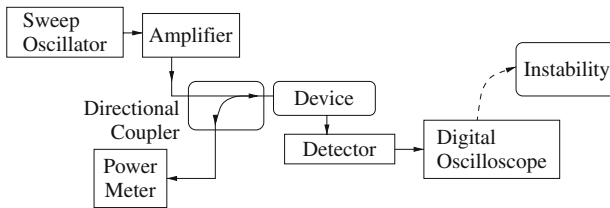


Fig. 9.3. Experimental configuration used to measure a high-power microwave passband by sweeping input frequency or to capture a time series at a constant input frequency and input power. Less than 10% of the power was reflected from the device and picked up by the power meter. (Reprinted with permission from [51]. Copyright 2000, American Institute of Physics.)

output voltage on a digital oscilloscope. When the oscilloscope is triggered along with the frequency sweep, the DC signal traced out on the oscilloscope is proportional to the RF power detected at f , thus giving us a measure of the transmission characteristics. The two-input parameter data set (P_{in} and f) can be viewed as a gray-scale density plot shown in Figure 9.4. By restricting ourselves to three grayscale levels, we highlight certain characteristic features:

- The lower edge of the passband is marked by dark circles that shift toward higher frequencies in accordance with Eq. (9.5).
- Around 17.5 dBm of input power, we observe that the white region extends down into the shaded areas in multiple “finger-like” regions.
- The vertical dots at 5.3 GHz are the locations at which we captured the microwave spectrum on a RF spectrum analyzer. From Figure 9.5, we observe that as we increase the input power and move into one of the white finger regions, the output signal develops additional frequency components and eventually becomes a broadband spectrum. Hence, we refer to these regions as *fingers of auto-oscillation*.

The broadband spectral characteristics are representative of highly nonlinear interactions within the spin wave manifold and serve to motivate our discussions in the latter parts of this chapter.

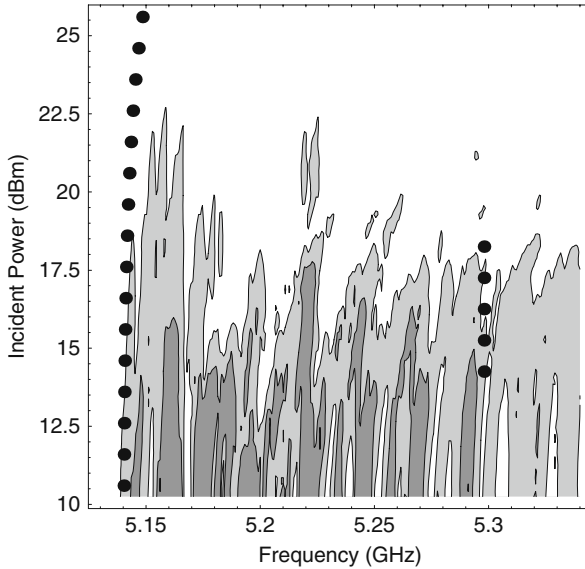


Fig. 9.4. Three level contour plot of the transmission characteristics of a SW delay line using different input RF power levels. The dark circles at the left mark the shift in the edge of the passband evaluated using Eq. (9.5) with $|\gamma| = 2\pi(28 \text{ GHz/T})$, $M_S = 140 \text{ kA/m}$, and $d = 5.9 \mu\text{m}$. (Reprinted with permission from [5]. Copyright 1998 by the American Physical Society.)

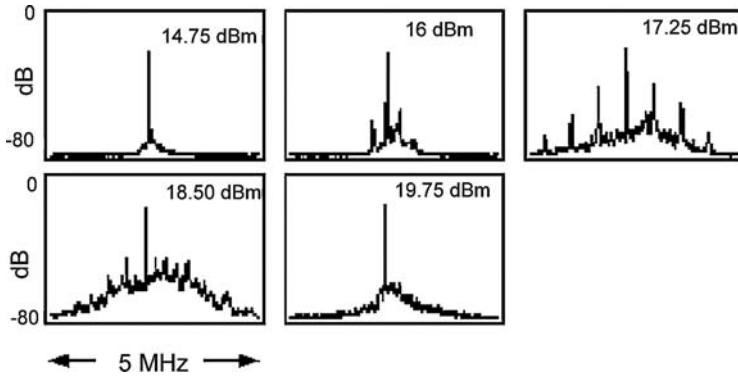


Fig. 9.5. Power spectrum of forward volume spin waves corresponding to the locations marked by the vertical dots at 5.3 GHz in Figure 9.4. (Reprinted with permission from [5]. Copyright 1998 by the American Physical Society.)

9.1.1 Foldover and Bistability

In 1958, while experimenting with YIG discs, Weiss postulated that above a “threshold signal level, the resonance response curve folds over to lower DC field values and to higher frequencies” [6]. Figure 9.6 shows the schematic progression from a typical low-frequency resonance to *foldover* as the pumping field is increased. The effects of large amplitude spin wave precession are best observed when the experimental device is tuned such that the critical input power for *bistability* lies below the threshold for other nonlinear effects [7, 8]. Calculations for SWs excited by a microstrip transducer in a yttrium–iron–garnet (YIG) film indicate that we can indeed establish the desired operating

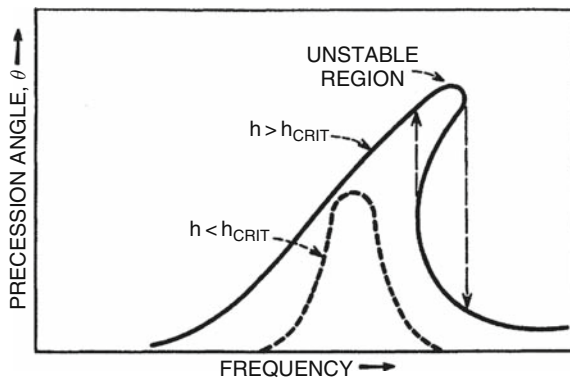


Fig. 9.6. Distortion in the FMR resonance response due to increased pump field, as envisaged by Weiss. (Reprinted with permission from [6]. Copyright 1958 by the American Physical Society.)

conditions. Such a bistable response was experimentally observed by Fetisov and Patton [3].

To gain an understanding of the origin of this foldover effect, we model the spin wave system as a nonlinear resonator. A resonator is usually classified in terms of its quality factor, Q , and the full width at half maximum, Δ , of its frequency response. The output power, P_{out} , is related to the low-power resonance frequency, f_0 , the input power, P_{in} , and input frequency, f , as

$$P_{\text{out}} = \frac{A P_{\text{in}}}{[f - f_0]^2 + \Delta^2} . \quad (9.6)$$

Q and the peak power in the resonator are defined by the constants A and Δ such that

$$Q = \frac{f_0}{2\Delta} \quad \text{and} \quad \lim_{f \rightarrow f_0} P_{\text{out}} \approx \frac{A P_{\text{in}}}{\Delta^2} . \quad (9.7)$$

Assuming that the output is proportional to the power in the spin wave excitations P_{SW} , we incorporate the dependence of the resonance frequency on SW amplitude by re-writing (9.6) as

$$P_{\text{SW}} = \frac{A' P_{\text{in}}}{[f - (f_0 + \alpha P_{\text{SW}})]^2 + \Delta^2} , \quad (9.8)$$

where αP_{SW} represents the linear shift in the observed frequency characteristics defined in (9.5) and A' represents the efficiency of coupling into the spin wave system. As described in Section 9.1, an increase in θ is accompanied by a reduction in the demagnetizing field within the thin-film sample [1]. For the case of SWs excited by a microstrip transducer, P_{in} and P_{SW} refer to the power per unit width. The coefficient α is obtained from Eq. (9.5) as

$$\alpha = \frac{1}{2\pi} \left(\frac{4|\gamma|}{\omega M_S d^2} \right) . \quad (9.9)$$

The cubic relation between P_{in} and P_{SW} , described by (9.8), is plotted in Figure 9.7.

A region of bistability is well defined when we obtain real values of P_{SW} that satisfy

$$\frac{\partial P_{\text{in}}}{\partial P_{\text{SW}}} = 0 . \quad (9.10)$$

Combining (9.8) and (9.10), we solve for the real roots of

$$3(\alpha P_{\text{SW}})^2 - 4\alpha P_{\text{SW}}(f - f_0) + \Delta^2 + (f - f_0)^2 = 0 \quad (9.11)$$

to obtain the following condition for observing bistability:

$$f > f_0 + \sqrt{3}\Delta . \quad (9.12)$$

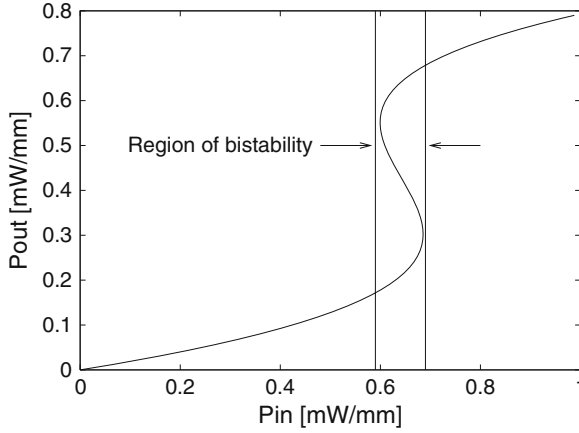


Fig. 9.7. Estimated response of a thin-film ferrite resonator with $A' = 1$, $2\Delta = 1.5$ MHz, $f - f_0 = 1.6$ MHz, and $\alpha = 2.5$ MHz mm/mW, assuming that $P_{\text{out}} = P_{\text{SW}}$. (Reprinted with permission from [9]. Copyright 1999, American Institute of Physics.)

FMR Response

To establish the similarity between the foldover of the FMR response and a bistability in the output power of the resonator, Eq. (9.11) is solved for the two cases

- (a) increasing and decreasing input power at a fixed input frequency and
- (b) sweeping input frequency up and down while keeping input power fixed.

Both calculations yield similar results and the latter case is shown in Figure 9.8. A bistability in P_{SW} occurs for values of $f - f_0$ that lie between the solid and dashed vertical lines.

Experimental verification of forward volume spin wave bistability in a ferrite resonator was obtained by Fetisov and co-workers [3] on a $1 \text{ mm} \times 1 \text{ mm} \times 4.9 \mu\text{m}$ YIG film. Figure 9.9 shows the results of the reflections from the resonator for various levels of input power as the input frequency is swept. The dashed line indicates the location of the FMR frequency at very low-power levels and, as expected, we observe a shift away from the resonance frequency as we increase the input power levels. Upon accounting for this shift and by pumping the resonator a fixed frequency away from the FMR resonance frequency, we observe, in Fig. 9.9(b), a change in reflected power of between 1 and 2 dB. By using pulsed power, Fetisov et al. also established that the bistability was intrinsic to the large-amplitude spin waves and not caused by thermal effects. In a more recent paper, Fetisov and Patton provide a detailed explanation of the foldover and bistability in FMR observations and the differences between experimental observations on thick and thin films [10].

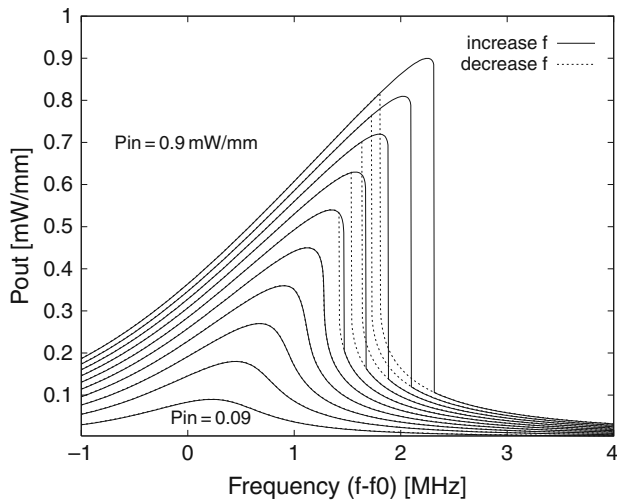


Fig. 9.8. Simulated foldover effect in the FMR response of a thin-film ferrite resonator with $\alpha = 2.5$ MHz mm/mW and $A' = 1$. The hysteretic response is obtained by solving (9.8) as $f-f_0$ is swept in opposite directions. (Reprinted with permission from [9]. Copyright 1999, American Institute of Physics.)

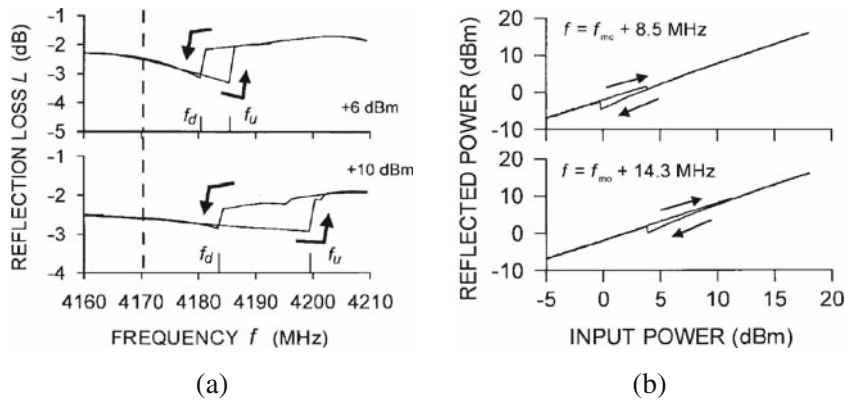


Fig. 9.9. Bistability in the FMR response from a thin-film YIG resonator (a) in the presence of a saturating magnetic field applied perpendicular to the film and (b) keeping the difference between the pumping and the resonance frequency constant. Further details of the experimental configuration and the measurement apparatus are available in [3]. (© 1999 IEEE.)

9.2 Hamiltonian Equations of Motion

In the classical mechanics of a particle, we typically use the dynamical variables q and p to represent the coordinate and momentum. The Hamiltonian equations for systems with a single degree of freedom have the form [11]

$$\dot{q} = \frac{\partial \mathcal{H}}{\partial p}, \quad \dot{p} = -\frac{\partial \mathcal{H}}{\partial q}, \quad (9.13)$$

where the dot specifies the total time derivative and \mathcal{H} is the Hamiltonian function. We recall from Eq. (1.43), that $\mathcal{H} = T + V$ is the system energy expressed as the sum of kinetic (T) and potential (V) energies. Consider the example introduced in Chapter 2, as part of our discussion on the simple harmonic oscillator, of a mass m connected to a spring with spring constant k . The Hamiltonian is formed by summing the kinetic energy of the mass with the potential energy of the spring:

$$\begin{aligned} \mathcal{H} &= \frac{1}{2}mv^2 + \frac{1}{2}kq^2 \\ &= \frac{p^2}{2m} + \frac{1}{2}kq^2, \end{aligned} \quad (9.14)$$

where q is the displacement and $p = mv = m\frac{dq}{dt}$ is the momentum. The Hamiltonian equations (9.13) become

$$\frac{dq}{dt} = \frac{\partial \mathcal{H}}{\partial p} = \frac{p}{m} \quad (9.15a)$$

and

$$\frac{dp}{dt} = -\frac{\partial \mathcal{H}}{\partial q} = -kq. \quad (9.15b)$$

The first equation restates our definition of the momentum, $p = mv$. The second equation is recognized as Newton's law $F = ma$, where $F = -kq$ is the force from the spring, and $\dot{p} = m\ddot{q}$.

Following the treatment by Cohen-Tannoudji et al. [12], we use canonical quantization to go over to quantum theory starting from classical theory. The recipe for canonical quantization consists of the following steps:

- identify a suitable Lagrangian and reproduce the equations of motion,
- identify the independent dynamical variables,
- obtain the canonical momenta conjugate to the independent variables,
- form the Hamiltonian, and
- replace the dynamical variables by the equivalent operators in a multidimensional space.

Let $\mathcal{L}(q_j, \dot{q}_j)$ be the Lagrangian (density) that describes some classical system. The generalized coordinates $q_j(t)$ and generalized velocities $\dot{q}_j(t)$ are the independent variables. The principle of least action² states that the equations of motion are obtained by minimizing the so-called action, S , given by:

$$S = \int_{t_1}^{t_2} dt \mathcal{L}(q_j, \dot{q}_j). \quad (9.16)$$

The canonical momentum p_j conjugate to \dot{q}_j is defined as:

$$p_j = \frac{\partial \mathcal{L}}{\partial \dot{q}_j} \quad (9.17)$$

with the the Hamiltonian

$$\mathcal{H} = \sum_j p_j \dot{q}_j - \mathcal{L}(q_j, \dot{q}_j). \quad (9.18)$$

The momenta and co-ordinates are considered as operators in a space of suitable dimension and satisfy the commutation relations

$$\begin{aligned} [p_j, q_i] &= \delta_{ij}, \\ [q_j, q_i] &= 0, \\ [p_j, p_i] &= 0. \end{aligned} \quad (9.19)$$

One advantage of the Hamiltonian equations (9.13) is that they lend themselves to a symmetrical representation when we introduce new canonical variables

$$a = \frac{1}{\sqrt{2}}(p + iq), \quad (9.20a)$$

$$a^* = \frac{1}{\sqrt{2}}(p - iq), \quad (9.20b)$$

such that (cf. Problem 9.1)

$$\dot{a} = i \frac{\partial \mathcal{H}}{\partial a^*}, \quad \dot{a}^* = -i \frac{\partial \mathcal{H}}{\partial a}. \quad (9.21)$$

The complex amplitudes, a^* and a , are the classical analogs of the creation and annihilation operators used in quantum mechanics, though we have used a slightly different notation than that used in Chapter 2. The present notation is chosen because of its similarity to the Landau–Lifshitz equation of motion, as we will see in Section 9.3. We will also see that these canonical variables are not unique and it is possible to use canonical transformations to obtain new variables that also satisfy the Hamiltonian equations of motion.

² This is analogous to minimizing the functional (7.27) in Section 7.3.

9.3 Spin Wave Interactions³

As the amplitude of spin wave precession increases, a number of nonlinear effects begin to surface. These effects manifest themselves in a variety of ways and can be observed experimentally and can also be exploited in the design of nonlinear devices.

In the absence of dissipation, the equation of motion for the magnetization is given by the lossless Landau–Lifshitz equation (3.104)

$$\dot{\mathbf{M}} = \gamma\mu_0 \mathbf{M} \times \mathbf{H}_{\text{eff}}. \quad (9.22)$$

The effective field \mathbf{H}_{eff} is defined as the functional derivative (cf. Eq. (7.8)) of the total energy density

$$\mathbf{H}_{\text{eff}} = -\frac{1}{\mu_0} \frac{\delta W}{\delta \mathbf{M}} = -\frac{1}{\mu_0} \left[\frac{\delta W}{\delta M_x} \hat{\mathbf{x}} + \frac{\delta W}{\delta M_y} \hat{\mathbf{y}} + \frac{\delta W}{\delta M_z} \hat{\mathbf{z}} \right]. \quad (9.23)$$

Consider a ferrite sample in the presence of a saturating field along the $\hat{\mathbf{z}}$ direction. We expect the magnetization will precess about $\hat{\mathbf{z}}$, subject to the condition

$$M_x^2 + M_y^2 + M_z^2 = M_S^2. \quad (9.24)$$

Because of this constraint, M_z can be expressed in terms of M_x , M_y so that the energy density W is only a function of M_x , M_y . In this form, $\delta W/\delta M_z = 0$, and M_x , M_y determine the dynamics of the system. The equations of motion for these components can be obtained from (9.22) combined with (9.23):

$$\dot{M}_x = \gamma M_z \frac{\delta W}{\delta M_y}, \quad (9.25a)$$

$$\dot{M}_y = -\gamma M_z \frac{\delta W}{\delta M_x}. \quad (9.25b)$$

Recall our discussion of Section 3.8, where we introduced the resonant and non-resonant eigenmodes of precession:

$$M_{\pm} = M_x \pm iM_y, \quad (9.26a)$$

such that

$$M_x = \frac{1}{2}(M_+ + M_-), \quad (9.26b)$$

$$M_y = \frac{-i}{2}(M_+ - M_-). \quad (9.26c)$$

Multiplying (9.25b) by i and adding the result to (9.25a) gives

³ This section relies on theory outlined by Schlömann [13] and by L'vov [14].

$$\dot{M}_+ = -i\gamma M_z \left(\frac{\delta W}{\delta M_x} + i \frac{\delta W}{\delta M_y} \right). \quad (9.27)$$

To express the right-hand side in terms of the variables M_\pm , we note that

$$\frac{\delta W}{\delta M_\pm} = \frac{\delta W}{\delta M_x} \frac{\partial M_x}{\partial M_\pm} + \frac{\delta W}{\delta M_y} \frac{\partial M_y}{\partial M_\pm}. \quad (9.28)$$

Using Eqs. (9.26b) and (9.26c) to obtain the partial derivatives in (9.28) leads to

$$2 \frac{\delta W}{\delta M_\pm} = \frac{\delta W}{\delta M_x} \mp i \frac{\delta W}{\delta M_y}. \quad (9.29)$$

Comparing this result with the right-hand side of (9.27) allows us to write

$$\dot{M}_+ = -2i\gamma M_z \frac{\delta W}{\delta M_-}. \quad (9.30a)$$

Similarly, we find that

$$\dot{M}_- = 2i\gamma M_z \frac{\delta W}{\delta M_+}. \quad (9.30b)$$

For small-precession angles $M_z \approx M_S$, and we observe that (9.30) takes on the canonical form (9.21) when

$$a = M_+ [-2\gamma M_S]^{-1/2} \quad (9.31a)$$

and

$$a^* = M_- [-2\gamma M_S]^{-1/2}. \quad (9.31b)$$

For larger precession angles, $M_z \approx M_S$ is no longer a good approximation. As was described in Section 9.1, we expect that M_z will decrease as the cone angle of precession increases, and the variables M_\pm will show a corresponding increase in magnitude. Since

$$M_+ M_- = M_x^2 + M_y^2, \quad (9.32)$$

(9.24) can be written as

$$M_z^2 = M_S^2 - M_+ M_- . \quad (9.33)$$

Our transformation from M_\pm to a, a^* in (9.31) must, therefore, incorporate a scaling function that depends on the square of the amplitude $|a|^2 = a^* a$. Thus, given the equations of motion (9.30), we want to find a transformation

$$M_+ = a f(a^* a) \sqrt{-2\gamma M_S}, \quad (9.34a)$$

$$M_- = a^* f(a^* a) \sqrt{-2\gamma M_S}, \quad (9.34b)$$

such that

$$\dot{a} = i \frac{\delta W}{\delta a^*}, \quad \dot{a}^* = -i \frac{\delta W}{\delta a}. \quad (9.35)$$

Since we must recover Eqs. (9.31) in the limit of a small-precession angle, we require $f(0) = 1$. To find $f(a^*a)$, we differentiate (9.34) with respect to time, use (9.35) for the resulting time derivatives \dot{a} and \dot{a}^* appearing on the right-hand side, and then express the variational derivatives $\delta W/\delta a$, $\delta W/\delta a^*$ in terms of $\delta W/\delta M_{\pm}$. The result is a differential equation for f which has a solution (see Problem 9.2 for details of this calculation)

$$f = \sqrt{1 + \frac{\gamma a a^*}{2M_S}}. \quad (9.36)$$

Using this expression, the z -component of the magnetization takes on an appealingly simple form in terms of a^*a :

$$\begin{aligned} M_z &= [M_S^2 - M_+ M_-]^{1/2} \\ &= [M_S^2 - a^* a f^2 (-2\gamma M_S)]^{1/2} \\ &= \left[M_S^2 + 2\gamma M_S a^* a \left(1 + \frac{\gamma a^* a}{2M_S} \right) \right]^{1/2} \\ &= [(M_S + \gamma a^* a)^2]^{1/2} \\ M_z &= M_S + \gamma a^* a. \end{aligned} \quad (9.37)$$

Combining (9.36) and (9.34) allows the variables M_{\pm} to be written

$$M_+ = a \sqrt{-2\gamma M_S} \sqrt{1 + \frac{\gamma a^* a}{2M_S}}, \quad (9.38)$$

$$M_- = a^* \sqrt{-2\gamma M_S} \sqrt{1 + \frac{\gamma a^* a}{2M_S}}. \quad (9.39)$$

In Chapter 2, we introduced the Holstein–Primakoff transformation [15] that related the spin raising and lowering operators \mathbf{S}_{\pm} to the spin deviation creation and annihilation operators a^* and a , respectively. Our transformation from M_{\pm} to a and a^* should be interpreted as the classical equivalent of the Holstein–Primakoff transformation, given by (2.149) and (2.150), with the canonical variables representing the complex amplitudes of classical spin wave excitations. Similarly, the pictorial representation of magnon interactions in Figure 2.4 is also applicable to the present classical formulation.

The energy density W when expressed in terms of a and a^* becomes the Hamiltonian function $\mathcal{H}(a, a^*)$. The canonical variables a and a^* are naturally suited to describe the total spin wave energy in the system. The functional $\mathcal{H}(a, a^*)$ can be expanded in a power series:

$$\mathcal{H}(a, a^*) = \mathcal{H}^{(0)} + \mathcal{H}^{(1)} + \mathcal{H}^{(2)} + \cdots, \quad (9.40)$$

where each term on the right is also a function of the canonical variables a and a^* . The lowest order term $\mathcal{H}^{(0)}(0, 0)$ does not shed any light on the dynamics since $\delta\mathcal{H}(0, 0)/\delta a = 0$. We assume that the medium is in equilibrium in the absence of spin waves, i.e., $\mathcal{H}(a^*, a)$ has a minimum for $a = a^* = 0$ such that the first-order term $\mathcal{H}^{(1)} = 0$. Hence, it is conventional to begin with contributions to the Hamiltonian that are second order in a and a^* . Let us first express the complex amplitudes as a linear combination of propagating spin wave modes using the Fourier transform pair (normalized with respect to the sample volume)

$$a_{\mathbf{k}} = \frac{1}{V} \int a(\mathbf{r}, t) e^{-i\mathbf{k} \cdot \mathbf{r}} d^3r, \quad (9.41a)$$

$$a(\mathbf{r}, t) = \sum_{\mathbf{k}} a_{\mathbf{k}}(t) e^{i\mathbf{k} \cdot \mathbf{r}}. \quad (9.41b)$$

The second-order Hamiltonian is written in the general form⁴

$$\mathcal{H}^{(2)} = \sum_{\mathbf{k}} \left(A_{\mathbf{k}} a_{\mathbf{k}}^* a_{\mathbf{k}} + \frac{1}{2} [B_{\mathbf{k}} a_{\mathbf{k}}^* a_{-\mathbf{k}}^* + B_{\mathbf{k}}^* a_{\mathbf{k}} a_{-\mathbf{k}}] \right), \quad (9.42)$$

where we are yet to determine the coefficients $A_{\mathbf{k}}$ and $B_{\mathbf{k}}$. In Section 9.3.2, we show how these coefficients can be derived starting from the Landau–Lifshitz equation of motion. Let us focus instead on interpreting the Hamiltonian equations of motion that now take the form,

$$\dot{a}_{\mathbf{k}} = i \frac{\partial \mathcal{H}}{\partial a_{\mathbf{k}}^*}, \quad \dot{a}_{\mathbf{k}}^* = -i \frac{\partial \mathcal{H}}{\partial a_{\mathbf{k}}}. \quad (9.43)$$

When we consider only the first term in $\mathcal{H}^{(2)}$, the equations (9.43) can be written as

$$\dot{a}_{\mathbf{k}} = i A_{\mathbf{k}} a_{\mathbf{k}}, \quad \dot{a}_{\mathbf{k}}^* = -i A_{\mathbf{k}} a_{\mathbf{k}}^*, \quad (9.44)$$

which have time harmonic solutions of the form $e^{\pm i\omega_{\mathbf{k}} t}$, where $\omega_{\mathbf{k}} \equiv A_{\mathbf{k}}$. However, when we include the second term of (9.42) and evaluate (9.43), the variables $a_{\mathbf{k}}$ and $a_{\mathbf{k}}^*$ represent elliptical, instead of circular, precession. To recover the resonant circular form, we must invoke a second change of variables via the *Bogoliubov transformation*. Let us define the new variables

$$b_{\mathbf{k}} = u_{\mathbf{k}} a_{\mathbf{k}} + v_{\mathbf{k}} a_{-\mathbf{k}}^* \quad (9.45a)$$

$$b_{\mathbf{k}}^* = u_{\mathbf{k}}^* a_{\mathbf{k}}^* + v_{\mathbf{k}}^* a_{-\mathbf{k}} \quad (9.45b)$$

and require that the Hamiltonian return to the diagonal form

$$\mathcal{H}^{(2)} = \sum_{\mathbf{k}} \omega_{\mathbf{k}} b_{\mathbf{k}}^* b_{\mathbf{k}}. \quad (9.46)$$

⁴ Here, $a_{\mathbf{k}}^* \equiv (a_{\mathbf{k}})^* = (a^*)_{-\mathbf{k}}$.

Factoring out a phase term in (9.45) does not affect the final form of (9.46), but allows us to assume that $u_{\mathbf{k}}$ is real while $v_{\mathbf{k}}$ is complex. Substituting (9.45) into (9.46), and requiring that the ensuing equation coincides with (9.42), results in the following conditions:

$$\omega_{\mathbf{k}}[u_{\mathbf{k}}^2 + |v_{\mathbf{k}}|^2] = A_{\mathbf{k}}, \quad (9.47a)$$

$$2\omega_{\mathbf{k}}u_{\mathbf{k}}v_{\mathbf{k}} = B_{\mathbf{k}}, \quad (9.47b)$$

$$2\omega_{\mathbf{k}}u_{\mathbf{k}}v_{\mathbf{k}}^* = B_{\mathbf{k}}^*. \quad (9.47c)$$

The above second and third equations ensure that $\omega_{\mathbf{k}}$ is real, as we would need it to be for a lossless spin wave mode. Furthermore, we ensure that the transformation is unitary by requiring that

$$u_{\mathbf{k}}^2 - |v_{\mathbf{k}}|^2 = 1. \quad (9.47d)$$

Solving Eqs. (9.47) yields the dispersion relation for the \mathbf{k} th mode:

$$\omega_{\mathbf{k}}^2 = A_{\mathbf{k}}^2 - |B_{\mathbf{k}}|^2. \quad (9.48)$$

The final rate equations, obtained from the diagonal Hamiltonian (9.46) are

$$\dot{b}_{\mathbf{k}} = i \frac{\partial \mathcal{H}}{\partial b_{\mathbf{k}}^*} = i\omega_{\mathbf{k}}b_{\mathbf{k}}, \quad (9.49a)$$

$$\dot{b}_{\mathbf{k}}^* = -i \frac{\partial \mathcal{H}}{\partial b_{\mathbf{k}}} = -i\omega_{\mathbf{k}}b_{\mathbf{k}}^*. \quad (9.49b)$$

Recalling our discussion accompanying Eq. (3.129), we can also introduce energy dissipation via the damping constant $\eta_{\mathbf{k}}$ for the \mathbf{k} th mode by allowing $\omega_{\mathbf{k}}$ to become complex. Since $b_{\mathbf{k}} \sim \exp(+i\omega_{\mathbf{k}}t)$, we make the substitution $\omega_{\mathbf{k}} \rightarrow \omega_{\mathbf{k}} + i\eta_{\mathbf{k}}$ in (9.49a), while in (9.49b) we make the substitution $\omega_{\mathbf{k}} \rightarrow \omega_{\mathbf{k}} - i\eta_{\mathbf{k}}$. The corresponding rate equations for lossy spin wave propagation become

$$\dot{b}_{\mathbf{k}} + [\eta_{\mathbf{k}} - i\omega_{\mathbf{k}}]b_{\mathbf{k}} = 0, \quad (9.50a)$$

$$\dot{b}_{\mathbf{k}}^* + [\eta_{\mathbf{k}} + i\omega_{\mathbf{k}}]b_{\mathbf{k}}^* = 0, \quad (9.50b)$$

where $\eta_{\mathbf{k}} = 1/T_{\mathbf{k}}$ can be estimated from phenomenological loss theory for volume or surface waves using (6.35b) or (6.26b), respectively.⁵ In Eq. (9.50) we are assuming steady-state excitations of the spin wave manifold, but allowing for a separate damping constant to be associated with each mode. This has technological implications for spin wave excitations in patterned structures, which we shall discuss further in Section 10.2.

As was previously mentioned, although we have motivated the rate equations using the Hamiltonian formalism, it is equally feasible to arrive at this

⁵ We typically assume energy dissipation to be small, i.e., $\eta_{\mathbf{k}} \ll \omega_{\mathbf{k}}$.

point from the Landau–Lifshitz equation by expanding the magnetization in terms of propagating modes and retaining nonlinear terms. In Section 9.3.2, we will demonstrate how Eq. (9.48) is analogous to the classical spin wave dispersion relation of (5.18). For now, it suffices to observe that

- the new canonical variables $b_{\mathbf{k}}$ and $b_{\mathbf{k}}^*$ have diagonalized $\mathcal{H}^{(2)}$,
- we once again have time harmonic solutions of the form $e^{(\pm i\omega_{\mathbf{k}}t)}$, and
- we have defined the dispersion relation $\omega_{\mathbf{k}}^2 = A_{\mathbf{k}}^2 - |B_{\mathbf{k}}|^2$ for each propagating spin wave mode.

To study higher order nonlinear interactions, we extend the Hamiltonian by including terms written in the general form

$$\mathcal{H}^{(3)} = \sum_{\mathbf{k}_1 \mathbf{k}_2 \mathbf{k}_3} V_{\mathbf{k}_1 \mathbf{k}_2 \mathbf{k}_3} a_{\mathbf{k}_1}^* a_{\mathbf{k}_2}^* a_{\mathbf{k}_3} + \text{c.c.} \quad (9.51a)$$

$$\mathcal{H}^{(4)} = \sum_{\mathbf{k}_1 \mathbf{k}_2 \mathbf{k}_3 \mathbf{k}_4} T_{\mathbf{k}_1 \mathbf{k}_2 \mathbf{k}_3 \mathbf{k}_4} a_{\mathbf{k}_1}^* a_{\mathbf{k}_2}^* a_{\mathbf{k}_3} a_{\mathbf{k}_4}, \quad (9.51b)$$

and then apply the Bogoliubov transformation $a_{\mathbf{k}} \rightarrow b_{\mathbf{k}}$ to each term. Although the three- and four-wave interactions of Eq. (9.51) seem to suggest an almost infinite interaction spectrum, momentum, and energy conservation will provide us with selection rules that allow us to determine which waves interact.

Let us consider the three-wave interaction term in Eq. (9.51a) under the conditions

$$\mathbf{k}_3 = \mathbf{k}_1 + \mathbf{k}_2, \quad (9.52a)$$

$$\omega_3 = \omega_1 + \omega_2. \quad (9.52b)$$

Now if we consider the uniform precession mode where $\mathbf{k}_3 = 0$, energy conservation would be satisfied when $\omega_1 = \omega_2 = \omega_3/2$ or the absorption of one magnon⁶ at ω_3 would create two magnons at half the frequency. The two magnons would then propagate in opposite directions to ensure momentum conservation. This three-wave process is illustrated in Figure 9.10(b). Note that the uniform precession mode would normally need to be driven at a frequency far from resonance so that $\omega_3/2 = \omega_p/2$ falls within the spin wave manifold. If the uniform precession mode is driven at resonance, then this process can only occur at sufficiently low fields such that $\omega_0/2$ falls within the manifold. It is common to refer to this phenomenon as the *Suhl first-order instability*, following the original article by Suhl [7], or as a *subsidiary absorption* with reference to experimental observations [19].

⁶ Following the quantum mechanical treatment in Chapter 2, we use the term *magnon* to represent a quantum of energy $\hbar\omega_k$ that can be absorbed or emitted when the k th mode interacts with other modes. An accurate quantum mechanical treatment involving interatomic exchange and dipolar interactions, see, e.g., Benson and Mills [16], is beyond the scope of our present discussion.

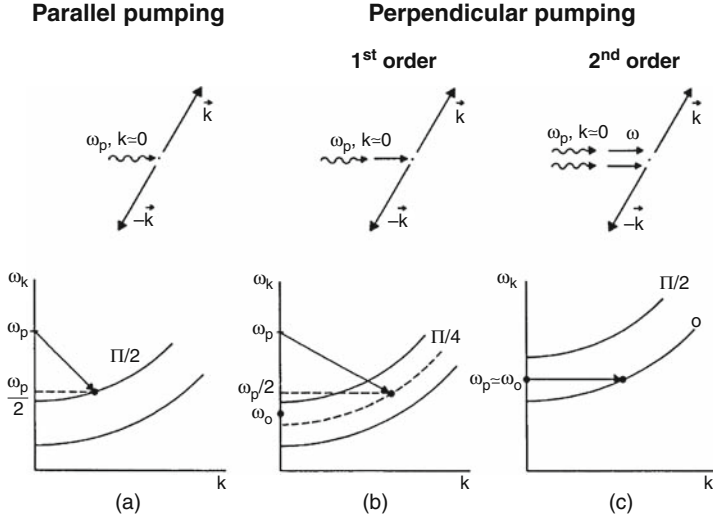


Fig. 9.10. First- and second-order nonlinear interaction processes in a ferrite sphere. (a) Parallel pumping. (b) Perpendicular pumping, subsidiary resonance (first-order Suhl processes). (c) Perpendicular pumping, premature saturation of the main resonance (second-order Suhl process) [17]. (© 1990 IEEE.)

In the above discussion, the uniform precession mode is excited by a small-signal driving field transverse to the magnetization. It is also possible to observe a nonlinear process when the driving field is parallel to the magnetization. This process is referred to as *parallel pumping*, and involves direct coupling from the driving field (a photon field with $\mathbf{k}_p = 0$) to spin waves with wave vectors $(-\mathbf{k}, \mathbf{k})$. This coupling is enabled by elliptical precession of the magnetization, causing a variation in M_z with twice the frequency of the precession.

In the same reference [7], Suhl also described a *second-order process*, wherein a $(-\mathbf{k}, \mathbf{k})$ spin wave pair is driven by two uniform mode magnons with $\mathbf{k} = 0$ and frequency $\omega_p = \omega_{\mathbf{k}}$ pumped by the microwave radiation. This is made possible by the four-magnon interaction as illustrated in Figure 9.10(c). This process limits the growth of the FMR absorption with increasing microwave power and is referred to as the premature saturation of the main resonance. For the four-wave interaction process, the simplest conservation laws are

$$\omega(\mathbf{k}_1) + \omega(\mathbf{k}_2) = \omega(\mathbf{k}_3) + \omega(\mathbf{k}_4), \quad (9.53a)$$

$$\mathbf{k}_1 + \mathbf{k}_2 = \mathbf{k}_3 + \mathbf{k}_4, \quad (9.53b)$$

i.e., two magnons collide to generate two new magnons, all within a narrow frequency spectrum. If we assume a narrow packet of spin waves linearly

excited in a thin film, such that we can linearize the dispersion relation $\omega(\mathbf{k})$ about the point $\mathbf{k}_3 = \mathbf{k}_4 = \mathbf{k}_0$, we can rewrite the conservation laws as

$$2\mathbf{k}_0 = \mathbf{k}_1 + \mathbf{k}_2, \quad (9.54a)$$

$$2\omega_0 = \omega_1 + \omega_2. \quad (9.54b)$$

Thus, a term of the form $a_{\mathbf{k}_1}a_{\mathbf{k}_2}(a_{\mathbf{k}_0}^*)^2$ in Eq. (9.51b) would correspond to the annihilation of magnons at ω_1 and ω_2 , while exciting two magnons at ω_0 . The special case when $\mathbf{k}_0 = 0$ and $\omega_0 = \omega_P$ is shown schematically in Figure 9.10(c) and is referred to as the *second Suhl instability*. We note that the reverse four-wave process, i.e., the annihilation of two magnons at ω_0 and the creation of magnons at ω_1 and ω_2 , is also likely to occur with equal probability. A similar argument also holds true for three-wave processes. The threshold power at which the different nonlinear processes become significant depends on the geometry of the sample (which determines the demagnetizing field), the direction of the excitation and static fields and the intrinsic loss mechanisms. We shall estimate the threshold for a simple three-wave interaction process in Section 9.3.1.

The mathematical formulation of Hamiltonians and canonical transformations might appear disconnected from our earlier discussions on precessing magnetic moments. However, the approach has its advantages and is gaining popularity among researchers. Krivosik et al. [18] have extended the nonlinear interaction formalism to include spatial variation in internal fields due to inhomogeneities. Of particular technological interest is their ability to predict the contribution of two magnon scattering to the measured FMR linewidth in NiFe thin films.

9.3.1 Decay Instability

In this section, we consider the three-magnon process shown in Figure 9.10(b) in more detail. As discussed previously, since $\mathbf{k}_3 = 0$ for the uniform precession mode, momentum conservation (9.52a) requires $\mathbf{k}_1 = -\mathbf{k}_2$. Further, since $\omega(\mathbf{k}) = \omega(-\mathbf{k})$, energy conservation (9.52b) requires $\omega_1 = \omega_2 = \omega_P/2$ where $\omega_3 = \omega_P$ is the frequency at which the uniform precession mode is driven. Let us begin with the Hamiltonian (9.51a) that describes a three-wave process. We affect the transformation (9.45) that diagonalizes $\mathcal{H}^{(2)}$ and rewrite $\mathcal{H}^{(3)}$ in terms of $b_{\mathbf{k}}$ and $b_{-\mathbf{k}}^*$. Further, since we require that the three-wave processes satisfy the conservation laws (9.52), the surviving terms in $\mathcal{H}^{(3)}$ take the form

$$\mathcal{H}^{(3)} = \frac{1}{2} \sum_{\mathbf{k}' \neq 0} \left[\hat{V}_{\mathbf{k}'} b_{\mathbf{k}'}^* b_{-\mathbf{k}'}^* b_0 + \hat{V}_{\mathbf{k}'}^* b_{\mathbf{k}'} b_{-\mathbf{k}'} b_0^* \right]. \quad (9.55)$$

The equations of motion can be written as

$$\dot{b}_{\mathbf{k}} = i \frac{\partial}{\partial b_{\mathbf{k}}^*} \left(\mathcal{H}^{(2)} + \mathcal{H}^{(3)} \right), \quad (9.56)$$

$$\dot{b}_{-\mathbf{k}}^* = -i \frac{\partial}{\partial b_{-\mathbf{k}}} \left(\mathcal{H}^{(2)} + \mathcal{H}^{(3)} \right). \quad (9.57)$$

Note that $\mathcal{H}^{(2)}$ in (9.42) is a summation over all values of \mathbf{k} , both positive and negative. Similarly, there are two terms in the sum of \mathbf{k}' in (9.55) that contribute to the equations of motion, i.e., $\mathbf{k}' = \pm \mathbf{k}$. Hence, using Eq. (9.42) with loss for $\mathcal{H}^{(2)}$, and (9.55) for $\mathcal{H}^{(3)}$, we obtain

$$\dot{b}_{\mathbf{k}} + [\eta_{\mathbf{k}} - i\omega(\mathbf{k})]b_{\mathbf{k}} = \frac{i}{2} \left[\hat{V}_{\mathbf{k}} + \hat{V}_{-\mathbf{k}} \right] b_0 b_{-\mathbf{k}}^*, \quad (9.58a)$$

$$\dot{b}_{-\mathbf{k}}^* + [\eta_{-\mathbf{k}} + i\omega(-\mathbf{k})]b_{-\mathbf{k}}^* = -\frac{i}{2} \left[\hat{V}_{\mathbf{k}}^* + \hat{V}_{-\mathbf{k}}^* \right] b_0^* b_{\mathbf{k}}. \quad (9.58b)$$

Assuming $\eta_{\mathbf{k}} = \eta_{-\mathbf{k}}$, $\omega(\mathbf{k}) = \omega(-\mathbf{k})$, and $\hat{V}_{\mathbf{k}} = \hat{V}_{-\mathbf{k}}$, the equations of motion (9.58) become

$$\dot{b}_{\mathbf{k}} + [\eta_{\mathbf{k}} - i\omega(\mathbf{k})]b_{\mathbf{k}} = i\hat{V}_{\mathbf{k}}b_0b_{-\mathbf{k}}^*, \quad (9.59a)$$

$$\dot{b}_{-\mathbf{k}}^* + [\eta_{\mathbf{k}} + i\omega(\mathbf{k})]b_{-\mathbf{k}}^* = -i\hat{V}_{\mathbf{k}}^*b_0^*b_{\mathbf{k}}. \quad (9.59b)$$

We seek solutions to the rate equations of the form

$$b_{\mathbf{k}}(t) \sim e^{(v+i\omega_P/2)t}, \quad (9.60)$$

$$b_{-\mathbf{k}}^*(t) \sim e^{(v-i\omega_P/2)t}, \quad (9.61)$$

where we are requiring that the growth rate of $b_{\mathbf{k}}$ and $b_{-\mathbf{k}}^*$ be the same, since both are generated by the decay of the same uniform precession mode. Substituting these solutions into the rate equations and using the fact that $\omega(\mathbf{k}) = \omega_P/2$, we obtain simultaneous equations in the coefficients with a unique solution when

$$\begin{vmatrix} \eta_{\mathbf{k}} + v & -i\hat{V}_{\mathbf{k}}b_0 \\ +i\hat{V}_{\mathbf{k}}^*b_0^* & \eta_{\mathbf{k}} + v \end{vmatrix} = 0. \quad (9.62)$$

This gives

$$v = -\eta_{\mathbf{k}} + |\hat{V}_{\mathbf{k}}b_0|, \quad (9.63)$$

which determines the threshold for the decay instability as

$$|\hat{V}_{\mathbf{k}}b_{\text{cr}}| = \eta_{\mathbf{k}}. \quad (9.64)$$

The coefficient $\hat{V}_{\mathbf{k}}$ can be shown to be proportional to $\sin \theta \cos \theta$, so that the spin wave modes with the lowest threshold occur at $\theta = \pi/4$ as shown in Figure 9.10(b).

9.3.2 $\mathcal{H}^{(2)}$ Coefficients

We now take on the final task of deriving the canonical rate equations for the magnetization from the Landau–Lifshitz equation and thus quantifying the coefficients $A_{\mathbf{k}}$ and $B_{\mathbf{k}}$ used in Eq. (9.42). Let us assume the motion of the fields without exchange or anisotropy, as was done in Section 3.7.2. We do not explicitly assume a time-dependent form and instead write the linearized equation of motion (3.109) as

$$\dot{\mathbf{m}} = [\omega_{\text{M}} \mathbf{h} - \omega_0 \mathbf{m}] \times \hat{\mathbf{z}}. \quad (9.65)$$

Let us now expand \mathbf{m} and \mathbf{h} , each as a Fourier series:

$$\mathbf{m} = \sum_{\mathbf{k}} \mathbf{m}_{\mathbf{k}} e^{i\mathbf{k} \cdot \mathbf{r}}, \quad (9.66a)$$

$$\mathbf{h} = \sum_{\mathbf{k}} \mathbf{h}_{\mathbf{k}} e^{i\mathbf{k} \cdot \mathbf{r}}. \quad (9.66b)$$

For a propagation angle θ with respect to $\hat{\mathbf{z}}$ and for $|k| \gg |k_0|$ (cf. Section 4.10 and Problem 4.6),

$$\mathbf{h}_{\mathbf{k}} \approx -\frac{\mathbf{k}(\mathbf{k} \cdot \mathbf{m})}{k^2}. \quad (9.67)$$

Expanding \mathbf{k} in spherical coordinates, we obtain

$$h_{\mathbf{k}x} = -\left[\sin^2 \theta \cos^2 \phi m_{\mathbf{k}x} + \frac{1}{2} \sin^2 \theta \sin(2\phi) m_{\mathbf{k}y} \right], \quad (9.68a)$$

$$h_{\mathbf{k}y} = -\left[\frac{1}{2} \sin^2 \theta \sin(2\phi) m_{\mathbf{k}x} + \sin^2 \theta \sin^2 \phi m_{\mathbf{k}y} \right]. \quad (9.68b)$$

Here, θ and ϕ are the polar angles describing the direction of spin wave propagation. Substituting (9.66) and (9.68) into (9.65) allows us to write the rate equations

$$\dot{m}_{\mathbf{k}x} = -\frac{\omega_{\text{M}}}{2} \sin^2 \theta \sin(2\phi) m_{\mathbf{k}x} - (\omega_0 + \omega_{\text{M}} \sin^2 \theta \sin^2 \phi) m_{\mathbf{k}y}, \quad (9.69a)$$

$$\dot{m}_{\mathbf{k}y} = (\omega_0 + \omega_{\text{M}} \sin^2 \theta \cos^2 \phi) m_{\mathbf{k}x} + \frac{\omega_{\text{M}}}{2} \sin^2 \theta \sin(2\phi) m_{\mathbf{k}y}. \quad (9.69b)$$

If we define the normalized elliptical variables

$$a_{\mathbf{k}}(t) = \frac{1}{M_{\text{S}}} [m_{\mathbf{k}x}(t) + i m_{\mathbf{k}y}(t)], \quad (9.70a)$$

$$a_{-\mathbf{k}}^*(t) = \frac{1}{M_{\text{S}}} [m_{\mathbf{k}x}(t) - i m_{\mathbf{k}y}(t)], \quad (9.70b)$$

the rate equations simply become (Problem 9.5)

$$\frac{d}{dt} \begin{pmatrix} a_{\mathbf{k}}(t) \\ a_{-\mathbf{k}}^*(t) \end{pmatrix} = i \begin{pmatrix} A_{\mathbf{k}} & B_{\mathbf{k}} \\ -B_{\mathbf{k}}^* & -A_{\mathbf{k}} \end{pmatrix} \begin{pmatrix} a_{\mathbf{k}} \\ a_{-\mathbf{k}}^* \end{pmatrix}, \quad (9.71)$$

where

$$A_{\mathbf{k}} = \omega_0 + \frac{1}{2}\omega_M \sin^2 \theta, \quad (9.72a)$$

$$B_{\mathbf{k}} = \frac{1}{2}\omega_M \sin^2 \theta e^{i2\phi}. \quad (9.72b)$$

We see from (9.72) that $A_{\mathbf{k}} = A_{-\mathbf{k}}$ and $B_{\mathbf{k}} = B_{-\mathbf{k}}$. Thus, we recognize that (9.71) is the equation of motion (9.43) resulting from the Hamiltonian in (9.42). Also recall that we had determined, as part of the Bogoliubov transformation (cf. Eq. (9.48)),

$$\omega_{\mathbf{k}}^2 = A_{\mathbf{k}}^2 - |B_{\mathbf{k}}|^2. \quad (9.73)$$

In the present case, this yields

$$\omega_{\mathbf{k}}^2 = \omega_0(\omega_0 + \omega_M \sin^2 \theta). \quad (9.74)$$

We have thus recovered the spin wave dispersion relation of Eq. (5.14).

The effects of the exchange interaction, described in Section 3.5, can be included by recognizing that for $\mathbf{k} \neq 0$, the exchange field $\mathbf{h}_{\text{ex}} = \lambda_{\text{ex}} \nabla^2 \mathbf{m}$ becomes

$$\mathbf{h}_{\text{ex}} = -\lambda_{\text{ex}} \sum_{\mathbf{k} \neq 0} k^2 \mathbf{m}_{\mathbf{k}} e^{i\mathbf{k} \cdot \mathbf{r}} \quad (9.75)$$

which we must add to the Fourier expansion for \mathbf{h} . We will find that in a manner similar to our discussion of Section 5.2, the inclusion of exchange interactions merely requires that we replace ω_0 with $\omega_0 + \omega_M \lambda_{\text{ex}} k^2$ in (9.72) and we will recover the dispersion relation of Eq. (5.18).

The nonlinear coefficients in $\mathcal{H}^{(3)}$ can be obtained by retaining the nonlinear term $\mathbf{m} \times \mathbf{h}$ in the torque equation. It is also possible to derive the coefficients of $\mathcal{H}^{(2)}$, $\mathcal{H}^{(3)}$, and $\mathcal{H}^{(4)}$ from the energy density W . For example, Bryant et al. [20] provide a comprehensive derivation of the various linear and nonlinear Hamiltonian coefficients for the case of a ferrite sphere.

Equations (9.42) and (9.51) are the starting point for the analysis of many nonlinear phenomena such as subsidiary absorption (or the first Suhl instability), auto-oscillations (beyond the second Suhl instability), parametric excitations, four-wave mixing, and eventually broadband chaos. In each case, the approach remains similar to what we have adopted, namely:

- determine the Hamiltonian for the specific excitation geometry,
- write the rate equations for the canonical variables,
- introduce energy dissipation into the rate equations,
- look for exponentially growing spin wave amplitudes, and
- identify the conditions under which the instability occurs.

Starting with Suhl [7] and Schlömann [13] and seminal contributions by Zakharov et al. [21], these phenomena have been explored under a variety of

geometries (spheres, discs, and thin films) and configurations (parallel and perpendicular pumping). The first- and second-order nonlinear spin wave processes are illustrated in Figure 9.10. L'vov [14] provides us with an understanding of wave turbulence, while Rezende and Aguiar [17], Wigen [22], and Marcelli and Nikitov [23] provide a summary of the different nonlinear phenomena in spin wave systems.

9.4 Nonlinear Schrödinger Equation

The onset of nonlinearity induces a frequency and wavevector modulation that requires us to rewrite the the general form for the dispersion relation as

$$G(\omega, \mathbf{k}) = G(\omega(k, |\psi|^2), k, |\psi|^2) = 0, \quad (9.76)$$

where we have introduced a correction factor $|\psi|^2 = (1/2)(m/M_S)^2$ to account for the reduction in magnetization along the direction of the applied bias field. The change in frequency (up to second-order corrections) is obtained from the Taylor series expansion,

$$\begin{aligned} \delta\omega &= \left(\frac{\partial\omega}{\partial k}\right)\delta k + \frac{1}{2}\frac{\partial^2\omega}{\partial k^2}\delta k^2 + \left(\frac{\partial\omega}{\partial|\psi|^2}\right)|\psi|^2 \\ &= v_g\delta k + \frac{D}{2}\delta k^2 + N|\psi|^2 \end{aligned} \quad (9.77)$$

where we introduce the dispersion and nonlinearity coefficients, D and N , respectively, in addition to the group velocity of Eq. (4.100). Assuming propagation of the form $\psi(z, t) = \psi_0 e^{i(\omega_0 t - k_0 z)}$, $\delta\omega$ and δk also correspond to the operators $i\frac{\partial}{\partial t}$ and $-i\frac{\partial}{\partial z}$. Thus, Eq. (9.77) can be rewritten as

$$i\left(\frac{\partial\psi}{\partial t} + v_g\frac{\partial\psi}{\partial z}\right) + \frac{1}{2}D\frac{\partial^2\psi}{\partial z^2} - N|\psi|^2\psi = 0 \quad (9.78)$$

which is identified as the nonlinear Schrödinger (NLS) equation. Consider the example of forward volume spin waves. From Eq. (5.53), we recall that waves propagate when the frequency lies in the range

$$\omega_0 \leq \omega \leq \sqrt{\omega_0(\omega_0 + \omega_M)}. \quad (9.79)$$

Accounting for the demagnetizing field in a thin film with surface normal along the z -axis, $\omega_0 = -\gamma\mu_0(H_0 - M_z)$. Consequently, the effect of nonlinearity on the envelope occurs predominantly through $M_z = M_S(1 - |\psi|^2)$ and we estimate $N \approx -\gamma\mu_0 M_S$, while dispersion is obtained by suitably differentiating Eq. (5.76b). Typical values for these coefficients in the case of spin wave excitations in YIG films are [24]

- group velocity $|v_g| \sim 10^6 \text{ cm s}^{-1}$,
- dispersion $|D| \sim 10^3 \text{ cm}^2 \text{ rad}^{-1} \text{ s}^{-1}$,
- nonlinearity $N \sim 10^{10} \text{ s}^{-1}$.

Equation (9.78) can be further simplified if we introduce a frame of reference moving at group velocity v_g such that

$$z' = z - v_g t \quad (9.80)$$

and we can describe the envelope $u(z', t) = \psi(z, t)$. Since z and t are independent variables, we can use the chain rule of differentiation

$$\frac{\partial \psi}{\partial z} = \frac{\partial u}{\partial z'} \frac{\partial z'}{\partial z} = \frac{\partial u}{\partial z'}, \quad (9.81)$$

$$\frac{\partial \psi}{\partial t} = \frac{\partial u}{\partial t} + \frac{\partial u}{\partial z'} \frac{\partial z'}{\partial t} = \frac{\partial u}{\partial t} - v_g \frac{\partial u}{\partial z'}, \quad (9.82)$$

to reduce Eq. (9.78) to

$$\frac{1}{2} D \frac{\partial^2 u}{\partial z'^2} - N |u|^2 u = -i \frac{\partial u}{\partial t}. \quad (9.83)$$

The above equation has been written in a form that lends itself to a quantum mechanical interpretation. Terms on the left side are identified as the kinetic and potential energy operators, respectively, while the right side represents the energy. Hence the reference to the Schrödinger equation which has the form $\mathcal{H}\Psi = \mathcal{E}\Psi$.

If we use scaled variables by setting $t = \frac{-tN}{2}$ and $z = z' \sqrt{\frac{-N}{D}}$, we reduce Eq. (9.83) to its canonical form

$$iu_t + u_{zz} + 2u^2 u^* = 0, \quad (9.84)$$

where the subscripts represent the partial derivatives. Note that it would have been just as easy for us to replace the Taylor series expansion (9.77) with

$$\delta k = k_1 \delta \omega + \frac{k_2}{2} \delta \omega^2 + \frac{\partial k}{\partial |\psi|^2} |\psi|^2, \quad (9.85)$$

where k_1 and k_2 are related to v_g and D , respectively. This leads us to an equivalent NLS equation (cf. Problem 9.6), with an exchange of variables $z \rightarrow t$ and $t \rightarrow z$, commonly used in the literature to describe pulse propagation in optical fibers [25].

9.4.1 Modulational Instability and Solitons

As we begin to pump ever increasing amounts of continuous wave RF power into the spin wave manifold, the linear theory described in previous chapters

breaks down. Experimentally, we observe that the continuous wave signal no longer retains a constant amplitude as it propagates and instead breaks down into an envelope of pulses. This phenomenon, also called *modulational instability*, is a precursor to the formation of shape-preserving pulses.

Let Eq. (9.84) possess the elementary solution

$$u = u_0(t) = a e^{2i|a|^2 t}, \quad (9.86)$$

for constant a about which small perturbations can respond. Let us start with a small perturbation $|\epsilon(z, t)| \ll 1$ and write

$$u(z, t) = u_0(t)(1 + \epsilon(z, t)) \quad (9.87)$$

which upon substitution in (9.84), and keeping only first-order terms in ϵ , yields the linear equation

$$i\epsilon_t + \epsilon_{zz} + 2|a|^2(\epsilon + \epsilon^*) = 0. \quad (9.88)$$

On account of the complex conjugate term ϵ^* , we look for solutions of the form

$$\epsilon(z, t) = \tilde{\epsilon}_+ e^{i(kz - \Omega t)} + \tilde{\epsilon}_- e^{-i(kz - \Omega t)}, \quad (9.89)$$

where $\tilde{\epsilon}_\pm$ are assumed to be real. Substituting $\epsilon(z, t)$ into (9.88) yields simultaneous equations in $\tilde{\epsilon}_+$ and $\tilde{\epsilon}_-$ which have a unique solution only when we satisfy

$$\Omega = \pm ik\sqrt{4|a|^2 - k^2}. \quad (9.90)$$

Consequently, any excitation that satisfies $4|a|^2 - k^2 > 0$ becomes exponentially unstable. This is observed as a modulational instability in response to a high-power continuous wave excitation [26].

A pulse that is limited in the time domain consists of many Fourier components. Dispersion which is a measure of the differential group velocities at different frequencies causes pulse broadening. Nonlinearity, on the other hand, causes an increase in regions of the pulse with larger amplitudes resulting in pulse shortening. Thus, under appropriate circumstances, these competing effects can compensate each other and pulses known as *solitons* can propagate through the dispersive nonlinear medium with an invariant shape. An analytic solution to Eq. (9.83) can be obtained under specific conditions using the inverse scattering method.⁷ Of particular interest to our current discussion are solutions of the form (cf. Problem 9.7)

$$u(z, t) = \eta \operatorname{sech}(\eta z) \exp(i\eta^2 t), \quad (9.91)$$

shown in Figure 9.11 for $\eta = 1, 2$ at $t = 0$. We observe that the order parameter η determines not only the soliton amplitude but also its width. It is possible to

⁷ See, e.g., Ablowitz and Clarkson [27].

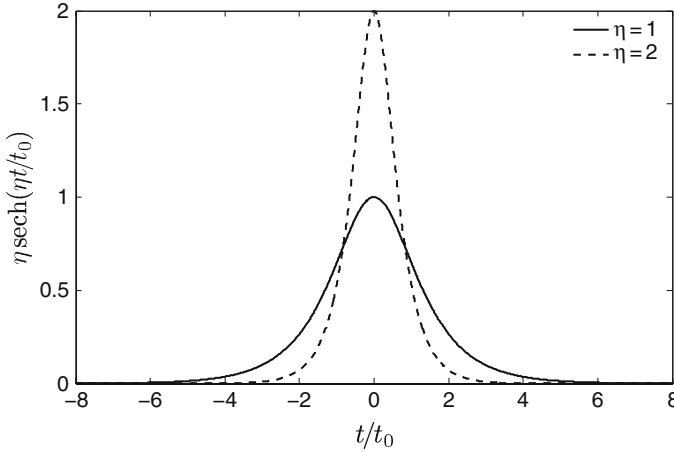


Fig. 9.11. Shape of first- and second-order solitons.

arrive at the analytic form for the lowest-order soliton by assuming a shape-preserving solution:

$$u(z, t) = v(z) \exp[i\phi(z, t)]. \quad (9.92)$$

Substituting $u(z, t)$ into (9.84), and separating the imaginary and real parts of the resulting equation, we obtain the simultaneous equations

$$2v_z\phi_z + v\phi_{zz} = 0, \quad (9.93a)$$

$$-v\phi_t + v_{zz} - v\phi_z^2 + 2v^3 = 0. \quad (9.93b)$$

The solution to (9.93a) is

$$\phi = k \int v^{-2} dz + f(t). \quad (9.94)$$

Consider the simplest case where $k = 0$ and $\phi = \eta^2 t$, such that $\phi_z = 0$. Equation (9.93b) can now be simplified and written as

$$v_{zz} = v\eta^2 - 2v^3. \quad (9.95)$$

This is a second-order differential equation with a solution $v(z) = \eta \operatorname{sech}(\eta z)$ (cf. Problem 9.8). Multiplying $v(z)$ with the phase $e^{i\phi}$ yields the form of the shape-preserving soliton pulse given in (9.91).

9.4.2 Split-Step Fourier Method⁸

The NLS equation does not lend itself to analytic solutions except in some special cases. The most common numerical approach to understanding the evolution of a soliton under different conditions is the Split-Step Fourier Method. Consider the NLS equation (9.83) written in the form

⁸ Following the method outlined in [25, p. 51].

$$\frac{\partial u}{\partial t} = (\hat{D} + \hat{N})u. \quad (9.96)$$

The differential and nonlinear operators, to lowest order, are

$$\hat{D} = \frac{i}{2} \left(\frac{\partial^2 \omega}{\partial k^2} \right) \frac{\partial^2}{\partial z^2} \quad (9.97)$$

and

$$\hat{N} = -i \left(\frac{\partial \omega}{\partial |u|^2} \right) |u|^2 \quad (9.98)$$

respectively. Higher-order effects can be incorporated by adding more terms from the Taylor series expansion for $k(\omega, |u|^2)$. Equation (9.96) has a formal solution $u(z+h, \tau) \approx e^{h\hat{D}} + e^{h\hat{N}} u(z, \tau)$, where $\tau = t - z/v_g$ and v_g is the group velocity. Although dispersion and nonlinearity act together, an approximate solution is obtained if we pretend that they act independently over a small distance h . The integration between z and $z+h$ is carried out in two steps:

- applying the nonlinearity with no dispersion, $v(z+h, t) = e^{h\hat{N}} u(z, t)$ and
- applying dispersion with no nonlinearity $u(z+h, t) = e^{h\hat{D}} v(z, t)$,

For the latter step, $\exp(h\hat{D})$ is evaluated in the Fourier domain as

$$e^{h\hat{D}} v(z, t) = \mathcal{F}^{-1} \left\{ e^{h\hat{D}(ik)} \mathcal{F} v(z, t) \right\}. \quad (9.99)$$

The order in which we apply the nonlinearity and the dispersion is fairly arbitrary. In the *symmetrized* split-step method, the nonlinearity is applied at the center of the integration step rather than at one end of the interval such that

$$u(z+h, t) = e^{h\hat{D}/2} \exp \left(\int_z^{z+h} \hat{N}(z') dz' \right) e^{h\hat{D}/2} u(z, t). \quad (9.100)$$

This procedure, shown pictorially in Figure 9.12, reduces the numerical error for the two non-commuting operators

$$e^{\hat{D}} e^{\hat{N}} = \exp \left(\hat{D} + \hat{N} + \frac{1}{2} [\hat{D}, \hat{N}] + \dots \right), \quad (9.101)$$

where the commutator $[\hat{D}, \hat{N}] = \hat{D}\hat{N} - \hat{N}\hat{D}$ is defined similar to that for quantum mechanical operators (cf. Eq. (1.54)). As a lowest-order approximation, the integral in (9.100) can be approximated by $\exp(h\hat{N})$. Further improvements to accuracy require evaluating the integral with more sophisticated iterative methods (see, e.g., Chapra and Canale [28]).

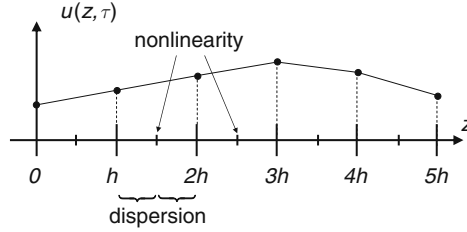


Fig. 9.12. Pictorial representation of the symmetrized split-step Fourier transform, corresponding to (9.100). The nonlinearity is applied at the half-interval points.

The phase distribution within the pulse is critical to the shape of the soliton. Very often, pulsed excitations do not begin with the form in Eq. (9.91), though they have similar amplitudes. The numerical solutions allow us to visualize the propagation of pulsed excitations. In Figure 9.13, we show the evolution of the second-order solution $2 \operatorname{sech}(2z/z_0)$ along with that of a soliton-like pulse $2 \operatorname{sech}(z/z_0)$ having equal amplitude at $z = 0$. We observe that the $\eta = 2$ soliton periodically recovers its shape, while the soliton-like pulse breaks into multiple peaks and the power distribution varies between the different peaks as the pulse propagates.

9.4.3 Anomalous Dispersion

Soliton formation requires that dispersion and nonlinearity compensate each other. This is mathematically represented as $DN < 0$, also referred to as the *Lighthill criterion* [29]. With $N > 0$, we seek particular frequencies where $D < 0$. Since D is typically a positive quantity, we often refer to regions, where $DN < 0$ as the anomalous dispersion regime. As was described in Section 5.2, the spin wave resonances cause a splitting of the dispersion equation into

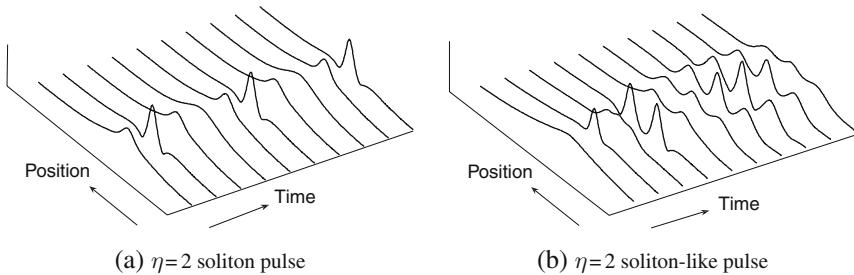


Fig. 9.13. Solutions of the split-step Fourier method for pulse propagation in the absence of dissipation. The position scale is in a coordinate system moving with the pulse envelope.

different branches. The theory of the dipole-exchange spin wave spectrum developed by Kalinikos and Slavin uses perturbation analysis to analyze the dispersion in the vicinity of a dipole gap. Assuming pinned spins at both surfaces of the film, the dispersion equation for forward volume spin waves can be written as [30]

$$(\omega_n^2 - \omega_{nn'}^2)(\omega_{n'}^2 - \omega_{nn'}^2) = \omega_M^2 \Omega_n \Omega_{n'} P_{nn'}^2, \quad (9.102)$$

where

$$\omega_n^2 = \Omega_n (\Omega_n + \omega_M P_{nn}), \quad (9.103a)$$

$$P_{nn'} = \frac{k_t^2}{k_{n'}^2} \delta_{nn'} + \frac{k_t^2}{k_n^2} \frac{k_{zn} k_{zn'}}{k_{n'}^2} \left(\frac{1 + (-1)^{n+n'}}{2} \right) F_n, \quad (9.103b)$$

$$F_n = \frac{2}{k_t d} [1 - (-1)^n e^{-k_t d}], \quad (9.103c)$$

and $\Omega_n = \omega_H + \lambda_{\text{ex}} \omega_M k_n^2$; $\omega_H = -\gamma \mu_0 H$; $\omega_M = -\gamma \mu_0 M_S$; $k_n^2 = k_t^2 + k_{zn}^2$; $k_{zn} = n\pi/d$, $n = 1, 2, 3, \dots$; d is the film thickness; k_t is the wave number in the plane of the film; and $\omega_{nn'}$ gives the frequencies for the two branches of the coupled-mode dispersion relation.

Equation (9.102) is plotted for $n = 1$ (lowest-order mode) and $n = 21$ in Figure 9.14. Since the Lighthill criterion requires that $DN < 0$ and since $N > 0$, we observe that soliton formation can only occur on the low-frequency side ($\omega < \omega_{nn}$) of a dipole gap where $D < 0$.

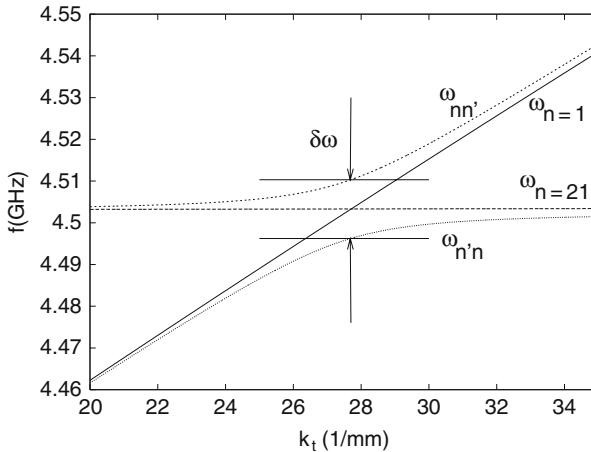


Fig. 9.14. The exchange splitting of the dispersion equation due to interaction between the $n = 1$ and $n' = 21$ modes calculated using Eq. (9.102). (Reprinted with permission from [5]. Copyright 1998 by the American Physical Society.)

9.4.4 Other Aspects

Observations of an instability in high-power continuous spin wave excitations [26] led to other experiments that explored soliton formation using microwave pulse excitations [24, 31, 32]. However, experimental observations are often limited by energy dissipation in the garnet film. To observe a decay-free soliton pulse train, Kalinikos et al. [33] relied on an interrupted feedback arrangement, similar to active mode locking in optical ring lasers. A typical setup used to generate a soliton train is shown in Figure 9.15. Switch 1 controls the gain in the loop and suppresses unwanted oscillations, while Switch 2 provides an RF input pulse to the loop. By adjusting the total gain in the loop (via the attenuator), Kalinikos et al. observed a decay-free pulse train. Figure 9.15 also shows the result of their experiment for two different gain settings.⁹

Today, the spin wave system continues to excite our imagination as it is a fertile ground for exploration of soliton self-generation [34], bright and dark soliton formation [35], and soliton fractals [36], and so on. On the theoretical front, further refinements to Eq. (9.78) are possible. We can derive the NLS equation in a 2D case, as was done recently for a ferromagnet with inhomogeneous exchange anisotropy [37]. There is evidence to suggest that a stable equilibrium between dispersion, diffraction and nonlinearity is not possible for the 2D case and the wave packet would collapse. However, if there was energy loss due to dissipation, we could envisage the formation of a quasi-stable and localized 2D wave packet called a *spin wave bullet* [38]. To account for an en-

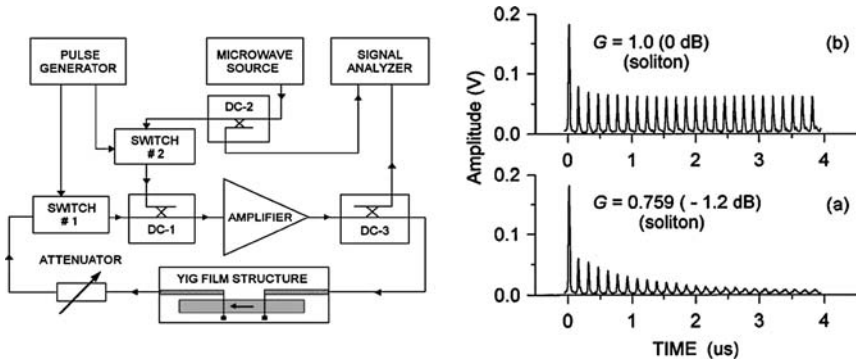


Fig. 9.15. Experimental setup (*left*) used to generate backward volume spin wave soliton pulse trains (*right*). At low values of gain (a) the feedback is insufficient to sustain the solitons beyond a few round-trips in the loop, while unity loop gain (b) results in a decay-free soliton pulse train. (Reprinted with permission from [33]. Copyright 1997 by the American Physical Society.)

⁹ Further experimental details are available in [33].

ergy loss mechanism, we must include a dissipation term $i\alpha\psi$ in the left side of Eq. (9.78). Similarly, we can also introduce higher order dispersion effects by retaining more terms in the Taylor series expansion for $\omega(\mathbf{k})$ [39].

Our description of the features inherent in the nonlinear Schrödinger equation is by no means complete. The literature covering both the theoretical and experimental aspects of this field is vast and beyond the scope of our limited discussion. It is perhaps prudent to attempt a pictorial summary of the nonlinear interactions using a power series expansion for the susceptibility

$$\mathbf{m}(t) = \bar{\chi}^{(1)}\mathbf{h}(t) + \bar{\chi}^{(2)}\mathbf{h}^2(t) + \bar{\chi}^{(3)}\mathbf{h}^3(t) + \dots \quad (9.104)$$

The linear susceptibility tensor $\bar{\chi}^{(1)}$ was defined in Eq. (3.114). For the second- and third-order interactions, we can define the response \mathbf{m} to the excitation \mathbf{h} in the Fourier domain as

$$m_i(\omega_m + \omega_n) = \sum_{jk} \sum_{mn} \chi_{ijk}^{(2)}(\omega_m + \omega_n, \omega_n, \omega_m) h_j(\omega_m) h_k(\omega_n), \quad (9.105)$$

$$m_i(\omega_m + \omega_n + \omega_o) = \sum_{jkl} \sum_{mno} \chi_{ijkl}^{(3)}(\omega_m + \omega_n + \omega_o, \omega_o, \omega_n, \omega_m) \times h_j(\omega_m) h_k(\omega_n) h_l(\omega_o), \quad (9.106)$$

where ijk refer to the Cartesian components of the fields and mn or mno refer to the summation over the different frequency components. The existence of higher-order susceptibility terms leads to a slew of nonlinear effects caused by the generation of sum and difference frequency components. Figure 9.16 is a pictorial representation of the possible combinations. Thus, the first Suhl instability, where one magnon at $\omega_0(\mathbf{k} = 0)$ interacts with two magnons at $\omega_p(\mathbf{k})$ and $\omega_p(-\mathbf{k})$, is an example of a $\chi^{(2)}$ process. We can similarly envisage other interaction processes for spin waves, e.g., in the forward volume wave configuration:

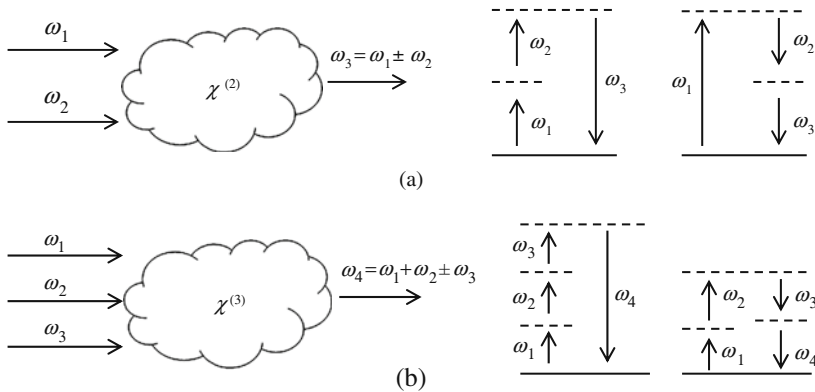


Fig. 9.16. Pictorial representation of second- and third-order interaction processes.

- (a) four-wave mixing ($\omega_1 + \omega_2 = \omega_3 + \omega_4$) easily satisfies $\mathbf{k}_1 + \mathbf{k}_2 = \mathbf{k}_3 + \mathbf{k}_4$,
- (b) parametric amplification ($\omega_1 = \omega_3 - \omega_2$) of solitons [40], where ω_2 is an *idler* wave that is generated during the parametric amplification of ω_1 .

Remember that not all possible processes shown in Figure 9.16 will satisfy momentum conservation. We also require that the resulting spin wave excitations lie within the spin wave manifold for the geometry of interest. Assuming that we pump enough energy into the system, it is conceivable that the different $\chi^{(2)}$ and $\chi^{(3)}$ processes will compete amongst each other leading to a possibly infinite set of coupled nonlinear rate equations. This leads us to our final topic of chaos among spin wave excitations.

9.5 Routes to Chaos

We have established that excitations of large-amplitude spin waves are the breeding ground for a variety of nonlinear interactions. Such interactions are not limited to spin waves and are in fact true for wave interactions ranging from acoustics to optics. However, the ease of conducting such experiments on ferrites has led us to a deeper understanding of a variety of phenomena such as modulational instabilities, period-doubling, auto-oscillations, and broadband chaos. In this section, we shall attempt to describe some of the characteristic features of nonlinear spin wave interactions in the forward volume wave configuration.

The group velocity $v_g = \frac{\partial \omega}{\partial k}$ in a thin ferrite film, in the region of exchange splitting, is shown in Figure 9.17. One immediately recognizes the shape as being similar to that of a notch in a microwave passband, as shown in Figure 9.2, where the location of the $n = 21$ gap was marked. Thus, in the vicinity of a notch, energy injected from one microstrip transducer into a dipole gap does not propagate efficiently through the film. This results in large-amplitude spin waves and a spatially localized build up of energy that can initiate a variety of nonlinear effects.

Although we cite the case of spin waves propagating in thin films above, similarly rich phenomena have been observed in YIG spheres and discs [41, 42]. Figure 9.18 is a map depicting the wide variety of nonlinear excitations found in YIG spheres [20]. In the rest of this section, we describe a few experiments that have allowed us to quantify some of the nonlinear interactions. The description is by no means complete as the existing literature on this topic is large.¹⁰

9.5.1 Center Manifold Theory

Returning to the rate equations of (9.59), we realize that as the number of interacting spin waves increases, we need to adopt different mathematical

¹⁰ We suggest [14, 22, 43–45] and the references therein.

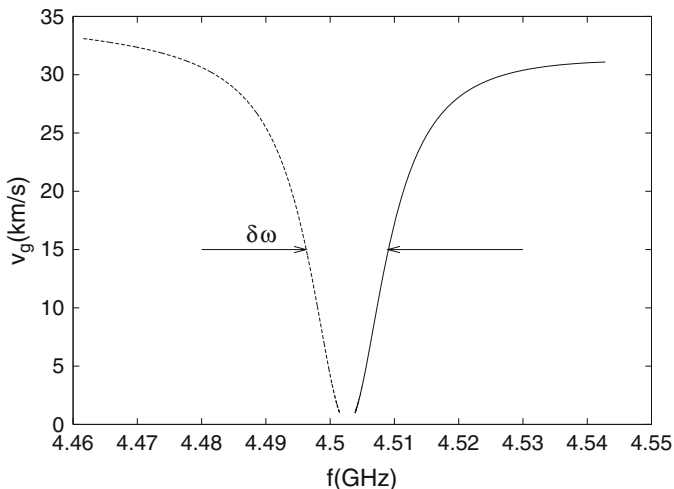


Fig. 9.17. Group velocity obtained by numerically differentiating the dispersion curves shown in Figure 9.14. (Reprinted with permission from [5]. Copyright 1998 by the American Physical Society.)

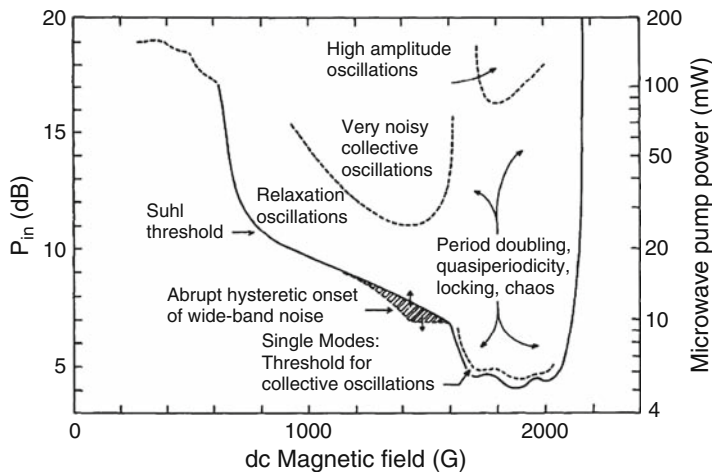


Fig. 9.18. Observed chaotic behavior in a YIG sphere over a 2D input parameter space comprising of RF excitation power and static external field. (Reprinted with permission from [20]. Copyright 1988 by the American Physical Society.)

tools to understand the behavior of the manifold.¹¹ To start, let us consider the dynamical process defined by

$$\dot{x} = V(\mu, x), \quad x \in \mathbb{R}^n \quad (9.107)$$

¹¹ The reader is referred to textbooks such as those by Robinson [46] and Glendinning [47] for a formal theory of nonlinear differential equations.

that describes the evolution of the system in an n -dimensional real-phase space when subject to a parameter μ . At $x = 0$, a Taylor series expansion yields

$$\dot{x} = V(\mu, 0) + D_x V(\mu, 0) \cdot x + O(x^2), \quad (9.108)$$

where $D_x V(\mu, 0)$ represents the partial derivative of V with respect to x , evaluated at $x = 0$. If $\mu = 0$ defines an equilibrium state such that $V(0, 0)$ vanishes, then we can study the linearized system

$$\dot{x} = D_x V(\mu, 0) \cdot x. \quad (9.109)$$

The above matrix equation can be diagonalized by a linear change of coordinates $x \rightarrow x'$ to find the eigenvalues $\lambda_1, \lambda_2, \dots, \lambda_n$ such that the general solution becomes

$$x'_n(t) = e^{\lambda_n t}. \quad (9.110)$$

λ_n can in general be complex. If $\text{Re}\{\lambda_n\} < 0$ then the system is asymptotically stable as $t \rightarrow \infty$ else we have a rapid growth in x'_n . Hence, the real axis in the complex λ plane, separating the asymptotically stable and unstable regions of phase space, plays an important role in describing the system.

Fixed points are the locations in \mathbb{R}^n where $\dot{x} = 0$, and depending on the value of μ it is possible to have one or more fixed points. If the system is perturbed from a fixed point, the value of λ determines whether the system will return to its original state or migrate to another fixed point or even keep continuously hopping between fixed points forming a *limit cycle*. As we vary μ , the system evolves and the λ 's change. A simple real eigenvalue $\lambda = 0$ describes a *steady-state bifurcation*. If we have a pair of simple conjugate eigenvalues satisfying $\text{Re}\{\lambda\} = \text{Re}\{\lambda^*\} = 0$, we have a *Hopf bifurcation* and the system begins to oscillate between two fixed points. One can imagine how further changes to μ can cause the system to split into four and then eight fixed points yielding a *period doubling cascade*. Another aspect worth considering is what happens when we look at the phase portrait of our dynamical system described by Eq. (9.107). The phase trajectories are the locus of velocity vectors \dot{x} . A closed-phase trajectory is a result of pure imaginary eigenvalues and gives rise to *auto-oscillations*, shown schematically in Figure 9.19.

While we have invoked the n -dimensional nature of spin wave excitations to motivate the above discussion, it is important to note that most features such as fixed points, bifurcations, and limit cycles are observable even in low-dimensional systems. In fact, Li and Yorke [49] established that even in a 1D system, a limit three cycle implies chaos.

Auto-Oscillations

Using the center-manifold theory on the degenerate spin wave manifold, Zhang and Suhl [8] estimated a threshold for the appearance of auto-oscillations (AO). Experimental observations for the case of forward volume SWs excited

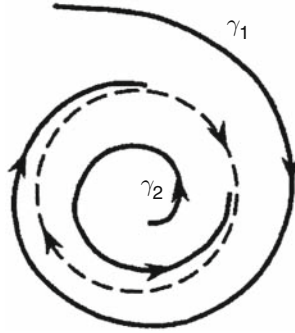


Fig. 9.19. Pictorial representation of trajectories in a 2D-phase space. The solid trajectories depict a system moving exponentially towards and away from a fixed-point, while the dotted line depicts an oscillatory system [48]. (With kind permission of Springer Science+Business Media.)

by a microstrip transducer appear to support the theoretical predictions for the auto-oscillation threshold power levels. The auto-oscillations are visible as subsidiary peaks in the RF spectrum shown in Figure 9.5. The threshold power per unit width for auto-oscillations at the resonance frequency, $\omega_0 = 2\pi f_0$, is given by [5]

$$P_{\text{AO}} = \frac{\omega_0 \omega_M d^2}{2|\gamma|^2 \mu_0 T_0}, \quad (9.111)$$

where $\omega_M = |\gamma| \mu_0 M_S$, d is the thickness of the film and the relaxation time T_0 can be estimated from FMR linewidth measurements (cf. Eq. (6.14)).

Zhang and Suhl also calculated the frequency of the limit cycle associated with AO and predicted that the square of the frequency would vary in a parabolic manner with an increase in the microwave signal amplitude. This behavior, shown in Figure 9.20, was observed close to the second Suhl instability threshold (P_{AO}) and persisted even when the system underwent a period-doubling bifurcation.¹²

9.5.2 Quantizing Low-Dimensional Chaos

Nonlinear interactions between a few propagating spin waves or standing wave modes leads us to the notion of low-dimensional chaos. This is separated from the notion of hyperchaos (with high-dimensional) or broadband noise. In fact, when viewing experimental data, the very metric of a chaotic dimension is subject to many definitions. In a simplistic manner, we can explain the notion

¹² The frequency of AO was calculated as the average separation between adjacent peaks in the output spectrum shown in Figure 9.5.

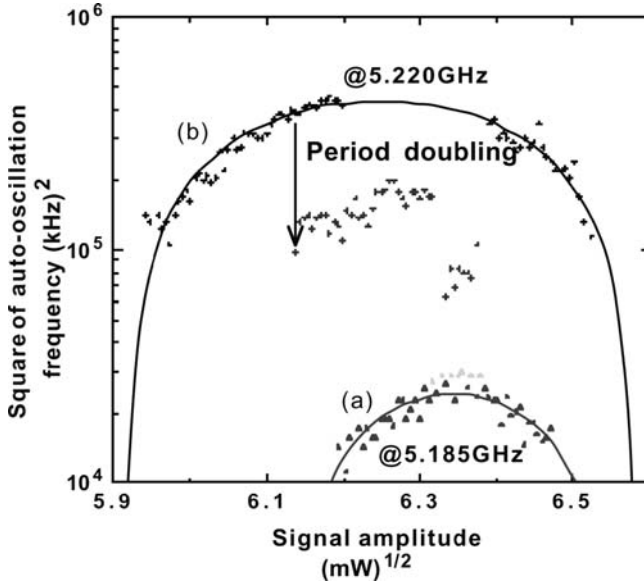


Fig. 9.20. Parabolic variation in AO frequency at the second Suhl instability threshold. Forward volume spin waves were excited in a rectangular YIG sample ($5\text{ mm} \times 10\text{ mm} \times 7.4\text{ m}$), with a constant magnetic field $H_{\text{dc}} = 3.48\text{ kG}$ applied perpendicular to the film plane. Separate low-power FMR measurements on the film indicated a linewidth of 0.9 Oe at 9.2 GHz suggesting a decay rate of 1.27 cm^{-1} . (Reprinted with permission from [50]. Copyright 1996, American Institute of Physics.)

of the fractal dimension in relation to the embedding dimension. Consider first a phase portrait that forms a noisy circle. It can be seen in two dimensions to occupy more than 1D and yet it leaves a large part of the 2D plane unoccupied. Now imagine the system of Eq. (9.107) described by vectors in \mathbb{R}^n . If we had a purely noisy system (referred to as having additive white Gaussian noise in engineering parlance), the experimental data that we collect would uniformly fill the \mathbb{R}^n volume. However, the dynamics of Eq. (9.107) dictate that only a fraction of this volume is occupied even as $t \rightarrow \infty$. Consequently, n becomes our embedding dimension and the volume fraction occupied by x in \mathbb{R}^n represents the fractal dimension.

In this section, we present the results of a dimensional analysis of the output waveform for propagating forward volume SWs over a two parameter input space consisting of microwave frequency (f) and power (P). We also present evidence to suggest that the instability in a finger depends on whether even or odd thickness modes interact with the predominantly excited zeroth order mode which has even symmetry. Near the AO threshold, nonlinear interactions between modes with like symmetry appear to cause a low-dimensional instability.

When we refer back to Figure 9.4, we observe *fingers of low transmission* (white regions) that appear to be extensions of the dipole gaps at low RF power levels. This correlation can be firmly established by measuring the amplitude of low-frequency oscillations at different points in the contour plot [5]. The experimental setup for such a measurement is shown by the dotted lines in Figure 9.3. A continuous wave signal at constant P and f was fed into the device and V_{pp} for the low frequency transmitted signal (< 500 MHz) was monitored. Auto-oscillations in the output signal manifest themselves as large values of V_{pp} . Figure 9.21 is a density plot that shows the variation in V_{pp} as we increment P and f in steps of 0.05 dB and 2 MHz, respectively. A time series snap-shot of the output from the detector was captured whenever $V_{pp} > 4$ mV. A total of 2074 sets of data were collected. Previously, our mode numbering scheme indicated the number of half-wave variations through the film thickness. Here, for consistency with [51], we use a convention where SW mode numbers refer to the number of zeros in the magnetostatic potential through the thickness of the film. In this convention, even dipole gaps correspond to interactions between the zeroth order mode and higher order even modes.

We observe that nonlinear interactions in the vicinity of an even dipole gap occur at a lower power than in the vicinity of an odd dipole gap. At higher power levels, the even and odd dipole gaps merge to form a single finger of AO.

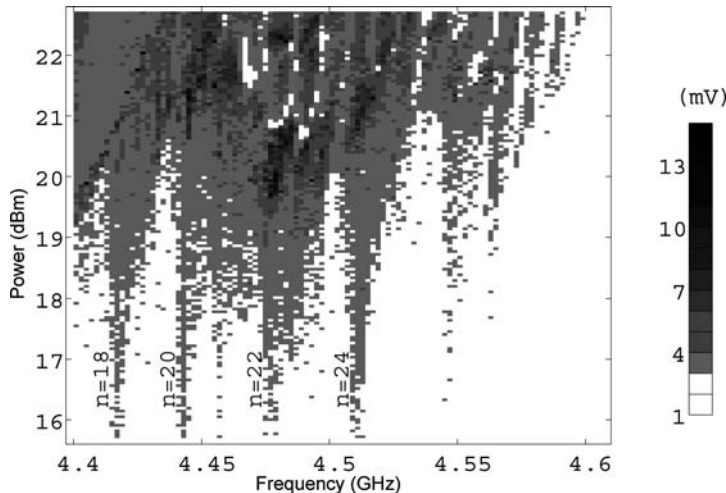


Fig. 9.21. Density plot of the peak-to-peak voltage of the output from the delay line as measured on the oscilloscope. The locations of the even dipole gaps at low-input power are marked on the plot. Here, a mode numbering scheme is used where $n = 0$ is the lowest-order mode in a film with pinned boundary conditions. (Reprinted with permission from [51]. Copyright 2000, American Institute of Physics.)

Analysis of Time Series Data

The time series data collected when $V_{pp} > 4 \text{ mV}$ were analyzed using nonlinear analysis tools which form part of the TISEAN package [52]. The analysis of a time series can become fairly complicated and we list the steps to follow below.

- (a) An appropriate delay length was determined using a reduction in mutual information as the criterion. Although similar to the auto-correlation, the mutual information also takes into account nonlinear correlations. The mutual information of a time series with N points is defined, in a manner similar to entropy, as

$$S = - \sum_{ij}^N p_{ij}(\tau) \ln \frac{p_{ij}(\tau)}{p_i p_j} \quad (9.112)$$

where for some partition on the real numbers p_i is the probability to find a time series value in the i -th interval and $p_{ij}(\tau)$ is the joint probability that an observation falls into the i -th interval and an observation a delay τ later falls into the j -th interval. The time step where the mutual information dropped to a fifth of its starting value is a reasonably good choice for the delay length of a particular time series and we can assume that the two series $x(t)$ and $x(t + \tau)$ are fairly independent [53].

- (b) The minimum embedding dimension, D , was then calculated using the method of false nearest neighbors [54]. The method relies on the fact that neighboring points in an m -dimensional space will get separated when they are embedded in an $m + 1$ -dimensional space. For each point \mathbf{s}_i , we look for its neighbor \mathbf{s}_j , the vector representing a point in m -dimensional space. At a later time instant, we have \mathbf{s}_{i+1} and \mathbf{s}_{j+1} . If the quantity

$$R_i = \frac{\|\mathbf{s}_{i+1} - \mathbf{s}_{j+1}\|}{\|\mathbf{s}_i - \mathbf{s}_j\|}, \quad (9.113)$$

where $\|\cdots\|$ represents the Euclidean norm, is above some threshold R_t , we have detected a *false nearest neighbor*. When the embedding dimension is sufficiently large, the fraction of points that have $R_i > R_t$ should be sufficiently small.¹³ While most of the sampled data had $D = 3$, for some combinations of f and P , the sampled data were well embedded within a 2D space. Since we are dealing with relatively short time series (4000 points), having a low dimension is highly beneficial. There exist fundamental limitations in numerically estimating the dimension [55], and Eckmann and Ruelle suggest that a maximum number for the dimension is $2 \log_{10} N$ [56].

¹³ Note that a time series of pure white noise will fill subspaces of all dimensions and the number of points satisfying $R_i > R_t$ will be of order N .

- (c) The nearest-neighbor information dimension, d , was calculated for each time series using the determined values of delay length and D [57]. A brief description of the information dimension is given below. The analysis of over 2000 datasets made the dimensional calculation statistically significant.

Information Dimension

The information dimension is one among many metrics used to quantify low-dimensional chaos, with the possibility of estimating each metric in different ways. The algorithm below, shared by Kostelich [58], allows us to estimate the information dimension from time series data. Given a reference point x on the attractor, one draws k_1 other points at random and without replacement from the attractor. A list of non-negative distances between x and each of the k_1 points is computed and sorted in increasing order. Fix the order p between 1 and k_1 and let $\delta_p(x, k_1)$ denote the distance between x and its p th nearest neighbor. Then add additional points, again at random and without replacement, to the previous collection for a total of k_2 points and calculate $\delta_p(x, k_2)$. The process continues for an increasing sequence of k_j 's until the distance between x and every other point on the attractor has been computed. The entire procedure is repeated for a collection of reference points $\{x_i\}_{i=1}^R$ and the mean distance,

$$\langle \delta_p(k) \rangle = \sum_{i=1}^R \delta_p(x, k) / R, \quad (9.114)$$

is calculated. The nearest-neighbor distances scale as

$$\langle \delta_p(k) \rangle \sim k^{-1/d}, \quad (9.115)$$

where d is the information dimension of the attractor. For small datasets, the value obtained for d (by fitting $\log(\langle \delta_p(k) \rangle)$ to a straight line) seemed to depend on our choice of p . However, we observed that d reached an asymptotic value as $p \rightarrow 50$. Our focus is on the variation in d with incremental changes in P and f , i.e., between datasets. Using $p = 50$ for each dataset ensured that the distribution for d over different datasets was unaffected.

Figure 9.22 is a histogram of d for all the time series sets collected. The bimodal distribution for d reveals a qualitative difference in the nonlinear interactions. The smaller cluster of 285 datasets, with $d < 2$, is indicative of low-dimensional interactions, possibly between two modes. Of interest to us are the combinations of P and f that yield a lower dimension for the output signal. Figure 9.23 is a bi-level density plot of d over the input space, with the darker shade referring to datasets with $d < 2$. By locating the frequencies that correspond to the dipole gaps on this density plot, we observe that the dark regions lie close to three even numbered dipole gaps. Values of $d > 2$ were

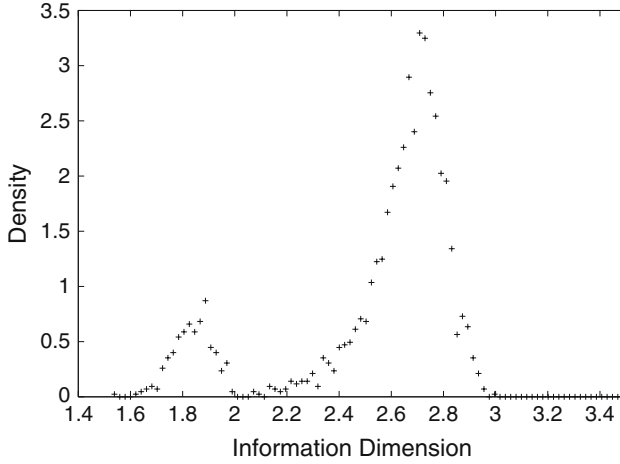


Fig. 9.22. Histogram of information dimension values calculated for each chaotic time series as input frequency and power were varied. A total of 2074 datasets were used with 285 sets having $d < 2$. (Reprinted with permission from [51]. Copyright 2000, American Institute of Physics.)

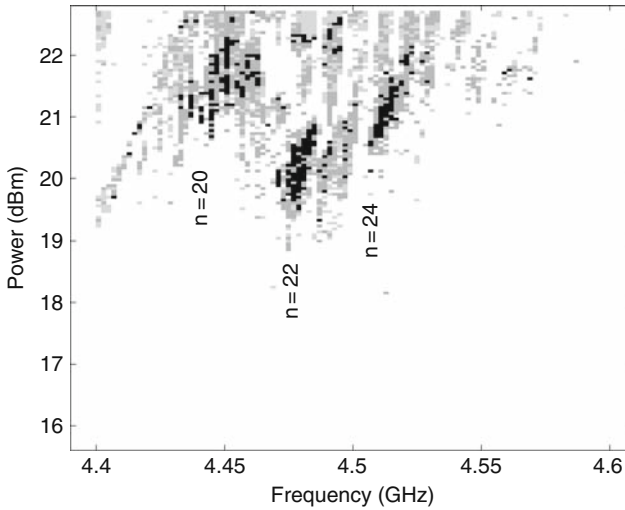


Fig. 9.23. Bi-level density plot of the information dimension, d , or equivalently a plot of the embedding dimension D . The dark clusters indicate datasets with $d < 2$ and lie close to the location of the even dipole gaps. d increases with an increase in power or a change in frequency. (Reprinted with permission from [51]. Copyright 2000, American Institute of Physics.)

observed with an increase in P or a change in f and are indicative of more complex interactions between SWs. Since most of the input power is coupled into the zeroth order mode, it is likely that the SW interactions near an even

dipole gap have a lower dimension than those at a comparable input power but near an odd dipole gap. However, this difference vanishes with further increases in P .

Problems

9.1. Show that the complex amplitude

$$a = \frac{1}{\sqrt{2}}(p + iq) \quad (9.116)$$

satisfies the equation of motion

$$\dot{a} = i \frac{\partial \mathcal{H}(a, a^*)}{\partial a^*}, \quad (9.117)$$

where p and q are canonical variables satisfying the Hamiltonian equations of motion in Eq. (9.13).

9.2. In this problem, we will solve for the scaling function f in (9.34).

(a) Take the time derivative of (9.34a) and show that

$$\dot{M}_+ = \dot{a}fC + af'[a^*\dot{a} + \dot{a}^*a]C, \quad (9.118)$$

where $C = \sqrt{-2\gamma M_S}$ and $f'(x) = df/dx$.

(b) Using the canonical equations (9.35) for the time derivatives on the right-hand side of (9.118), show that

$$\dot{M}_+ = iC[f + f'a^*a] \frac{\delta W}{\delta a^*} - iCa^2f' \frac{\delta W}{\delta a}. \quad (9.119)$$

(c) Using the chain rules

$$\frac{\delta W}{\delta a} = \frac{\delta W}{\delta M_+} \frac{\partial M_+}{\partial a} + \frac{\delta W}{\delta M_-} \frac{\partial M_-}{\partial a}, \quad (9.120a)$$

$$\frac{\delta W}{\delta a^*} = \frac{\delta W}{\delta M_+} \frac{\partial M_+}{\partial a^*} + \frac{\delta W}{\delta M_-} \frac{\partial M_-}{\partial a^*}, \quad (9.120b)$$

show that

$$\frac{\delta W}{\delta a} = C(f + a^*af') \frac{\delta W}{\delta M_+} + C(a^*)^2f' \frac{\delta W}{\delta M_-}, \quad (9.121a)$$

$$\frac{\delta W}{\delta a^*} = Ca^2f' \frac{\delta W}{\delta M_+} + C(f + a^*af') \frac{\delta W}{\delta M_-}. \quad (9.121b)$$

(d) Substitute the results of part (c) into the result of part (b) and show that

$$\dot{M}_+ = -i2\gamma M_S (f^2 + 2ff'a^*a) \frac{\delta W}{\delta M_-}. \quad (9.122)$$

- (e) Show that the result of part (d) has the same form as the equation of motion (9.30a) provided f satisfies the differential equation

$$\frac{d}{dx}(xf^2) = f^2 + 2xf f' = \sqrt{1 + \frac{2\gamma x f^2}{M_S}}, \quad (9.123)$$

where $x = a^* a$.

- (f) Using direct substitution, show that

$$f(x) = \sqrt{1 + \frac{\gamma x}{2M_S}} \quad (9.124)$$

is a solution to the differential equation in part (e).

9.3. The magnetic energy density for small signal excitations about equilibrium ($\mathbf{M} = M_S \hat{z}$) can be expanded into a quadratic variation [59]

$$W = \frac{H_x M_x^2 + H_y M_y^2}{2M_S} \quad (9.125)$$

where H_x and H_y are the effective fields ($-\frac{1}{\mu_0} \frac{\partial W}{\partial \mathbf{M}}$) in the $\hat{\mathbf{x}}$ and $\hat{\mathbf{y}}$ directions, respectively. Assuming a very thin film along $\hat{\mathbf{x}}$ with both applied and uniaxial anisotropy along $\hat{\mathbf{z}}$, show that the variables

$$M_x = \sqrt{\frac{|\gamma| M_S}{2}} (a^* + a), \quad M_y = i \sqrt{\frac{|\gamma| M_S}{2}} (a^* - a), \quad (9.126)$$

describe a Hamiltonian of the form

$$\mathcal{H} = A a^* a + \frac{B}{2} (a a + a^* a^*) \quad (9.127)$$

where $A = |\gamma|(H_x + H_y)/2$ and $B = |\gamma|(H_x - H_y)/2$.

9.4. Prove the results of the Bogoliubov transformation:

- (a) Substituting (9.45) into (9.46), show that we obtain the general (non-diagonal) form of the second-order Hamiltonian given in Eq. (9.42). Identify the appropriate terms to yield Eqs. (9.47).
 (b) Solving (9.47), show that

$$u_{\mathbf{k}} = \sqrt{\frac{A_{\mathbf{k}} + \omega_{\mathbf{k}}}{2\omega_{\mathbf{k}}}} \quad \text{and} \quad v_{\mathbf{k}} = \frac{B_{\mathbf{k}}}{|B_{\mathbf{k}}|} \sqrt{\frac{A_{\mathbf{k}} - \omega_{\mathbf{k}}}{2\omega_{\mathbf{k}}}}. \quad (9.128)$$

- (c) Use (9.46) to write down, in matrix notation, the rate equations for $b_{\mathbf{k}}$ and $b_{-\mathbf{k}}^*$. Show that the transformation

$$\begin{pmatrix} b_{\mathbf{k}} \\ b_{-\mathbf{k}}^* \end{pmatrix} = \begin{pmatrix} u_{\mathbf{k}} & v_{\mathbf{k}} \\ v_{\mathbf{k}}^* & u_{\mathbf{k}} \end{pmatrix} \begin{pmatrix} a_{\mathbf{k}} \\ a_{-\mathbf{k}}^* \end{pmatrix}, \quad (9.129)$$

will yield the corresponding rate equations $(\dot{a}_{\mathbf{k}} \quad \dot{a}_{-\mathbf{k}}^*)^T$.

9.5. The Landau–Lifshitz equation of motion can be used to derive the various coefficients in the Hamiltonian for the spin wave manifold. Using (9.70), write the small-signal magnetization in terms of the canonical variables as

$$\frac{m_{\mathbf{k}x}}{M_S} = \frac{a_{\mathbf{k}} + a_{-\mathbf{k}}^*}{2} \quad \text{and} \quad \frac{m_{\mathbf{k}y}}{M_S} = \frac{a_{\mathbf{k}} - a_{-\mathbf{k}}^*}{2i}. \quad (9.130)$$

Substitute this into Eqs. (9.69) to derive $A_{\mathbf{k}}$ and $B_{\mathbf{k}}$ in (9.72).

9.6. Start with the dispersion relation

$$[k - k(\omega, |\psi|^2)] \psi = 0. \quad (9.131)$$

For a slowly varying amplitude ψ , a small deviation due to dispersion drives the wave number $k(\omega_0)$ to $k = k(\omega_0) + \delta k$.

- (a) Using the Taylor expansion (9.85), and identifying $z' = z - v_g t$, derive the canonical NLS equation for a wave of the form $u(z, t)$ as

$$i \frac{\partial u}{\partial z} = \frac{k_2}{2} \frac{\partial^2 u}{\partial t^2} - \gamma^2 |u|^2 u, \quad (9.132)$$

where k_2 and γ are the dispersion and nonlinearity coefficients, respectively.

- (b) Verify, by substitution, that

$$u(z, t) = u_0 \operatorname{sech}(t/t_0) e^{i\kappa z} \quad (9.133)$$

is a solution to the NLS equation where the pulse amplitude u_0 and the width t_0 are related according to

$$|u_0|^2 = \frac{k_2}{\gamma t_0^2} \quad \text{and} \quad \kappa = \frac{k_2}{2t_0^2}. \quad (9.134)$$

- (c) A physical pulse must have positive amplitude, i.e., $k_2 \gamma > 0$. For forward volume spin waves, verify that this criterion is satisfied under the anomalous dispersion regime.

9.7. (a) Using the hyperbolic trigonometric identities listed in Appendix D, show by direct substitution that (9.91) is a solution to the nonlinear Schrödinger equation (9.84).

- (b) If $u(z, t)$ is a solution to the NLS equation, show that $\varepsilon u(\varepsilon z, \varepsilon^2 t)$ is also a solution. The arbitrary scaling factor ε accounts for the existence of higher order solitons, with the fundamental soliton obtained by choosing $u(0, 0) = 1$ and $\varepsilon = 1$.

9.8. Multiply Eq. (9.95) by $2(dv/dz)$ and integrate both sides to obtain

$$v_z = [v^2 \eta^2 - v^4 + C]^{1/2}, \quad (9.135)$$

where C is a constant of integration. Requiring that both v and v_z vanish as $z \rightarrow \infty$ yields $C = 0$. Using $v = 1/s$ and $s = \eta^{-1} \cosh \theta$, integrate (9.135) to obtain $\theta = -\eta z$ and thus, $v(z) = \eta \operatorname{sech} \eta z$.

References

- [1] A. Cash and D. D. Stancil, "Measurement of magnetostatic wave profiles using the interaction with transverse optical guided modes," *IEEE Trans. Mag.*, vol. 32, p. 5188, 1996.
- [2] D. J. Seagle, S. H. Charap, and J. O. Artman, "Foldover in YIG," *J. Appl. Phys.*, vol. 57, p. 3706, 1985.
- [3] Y. K. Fetisov, C. E. Patton, and V. T. Synogach, "Nonlinear ferromagnetic resonance and foldover in yttrium iron garnet thin films – inadequacy of the classical model," *IEEE Trans. Mag.*, vol. 35, p. 4511, 1999.
- [4] Y. T. Zhang, C. E. Patton, and M. V. Kogekar, "Ferromagnetic resonance foldover in single crystal YIG films – sample heating or Suhl instability," *IEEE Trans. Mag.*, vol. 22, p. 993, 1986.
- [5] A. Prabhakar and D. D. Stancil, "Auto-oscillation thresholds at the main resonance in ferrimagnetic films," *Phys. Rev. B*, vol. 57, p. 11483, 1998.
- [6] M. Weiss, "Microwave and low-frequency oscillation due to resonance instabilities in ferrites," *Phys. Rev. Lett.*, vol. 1, p. 239, 1958.
- [7] H. Suhl, "The theory of ferromagnetic resonance at high signal powers," *J. Phys. Chem. Solids*, vol. 1, p. 209, 1957.
- [8] X. Y. Zhang and H. Suhl, "Theory of auto-oscillations in high power ferromagnetic resonance," *Phys. Rev. B*, vol. 38, p. 4893, 1988.
- [9] A. Prabhakar and D. D. Stancil, "Nonlinear microwave-magnetic resonator operated as a bistable device," *J. Appl. Phys.*, vol. 85, p. 4859, 1999.
- [10] Y. K. Fetisov and C. E. Patton, "Microwave bistability in a magnetostatic wave interferometer with external feedback," *IEEE Trans. Mag.*, vol. 35, no. 2, pp. 1024–1036, Mar 1999.
- [11] H. Goldstein, C. P. Poole, and J. L. Safko, *Classical Mechanics*, 3rd ed. Cambridge, MA: Addison-Wesley, 2001.
- [12] C. Cohen-Tannoudji, J. Dupont-Roc, and G. Grynberg, *Photons and Atoms: Introduction to Quantum Electrodynamics*. New York, NY: Wiley & Sons, 1997.
- [13] E. Schlömann, "Ferromagnetic resonance at high power levels," Raytheon Corporation, Tech. Rep., 1959.
- [14] V. S. L'vov, *Turbulence Under Parametric Excitation, Applications to Magnets*. Berlin: Springer-Verlag, 1994.
- [15] T. Holstein and H. Primakoff, "Field dependence of the intrinsic domain magnetization of a ferromagnet," *Phys. Rev.*, vol. 58, no. 12, pp. 1098–1113, Dec 1940.
- [16] H. Benson and D. L. Mills, "Spin waves in thin films; dipolar effects," *Phys. Rev.*, vol. 178, no. 2, pp. 839–847, Feb 1969.
- [17] S. M. Rezende and F. M. Aguiar, "Spin-wave instabilities, auto-oscillations, and chaos in yttrium-iron-garnet," *Proc. IEEE*, vol. 78, p. 893, 1990.

- [18] P. Krivosik, N. Mo, S. Kalarickal, and C. E. Patton, "Hamiltonian formalism for two magnon scattering microwave relaxation: Theory and applications," *J. Appl. Phys.*, vol. 101, p. 083901, 2007.
- [19] H. Suhl, "Subsidiary absorption peaks in ferromagnetic resonance at high signal levels," *Phys. Rev.*, vol. 101, pp. 1437–1438, 1956.
- [20] P. H. Bryant, C. D. Jeffries, and K. Nakamura, "Spin-wave dynamics in a ferrimagnetic sphere," *Phys. Rev. A*, vol. 38, p. 4223, 1988.
- [21] V. E. Zakharov, V. S. L'vov, and S. S. Starobinets, "Instability of monochromatic spin waves," *Sov. Phys. Solid State*, vol. 11, p. 2368, 1970.
- [22] P. Wigen, Ed., *Nonlinear Phenomena and Chaos in Magnetic Materials*. Singapore: World Scientific, 1994.
- [23] R. Marcelli and S. A. Nikitov, Eds., *Nonlinear Microwave Signal Processing: Towards a New Range of Devices*. Dordrecht: Kluwer Academic Publishers, 1996.
- [24] M. A. Tsankov, M. Chen, and C. E. Patton, "Forward volume wave microwave envelope solitons in yttrium iron garnet films: Propagation, decay and collision," *J. Appl. Phys.*, vol. 76, p. 4274, 1994.
- [25] G. P. Agrawal, *Nonlinear Fiber Optics*. New York, NY: Academic Press, 2006.
- [26] B. A. Kalinikos, N. G. Kovshikov, and A. N. Slavin, "Spin-wave solitons in ferromagnetic films: observation of a modulational instability of spin-waves during continuous excitation," *JETP Lett*, vol. 10, p. 392, 1984.
- [27] M. J. Ablowitz and P. A. Clarkson, *Solitons, Nonlinear Evolution Equations and Inverse Scattering*. New York, NY: Cambridge University Press, 1991.
- [28] S. C. Chapra and R. P. Canale, *Numerical Methods for Engineers*, 5th ed. New York, NY: McGraw-Hill, 2005.
- [29] M. J. Lighthill, "Contributions to the theory of waves in nonlinear dispersive systems," *J. Inst. Maths Applics.*, vol. 1, p. 269, 1965.
- [30] B. Kalinikos and A. N. Slavin, "Theory of dipole exchange spin-wave spectrum for ferromagnetic films with mixed exchange boundary conditions," *J. Phys. C: Solid State Phys.*, vol. 19, p. 7013, 1986.
- [31] A. N. Slavin, "Thresholds of envelope soliton formation in a weakly dissipative medium," *Phys. Rev. Lett.*, vol. 77, p. 4644, 1996.
- [32] R. A. Stuadinger, P. Kabos, H. Xia, B. T. Faber, and C. E. Patton, "Calculation of the formation time for microwave magnetic envelope solitons," *IEEE Trans. Mag.*, vol. 34, p. 2334, 1998.
- [33] B. A. Kalinikos, N. G. Kovshikov, and C. E. Patton, "Decay free microwave magnetic envelope soliton pulse trains in yttrium iron garnet thin films," *Phys. Rev. Lett.*, vol. 78, no. 14, pp. 2827–2830, 1997.
- [34] B. Kalinikos, N. V. Kovshikov, and C. E. Patton, "Self-generation of microwave magnetic envelope soliton trains in yttrium iron garnet thin films," *Phys. Rev. Lett.*, vol. 80, p. 4301, 1998.

- [35] B. A. Kalinikos, N. G. Kovshikov, and C. E. Patton, "Excitation of bright and dark microwave magnetic envelope solitons in a resonant ring," *Appl. Phys. Lett.*, vol. 75, p. 265, 1999.
- [36] M. Wu, B. A. Kalinikos, L. D. Carr, and C. E. Patton, "Observation of spin wave soliton fractals in magnetic film active feedback rings," *Phys. Rev. Lett.*, 2006.
- [37] Y. Xu, G. Su, D. Xue, H. Xing, and F. shen Li, "Nonlinear surface spin waves on ferromagnetic media with inhomogeneous exchange anisotropies: soliton solutions," *Phys. Lett. A*, vol. 279, pp. 385–390, 2001.
- [38] O. Büttner, M. Bauer, S. O. Demokritov, B. Hillebrands, Y. S. Kivshar, V. Grimalsky, Y. Rapoport, M. P. Kostylev, B. A. Kalinikos, and A. N. Slavin, "Spatial and spatiotemporal self-focusing of spin waves in garnet films observed by space- and time-resolved brillouin light scattering," *J. Appl. Phys.*, vol. 87, pp. 5088–5090, 2000.
- [39] R. Gong, Y. Cheng, and H. Li, "Variational analysis of evolution for magnetostatic envelope bright soliton with higher-order dispersion," *J. Magn. Magn. Matl.*, vol. 313, pp. 122–126, 2007.
- [40] B. Kalinikos and M. P. Kostylev, "Parametric amplification of spin wave envelope solitons in ferromagnetic films by parallel pumping," *IEEE Trans. Mag.*, vol. 33, no. 5, p. 3445, 1997.
- [41] G. Gibson and C. Jeffries, "Observation of period doubling and chaos in spin-wave instabilities in yttrium iron garnet," *Phys. Rev. A*, vol. 29, p. 811, 1984.
- [42] R. D. McMichael and P. E. Wigen, "High power ferromagnetic resonance without a degenerate spin-wave manifold," *Phys. Rev. Lett.*, vol. 64, p. 64, 1990.
- [43] A. Borovik-Romanov and S. Sinha, Eds., *Spin Waves and Magnetic Excitations*. Amsterdam: North Holland Physics, 1988.
- [44] M. Cottam, Ed., *Linear and Nonlinear Spin Waves in Magnetic Films and Superlattices*. Singapore: World Scientific, 1994.
- [45] G. Srinivasan and A. N. Slavin, Eds., *High Frequency Processes in Magnetic Materials*. Singapore: World Scientific, 1995.
- [46] C. Robinson, *Dynamical Systems*. Boca Raton, FL CRC Press Inc., 1995.
- [47] P. Glendinning, *Stability, Instability and Chaos*. Cambridge Cambridge University Press., 1994.
- [48] J. I. Neimark, *Mathematical Models in Natural Science and Engineering*. Berlin: Springer, 2003, ch. 4.
- [49] T. Y. Li and J. A. Yorke, "Period three implies chaos," *Amer. Math. Monthly*, vol. 82, pp. 985–992, 1975.
- [50] A. Prabhakar and D. D. Stancil, "Variations in auto-oscillation frequency at the main resonance in rectangular YIG films," *J. Appl. Phys.*, vol. 79, p. 5374, 1996.

- [51] A. Prabhakar and D. D. Stancil, "Information dimension analysis of chaotic forward volume spin waves in a yttrium-iron-garnet thin film," *J. Appl. Phys.*, vol. 87, p. 5091, 2000.
- [52] R. Hegger and H. Kantz, "Practical implementation of nonlinear time series methods: The TISEAN package," *Chaos*, vol. 9, no. 2, pp. 413–435, 1999.
- [53] H. D. I. Abarbanel, R. Brown, J. J. Sidorowich, and L. S. Tsimring, "The analysis of observed chaotic data in physical systems," *Rev. Mod. Phys.*, vol. 65, no. 4, p. 1331, 1993.
- [54] M. Kennel, R. Brown, and H. D. I. Abarbanel, "Determining embedding dimension for phase-space reconstruction using a geometrical construction," *Phys. Rev. A*, vol. 45, p. 3403, 1992.
- [55] I. Procaccia and M. Shapiro, Eds., *Chaos and Related Nonlinear Phenomena*. New York: Plenum, 1987, ch. Practical Considerations in estimating dimension from time series data.
- [56] J. P. Eckmann and D. Ruelle, "Fundamental limitations for estimating dimensions and Lyapunov exponents in dynamical systems," *Physica D*, vol. 56, p. 185, 1992.
- [57] R. Badii and A. Politi, "Statistical description of chaotic attractors: the dimension function," *J. Stat. Phys.*, vol. 40, p. 725, 1985.
- [58] E. J. Kostelich, "Nearest neighbour algorithm," personal communication.
- [59] H. N. Bertram, V. L. Safonov, and Z. Jin, "Thermal magnetization noise, damping fundamentals, and mode analysis: Application to a thin film GMR sensor," *IEEE Trans. Mag.*, vol. 38, pp. 2514–2519, 2002.

Novel Applications

Gedanken (or thought) experiments are often followed by practical demonstrations of underlying physics. Once laboratory experiments establish the physics, we could witness the emergence of a new technology. In parallel, as existing technologies mature, there is a rebirth of established ideas with the possibility of new applications. This chapter attempts to describe a few areas of current research in spin-waves, where the fate of novel physics and emerging technology are closely intertwined. For example, the advent of submicron lithographic techniques has given rise to nano-contact spin-wave generation structures using current-driven spin-transfer torques. Also, an improved understanding of spin-wave excitations helps describe noise in patterned nano-structures, and new techniques such as the Magneto-Optic Kerr Effect (MOKE) make it possible to probe the modes of patterned structures. Finally, the properties of backward spin-waves make it possible to observe the long-predicted inverse *Doppler effect*. Since these are all “hot topics,” we cannot do full justice to them or cover all the frontier areas of research. However, in this chapter, we shall attempt to provide self-contained descriptions of a few topics while referring the reader to recently published literature for a more complete account of the theoretical and technological nuances.¹

10.1 Nano-Contact Spin-Wave Excitations

In recent years, the excitation of spin-waves using current injection through nano-contacts has garnered much interest. These devices hold the promise of a new generation of tunable microwave sources. To understand the physics behind the operation of these technologically advanced devices, we must first embark on a short journey into the area of magnetoelectronics. Thereafter, we

¹ A few topics in quantum mechanics, related to the tunneling of electrons, are described in Appendix B.

will describe the results of an experiment that validates our understanding of spin polarized current-induced spin-wave excitations.

10.1.1 Current-Induced Spin Torque

Seminal work by Slonczewski [1] and Berger [2] laid the foundations of our understanding of current-induced spin torque in ferromagnetic multilayers. Earlier work by Stearns [3] on the tunneling of electrons from a ferromagnet across a barrier presented an explanation of the spin polarization of the tunneling current based on band-splitting in the ferromagnet. The intrinsic magnetic moment in a ferromagnetic material causes “spin-down” electrons (with magnetic moment parallel to magnetization of the ferromagnet) to have a lower energy than “spin-up” electrons (with moment antiparallel to the magnetization), or in other words a splitting of the conduction band, as shown in Figure 10.1. In fact, the magnetization can be defined as

$$M = \mu_B \int_0^{\infty} [g_{\downarrow}(E) - g_{\uparrow}(E)] f(E) dE, \quad (10.1)$$

where $g(E)$ is the *density of states* and $f(E)$ is the Fermi–Dirac distribution (cf. Appendix B). We expect the population of spin-down electrons to be higher than that of spin-up electrons, leading to the terms majority and minority spin carriers, respectively. The spin-down states (with up moment) are lower in energy and the spin-up (with down moment) are higher in energy, each by an amount $\mu_0 \mu_B H_m$. The asymmetry in $g(E)$ at the *Fermi energy* is also used to define the spin polarization of a metal as

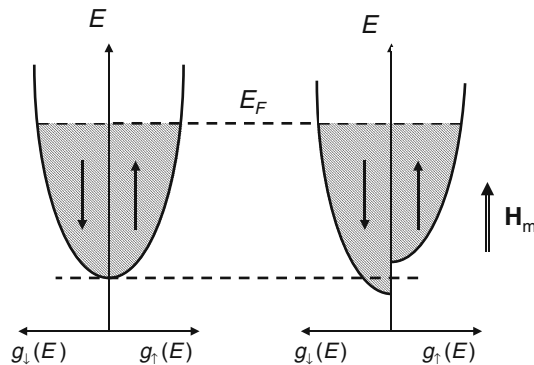


Fig. 10.1. The parabolic band approximation in the free electron model. The splitting in the density of states $g(E)$ in the presence of a magnetic field is $\pm \mu_0 \mu_B H_m$. In a ferromagnetic metal, splitting occurs from the effective exchange field, or molecular field, that is parallel to the magnetization.

$$P = \frac{g_{\uparrow}(E_F) - g_{\downarrow}(E_F)}{g_{\uparrow}(E_F) + g_{\downarrow}(E_F)}. \quad (10.2)$$

This is a very elementary picture applicable only to a split in the band of free electrons. In reality, $g(E)$ in transition elements like Ni and Fe is fairly complicated and the Fermi energy overlaps with both the s and d orbitals. The resulting exchange interaction is strong enough to require the use of collective-electron and rigid-band models [4, 5].

Consider now two ferromagnetic layers separated by a paramagnetic or insulating barrier. In a rather simplified picture of spin-torque, we can argue that if we manage to transfer only spin-up electrons from one ferromagnetic layer into another ferromagnetic layer, we could affect a change in number of majority and minority spin carriers in the second layer. We compensate for the resulting imbalance in spin angular momentum by introducing an additional torque term in the LLG equation that describes the magnetization dynamics of the second layer.

To pursue this further, consider the geometry shown in Figure 10.2, where a spin-polarized current from ferromagnetic layer F_1 is injected through a thin barrier of a normal metal into a second ferromagnetic layer F_2 . The dashed box represents a thin volume near the interface of F_2 . If the angular momentum of the *spin currents* leaving the box differs from that of the spin currents entering the box, then conservation of angular momentum requires that a torque be exerted on the spins \mathbf{S}_2 in this layer. This torque results in a current-induced precession of \mathbf{S}_2 .

Although we are concerned with a tunnel junction, the origin of the current-driven precession phenomenon can be understood by considering the somewhat simpler problem of reflection and transmission at the boundary between the normal metal and ferromagnet 2. Consequently, we will concentrate on the dynamics at this interface in the following discussion. Reflection and transmission of a particle current density without spin polarization at

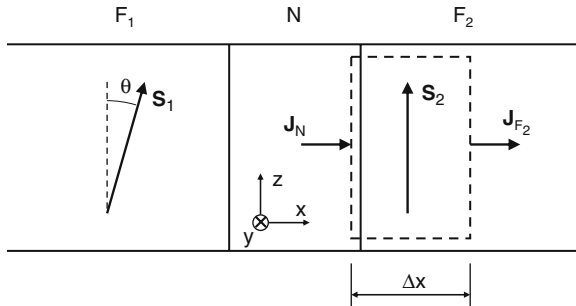


Fig. 10.2. Pictorial representation of the transfer of spin angular momentum from one ferromagnet to another, across a non-magnetic barrier. The picture highlights the notion that momentum transfer is caused by scattering and is largely an interface effect.

a potential barrier is a standard treatment in quantum mechanics [6, 7]. Appendix B describes how we can calculate the reflection and transmission coefficients at a boundary between two media.

In the context of spin-wave generation, we are primarily interested in the form of the spin torque term ($\boldsymbol{\tau}$) to be included in the LLG equation. To understand this, we define the *spin density*

$$\mathbf{S}(\mathbf{r}) = \frac{\hbar}{2} \psi^\dagger \boldsymbol{\sigma} \psi \quad (10.3)$$

and the *spin current density*²

$$\mathbf{J} = \mathbf{v} \otimes \mathbf{s} = \frac{\hbar^2}{2m} \text{Im}(\psi^\dagger \boldsymbol{\sigma} \otimes \nabla \psi), \quad (10.4)$$

where $\mathbf{s} = \frac{\hbar}{2} \boldsymbol{\sigma}$ and $\boldsymbol{\sigma}$ is the Pauli spin vector (cf. Problems 1.5 and 10.1). Here, we have introduced the notion of the inner product between two sub-spaces denoted by the symbol \otimes . In the present context, this refers to the position and spin subspaces. Operators such as ∇ and $\boldsymbol{\sigma}$ operate only on the part of the wavefunction that belongs to their respective subspaces (recall a similar approach in Section 2.4). Thus, the wavefunction of a free-electron with spin has the form

$$\psi = a \frac{e^{ik_\uparrow x}}{\sqrt{k_\uparrow}} \chi_\uparrow + b \frac{e^{ik_\downarrow x}}{\sqrt{k_\downarrow}} \chi_\downarrow, \quad (10.5)$$

where the spin-up and spin-down states (defined in Problem 1.5) have amplitudes a and b , respectively, and the normalization $1/\sqrt{k_{\uparrow,\downarrow}}$ assures unit particle flux. Note that \mathbf{J} is a tensor quantity. Referring to (10.4), the first index comes from the Pauli spin vector and represents the spin direction, while the second index comes from the gradient operator and represents the direction of the current. For example, J_{xy} refers to the y component of the spin current that has a spin along x .

The spin density and spin current density have forms that are similar to the more familiar charge density and current density given by

$$\rho(\mathbf{r}) = q \psi^\dagger \psi \quad (10.6)$$

and

$$\mathbf{j}(\mathbf{r}) = q \frac{\hbar}{m} \text{Im}(\psi^\dagger \nabla \psi), \quad (10.7)$$

where q is the electronic charge (negative). These quantities satisfy the conservation equation (cf. Eq. (4.25a))

$$\int_V \frac{\partial \rho}{\partial t} dv = - \oint_A \mathbf{j} \cdot d\mathbf{a}, \quad (10.8)$$

² Mita shows how the spin probability current is a virtual current, i.e., it does not contribute to the particle's kinetic energy, and can be derived from the expectation value of the spin operator $\langle \mathbf{s} \rangle$ [8].

where A is the surface enclosing the volume V . In a similar fashion, if no other torques are acting on the system, the spin quantities satisfy the conservation equation

$$\int_V \frac{\partial \mathbf{S}}{\partial t} dv = - \oint_A \mathbf{J} \cdot d\mathbf{a}. \quad (10.9)$$

Let us apply this conservation equation to the volume enclosed by the dashed lines in Figure 10.2. We will assume that the left boundary of the surface is infinitesimally to the left of the interface, but that the right boundary extends a distance Δx into F_2 . Equation (10.9) then becomes

$$\begin{aligned} \frac{\partial \mathbf{S}_2}{\partial t} A_x \Delta x &= - [\mathbf{J}_{F_2} \cdot \hat{\mathbf{x}} + \mathbf{J}_N \cdot (-\hat{\mathbf{x}})] A_x \\ &= - [\mathbf{J}_{F_2} - \mathbf{J}_N] \cdot \hat{\mathbf{x}} A_x \\ &= [\mathbf{J}^{\text{in}} + \mathbf{J}^{\text{ref}} - \mathbf{J}^{\text{tr}}] \cdot \hat{\mathbf{x}} A_x, \end{aligned} \quad (10.10)$$

or

$$\frac{\partial \mathbf{S}_2}{\partial t} \Delta x = [\mathbf{J}^{\text{in}} + \mathbf{J}^{\text{ref}} - \mathbf{J}^{\text{tr}}] \cdot \hat{\mathbf{x}} \equiv \mathbf{N}. \quad (10.11)$$

Here, A_x is the cross-sectional area perpendicular to the x -axis, $\mathbf{J}_N = \mathbf{J}^{\text{in}} + \mathbf{J}^{\text{ref}}$ is the total spin current in the normal metal, $\mathbf{J}_{F_2} = \mathbf{J}^{\text{tr}}$ is the spin current transmitted into ferromagnet F_2 , and Δx is sufficiently small that any current crossing the top and bottom surfaces can be neglected.

Recalling the discussion in Section 1.4.3, we realize that the appropriate direction for quantization of the electron spin in F_2 is along \mathbf{S}_2 . We will assume that the spin current incident on the interface with F_2 is polarized parallel with \mathbf{S}_1 , so we must construct a representation of this current in the coordinate system of \mathbf{S}_2 . We can do this by rotating the state χ_{\uparrow} about the $\hat{\mathbf{y}}$ axis, shown in Figure 10.2. In general, a spinor χ can be rotated about the axis $\hat{\mathbf{n}}$ through an angle θ using the operator [7]

$$\begin{aligned} U_R &= \exp \left(-i \frac{\theta}{2} \hat{\mathbf{n}} \cdot \boldsymbol{\sigma} \right) \\ &= \mathbf{I} \cos \frac{\theta}{2} - i \hat{\mathbf{n}} \cdot \boldsymbol{\sigma} \sin \frac{\theta}{2}, \end{aligned} \quad (10.12)$$

where \mathbf{I} is the identity matrix. For rotations about the y -axis, this becomes

$$U_R = \begin{bmatrix} \cos(\theta/2) & -\sin(\theta/2) \\ \sin(\theta/2) & \cos(\theta/2) \end{bmatrix}. \quad (10.13)$$

The construction of a properly oriented spinor then proceeds as follows:

$$\begin{aligned}
U_R \chi_\uparrow &= \begin{bmatrix} \cos(\theta/2) & -\sin(\theta/2) \\ \sin(\theta/2) & \cos(\theta/2) \end{bmatrix} \begin{bmatrix} 1 \\ 0 \end{bmatrix} \\
&= \begin{bmatrix} \cos(\theta/2) \\ \sin(\theta/2) \end{bmatrix} \\
&= \cos(\theta/2) \begin{bmatrix} 1 \\ 0 \end{bmatrix} + \sin(\theta/2) \begin{bmatrix} 0 \\ 1 \end{bmatrix} \\
&= \cos(\theta/2) \chi_\uparrow + \sin(\theta/2) \chi_\downarrow.
\end{aligned} \tag{10.14}$$

The wavefunctions for the incident, reflected, and transmitted spin currents can now be written as

$$\psi_{\text{in}} = \frac{e^{ikx}}{\sqrt{k}} \left(\cos(\theta/2) \chi_\uparrow + \sin(\theta/2) \chi_\downarrow \right), \tag{10.15a}$$

$$\psi_{\text{ref}} = \frac{e^{-ikx}}{\sqrt{k}} \left(r_\uparrow \cos(\theta/2) \chi_\uparrow + r_\downarrow \sin(\theta/2) \chi_\downarrow \right), \tag{10.15b}$$

$$\psi_{\text{tr}} = t_\uparrow \cos(\theta/2) \frac{e^{ik_\uparrow x}}{\sqrt{k_\uparrow}} \chi_\uparrow + t_\downarrow \sin(\theta/2) \frac{e^{ik_\downarrow x}}{\sqrt{k_\downarrow}} \chi_\downarrow, \tag{10.15c}$$

with the normalized amplitudes $r_{\uparrow,\downarrow}$ and $t_{\uparrow,\downarrow}$. Here, we have assumed that in the normal metal $k_\uparrow = k_\downarrow = k$. Substituting (10.15) into (10.4) yields the incident, reflected, and transmitted spin current densities (cf. Problem 10.2). Using these current densities, the areal torque density from Eq. (10.11) is given by

$$\begin{aligned}
\mathbf{N} &= [\mathbf{J}^{\text{in}} + \mathbf{J}^{\text{ref}} - \mathbf{J}^{\text{tr}}] \cdot \hat{\mathbf{x}} \\
&= \frac{\hbar^2 \sin \theta}{2m} \left\{ \hat{\mathbf{x}} \left[1 - \text{Re} \left(r_\uparrow^* r_\downarrow + \frac{(k_\uparrow + k_\downarrow)}{2\sqrt{k_\uparrow k_\downarrow}} t_\uparrow^* t_\downarrow e^{i(k_\downarrow - k_\uparrow)x} \right) \right] \right. \\
&\quad \left. - \hat{\mathbf{y}} \text{Im} \left(r_\uparrow^* r_\downarrow + \frac{(k_\uparrow + k_\downarrow)}{2\sqrt{k_\uparrow k_\downarrow}} t_\uparrow^* t_\downarrow e^{i(k_\downarrow - k_\uparrow)x} \right) \right\}.
\end{aligned} \tag{10.16}$$

To better understand the above equation, consider the case when there is no splitting of the spin-up and spin-down bands, i.e., $t_\uparrow = t_\downarrow = t$, $k_\uparrow = k_\downarrow = k$, and $r_\uparrow = r_\downarrow = r$. Consequently,

$$\text{Im} \left(r_\uparrow^* r_\downarrow + \frac{(k_\uparrow + k_\downarrow)}{2\sqrt{k_\uparrow k_\downarrow}} t_\uparrow^* t_\downarrow e^{i(k_\downarrow - k_\uparrow)x} \right) = \text{Im}(|r|^2 + |t|^2) = 0, \tag{10.17a}$$

$$\text{Re} \left(r_\uparrow^* r_\downarrow + \frac{(k_\uparrow + k_\downarrow)}{2\sqrt{k_\uparrow k_\downarrow}} t_\uparrow^* t_\downarrow e^{i(k_\downarrow - k_\uparrow)x} \right) = \text{Re}(|r|^2 + |t|^2) = 1, \tag{10.17b}$$

which yield $\mathbf{N} = 0$, i.e., there is no net transfer of spin. Further, note that the above condition on the real part is merely a statement of particle flux conservation.

Our calculation assumed a single electron with wavenumber k and traveling along $\hat{\mathbf{x}}$. In reality, we must average \mathbf{N} over all the electrons close to the Fermi surface, each with a different \mathbf{k} in a 3D space. Such a calculation is beyond the scope of our present discussion. However, to a good approximation, a first principle calculation [9] yields the average quantities

$$\langle r_{\uparrow}^* r_{\downarrow} \rangle \approx \left\langle \frac{(k_{\uparrow} + k_{\downarrow})}{2\sqrt{k_{\uparrow} k_{\downarrow}}} t_{\uparrow}^* t_{\downarrow} e^{i(k_{\downarrow} - k_{\uparrow})x} \right\rangle \approx 0. \quad (10.18)$$

As a result, the transfer of angular momentum into \mathbf{F}_2 , in the lowest-order approximation, is simply related to the angle between the two ferromagnetic layers, i.e.,

$$\mathbf{N} = \hat{\mathbf{x}} \frac{\hbar^2}{2m} \sin \theta. \quad (10.19)$$

The proportionality to $\sin \theta$ suggests that the right-hand side of (10.19) could be represented in terms of the cross-product of \mathbf{S}_1 and \mathbf{S}_2 . However, a moment's consideration shows that $\mathbf{S}_1 \times \mathbf{S}_2$ points in the $-\hat{\mathbf{y}}$ direction instead of the $\hat{\mathbf{x}}$ direction. The proper direction can be restored using an additional cross-product, as proposed by Slonczewski [1]:

$$\frac{d\mathbf{S}_2}{dt} \propto \mathbf{S}_2 \times (\mathbf{S}_1 \times \mathbf{S}_2). \quad (10.20)$$

10.1.2 Magnetic Precession

Let us focus our attention on understanding some of the effects of spin-polarized currents traversing a ferromagnetic film. Consider the geometry of Figure 10.3, where a current is passed through two layers both with easy axes along $\hat{\mathbf{z}}$. We will assume that the layer thicknesses $d_{1,2}$ are sufficiently thin that significant relaxation of the spin polarization of the currents does not

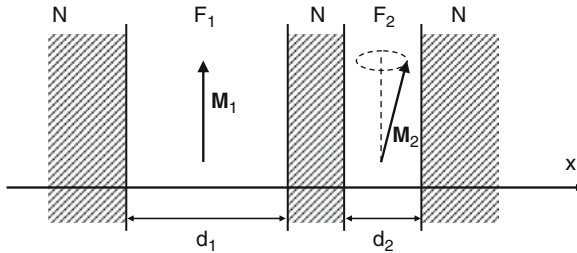


Fig. 10.3. Schematic representation of a five layer spin-transfer tunneling structure. Ferromagnetic layer \mathbf{F}_1 is assumed to be pinned, while the magnetization in ferromagnetic layer \mathbf{F}_2 is free to precess. The direction of positive current is to the right.

occur within the layers. Combining (10.11), (10.19), and (10.20) with $\Delta x = d_2$ gives³

$$\frac{d\mathbf{S}_2}{dt} = \frac{\hbar^2}{2md_2} \hat{\mathbf{S}}_2 \times (\hat{\mathbf{S}}_1 \times \hat{\mathbf{S}}_2), \quad (10.21)$$

where $\hat{\mathbf{S}}_{1,2}$ are unit vectors in the directions of $\mathbf{S}_{1,2}$. Slonczewski also showed there is a torque on layer F_1 given by

$$\frac{d\mathbf{S}_1}{dt} = \frac{\hbar^2}{2md_1} \hat{\mathbf{S}}_1 \times (\hat{\mathbf{S}}_1 \times \hat{\mathbf{S}}_2). \quad (10.22)$$

In the following, we assume that the spin in layer F_1 is fixed, either because of a large thickness $d_1 \gg d_2$, large damping, or large anisotropy. Consequently, we will concentrate on the dynamics of layer F_2 .

Since \mathbf{S} is a spin density, Eq. (10.21) can be expressed in terms of the magnetization using $\mathbf{M} = \gamma\mathbf{S}$, where $\gamma = q/m$ (negative). It follows that $\hat{\mathbf{S}}_1 = -\hat{\mathbf{M}}_1$. The spin torque (10.21) becomes

$$\frac{d\mathbf{M}_2}{dt} = -\frac{\gamma\hbar^2}{2md_2} \hat{\mathbf{M}}_2 \times (\hat{\mathbf{M}}_1 \times \hat{\mathbf{M}}_2). \quad (10.23)$$

Since we assume the magnetization in layer 1 is fixed, $\hat{\mathbf{M}}_1 = \hat{\mathbf{z}}$, and we can write

$$\frac{d\mathbf{M}_2}{dt} = -\frac{\gamma\hbar^2}{2mM_S^2d_2} \mathbf{M}_2 \times (\hat{\mathbf{z}} \times \mathbf{M}_2), \quad (10.24)$$

where M_S is the saturation magnetization of the free layer F_2 .

Up to this point, we have been considering the torque resulting from a unit particle flux. If the volume density of injected spin-polarized electrons is instead N , then the right-hand side of Eq. (10.24) is increased by this factor. The resulting torque can be related to the injected current density by noting that the current density across the interface can be written⁴ $j = qN'\hbar/m$, where $N' > N$ is the density of electrons contributing to the electric current. Thus, after multiplying by N , the coefficient in (10.24) can be written

$$\begin{aligned} \frac{\gamma N \hbar^2}{2mM_S^2d_2} &= \frac{\gamma \hbar (N/N')}{2qM_S^2d_2} \frac{qN'\hbar}{m} \\ &= \frac{\gamma \hbar \varsigma j}{2qM_S^2d_2} \\ &= \frac{\beta j}{M_S}, \end{aligned} \quad (10.25)$$

where the constant β is given by [10]

³ Here, $\partial/\partial t = d/dt$ since the surfaces and volumes under consideration are stationary.

⁴ In general, the current density is $j = qN'\hbar k/m$. However, in our calculation, the k was removed by our choice of wavefunction normalization (10.5).

$$\beta = \frac{\gamma\zeta\hbar}{2qM_S d_2}, \quad (10.26)$$

and $\zeta = N/N'$ is a spin-transfer efficiency. The form of (10.24) allows us to introduce an effective field from the spin-transfer current into the first term of the Landau–Lifshitz equation (3.127):

$$\mathbf{H}_{\text{STI}} = \frac{\beta j}{\omega_M} \hat{\mathbf{z}} \times \mathbf{M}, \quad (10.27)$$

where $\omega_M = -\gamma\mu_0 M_S$. The spin-transfer torque can now be written

$$\frac{d\mathbf{M}_2}{dt} = \gamma\mu_0 \mathbf{M}_2 \times \mathbf{H}_{\text{STI}}. \quad (10.28)$$

The total torque on \mathbf{M}_2 must also consider the effective field \mathbf{H}_{eff} as well as damping. The effective field may include magnetocrystalline anisotropy, shape anisotropy, an exchange bias field, and an externally applied bias field as well as the time-varying small-signal field. The total torque on \mathbf{M}_2 is, therefore,

$$\frac{d\mathbf{M}_2}{dt} = \gamma\mu_0 \mathbf{M}_2 \times \mathbf{H}_{\text{eff}} + \frac{\alpha}{M_S} \mathbf{M}_2 \times \frac{d\mathbf{M}_2}{dt} + \gamma\mu_0 \mathbf{M}_2 \times \mathbf{H}_{\text{STI}}. \quad (10.29)$$

Referring to Figure 10.4, the STI torque is collinear with the damping torque. Consequently, it is possible to overcome the damping and realize a current-induced precession. The threshold for this precession occurs when the last two terms in (10.29) cancel:

$$\frac{\alpha}{M_S} \mathbf{M}_2 \times \frac{d\mathbf{M}_2}{dt} = -\gamma\mu_0 \mathbf{M}_2 \times \mathbf{H}_{\text{STI}}. \quad (10.30)$$

To solve this, it is convenient to linearize the equation by writing

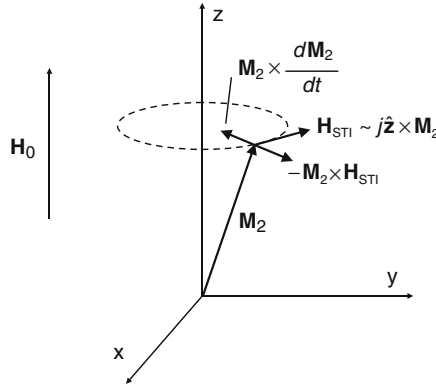


Fig. 10.4. The STI torque is collinear with the damping torque. The STI torque may aid or oppose damping depending on the sign of the current density j .

$$\mathbf{M}_2 \approx \hat{\mathbf{z}}M_S + \mathbf{m} \quad (10.31)$$

and keeping only terms to first-order in small quantities. Thus

$$\alpha \hat{\mathbf{z}} \times \frac{d\mathbf{m}}{dt} \approx \beta j \hat{\mathbf{z}} \times (\hat{\mathbf{z}} \times \mathbf{m}) \quad (10.32)$$

or

$$\alpha \frac{d\mathbf{m}}{dt} \approx \beta j (\hat{\mathbf{z}} \times \mathbf{m}). \quad (10.33)$$

Letting $\mathbf{m} = \hat{\mathbf{x}}m_x + \hat{\mathbf{y}}m_y$, Eq. (10.33) can be cast into the form

$$\begin{bmatrix} i\omega\alpha & -\beta j \\ \beta j & i\omega\alpha \end{bmatrix} \begin{bmatrix} m_x \\ m_y \end{bmatrix} = 0. \quad (10.34)$$

This has a non-trivial solution when the determinant of the coefficient matrix vanishes, leading to the critical current

$$j_c = \frac{\omega\alpha}{\beta}. \quad (10.35)$$

Recall from Section 3.8 that damping could be added to the Gilbert form of the Landau–Lifshitz equation by making the replacement $\omega_0 \rightarrow \omega_0 - i\omega\alpha$ where ω_0 is the frequency of resonant precession. Comparison with Eq. (10.35) shows that the numerator is equal to the imaginary part of the resonant frequency that represents loss. Since the spin transfer torque is proportional to β , we see that the critical current is proportional to the ratio of the loss to spin-transfer torque. We have also seen that loss can be introduced into the dynamics of the \mathbf{k} th spin-wave mode by making the substitution $\omega_{\mathbf{k}} \rightarrow \omega_{\mathbf{k}} - i\eta_{\mathbf{k}}$, so we expect the critical current more generally to be given by $j_{\mathbf{k},c} = \eta_{\mathbf{k}}/\beta$. We will return to this observation shortly.

Also note that (10.35) shows that j_c is positive, indicating that the particle flow is actually to the left in Figure 10.3 rather than to the right as we assumed in our initial analysis. Thus, to create an instability in layer 2, we must inject positive current into the layer from an adjacent layer with fixed magnetization.

In the above discussion, we neglected the effects of the demagnetizing field on the dynamics of the magnetization in the film for simplicity. However, we know from Section 5.3.2 that the demagnetizing field will significantly shift the frequency of resonant precession. Now that we have a handle on the basic physics, let us re-examine the present tunneling problem taking the demagnetizing fields into account. The first step is to linearize the complete torque equation (10.29). Similar to Eq. (10.31), we express the total effective field as a static component plus a small time-varying perturbation:

$$\mathbf{H}_0 \approx \hat{\mathbf{z}}H_0 + \mathbf{h}. \quad (10.36)$$

Following a similar procedure to that leading to Eq. (5.23), we substitute (10.31) and (10.36) into the total torque equation (10.29) and keep terms that are linear in small quantities. The result is

$$\mathbf{h} = \bar{\chi}^{-1} \cdot \mathbf{m} = \frac{1}{\omega_M} \begin{bmatrix} \omega_0 - i\omega\alpha & i\omega + \beta j \\ -i\omega - \beta j & \omega_0 - i\omega\alpha \end{bmatrix} \begin{bmatrix} m_x \\ m_y \end{bmatrix}. \quad (10.37)$$

Here, $\omega_0 = -\gamma\mu_0 H_0$. As in Section 5.3.2, another relation between \mathbf{h} and \mathbf{m} is given by the demagnetizing tensor. For the present geometry, we have

$$\mathbf{h} = -\bar{\mathbf{N}}_d \cdot \mathbf{m} = - \begin{bmatrix} 1 & 0 \\ 0 & 0 \end{bmatrix} \begin{bmatrix} m_x \\ m_y \end{bmatrix}. \quad (10.38)$$

Combining the requirements of Eqs. (10.37) and (10.38) gives

$$[\bar{\mathbf{N}}_d + \bar{\chi}^{-1}] \cdot \mathbf{m} = 0, \quad (10.39)$$

which can also be written in the form

$$\begin{bmatrix} \omega_M + \omega_0 - i\omega\alpha & i\omega + \beta j \\ -i\omega - \beta j & \omega_0 - i\omega\alpha \end{bmatrix} \begin{bmatrix} m_x \\ m_y \end{bmatrix} = 0. \quad (10.40)$$

As before, non-trivial solutions exist when the determinant of the coefficient matrix vanishes. Requiring the real part of the determinant to vanish gives the resonant frequency (cf. Eq. (5.28))

$$\omega = \sqrt{\omega_0(\omega_0 + \omega_M)}, \quad (10.41)$$

while requiring the imaginary part to vanish gives the critical current density

$$j_c = \frac{\eta_{\parallel}}{\beta}, \quad (10.42)$$

where

$$\eta_{\parallel} = \frac{1}{T_{\parallel}} = \alpha \left(\omega_0 + \frac{\omega_M}{2} \right). \quad (10.43)$$

Thus, the resonant precession frequency corresponds to the top of the volume wave manifold, and Eq. (10.43) can be recognized as the corresponding relaxation frequency (cf. Eqs. (6.26b) and (6.35b) evaluated at the frequency (10.41)).

A full mathematical description for the spin dynamics of a multiple layer structure such as that used in our example requires consideration of nonlinear terms in the torque equation that we have neglected. These nonlinear effects determine the steady-state precession angle, and give rise to current-dependent shifts in the resonant frequency. The mathematical approach for spin wave interactions discussed in Section 9.3 is often used to treat the lowest-order nonlinear effects. This approach is based on coupling between rate equations for the spin wave mode amplitudes. Fortunately, the spin-transfer torque can be easily incorporated into the rate equations using the knowledge that it acts in a direction opposite to dissipation. The rate equation (9.50) for the k th spin-wave mode then takes the form [10]

$$\frac{db_{\mathbf{k}}}{dt} = i\omega_{\mathbf{k}}b_{\mathbf{k}} - (\eta_{\mathbf{k}} - \beta j)b_{\mathbf{k}}. \quad (10.44)$$

As in the previous discussion, when the current density exceeds a critical value

$$j_c = \eta_{\mathbf{k}}/\beta, \quad (10.45)$$

we expect to see an exponential growth in the \mathbf{k} th spin wave mode. As was described in Section 6.2, $\eta_{\mathbf{k}} = \eta_k$ is independent of k for surface waves but for both surface and volume waves, $\eta_k = 1/T_k$ increases with ω_0 . This implies a dependence of the critical current j_c on the applied field.

The first observations of magnetic excitations by pumping electric current used a point contact on Co/Cu multilayers [11]. In this geometry, radiation of spin waves away from the excitation region represents an additional source of loss that must be overcome, increasing the threshold by an order of magnitude above that given by (10.45) [12]. The analysis leading to Eq. (10.45) is applicable to a multilayer pillar in which both the current and the spin waves are confined to the same region. The size of the pillar will also quantize the allowed values of spin wave \mathbf{k} . Today, in addition to metallic non-magnetic/ferromagnetic interfaces, the use of an epitaxially grown MgO insulator between two ferromagnets is a prime candidate for spin-torque-based devices [13]. A clear example of time-domain oscillations induced by a current-driven spin transfer torque is shown in Figure 10.5 [14]. The oscillations were measured in the voltage across a permalloy–Cu–permalloy stack. The voltage variations were caused by changes in resistance from the giant magnetoresistance effect (GMR).

Of interest to the microwave community is the ability to generate coherent spin-wave excitations when a number of such devices are fabricated in close proximity forming nano-oscillators. A schematic geometry for the nano-oscillators is shown in Figure 10.6 [15]. The current injected from the pinned (or fixed) ferromagnetic underlayer is polarized along $\hat{\mathbf{z}}$ and affects a transfer of angular momentum into the free layer, causing the magnetizations \mathbf{M}_1 and \mathbf{M}_2 to precess. However, a coherent precession between adjacent oscillators, leading to the generation of a microwave signal, is possible only if the oscillators are coupled together. Rezende et al. used the mathematics of four-wave interactions between excited spin waves to describe the nonlinear coupling and resulting coherent precession of these nano-oscillators [15].

Berger coined the catchy acronym SWASER (spin wave amplification by stimulated emission of radiation) to describe current-induced spin wave generation. In addition to GMR, methods for detecting the spin wave oscillations include inductive coupling to a microstrip circuit, and changes in the anisotropic magnetoresistance (AMR) with spin precession [16]. The inverse effect, i.e., excitation of a magnetic layer by an external microwave signal leading to the generation of a measurable DC voltage across the film, is also possible [17].

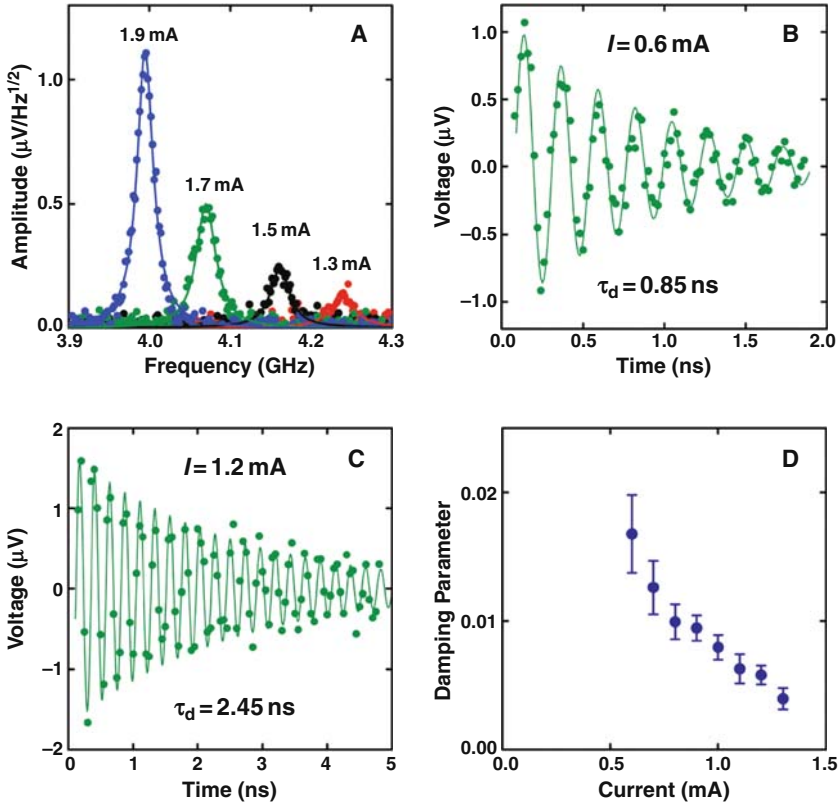


Fig. 10.5. Voltage oscillations caused by current-induced spin transfer in a permalloy-copper-permalloy sample. (Reprinted with permission from [14]. Copyright 2005 by the American Association for the Advancement of Science.)

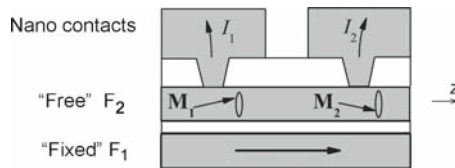


Fig. 10.6. Schematic representation of two nano-contact oscillators. The arrows represent positive current pumped from a ferromagnetic underlayer pinned along the \hat{z} direction. The magnetization in the free layer experiences a torque due to the spin-polarized current and begins to precess. (Reprinted with permission from [15]. Copyright 2007 by the American Physical Society.)

10.2 Magnetic Precession in Patterned Structures

The use of planar thin films and submicron lithography has led to the study of magnetization dynamics in patterned structures. The normal modes of excitation of a patterned structure can significantly affect the signal-to-noise ratio of the readback signal in hard-disk drives. Researchers often use micromagnetic simulations to study the dynamics of such patterned structures. Bertram et al. [18] have predicted the existence of normal modes of oscillation in a rectangular film of permalloy and demonstrated that the power spectral density of the thermal noise in the device can degrade the performance of a hard-disk drive.

The mathematics we developed in previous chapters can assist us in understanding the modes of oscillation that contribute to the noise in a patterned structure. In Section 3.8 we introduced the notion of magnetic damping, but used an aggregate measure α that was independent of the spin-wave mode. In a patterned structure, the spin-wave modes are likely to be standing waves that satisfy pinned boundary conditions on the external surface. If we identify each such mode by the subscript \mathbf{k} , we can return to (9.50) and introduce thermal fluctuations in $b_{\mathbf{k}}$ in a stochastic manner. The *equipartition theorem* from classical statistical mechanics states that, at a temperature T , the mean value of each independent quadratic term in energy is equal to $\frac{1}{2}k_B T$. This applies equally to both the kinetic and potential energy terms of a harmonic oscillator. The Hamiltonian \mathcal{H} in (9.50) is the total energy of the \mathbf{k} th oscillator, with each energy term contributing $\frac{1}{2}k_B T$. If we assume that the oscillator is in contact with a thermal reservoir at temperature T , $b_{\mathbf{k}}$ approaches a lower bound determined by $\omega_0|b_0|^2 = k_B T$. When $|b_k| \sim |b_0|$, the dynamics are governed by a stochastic differential equation and we must include a random forcing function to imitate thermal noise so that Eq. (9.50) becomes

$$\frac{db_{\mathbf{k}}^*}{dt} + [\eta_{\mathbf{k}} + i\omega_{\mathbf{k}}]b_{\mathbf{k}}^* = f_{\mathbf{k}}(t), \quad (10.46)$$

where $f_{\mathbf{k}}$ is a randomly applied force, with mean value of zero, but applied so that $\omega_k|b_k|^2 \rightarrow k_B T$ as $k \rightarrow 0$. To fully understand the statistical nature of such a random forcing function and its consequences, we suggest that the reader further explore the topic of Langevin dynamics in statistical mechanics.⁵

Taking the Fourier transform in time of (10.46) yields

$$-i\omega b_{\mathbf{k}}^* + [\eta_{\mathbf{k}} + i\omega_{\mathbf{k}}]b_{\mathbf{k}}^* = f_{\mathbf{k}} \quad (10.47)$$

or

$$b_{\mathbf{k}}^* = \frac{if_{\mathbf{k}}}{\omega - \omega_{\mathbf{k}} + i\eta_{\mathbf{k}}}. \quad (10.48)$$

The magnitude squared (proportional to the power) is

⁵ See, e.g., Reif [19, Chapter 15].

$$|b_{\mathbf{k}}|^2 = \frac{|f_{\mathbf{k}}|^2}{(\omega - \omega_{\mathbf{k}})^2 + \eta_{\mathbf{k}}^2}. \quad (10.49)$$

This gives a Lorentzian-shaped peak about each resonant mode (note that the discrete values of \mathbf{k} result from the boundary conditions of the sample, so each \mathbf{k} represents a resonant mode of the structure). Figure 10.7 shows the result of micromagnetic simulations on a rectangular magnetic element where the noise power spectral density is the sum of the Lorentzian peaks of the dominant noise modes.

An alternate way of obtaining the complete curve shown in Figure 10.7 is to take the inverse Fourier transform with respect to space of $b_{\mathbf{k}}$ to obtain $b(\mathbf{r})$, and then average the magnitude squared of $b(\mathbf{r})$ over the sample:

$$\begin{aligned} \langle |b(\mathbf{r}, \omega)|^2 \rangle &= \frac{1}{V} \int_V d^3r \sum_{\mathbf{k}, \mathbf{k}'} b_{\mathbf{k}} b_{\mathbf{k}'}^* e^{i(\mathbf{k} - \mathbf{k}') \cdot \mathbf{r}} \\ &= \sum_{\mathbf{k}, \mathbf{k}'} b_{\mathbf{k}} b_{\mathbf{k}'}^* \frac{1}{V} \int_V e^{i(\mathbf{k} - \mathbf{k}') \cdot \mathbf{r}} d^3r \\ &= \sum_{\mathbf{k}, \mathbf{k}'} b_{\mathbf{k}} b_{\mathbf{k}'}^* \delta_{\mathbf{k}, \mathbf{k}'} \\ &= \sum_{\mathbf{k}} |b_{\mathbf{k}}|^2 \\ \langle |b(\omega)|^2 \rangle &= \sum_{\mathbf{k}} \frac{|f_{\mathbf{k}}|^2}{(\omega - \omega_{\mathbf{k}})^2 + \eta_{\mathbf{k}}^2}. \end{aligned} \quad (10.50)$$

Here, the brackets indicate a spatial average. Note that the above equation gives a series of peaks corresponding to the modes of the sample as shown in Figure 10.7. The amplitudes of the peaks will depend on the excitation

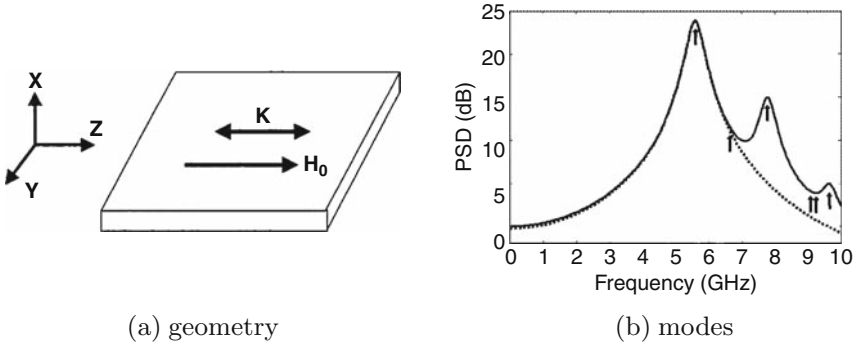


Fig. 10.7. Noise power spectral density in a patterned thin-film structure [18]. In part (a), the double-ended arrow labeled \mathbf{K} indicates the uniaxial anisotropy axis. The dimensions of the film for the simulation were $200 \text{ nm} \times 120 \text{ nm} \times 4 \text{ nm}$. (© 2002 IEEE.)

spectrum from the random fluctuations $f_{\mathbf{k}}$ as well as the damping of each mode determined by $\eta_{\mathbf{k}}$.

The magneto-optic Kerr effect (MOKE) has established itself as a popular technique to directly observe the magnetization dynamics in patterned structures. MOKE measurements can be used to determine the properties of patterned thin-film samples. In a typical setup, the magnetization of the film is oriented along a particular direction using a strong external applied field and then the dynamics are observed as a response to a short-magnetic pulse, delivered by sending a current pulse through a microstrip line kept in proximity to the sample. Different excitation geometries, with the magnetization in the plane at different angles or even out of the film plane, are possible. The frequency of precession is obtained from the power spectral density of the time series MOKE signal reflected from the sample.

Figure 10.8 shows the result of one such series of measurements along with a schematic of the excitation fields. The four peaks in the observed MOKE signal, as we vary the angle of the static applied field \mathbf{H} with respect to the magnetic pulse $\mathbf{h}(t)$ are indicative of four angles at which the internal magnetic field is a maximum. Hence, we expect the sample to have a fourfold symmetry in the magnetic anisotropy, reflecting the symmetry of the square sample. Thus, the measurements suggest an anisotropic energy density of the form [20]

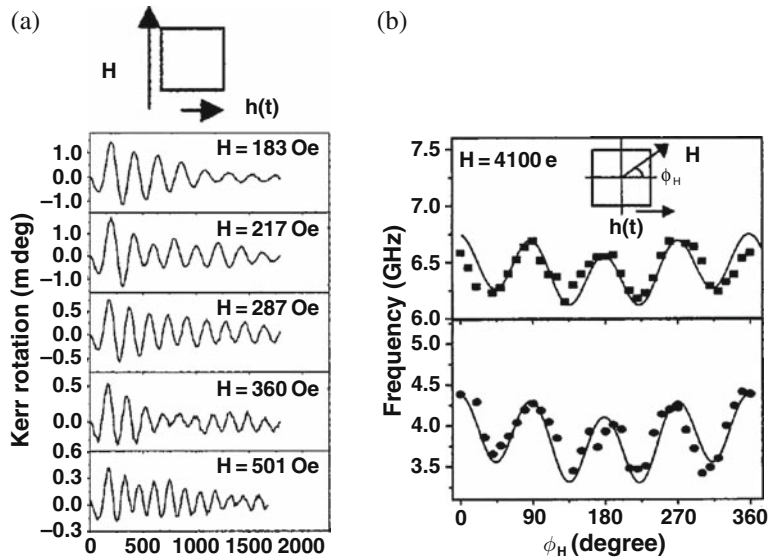


Fig. 10.8. (a) MOKE response on a $10\mu\text{m}$ square permalloy element as a function of the applied static field \mathbf{H} , when $\mathbf{H} \perp \mathbf{h}(t)$, with a time delay in picoseconds after $\mathbf{h}(t)$ is applied. (b) Frequency response as a function of angle between static and pulsed fields. (Reprinted with permission from [20]. Copyright 2003, American Institute of Physics.)

$$\mathcal{E}_k = -K_{u1}(\hat{\mathbf{u}} \cdot \hat{\mathbf{k}})^2 + K_{u2}(u_x^4 + u_y^4), \quad (10.51)$$

where K_{u1} and K_{u2} are the uniaxial anisotropy constants (cf. Eq. (3.68)), $\hat{\mathbf{u}}$ and $\hat{\mathbf{k}}$ are unit vectors in the plane of the film and along the direction of the magnetization and the easy-axis, and x and y define the edges of the sample.

10.3 Inverse Doppler Effect in Backward Volume Waves

The *Doppler shift* [21] is familiar in common experience as an increase in audio pitch when we move towards a source such as a siren. This phenomenon occurs for electromagnetic waves as well as sound waves, and is used in applications such as radar and motion detection. In 1968, Veselago pointed out that an inverse Doppler shift should occur in media for which the electric field intensity \mathbf{E} , the magnetic field intensity \mathbf{H} , and the direction of the movement of the constant phase planes (described by the wave vector \mathbf{k}) form a left-handed coordinate system – in contrast to the right-handed system formed by these vectors in an ordinary medium [22]. Veselago specifically considered a material in which the permittivity and permeability were simultaneously negative, i.e., $\varepsilon < 0$ and $\mu < 0$. Such materials exhibit a number of other interesting properties, including an inverse Cerenkov effect and negative refraction as well as an inverse Doppler effect. In the present context, we find that backward volume spin-waves have fields described by a left-handed coordinate system. The short wavelengths of the spin-waves enhance the magnitude of the Doppler shift by factors of 50–70 over what would be expected from electromagnetic waves in free space at the same frequency.

To understand the origin of the inverse Doppler effect, we note that the shift in frequency is determined by the relative directions of the phase velocity of the wave and the direction of motion, and in the non-relativistic limit is given by [21]

$$\Delta f = -\frac{v}{\lambda} \cos \theta, \quad (10.52)$$

where v is the velocity magnitude (speed) of the observer, λ is the wavelength, and θ is the angle between the velocity of the observer and the phase velocity of the wave. Consequently, when the direction of either the observer velocity or the phase velocity of the wave reverses, the Doppler shift changes sign.

Consider an experiment on spin-waves in a magnetic thin film using the apparatus shown in Figure 10.9. A receiving probe on a rotating element periodically moves across the surface of the film, creating relative motion between the source and the observer. As described in Section 5.5, backward volume waves propagate in a thin film with saturated in-plane magnetization when the direction of propagation is parallel or antiparallel to the applied magnetic field. A YIG film epitaxially grown on a substrate of GGG is used to support the left-handed spin-waves. The in-plane magnetic bias field is supplied by the permanent magnet below the magnetic thin film. The magnet can be rotated

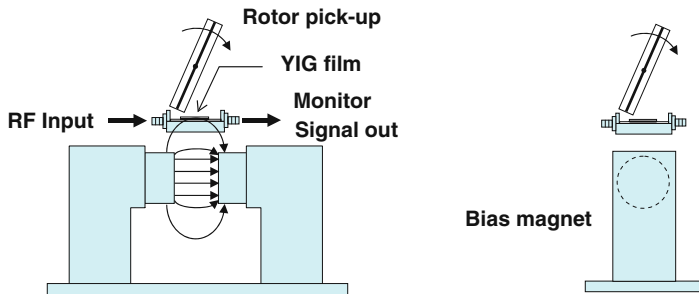


Fig. 10.9. Experimental configuration for the Doppler shift measurements. Spin-waves are excited in the magnetic thin film and sensed by a moving microstrip antenna on a rotating pickup. Diagram of test geometry with bias magnet in the orientation for backward (*left*) and forward (*right*) waves. (Reprinted with permission from [24]. Copyright 1998 by the American Physical Society.)

about a vertical axis so that the field can be either parallel (to excite backward volume waves) or transverse (to excite surface waves⁶) to the direction of propagation. The spin-waves are excited by placing the magnetic sample film side-down on a microstrip antenna fabricated on an alumina substrate. Above the film is a rotor with an antenna fabricated on a flexible microstrip substrate, to allow conformance to the shape of the rotor. The signal from this rotating pick-up antenna is coupled back to the measuring instrumentation using a rotary coaxial joint. An auxiliary output is also available on the stationary microstrip circuit to permit characterization of the spin-waves excited in the film independent of the rotating pick-up.⁷

Let us define our geometry such that the magnetic film is placed in the x - z plane between two semi-infinite dielectric regions, with an in-plane static magnetic bias field applied along the \hat{z} -direction. Backward volume waves are guided along the \hat{z} -direction by reflecting from the top and bottom surfaces of the film. Recall the magnetostatic approximation,

$$\mathbf{h} = -\nabla\psi(y, z), \quad (10.53)$$

where ψ is a scalar potential function and we assume that no x -variations exist since the propagation is entirely in the y - z plane. It follows that there is no x -component of the magnetic field intensity, so the field components contributing to the *Poynting vector* $\mathbf{S} = \frac{1}{2}\text{Re}\{\mathbf{e} \times \mathbf{h}^*\}$ along the z -direction are e_x, h_y . Within the film ($|y| < d/2$), the potential function ψ , for the lowest-order ($n = 1$) backward wave mode in this geometry, is given by (cf. Eq. (5.99))

$$\psi(\mathbf{r}) = \psi_0 \sin(k_y y) e^{ik_z z}. \quad (10.54)$$

⁶ The Doppler shift from these forward surface waves has been previously reported [23].

⁷ We refer the reader [24] for further details on the experimental setup.

Substituting ψ into (10.53) yields

$$h_y = -\psi_0 k_y \cos(k_y y) e^{ik_z z}. \quad (10.55)$$

Since there is no variation along the x -direction, $h_x = 0$ and, according to Eq. (5.91), we can now write the constitutive relation

$$b_y = \mu_0(1 + \chi)h_y = \mu_{22}h_y \quad (10.56)$$

where, as in previous chapters,

$$\chi = \frac{\omega_0 \omega_M}{\omega_0^2 - \omega_M^2}. \quad (10.57)$$

From Faraday's law, Eqs. (4.7) and (4.141), we find that $e_x/h_y = \omega\mu_{22}/k_z$. Defining $\beta = k_z \hat{\mathbf{z}}$, it follows that $\beta \cdot (\mathbf{e} \times \mathbf{h}^*) < 0$ when $\mu_{22} < 0$. Thus, the phase and energy velocities are oppositely directed and the waves are left-handed in nature within the film. To better understand the manifold of propagating spin-waves, let us use (10.57) to write the permeability element

$$\mu_{22} = \mu_0 \frac{\omega_0(\omega_0 + \omega_M) - \omega^2}{\omega_0^2 - \omega^2}. \quad (10.58)$$

The frequencies at which the numerator and denominator vanish correspond to the upper and lower edges, respectively, of the spin-wave manifold. Consequently, $\mu_{22} < 0$ in the magnetic film over the entire spin-wave manifold. To demonstrate the net left-handed nature of the waves, the direction of the Poynting vector outside the film must also be considered. It can be shown (Problem 10.4) that the integral of the Poynting vector over all y does, indeed, give left-handed behavior. It follows that the waves exhibit an inverted Doppler shift, as argued by Veselago.

In the experiment shown in Figure 10.9, the phase shift as a function of frequency can be measured using the auxiliary output. This phase shift results from spin-wave propagation from the input to the output. Since $\phi(\omega) = k(\omega)L$, where L is the propagation distance, the dispersion relation can be obtained after adding or subtracting multiples of 2π to the phase to form a continuous function. (This process is referred to as “unwrapping.”) The dispersion relations so obtained for surface and backward volume spin-waves are shown in Figure 10.10. The solid lines are the theoretical dispersion relations for surface waves and backward volume waves from (5.111b) and (5.95), respectively. This plot highlights an important point not apparent from dispersion relation plots such as Figure 5.13. We see from Figure 10.10 that the group velocity (slope) is always positive – the *phase velocity* is the quantity that reverses in backward waves. This follows from the observation that the energy always goes from input to output.

In the present experiment, the coupling to the spin-waves occurs only during a small portion of the rotation cycle when the pick-up is closest. Hence, to

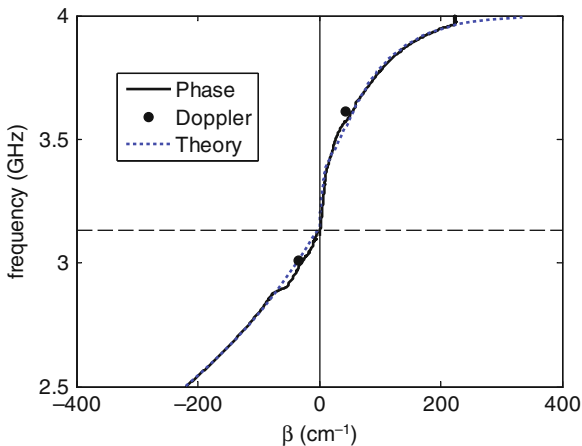


Fig. 10.10. Dispersion relations for surface waves and backward volume waves excited in the Doppler experiment. The solid line was determined from the measured phase, the circles were determined from the Doppler measurement, and the dashed lines are from theory. (Reprinted with permission from [24]. Copyright 1998 by the American Physical Society.)

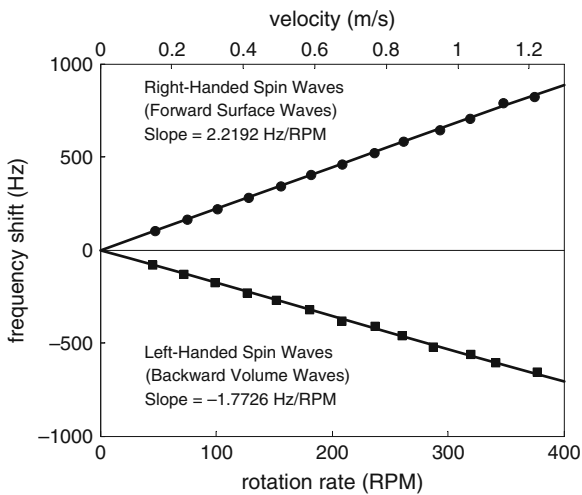


Fig. 10.11. Doppler shifts obtained as the rotation rate is varied. The tangential linear velocity is given across the top axis. The left-handed waves generate a negative shift, while the right-handed waves generate a positive shift. (Reprinted with permission from [24]. Copyright 1998 by the American Physical Society.)

a good approximation, the tangential velocity is parallel ($\theta = 0$) or antiparallel ($\theta = \pi$) to the wave vector when the signal is detected. Thus, the Doppler shift is

$$\Delta f = \mp v/\lambda, \quad (10.59)$$

where v is the tangential velocity of the rotating pick-up antenna. The sense of rotation was such that the pick-up was always moving toward the source of the spin-waves. The observed Doppler shift is shown in Figure 10.11, confirming the left-handed nature of backward volume spin-waves. The Doppler shifts were measured at the points on the dispersion curves marked by circles in Figure 10.10.

This brings us to the conclusion of our journey through many different topics. The list of novel applications that we have described is by no means complete. We have chosen to describe a select few and have provided somewhat brief mathematical details of the underlying physical interactions. The objective was to introduce you to the emerging facets of spin-wave applications with suitable references for further reading and we hope that we have succeeded in piquing your interest.

Problems

10.1. The Pauli matrices $\boldsymbol{\sigma}$, introduced in Problem 1.5, act as rotation operators on the spinor state. A rotation by an angle θ about the axis $\hat{\mathbf{n}}$ is written as [7]

$$U_R = \mathbf{I} \cos \frac{\theta}{2} - i \hat{\mathbf{n}} \cdot \boldsymbol{\sigma} \frac{\sin \theta}{2} \quad (10.60)$$

where \mathbf{I} is the identity matrix and

$$\sigma_1 = \begin{bmatrix} 0 & 1 \\ 1 & 0 \end{bmatrix}, \quad \sigma_2 = \begin{bmatrix} 0 & -i \\ i & 0 \end{bmatrix}, \quad \sigma_3 = \begin{bmatrix} 1 & 0 \\ 0 & -1 \end{bmatrix}. \quad (10.61)$$

Using the notation

$$\chi_{\uparrow} = \begin{bmatrix} 1 \\ 0 \end{bmatrix}; \quad \chi_{\downarrow} = \begin{bmatrix} 0 \\ 1 \end{bmatrix}, \quad (10.62)$$

show that

$$\begin{aligned} \sigma_1 \chi_{\uparrow} &= \chi_{\downarrow}, \\ i\sigma_2 \chi_{\uparrow} &= -\chi_{\downarrow}, \\ \sigma_3 \chi_{\uparrow} &= \chi_{\uparrow}, \end{aligned}$$

and derive the equivalent operations on χ_{\downarrow} .

10.2. Show that substituting Eq. (10.15) into (10.4) yields

$$\mathbf{J}^{\text{in}} \cdot \hat{\mathbf{x}} = \frac{\hbar^2}{2m} \left[\hat{\mathbf{x}} \sin \theta + \hat{\mathbf{z}} \cos \theta \right], \quad (10.63a)$$

$$\mathbf{J}^{\text{ref}} \cdot \hat{\mathbf{x}} = \frac{\hbar^2}{2m} \left[-\hat{\mathbf{x}} \operatorname{Re}(r_{\uparrow}^* r_{\downarrow}) \sin \theta - \hat{\mathbf{y}} \operatorname{Im}(r_{\uparrow}^* r_{\downarrow}) \sin \theta - \hat{\mathbf{z}} \left(|r_{\uparrow}^2| \cos^2(\theta/2) - |r_{\downarrow}^2| \sin^2(\theta/2) \right) \right], \quad (10.63b)$$

$$\mathbf{J}^{\text{tr}} \cdot \hat{\mathbf{x}} = \frac{\hbar^2}{2m} \left[\hat{\mathbf{x}} \left(\frac{k_{\downarrow} + k_{\uparrow}}{2\sqrt{k_{\downarrow}k_{\uparrow}}} \right) \operatorname{Re}(t_{\uparrow}^* t_{\downarrow} e^{i(k_{\downarrow} - k_{\uparrow})x}) \sin \theta \right. \quad (10.63c)$$

$$+ \hat{\mathbf{y}} \left(\frac{k_{\downarrow} + k_{\uparrow}}{2\sqrt{k_{\downarrow}k_{\uparrow}}} \right) \operatorname{Im}(t_{\uparrow}^* t_{\downarrow} e^{i(k_{\downarrow} - k_{\uparrow})x}) \sin \theta + \hat{\mathbf{z}} \left(|t_{\uparrow}^2| \cos^2(\theta/2) - |t_{\downarrow}^2| \sin^2(\theta/2) \right) \left. \right]. \quad (10.63d)$$

10.3. Use the results of Problem 10.2 to evaluate $\mathbf{N} = [\mathbf{J}^{\text{in}} + \mathbf{J}^{\text{ref}} - \mathbf{J}^{\text{tr}}] \cdot \hat{\mathbf{x}}$, and verify Eq. (10.16).

10.4. The direction of the phase velocity is the same as the direction of the in-plane wave vector defined by $\boldsymbol{\beta} = k_z \hat{\mathbf{z}}$. To establish whether or not the wave is left-handed, we therefore examine the sign of the quantity $\boldsymbol{\beta} \cdot (\mathbf{e} \times \mathbf{h}^*)$. If this quantity is negative, the transverse components of \mathbf{e} and \mathbf{h} necessarily form a left-handed triplet with $\boldsymbol{\beta}$.

(a) By deriving the relevant expression for \mathbf{e} and \mathbf{h} for all y , show that

$$\boldsymbol{\beta} \cdot (\mathbf{e} \times \mathbf{h}^*) < 0, \quad |y| < d/2 \quad (10.64)$$

$$\boldsymbol{\beta} \cdot (\mathbf{e} \times \mathbf{h}^*) > 0, \quad |y| > d/2 \quad (10.65)$$

indicating left-handed fields within the film and right-handed fields outside the film.

(b) Show that

$$\int_{-\infty}^{\infty} \boldsymbol{\beta} \cdot (\mathbf{e} \times \mathbf{h}^*) dy < 0, \quad (10.66)$$

and thus that the guided wave exhibits a net left-handed behavior.

References

- [1] J. C. Slonczewski, "Current-driven excitation of magnetic multilayers," *J. Magn. Magn. Matl.*, vol. 159, p. L1, 1996.
- [2] L. Berger, "Emission of spin-waves by a magnetic multilayer traversed by a current," *Phys. Rev. B*, vol. 54, p. 9353, 1996.

- [3] M. B. Stearns, "Simple explanation of tunneling spin-polarization of Fe, Co, Ni and its alloys," *J. Magn. Magn. Matl.*, vol. 5, pp. 167–171, 1977.
- [4] W. H. Butler, O. Heinonen, and X.-G. Zhang, *The Physics of Ultra-High-Density Magnetic Recording*. Berlin: Springer-Verlag, 2001, ch. 10.
- [5] N. Spaldin, *Magnetic Materials – Fundamentals and Device Applications*. Cambridge: Cambridge University Press, 2003, ch. 6.
- [6] H. Imamura and S. Maekawa, "Theory of spin-dependent tunneling," in *Handbook of Magnetism and Advanced Magnetic Materials: Fundamentals and Theory*, H. Krommüller and S. Parkin, Eds. New York, NY: John Wiley & Sons, 2007.
- [7] E. Merzbacher, *Quantum Mechanics*, 3rd ed. New York, NY: John Wiley & Sons, 1998.
- [8] K. Mita, "Virtual probability current associated with the spin," *Am. J. Phys.*, vol. 68, p. 259, 2000.
- [9] M. Stiles and A. Zangwill, "Anatomy of spin-transfer torque," *Phys. Rev. B*, vol. 66, p. 014407, 2002.
- [10] S. M. Rezende, F. M. de Aguiar, and A. Azevedo, "Spin-wave theory for the dynamics induced by direct currents in magnetic multilayers," *Phys. Rev. Lett.*, vol. 94, p. 037202, 2005.
- [11] M. Tsoi, A. G. M. Jansen, J. Bass1, W.-C. Chiang, M. Seck1, V. Tsoi, and P. Wyder, "Excitation of a magnetic multilayer by an electric current," *Phys. Rev. Lett.*, vol. 80, pp. 4281–4284, 1998.
- [12] J. C. Slonczewski, "Excitation of spin-waves by an electric current," *J. Magn. Magn. Matl.*, vol. 195, p. L261, 1999.
- [13] J. Z. Sun, "Spin angular momentum transfer in current-perpendicular nanomagnetic junctions," *IBM J. Res. Dev.*, vol. 50, pp. 81–100, 2006.
- [14] I. N. Krivorotov, N. C. Emley, J. C. Sankey, S. I. Kiselev, D. C. Ralph, and R. A. Buhrman, "Time-domain measurements of nanomagnet dynamics driven by spin-transfer torquess," *Science*, vol. 307, p. 228, 2005.
- [15] S. M. Rezende, F. M. de Aguiar, R. L. Rodriguez-Suarez, and A. Azevedo, "Mode locking of spin-waves excited by direct currents in microwave nano-oscillators," *Phys. Rev. Lett.*, vol. 98, no. 8, p. 087202, 2007.
- [16] M. V. Costache, S. M. Watts, M. Sladkov, C. H. van der Wal, and B. J. van Wees, "Large cone angle magnetization precession of an individual nanopatterned ferromagnet with dc electrical detection," *Appl. Phys. Lett.*, vol. 89, p. 232115, 2006.
- [17] L. Berger, "Generation of dc voltages by a magnetic multilayer undergoing ferromagnetic resonance," *Phys. Rev. B*, vol. 59, p. 11465, 1999.
- [18] H. N. Bertram, V. L. Safonov, and Z. Jin, "Thermal magnetization noise, damping fundamentals, and mode analysis: Application to a thin film GMR sensor," *IEEE Trans. Mag.*, vol. 38, pp. 2514–2519, 2002.
- [19] F. Reif, *Fundamentals of Statistical and Thermal Physics*. New York: McGraw Hill Intl. Ed., 1985.
- [20] A. Barman, V. V. Kruglyak, R. J. Hicken, A. Kundrotaite, and M. Rahman, "Anisotropy, damping, and coherence of magnetization

- dynamics in a $10\text{ }\mu\text{m}$ square $\text{ni}_{81}\text{fe}_{19}$ element,” *Appl. Phys. Lett.*, vol. 82, pp. 3065–3067, 2003.
- [21] J. D. Jackson, *Classical Electrodynamics*, 3rd ed. Singapore: John Wiley and Sons, 1999.
- [22] V. G. Veslago, “The electrodynamics of substances with simultaneously negative values of ϵ and μ ,” *Sov. Phys. Usp.*, vol. 10, p. 509, 1968.
- [23] N. L. Koros, D. D. Stancil, and N. Bilaniuk, “Linear motion sensor using the Doppler effect with magnetostatic waves,” *J. Appl. Phys.*, vol. 67, p. 511, 1990.
- [24] D. D. Stancil, B. E. Henty, A. G. Cepni, and J. P. V. Hof, “Observation of an inverse Doppler shift from left-handed dipolar spin-waves,” *Phys. Rev. B (Condensed Matter and Materials Physics)*, vol. 74, no. 6, p. 060404, 2006.

Appendix A

Properties of Yttrium–Iron–Garnet (YIG)

Structure and Physical Properties		
Chemical formula		Y ₃ Fe ₅ O ₁₂
Crystal structure		Cubic
Number of formula units per unit cell		8
Lattice constant (25 °C)		12.376 Å
Mass density (25 °C)		5172 kg/m ³
Octahedral Sublattice		
Site density	N_a	$8.441 \times 10^{27} \text{ m}^{-3}$
Angular momentum	J_a	5/2
Landé g factor	g_a	2
Magnetization at 0 K	M_a (0 K)	391.5 kA/m
Tetrahedral Sublattice		
Site density	N_d	$12.66 \times 10^{27} \text{ m}^{-3}$
Angular momentum	J_d	5/2
Landé g factor	g_d	2
Magnetization at 0 K	M_d (0 K)	587.2 kA/m
Molecular Field Constants [1]		
Octahedral	λ_{aa}	735.84
Tetrahedral	λ_{dd}	344.59
Nearest-neighbor	λ_{ad}	1100.3
Phenomenological Exchange Constant [2]		
Defined by $h_{\text{ex}} = \lambda_{\text{ex}} \nabla^2 m$ (3.104)	λ_{ex}	$3 \times 10^{-16} \text{ m}^2$
Macroscopic Magnetic Properties		
Magnetization at 0 K	M_{tot} (0 K)	196 kA/m
Magnetization at 298 K	M_{tot} (298 K)	140 kA/m
Curie temperature	T_c	559 K

Anisotropy Constants		
First-order cubic (4.2 K) [3]	K_{c1} (4.2 K)	-2480 J/m^3
First-order cubic (295 K) [3]	K_{c1} (295 K)	-610 J/m^3
Second-order cubic (4.2 K) [4]	K_{c2} (4.2 K)	-118.0 J/m^3
Second-order cubic (273 K) [4]	K_{c2} (273 K)	-26.0 J/m^3
Optical Properties [5–7]		
Refractive index (1.2 μm)	n	2.2
Faraday rotation (1.2 μm)	ϕ_F	240 deg/cm
Absorption coefficient (1.2 μm)	α	0.069 cm^{-1}
Cotton–Mouton tensor elements (1–3 μm)	$g_{44} M_S^2$	-1.14×10^{-4}
	$\Delta g M_S^2$	5.73×10^{-5}
Cotton–Mouton rotation (1.14 μm)	Φ_{CM}	-160 deg/cm

References

[1] E. E. Anderson, “Molecular field model and magnetization of YIG,” *Phys. Rev.*, vol. 134, p. A1581, 1964.

[2] E. H. Turner, “Interaction of phonons and spin waves in yttrium iron garnet,” *Phys. Rev. Lett.*, vol. 5, p. 100, 1960.

[3] P. Hansen, “Anisotropy and magnetostriction of gallium-substituted yttrium iron garnet,” *J. Appl. Phys.*, vol. 45, p. 3638, 1974.

[4] P. Escudier, “L’anisotropie de l’aimantation; un paramètre important de l’étude de l’anisotropie magnétocristalline,” *Ann. Phys. (Paris)*, vol. 9, p. 125, 1975.

[5] M. J. Weber, Ed., *CRC Handbook of Laser Science and Technology, Vol. IV Optical Materials Part 2: Properties*. Boca Raton, FL: CRC Press, 1986, p. 291.

[6] R. V. Pisarev, I. G. Sinii, N. N. Kolpakova, and Y. M. Yakovlev, “Magnetic birefringence of light in iron garnets,” *Sov. Phys. JETP*, vol. 33, p. 1175, 1971.

[7] G. A. Smolensky, R. V. Pisarev, I. G. Sinii, and N. N. Kolpakova, “Cotton-Mouton birefringence of ferrimagnetic garnets,” *J. Physique Colloque*, vol. C1 32, pp. c1–1048, 1971.

Appendix B

Currents in Quantum Mechanics

B.1 Density of States

The valence electrons in a metal can be modeled as free electrons contained in a box the size of the sample. Because of the boundary conditions at the faces of the box, the allowed values of wave number k are quantized. The actual conditions at the surface of a metal may be very complicated, but much of solid-state physics depends primarily on the fact that the modes are quantized, rather than on exactly what the boundary conditions of a particular sample happen to be. Consequently, it is common to make the simple assumption of periodic boundary conditions. In this assumption, the wave function of an electron at $x = L$ should equal to that at $x = 0$, where L is the length of the sample along the x -direction. For this to be true, we have $\exp(ikL) = \exp(0) = 1$, which gives the discrete values of wave number $k = 2\pi n/L$, where n is an integer. In \mathbf{k} space, the total number of states N in a sphere of radius $|\mathbf{k}|$ is given by the volume of the sphere divided by the volume occupied by one state. Thus

$$N = 2\frac{4}{3}\pi k^3 \frac{1}{(2\pi/L)^3} = 2\frac{4\pi k^3 L^3}{3(2\pi)^3}, \quad (\text{B.1})$$

where we have assumed the sample is a cube with length L on each side so that the minimum volume in k space is $\Delta k_x \Delta k_y \Delta k_z = (2\pi/L)^3$. The factor of 2 accounts for the degeneracy in the energy of spin-up and spin-down electrons.¹

In the free electron approximation, the Hamiltonian \mathcal{H} is merely the kinetic energy operator (cf. Table 1.1)

$$\mathcal{H} = \frac{p^2}{2m} = -\frac{\hbar^2}{2m} \nabla^2, \quad (\text{B.2})$$

¹ When we consider ferromagnetic metals, this degeneracy is lifted by the interaction with the internal exchange field causing a splitting of the energy band diagram.

and when we assume an electron wavefunction of the form $\psi \sim e^{i\mathbf{k}\cdot\mathbf{r}}$, the Schrödinger equation $\mathcal{H}\psi = E\psi$ yields

$$\frac{\hbar^2 k^2}{2m} = E. \quad (\text{B.3})$$

Combining (B.1) and (B.3), the number of states with energy less than E can be written

$$N = 2 \frac{4\pi L^3}{3(2\pi)^3} \left(\frac{2m}{\hbar^2} \right)^{3/2} E^{3/2}. \quad (\text{B.4})$$

The density of states is defined as the number of states per unit energy, or

$$g(E) = \frac{dN}{dE}. \quad (\text{B.5})$$

Thus, the density of states is given by

$$g(E) = 2 \frac{4\pi L^3}{3(2\pi)^3} \left(\frac{2m}{\hbar^2} \right)^{3/2} \left(\frac{3}{2} E^{1/2} \right) \quad (\text{B.6})$$

$$= \frac{L^3}{2\pi^2} \left(\frac{2m}{\hbar^2} \right)^{3/2} \sqrt{E}. \quad (\text{B.7})$$

The Fermi energy is defined as the highest occupied energy state by an electron, at absolute zero temperature. Interactions at higher temperatures typically occur near the Fermi energy, $E_F = \hbar^2 k_F^2 / (2m)$, since electrons at the Fermi energy have nearby empty states. Consequently, the current is often calculated at the Fermi energy while assuming the parabolic band approximation $g(E) \propto E^{1/2}$. Multiplying and dividing (B.7) by E and comparing the result with (B.4), we see that the relationship between the Fermi energy and the density of states can be expressed

$$g(E_F) = \frac{3}{2} \frac{N}{E_F}. \quad (\text{B.8})$$

At finite temperature, some of the electrons will be excited to states above the Fermi level. In this case, the density of states is related to the number of particles by

$$N = \int_0^\infty g(E) f(E) dE, \quad (\text{B.9})$$

where

$$f(E) = \left(1 + e^{(E-E_F)/(k_B T)} \right)^{-1} \quad (\text{B.10})$$

is the Fermi–Dirac distribution describing the probability of finding an electron with energy E at temperature T and $k_B = 1.38 \times 10^{-23} \text{ J/K}$ is the Boltzmann constant.

Note that the above expressions assume degenerate spin-up and spin-down subbands. In a ferromagnetic metal, the molecular field interacting with the electron spin splits the bands as illustrated in Figure 10.1. If the magnetization is oriented upwards, then the Hamiltonian with the effects of the molecular field is (cf. Eq. (2.30))

$$\mathcal{H} = \frac{-\hbar^2}{2m} \left(\frac{d}{dx} \right)^2 + \mu_0 \mu_B \sigma H_m, \quad (\text{B.11})$$

where H_m is the molecular field and $\sigma = \pm 1$. Defining $E_m = \mu_0 \mu_B \sigma H_m$, the density of states for the spin subbands can be expressed

$$g_\sigma(E) = \frac{1}{2} g(E - \sigma E_m), \quad (\text{B.12})$$

and the total density of states is given by

$$g(E) = \sum_{\sigma} g_{\sigma}(E) \quad (\text{B.13})$$

$$= g_{\uparrow}(E) + g_{\downarrow}(E) \quad (\text{B.14})$$

$$= \frac{1}{2} [g(E - E_m) + g(E + E_m)]. \quad (\text{B.15})$$

$$(\text{B.16})$$

B.2 Electric and Spin Current Densities

Consider ψ to be a solution of the 1D Schrödinger equation

$$i\hbar \frac{\partial \psi}{\partial t} = -\frac{\hbar^2}{2m} \nabla^2 \psi. \quad (\text{B.17})$$

Multiplying (B.17) by ψ^* and subtracting the complex conjugate of the resulting equation, we obtain

$$\frac{\partial}{\partial t}(\psi^* \psi) + \frac{-i\hbar}{2m} \nabla \cdot [\psi^* \nabla \psi - \psi \nabla \psi^*] = 0. \quad (\text{B.18})$$

In obtaining (B.18), we have used the vector identity

$$\nabla \cdot (f \nabla g) = \nabla f \cdot \nabla g + f \nabla^2 g. \quad (\text{B.19})$$

If we define the probability density of finding an electron as $\psi^* \psi$, we can express the charge density as $\rho = q\psi^* \psi$. We can also define a current density \mathbf{j} that satisfies the conservation equation

$$\frac{\partial \rho}{\partial t} + \nabla \cdot \mathbf{j} = 0. \quad (\text{B.20})$$

Multiplying (B.18) by the electronic charge q and comparing with (B.20), we make the identification

$$\begin{aligned}\mathbf{j} &= \frac{-i\hbar q}{2m} [\psi^* \nabla \psi - \psi \nabla \psi^*] \\ &= \frac{\hbar q}{m} \text{Im}(\psi^* \nabla \psi).\end{aligned}\tag{B.21}$$

Choosing $\psi = 1/\sqrt{k}e^{ikx}$ for the 1D case ensures the normalization

$$\text{Im}\left(\psi^* \frac{d\psi}{dx}\right) = 1.\tag{B.22}$$

Under the two-band approximation, we treat the spin-up and spin-down carriers as being independent. Under this two-channel approximation, we can borrow standard techniques from quantum mechanics to solve for the probability of carrier transmission across an interface, or even through a barrier with multiple interfaces.

B.3 Reflection and Transmission at a Boundary

Consider an electron that is incident on a planar interface between two media as illustrated in Figure B.1. The electron will be reflected with probability

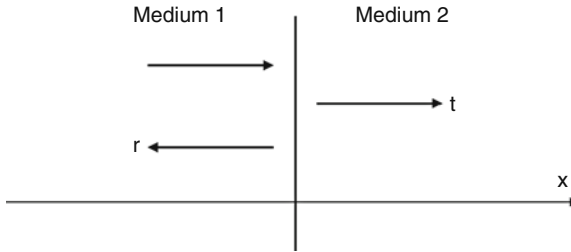


Fig. B.1. Geometry for calculating the reflection and transmission coefficients of a particle at a boundary between two materials.

amplitude r , and transmitted with probability amplitude t . In medium 1, the wave function is

$$\psi_1 = \psi_{\text{inc}} + \psi_{\text{ref}}\tag{B.23}$$

$$= \frac{1}{\sqrt{k_1}} (e^{ik_1x} + r e^{-ik_1x}),\tag{B.24}$$

$$\tag{B.25}$$

while in medium 2, the wave function is

$$\psi_2 = \psi_{\text{tr}} = \frac{t}{\sqrt{k_2}} e^{ik_2 x}. \quad (\text{B.26})$$

The reflection and transmission coefficients can be found by requiring both the wave function and its derivative to be continuous at the boundary $x = 0$. Requiring $\psi_1(0^-) = \psi_2(0^+)$ gives

$$\frac{1}{\sqrt{k_1}} (1 + r) = \frac{1}{\sqrt{k_2}} t. \quad (\text{B.27})$$

Similarly, requiring $d\psi/dx$ to be continuous at $x = 0$ gives

$$\sqrt{k_1} (1 - r) = t \sqrt{k_2}. \quad (\text{B.28})$$

Solving (B.27) and (B.28) simultaneously gives the desired reflection and transmission amplitudes:

$$r = \frac{k_1 - k_2}{k_1 + k_2}, \quad (\text{B.29})$$

$$t = \frac{2\sqrt{k_1 k_2}}{k_1 + k_2}. \quad (\text{B.30})$$

It is straightforward to show that the probabilities of reflection and transmission sum to 1:

$$r^2 + t^2 = 1. \quad (\text{B.31})$$

These equations can be readily applied to the transmission and reflection of spin-up and spin-down electrons at an interface between a normal metal and a ferromagnetic metal. To do this, we make the identifications $k_1 = k_N$ and $k_2 = k_\sigma$. Thus, we have

$$r_\sigma = \frac{k_N - k_\sigma}{k_N + k_\sigma}, \quad (\text{B.32})$$

$$t_\sigma = \frac{2\sqrt{k_N k_\sigma}}{k_N + k_\sigma}, \quad (\text{B.33})$$

and

$$r_\sigma^2 + t_\sigma^2 = 1. \quad (\text{B.34})$$

B.4 Tunneling Through a Barrier²

Consider the quantum mechanical tunneling of particles with energy E through a potential barrier

$$U(x) = \begin{cases} V & -a/2 < x < a/2, \\ 0 & \text{elsewhere.} \end{cases}$$

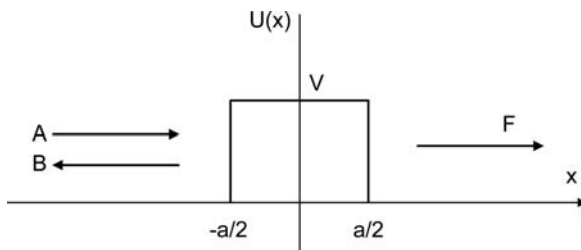


Fig. B.2. Tunneling through a potential barrier. A particle incident from the left has a finite probability of tunneling through the barrier, even though the particle energy E is less than the barrier height V .

where $V > E$ (Figure B.2). Assuming a free particle solution to the Schrödinger equation $\mathcal{H}\psi = E\psi$, the wavefunction will have the form (for 1D problem)

$$\psi = A e^{+ikx} + B e^{-ikx}, \quad (\text{B.35})$$

where the two terms represent plane waves of amplitude A and B traveling along the $+\hat{x}$ and $-\hat{x}$ directions, respectively. The wavenumber k is a measure of the oscillatory nature of ψ and can be obtained by substituting (B.35) into the Schrödinger equation

$$-\frac{\hbar^2}{2m} \nabla^2 \psi + U(x) = E\psi \quad (\text{B.36})$$

to yield

$$k(x) = \frac{1}{\hbar} \sqrt{2m(E - U(x))}. \quad (\text{B.37})$$

We write the wavefunction for the particle in the three regions as³

$$\psi(x) = \begin{cases} A e^{ikx} + B e^{-ikx} & x < -a/2, \\ C e^{-\kappa x} + D e^{\kappa x} & -a/2 < x < a/2, \\ F e^{ikx} & a/2 < x. \end{cases} \quad (\text{B.38})$$

Since $U(x)$ is piecewise constant, we can define

$$k = \frac{1}{\hbar} \sqrt{2mE} \quad (\text{B.39})$$

outside the barrier, where $U(x) = 0$, and within the barrier $U(x) = V$ and we define the real quantity κ :

$$\kappa = \frac{1}{\hbar} \sqrt{2m(V - E)}. \quad (\text{B.40})$$

² We rely heavily on the mathematics in [1].

³ The normalization is not important in this case, since we are interested in the ratio of the transmitted to incident amplitudes, and the initial and final media both have the same k .

We interpret $1/\kappa$ as an exponential decay length characteristic of tunneling through a barrier. The wavefunction in each region is determined by requiring that both ψ and $d\psi/dx$ be continuous across the interfaces $x = -a/2$ and $x = a/2$. The boundary conditions at $x = -a/2$ yield the equations

$$A e^{-ika/2} + B e^{ika/2} = C e^{\kappa a/2} + D e^{-\kappa a/2}, \quad (\text{B.41})$$

$$ikA e^{-ika/2} - ikB e^{ika/2} = -\kappa C e^{\kappa a/2} + \kappa D e^{-\kappa a/2}, \quad (\text{B.42})$$

while the boundary conditions at $x = a/2$ give

$$C e^{-\kappa a/2} + D e^{\kappa a/2} = F e^{ika/2}, \quad (\text{B.43})$$

$$-\kappa C e^{-\kappa a/2} + \kappa D e^{\kappa a/2} = ikF e^{ika/2}. \quad (\text{B.44})$$

Normalizing the equations by A , we have four equations in the four unknown normalized coefficients.

The ratio of the transmitted and incident wave amplitudes can thus be uniquely determined as [1]

$$\frac{F}{A} = \frac{e^{-ika}}{\cosh \kappa a + i(\varepsilon/2) \sinh \kappa a}, \quad (\text{B.45})$$

where

$$\varepsilon = \frac{\kappa}{k} - \frac{k}{\kappa}. \quad (\text{B.46})$$

We are usually interested in quantities such as the transmissivity of the barrier defined as

$$T = \left| \frac{F}{A} \right|^2. \quad (\text{B.47})$$

For a high and wide barrier ($\kappa a \gg 1$), we obtain

$$T \approx 16 e^{-2\kappa a} \left(\frac{\kappa k}{k^2 + \kappa^2} \right)^2. \quad (\text{B.48})$$

Note, however, that when we apply a bias between the two ferromagnetic electrodes, the potential $U(x)$ will contain a linear term. Consequently, the solutions for $\psi(x)$ within the barrier will no longer have the exponential form $e^{\pm \kappa x}$ and will instead be replaced by Airy functions.

References

- [1] E. Merzbacher, *Quantum Mechanics*, 3rd ed. New York: John Wiley & Sons, 1998.

Appendix C

Characteristics of Spin Wave Modes

This appendix provides a summary of the characteristics of spin wave modes, as described in Chapters 5 and 6. We identify

- H_0 as the total internal field,
- M_S as the saturation magnetization,
- H_{DC} as the applied DC bias field,
- g as the Lande' g factor (2 for spin),
- q and m as the charge (negative) and effective mass, respectively, of an electron, and
- d as the film thickness
- w as the width of the microstrip transducer
- s as the separation between the transducer and the surface of a magnetic film

and define

$$\begin{aligned}\omega_0 &= -\gamma\mu_0 H_0, \\ \omega_M &= -\gamma\mu_0 M_S, \\ \gamma &= \frac{gq}{2m} \quad (\text{which is negative}).\end{aligned}$$

The coordinate system is generally defined so that H_0 and H_{DC} are along the \hat{z} direction. For simplicity, magnetocrystalline anisotropy is neglected in the following equations.

C.1 Constitutive Tensors

C.1.1 Polder Susceptibility Tensor

$$\bar{\chi} = \begin{bmatrix} \chi & -i\kappa \\ i\kappa & \chi \end{bmatrix},$$

where

$$\chi = \frac{\omega_0 \omega_M}{\omega_0^2 - \omega^2} \quad \text{and} \quad \kappa = \frac{\omega \omega_M}{\omega_0^2 - \omega^2}.$$

C.1.2 Permeability Tensor

$$\bar{\boldsymbol{\mu}} = \mu_0 \begin{bmatrix} 1 + \chi & -i\kappa & 0 \\ i\kappa & 1 + \chi & 0 \\ 0 & 0 & 1 \end{bmatrix}.$$

C.2 Uniform Precession Mode Frequencies

- Normally magnetized film with $H_0 = H_{\text{DC}} - M_{\text{S}}$,

$$\omega = \omega_0 = -\gamma\mu_0(H_{\text{DC}} - M_{\text{S}}).$$

- Tangentially magnetized film with $H_0 = H_{\text{DC}}$,

$$\omega = [\omega_0(\omega_0 + \omega_M)]^{1/2}.$$

- Sphere,

$$\omega = -\gamma\mu_0 H_{\text{DC}}.$$

C.3 Spin Wave Resonance Frequencies

Assuming pinned boundary conditions:

- Normally magnetized film with $H_0 = H_{\text{DC}} - M_{\text{S}}$,

$$\omega_n = \omega_0 + \omega_M \lambda_{\text{ex}} \left(\frac{n\pi}{d} \right)^2, \quad n = 1, 2, 3, \dots$$

- Tangentially magnetized film with $H_0 = H_{\text{DC}}$,

$$\omega_n = \left[\left(\omega_0 + \omega_M \lambda_{\text{ex}} \left(\frac{n\pi}{d} \right)^2 \right) \left(\omega_0 + \omega_M \lambda_{\text{ex}} \left(\frac{n\pi}{d} \right)^2 + \omega_M \right) \right]^{1/2},$$

$$n = 1, 2, 3, \dots$$

C.4 General Magnetostatic Field Relations

$$\mathbf{h} = -\nabla\psi,$$

$$\mathbf{m} = \bar{\boldsymbol{\chi}} \cdot \mathbf{h},$$

$$\mathbf{b} = \mu_0 (1 + \bar{\boldsymbol{\chi}}) \cdot \mathbf{h},$$

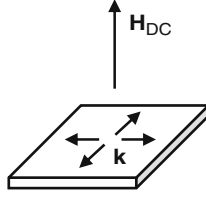
$$\nabla \times \mathbf{e} = i\omega \mathbf{b},$$

$$\mathbf{h} = -\frac{\mathbf{k}\mathbf{k} \cdot \mathbf{m}}{k^2},$$

$$\mathbf{e} = -\frac{\omega\mu_0}{k^2} \mathbf{k} \times \mathbf{m}.$$

C.5 Forward Volume Spin Waves

Normally magnetized film



$$H_0 = H_{DC} - M_S$$

Dispersion relation:

$$\omega^2 = \omega_0 \left[\omega_0 + \omega_M \left(1 - \frac{1 - e^{-k_t d}}{k_t d} \right) \right].$$

Group velocity:

$$\frac{1}{v_g} = \frac{\chi \kappa}{(1 + \chi) \omega_M d} \left[\frac{2}{\chi} - k_t d \right].$$

For lowest order $n = 0$ mode,

$$\frac{1}{v_g} \Big|_{k_t d=0} = \frac{4}{\omega_M d}.$$

Loss:

$$\frac{1}{T_k} = |\gamma| \mu_0 \Delta H \frac{\omega_0^2 + \omega^2}{4 \omega_0 \omega} = \alpha \frac{\omega_0^2 + \omega^2}{2 \omega_0}.$$

Potential function:

$$\psi^{(e)}(\mathbf{r}) = \begin{cases} \psi_0 e^{k_t d/2} \cos(\sqrt{-(1+\chi)} k_t d/2) e^{i\mathbf{k}_t \cdot \mathbf{r} - k_t z}, & z > d/2, \\ \psi_0 \cos(\sqrt{-(1+\chi)} k_t z) e^{i\mathbf{k}_t \cdot \mathbf{r}}, & |z| \leq d/2, \\ \psi_0 e^{k_t d/2} \cos(\sqrt{-(1+\chi)} k_t d/2) e^{i\mathbf{k}_t \cdot \mathbf{r} + k_t z}, & z < -d/2. \end{cases}$$

Normalization: For a mode power of P , mW/mm,

$$\psi_0 = \sqrt{\frac{4P}{-(1+\chi)\omega\mu_0 k d}}.$$

Radiation resistance of m th mode with wavenumber k_m :

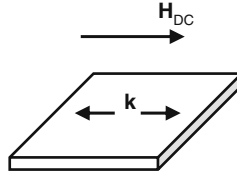
$$r_{rm} = \begin{cases} \frac{\omega\mu_0}{[-(1+\chi)]k_md} \cos^2 \left[\frac{k_md}{2} \sqrt{-(1+\chi)} \right] \left| \frac{F}{I} \right|^2, & m = 0, 2, 4, \dots, \\ \frac{\omega\mu_0}{[-(1+\chi)]k_md} \sin^2 \left[\frac{k_md}{2} \sqrt{-(1+\chi)} \right] \left| \frac{F}{I} \right|^2, & m = 1, 3, 5, \dots, \end{cases}$$

where

$$\frac{F}{I} = e^{-k_ms} \frac{\sin(k_m w/2)}{k_m w/2}.$$

C.6 Backward Volume Spin Waves

Tangentially magnetized film



$$H_0 = H_{DC}$$

Dispersion relation:

$$\omega^2 = \omega_0 \left[\omega_0 + \omega_M \left(\frac{1 - e^{-k_z d}}{k_z d} \right) \right].$$

Group velocity:

$$\frac{1}{v_g} = \frac{\chi\kappa}{\omega_M d} \left[\frac{2}{\chi} + \frac{k_z d}{1 + \chi} \right].$$

For lowest order $n = 1$ mode,

$$\frac{1}{v_g} \bigg|_{k_z d=0} = -\frac{4}{\omega_M d} \frac{\sqrt{\omega_0(\omega_0 + \omega_M)}}{\omega_0}.$$

Loss:

$$\frac{1}{T_k} = |\gamma| \mu_0 \Delta H \left(\frac{\omega_0^2 + \omega^2}{4\omega_0 \omega} \right) = \alpha \frac{\omega_0^2 + \omega^2}{2\omega_0}.$$

Potential function:

$$\psi^{(o)}(\mathbf{r}) = \begin{cases} \psi_0 e^{k_z d/2} \sin(k_y d/2) e^{i\nu k_z z - k_z y}, & y > d/2, \\ \psi_0 \sin(k_y y) e^{i\nu k_z z}, & |y| \leq d/2, \\ -\psi_0 e^{k_z d/2} \sin(k_y d/2) e^{i\nu k_z z + k_z y}, & y < -d/2. \end{cases}$$

Normalization: For a mode power of P , mW/mm,

$$\psi_0 = \sqrt{\frac{4P}{\omega\mu_0 k_z d}}.$$

Radiation resistance of m th mode with wavenumber k_m :

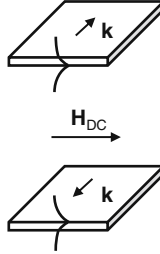
$$r_{rm} = \begin{cases} \frac{\omega\mu_0}{k_m d} \sin^2 \left[\frac{k_m d}{2\sqrt{-(1+\chi)}} \right] \left| \frac{F}{I} \right|^2, & m = 1, 3, 5, \dots, \\ \frac{\omega\mu_0}{k_m d} \cos^2 \left[\frac{k_m d}{2\sqrt{-(1+\chi)}} \right] \left| \frac{F}{I} \right|^2, & m = 2, 4, 6, \dots, \end{cases}$$

where

$$\frac{F}{I} = e^{-k_m s} \frac{\sin(k_m w/2)}{k_m w/2}.$$

C.7 Surface Spin Waves

Tangentially magnetized film



$$H_0 = H_{DC}$$

Dispersion relation ($k > 0$):

$$\omega^2 = \omega_0(\omega_0 + \omega_M) + \frac{\omega_M^2}{4} [1 - e^{-2kd}].$$

Or equivalently,

$$k = -\frac{1}{2d} \ln \left[1 + \frac{4}{\omega_M^2} [\omega_0(\omega_0 + \omega_M) - \omega^2] \right].$$

Group velocity:

$$\frac{1}{v_g} = \frac{4\omega}{\omega_M^2 d} e^{2kd}$$

$$\frac{1}{v_g} \Big|_{k_z d=0} = \frac{4}{\omega_M d} \frac{\sqrt{\omega_0(\omega_0 + \omega_M)}}{\omega_M}.$$

Loss:

$$\frac{1}{T_k} = \frac{|\gamma| \mu_0 \Delta H}{4\omega} (2\omega_0 + \omega_M) = \alpha(\omega_0 + \omega_M/2).$$

Potential function:

$$\psi_\nu(\mathbf{r}) = \begin{cases} \psi_0 (e^{kd} + p(\nu)) e^{-ky + i\nu kx}, & y > d/2, \\ \psi_0 (e^{ky} + p(\nu) e^{-ky}) e^{i\nu kx}, & |y| \leq d/2, \\ \psi_0 (1 + p(\nu) e^{kd}) e^{ky + i\nu kx}, & y < -d/2, \end{cases}$$

where $p(\nu) \equiv \frac{\psi_{0-}}{\psi_{0+}} = \frac{\chi - \nu\kappa}{\chi + 2 + \nu\kappa} e^{-kd},$

$$p(\nu) = \frac{\chi + 2 - \nu\kappa}{\chi + \nu\kappa} e^{kd}.$$

Normalization: For a mode power of P , mW/mm,

$$\psi_{0\nu} = \sqrt{\frac{P}{-(1 + \chi)\omega\mu_0 p(\nu)kd}}.$$

Radiation resistance:

$$r_r^{(\nu)} = \frac{\mu_0 \omega}{2kd} \left[\frac{1 + \chi}{(1 + \nu\kappa)^2 - (1 + \chi)^2} \right] \left| \frac{F}{I} \right|^2, \quad \nu = \pm 1.$$

where, for a SW mode with wavenumber k ,

$$\frac{F}{I} = e^{-ks} \frac{\sin(kw/2)}{kw/2}.$$

Appendix D

Mathematical Relations

D.1 Trigonometric Identities

$$2 \cos \alpha \cos \beta = \cos(\alpha + \beta) + \cos(\alpha - \beta)$$

$$2 \sin \alpha \sin \beta = \cos(\alpha - \beta) - \cos(\alpha + \beta)$$

$$2 \sin \alpha \cos \beta = \sin(\alpha + \beta) + \sin(\alpha - \beta)$$

$$\tan(\theta - \pi/2) = -\cot \theta$$

$$\sin 2\theta = 2 \sin \theta \cos \theta$$

$$\cos 2\theta = \cos^2 \theta - \sin^2 \theta$$

$$\cosh^2(x) - \sinh^2(x) = 1$$

$$\tanh^2(x) + \operatorname{sech}^2(x) = 1$$

$$\coth^2(x) - \cosh^2(x) = 1$$

D.2 Vector Identities and Definitions

$$\nabla \cdot (\nabla \times \mathbf{A}) = 0$$

$$\nabla \times \nabla \varphi = 0$$

$$\nabla \cdot \nabla \varphi = \nabla^2 \varphi$$

$$\mathbf{A} \cdot (\mathbf{B} \times \mathbf{C}) = \mathbf{C} \cdot (\mathbf{A} \times \mathbf{B}) = \mathbf{B} \cdot (\mathbf{C} \times \mathbf{A})$$

$$\nabla \cdot (\mathbf{A} \times \mathbf{B}) = \mathbf{B} \cdot (\nabla \times \mathbf{A}) - \mathbf{A} \cdot (\nabla \times \mathbf{B})$$

$$\nabla \times (\mathbf{A} \times \mathbf{B}) = \mathbf{A} \nabla \cdot \mathbf{B} - \mathbf{B} \nabla \cdot \mathbf{A} + (\mathbf{B} \cdot \nabla) \mathbf{A} - (\mathbf{A} \cdot \nabla) \mathbf{B}$$

$$\nabla \cdot (f \mathbf{G}) = \mathbf{G} \cdot (\nabla f) + f(\nabla \cdot \mathbf{G})$$

$$\nabla \cdot (f \nabla g) = \nabla f \cdot \nabla g + f \nabla^2 g$$

$$(\mathbf{M} \times \nabla) \times \mathbf{r} = -2\mathbf{M}$$

$$\begin{aligned}
\bar{\mathbf{k}} \cdot \bar{\mathbf{k}} &= \mathbf{k} \mathbf{k} - k^2 \bar{\mathbf{I}} \\
(\mathbf{k} \mathbf{k})_{ij} &= k_i k_j \\
\bar{\mathbf{k}} \equiv \mathbf{k} \times \bar{\mathbf{I}} &= \begin{bmatrix} 0 & -k_z & k_y \\ k_z & 0 & -k_x \\ -k_y & k_x & 0 \end{bmatrix} \\
\mathbf{k} \times \mathbf{A} &= \bar{\mathbf{k}} \cdot \mathbf{A}
\end{aligned}$$

$$\text{Divergence Theorem:} \quad \oint_S \mathbf{A} \cdot d\mathbf{s} = \int_V \nabla \cdot \mathbf{A} \, dv.$$

$$\text{Stokes Theorem:} \quad \int_S (\nabla \times \mathbf{A}) \cdot d\mathbf{s} = \oint_C \mathbf{A} \cdot d\mathbf{l}.$$

D.3 Fourier Transform Definitions

$$\begin{aligned}
f(t) &= \int_{-\infty}^{\infty} \frac{d\omega}{2\pi} e^{-i\omega t} f(\omega), & f(\omega) &= \int_{-\infty}^{\infty} dt \, e^{i\omega t} f(t), \\
f(\mathbf{r}) &= \int_{-\infty}^{\infty} \frac{d^3 k}{(2\pi)^3} e^{i\mathbf{k} \cdot \mathbf{r}} f(\mathbf{k}), & f(\mathbf{k}) &= \int_{-\infty}^{\infty} d^3 r \, e^{-i\mathbf{k} \cdot \mathbf{r}} f(\mathbf{r}).
\end{aligned}$$

Index

- Angular momentum, 6–12, 37
 - addition of, 20
 - orbital, 10, 11, 16
- Anisotropic Bragg diffraction, 253
- Anisotropic medium, 113
- Anisotropy
 - cubic, 86
 - energy density, 84
 - field, 85, 86, 90, 107
 - tensor, 87
 - uniaxial, 303, 323, 325
- Annihilation operator, 57
- Anomalous dispersion, 289
- Antiferromagnetism, 4
- Array factor, 191
- Asteroid, 103
- Auto-oscillations, 295
 - fingers, 266
- Backward volume waves, 158, 160, 161, 328
 - dispersion relation, 159, 167
 - group velocity, 160
 - insertion loss, 197
 - normalization, 182
 - orthogonality relation, 181
 - potential functions, 160
 - radiation resistance, 195, 196, 200
 - return loss, 196
 - solitons, 291
 - stationary formulas, 213
- Bifurcation
 - Hopf, 295
 - steady state, 295
- Birefringence
 - circular, 223
 - linear, 223
- Bistability, 267, 268
- Bogoliubov transformation, 276, 278, 303
- Bohr magneton, 23, 70
- Boltzmann factor, 70
- Bose-Einstein statistics, 43
- Bosons, 43, 57
- Boundary conditions, 206, 208
- Bragg diffraction, 253
- Brillouin function, 72, 73, 77, 79, 107
- Brillouin zone, 49
- Canonical equations, 302
- Canonical variables, 35, 54, 271, 272, 275, 276, 278, 302, 304
- Charge density, 112
- Circular polarization, 123
- Commutation relation, 15, 16, 21, 54, 59, 272
- Commutator, 15–18
- Compensation point, 78
- Conservation of charge, 121
- Constitutive relations, 112, 113, 139
- Continuity equation, 115, 121
- Conversion length, 251, 260
- Cotton-Mouton effect, 223, 252, 253, 334
- Coulomb gauge, 34, 37
- Coulomb potential, 24
- Coupled-mode equations, 238

- Coupling coefficient, 247, 251
- Creation operator, 57
- Cubic anisotropy, 86
- Curie Law, 72
- Curie temperature, 5, 73, 82
- Curie-Weiss law, 73
- Damping, 94
- Decay instability, 280
- Demagnetizing field, 145, 318
- Demagnetizing tensor, 146, 149, 150, 319
- Density of states, 310
- Diamagnetism, 3, 11, 67
 - susceptibility, 106
- Dielectric waveguide, 224
- Dipolar spin waves, 134, 142
- Dipole gap, 265, 290, 293, 298, 300–302
- Dispersion energy density, 211
- Dispersion relation, 49, 55, 64, 122
 - backward volume waves, 159, 167
 - dielectric waveguide, 227, 228, 257, 258
 - ferrite, 128, 130
 - forward volume waves, 166
 - isotropic medium, 122
 - magnetostatic wave, 140, 142
 - surface waves, 163, 167
- Dispersive medium, 113
- Divergence theorem, 114, 229
- Domains, 3–5
- Doppler effect, 309, 325, 327
- Dyadic product, 122
- Dynamical interaction, 62
- Effective magneton number, 72
- Eigenfunction, 14–17
- Eigenvalue, 14, 17, 18, 21–23, 29
- Electric energy density, 119
- Electric field intensity, 111
- Electric flux density, 111
- Electric volume current density, 111
- Electromagnetic wave, 142
 - extraordinary, 135
 - ordinary, 135
- Elliptical polarization, 123
- Energy density
 - electric, 119
 - magnetic, 119
- Energy velocity, 127, 169, 170
- Equipartition theorem, 322
- Euler-Lagrange equation, 35, 205, 208
- EuO, 75, 76
- Exchange interaction, 3, 33, 76, 141, 311
 - energy, 81, 82
 - field, 81, 82, 93
 - Pauli spin exchange operator, 45, 64
 - YIG, 142
- Exchange spin waves, 141
- False nearest neighbor, 299
- Faraday rotation, 135, 223, 236, 240
- Faraday's law, 34, 68, 225, 259
- Fermi energy, 310, 336
- Fermi-Dirac distribution, 336
- Fermi-Dirac statistics, 43, 310
- Fermions, 43
- Ferrimagnetism, 4
- Ferromagnetic resonance, 98, 108
 - foldover, 267
 - line width, 199
- Ferromagnetism, 3
- Field displacement non-reciprocity, 165, 197
- Foldover, 267, 269
- Forward volume waves, 155, 157
 - bistability, 269
 - dispersion relation, 166
 - group velocity, 155
 - insertion loss, 192, 193
 - normalization, 180
 - orthogonality relation, 179
 - potential function, 156
 - radiation resistance, 191, 192, 200
 - return loss, 192
 - stationary formulas, 212, 214
- Fourier transform, 58, 96, 124, 125, 191, 242, 276, 289, 322, 323
- Functional, 204, 208
- Functional derivative, 205
- Gadolinium gallium garnet, 184
- Gilbert damping, 95
- Group velocity, 126, 171
 - backward volume waves, 160
 - forward volume waves, 155
 - surface waves, 163

- Gyromagnetic ratio, 9–12, 69
- Hamiltonian, 14, 36–38, 42, 46, 47, 54, 58, 63
- Harmonic oscillator, 50, 62
 - classical, 50, 271
 - eigenfunction, 51, 52
 - operators, 56, 57
 - quantum mechanical, 50
- Heisenberg Hamiltonian, 39, 44, 46, 64
- Heisenberg uncertainty principle, 13, 16, 23
- Hermite polynomials, 51
- Hermitian matrices, 117
 - adjoint, 55
 - conjugate, 63
- Hilbert transforms, 187
- Holstein-Primakoff transformation, 57, 275
- Hund's rules, 26, 28
 - ground state, 74, 75
- Impedance, 185, 186
- Information dimension, 300
- Inner product, 46
- Insertion loss, 187
- Interaction bandwidth, 256
- Iron group, 28
- Isotropic medium, 113, 122
- Kerr effect, 252, 324
- Kinematical interaction, 62
- Kramers-Kronig relations, 187
- Kronecker delta, 88
- Lagrange multipliers, 219, 220
- Lagrangian, 35, 206, 210, 212, 220, 263, 271, 272
- Landé g factor, 12, 22, 30, 72
- Landau-Lifshitz equation, 91, 95, 104, 108, 151, 282, 311
- Langevin diamagnetism, 69
- Larmor precession, 11, 38, 104
- Left-hand polarization, 123
- Legendre equation, 147
 - polynomials, 148
- Lenz's law, 3, 67
- Limit cycle, 295, 296
- Linear polarization, 123
- Lorentz reciprocity theorem, 229
- Lowering operator, 53
- Lumped element model, 185
- Magnetic circular birefringence, 223
- Magnetic energy density, 119, 211
- Magnetic field intensity, 111
- Magnetic flux density, 112
- Magnetic linear birefringence, 223
- Magnetic susceptibility tensor, 67
- Magnetization, 69
- Magnetocrystalline anisotropy, 84
- Magnetoquasistatics, 139
- Magnetostatic approximation, 132, 169
- Magnetostatic limit, 132
- Magnetostatic modes, 140
- Magnetostatic scalar potential, 140
- Magnetostatic waves, 142
- Magnons, 50, 57, 62, 63
- Maxwell's equations, 34, 111, 112, 120–122, 129, 132, 151, 209, 225, 231, 237, 243, 258
- Micromagnetics, 104, 322, 323
 - mid-point rule, 105
- Microstrip, 183, 184
- Modulational instability, 286
- Molecular field, 73, 75, 76
- Néel temperature, 5, 79
- Néel theory of ferrimagnetism, 76
- Nonlinear Schrödinger equation, 304
- Orbital, 24
- Orbital angular momentum, 68
- Orthogonality relation, 178
 - backward volume waves, 180
 - forward volume waves, 178
 - surface waves, 182
 - TE modes, 230
 - TM modes, 230
- Paramagnetic susceptibility, 72, 78, 107
- Paramagnetism, 3, 70
- Pauli exclusion principle, 42, 57
- Pauli spin matrices, 29
- Permeability, 112, 113
 - tensor, 139

- Permittivity, 112, 113, 236, 237, 258, 259
 - tensor, 135
- Phase matching, 240, 253
- Phase velocity, 120
- Polarization, 122
 - circular, 123
 - density, 112
 - elliptic, 123
 - left-hand, 123
 - linear, 123
 - right-hand, 123
- Polder susceptibility tensor, 92
- Poynting theorem, 115, 117
- Poynting vector, 115, 126, 170, 326
- Precession frequency, 7, 9–11, 29, 166, 318, 319, 324
- Propagation loss, 176
- Pseudo-energy density, 210, 211

- Quantum numbers, 24
- Quasi-particle number density, 212

- Radiation reactance, 187
- Radiation resistance, 188
 - backward volume waves, 195, 196, 200
 - forward volume waves, 191, 192, 200
 - surface waves, 196, 198
- Raising operator, 53
- Rare earths, 28
- Reciprocal lattice vector, 49
- Reflection coefficient, 187, 339
- Relaxation time, 171, 172
- Residue theorem, 97
- Resonance frequency, 93
 - line width, 101, 108
- Return loss, 187
- Right-hand polarization, 123
- Russell-Saunders coupling, 84

- Saturation magnetization, 85
- Schrödinger equation, 47, 50, 51, 285
 - time dependent, 36
 - time independent, 14, 33
- Screening, 24
- Shell, 24, 26, 27
- Soliton, 286, 287, 304
 - Lighthill criterion, 289
 - pulse train, 291
 - spin wave bullet, 291
- Spin current, 311–314
 - density, 312, 314, 337
- Spin torque, 310, 312, 316, 317
- Spin transfer torque, 319
- Spin wave manifold, 64, 151
- Spin wave resonance, 142, 143, 166
- Spin waves, 33, 134, 141
- Spin-orbit coupling, 26, 84
- Spinors, 30
- Stationary formulas, 41, 212
- Stoke's theorem, 233
- Stoner-Wohlfarth model, 102, 108
- Subshell, 24–26
- Subsidiary absorption, 278
- Suhl processes, 278
 - first instability, 292
 - first order, 278
 - second instability, 280, 296
 - second order, 279
 - subsidiary absorption, 278
- Surface waves, 158, 162, 164, 166, 328
 - dispersion relation, 163, 167
 - group velocity, 163
 - insertion loss, 199
 - normalization, 183
 - orthogonality relation, 182
 - potential function, 165
 - radiation resistance, 196, 198
 - return loss, 198
 - stationary formulas, 212
- Susceptibility, 73
 - antiferromagnet, 79
 - diamagnetism, 69, 106
 - EuO, 75
 - paramagnetism, 72, 78, 107
 - tensor, 67, 91, 92

- TE modes, 224
- Thermal average, 71
- Torque, 6, 68, 106, 311, 317
 - current loop, 8
- Torque equation, 92, 93, 145, 150, 151, 210, 283, 318
- Total angular momentum, 21
- Transducer, 184, 185
- Transduction loss, 187
- Transition elements, 28

- Transmission line, 185
- Transverse susceptibility, 94
- Uniaxial anisotropy, 84
- Uniform plane waves, 120
- Uniform precession mode, 144, 166, 171
- Variational derivative, 205
- Walker's equation, 139, 140, 158, 162, 220
- Wave equations, 122
- Wave function, 13, 24
- Wave impedance, 134
- Wave number, 120
- Wave packet, 126
- Wave vector diagram, 253
- Wavelength, 120
- Weiss theory of ferromagnetism, 73
- Yttrium iron garnet, 5, 23, 28, 78, 333
 - exchange constant, 142
- Zeeman energy, 37, 70, 82, 102, 210, 220